REPORT

Tonkin+Taylor

National Liquefaction Model (NLM)

Final technical report

Prepared for
Natural Hazards Commission Toka Tū Ake
Prepared by
Tonkin & Taylor Ltd
Date
May 2026
Job Number
1017473 v5.2

Together we create and sustain a better world
www.tonkintaylor.com

Document control

Title: National Liquefaction Model (NLM)					
Date	**Version**	**Description**	**Prepared by:**	**Reviewed by:**	**Authorised by:**
11/11/24	1.0	Draft for client and peer review	M. Millen	M. Jacka	J. Russell
10/02/25	2.0	Draft for client and peer review	M. Millen	M. Jacka	J. Russell
24/04/25	3.0	Updated draft incorporating peer review feedback – for client and peer review	M. Millen	M. Jacka	J. Russell
30/06/25	4.0	Final report incorporating final peer review feedback	M. Millen	M. Jacka	J. Russell
02/07/25	5.0	Final Technical Report	M. Millen	M. Jacka	J. Russell
25/03/26	5.1	Added data attributions (section 13)	M. Millen	M. Jacka	J. Russell
21/05/26	5.2	Updated section 11 scenario output figures	M. Millen	M. Jacka	J. Russell

Key contributions by:

- P. Anithottam
- J. Bennett
- J. Beetham
- C. Cappellaro
- R. Dhakal
- J. Dickson
- T. Forstner
- C. Handley
- Q. Hornblow
- B. Karl
- B. Kennerley
- V. Lacrosse
- N. McDougall
- H. Lustiger
- M. Ogden
- D. Solovyeva
- K. Spencer-Edgar
- S. van Ballegooy
- K. Williams

Distribution:

Natural Hazards Commission Toka Tū Ake	1 electronic copy
Tonkin & Taylor Ltd (FILE)	1 electronic copy

Table of contents

Acknowledgements

The development of the National Liquefaction Model (NLM) was a significant undertaking that would not have been possible without the funding, guidance, and collaboration of numerous individuals and organisations. The authors wish to extend their sincere gratitude to all who contributed to this project.

This work was formally funded by the Natural Hazards Commission Toka Tū Ake (NHC). We gratefully acknowledge NHC's vision and investment in this model, which have been fundamental to its success. We particularly thank Jo Horrocks, Natalie Balfour, Richard Woods, Caleb Dunne and Wendy Saunders for their vision, guidance and project stewardship.

We extend our sincere thanks to the members of the Peer Review Team (PRT): Rick Wentz (Wentz Pacific Ltd.), Professor Ellen Rathje (University of Texas at Austin), and Associate Professor Brett Maurer (University of Washington). Their rigorous technical review and invaluable insights significantly enhanced the robustness and integrity of the model.

The strategic oversight provided by the Steering Group (SG) was instrumental in aligning the NLM with national priorities and ensuring its practical relevance. We thank Robert Buxton and Simon Cox (GNS Science), Sue-Ellen Fenelon and Jenny Christie (Ministry for the Environment), Helen Jack (Environment Canterbury), Sam Ketley (Aon), and Kiran Saligame (Ministry of Business, Innovation and Employment) for their expertise and continued engagement.

The usability and applicability of the NLM were greatly improved by the practical feedback from the End User Group (EUG). We thank its diverse members from central and local government, consultancies, research institutions, and the insurance sector for their time and constructive input.

This work relies on extensive datasets, and we thank the following organisations for making their data available: GNS Science Te Pū Ao for the QMAP series, the National Seismic Hazard Model and local groundwater models; Land Information New Zealand (LINZ) for elevation, LiDAR, and hydrographic data; the Ministry of Business, Innovation and Employment (MBIE) for its stewardship of the New Zealand Geotechnical Database (NZGD) and seismic hazard layers from Professor Brendon Bradley’s research group. We also offer a special thanks to the many regional and territorial authorities across New Zealand who provided information, particularly those who responded to direct requests for data not available on public portals.

The data processing, analysis, and modelling for this project were performed using the Python programming language. We specifically acknowledge the use of key open-source libraries, including NumPy, SciPy, Pandas, scikit-learn, PyKrige, and GSTools, which were instrumental in the development of the NLM.

Finally, we wish to acknowledge the dedicated project team at Tonkin + Taylor (listed as key contributors above) and wider contributions from domain experts, data scientists, software developers and support staff. We are also grateful to our former T+T colleagues Sjoerd van Ballegooy (Infinity Studio Ai) and Eric Bird (WSP) who made a huge contribution laying the foundations for this project.

Glossary

- **Bayesian updating**: a statistical method to revise the probability of an estimate using additional data based on the likelihood of the additional data.
- **BDR**: Building Damage Ratio.
- **BH**: Borehole, a type of Ground Investigation (GI).
- **Boundary uncertainty:** The increase in uncertainty of a parameter near a boundary.
- **Codebase**: The implementation of a digital workflow (i.e. the entire source code of the project).
- **Component**: A distinct element of a model (this can be another model, e.g. the GW model is a component of the liquefaction model).
- **CPT**: Cone Penetration Test – a type of GI.
- **CSO**: Consultancy Services Order.
- **Decoupled**: each module/output/component is self-contained, is independent of the implementation details of its inputs, and is independent of any downstream processes.
- **DEM**: Digital Elevation Model.
- ***density_status***: A category for BH logs to identify whether the layer description indicates that the soil has high, low or medium density.
- **DEST**: Determination of Earth surface Structures (algorithm).
- **Dirty CPT**: A dirty CPT is a CPT that was performed with a cone that was not properly cleaned prior to the test. This can result in very low sleeve friction values (sometimes negative), which usually results in soil appearing more liquefiable.
- **EUG**: End User Group.
- **f_s**: Sleeve friction – a measure outputted from a CPT.
- **FOS_{liq}**: The ratio of cyclic resistance of soil to liquefaction to the cyclic demand.
- **Geology**: The content of a deposit (3D).
- **Geomorphology model**: A series of spatial areas with a geomorphological class (i.e. soil type and depositional environment).
- **GI**: Ground Investigation - measures soil properties vs depth at a location.
- **GW**: Groundwater - water below the ground surface.
- **GWD**: Groundwater Depth - the depth from the ground surface to the unconfined GW table.
- **GWL:** Groundwater Level (also referred to as GW elevation and water table) – the elevation of the surface of the GW above mean sea level.
- **Groundwater flux:** The movement of GW through soil or rock, typically measured as flow per unit area.
- **Groundwater head:** The total energy per unit weight of GW at a specific point, influencing flow direction and pressure.
- **Groundwater source:** A location where GW is replenished through recharge processes.
- **I_c:** Soil behaviour type index – correlated to CPT tip resistance (q_c) and sleeve friction (f_s).
- **I_{c10}:** Soil behaviour type index (I_c) averaged over the top 10 m of the CPT soil profile.
- **Kriging**: A geostatistical interpolation technique that predicts values at unsampled locations and provides an estimate of the prediction error. It relies on variogram analysis to quantify spatial dependency set interpolation weights of surrounding data points.

- **LDFC:** Land Damage Fragility Curve – A relationship that estimates the probability of a land damage state for a given input measure (e.g. LSN).
- **LDM**: Liquefaction Damage Measure - A single number to represent the expected extent of liquefaction-induce ground damage (e.g. LSN, SV1D, LPI).
- **LENZ**: Land Environments of New Zealand.
- **LiDAR**: Light Detection and Ranging.
- **Liquefaction response uncertainty:** The uncertainty related to the prediction of liquefaction response.
- **LSN**: Liquefaction Severity Number (van Ballegooy, Malan, et al., 2014), an LDM.
- **LV**: Liquefaction Vulnerability.
- **LVM**: Liquefaction Vulnerability Model.
- **Map**: A static file displaying the geospatial variation of an attribute.
- **MBIE**: The Ministry of Business Innovation and Employment - the New Zealand government ministry that administers building regulation.
- **MfE**: Ministry for the Environment.
- **Misclassification uncertainty:** The uncertainty in the assignment of classes or categories.
- **ML**: Machine Learning.
- **Model**: A digital query-able output (e.g. GIS file).
- **Module**: A part of the codebase covering a particular domain (e.g. GW module).
- **MLR:** Multi-Linear Regression. A statistical method used to develop an equation between a dependent variable and two or more independent variables.
- **Mw**: Moment magnitude.
- **NWT:** National Water Table (model created by GNS).
- **NHC**: Natural Hazards Commission Toka Tū Ake.
- **NLM**: National Liquefaction Model.
- **NSHM**: National Seismic Hazard Model.
- **NZGD**: New Zealand Geotechnical Database (national database of GIs).
- **Parquet**: An efficient computer file type for storing tabular data.
- **PGA**: Peak Ground Acceleration.
- **P_L**: Probability of liquefaction as defined in Boulanger & Idriss (2014), expressed as a percentage from 0 to 100%.
- ***plasticity_status***: A category for BH logs to identify whether the layer description indicates that the soil has high or low plasticity.
- **PRT**: Peer Review Team.
- **PRUE**: Natural Hazards Commission Toka Tū Ake's catastrophe loss model suite.
- **q_c:** Tip resistance – a measure outputted from a CPT.
- **q_{c1N}**: Normalised equivalent cone tip resistance of a CPT.
- **q_{c1Ncs}**: Normalised clean sand equivalent cone tip resistance of a CPT. Where q_{c1Ncs} is a measure of liquefaction resistance for any frictional soil converted to an equivalent sand.
- **QMAP:** The digitised quarter million (1:250000) geological maps of New Zealand from a GNS-led project.

- **Realisation**: A single simulation of a random process representing one possible outcome. In loss modelling it is common to produce several realisations of an event to understand the range of outcomes due to some aspects of the model using random sampling.
- **RMA**: Resource Management Act, 1991 act administered by the Ministry for the Environment (MfE) in New Zealand.
- **SCPT**: Seismic Cone Penetration Test – a type of GI.
- **SG**: Steering Group.
- **SLR**: Sea-Level Rise.
- **Spatial variability**: The variation of a parameter within an area.
- **SPT**: Standard Penetration Test – a type of GI.
- **SSP**: Similar Soil Polygon - A polygon where the soil properties are considered similar for the purpose of evaluating liquefaction.
- **T+T**: Tonkin + Taylor.
- **term_high_q:** A flag to indicate that a CPT terminated in dense soil.
- **Transform:** A mapping of one value or class to another.
- **TTGD**: Tonkin + Taylor Geotechnical Database.
- **USGS**: United States Geological Survey.
- **Variogram**: A function that quantifies the spatial variability of a dataset by describing how the semi-variance between data points changes with distance and direction.
- **Voronoi expansion**: More commonly referred to as a Voronoi diagram, this process partitions 2D space around a set of input points, creating a cell for each point. The cell geometry is defined such that any location within the cell is at least as close to the cell's defining point as it is to any other of the original points.

Executive summary

The National Liquefaction Model (NLM) has been developed to deliver a consistent, data-driven framework for modelling liquefaction hazard across New Zealand. Development of the model was funded by the Natural Hazards Commission Toka Tū Ake (NHC). The NLM responds to key national needs identified following the Canterbury Earthquake Sequence: improving the accuracy of earthquake loss modelling, supporting informed decision-making about land-use planning, furthering research into liquefaction science, and enhancing public understanding of liquefaction hazards.

The NLM integrates multiple geotechnical, geospatial, and Groundwater (GW) datasets within a modular software architecture. The model draws on a national inventory of over 50,000 Ground Investigations (GIs), and undertakes more than 15 million liquefaction triggering analyses, to estimate the severity and likelihood of liquefaction across the country's flatland areas.

Key outputs include:

1 **Liquefaction Vulnerability Model (LVM):** used as a key input to NHC's loss modelling platform (PRUE), this model generates earthquake scenario and return-period-based outputs.

2 **Land damage probability maps:** to support informed land-use planning to manage liquefaction-related risk.

3 **National Flatland, Geomorphology and GW models:** to understand the inputs to the LVM and support other research.

4 **Key relationships to quantify liquefaction:** including liquefaction-induced Land Damage Fragility Curves (LDFCs), the quantification of liquefaction spatial variability, and relationships that model the change in liquefaction hazard for different relevant inputs.

The NLM framework is designed for future refinement: it is modular, readily updatable with new data, and adaptable to new scientific methods. It has the potential to be used to enable the modelling of additional infrastructure, although the primary focus of this phase is the modelling of residential houses. By decoupling the liquefaction model from seismic hazard models, the NLM remains resilient to future updates of the National Seismic Hazard Model (NSHM) and changes to GW, which are expected to occur due to climate change.

This first phase of model development has primarily focused on the development of the model framework to support regular updates and produce useable outputs for multiple end use cases. Throughout the report, potential future improvements have been identified to guide future development of the model. These are not recommendations for updates within the current phase of work but should be considered and prioritised for inclusion in the future model updates. The intention is for the model to be maintained and updated for years to come, and accordingly NHC is taking a long-term view on its investment.

Development of the model involved extensive stakeholder engagement, including guidance from a Peer Review Team (PRT), oversight from a Steering Group (SG), and input from a diverse End User Group (EUG). Their contributions ensured that the model is scientifically robust, practically useful, and broadly supported.

The release of the NLM enables a nationally-consistent approach to liquefaction assessment, that can be used to inform and enhance region-specific practices with a transparent and scalable system. The model can be used to support critical applications including pre-event planning, post-disaster response, infrastructure investment, and regulatory compliance, while also offering a foundation for ongoing research and refinement.

As with all models, there are important limitations that need to be understood when using the model. Many of these stem from the fact that the model has been developed at a national to

regional scale, and as a result, it is not appropriate to apply the NLM to higher resolution assessments (e.g. individual property or subdivision scales). The limitations subsections outline specific limitations related to each module and should be read in conjunction with the general limitations. These limitations are important and should be clearly understood and adhered to before the model is implemented for any particular purpose.

Liquefaction assessment is a complex and highly specialised undertaking. Furthermore, this model and the associated codebase are complex and outside the scope of routine geotechnical engineering expertise. Therefore, if this model and its outputs are utilised by others it is important that the context for any work is clearly defined, and that it is undertaken by a team with suitable competency and experience in earthquake geotechnical engineering and data science.

This technical report documents the development of the NLM, detailing its methodology, model architecture, data sources, outputs, and applications. This report has been developed for a technical audience to communicate the details of the framework that have been developed. It is not intended for a non-technical audience.

Our vision for the NLM is for it to become established as a key tool that supports natural hazard resilience in New Zealand.

1 Introduction

Tonkin & Taylor Ltd (T+T) was commissioned by Natural Hazards Commission Toka Tū Ake (NHC) in May 2023 to develop Aotearoa New Zealand's first National Liquefaction Model (NLM). The project is expected to be completed by 30 June 2025, but it is anticipated that the NLM will continue to be incrementally enhanced over time into the future.

1.1 Report purpose

The purpose of this report is to document the development of the NLM, detailing its methodology, model architecture, data sources, outputs, applications and limitations. This report has been developed for a technical audience to communicate the details of the framework that has been developed. It is not intended for a non-technical audience.

1.2 Study area

The NLM has been developed as an input into PRUE, NHC's catastrophe loss model suite, to assess consequential liquefaction damage to one and two-storey residential buildings across the "flatland" areas of New Zealand. Extensive liquefaction is generally not expected to occur in the "non-flatland" areas, and therefore the flatland defines the extent of the model. Figure 1.1 shows the extent of flatland in New Zealand determined from the Flatland Model (presented in Section 5). Flatland encompasses approximately 30% (~80,400 km^2) of New Zealand's total land area. Approximately 90% of buildings in New Zealand are located on flatland.

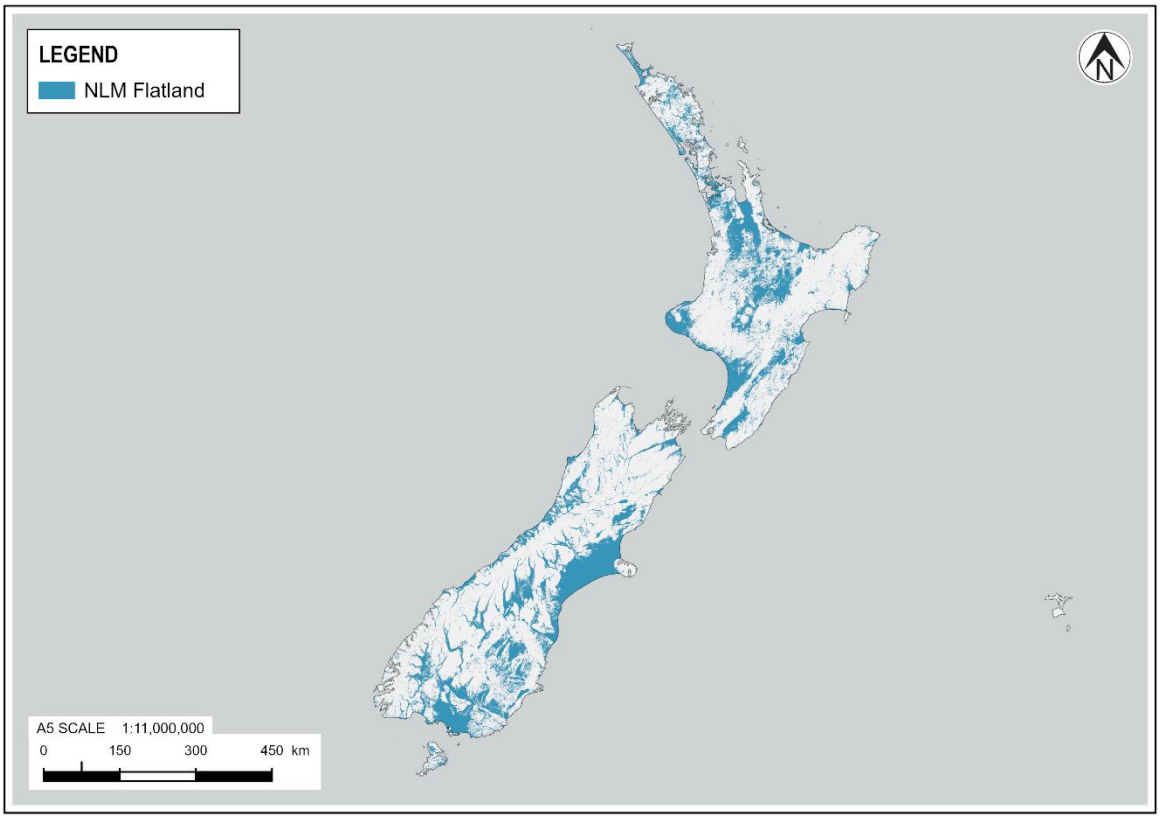

Figure 1.1: Flatland areas within New Zealand determined by slope analysis

1.3 Objectives of the NLM

The NLM will be used to support the development of NHC's earthquake loss modelling. A better understanding of the potential losses will assist NHC in securing risk financing, which will help provide affordable natural hazards insurance cover to homeowners.

The NLM aims to improve the knowledge of New Zealand's liquefaction-related risk in a way that is suitable to inform a range of end-user applications, including local government planning, public engagement and education, and other loss modelling exercises.

Additional objectives of the NLM include:

- Improve the state of knowledge about New Zealand's liquefaction hazards.
- Storage of input data in a consistent format which enables the inclusion of new data as it becomes available or is improved.
- Functionality that enables the model to be readily updated as new data becomes available or liquefaction methodologies evolve.
- The ability for the model to generate outputs in a variety of different formats.
- Well documented model development and accessible codebase, available upon request.

1.4 Report structure

The main sections of this report are structured as follows:

- **Context and background** (Section 2): Project background, scope, key stakeholders, intended users and use cases, regulatory context, existing liquefaction information, and limitations of the model.
- **Base information** (Section 3): Details of the foundational data used in model development, including ground surface levels, geology and geomorphology, geotechnical investigations, Groundwater (GW), seismic hazard, and historical observations of liquefaction.
- **Model structure and development** (Sections 4 to 11): Details the design and implementation of the different modules of the NLM including: flatland, geomorphology, Ground Investigations (GIs), Liquefaction Vulnerability (LV), GW, land damage fragility assessment, and scenario outputs.
- **Use of outputs** (Section 12): Discusses the use of the model outputs, key enhancements to liquefaction understanding, limitations and future opportunities and research needs.
- **Conclusions** (Section 14).

There are 9 digital supplements that accompany the report and provide examples related to some of the work described in the sections listed above. These are referenced in the report where necessary.

The technical sections that cover the NLM modules (Sections 5 to 10) generally follow a consistent structure where the purpose of the module is discussed followed by a description of the data schema of the outputs of the module (typically the output is a model). Three other subsections are presented at the end of each section, which cover validations, limitations and potential future improvements.

The validations subsections present validation exercises that were performed on the module outputs or parts of the module development process. As this is the first time a nationally-consistent model of LV has been developed for New Zealand, there are no previous versions against which to validate it. Therefore, validation can only be undertaken where other models are available and those models that are available have been undertaken at a different scale, under a different context, and using a different methodology. This limits the conclusions that can be drawn from this validation process.

For future development of the NLM, the previous versions of the model will serve as “baseline” datasets to validate against.

The limitations subsections outline specific limitations related to that module and should be read in conjunction with the general limitations (Section 2.7). These limitations are important and should be clearly understood and adhered to before the model is implemented for any particular purpose.

The potential future improvements subsection provides potential tasks that could be undertaken to improve future releases of the model. These future improvements are not recommendations for updates within the current phase of work but should be considered and prioritised for inclusion in the future model updates.

This document is presented in the order of the model build process; however, some concepts require information that is only presented later in the text. In general, these sections have been cross-referenced for the reader. In some instances, some details and decisions impact other model outcomes. The discussion of these impacts requires significant context. To aid the reader, these discussions are presented in orange text boxes like the one below.

Orange text boxes are uses to indicate that the text refers to concepts that are outside of the current context and may not have been presented yet in the document. These boxes often discuss details and decisions that impact model outputs and require a holistic understanding of the full model build process.

2 Context

2.1 Background to this project

Following the Canterbury earthquake sequence (2010 – 2011) and the significant damage caused by liquefaction, there has been increased focus on managing New Zealand’s liquefaction hazard. This increased focus has been led by NHC, the Ministry of Business, Innovation and Employment (MBIE), the Ministry for the Environment (MfE), local councils, insurers, reinsurers and crown research institutes (e.g. GNS).

In 2011, MBIE published guidance for repairing and rebuilding houses affected by the Canterbury earthquake sequence in the Canterbury region (MBIE, 2012). This document provides guidance about how to take liquefaction into account when subdividing land, designing houses and processing building consents. While the scope of the guidance is limited to the Canterbury region, in practice many of the recommendations are routinely applied for design purposes throughout New Zealand.

In 2015, NHC (formerly known as the Earthquake Commission) began work to revise their loss models to explicitly incorporate the effects of liquefaction. Previous models had not accounted for the effects of liquefaction which led to a significant under-prediction of potential losses from the Canterbury earthquake sequence.

In 2017, MBIE and the MfE published national guidance on undertaking liquefaction assessments to support better land-use and development planning (MBIE/MfE, 2017). The scope of the MBIE/MfE Guidance (2017) is focused on the legislation and policy associated with the Resource Management Act (RMA) and the Building Act.

In 2019, MBIE made changes to the Building Code (MBIE, 2019) (changing the definition of “Good Ground” in NZS 3604:2011 (Standards New Zealand, 2011)) which came into effect at the end of 2021 and requires all territorial authorities to consider liquefaction when processing building consents for residential dwellings.

In 2021, MBIE in collaboration with the New Zealand Geotechnical Society, published the Geotechnical Engineering Practice Series to provide updated guidance on earthquake geotechnical engineering in New Zealand (MBIE, 2021, p. 1). This series outlines best-practice approaches for assessing and mitigating geotechnical hazards such as liquefaction, lateral spreading, and ground shaking, with a focus on improving the seismic resilience of buildings and infrastructure.

Accordingly, there are two main drivers that have led to NHC commissioning the NLM:

1 **Loss modelling**: NHC is developing a loss model that specifically accounts for liquefaction damage to residential houses. This model is probabilistic and uses the expected level of liquefaction severity to predict the extent and additional cost of damage caused by liquefaction (i.e. the additional cost over and above the cost of the building shaking damage). The liquefaction loss model therefore requires maps of liquefaction severity as a key input. Currently, these are only internally available for NHC for Wellington, Hawke's Bay, and Christchurch, having been developed as part of the loss modelling work carried out previously by T+T. The NLM will enable this loss modelling to be carried out nationally, both for future loss estimation and for event response.

2 **Regulatory functions**: The RMA requires an assessment of natural hazard risk to support applications for subdivision consenting, and therefore there is a need to understand whether that land is likely to be affected by liquefaction. While the driver for the NLM is primarily in relation to regional scale loss modelling, the model may also be able to help inform the development of a territorial authority's MBIE/MfE Guidance (2017) maps[1].

In addition to this, there are other potential benefits from developing the NLM, such as loss modelling assessment of other assets (e.g. pipe networks, and multi-storey buildings), scenario modelling to support Civil Defence and Emergency Management planning exercises, and public education initiatives[2]. Accordingly, the NLM is being developed in a modular way to facilitate future development for these additional benefits.

2.2 Scope of works

The original scope of works is set out in the Consultancy Services Order (CSO) titled *National Liquefaction Model* and dated *23 May 2023*. Due to the uncertain nature of this novel project, the CSO was written to allow for significant stakeholder engagement, allowing the scope to be refined over time.

The main outputs of the NLM include:

- A Liquefaction Vulnerability Model (LVM) that is suitable for ingestion into NHC's catastrophe loss model suite PRUE.

[1] It is not appropriate to apply the NLM at an individual property level, or to directly translate the model outputs to MBIE/MfE liquefaction vulnerability (LV) categories or vulnerability maps. Rather, the NLM can be one source of information which if used to help inform MBIE/MfE regional mapping, must be critically assessed and verified by suitably qualified and experienced geo-professionals, alongside other relevant information such as factual data specific to the area in question. Where the NLM is used to help inform development of MBIE/MfE guidance maps, it is important to appreciate the low level of detail in the input data and the significant uncertainties in the model outputs, including the limitations detailed in Section 2.7. The development of MBIE/MfE maps is discussed further in Section 12.2. The NLM model outputs are likely to only be relevant to help inform development of Level A maps (basic desktop assessment), or Level B maps (calibrated desktop assessment) in conjunction with additional ground truthing and qualitative analysis. Development of Level C and Level D maps requires location-specific mapping of geology and geomorphology, subsurface investigations and quantitative analysis (refer Table 3.2 of MBIE/MfE (2017)), and this more detailed information would supersede any outputs from the NLM.

[2] The NLM may not be directly applicable/useable for these other applications and may require modification or further development before it is suitable for the alternative use cases. Please refer to Section 2.7 for more information about limitations of the NLM.

- Outputs to help generate maps to support land-use planning processes consistent with the format provided in the document *Planning and engineering guidance for potentially liquefaction prone land* (MBIE/MfE, 2017).
- Liquefaction maps for various earthquake return periods based on the National Seismic Hazard Model (GNS Science, 2022c). 25-year, 100-year, 500-year and 2,500-year return period intervals.
- Liquefaction maps for the four historical earthquake events (Darfield 4 September 2010 Mw7.1, Christchurch 22 February 2011 Mw6.2, Christchurch 14 February 2016 Mw5.7 and Kaikōura 14 November 2016 Mw7.8).
- Liquefaction maps for an Alpine Fault earthquake event.
- Loss analysis due to ground shaking and liquefaction-induced damage for each of the historical earthquake scenarios for New Zealand's one to two-storey residential building portfolio. Note, the loss analysis is not covered as part of this technical report.
- Nationally consistent Flatland, Geomorphology and GW models[3].
- A report documenting the structure of the model and its development. The codebase from which the NLM is generated will be made available on request.

2.3 Key stakeholders and engagement

In addition to NHC and T+T, three other groups have been engaged in the NLM project:

1 **The Peer Review Team (PRT)** consists of Rick Wentz (Wentz Pacific Ltd.), Prof. Ellen Rathje (University of Texas at Austin), and Assoc. Prof. Brett Maurer (University of Washington). The role of the PRT is to provide recommendations to NHC relating to technical aspects of the NLM. Rick Wentz is the Lead Peer Reviewer for the PRT.

2 **The Steering Group (SG)** is a stakeholder group that consists of Robert Buxton (GNS Science Te Pū Ao), Simon Cox (GNS Science Te Pū Ao), Sue-Ellen Fenelon (MfE), Jenny Christie (MfE), Helen Jack (Environment Canterbury), Sam Ketley (Aon), Kiran Saligame (MBIE), and Geoffrey Spurr (NHC). The role of the SG is to provide specialist oversight and recommendations during the development of the NLM.

3 **The End User Group (EUG)** is a stakeholder group that consists of a wide range of end users from representative organisations such as central and local government, insurers, consultants, and researchers. The key objectives of forming and engaging with the EUG are:

   - Ensure end users are aware of the model, including why it's needed, why NHC funded it, its scope, and limitations.
   - Provide an opportunity for end users to provide feedback on the model focused on how they may engage with it once it is released.
   - Promote the use of the model amongst relevant stakeholder groups with the goal of creating "champions" who engage with the model regularly.
   - Manage risks associated with the use and application of the model.

2.4 Intended users and use cases

There are several intended users and associated use cases of the NLM. The examples listed below are not intended to be exhaustive, and it is likely that other users will be identified as the model starts to be used in practice and continues to evolve.

[3] The GW Model includes estimates of the present-day GW level and a future GW level assuming 1 m of sea-level rise (SLR).

2.4.1 Natural Hazards Commission Toka Tū Ake (NHC)

NHC intend to use the NLM for a range of different applications. They and their agents (e.g. researchers and consulting engineers) will use the NLM as an input to their loss modelling software, PRUE, to help understand their potential exposure for a range of earthquake scenarios and to help set their requirements for appropriate levels of reinsurance.

They will use the outputs to help support the generation of nationally-consistent maps in the MBIE/MfE Guidance (2017) format to facilitate consultation with central and local government, their agents, and the wider community. How these outputs will be shared with these stakeholders is yet to be determined because this requires validation of the output and communication with these parties. It is envisaged the ongoing engagement with the EUG will be an important part of this process, and a communication plan is currently being developed by NHC.

Similarly, they will use the analysis from the earthquake return periods and earthquake scenarios to facilitate consultation with a range of stakeholders. For example, the analysis will be useful for Civil Defence and Emergency Management planning exercises, public education initiatives, and land-use planning activities. Additional return periods and scenarios could also be modelled; however, this is currently out of scope for this project.

2.4.2 Councils and their agents

It is intended that councils and their agents (e.g. consulting engineers and planners) will interact with the NLM by providing inputs and interpreting the outputs. The objective is that they will provide inputs in the specified format to the model (e.g. geomorphology maps and GW models) to enable periodic updates of the NLM to produce more refined outputs over time.

The NLM outputs can support councils with the development of MBIE/MfE Guidance (2017) maps and to validate their existing liquefaction maps. Ultimately, the MBIE/MfE maps may then be used to support regulatory processes (e.g. reviewing resource and building consent applications, and land-use planning purposes) following detailed evaluation and assessment by councils and their agents[4].

Finally, councils may choose to use the NLM outputs to support their own loss modelling exercises. For example, councils have previously engaged consultants to undertake loss modelling for Three Waters infrastructure. In each instance, this has required the development of a LVM specifically for this purpose. Further development of the NLM is required to facilitate the use of the model for this specific purpose (e.g. estimation of the extent and severity of lateral spreading), however, it has been developed in a way that can readily facilitate this.

2.4.3 Insurers, banks, and large asset owners

Insurers, banks, and large asset owners are often interested in their exposure to natural hazards to help support evaluation of the associated risk. They could use the NLM to assess the exposure of their assets to liquefaction for loss modelling, event response planning, and portfolio management. Depending on the asset type under consideration, further development of the NLM may be required to facilitate the use of the model for this purpose (e.g. estimation of the extent and severity of lateral spreading).

2.4.4 Researchers

Researchers and the academic community will be interested in many aspects of the NLM. The novel aspects of the NLM (see Section 12.3) will likely be of particular interest and could be developed

[4]The outputs of the NLM should not be used to generate MBIE/MfE maps without consideration of the local context and other information, which will require careful assessment by council and its agents. Please refer to Section 2.7 for more information about limitations of the NLM.

further. The data that is created as inputs to the NLM (e.g. GW models and geomorphology maps) could be utilised for research into both liquefaction and other applications (e.g. impacts of Sea-Level Rise (SLR) on GW). The outputs of the NLM (e.g. the loss model input and the scenario analysis) will be valuable resources for research projects.

2.5 Regulatory context

Central and local government agencies have important roles in the management of Natural Hazards in New Zealand. Reference to these agencies is provided throughout this report and therefore this section provides context to the role of these agencies and their jurisdiction, and the regulatory framework within which they operate as it is relevant to the NLM.

2.5.1 Central government

Central government agencies that are key stakeholders in the NLM include NHC, MfE, and MBIE. Their roles and relevant legislation and policy documents are introduced at a high level below[5].

- **NHC** is the crown entity established under the Earthquake Commission Act 1993 that invests in Natural Disaster research to help communities reduce their natural hazard risk. They provide residential property insurance for natural hazards following an event. From July 2024, NHC operates under new legislation, the Natural Hazards Insurance Act 2023. The new legislation has three key objectives; enabling better community recovery from natural hazards, clarifying NHC's role and the insurance cover provided by the Act, and enhancing the future durability and flexibility of legislation.
- **MfE** is the Government's primary advisor on environmental matters, and it has a stewardship role for the environment. MfE is responsible for the RMA which is the primary legislation in New Zealand for managing the environment. The RMA lists the management of natural hazards as a matter of national importance and includes provision for territorial authorities to refuse a resource consent for subdivision if the land is at significant risk from natural hazards. In September 2023, MfE published the first proposed National Policy Statement for Natural Hazard Decision-Making (NPS-NHD) (MfE, 2023) which aims to direct how decision-makers consider natural hazard risk in planning decisions relating to new development under the RMA.
- **MBIE** is an agency with multiple cross-government functions including acting as the steward and the central regulator for the building regulatory system in New Zealand. The Building Act 2004 is the primary legislation underpinning the building regulatory system. The Building Code (Building Regulations 1992) sets the minimum performance standards that buildings must meet to comply with the Building Act.

2.5.2 Local government

Local government in New Zealand is made up of 11 regional councils, 61 territorial authorities, and 6 unitary authorities. Regional councils typically serve a large area and have a key regulatory function by making decisions about land-use to reduce the impact from natural hazards. Territorial authorities consist of city and district councils which typically serve a smaller area. They have a key role in the regulation of natural hazards as consenting authorities for both resource and building consents. Unitary authorities are territorial authorities with regional council responsibilities. They include Auckland Council, Chatham Islands Council, Gisborne District Council, Marlborough District Council, Nelson City Council, and Tasman District Council.

[5] Legislation and policy on regulatory matters are subject to reform and change (e.g. RMA reforms). The reader should refer to the relevant legislation and associated policy, and seek appropriate advice, when considering application of the NLM to any regulatory context. Please refer to Section 2.7 for more information about limitations of the NLM.

Figure 2.1 shows the territorial authority and regional council boundaries. Note that some territorial authority and regional council boundaries do not align meaning that some territorial authorities are in the jurisdiction of more than one regional council.

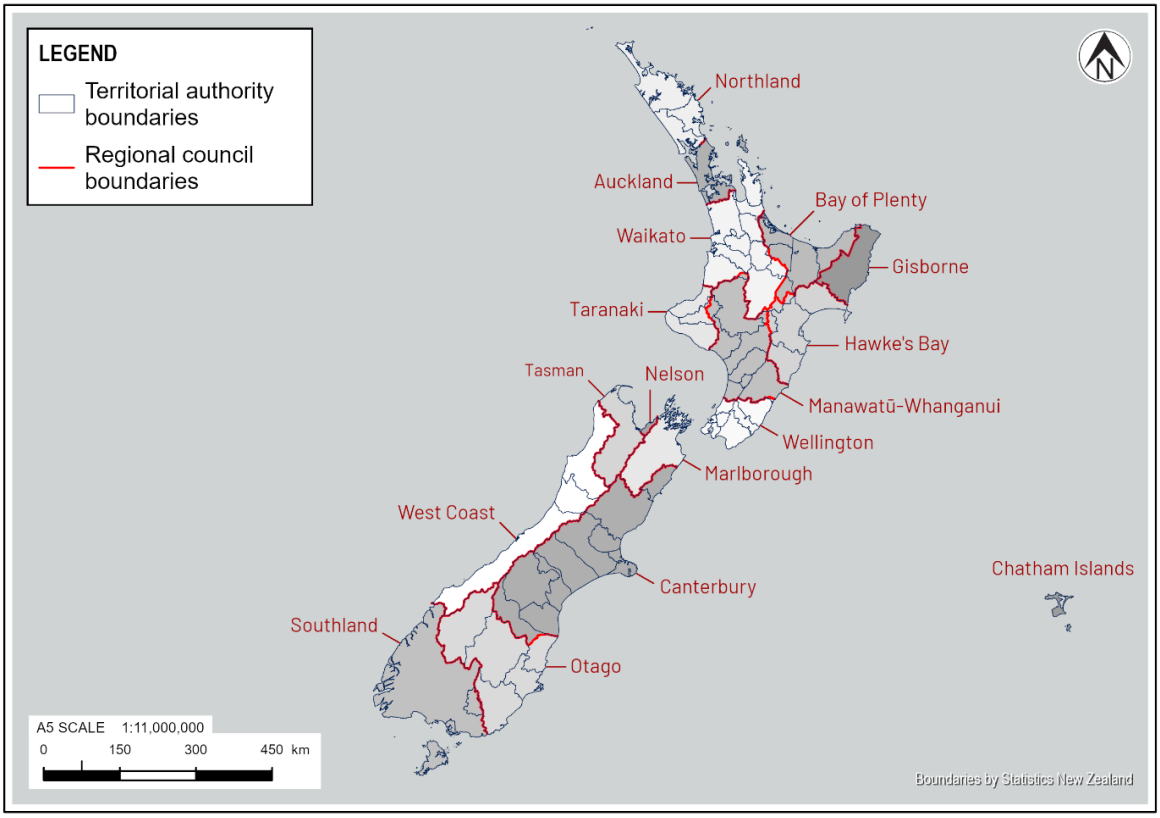

Figure 2.1: Territorial authority and regional council boundaries in New Zealand

2.6 Existing information about liquefaction

Nationally, there is a large amount of pre-existing information about liquefaction available. This information can be broadly categorised as follows:

- **Liquefaction maps** prepared prior to the release of the MBIE/MfE Guidance (2017). These maps have been produced by a variety of different authors for a variety of different uses. As a result, they typically do not share a common format or a consistent basis for categorising the liquefaction potential of the land assessed. Many of these maps were prepared prior to, or immediately following, the Canterbury earthquake sequence. Therefore, the authors did not have the benefit of the subsequent advances in liquefaction assessment methods, the increased availability of data facilitated by the New Zealand Geotechnical Database (NZGD), or the ability to refer to a common national guidance detailing how to undertake the assessment.
- **LV maps** consistent with the format of the MBIE/MfE Guidance (2017). 43 of the 67 Territorial authorities across New Zealand have published such maps which have been commissioned either by the local regional council or the territorial authority (see Figure 2.2). The majority (39) of these cover the full extent of the territory. The territory-wide assessments are typically undertaken to a Level A (Basic desktop), or Level B (Calibrated desktop) level of detail as specified in the MBIE/MfE Guidance (2017). There are some more detailed assessments published, for example a Level C (Detailed area-wide assessment) for Glenorchy (Tonkin + Taylor, 2022a), but they cover relatively small areas of land.

  - These maps are typically more useful for their intended purpose than other forms of mapping because they have been prepared with reference to common guidance, and with the benefit of improved assessment methods and access to data. Despite these benefits, due to differences in interpretation of the MBIE/MfE Guidance (2017), there are inconsistencies between some of the assessments. Furthermore, the maps are also limited because they are static representations of the understanding of LV at the time the assessment was undertaken. Subsequent changes (e.g. new data, changes in liquefaction science etc.) could require a reassessment of the LV of the land. The recent update to the NSHM is a prime example of this (GNS Science, 2022b).

- **LVMs** suitable for ingestion into NHC's catastrophe loss model suite PRUE. These models have been developed by T+T for the Wellington, Hawke's Bay, and Christchurch regions. While they are robust models, the spatial extent they cover limits their usefulness for NHC's purposes and there is the opportunity for further development of the methodology. The NLM, with its national scope, enables the modelling of many more scenarios and makes use of more of the available data across New Zealand.
- **Other national-scale models** have been developed for research purposes in New Zealand. Notable studies include the work by (Lin et al., 2019), which evaluates the exposure of New Zealand's transportation and power transmission networks to liquefaction.

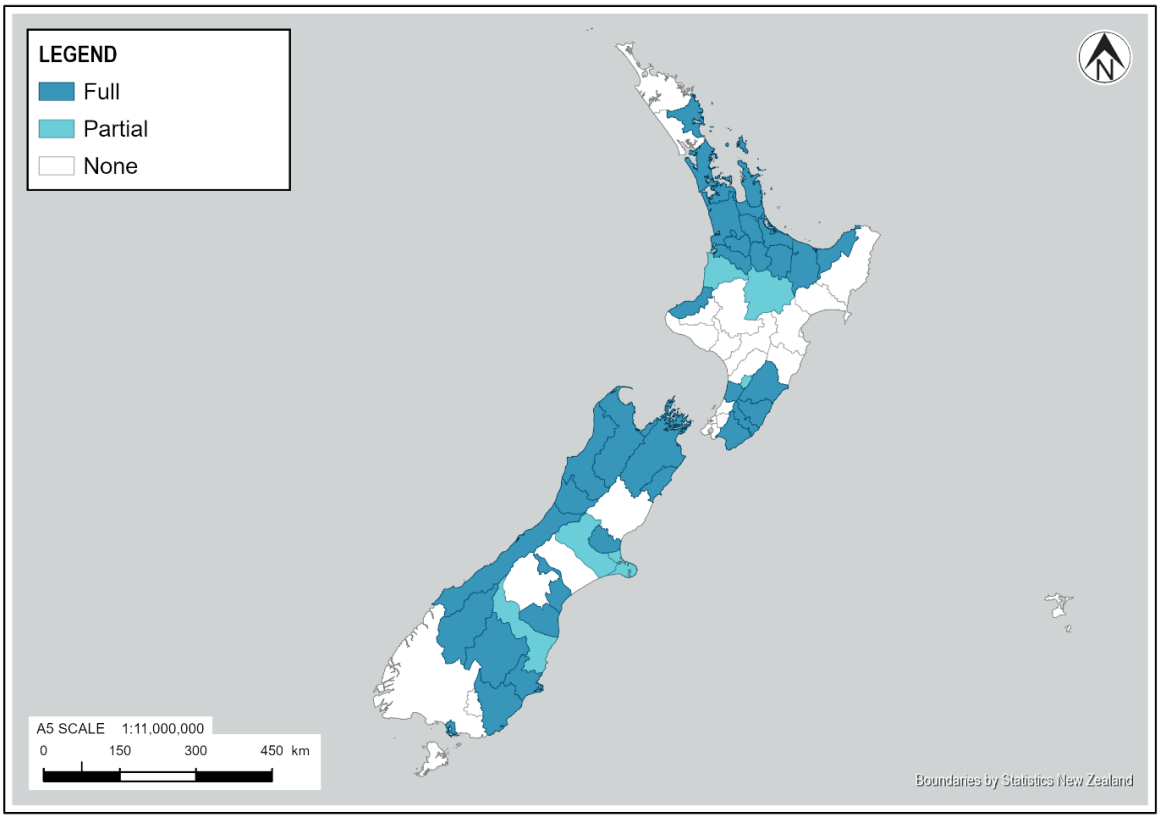

Figure 2.2: National coverage of MBIE/MfE Guidance (2017) maps (by territorial authority), with the colour shading denoting whether mapping covers the full region or only part

2.7 Limitations of the NLM

All models have limitations, however if these limitations are understood then the model can still be useful. Each of the technical sections discuss limitations associated with the sub-model discussed in each. The limitations listed here identify key limitations in the inputs, the outputs and the overall

methodology. This section should be read in conjunction with the model limitations section for each sub-model.

Key limitations of the NLM include the following:

1 **Scale of application:** This version of the NLM has been developed at a national to regional scale and it is not appropriate to apply the NLM to higher resolution assessments (e.g. individual property or subdivision scales). Even for development of regional scale maps, the NLM should only be viewed as one source of information which must be critically assessed and verified by suitably qualified and experienced geo-professionals, alongside other relevant information such as factual data specific to the area in question.

   This also applies to sub-models of this version of the NLM (e.g. Flatland, Geomorphology, GI and GW) which have been developed for the purpose of regional scale LV assessment and therefore should not be relied upon for other purposes without careful consideration of other site-specific information.

2 **Distribution of investigation data:** Ground and GW investigations are not evenly distributed and vary considerably between regions and within cities and towns (e.g. clusters in new subdivisions). This limits the development of representative prediction models in areas with low or no data and these areas may be mis-represented in NLM outputs.

3 **Use of the model:** Liquefaction assessment is a complex and highly specialised undertaking. Furthermore, this model and the associated codebase are complex and outside the scope of routine geotechnical engineering expertise. Therefore, if this model and its outputs are utilised by others it is important that the context for any work is clearly defined, and that it is undertaken by a team with suitable competency and experience in earthquake geotechnical engineering and data science.

4 **Regulatory context:** This report refers to relevant regulation (e.g. legislation and policies) that are, to the best of the authors knowledge, current as at the date of writing. Legislative and policy reform are ongoing in New Zealand and the reader should undertake their own review of such information as it is relevant to their context (e.g. MBIE, 2021; MBIE/MfE, 2017).

5 **Other sources of information:** There are many other sources of information about liquefaction available throughout New Zealand (e.g. site-specific assessment, regional land-use studies, and national technical guidance). Any application of the NLM needs to also consider other information about liquefaction that may be relevant to the context within which it is being used.

6 **Loss modelling:** This version of the NLM is only suitable for loss modelling in PRUE for one to two-storey residential dwellings. Further development that is outside of the scope of this project may be required to make it suitable for loss modelling of other assets (e.g. pipe networks and multi-storey buildings) and/or in other catastrophe loss modelling suites/programmes (e.g. vendor models developed by Moody's RMS and Verisk AIR).

7 **Lateral spreading:** This version of the NLM does not include a module that estimates land vulnerability to lateral spreading (i.e. it does not model the intensity or degree of lateral spreading), nor does it identify areas where lateral spreading has the potential to occur. Further work would be required to incorporate this module into the NLM in the future.

8 **Data-driven approach:** The choice to use an automated approach has benefits in that it reduces human-introduced biases but does not allow modifications to outputs and processes due to local knowledge and professional judgement. In some areas, particularly areas with a low density of investigations, local knowledge and judgement could significantly inform more detailed liquefaction assessment.

9 **Development of MBIE/MfE Guidance (2017) maps:** The automated NLM outputs are not suitable for directly converting to the MBIE/MfE Guidance (2017) maps without further

manual review (and likely localised adjustments) by suitably qualified geo-professionals. This is because some of the limitations listed in the data-driven approach (item 8 above) do not address key aspects of the MBIE/MfE Guidance (2017). Also, the MBIE/MfE Guidance (2017) is a risk-based approach that includes stakeholder engagement and consideration of the local context and other relevant information, which is outside of the scope of this project.

10 **Liquefaction Damage Measures:** The current version of the NLM relies on Liquefaction Damage Measures (LDMs) that have been computed in aggregate without the specific quality control that would be performed for site-specific work. Therefore, the LDMs of individual GIs, as well as the derived outputs, are not suitable for site-specific assessment.

11 **LVM uncertainty:** The LVM produces an estimate of uncertainty, however, the GIs in each geomorphology are not uniformly distributed. In cases where there are no local GIs to constrain estimates, these areas may have larger uncertainty than what is captured by the geospatial model. The future inclusion of GIs in these areas may result in significant changes to predictions in the future releases of the model. Areas with no refined geomorphology model and very few digital Cone Penetration Tests (CPT) and Boreholes (BH) are associated with particularly high uncertainty (e.g. Upper Hutt).

12 **GW model uncertainty:** The NLM GW Model produces an estimate of uncertainty, however, the GW investigation dataset does not sample the full extent of the NLM Flatland Model and therefore some estimates are extrapolations (rather than interpolations). Extrapolations have higher uncertainty associated with them than what is reflected in the GW uncertainty distribution. The areas with extrapolation predictions are not easily identified due to the multi feature regression approach adopted but are in areas with a low density of GW measurements.

13 **Data source limitations:** The LVM and GW Model rely on GIs and static water depths, the majority of which are sourced from the NZGD. The limitations on accuracy and disclaimers for the NZGD are applicable to the NLM output.

14 **Error guides:** The error guides in Section 4.3.1 and approximate uncertainty levels for each tier of Similar Soil Polygon (SSP) in Section 8.6 are only guides and bias can compound, especially at individual property level. These limits have been set for the purpose of regional loss modelling and the model outputs are not suitable for assessing individual properties.

3 Base information

This section details the base information used to develop or validate the sub-models of the NLM.

3.1 Ground surface levels

A ground surface elevation model and ground slope model are needed to help identify areas of flatland (see Section 5) and as a training feature for the NLM GW Model (see Section 9). The sections below explain how the national ground surface elevation and slope models were developed for the purpose of the NLM.

3.1.1 National 8 m DEM

The New Zealand 8 m Digital Elevation Model (DEM) (LINZ, 2012) was developed by Toitū Te Whenua Land Information New Zealand (LINZ) and Geographx. It incorporates data from the LINZ Topo50 20 m contours recorded in January 2012 and includes 3-second Shuttle Radar Topography Mission data from the United States Geological Survey (USGS), which provides high-resolution topographic information. The model creation process involved constrained triangulation and the application of the Determination of Earth Surface Structures (DEST) algorithm, a technique for creating DEMs that aims to accurately represent natural landforms[6]. It covers most of mainland New Zealand but excludes some Islands such as the Chatham Islands (see Figure 3.1).

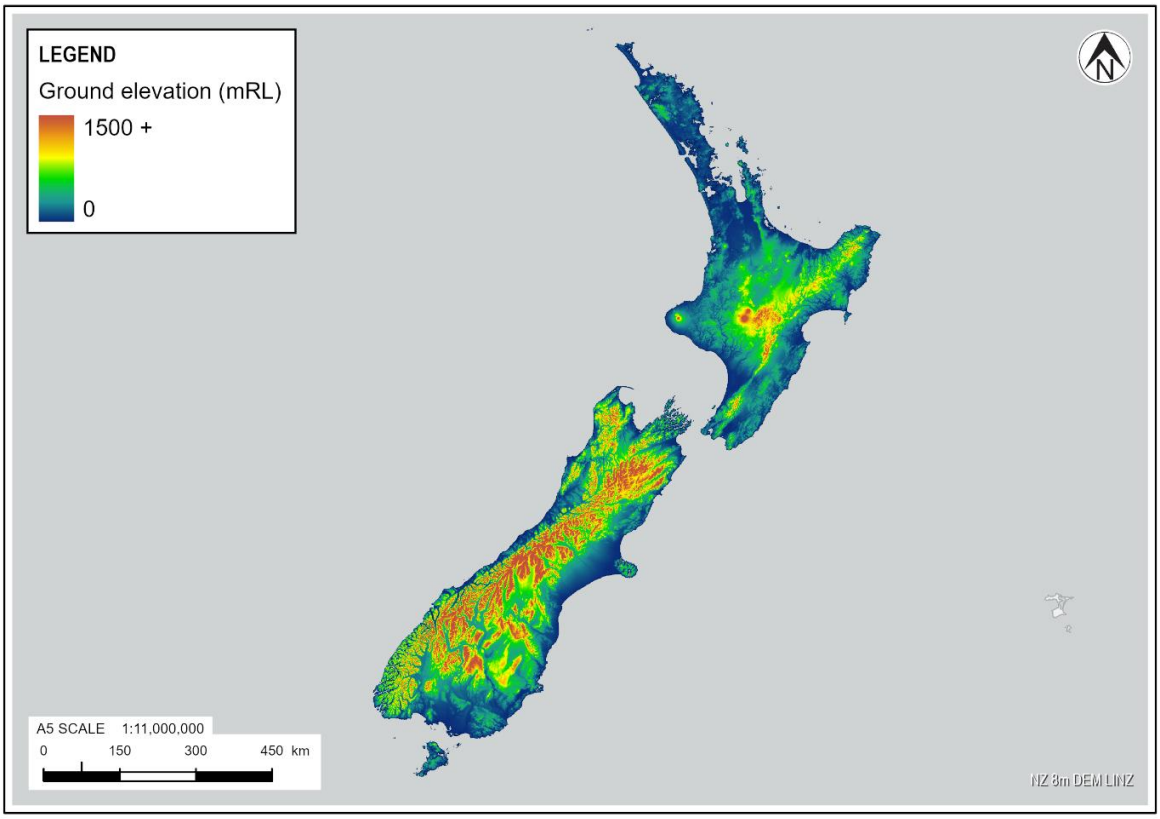

Figure 3.1: National 8 m DEM map of New Zealand

Designed primarily for use in cartographic visualisation, this DEM provides a representation of New Zealand's topography. It can also be used for preliminary assessments in terrain analysis, prior to the

[6] More specifically, the DEST algorithm is an established method that was developed to reconstruct digital terrain models of complex landforms from topographic data, such as contour lines and spot heights.

acquisition of more detailed, high-resolution data. The New Zealand 8 m DEM conforms to the spatial accuracy of the LINZ data it is based on.

3.1.2 LiDAR-derived 1 m DEM

The 1 m LiDAR-derived DEMs, a collection of 102 datasets with 95 publicly available sources collected between 2007 and 2024, are hosted by LINZ through the LINZ Data Service. The public datasets in this collection cover 67% of New Zealand's land area (see Figure 3.2). The majority of New Zealand's residential property portfolio has LiDAR data available. Created using Light Detection and Ranging (LiDAR) technology, these datasets map the Earth's surface by emitting laser pulses from airborne systems and measuring the reflected signals. These LiDAR-derived DEMs are significantly more accurate than the National 8 m DEM.

Each dataset in the collection is presented at a 1 m resolution. Within these datasets, there is a variation in point density. The dataset from Mackenzie, Canterbury in 2015 has the lowest point density at 1.30 points per square metre, while the Wānaka, Otago dataset for 2022-2023 has one of the highest point densities at 40.65 points per square metre. Unlike the National 8 m DEM, these datasets provide elevation data that is generally suitable for detailed terrain analysis.

The accuracy of LiDAR-derived DEMs is influenced by several factors inherent to the methodology:

1 Measurement errors may occur during the LiDAR point cloud collection process.

2 In areas with sparse ground classified points, interpolation may lead to localised inaccuracies.

3 The DEM's spatial resolution impacts precision of ground surface elevation representation.

Additionally, LiDAR effectiveness at penetrating water surfaces is limited and changes in ground surface elevation over time due to natural and anthropogenic activity may affect the datasets (e.g. landslides, sediment deposition from flooding, cut and fill activities).

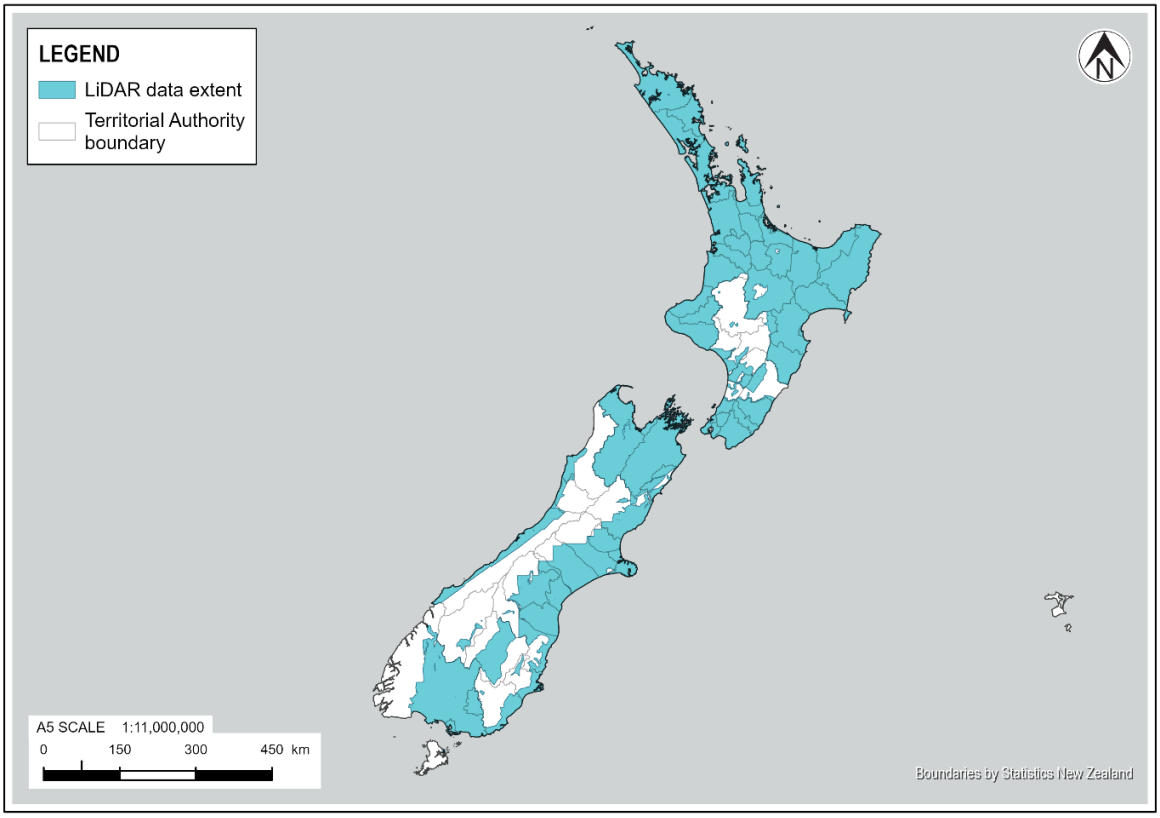

Figure 3.2: Map showing availability of national LiDAR derived 1 m DEM in New Zealand, sourced from LINZ and OpenTopography (accessed date 11 November 2024)

3.1.3 T+T National DEM and slope model

T+T has an internal process to create a mosaic of the national 8 m DEM and LiDAR-derived 1 m DEMs. Two thirds of New Zealand's land area is covered by the LiDAR-derived 1 m DEMs, including most of the populated areas in New Zealand. This represents 77% of the flatland in New Zealand (see Section 5). For the remaining areas, the 8 m DEM, created from 20 m contours, is used.

In areas with overlap of LiDAR-derived 1 m DEMs, the most recent dataset is used. The datasets were sourced on May 2024 and two datasets are excluded, the DEM created in Hawke's Bay after cyclone Gabrielle and the DEM from the Nelson 2022 flood event. These datasets are localised and were captured for the primary purpose of supporting storm recovery, and there is uncertainty around their suitability for the purpose of terrain analysis. For example, the Nelson 2022 event capture has a pulse density of less than 3 points per square metre compared with 8 points per square metre for the Nelson 2021 LiDAR.

To create the mosaiced DEM, the rasters are resampled using two-way linear interpolation. Using a second order central difference approximation as outlined in Zevenbergen & Thorne (1987), the mosaiced DEM is used to calculate the slope angle for the national slope model, which in turn is used to determine the areas of flatland within New Zealand. The output of the national slope model is presented in Figure 3.3 and discussed in Section 5.

Merging DEM datasets with different base resolutions is not without challenges. Steps or sharp transitions at the boundary between the two sources can be created due to the difference in vertical accuracy. This is not an issue for discrete sampling (like ground elevation at BH) but can create false artifacts in secondary outputs such as slope maps (e.g. a steep slope or cliff would be created if there is a large elevation difference).

The accuracy of the elevation and slope models is linked to the quality of the underlying LiDAR DEM and national contour data. Furthermore, the use of two-way linear interpolation in the final DEM development introduces statistical uncertainty. To manage this problem, the outputs are also resampled to lower resolutions for different use cases. This strikes a balance between the accuracy of LiDAR and ensuring a smooth transition between datasets. Two DEM resolutions have been used within the NLM. A resampled 10 m version is used for flatland predictions, whereas the DEM (and slope model) for GW predictions was resampled at a 100 m scale to match the output resolution.

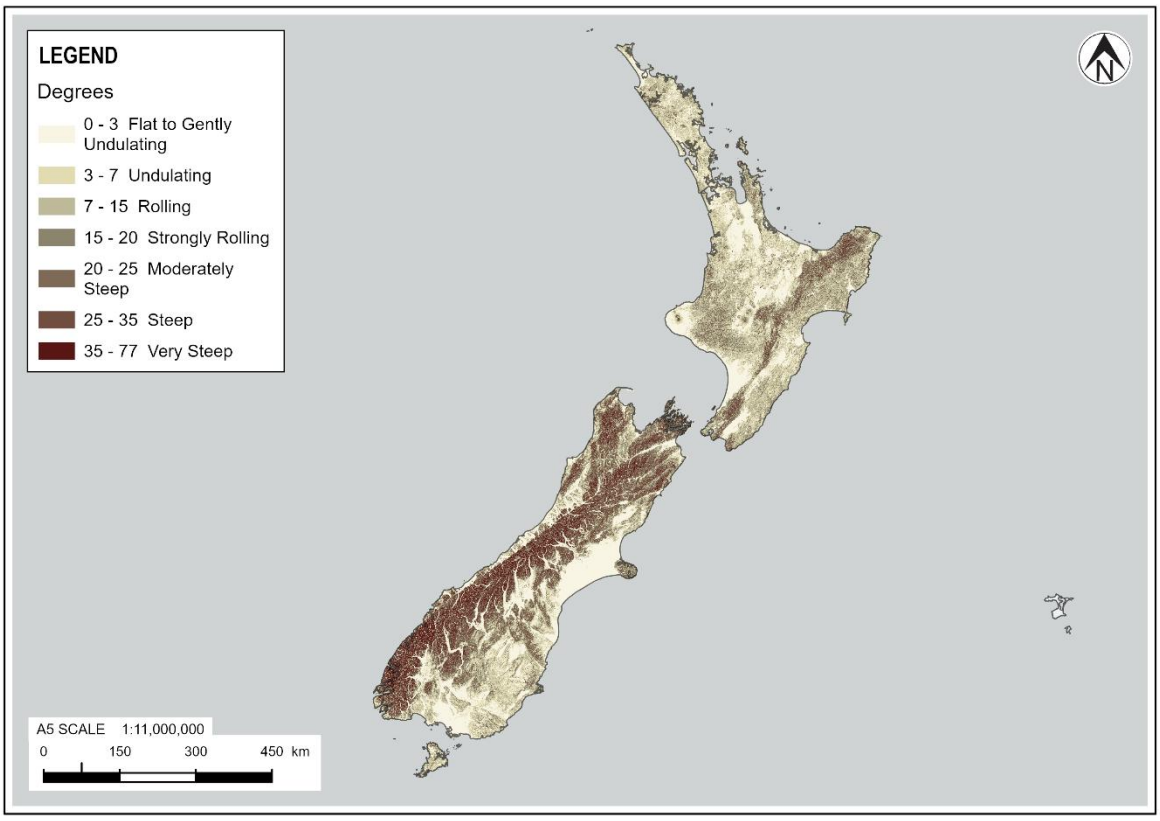

Figure 3.3: T+T National slope model of New Zealand

3.2 Geology and geomorphology classifications

Geomorphology maps categorise a landscape into a series of terrains (polygons) with similar near-surface ground conditions, depending on their depositional settings. The maps are used as the basis for the geomorphology model, which is used to group GIs and provide spatial boundaries and liquefaction predictions based on the geomorphology categories (see Section 6).

The accuracy and precision of geomorphology maps is influenced by several factors:

- **The definition of the boundaries between terrains.** This can result in the incorrect categorisation of the land. Where specified, the scale of mapping provides an indication of the accuracy. For some maps, areas where there is more uncertainty associated with the location of the boundary have been identified.
- **Unmapped anthropogenic landform changes.** Some anthropogenic landform changes can result in changes to the underlying ground conditions. In some cases, these changes will reduce LV (e.g. ground improvements) and in some cases these changes will increase LV (e.g. reduction of the ground surface elevation resulting in a reduced depth to GW or increasing the ground surface elevation on top of liquefiable deposits adjacent to water bodies).

3.2.1 Geological map (QMAP)

The New Zealand 1:250K Geology (4th Edition) (Heron, 2023) developed by GNS Science Te Pū Ao (GNS) is a geological map that was created as part of the QMAP[7] project from 1995 to 2012. The process involved compiling data from various sources, using GIS software for digitisation, and conducting several verification steps, including alignment with LINZ topographic data. The map comprehensively covers all of mainland New Zealand and the Chatham Islands at a 1:250,000 scale (see Figure 3.4).

The map is intended for use in geological studies and serves as a resource for understanding the geomorphology, stratigraphy, tectonic history, and geological aspects of New Zealand. It is designed to support scientific research and regional geological analysis. The accuracy of the map is influenced by multiple factors, including the quality and resolution of underlying data sources, the extent of field verification, the level of generalisation required for national-scale mapping, and the consistency of interpretation across different geological units. The compilation process involved fieldwork, research, and various validation steps. The map adheres to the GeoSciML[8] 4.1 standards and employs CGI[9] Controlled Vocabularies, contributing to the robustness of its geological representation.

The map has undergone updates to include new geological information and to align with current topographic data. Updates will continue to be made into the future, and this is one of the specific motivations for developing an automated data-driven approach for the NLM.

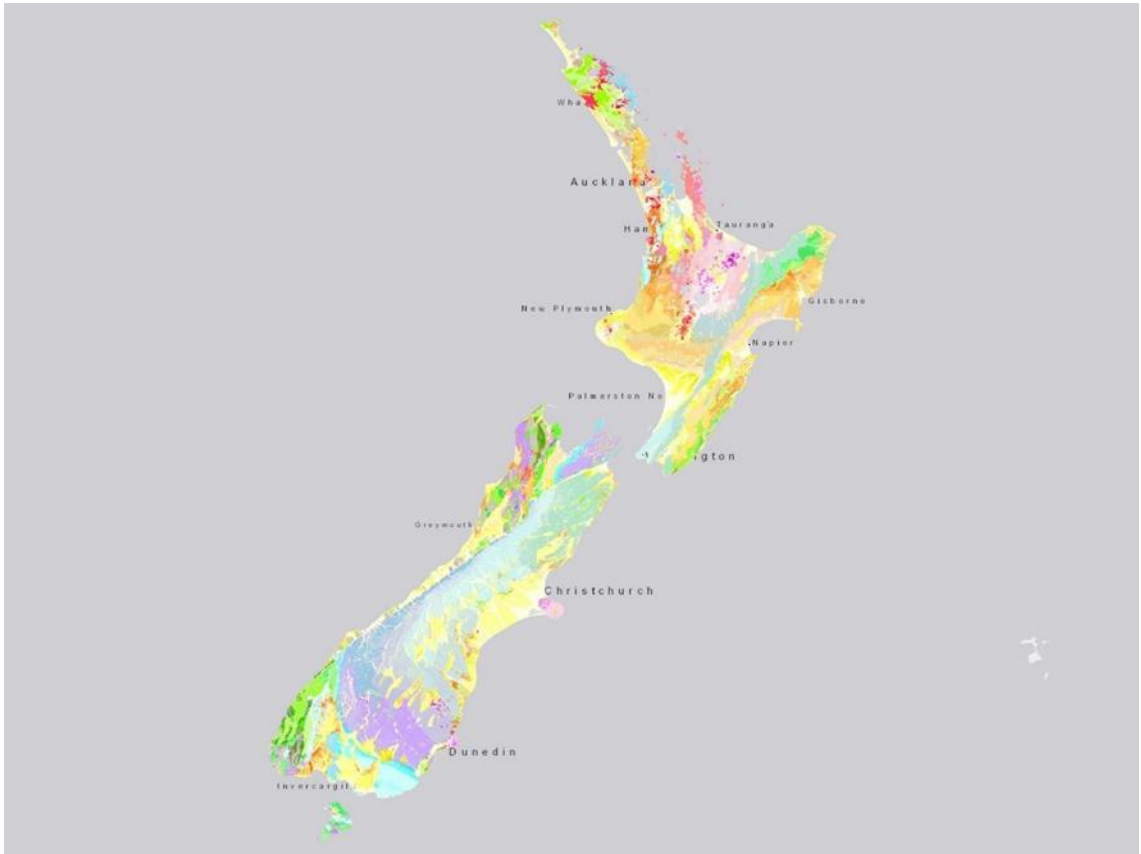

[7] QMAP is the shorthand reference for the digitised quarter million (1:250000) geological maps of New Zealand from a GNS-led project.
[8] GeoSciML is a data model and data transfer standard for geological data. It can be used for a range of applications from basic map data to complex relational geological databases.
[9] CGI or the Commission for the Management and Application of Geoscience Information is an international organisation that shares resources about data sharing, standards, and best practice in geoscience information management.

Figure 3.4: GNS 1:250k Geology, Geological Units 250k, image taken from https://data.gns.cri.nz/geology/ (Access date 8 November 2024)

3.2.2 GNS refined maps

GNS has undertaken more detailed geological and geomorphology mapping in certain areas around the country. The scale of this mapping varies between 1:25,000 to 1:75,000 and, in many locations, has been incorporated into QMAP v4. The refined maps offer higher resolution in specific regions. However, their accuracy depends on factors such as the quality of field validation, the resolution of the base datasets, and the methods used in their development. The accuracy of these maps can sometimes surpass that of the QMAP, particularly in regions where additional fieldwork and higher-resolution datasets have been considered.

Following consultation with GNS, four higher resolution maps were identified that were available, were not already included within the current QMAP v4, and had a suitable data schema to allow them to be transformed into the NLM data schema. The four maps are listed below with associated references:

1 **Hawke's Bay (Napier-Hastings)** – https://www.gns.cri.nz/our-science/land-and-marine-geoscience/te-riu-a-maui-our-continent/geology-of-new-zealand/urban-geological-maps/napier-hastings/ (GNS Science, 2022a)

2 **Kapiti Coast** – https://geodata.nz/geonetwork/srv/api/records/CCD1C820-4020-40FA-BB95-37F116C823CB (GNS Science, 2016)

3 **Nelson** – This model has not been formally published yet but was made available to the NLM project by GNS.

4 **Christchurch** – https://www.gns.cri.nz/our-science/land-and-marine-geoscience/te-riu-a-maui-our-continent/geology-of-new-zealand/urban-geological-maps/christchurch/ (GNS Science, 2015)

While these refined maps provide improved geological detail at a local scale, their integration into the national-scale QMAP requires generalisation to maintain consistency across broader regions. This process inherently influences how detailed geological features are represented in the national dataset. Therefore, both map types have their respective strengths, with QMAP providing a consistent national framework and the refined maps offering enhanced resolution for specific regions.

3.3 Geotechnical investigations

3.3.1 New Zealand Geotechnical Database (NZGD)

The NZGD is an online platform for storing and accessing geotechnical data. Established following the Canterbury earthquakes, it allows registered users to search, download, and contribute geotechnical information. The database operates on a reciprocal data-sharing basis and is free for registered users. It is currently funded by MBIE.

The NZGD includes various types of geotechnical investigations including CPTs, BHs and associated Standard Penetration Tests (SPT), hand augers, Seismic Cone Penetration Tests (SCPT), seismic dilatometer test, surface wave surveys, scala penetrometer tests, test pits, and vertical seismic profiles. The metadata for each investigation often contains an observed Groundwater Level (GWL) at the time of testing. The data sources used for the NLM are the CPT, BH and SPT data.

There are several automated and manual data checks performed on uploaded data, however, there is no required format for data to be uploaded. There are only warnings about duplicate location data and no (or limited) cleaning of duplicate locations or duplication of readings. Table 3.1 shows the

number of CPT and BH by region on the NZGD. Figure 3.5 shows the number of CPT across the territorial authorities of New Zealand. Data is added to the NZGD on a regular basis and the data presented in this table and figure are current as of 11 March 2025. The data provides the following insights:

- The Canterbury region has the most geotechnical investigations on the NZGD including more than half of all CPT and just under half of all investigation types. This disproportionate distribution is a direct result of the response to the Canterbury earthquake sequence where large numbers of investigations were undertaking to support the recovery process.
- Regions with larger urban centres have more investigations overall than those with smaller rural communities. Auckland (Auckland City), Waikato (Hamilton City), Bay of Plenty (Tauranga City), and Canterbury (Christchurch City) all have more than 3,000 investigations. Wellington (Wellington City and Lower Hutt) is a notable exception with approximately 1,800 investigations. This is likely attributable to the smaller geographic area, steeply sloping terrain (being less favourable to development) and relatively higher population density in the main urban centres of Wellington City and Lower Hutt.
- In most regions, there are more CPT than BH except for Auckland and Wellington where there are more BH than CPT. This could be attributed to several factors such as the ground conditions in each region, the nature and location of infrastructure being designed and built, and the practice of geo-professionals in each region.
- The distribution of GIs is not spatially uniform. They are typically concentrated around new developments. Furthermore, CPT are only performed in penetrable ground, which means that non-penetrable ground is under-represented in the data. The biases that are introduced due to the spatial sampling are addressed in several sections throughout the development of the NLM, particularly in Sections 8.4.3, 8.6.3, 8.6.4, and 8.7.3.

Table 3.1: CPT and BH count by region on the NZGD (as at 11 March 2025)

Region	CPT count (No.)	BH count (No.)	Total
Canterbury	30,996	3,385	34,381
Bay of Plenty	5,246	130	5,376
Auckland	3,768	1,552	5,320
Waikato	3,840	50	3,890
Wellington	1,383	451	1,834
Hawke's Bay	1,262	147	1,409
Manawatū-Whanganui	811	182	993
Otago	703	72	775
Marlborough	438	41	479
Northland	410	44	454
Nelson	268	21	289
Southland	262	3	265
Gisborne	246	2	248
Taranaki	213	7	220
West Coast	120	31	151
Tasman	115	0	115
Total	**50,081**	**6,118**	**56,199**

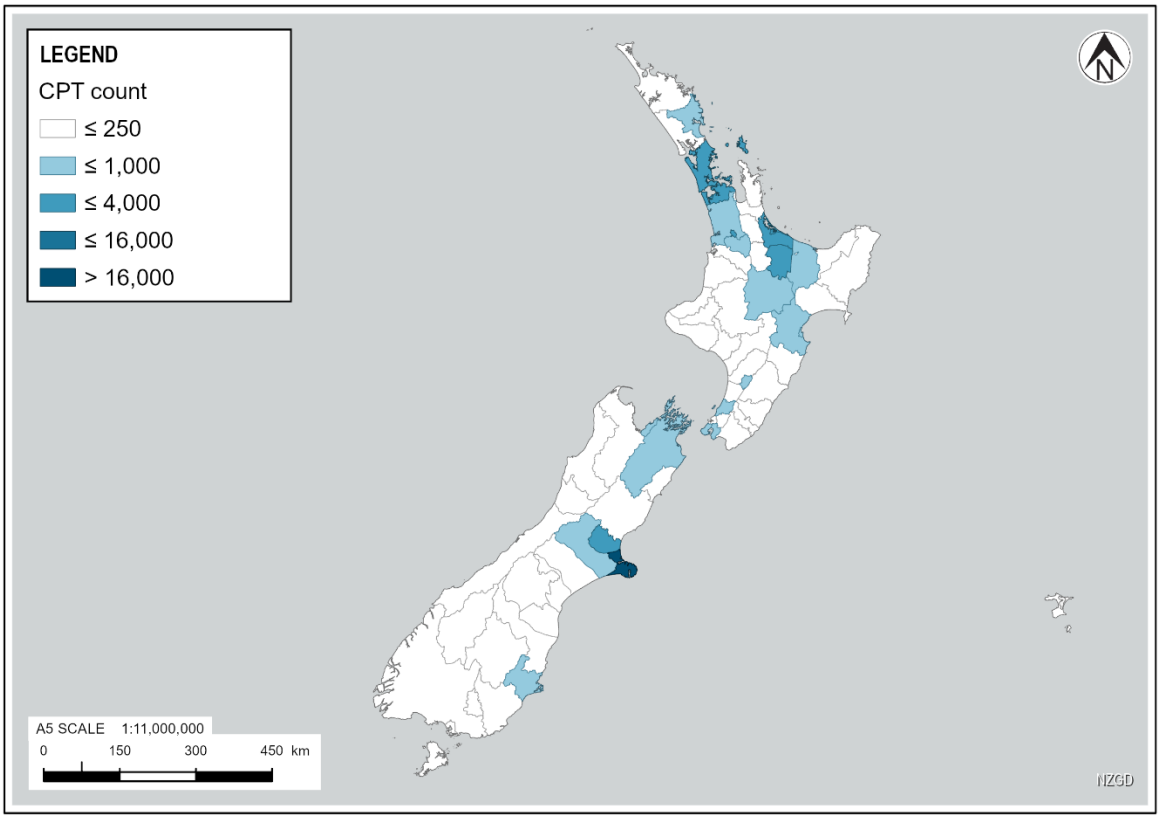

Figure 3.5: National count of CPT on NZGD by territorial authority in New Zealand

3.3.2 Tonkin + Taylor's Geotechnical Database (TTGD)

The TTGD is the primary geotechnical site investigation library for T+T for additional data that is not publicly available on the NZGD. Table 3.2 shows the additional number of CPT, and BH by region on the TTGD. Figure 3.6 shows the additional number of CPT across the territorial authorities of New Zealand on the TTGD. The summary of data readings by regions shows:

- Unlike the NZGD, the Canterbury region does not hold the largest share of geotechnical investigations in the TTGD. The Auckland region has the highest share of geotechnical investigations.
- Regions with larger urban centres, such as Auckland, Waikato and Bay of Plenty still show more geotechnical investigations compared to rural areas. Wellington is an exception with a lower-than-expected count for a major urban area, reflecting its unique geographical constraints and urban density.
- The benefit of incorporating data from the TTGD (to augment the NZGD data) varies from region to region. For example, in the Canterbury region it adds only an additional 4% to the total number of investigations whereas in the Gisborne region it adds an additional 70% to the total number of investigations and an additional 176% to the number of CPT.

Table 3.2: Additional CPT, and BH count by region on the TTGD (as at 11 March 2025)

Region	CPT count (No.)	BH count (No.)	Total
Canterbury	1,042	3,746	4,788
Bay of Plenty	1,362	200	1,562
Auckland	3,622	4,895	8,517
Waikato	1,722	280	2,002
Wellington	744	638	1,382
Hawke's Bay	747	322	1,069
Manawatū-Whanganui	252	132	384
Otago	161	117	278
Marlborough	74	134	208
Northland	226	318	544
Nelson	35	51	86
Southland	25	4	29
Gisborne	316	65	381
Taranaki	498	149	647
West Coast	71	48	119
Tasman	17	15	32
Total	**10,914**	**11,114**	**22,028**

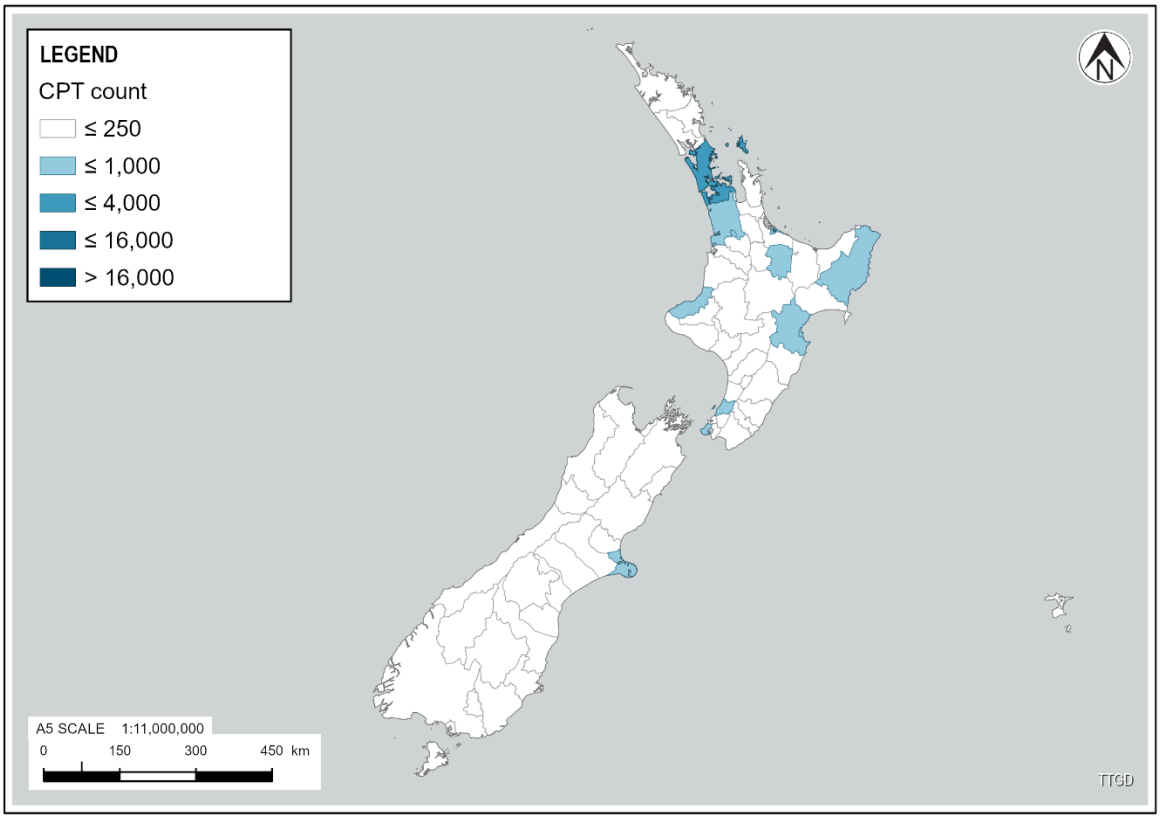

Figure 3.6: National count of CPT on TTGD by territorial authority in New Zealand

3.3.3 Investigation data quality

Each geotechnical investigation has the possibility for inherent issues in data quality. Some of these are readily identifiable, are logged as part of the investigation and can be accounted for in the analysis (e.g. post-ground improvement investigations and portions of predrilled CPT). Others are not readily identifiable without being able to manually review the data source (e.g. duplication of readings or incorrectly logged BH data).

To provide a more consistent basis for use in the NLM, an initial filtering process has been applied to the GI dataset used for the calculation of LV parameters. This is discussed further in Section 7.5.2.

3.4 Groundwater (GW)

A national GW model has been created for the purpose of the NLM, herein referred to as the NLM GW Model. This section outlines the core data used to build and validate this model. It explains the role of GW information, such as static and temporal water level measurements, in estimating Groundwater Depth (GWD). The existing models that are listed below are used as a benchmark and as a comparison against the NLM GW Model. They are discussed further in Section 9.4.

3.4.1 GW data

GW data comes from two primary sources:

1 Static water level data from drilled bores.

2 Temporal water levels at specified intervals (i.e. daily or monthly) from monitoring wells.

Due to the nature of collecting and maintaining a temporal record, there are significantly fewer monitoring wells than static water level locations (often representing less than 1% of the total

primary GW data available in a region). However, these monitoring locations are important in understanding the expected variation in GWL within a local area or type of geomorphology. The following sections discuss the known sources of GW data.

3.4.1.1 Static water depth data

Static water depth data can be obtained from the following sources:

- **Regional council databases:** Static water depth data is often published by regional councils for downloading. In some cases, the data is not publicly available and requires a request to the councils to gain access. The sources of data used in the model are listed in Section 9.2.1.
- **NZGD:** Spatially distributed BH data containing GWLs is also sourced from the NZGD. More information about the NZGD can be found in Section 3.3.1.
- **Other available databases:** Spatially distributed BH data can also be found from other sources, which may be made available through local councils, or other private sources, such as the TTGD (see Section 3.3.2).

3.4.1.2 Monitoring wells data

Temporal data from monitoring wells can be more difficult to store and access. This is expected, given the difficulties associated with hosting and maintaining a public server to access temporal, continuously updating data. In the past, councils have provided snapshots of temporal data when requested. In some cases, the data is available to query from public servers, such as Wellington's hilltop server. However, it is not always straightforward to query. This data has been used in specific regions, where available.

3.4.1.3 Uncertainty and limitations of GW data

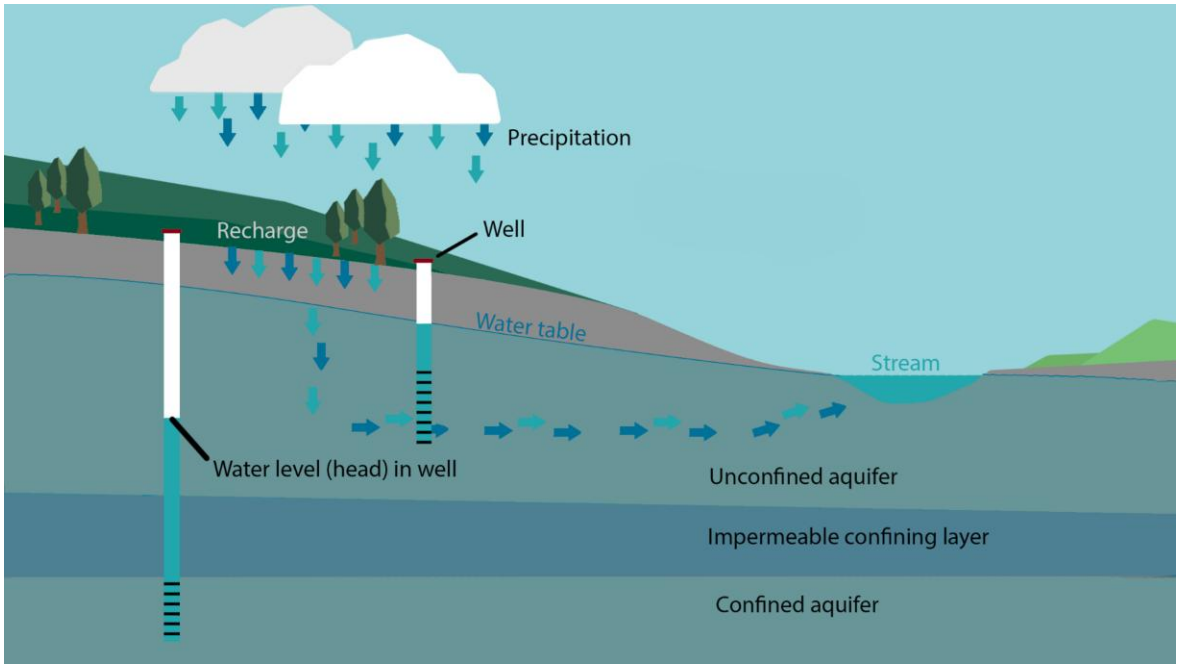

Figure 3.7: Aquifer schematic for water level in confined and unconfined aquifer (LAWA, 2020)

There are many known limitations and uncertainties of BH GW data associated with the collection process and storage. This includes, but is not limited to:

- **Confined vs unconfined aquifer:** Most regional council GW monitoring data is of the deeper confined aquifers (see Figure 3.7) for the purpose of managing the GW resource for extraction purposes. This is not a measurement of the upper unconfined aquifer relevant for liquefaction. Therefore, data vetting is required to identify data from monitoring wells and BHs that measure the near surface unconfined GW.
- **Limited data integration:** BH data is collected by different entities and stored in disparate formats, making it challenging to integrate and analyse comprehensively. This includes the use of different vertical datums and different methods of measurement.
- **Data availability and accessibility:** There can be gaps in data due to the limited number of BHs in certain regions, and access to existing data can be restricted or limited.
- **Impact of human activities:** The influence of nearby human activities, such as pumping or contamination, can alter GW conditions, introducing further uncertainty in data interpretation.
- **Long-term changes:** GW fluctuates and can change over extended time periods. This can make some measurements obsolete, and measurements may need to be corrected to remove short term (e.g. tidal) and seasonal fluctuations.

Further detail on the data cleaning steps undertaken for the GW modelling process is in Section 9.

3.4.2 Local GW models

While many areas in NZ have existing regional and local GW models, many of these models have been focused on the resource management and monitoring of productive confined aquifers (i.e. Heretaunga Plains, Lower Hutt, Wairau, lower Canterbury Plains). These models typically do not provide an estimate of the depth to GW. However, there are local models across New Zealand that do provide depth to GW, referred to here as shallow GW models, which have been created by various organisations for a range of different applications. A review of the currently known sources identified that 16 of the 67 territorial authorities across New Zealand have some form of local shallow GWL model available (see Figure 3.8).

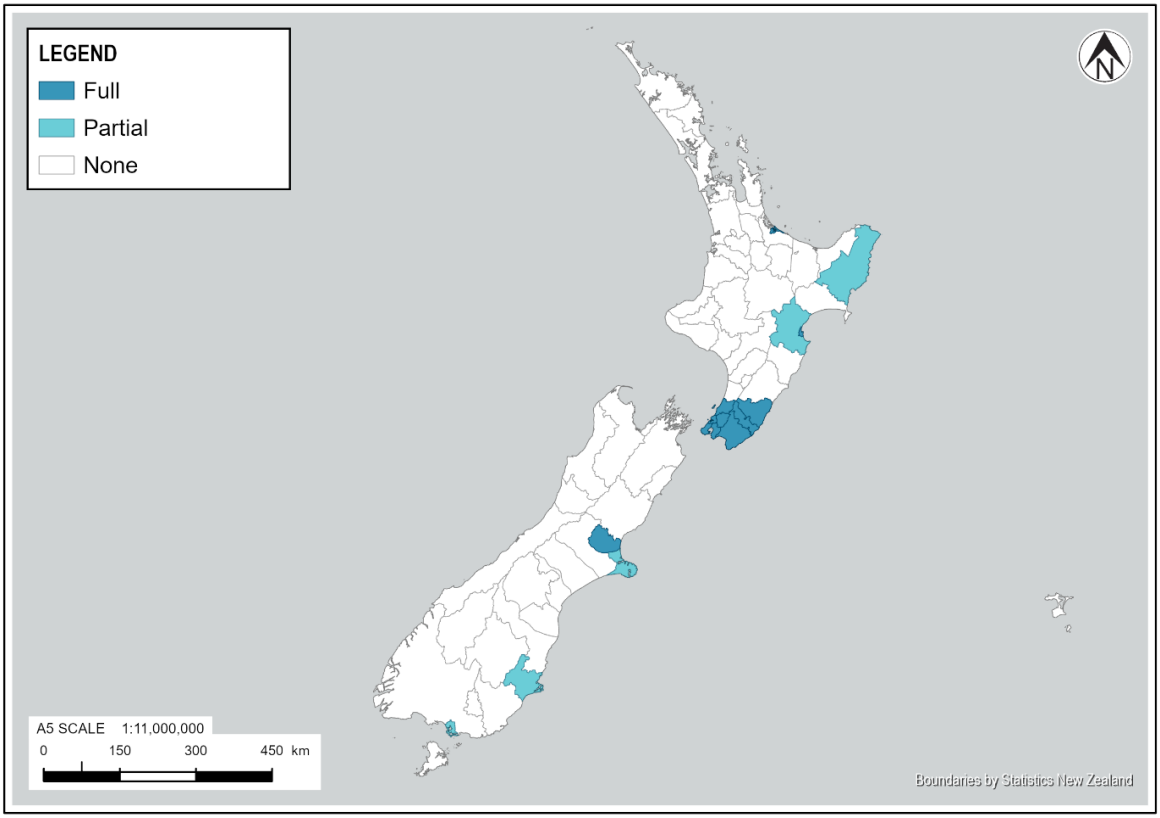

Figure 3.8: National coverage of local GWL models by territorial authority

The methodology applied to develop each local national GWL model varies depending on the application. For example, a relatively simple approach was applied to create the GWL model for the Wairarapa Region (see Figure 3.9), whereas a relatively complex approach was applied to create the GWL model for Tauranga City Council (see Figure 3.10). Table 3.3 summarises some of the differences between these two models.

Table 3.3: Summary of differences between the GWL models developed for the Wairarapa Region and Tauranga City

	Wairarapa Region	Tauranga City
Purpose	Input to earthquake loss modelling	Assessing the impacts of shallow GW on infrastructure
Data utilised	Readily available data from a variety of sources (primarily static measurements)	GW monitoring data collected specifically for the project (temporally varying GW)
Output	A single GWD estimate	Statistically varying GW scenarios (e.g. median and 95th percentile estimates)
SLR	Not included	Projections for future time horizons included

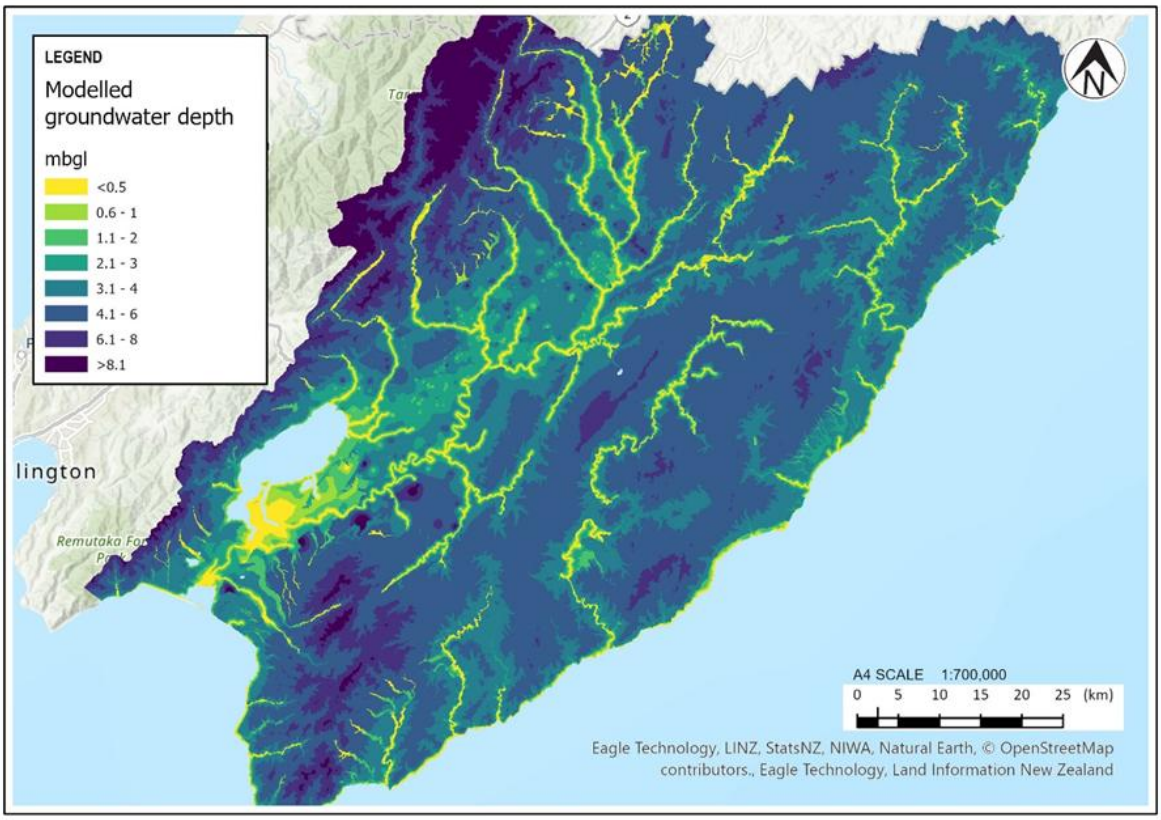

Figure 3.9: Model of GWD for the Wairarapa Region, sourced from report for Aon New Zealand (Tonkin + Taylor, 2022b)

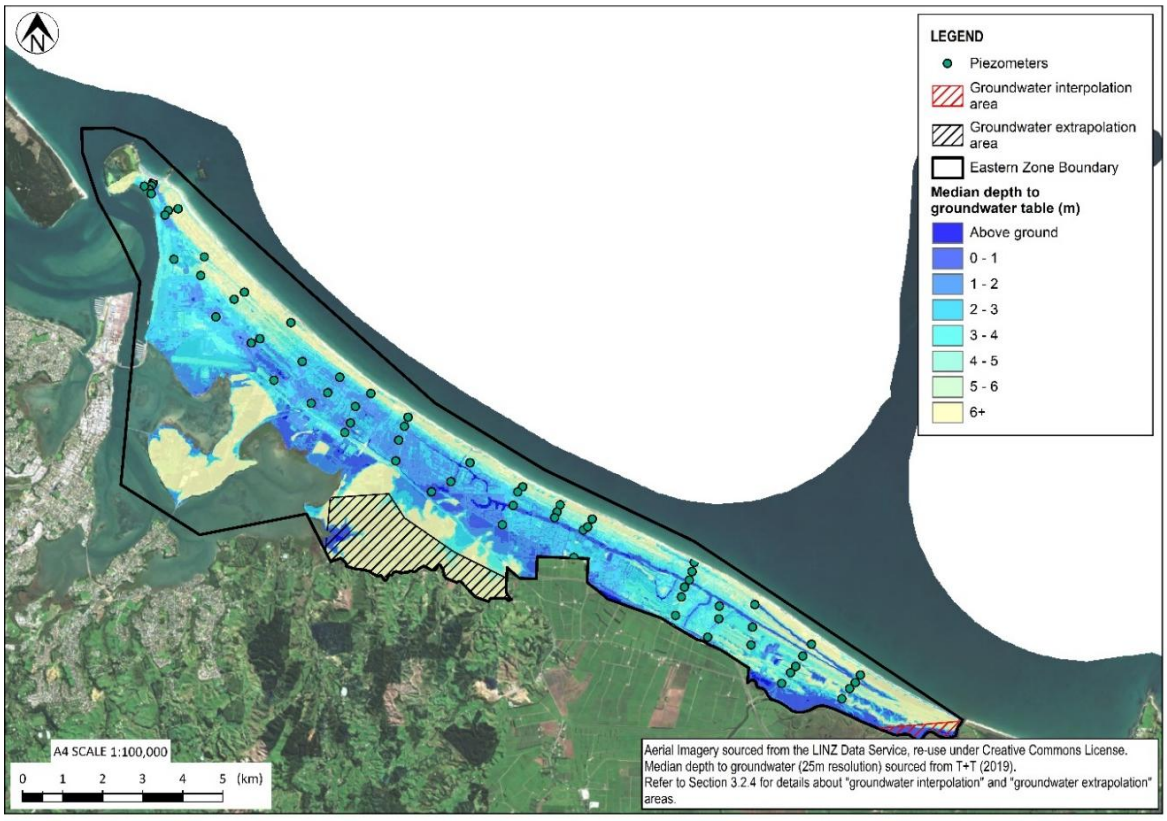

Figure 3.10: Model of GWD for Tauranga City, sourced from report for Tauranga City Council (Tonkin + Taylor, 2020)

3.4.2.1 Selected models for validation and calibration of NLM GW Models

For validating and evaluating the NLM median shallow GW Model, several existing shallow GW models were selected that were easily available and were developed by a range of organisations. Additionally, two SLR models were identified for the purpose of calibration of the NLM SLR model. Table 3.4 lists the selected existing models, their source and the purpose of their use for the NLM project, with further details provided in subsequent subsections.

Table 3.4: Existing models used as validation and calibration for the NLM GW Model

Model	Coverage	Source	Purpose	Section
National Water Table (NWT) model	National	(Westerhoff et al., 2018)	Validation	9.4.2
Hawke's Bay unconfined GW	Regional	(Rosser & Dellow, 2017)	Validation	9.4.3
South Dunedin shallow GW current and SLR models	Regional	(Cox et al., 2023)	Validation & Calibration of SLR model	9.4.4
Christchurch shallow GW SLR model	Regional	(Rutter, 2020)	Validation & Calibration of SLR model	9.4.5
Christchurch event-specific shallow GW models	Regional	(Tonkin + Taylor, 2013)	Validation	9.4.6

National coverage of shallow GW conditions for the purpose of local scale liquefaction assessment is currently lacking at the time of writing this report. As such, a separate modelling approach which aims to capture local-scale median shallow GW conditions at a national scale has been developed.

Shallow GW conditions vary nationally due to the heterogeneity of the subsurface, climatic influences, surface water features, and anthropogenic activities. As such, they are complex physical systems. While numerical approaches to model GW are possible, these are significantly more computationally demanding. Geostatistical approaches that use expert-knowledge of GW systems can produce semi-automated models for estimating median shallow GW conditions that include measurement of the prediction error.

National and regional GW models used for validation (all models) and calibration (only South Dunedin and Christchurch models) are described below and their comparisons against the NLM GW Model are presented in Section 9.4.

3.4.2.2 National Water Table (NWT) model

The NWT model (GNS Science, 2018), aims to provide a nationwide overview of GWLs across New Zealand. It is designed to bridge the gap between highly detailed local models, which are often expensive, and oversimplified global-scale models. The model offers a steady state mean GW table depth representation with a spatial resolution of 250 m, covering the entirety of mainland New Zealand, as shown in Figure 3.11.

The development of the model involved leveraging existing global-scale GW flow models as a foundational framework. Key enhancements included the integration of national input data specific to New Zealand's terrain, geology, and recharge patterns (Westerhoff et al., 2018).

Adjustments in model parametrisation and rigorous testing were integral to refining the model's accuracy. The dataset encompasses information on hydraulic head (measured in metres above sea-level) and GW table depth (measured in metres below ground level), mapped using the New Zealand Transverse Mercator projection for spatial accuracy.

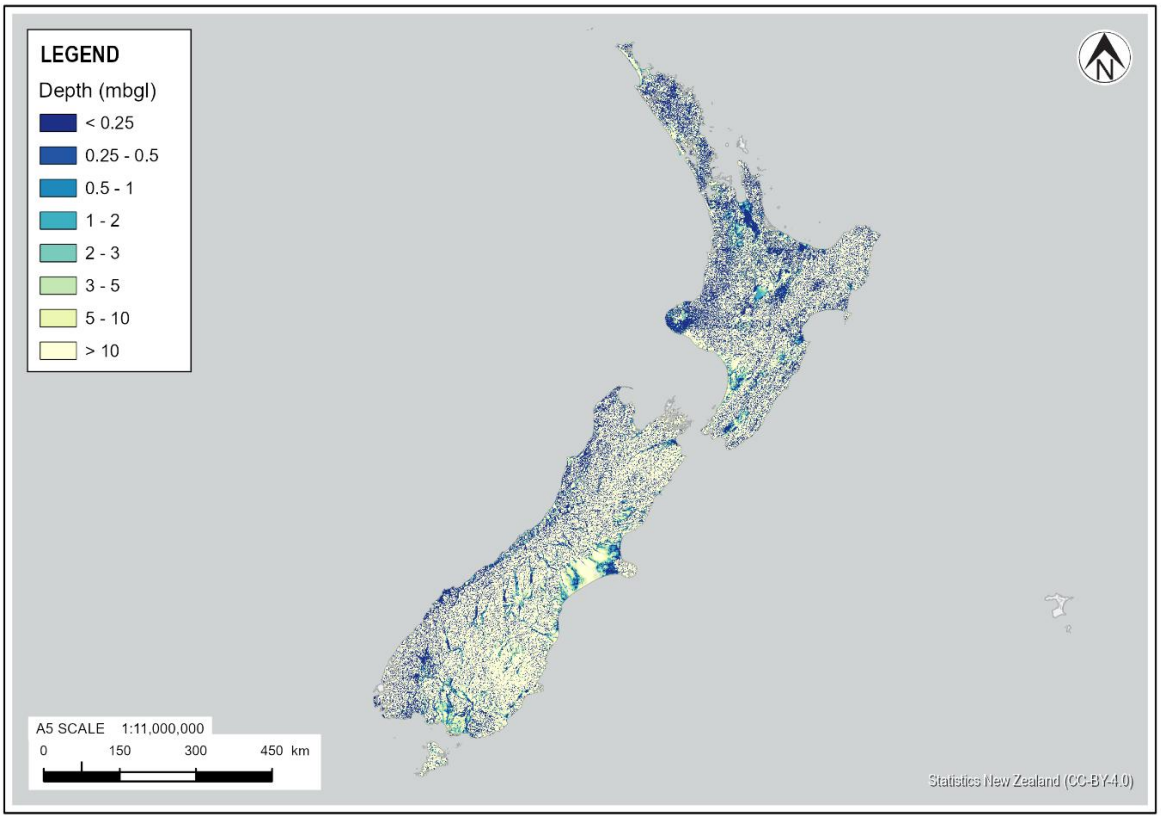

Figure 3.11: National GW table depth (metres below ground level) from GNS (2018)

Despite the national coverage of the model (GNS Science, 2018), it is subject to limitations inherent to large-scale models, particularly due to its coarse spatial resolution which does not fully capture local-scale variability and specific hydrogeological features that require finer-scale analysis. It serves as a useful national base model for comparison and validation but on its own cannot be relied on for accurate estimates of GWDs which are required for liquefaction assessments.

Comparative analysis between the NWT's modelled values and measured GWDs from site investigation data have shown significant discrepancies on the scale of tens of metres. Based on comparisons with static water level data from monitoring wells and drilled bores, the NWT model appears to capture regional trends but lacks the local scale variability seen in observations. Although static heads can be unreliable due to a number of factors (see Section 9.2.2), the coarse resolution of the model, input data assumptions (i.e. recharge model), and likely unaccounted for local spatial heterogeneity of hydraulic conductivity likely all contribute to the high observed residuals.

Given its large spatial coverage and the need to compare approaches, the NWT model was used as the main benchmark for validating the NLM GW Model. As the NLM GW Model uses a data-driven approach which doesn't account for GW flow properties, regional trends and patterns of modelled GWD are compared against the NWT to "ground truth" the NLM GW Model predictions in areas of scarce observations.

3.4.2.3 Hawke's Bay unconfined GW model

A depth to GW model was developed for three zones across Hawke's Bay, including the Heretaunga Plains. The development of the model was based on a methodology used to model shallow GW in Christchurch (van Ballegooy, Cox, Simon C., et al., 2014). Following testing of three different interpolation methods, a kriging method with linear drift was used with a search area of 10 km and a Gaussian variogram. The grid size has a resolution of 250 m and coastlines and rivers were set as break lines at ground level. The interpolation was performed in metres below ground level and clipped to the study area.

3.4.2.4 South Dunedin shallow GW model and Sea-Level Rise (SLR) predictions

Two GW models have been developed to represent shallow GW conditions in South Dunedin based on data-driven and process-based models (Cox et al., 2023). The data-driven model is based on a statistical interpolation of median GW elevations, where depth to GW is derived by subtracting the GW elevation grids from the DEM. The depth to GW surfaces are at an 8 m resolution and based on data captured between 2019 and 2023.

The impact of SLR is modelled as a change in the elevation of the median GW surface based on the assumption of a "flux-controlled" system, whereby the surface increases by the same magnitude as SLR. This SLR prediction is termed the "geometric model" within their report. Tidal and storm surge influences have been included by deriving present-day tide and storm-surge anomalies and tidal efficiency grids.

In addition to the geometric model, a numerical GW model was redeveloped (Chambers et al., 2023) from a previous South Dunedin GW model (Rekker, J., 2012). The more recently developed model incorporates new observation, stormwater pumping outflows, and a wider range of aquifer properties captured in a highly parameterised Bayesian framework. In the numerical model, SLR driven probability of GW reaching the model top is mitigated by waste/stormwater drainage networks which generates conditions more similar to "head-controlled" systems.

Therefore, both the geometric and numerical models capture two endmembers of GWL rise mechanisms from "flux-controlled" and "head-controlled" systems.

3.4.2.5 Christchurch shallow GW SLR predictions

The Christchurch GW model is a high-level, three-dimensional, block-centred, finite difference GW flow model built using MODFLOW-NWT numerical code (Rutter, 2020).

SLR scenarios were modelled using a steady-state version of the Christchurch GW model. SLR was modelled by adjusting the constant head boundaries of the estuary and coastline to the corresponding predicted SLR projection. The change in GWL surface was calculated as the difference between the original steady-state model (i.e. no SLR) and including a SLR scenario. Vertical land movement at the coast was not taken into consideration for the SLR scenarios.

3.4.2.6 Christchurch event-specific GW models

For the purpose of LV mapping, several earthquake-specific GWL surfaces were created (Tonkin + Taylor, 2013). The earthquake-specific surfaces were created following a similar methodology as Ballegooy et al. (similar to the 2013 version 1 of van Ballegooy, Cox, Simon C., et al., 2014). These maps were created by modelling an event based offset value which represents the GWL above or below the median GW surface modelled by Ballegooy et al. (using the 2013 version 1 of van Ballegooy, Cox, Simon C., et al., 2014). The earthquake specific GW surfaces were modelled by adding the event specific offset surface to the median GW surface.

To model the offset surfaces, GW observations were filtered to only capture observations which had records of GWLs within the month immediately before the respective earthquake events. For the September 2010 and February 2011 earthquakes, the spread of observations was relatively scarce, and therefore river monitoring stations were included to provide control points in the interpolation. Where observations were available, the offset was calculated as the difference between the GWL at a specific time and the median surface. Offset observations were then interpolated to create an offset surface.

3.4.3 Mapped waterbodies

The Topo50 map series by Land Information New Zealand (LINZ) includes the New Zealand River Centrelines (LINZ, 2011c), New Zealand River Polygons (LINZ, 2011d), New Zealand Lake Polygons (LINZ, 2011b), and New Zealand Coastlines datasets (LINZ, 2011a). It provides generally consistent mapping of New Zealand's rivers, lakes, and coastal areas at a 1:50,000 scale, encompassing the mainland and offshore islands. This data source has been developed from topographic mapping techniques, incorporating aerial imagery, satellite data, and GIS technology. These mapped waterbodies are used as inputs into the NLM Geomorphology Model (see Section 6.3.1) and the NLM GW Model (see Section 9.2.1).

Precision and accuracy in this data are linked to the mapping processes, and there may be variations depending on the methods and scale of data collection, and temporal changes to waterbodies since they were mapped. Common reasons for differences between these Topo50 data and underlying aerial imagery include:

- Transposition errors associated with the georectification of the data.
- Inaccurate mapping at the time of data collection.
- Temporal changes in waterbodies since the mapping was undertaken.
- Differences in methodology for mapping each of the different datasets.

Figure 3.12 a) – d) shows examples where the Topo50 data differs from aerial imagery and differences between the different datasets. In some instances, the reason for the difference can be inferred (e.g. temporal changes in braided river systems), but in many instances it will not be possible to infer the reason for the difference. Note that the water body boundaries from the Topo50 map series differ from the boundaries in QMAP.

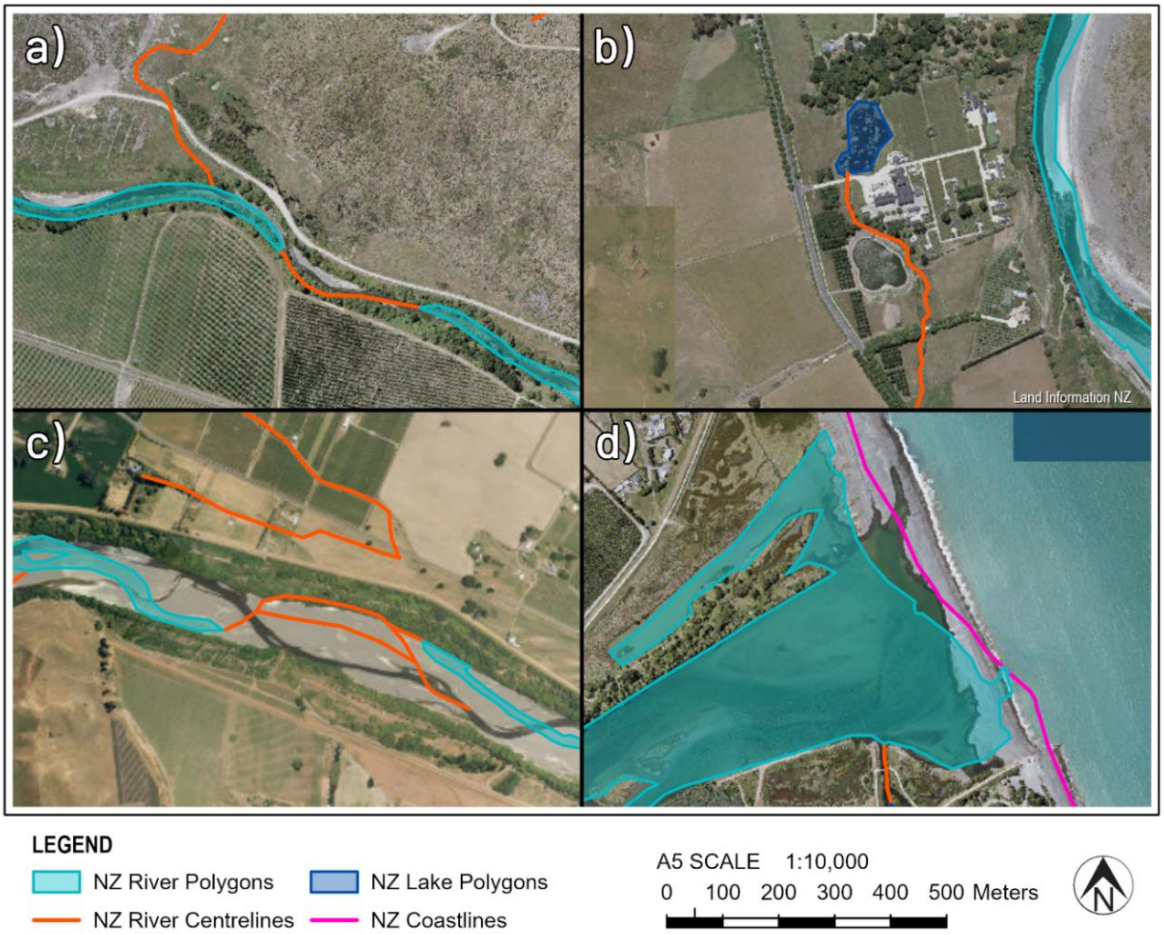

Figure 3.12: Examples where the Topo50 data differs from aerial imagery. a) Transition between New Zealand River Centrelines and New Zealand River Polygons, b) Unmapped waterbodies in New Zealand Lake Polygons, c) Different mapping of river channel in New Zealand River Centrelines and New Zealand River Polygons (inferred to be due to temporal changes in a braided river system), and d) Differences at a river mouth between New Zealand River Polygons and New Zealand Coastlines

3.5 Seismic hazard

The recent update of modelled seismic hazard in the NSHM (GNS Science, 2022c) is in the process of being incorporated into New Zealand's building regulatory system via the draft technical specification TS1170.5 (Standards New Zealand, 2024). The NSHM and TS1170.5 are of relevance as they are being used as inputs for scenario modelling of potential future events (see Section 11.2).

New Zealand's tectonic setting is defined by its location on the boundary between the Pacific and Australian tectonic plates (see Figure 3.13). Two key features of this setting are the Hikurangi Subduction Zone, where the Pacific Plate subducts beneath the Australian Plate, and the Alpine Fault, a major fault running through the South Island. The interaction of these plates significantly influences the seismic and volcanic activity in the region.

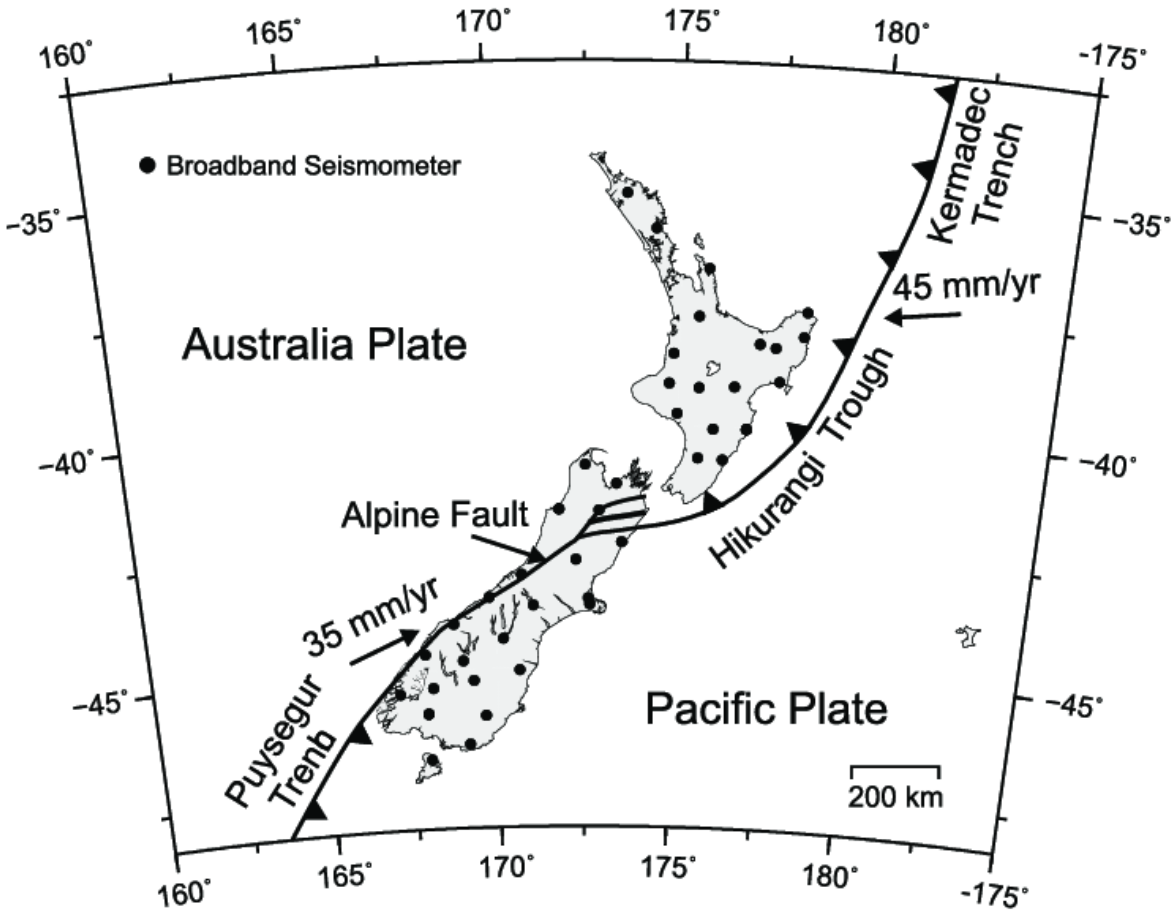

Figure 3.13: Overview of the tectonic setting of New Zealand (Ristau, 2008)

3.5.1 National Seismic Hazard Model (NSHM)

The NSHM for New Zealand (GNS Science, 2022c) was initially developed in the 1980s. Its creation involved integrating seismic data, geological understanding, and advancements in seismology. The model has seen updates, including a significant update in 2002 that influenced the seismic loading requirements in the NZS1170.5:2004 Building Code (New Zealand Standards Executive, 2004), and a 2010 update that incorporated new data with minimal changes to the scientific methodology. A 2020 review of the model led to the 2022 update, incorporating new scientific insights and data, including learnings from recent earthquakes.

Covering the entire country, the NSHM estimates the likelihood and strength of earthquake shaking that may occur in different parts of New Zealand over specified time periods. The NSHM is used to inform technical standards for earthquake engineering design as well as providing critical information for earthquake risk management relevant to insurance, infrastructure management and emergency planning and response.

The NSHM is periodically updated to reflect new scientific findings and data, enhancing its reliability. However, as with any model predicting natural phenomena, there is an inherent level of uncertainty.

3.5.2 Seismic demands from TS1170.5

The draft technical specification TS1170.5 (Standards New Zealand, 2024) provides seismic demand parameters for structures and some geotechnical systems. The draft contains updated seismic

demands based on the latest science from the NSHM update (GNS Science, 2022c). The previous major updates to the underlying seismic hazard model used in NZS1170.5:2004 were made in 2002.

A key output of TS1170.5 is earthquake demand parameters for engineering design at a given location in New Zealand, for a limit state under consideration (i.e. annual probability of exceedance), and for given local soil conditions determined primarily from Vs30 (time-averaged shear-wave velocity to 30 m depth below the ground surface). Key demand parameters that can be extracted for geotechnical application include moment magnitude (Mw) and Peak Ground Acceleration (PGA).

Once TS1170.5 is published, NZS 1170.5:2004 will remain the referenced standard for compliance with the New Zealand Building Code. However, TS1170.5 provide a means for engineers to voluntarily test, and put into practice, new technical specifications within the context of the updated NSHM. This will allow time for it to be “road tested” before potential integration in a subsequent development of a standard.

3.6 Historical observations of liquefaction

As part of a QuakeCoRE funded project, records of liquefaction following large earthquakes in New Zealand have been collated and digitised into an online GIS-based database (Bastin et al., 2021). The creation of the database involved collecting data from a variety of sources, including museum archives, newspaper articles, photographs, diaries, post-event publications, and technical reports. The objective was to assemble a comprehensive record of liquefaction observations associated with significant earthquakes in New Zealand since European settlement.

As shown in Figure 3.14, the database includes observations from the following earthquakes:

- 1848 Marlborough Earthquake (Mw ~7.4-7.5).
- 1855 Wairarapa Earthquake (Mw ~8.1).
- 1901 Cheviot Earthquake (Mw ~7.0).
- 1929 Murchison Earthquake (Mw 7.3).
- 1931 Napier Earthquake (M ~7.4-7.8).
- 1968 Inangahua Earthquake (Mw 7.1).
- 1987 Edgecumbe Earthquake (Mw 6.5).
- 2007 Gisborne Earthquake (Mw 6.0).
- 2010 – 2011 Canterbury Earthquake Sequence.
- 2013 Lake Grassmere (Mw 6.6).
- 2016 Kaikōura Earthquake (Mw 7.8).

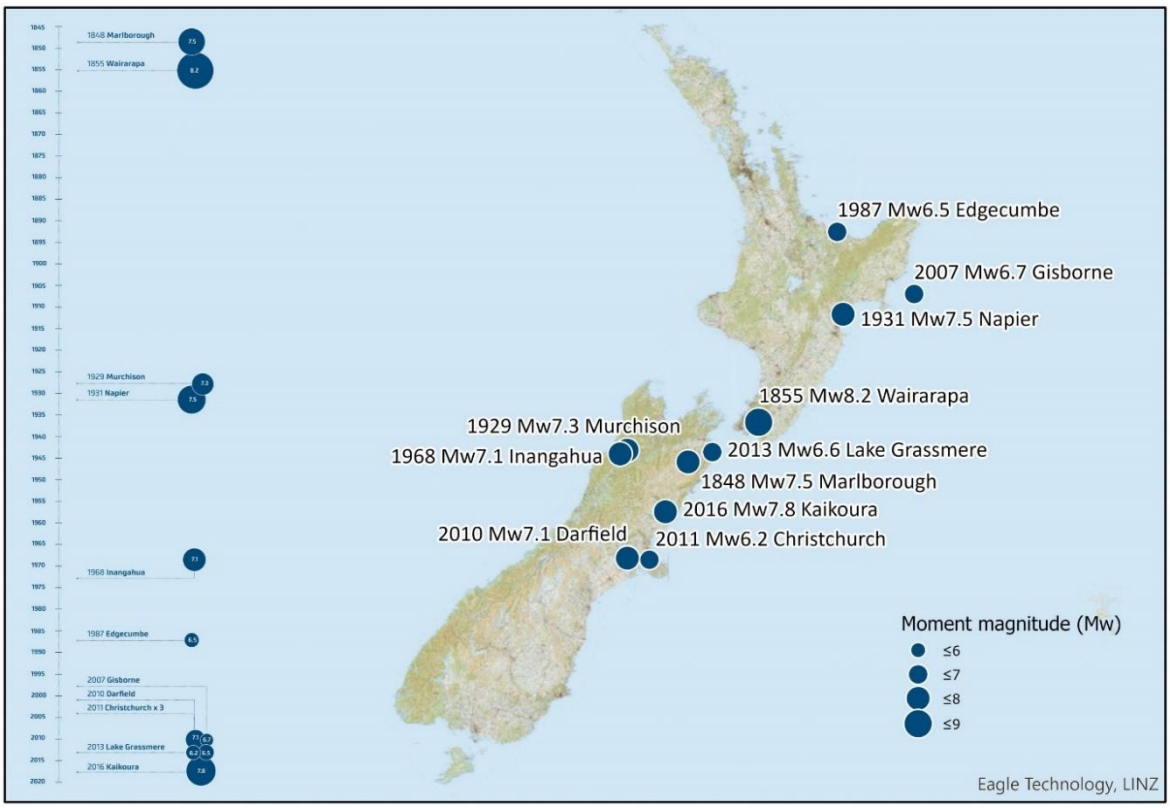

Figure 3.14: Spatial distribution of earthquakes in New Zealand since European settlement with associated liquefaction observations that are included in the database with their corresponding Mw (Image from QuakeCore (2024))

As shown in Figure 3.15, the observations have been recorded as either a point or a polygon and assigned one of five categories:

1 Liquefaction with Lateral Spreading.

2 Liquefaction without Lateral Spreading.

3 Ground Cracking.

4 Ground Surface Distortion.

5 No Observed Land Damage.

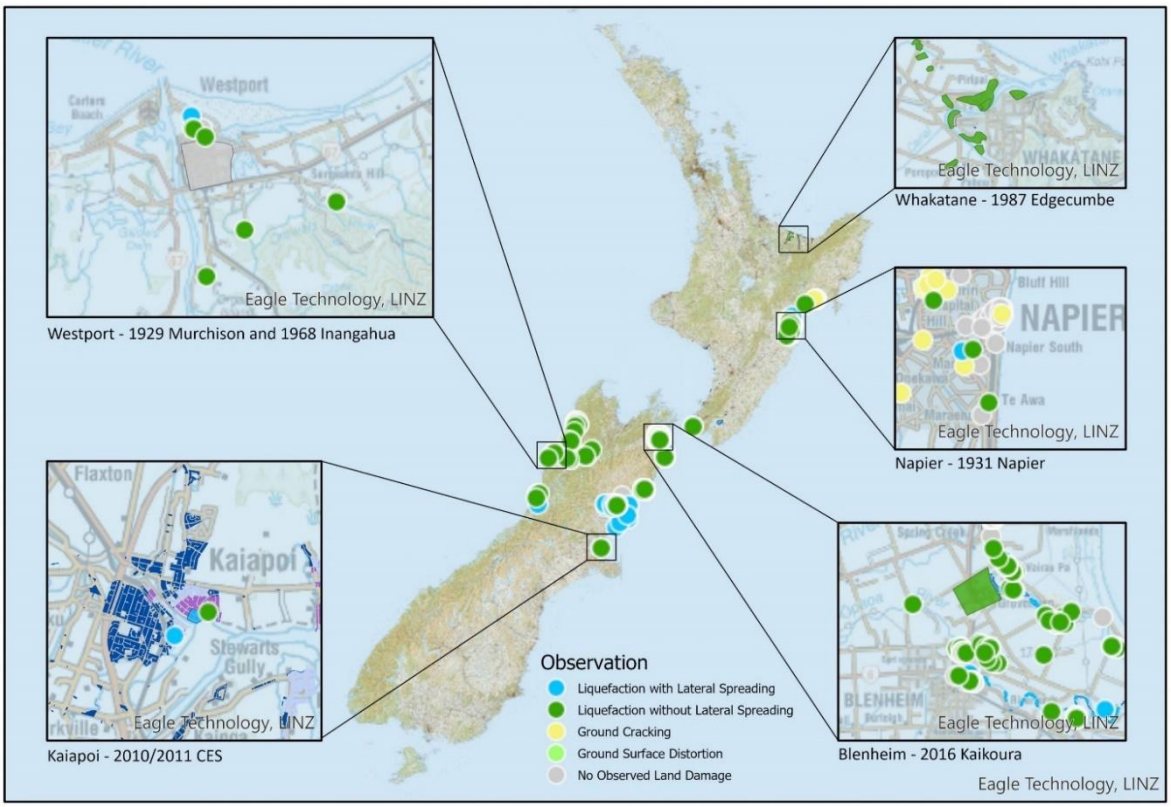

Figure 3.15: Spatial distribution of liquefaction observations that are included in the database (Image from QuakeCore (2024))

The data can be used to inform the settings and soil types where liquefaction has historically occurred, to aid in future event predictions and preparations. The data is considered suitable for use by the authors in the implementation of the MBIE/MfE Guidance (2017) for liquefaction assessment.

The accuracy of this data varies depending on the specific earthquake event and the quality of the historical records available:

- **Earlier Earthquakes** (Pre-20th Century): The data mainly consists of qualitative descriptions sourced from written and oral records and historic photographs.
- **Later Earthquakes** (Post-20th Century): The records are more detailed, incorporating quantitative data and observations from focused reconnaissance and mapping methods. For example, the 2016 Kaikōura earthquake includes detailed mapping of localised liquefaction in alluvial plains near rivers, noting specific soil compositions.

This variance in detail and reliability is indicative of the progression of data collection and seismic analysis methods over time. The level of confidence in the location and that the observation relates to liquefaction was documented for each observation. Locations where liquefaction was well documented have lower levels of uncertainty whereas reports loosely associated with a property or region have higher levels of uncertainty.

4 Model overview

The NLM collectively refers to the digital query-able GIS files that quantify LV across the country. The outputs are generated through a series of processes implemented within a series of modules. There are several outputs, the two primary outputs being the LVM for loss modelling, and outputs to support the creation of MBIE/MfE Guidance (2017) land classification category maps (i.e. probability of liquefaction-induced land damage maps). The secondary outputs consist of national models quantifying flatland, geomorphology, and GW as well as liquefaction-induced Land Damage Fragility Curves (LDFCs). The processes used to generate the outputs are implemented in Python[10] and are referred to collectively as the codebase.

4.1 High-level framework

Figure 4.1 provides the high-level steps for development and application of the NLM to produce the key model outputs. The model development steps and run time steps (i.e. steps to produce outputs using the model) are covered briefly below.

Development steps:

1 **Develop a National Flatland Model**, which identifies flatland across the country and defines the extent of the NLM (see Section 5).

2 **Develop a National Geomorphology Model** (as described in Section 6), which identifies geomorphology across the country as defined by the terms established by Youd and Perkins (1978, referred to as YP78 in this document)[11] for liquefaction evaluation (i.e. geomorphology and epoch), and an additional primary rock mapping classification obtained primarily from QMAP v4 from GNS (Heron, 2023).

3 **Liquefaction triggering analysis of over 50,000 GIs** (CPT, BH and SPT) from the NZGD for a range of PGA, Mw and GWD, resulting in over 15 million analyses (see Section 7).

4 **Develop the LVM** (see Section 8), which provides estimates of LDMs (e.g. Liquefaction Severity Number (LSN)) for different PGA, Mw and GW combinations across the extent of the National Flatland Model. The model combines estimates from both the geospatial model and local GIs and produces output in terms of a lognormal distribution of LSN for each PGA, Mw and GWD combination.

5 **Develop a geospatial model** (see Section 8.4), which provides LV estimates using relationships between the aggregated national dataset of GIs and geospatial features.

6 **Develop a National GW Model** (see Section 9), which provides estimates of the median free GWD, an estimate of uncertainty in that depth, and a seasonal variability trend. Additionally, a model that reflects 1 m of SLR was developed.

[10] Python is a high-level, interpreted programming language known for its readability and versatility, it is used widely in a range of applications including web development, data analysis, and AI.
[11] Referred to as YP78 in this document.

Run time steps:

1 **Select the seismicity map of PGA and Mw** (either a return period output or an event scenario).

2 **Estimate the likely distribution of an LDM at each location of interest**, by combining the PGA map, event Mw (or Mw map for return period calculations), GWD map, and the LVM.

3 **Estimate the probability of land damage** from fragility functions, or estimation of building damage using published building damage fragility functions that are not covered in this project or report.

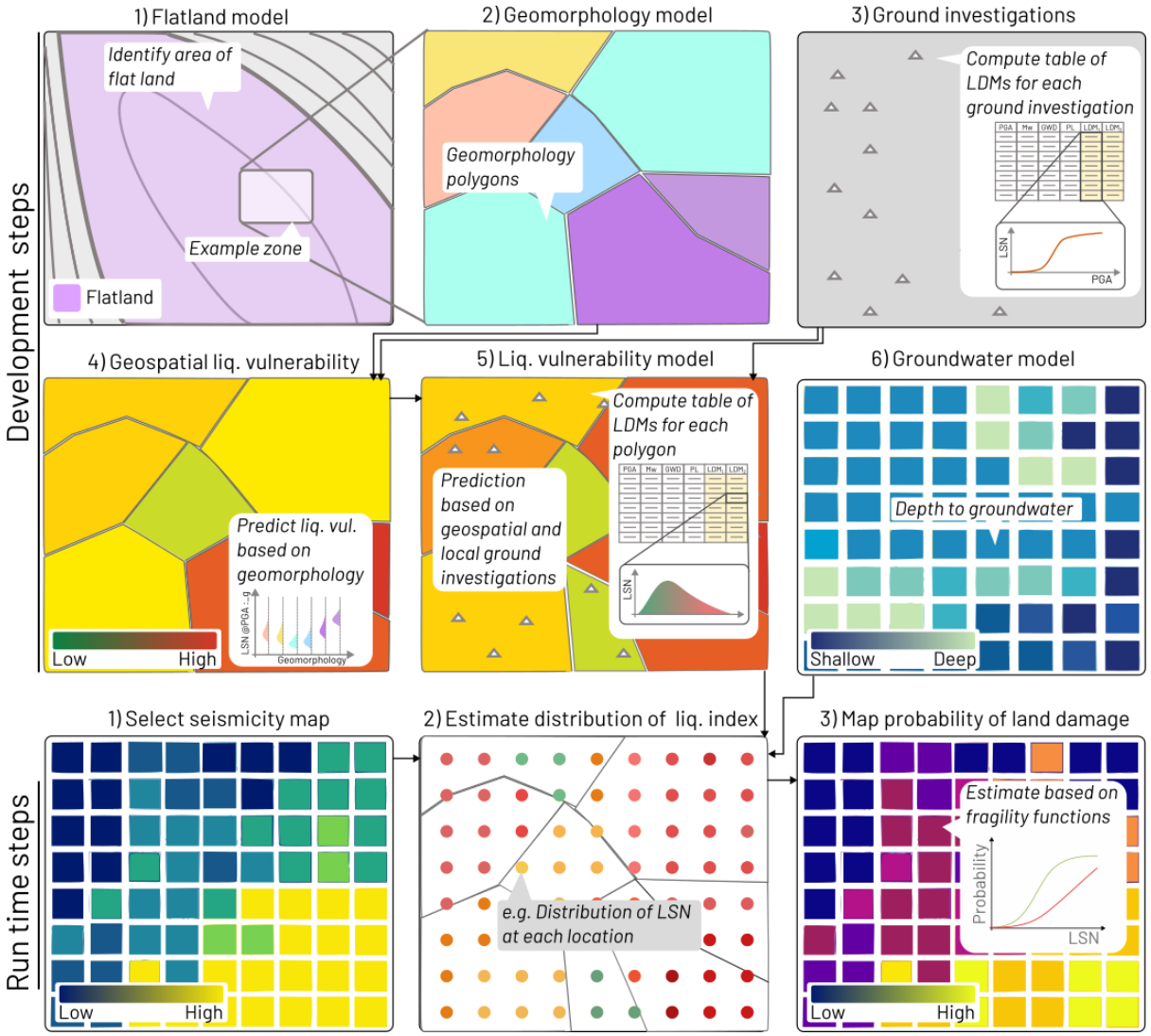

Figure 4.1: Overview of key steps in the generation of outputs

The modules are designed to be independent to enable updates to science and processes, however, there is some level of upstream dependence for the LVM and land damage calculations. For example, the LVM requires geomorphology categories that are hierarchical to build the geospatial model predictions in the absence of Geotechnical Investigation (GI) data within that geomorphology category.

The technical sections of this report are arranged based on the steps outlined in Figure 4.1, with the exception that the LV geospatial model is presented within the LV module, and the LDFCs are

presented in their own section (Section 10) prior to covering the runtime steps for generating scenario outputs in Section 11.

4.2 Requirements for the development of the NLM framework

The overarching requirement for the NLM framework is the ability to support multiple use cases. In particular, the uses cases of loss modelling and land-use planning were the primary focus. Specific details of those end use requirements are covered in Sections 4.2.1 and 4.2.2 respectively. Notably, the requirements for accuracy and precision for loss calculations are different to those for land-use planning. For example, an unbiased best estimate with sufficient precision to see meaningful trends may be adopted for loss calculations. Conversely, a regulatory application may require a conservative estimate for engineering design purposes or a mechanism that identifies the degree of uncertainty in the assessment for land-use planning purposes. To manage the competing demands of multiple use cases a strong focus was put on reducing bias and quantifying the uncertainty in the outputs. By quantifying the uncertainty in the outputs, it allows end users to select the appropriate precision and bias for their selected use case. The other primary requirements were that the framework should have a consistent national approach and be modular in design. The details and benefits of the consistent modular approach are outlined in Section 4.2.3.

4.2.1 Loss modelling

The NLM is needed for the estimation of liquefaction-induced losses and has several requirements which are outlined in Table 4.1, along with how they are addressed in the framework.

Table 4.1: Requirements for loss modelling

Requirement	Addressed by
Estimate the distribution of LSN for potential future seismic events for use in regional scale loss modelling, particularly with residential house liquefaction-induced loss curves.	The framework produces several different distributions of LSN. Specific considerations for this are outlined in Section 4.2.1.1 below.
Be decoupled from the estimated GWD – to allow different seasonal and SLR scenarios to be considered.	The LVM model precomputes LSN responses for different GWDs, and the NLM GW Model produces estimates of different GWD for different scenarios. Different LSN values can be quickly obtained using the lookup tables in the LVM as discussed in Section 8.1.
Be decoupled from the estimated seismic hazard – to allow different seismic hazard scenarios to be considered.	The LVM model precomputes LSN responses for different combination of PGA and Mw. Therefore, different earthquake scenario PGA maps can be used and the LSN values can be quickly obtained using the lookup tables in the LVM as discussed in Section 8.1.
Be ingestible within NHC's PRUE software.	PRUE requires estimates of liquefaction response in terms of LSN and the seismic demand from PGA and Mw. Additionally, there are implicit requirements on not producing very large files that would be slow to use during runtime.

4.2.1.1 Considerations for quantifying LSN for loss modelling

The distribution of LSN for loss modelling is primarily concerned with providing:

1 Spatial trends in the variation of LSN at the suburb-scale. While the objective was to provide models appropriate for regional-scale modelling, suburb level scale was considered suitable for resolving spatial trends. Suburb-scale was chosen since property values (and thus loss values) vary at this scale (i.e. adjacent suburbs can have very different property values). Furthermore, the response/damage of a dwelling due to liquefaction is driven by the construction and typology of the dwelling and its foundation, which can also vary at the suburb-scale (i.e. some suburbs have been developed at a similar time using similar construction).

2 An appropriate estimate of the probability distribution of LSN for a residential dwelling.

The first concern is primarily driven by both accuracy and for the ability to evaluate multiple events. Regarding accuracy, if there is poor resolution of spatial trends in LSN, then the uncertainty in loss estimates generally increases. However, resolving spatial trends to a precision finer than suburb-scale may not result in reduced uncertainty in loss estimates (since overestimating and underestimating LSN at the suburb-scale would generally cancel out, so increased precision of LSN may lead to a similar result).

The importance of evaluating impacts from multiple events was exemplified in the Christchurch earthquake sequence (2010-2012). Some areas experienced severe liquefaction from multiple events, however, in some cases, the dwellings in those areas were demolished after the first event, so no further losses were incurred. A broad scale geospatial estimate may provide a reasonable estimate of the LSN distribution across the city for an event by randomly sampling from a wide distribution. However, if a second event is also randomly sampled, then losses may be overrepresented as the sites with severe liquefaction would occur randomly at different places to the first event. To address the concern around spatial trends, the NLM framework produces spatial estimates of LSN using polygons, which where possible, quantify spatial trends at the suburb-scale. Note that this does not mean that the NLM can provide accurate suburb level loss estimates.

The second concern is not about providing realistic estimates of LSN, it is about providing the flexibility to compute a suitable distribution of LSN for loss modelling. This recognises that most loss functions have some implicit level of uncertainty of LSN within them. Excessive uncertainty generally results in an overestimation of losses for small demands and an underestimation for large demands. This important bias from uncertainty is conceptually demonstrated in Figure 4.2. The top row of Figure 4.2 shows a hypothetical fragility curve for an asset for some damage state (e.g. unrepairable). Figure 4.2b shows two lognormal distributions of LSN, and Figure 4.2c shows the cumulative probability of the damage state for those two LSN distributions. Both distributions have the same median, however, the wider distribution produces a higher probability of damage (25%). Conversely, in Figure 4.2e and f, the wider distribution results in a lower probability of damage. Perhaps contrary to intuition, intra-event uncertainty in asset response can reduce variability in inter-event estimates of total losses for regional loss calculations. At a more immediate level, the overestimation of uncertainty generally overestimates losses from small events which can have a significant impact on annualised average loss estimates.

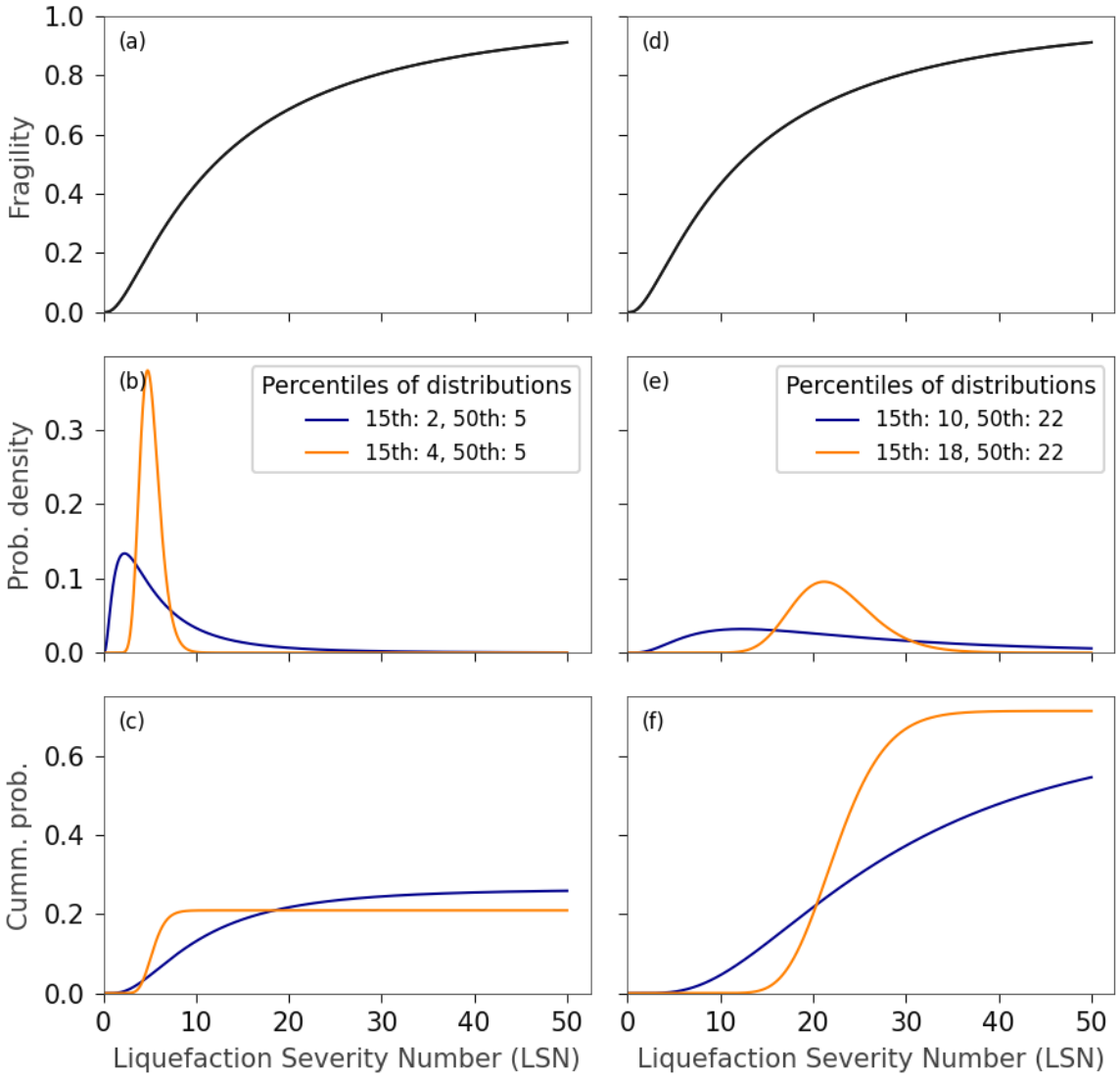

Figure 4.2: Evaluation of uncertainty on probability of occurrence (top) fragility curve for a damage state, (middle) LSN distributions (bottom) cumulative probability of damage considering the distribution of LSN, (left) examples for low LSN, (right) examples for high LSN

To reduce double counting uncertainty for the purposes of loss modelling, the loss modeller may adopt a narrower range of LSN (or simply the median). This can be a simple exercise when only evaluating total loss, as the distribution of loss per asset for a particular realisation is not critical. However, the loss modelling within PRUE needs to account for NHC's payout limit (i.e. capped losses[12]) on exposed loss for residential dwellings. Therefore, the adoption of the mean Building Damage Ratio (BDR) or loss is not suitable. This is conceptually demonstrated in Figure 4.3 where the variation in BDR and asset values for an event result in a large spread in losses. Some losses per asset are below the cap, whereas the mean values result in the whole population being over cap. There is a significant monetary difference between a conclusion which results in the whole population being over cap and a more refined individual asset assessment.

[12] The NHC cap for residential buildings is $300,000 plus GST. That is the maximum that NHC pay towards repairing and/or rebuilding an insured dwelling. Any eligible cover over that amount is provided by the private insurer. Note, the cap amount increased from $150,000 to $300,000 in 2022 (Natural Hazards Commission Toka Tū Ake, 2024).

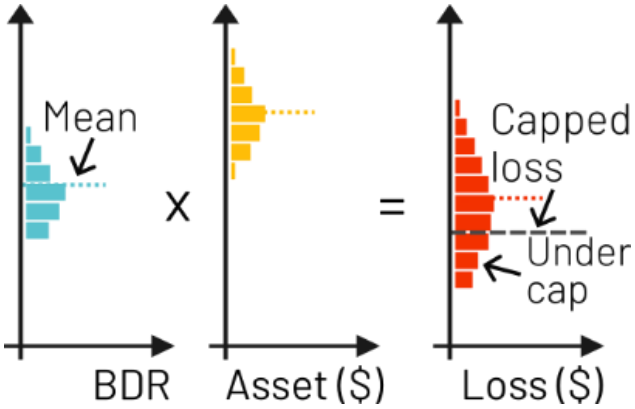

Figure 4.3: Conceptual difference between population-based loss calculations and individual asset-based in relation to capped losses. The mean values are represented by the dotted lines

To handle these competing requirements, the framework attempts to accurately quantify variability at different steps throughout the model development and provides as output several different measures of the LSN distribution at a site. The loss modeller can then evaluate and post-process the LSN distributions for their particular use case.

4.2.2 Support development of land-use planning maps

The MBIE/MfE Guidance (2017)) provides a nationally-consistent methodology to carry out liquefaction assessments, with a specific focus on the RMA and Building Act aspects. The MBIE/MfE Guidance (2017) provides specific guidance on targeting particular return periods and probabilities of different damage states, as well as guidance on GI density, consideration of geomorphology, previous earthquake events, and SLR. Finally, it establishes a framework to balance accuracy and precision in distinct LV Categories and Level of Detail categories. The requirements from the loss modelling directly fulfil some of the needs for supporting the development of MBIE/MfE maps[13], i.e. the outputs support the consideration of different seismic demands from different return periods and different GWD scenarios. However, the low spatial accuracy requirements (i.e. trends at suburb-scale) mean that the NLM outputs would not be suitable for MBIE/MfE maps without additional evaluation of boundary uncertainty (this is not directly accounted for within the framework but could be performed by post-processing the NLM output as outlined in Section 12.2). To support the development of MBIE/MfE maps, the NLM framework produces probability of land damage maps for various return periods with different considerations of GWD and using different methods to establish the LSN distributions.

4.2.3 Consistent modular approach

A consistent modular approach was established as a requirement to produce the following benefits:

- Provide a nationally-consistent approach to mapping liquefaction hazard to reduce variations in outputs that occur between different analyses and interpretation, and variations that occur over time due to data and science updates.
- Provide nationally-consistent nomenclature and data schemas.
- Enable ease of maintenance.
- Allow multiple different processes to be implemented in parallel, thus future proofing to allow inclusion of future scientific updates (e.g. new liquefaction triggering analysis).

[13] This is not saying that the NLM outputs can be directly converted into MBIE/MfE outputs, since there are a number of non-technical requirements that need to be considered for MBIE/MfE outputs as well as limitations in the NLM that need to be considered as outlined later in Section 12.2.

- Reduce the amount of additional software development required to allow new use cases (e.g. liquefaction damage to pipe networks) to be implemented.
- Allow the generation of stand-alone secondary outputs (e.g. national geomorphology model) and sub-versioning of these.
- Allow each of the modules and the corresponding outputs to be updated in a decoupled manner that only influences downstream modules and outputs (see Section 4.4).
- Allow scenario modelling and futureproofing for inevitable changes in the codified and scientific understanding of seismic hazard by decoupling the liquefaction model from the seismic hazard model.

The consistent approach is achieved by making all the processes data-driven, in that the process remains unchanged and only the input data drives the output of the model. To achieve modularity, the framework presented in Section 4.1 was developed. Furthermore, modularity was applied within each module by splitting large processes into a series of sub processes, decoupling the model inputs and outputs from the processes by using data schemas, and modularising the codebase using object-oriented software architecture where appropriate.

4.3 Key framework decisions

To balance the multiple design requirements, the LVM was developed with the following considerations:

- Liquefaction response was quantified spatially using polygons – as opposed to raster grids or points. The reasoning behind this is discussed in detail in Section 8.3.1.
- Liquefaction response was precomputed for predefined PGA, Mw and GWDs to de-couple the LVM from the seismic demand and GW (both of which are uncertain and differ for different scenarios). Precomputed values are defined in Section 7.4.
- Liquefaction response uncertainty was quantified using multiple different distributions of LSN – allowing different use cases to adopt different distributions for the specific end use. The different distributions are defined in Section 8.1.

The NLM GW Model achieved the requirements by providing representative GWD outputs for both current median conditions and 1 m of SLR on regular 100 m grid. The seasonal variability of GW was quantified as a simple sine function. The uncertainty in GWD was quantified as a distribution to allow different use cases to select the most appropriate GWD.

Flexibility in handling uncertainty is provided in the estimation of land damage, in that two different sets of LDFCs were developed. The first was directly fitted to the data, whereas the second removed some uncertainty related to the input GW. The end user can then select the most appropriate set of curves for their end use case.

Collectively, the different options provide 12 ways[14] to compute land damage directly from the NLM for an extensive range of PGA, Mw and GWD combinations. However, the layers can easily be augmented (e.g. selection of a certain percentile GWD, adjustments to LSN distributions, adjustments to fragility functions) to produce specific outputs for different end uses.

Given the significant focus on reducing bias and quantifying uncertainty, Section 4.3.1 provides high-level details on how this was handled across the modules.

4.3.1 Handling uncertainty

The model build process involves thousands of modelling choices (referred to here as equations) that involve some uncertainty and/or error/bias. The handling of uncertainty is primarily focused on

[14] The 12 ways come from the product of three different types of LSN distributions, two different sets of fragility curves, and two different probabilities of liquefaction.

input uncertainty and model uncertainty[15]. Given that there are a series of equations, the uncertainty in the output of one equation becomes the input uncertainty for the next equation in the series and uncertainties can compound. To manage the propagation of uncertainty through the model, the uncertainty was considered both at the system (module level and whole of NLM level) and at the equation level, with the primary goal of minimising bias and uncertainty in the NLM outputs.

One of the key challenges is that quantifying input uncertainty can be very difficult for some equations as the relevant information is not often provided in raw datasets. Since many of the NLM equations were developed using empirical data which have uncertainty in the predictor variables, this uncertainty is implicitly included in the equation if the equation is directly fitted to the data. Therefore, explicitly modelling the input uncertainty (e.g. by randomly sampling an error term) may double count the uncertainty in predictor variables since it is already implicitly considered. Different approaches (i.e. implicitly or explicitly) for handling input uncertainty are adopted for different equations throughout the NLM due to practicalities of quantifying input uncertainty and reducing the double-counting.

A brief discussion is provided here outlining how the propagation of uncertainty is handled within and across the various NLM modules. For clarity, three uncertainties that are discussed widely in the report deserve a special mention here to improve readability:

- Boundary uncertainty: The increase in uncertainty of a parameter near a boundary. In the LVM (Section 8), the uncertainty in an LDM is assumed constant within a polygon but in reality, the uncertainty in an LDM is lower near GIs and higher near polygon boundaries[16].
- Misclassification uncertainty: The uncertainty in the assignment of classes or categories. This can either be quantified explicitly (e.g. using probabilities of being in each class) or handled implicitly in later equations[17].
- Liquefaction response uncertainty: The uncertainty related to the prediction of liquefaction response. This is sometimes specifically quantified as the probability of a given land damage state or with a probability distribution of an LDM.

The flatland and ground investigations modules do not explicitly quantify the uncertainty in their outputs (i.e. there is no specific quantification of boundary uncertainty or misclassification uncertainty). The geomorphology model does quantify the misclassification uncertainty, however, in this version of the NLM it is not used in later stages. The primary reason for not using these uncertainties is because they are implicitly captured in the LV model (i.e. increased misclassification uncertainty results wider distributions in the LV geospatial model). Additionally, the uncertainty can be accounted for explicitly as a post-processing step (e.g. buffering outputs with a high uncertainty overlay near the boundary of flatland).

The LV model explicitly quantifies uncertainty by providing several different distributions for the expected LDM that reflect different measurements of uncertainty. The misclassification uncertainty from the NLM Geomorphology Model is implicitly accounted for in the geospatial model predictions. Boundary uncertainty is not explicitly considered in the LV model in that the uncertainty is assumed constant within a polygon. However, there are different tiers of polygons to reflect different levels of

[15] Input uncertainty refers to the uncertainty in the predictor variables for forward modelling (not uncertainty in the predictor variables when developing the equation), whereas model uncertainty is the uncertainty in the predicted output due to unmodelled phenomenon.

[16] An alternative definition (not adopted) would be the uncertainty in the position of boundary. This was not adopted since the boundary of non-flatland to flatland, or from one geomorphology to another, or from one liquefaction response to another, is more nuanced (e.g. a gradual transition).

[17] This is particularly relevant in the assignment of geomorphology classes within NLM Geomorphology Model (Section 6) and the LV geospatial model (Section 8.4), and the assignment of land damage observations in the development of LDFCs (Section 10) and historical scenario validations (Section 11.1).

uncertainty. The different tiers use different algorithms to balance boundary uncertainty versus precision. The different tiers also correspond to different levels of liquefaction response uncertainty (see Table 8.2 for details).

As covered in Section 4.3, the GW Model explicitly quantifies the uncertainty in GWD, and different LDFCs are provided to allow the user to explicitly or implicitly consider GWD uncertainty. Notably, uncertainty related to the determination of LSN (e.g. differences between CPT and BH, between testing equipment rigs, corrections for tip sizes, uncertainty in GWD during the investigation, corrections for short GI, and three-way interpolation error) manifest in both the LSN distributions of the LV model and in the LDFCs. This double counting of uncertainty is discussed in relation to the outputs in Section 11.1.1 and future work may address it within the NLM. Some general comments on handling of the different uncertainties for loss modelling and land-use planning maps are provided in Sections 12.1 and 12.2 respectively.

There are other uncertainties that may not have been accounted for and could be better quantified and addressed in the future. Most of these uncertainties have also been noted in the model limitation statements. The terms aleatory (meaning random or inherent) and epistemic (meaning due to lack of knowledge) uncertainty have been avoided in this report due to a lack of consistent understanding and widespread acceptance on what constitutes aleatory uncertainty. Instead, uncertainties have been labelled based on how they manifest at each point in the model build process and explanations have been provided on how they impact model outputs.

4.3.1.1 Guidance for limiting uncertainty and bias

Ideally, LSN distributions would be very narrow and the LDFCs very steep (reflecting low uncertainty). However, lack of data, issues with the quality of the data, and simplifications in assessment processes (both to manage data storage requirements and simplifications in processes found in existing literature) all contribute to increasing uncertainty in the behaviour of the NLM. This section outlines some high-level guidance for the development of each of the modules in terms of managing both uncertainty and bias.

Unlike a systematic bias (i.e. a bias that occurs across all inputs), if a modelling decision results in over-prediction at some hazard levels and under-prediction at others, then this is unlikely to cause bias when aggregated for a seismic event or across a series of seismic events. Instead, it will increase the quantified uncertainty. Given there is already considerable spatial variability of soil properties, modelling simplifications that increase uncertainty may have only limited impact on the uncertainty in the model output[18].

The model framework generally quantifies liquefaction response in terms of LSN, which is converted to probabilities of land damage categories using LDFCs. The direct use of a linear LSN scale to quantify biases and uncertainties generally does not balance differences suitably across the damage spectrum. For example, the difference between LSN of 1 and 2 would be seen as of equal importance as the difference between 51 and 52, but the former results in a more impactful change in the probability of land damage. As justified later in Section 10.4.1.3, the evaluation of uncertainty and bias was instead quantified in terms of the natural log of LSN, log(LSN). Note that in all cases in this report log is natural log. The use of log(LSN) puts a significantly greater focus on quantifying variability in LSN at low LSN compared to using a linear scale for LSN. Given that differences in log(LSN) are unfamiliar for most readers, Table 4.2 has been produced as a reference of several comparisons between log(LSN) differences compared to differences in LSN.

[18] The uncertainty from the combination of two independent variables with normally distributed uncertainty is calculated as the square root sum of the squares of the standard deviations of the two variables. In this case, spatial variability is assumed to be independent of uncertainty generated by modelling decisions.

Table 4.2: Comparison of differences in natural log of LSN versus linear scale LSN

log(LSN) difference	Examples of difference in LSN
0.05	1-1.05, 5-5.3, 30-32, 50-53
0.1	1-1.1, 5-5.5, 30-33, 50-55
0.3	1-1.3, 5-6.7, 30-40, 50-67
0.6	1-1.8, 5-9.1, 30-55, 50-91
1	1-2.7, 5-14, 30-82, 50-140
1.5	1-4.5, 5-22, 30-130, 50-220

The target range of uncertainty and bias in log(LSN) was developed for different spatial and analysis scales. The target range considered the significant spatial variability of LSN, as well as the limitations of LSN in predicting land damage (see Section 7.8.3 for details). The general guidance applied was that modelling decisions should ideally not result in:

- City-scale bias for a single seismic event.
- Suburb level bias when considering a range of seismic events.
- At polygon level:
  - Bias of the median exceeding log(LSN) of 0.05 for an individual polygon at a single seismicity level.
  - Standard deviation in uncertainty from that decision exceeding 0.1.
- At GI level:
  - Bias exceeding log(LSN) of 0.07 at a single seismicity level.
  - Standard deviation in uncertainty of log(LSN) of 0.15 at a single seismicity level.

The guidance for bias and uncertainty was not straightforward to apply since many relationships are highly non-linear, such that an uncertainty in one parameter can result in a biased estimate of a dependent variable. Furthermore, the uncertainty in the input data was not always quantified. Finally, the LSN calculation has thresholds (e.g. no contribution from a layer if the liquefaction factor of safety is greater than 2), therefore, it is not necessarily valid to evaluate differences in log(LSN) at very low LSN values. In general, a lower limit of LSN = 0.1 was adopted for a high seismicity and high GW scenario (e.g. PGA = 0.6 g, Mw = 7.5 and GWD = 1 m) when evaluating adherence to guidance. However, different thresholds were sometimes adopted as detailed in this report.

4.4 Future model updates

The intention is that NLM would be regularly updated to include new data and processes and provide general enhancements. Each of the technical sections of this report identifies potential future improvements to help outline the direction of future updates. These future improvements are not recommendations for updates within the current phase of work but should be considered and prioritised for inclusion in the future model updates.

This first phase of model development has primarily focused on developing a model framework that can support regular updates and produce useable outputs for multiple end use cases. There has been considerable effort to develop automated cleaning and filtering of the input data to produce a useable first version of the model, however, as noted throughout the report, a review and update of the data cleaning and filtering processes may yield further improvements.

The tuning of model parameters (i.e. coefficients that are used for interpreting and converting the raw data into a model that produces estimates of liquefaction-induced damage) has been done with a focus on producing a model that has minimal bias to over or under predict liquefaction at a regional scale. In the future versions of the model, it could be expected that these parameters would be adjusted to improve model outputs, noting that in many cases the relationships needed to constrain the model parameters are not yet established in published literature.

4.4.1 Versioning

The current system has a single version release number for all outputs (i.e. everything is at version 2025.0), and the source code maintains its own version per module. However, with future revisions, the version numbers of the different outputs could differ (e.g. GW Model could be at version 2026.2, while Flatland Model could be at version 2025.2). In the case where the LV model version becomes out-of-sync with the input sub models, the version of each sub model used to build the LV model would then be stored as meta data.

4.4.2 Data updates

The automated approach to the creation of the liquefaction model and sub-models means it is setup to efficiently incorporate additional data as it is collected (such as geotechnical and GW data). However, there are several challenges to incorporating additional data beyond automating the model build process. The primary challenges are consistency of data format, the accuracy/audit of the data and merging data. Future data and models may be generated by different parties (for example consultants working on behalf of councils) and may be at different spatial scales and levels of detail to existing data.

To address these issues:

- Data schemas have been developed for each data type and model output.
- Where possible, automated data merging rules and data auditing has been implemented, with run reports that identify issues that require human intervention (e.g. significant changes in predictions).

When data is updated, it influences all downstream components, such that all downstream sections should be re-run to reflect the changes.

4.4.3 Process updates

The processes are decoupled from the data and models using data schemas. This allows individual processes to be updated or replaced without rebuilding the whole source code. However, different changes require different levels of updating. These have been categorised as minor and major below.

A typical minor update could include:

- Addition of data in a new format.
- Addition of more data that conflicts with existing data.
- Inclusion of a new method to obtain an existing derived input/component.
- A patch to the model to fix a bug that is known to affect outputs.

A typical major update could include the creation of a new component (or many components). For example, a major update would be where a request is made to include liquefaction indices for pipes quantified through lateral spreading. This would require a new input component to quantify ground slope, a new type of Similar Soil Polygon (SSP) that would account for similarity of slope, and a new lookup table quantifying lateral spreading.

4.5 Model validations

The technical sections of the report describe validation exercises that were conducted. The validations are primarily cross-checks with existing published outputs or internal validations, noting that there is often no source of truth. The primary purpose of these validation exercises was error detection, by checking that results were similar to existing published outputs and/or adhered to expected behaviour (e.g. GIs that are close together are generally more similar than ones that are further apart). In the future releases of the model, it is expected that these validation exercises would be repeated and comparisons between versions would provide insight into how the model is improving between releases.

4.6 Model refinement guide

Given practical and budget limitations of applying a detailed model build approach for the GW and geomorphology models, a model refinement guide was established to prioritise the regions where additional detail is required. The following conditions were used as a guide to focus model development efforts:

1 Flatland areas.

2 Large urban areas and surrounding land.

3 Areas with significant expected urban growth in the upcoming decades.

4 Areas with large amounts of GW data or GIs.

Using these conditions as a guide, locally refined GW models were developed in selected regions and greater focus was put on these areas when developing the transformations used in the geomorphology model.

5 Flatland module

Flatland modelling uses topographic data to provide an initial screen of land areas that may include ground conditions in which liquefaction could occur. The model's primary function is to discern flat, low-lying areas (including river and stream valleys), as opposed to hilly terrain where landslide analysis is more relevant.

5.1 Module output

The Flatland Module produces the NLM Flatland Model which identifies areas of flat land nationwide. It is stored as a single GIS vector file. Figure 5.1 and Figure 5.2 show Flatland Model outputs for Wellington and Napier and their surrounding areas respectively.

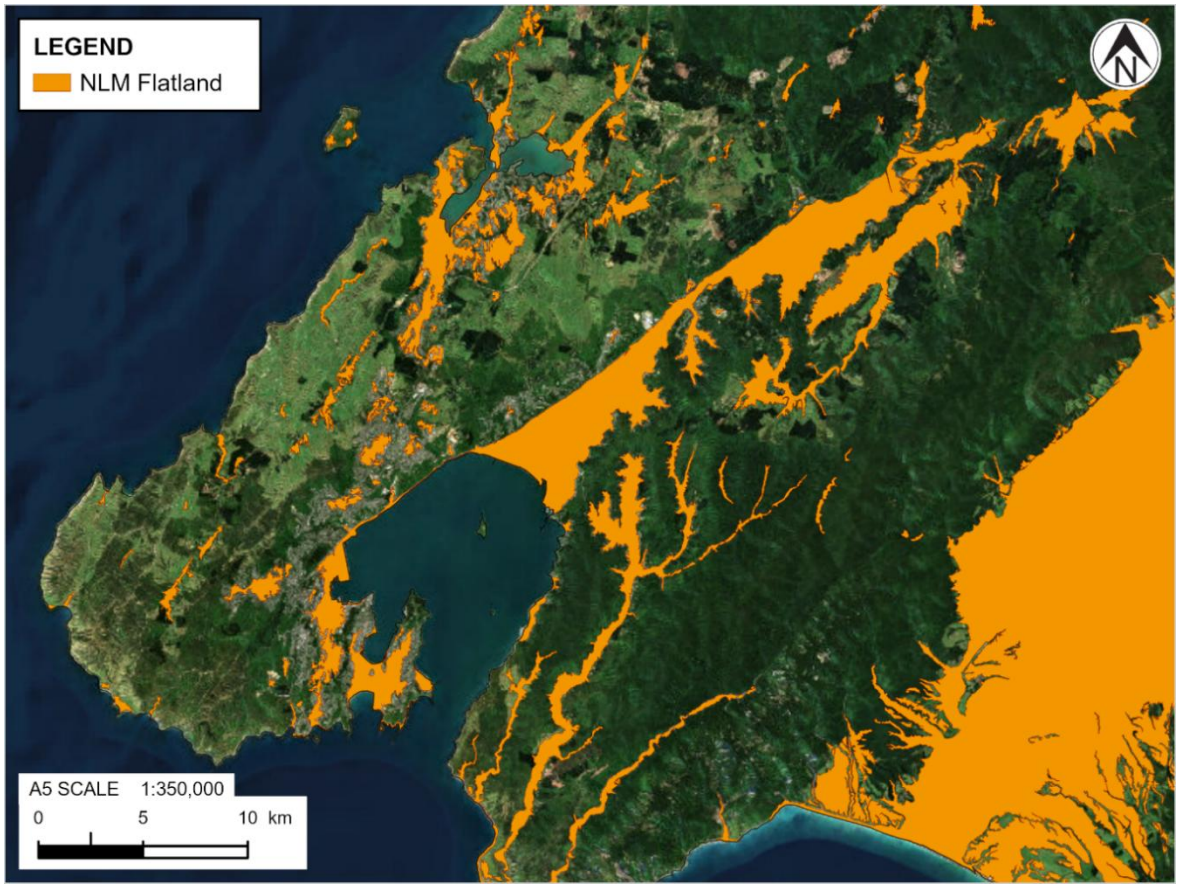

Figure 5.1: Output of NLM Flatland Model showing Wellington and surrounding areas

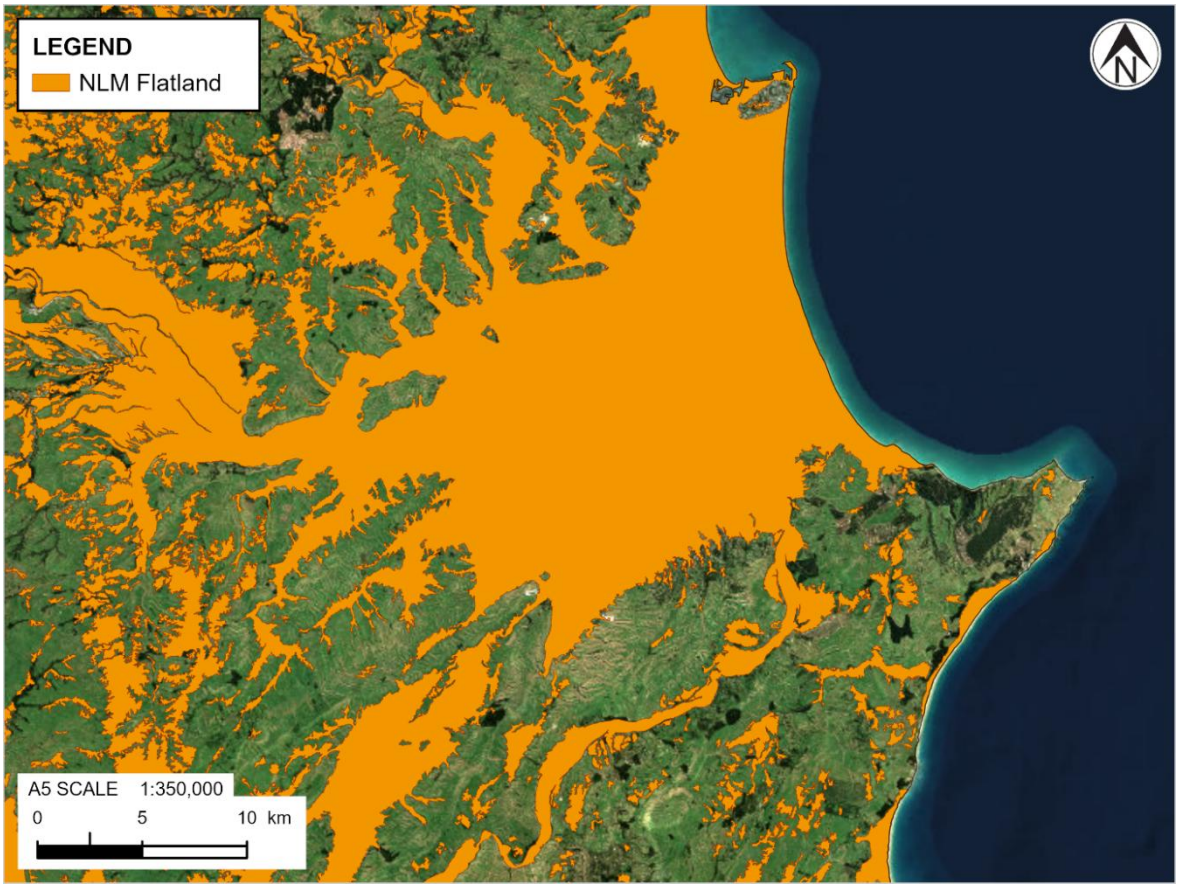

Figure 5.2: Output of NLM Flatland Model showing Napier and surrounding areas

5.2 Existing algorithms and models

Several existing algorithms and models to identify flatland were explored, the two most promising are covered briefly here, although neither were adopted for reasons stated below.

5.2.1 Geomorphon method

The geomorphon method, initially proposed by Stepinski & Jasiewicz (2011), is a technique used to analyse local elevation gradients. It involves defining a central point and then examining lines of sight in eight directions using a predetermined search radius known as the lookup distance. Within this radius, the zenith (maximum) and nadir (minimum) angles of elevation are calculated for each line of sight. Based on these angles and a set threshold, each direction is classified into one of three categories: elevation increase, decrease, or same elevation, represented by "+", "-", or "0", respectively. This classification helps in understanding the local elevation profile and landform categorisation.

The effectiveness of this method depends on two key parameters: the lookup distance and the zenith-nadir angle difference threshold. The lookup distance determines the extent of the area considered for each line of sight, influencing the scale of topographic features analysed. The angle threshold affects how distinctly different geomorphon features are identified. The choice of these parameters is critical and varies depending on the terrain and landforms of interest.

This method was evaluated but not selected due to two reasons:

1 The approach requires manual adjustment of parameters, such as the zenith-nadir angle and lookup distance, for each specific region to ensure optimal outcomes.

2 Despite careful tuning, certain areas require manual correction to achieve desired results.

These limitations didn't fit with the design philosophy of a data-driven automated approach. Therefore, the Geomorphon method was not adopted.

5.2.2 National Slope Map

The National Slope Map (LENZ, 2010) shown in Figure 5.3 was developed by Manaaki Whenua Landcare Research Ltd (Landcare Research). The slope data layer is an integral part of the Land Environments of New Zealand (LENZ) classification. It was constructed from a 25 m DEM, which was derived from 20 m digital contour data taken from the New Zealand Mapping Service 260 map series.

The DEM was produced using software developed at Landcare Research. The original contours, photogrammetrically derived from stereo photographs for map production at a scale of 1:50,000, were supplemented with additional intermediate contours, spot heights, and coastal features for lakes over 10 hectares, to improve the accuracy of the DEM for terrain surrounding water bodies. A linear interpolation method was used, assigning cells intersected by contours the elevation of those contours, especially in areas of steep terrain.

Slope was calculated from the elevation model using a second order central difference approximation as outlined in Zevenbergen & Thorne (1987). It covers most of mainland New Zealand but excludes some islands (e.g. the Chatham Islands).

A visual comparison of the "Flat to Gently Undulating" areas from the LENZ National Slope Map to areas of manually determined flatland highlighted that this map was coarse, predominantly due to the low resolution of the inputs. Therefore, this map was deemed to be not detailed enough, and hence, not suitable for the identification of liquefiable land, particularly in urban environments. However, the map does provide a useful reference for validation purposes.

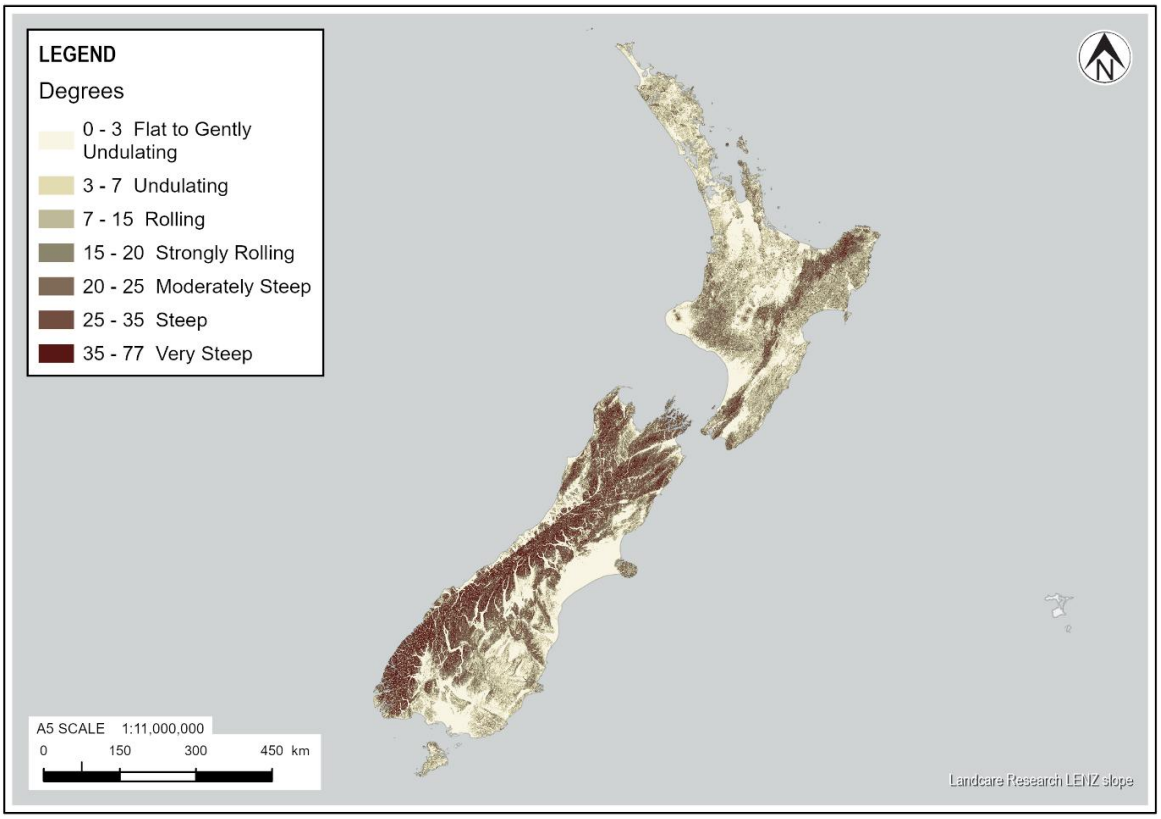

Figure 5.3: LENZ National Slope Map of New Zealand

5.3 Model development

The Flatland Model is built using five steps:

1 Identify sloping land and flatland (see Section 5.3.3)
2 Convert hilltop flatland to sloping land (see Section 5.3.4)
3 Remove small regions (see Section 5.3.5)
4 Convert to flatland polygons (see Section 5.3.6)
5 Trim flatland to coastal boundary (see Section 5.3.7)

5.3.1 Model inputs

The following two sources are inputs in the NLM Flatland Model:

1 T+T DEM model (see Section 3.1.3).
2 New Zealand coastal boundaries (see Section 3.4.3).

5.3.2 Definition of flatland

For the purposes of the NLM flatland was defined as any land that was not considered sloping. Sloping land was defined using two criteria:

1 10% (5.7°) or greater gradient for at least 200 m in any direction; or
2 Land on top of a mountain (there is a point 100 m below the current location, within 1 km).

The above criteria were developed by testing different algorithms and conditions on small areas of the country. The output was compared with expected behaviour, determined from existing liquefaction hazard maps where sloping land has been classified as ***Liquefaction Damage is Unlikely*** using MBIE/MfE Guidance (2017) maps.

The criteria are related to ground composition, and the mechanics of liquefaction. Increased slope tends to correspond to larger particle size or highly cohesive material, as well as high shear wave velocities (Foster et al., 2019). These ground conditions are generally less likely to be susceptible to liquefaction. The depth within the soil deposit that these relationships are valid for is dependent on the length of the slope. The length of 200 m was adopted based on visual comparison with elevation data. The algorithm outputs using different lengths were compared to existing MBIE/MfE Guidance (2017) maps.

5.3.3 Identify sloping land and flatland

An algorithm was developed to identify land that matched the sloping land criteria as detailed below. This produces a raster where each cell is identified as either sloping or flat.

From the first criteria, there are two attributes to identify a slope:

1 A slope threshold, st, (10%).
2 A distance threshold, dt, (200 m).

The following process was applied to each raster pixel of the DEM:

1 Find the slope in each of the 8 cardinal directions to a point at 3 distances (Figure 5.4):
    a A coarse distance (0.75 dt).
    b An intermediate distance (0.25 dt).
    c And a fine distance (DEM cell size).
2 Evaluate four slope criteria:

a Unidirectional coarse distance criterion (absolute slope from coarse distance > st).

b Unidirectional intermediate distance criterion (absolute slope from intermediate distance > st].

c Unidirectional fine distance criterion (absolute slope from fine distance > st).

d The overlap criterion (criteria (b) is true, criteria (b) for the opposing direction is true, and slope has the same gradient in opposing directions).

3 Each of the 8 cardinal directions is then checked, if all of a, b and c are met or d is met, the direction is considered sloping.

4 The pixel is considered flat if none of the lookup directions are sloping.

5 Figure 5.5 provides an example of the application of the criteria on a 1D test case, showing how the different criteria interact to correctly identify sloping areas and flatland. (a) has the 1D input elevation profile. This is coloured by which areas are expected to be sloping. (b) has the modelled flatland, expected flatland, and where each of the slope criteria are met, along the elevation profile. Where the coarse, intermediate and fine criteria are met, the lines overlap and the model considers the profile to be sloping. The model also considers anywhere where the overlap criterion is met to be sloping.

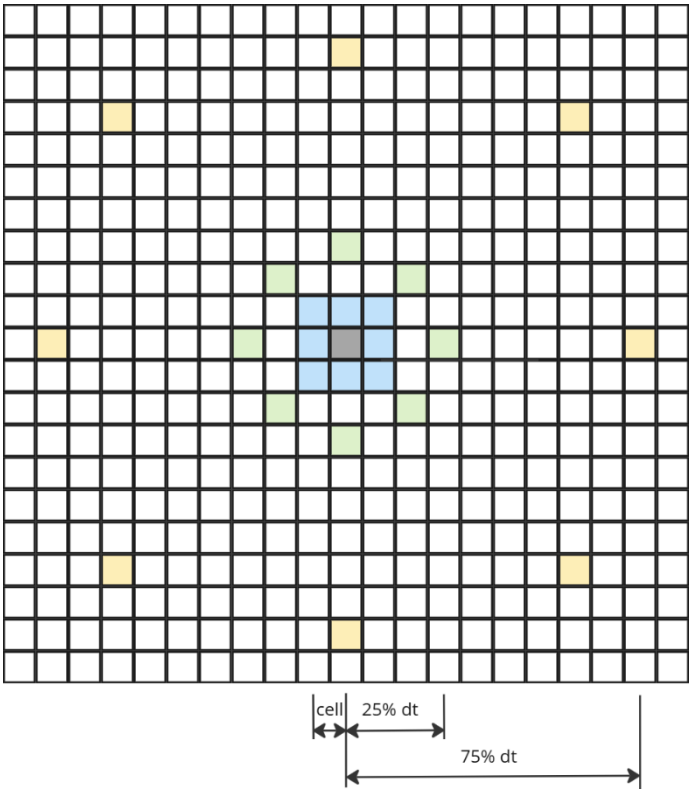

Figure 5.4: Fine, intermediate and coarse lookup distances used to calculate slope

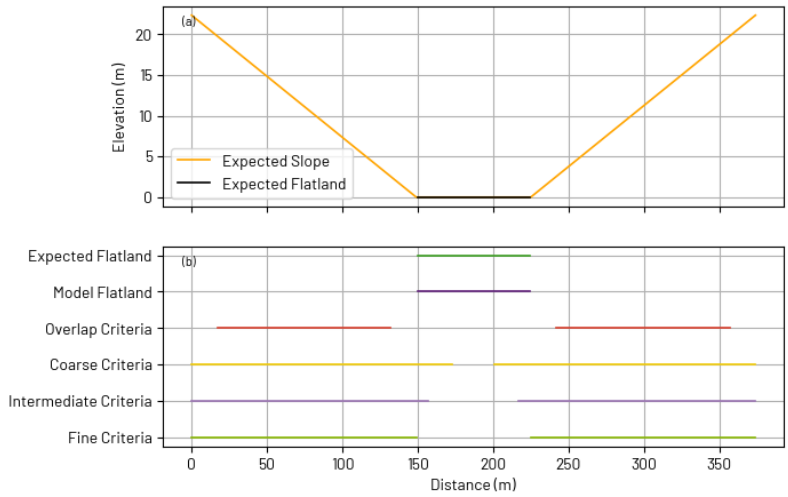

Figure 5.5: Example of a 1D comparison case showing a) The 1D geometry, and b) The results of all the criteria and the final classification

5.3.4 Convert hilltop flatland to sloping land

Any point that has another point 100 m lower in elevation below the location under consideration within a 1000 m radius is considered hilltop. Hilltop flatland cells are reclassified to sloping.

The selected change in elevation and radius was chosen based by trialling several different elevation changes with a radius corresponding to 10% slope. The different options were evaluated in terms of their effectiveness to remove easily identified hill tops without removing areas that would be considered flatland near a steep slope. The chosen elevation change was considered suitable though some flat areas on top of hills/mountains was not removed. This area was generally in low population areas or was a small area that was removed due to the small areas filter. An additional larger elevation change (e.g. 400 m) with correspondingly larger radius could be added to further identify these flat hilltops.

5.3.5 Remove small areas

Areas smaller than d_t^2 (i.e. 40,000 m^2) are reclassified to match their surroundings. First, small areas of flatland surrounded by sloping land are reclassified to sloping land. Second, small areas of sloping land surrounded by flatland are reclassified to flatland. This means significant slopes with small flat features are more likely to be considered sloping.

The reclassification process is undertaken so a higher degree of spatial accuracy is not inferred from the model. The choice of 40,000 m^2 is a reasonable proxy for the size of a large rural-residential lot in New Zealand (i.e. as per Table 3.5 of MBIE/MfE (2017)), and therefore identifying areas of flat land smaller could infer a degree of accuracy at a site-specific scale. The small area reclassification process also reduces the impact of occasional misclassification errors in the algorithm and decreases computational time in downstream NLM calculations (discussed in Section 5.5). As the NLM model is refined in the future, the threshold for small areas could be reviewed.

5.3.6 Convert to flatland polygons

The flatland raster is converted into a series of polygons by taking contours around the flatland boundary. This results in a smoother boundary than if raster pixels were used to determine flatland polygons.

The scikit-image implementation of the marching squares algorithm (Scikit-image) is used to find contours. Contours are created at the midpoint between flatland and sloping pixels. A 1-pixel buffer of flatland is then applied around the edges of the contour to ensure no flatland areas is missed. Subsequent slope and flatland contours are subtracted from this to give the nested flatland polygons.

5.3.7 Trim flatland polygons to coastal boundary

The flatland polygons are clipped to the LINZ coastal boundary. Flatland polygons smaller than the d_t^2 (40,000 m^2), outlined in Section 8.6.2, are then removed. This prevents the creation of small areas where flatland intersects with the coastline, caused by the pixelation of the flatland output.

5.4 Model validations

5.4.1 Comparison to the National Slope Map

The Flatland Model is validated through a comparison with flatland identified from the LENZ National Slope Map (Table 5.1). More information about the LENZ National Slope Map can be found in Section 5.2. Note that the flatland is identified in the NLM Flatland Model using a 10% slope threshold (corresponding to 5.7 degrees), and therefore, this is compared to areas in the LENZ National Slope Map with slope angle classified as 6 degrees or less.

Table 5.1: Comparing the amount of land defined as "flatland" as a percentage of the total land area for a given region for both the NLM Flatland Model and the LENZ National Slope Map

Region	% of land defined as flat in the NLM Flatland Model	% of land defined as flatland in NLM but not in LENZ	% of land defined as flatland in LENZ but not in NLM
Auckland	40.6	2.6	12.5
Bay of Plenty	30.1	1.6	8.0
Gisborne	9.7	0.9	4.5
Hawke's Bay	20.6	1.4	8.4
Manawatū-Whanganui	29.4	1.8	4.1
North Canterbury	34.2	1.1	2.0
Northland	32.2	1.8	13.0
Otago	29.8	1.7	5.1
South Canterbury	41.8	1.1	2.9
Southland	32.6	1.6	4.1
Taranaki	37.2	1.1	6.1
Tasman Nelson Marlborough	12.0	1.1	2.0
Waikato	44.8	1.9	7.6
Wellington	23.1	1.1	4.7
West Coast	22.4	1.4	1.8

There is significantly less land classified as flatland in the NLM Flatland Model relative to the LENZ National Slope Map. For all regions, the percentage of land classified as flatland by LENZ but not the NLM is greater than the percentage of land classified as flatland by the NLM but not LENZ (i.e. the

percentages in the fourth column of Table 5.1 are always greater than those is the third column). This is particularly the case in the Auckland and Northland regions. This difference could be explained by the high proportion of small rolling hills Figure 5.6 and Figure 5.7.

The LENZ National Slope Map is more likely to classify areas as flatland for the following reasons:

- The LENZ method uses 20 m contours to identify slope while the NLM Flatland Model uses a higher resolution DEM. Small depressions or hilltops may appear flat in contours but not in the DEM.
- The NLM Flatland Model reclassifies flatland areas smaller than 40,000 m^2. Rolling terrain has many small flat areas which would be reclassified.
- The NLM Flatland Model reclassifies hilltop flatland.

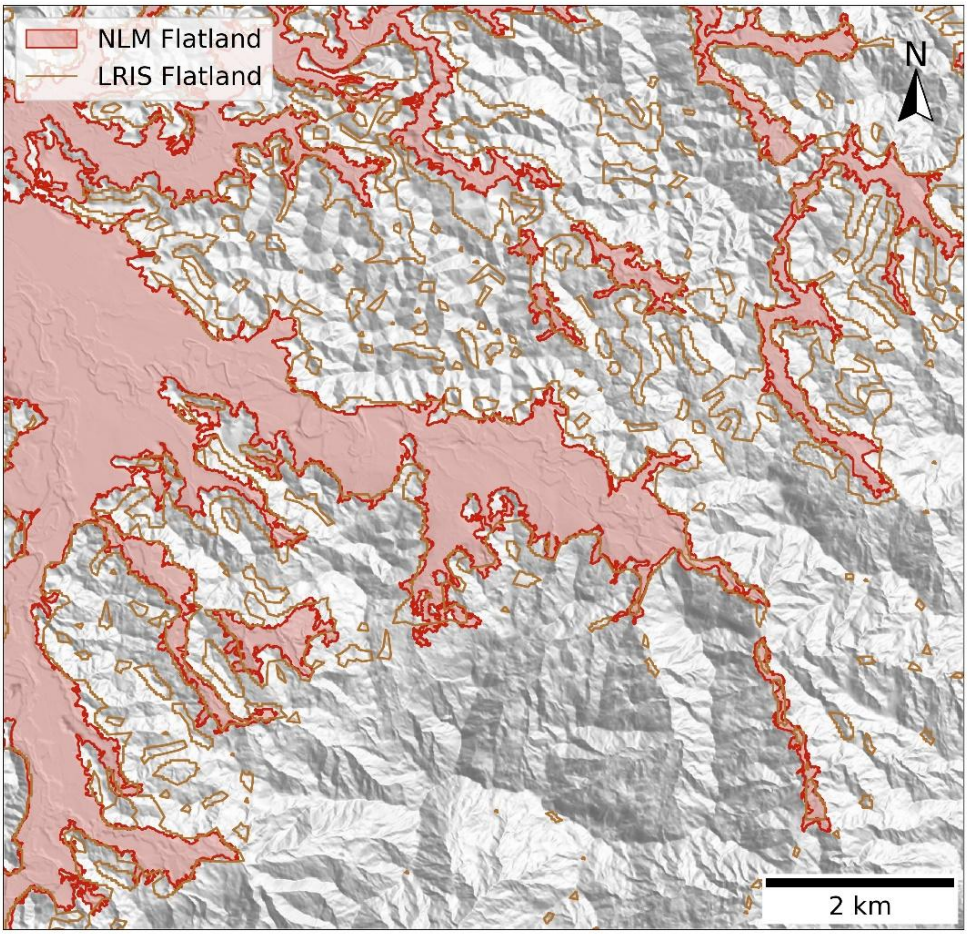

Figure 5.6: Area of Northland showing NLM Flatland Model (red) compared against flatland from the LENZ National Slope Map (orange line)

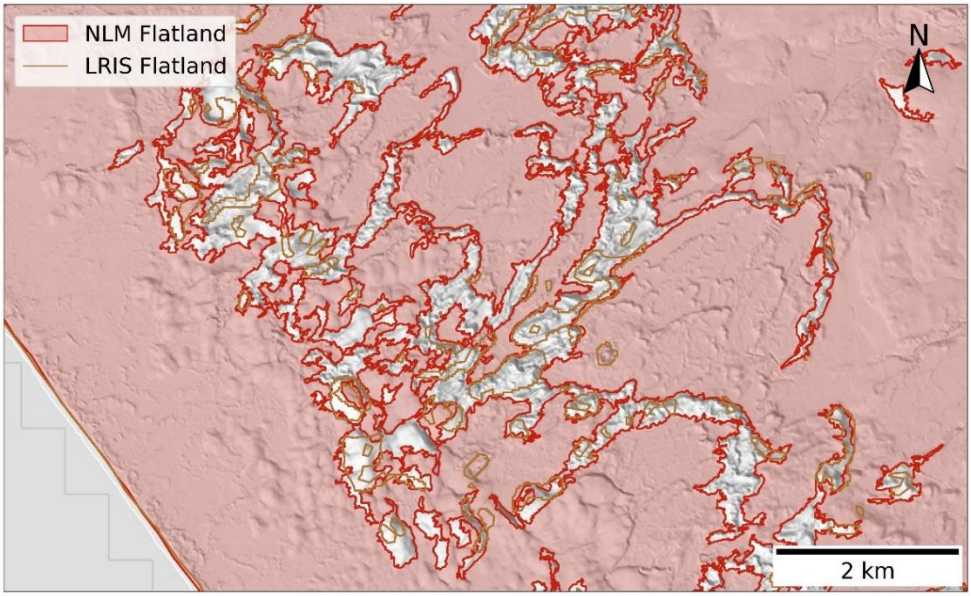

Figure 5.7: Another area of Northland showing NLM Flatland Model (red) compared against flatland from the LENZ National Slope Map (orange line)

Figure 5.8 and Figure 5.9 compare the NLM Flatland Model and LENZ National Slope Map for areas of Christchurch and Nelson respectively. The LENZ model cuts off important features that are captured by the NLM Flatland Model.

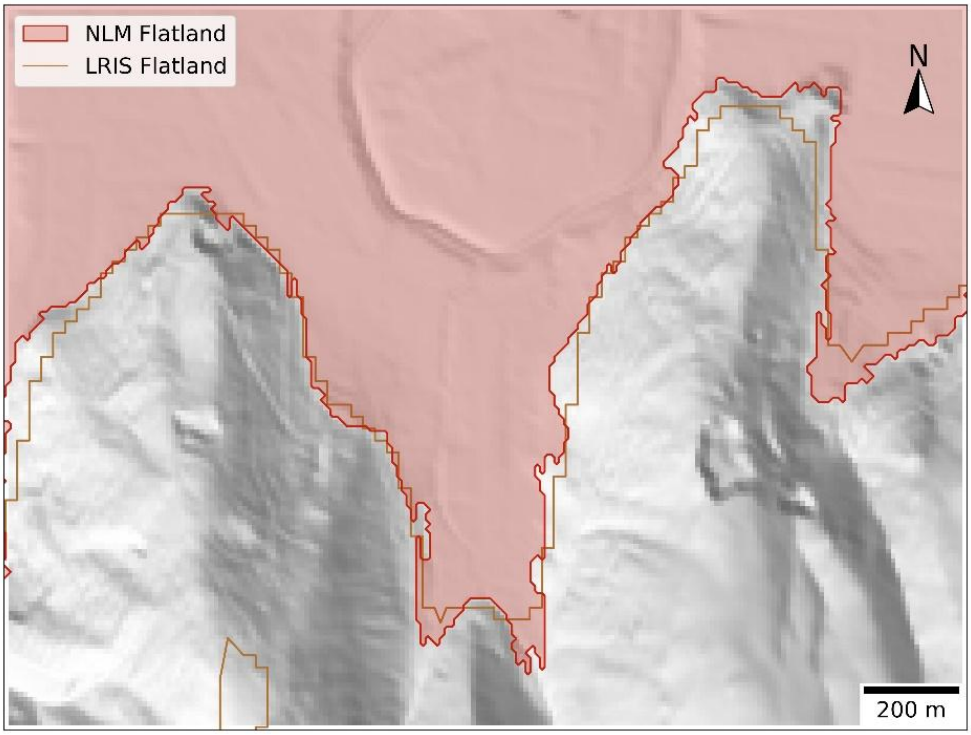

Figure 5.8: Area of Christchurch showing NLM Flatland Model (red) compared against flatland from the LENZ National Slope Map (orange line)

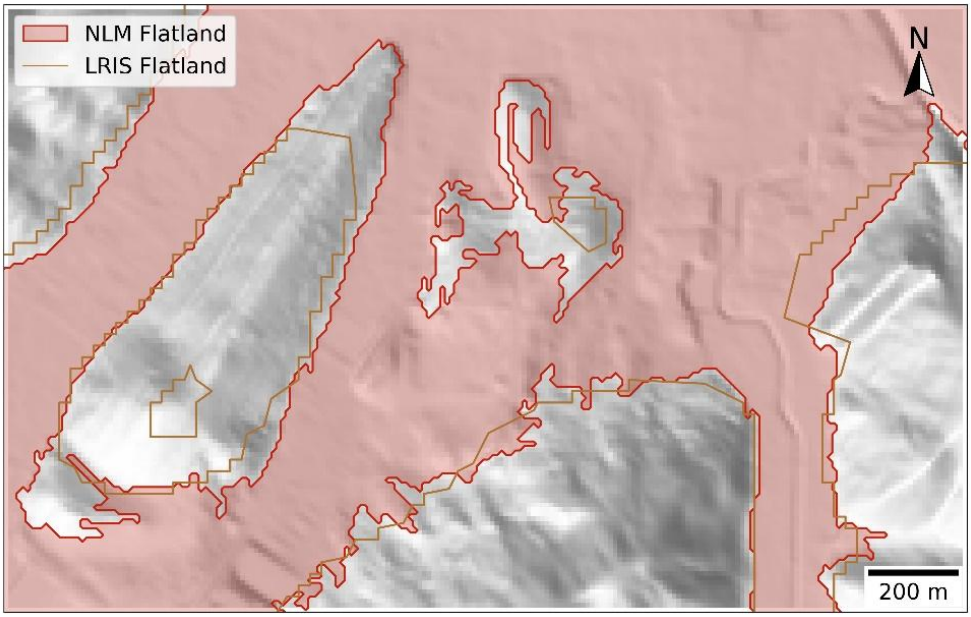

Figure 5.9: Area of Nelson showing NLM Flatland Model (red) compared against flatland from the LENZ National Slope Map (orange line)

5.4.2 Comparison to artificial geometries

A series of verification problems were also used to validate that the algorithm correctly identified flatland around simple landforms (i.e. artificially generated 1D and 2D landforms where the expected correct identification is easily identified by a human). The verification problems were also expanded to determine how resilient the model was to noise in the DEM (e.g. houses). These validations are provided in Digital Supplement A: *Flatland-comparisons*, and are similar to the output in Figure 5.5.

5.5 Limitations

The NLM Flatland Model has several limitations that must be acknowledged.

1 The accuracy of the Flatland Model is dependent on the accuracy of the DEM which is linked to the quality of the underlying LiDAR and national contour data. Areas based on the national 8 m DEM rather than the LiDAR-derived 1 m DEM (see Section 3.1) therefore have lower accuracy.

2 The removal of small areas (< 40,000 m^2) does limit the identification of small flatland areas, particularly along the coast (e.g. small bays).

3 The use of a 10 m spacing DEM theoretically allows the algorithm to identify the start of a slope to within 10 m, however, the irregular (noisy) output of DEM data means that true accuracy would be closer to an intermediate distance ~50 m.

4 The ground surface elevation may change over time due to natural and anthropogenic activity (e.g. landslides, sediment deposition from flooding, cut and fill activities), which may change the flatland extent.

5 The definition of what is not flatland land (Section 5.3.2) may not be appropriate for all soil deposits and for all applications.

6 The flatland algorithm has a “hole” where slopes between 50-100 m horizontal length can be incorrectly classified as sloping. Figure 5.10 shows a step of 7.5 m across 75 m (slope of 10%). According to the flatland definition presented in Section 5.3.2, this should not be mapped as

sloping, however, due to the overlap criteria there is a small portion mapped as sloping. In general, removing small polygons prevents this issue but the algorithm is slightly inconsistent with the definition.

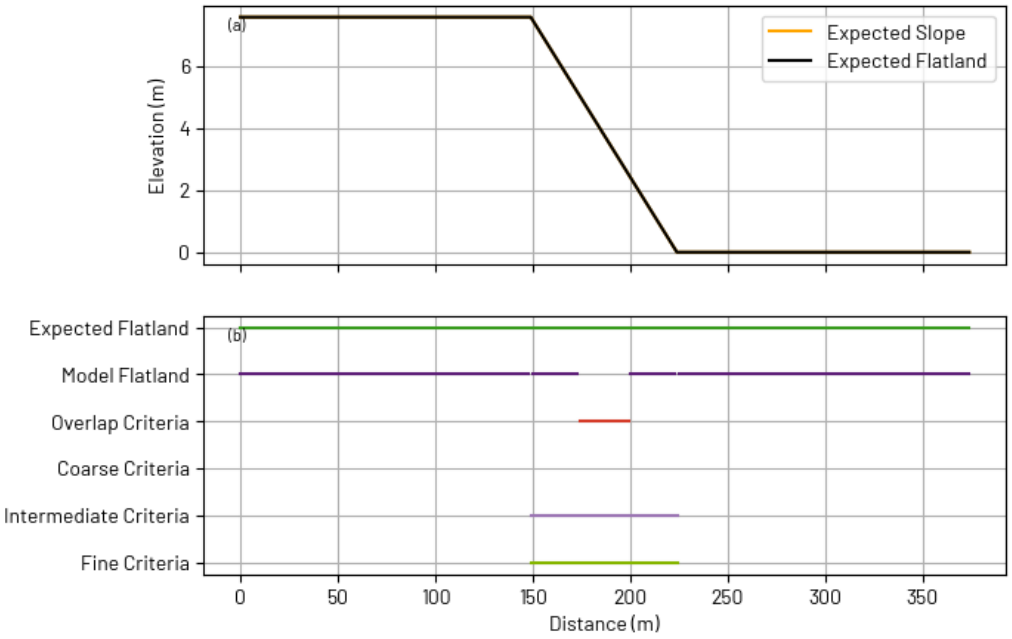

Figure 5.10: 1D example of the algorithm "hole", with a) Input elevation, and b) Model results

The NLM Flatland Model has been developed for the purpose of LV and has been developed with an emphasis on classifications important to liquefaction assessment, therefore it should not be relied upon for other purposes.

5.6 Potential future improvements

To enhance the Flatland Model and address its current limitations, several potential future improvements have been identified:

1 **Incorporate higher resolution LiDAR-derived DEM.** As new LiDAR-derived 1 m DEM becomes available, incorporate it into the Flatland Model as part of regular updates.

2 **Periodic review of the methodology for identifying flatland.** As new methodologies become available (e.g. geomorphon method), review these and see if they are more suitable than the methodology which has been specifically developed for this the development of the NLM Flatland Model.

3 **Removal of more small areas in non-urban areas** (e.g. in Fiordland) from the study area since these add computational time to downstream processes. In rural areas, the threshold for removing small areas could be increased to greater than 40,000 m^2.

6 Geomorphology module

Geomorphology mapping is the process of categorising a landscape into a series of terrains (polygons) with similar near-surface ground conditions, depending on their depositional settings. The categorised polygons are used to group GIs for developing the liquefaction geospatial model, providing a boundary for developing SSP and assigning an initial estimate of liquefaction based on the geospatial model. The model development builds largely off QMAP (See Section 3.2.1) and follows closely the geomorphology classifications for liquefaction developed in YP78.

6.1 Module output

The geomorphology module produces the NLM Geomorphology Model which is stored as a single GIS file that encapsulates the entire geomorphology data schema shown in Figure 6.1 and example regional outputs in Figure 6.2 and Figure 6.3.

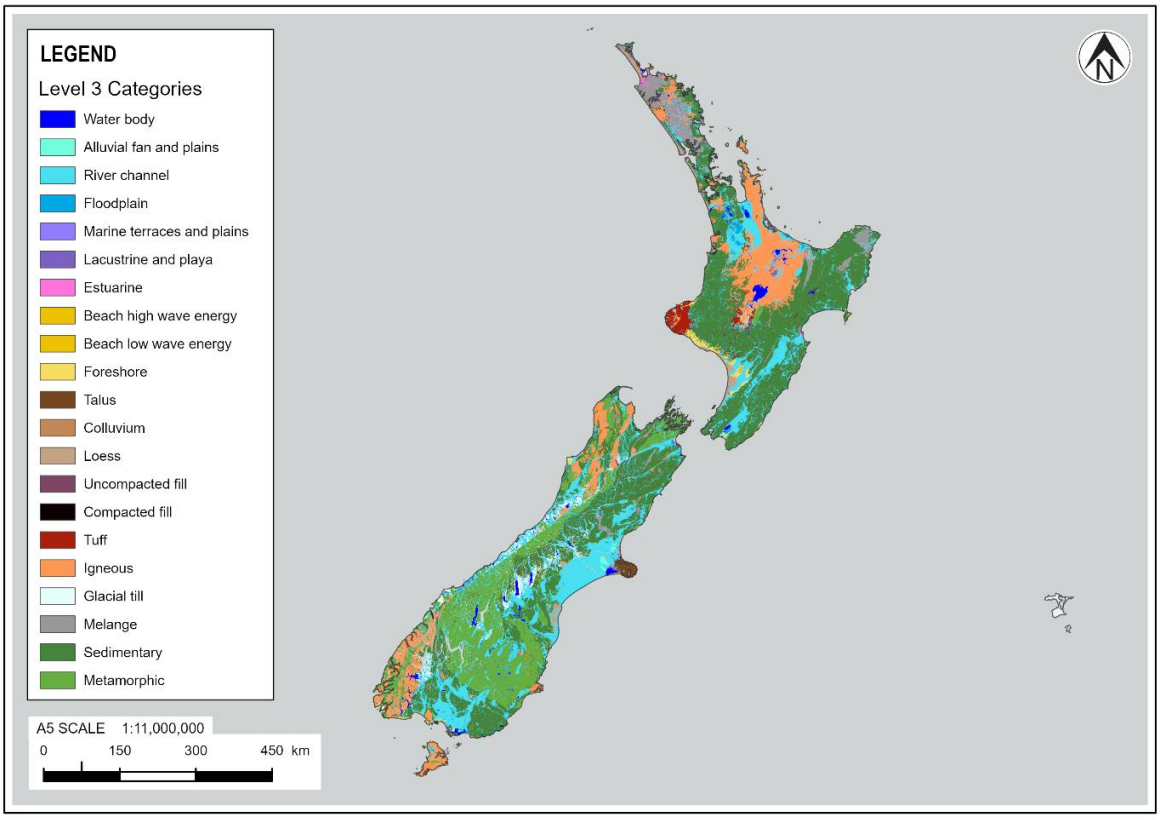

Figure 6.1: National NLM Geomorphology Model shown using Level 3 categories

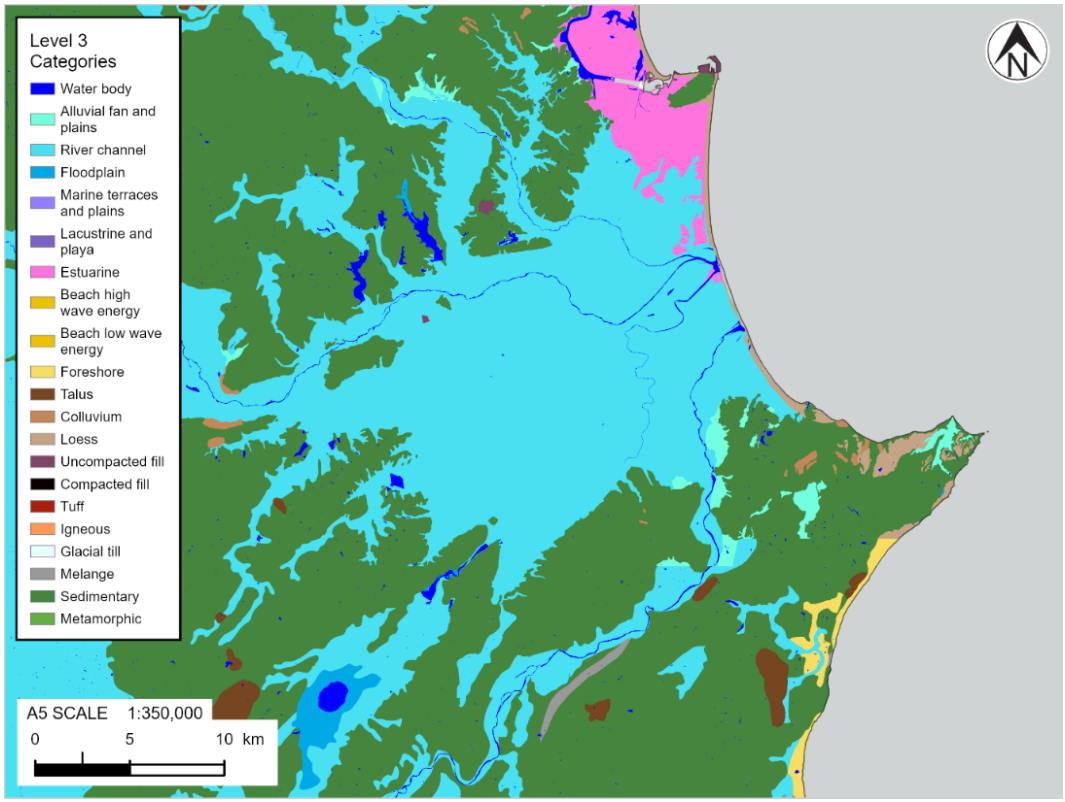

Figure 6.2: Sample output of the NLM Geomorphology Model for Hawke's Bay urban area

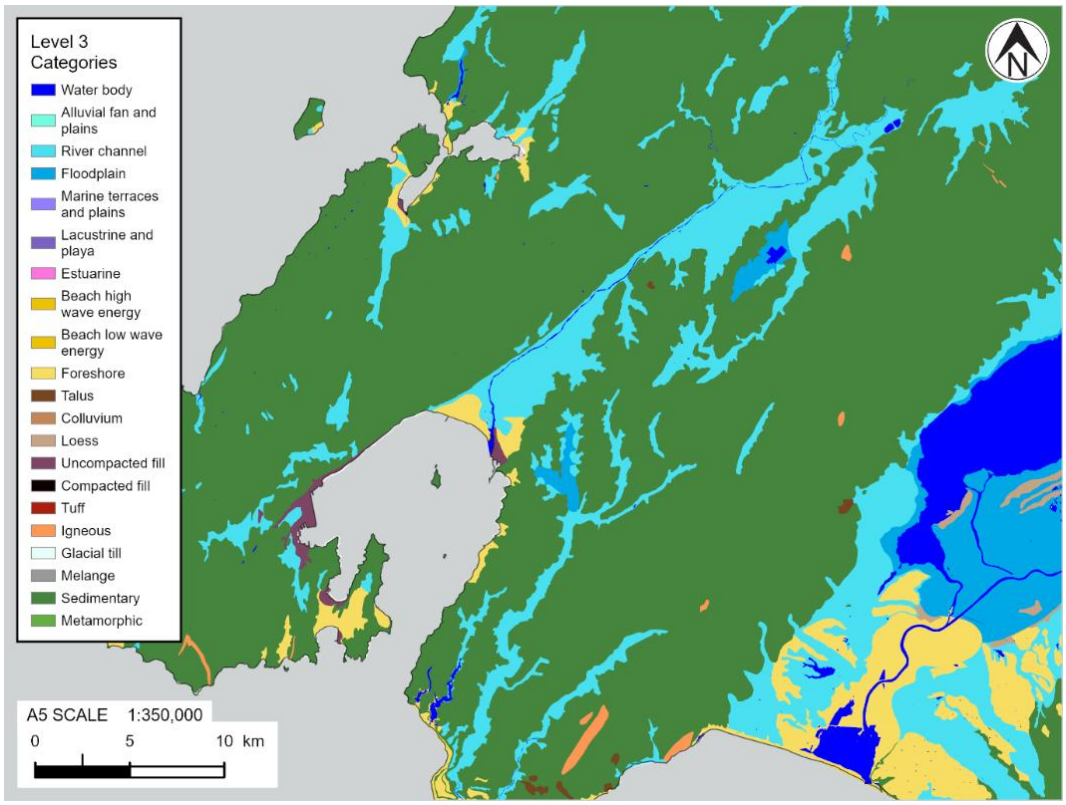

Figure 6.3: Sample output of the NLM Geomorphology Model for Wellington urban area

6.1.1 Data schema

The standardised, nationally-consistent schema applied in the NLM Geomorphology Model is presented in Table 6.1. This schema categorises geomorphology at multiple scales—Levels 1, 2, and 3—and includes fields for epoch and liquefaction susceptibility (geomorph_liq_susc), the latter derived from the YP78 classification. Key attributes, such as simple_name, description, and main_rock, are incorporated from QMAP and further refined with localised mapping. The confidence field indicates the qualitative uncertainty associated with the YP78 classification, while the geometry field defines the polygon boundaries within the model.

Table 6.1: Data schema for NLM geomorphology Model

Attribute	Description
l1_yp	Level 1: Broad classifications of geomorphology, including categories such as continental deposits, coastal zone deposits, fill materials, volcanic deposits, and areas identified as non-liquefiable. These categories are aligned with the YP78 qualitative system.
l2_geomorphology	Level 2: More specific geomorphology mapped at a regional scale, tailored to the NLM model. These classifications are unique to the NLM and are not part of the YP78 qualitative system.
l3_yp	Level 3: This level provides detailed geomorphology classifications, drawing from an expanded and adapted version of the YP78 “type of deposit” qualitative system. Categories include a broad range of geomorphology features relevant to New Zealand’s unique landscape, such as coastal features (e.g. "Beach high wave energy," "Estuarine"), fluvial environments ("River channel," "Floodplain"), and unique geological formations (e.g. "Igneous," "Melange," "Landslide"). Other entries like "Residual soils," "Tephra", and "Compacted fill" capture diverse depositional and man-made environments. While based on YP78, the list has been extended to include subcategories (e.g. "Igneous" and "Melange" under "Hills, ranges, and mountains") and New Zealand-specific geomorphology features. Not all original YP78 categories were used, as the overlap of liquefaction susceptibility and the difficulty in distinguishing features based on QMAP descriptions have led to the NLM categorisation not needing all YP78 categories.
epoch	The inferred age of the deposit, based on QMAP data, categorised according to the YP78 epoch system: < 500 years/Modern, Holocene, Pleistocene, or Pre-Pleistocene.
l4_yp	Level 4: The l3_yp classification combined with epoch.
geomorph_liq_susc	The estimated liquefaction susceptibility, derived from the YP78 qualitative system, with values ranging from Very Low, Low, Moderate, High, to Very High.
main_rock	The primary rock type associated with each geomorphology polygon, identified in QMAP and further refined maps.
simple_name	The simplified name provided in QMAP and refined maps, representing the geomorphology type.
description	A brief, one-to-two sentence description provided in QMAP and refined maps, detailing the geology and depositional environment of each geomorphology type.
confidence	A measure of the misclassification uncertainty. The level of confidence assigned by geo-professionals when linking l3_yp classifications to simple_name categories. Values include Low, Medium, and High, indicating the certainty of this correlation.
geometry	Spatial coordinates defining the extent of each polygon or multi-polygon within the model.

The “confidence” attribute is not currently used in later modules of the NLM but has been created to allow misclassification uncertainty to be utilised and reflected in the outputs. Currently misclassification uncertainty manifests itself implicitly in the LVM through the LV geospatial model (Section 8.4), where misclassifications result in wider distributions of LSN. The implicit inclusion means that a local misclassification of a single geomorphology polygon influences the prediction of that whole geomorphology class. Later versions of the LV geospatial model may consider GIs from lower confidence polygons with lower weight in the development of the LSN distributions. However, then the width of distributions for lower confidence polygons should be artificially increased to reflect the misclassification uncertainty. The increase in the width of the distributions is non-trivial in that a misclassification may result in no significant change in LSN if the true classification has a similar liquefaction response to the adopted classification.

6.2 Existing models, previous algorithms

Currently, there is no publicly available geomorphology map that covers the entire land area of New Zealand. While several region-specific geomorphology maps exist for certain regions, they have been prepared on a case-by-case basis and without reference to a consistent methodology or data-schema.

The most comprehensive relevant dataset available is the nationally-consistent geological map series known as QMAP. As detailed in Section 3.2.1, information contained within the QMAP dataset can be used to establish high-level geomorphology classifications across New Zealand. However, it is important to note that GNS Science provides the following disclaimer associated with their QMAP series:

> *"This 1:250,000 map is a regional scale map and should not be used alone for land-use planning, planning or design of engineering projects, earthquake risk assessment, or other work for which detailed site investigations are necessary. Some datasets (e.g. GERM) have been compiled from old or unchecked information of lesser reliability."*

While QMAP is available nationally, on its own, it cannot be used directly for liquefaction assessment purposes. Therefore, the NLM uses QMAP as a starting point for geology data and combines it with refined local maps to yield a national Geomorphology Model.

6.3 Model development

The development of the NLM Geomorphology Model involves a multi-step process that first utilises the QMAP dataset and then integrates local refined maps where available.

The high-level methodology includes:

1 **Development of National Schema**: Create a standardised nationally-consistent geomorphology schema for the purpose of assessing LV (Section 6.1.1).

2 **QMAP Conversion**: Transform the geological data from the latest version of QMAP into the standardised national schema of geomorphology categories as defined by YP78, including attribute mapping of epoch and main rock.

3 **Merging of Local Refined Maps**: Incorporate existing local refined maps and map their attributes to the standardised national schema.

4 **Geometry Refinement and Incorporation of Water Bodies**: Incorporate water bodies into the resulting intermediate output of Steps 2 and 3 to give the final NLM Geomorphology Model.

This approach ensures consistency across different datasets and scales, enabling the use of larger scale geomorphology maps where available. It focuses on making the best use of available data while allowing for future updates as more accurate geomorphology data becomes available.

6.3.1 Model inputs

The primary inputs for the NLM Geomorphology Model are:

1 **QMAP Geological Data:** Provides nationwide geological information that serves as the base layer for geomorphology classification.

2 **Existing Local Geomorphology Maps**: Publicly available maps prepared for specific areas, which are integrated into the model. These have been obtained from GNS and represent the outputs of their more detailed (typically 1:50k) mapping. The current version of the NLM Geomorphology Model includes local refined geomorphology maps for Hawke's Bay, Kapiti Coast, Nelson, and Christchurch.

3 **LINZ Water Bodies**: Publicly available (through LINZ) polygon datasets representing water bodies. Includes lakes, rivers, ponds, canals, and swamps. See Section 3.4.3.

6.3.2 Development of national geomorphology schema

There are several widely used schemas for geomorphology, e.g. the terrain-based categories from Iwahashi & Pike (2007) and the geology-based categories from Ahdi et al. (2017), both of which are primarily used for estimating shear wave velocity. The most widely used categories for LV are those from YP78. The YP78 categories are adopted in numerous US national standards including the American Society of Civil Engineers (2023), and are referenced in the MBIE/MfE Guidance (2017).

Despite the widespread use of YP78, there appear to be no formal definitions of the YP78 classifications either in the original texts from YP78, or in the documents that have adopted the categories. To support the development of conversions from New Zealand maps, a set of definitions were developed and adopted as detailed in Table 6.2.

Not all geomorphology categories from YP78 were used in the NLM Geomorphology Model because there were several similar categories that could not be distinguished based on QMAP descriptions and resulted in the same or similar liquefaction susceptibility class based on YP78. Furthermore, several additional classes were added, particularly to capture the hills, ranges and mountains, which are prominent in QMAP even on land categorised as "flatland" in the Flatland Model.

The classification system is tiered to allow comparison between similar geomorphologies. The tier classes are as follows (with level 1, level 3 and level 4 adopted from YP78):

- **Level 1**: Broad categorisations, including:
  - Continental deposits.
  - Coastal zone deposits.
  - Fill materials.
- **Level 2**: More specific geomorphology classifications mapped at a regional scale (typically 1:25,000 – 1:50,000). This level was determined as an intermediate level between level 1 and 3.
- **Level 3**: Detailed geomorphology classifications.
- **Level 4**: Epoch – Classifies polygons into one of four categories describing geological age:
  - **Modern**: Formed within the last 500 years, often by human activity.
  - **Holocene**: Developed within the last 500 to 11,700 years.
  - **Pleistocene**: Developed between 2.6 million and 11,700 years ago.

– **Pre-Pleistocene**: Formed more than 2.6 million years ago.

Table 6.2: Adopted geomorphology classification definitions

Level 3	Level 2	Level 1	Definition
Estuarine	Coastal lowlands	Coastal zone deposits	Estuaries, where freshwater from rivers meets and mixes with saltwater from the sea. These environments are characterised by tidal fluctuations, sediment deposition, and often support diverse ecosystems.
Beach high wave energy	Coastal lowlands	Coastal zone deposits	Beaches subjected to high wave energy, resulting in well-sorted, coarse sediments like gravel and sand. These beaches typically have steep profiles and strong backwash.
Beach low wave energy	Coastal lowlands	Coastal zone deposits	Beaches experiencing low wave energy, leading to the deposition of finer sediments such as silt and fine sand. These beaches often have gentle slopes and more stable conditions.
Lagoonal	Coastal lowlands	Coastal zone deposits	Lagoons are shallow bodies of water separated from larger bodies of water by barriers such as sandbars, coral reefs, or barrier islands. Lagoonal environments are often characterised by limited wave action and varied salinity.
Foreshore	Coastal lowlands	Coastal zone deposits	The part of the shore lying between the high and low tide lines, which is regularly exposed to tidal action. It is typically a dynamic area of sediment deposition and erosion.
River channel	Alluvial plains and river flats	Continental deposits	The physical confinement of a river or stream, encompassing the bed and banks, through which the river's flow is directed. River channels are shaped by the flow of water and sediment transport.
Floodplain	Alluvial plains and river flats	Continental deposits	Flat or nearly flat land adjacent to a river or stream, which is periodically flooded. Floodplains are formed by sediment deposition during flooding events.
Alluvial fan and plains	Alluvial plains and river flats	Continental deposits	Alluvial fans are cone-shaped deposits of sediment formed where a stream flows out from a steep slope onto a flatter plain. Alluvial plains are extensive, flat regions formed by the lateral coalescence of alluvial fans.
Delta and fan delta	Alluvial plains and river flats	Continental deposits	A delta is a landform formed at the mouth of a river where it deposits sediment as it enters a standing body of water like an ocean or a lake. A fan delta is similar but forms where a river enters a standing body of water at the foot of a mountain range, typically at the exit of a canyon or steep valley.

Level 3	Level 2	Level 1	Definition
Loess	Loess	Continental deposits	Wind-blown silt deposits that form extensive, unstratified, and fertile layers. Loess is often found in regions downwind of glacial or desert areas where fine particles are available.
Colluvium	Hill slope deposits	Continental deposits	Colluvium and landslide deposits.
Talus	Hill slope deposits	Continental deposits	Accumulation of rock debris at the base of cliffs or steep slopes, typically formed by physical weathering processes like frost action.
Glacial till	Glacial deposits	Continental deposits	Unsorted glacial sediment deposited directly by glacial ice. Till consists of a mix of clay, silt, sand, gravel, and boulders.
Tuff	Volcanic deposits	Continental deposits	A type of rock made of volcanic ash ejected from a vent during a volcanic eruption. The ash is subsequently compacted and cemented into a solid mass.
Tephra	Volcanic deposits	Continental deposits	Fragmented material produced by a volcanic eruption, regardless of composition, size, or emplacement mechanism. Tephra includes ash and lapilli.
Igneous	Hills, ranges and mountains	Continental deposits	Landforms created through the cooling and solidification of magma or lava.
Melange	Hills, ranges and mountains	Continental deposits	Landforms that consist of a chaotic mixture of rock types, typically formed in areas of tectonic activity, such as subduction zones. Melanges often contain a jumble of various rock fragments, including oceanic crust, sediments, and other material caught in the complex movement of tectonic plates.
Sedimentary	Hills, ranges and mountains	Continental deposits	Landforms created by the accumulation and compaction of sediments, which are typically particles of rock, minerals, or organic material transported by wind, water, or ice. These rocks are often layered and can contain fossils.
Metamorphic	Hills, ranges and mountains	Continental deposits	Landforms that have been created by high heat, pressure, or chemical processes from an existing rock type (either igneous, sedimentary, or another metamorphic rock). The original structure and composition of the rock are altered, forming new minerals and textures.
Lacustrine and playa	Lacustrine lowlands	Continental deposits	Lacustrine refers to lake environments, often characterised by fine sediment deposition. Playas are dry, flat lake beds found in arid regions, where evaporative processes dominate.
Residual soils	Residual soils	Continental deposits	Soils that form in place through the weathering of underlying bedrock, retaining

Level 3	Level 2	Level 1	Definition
			many characteristics of the parent rock material.
Marine terraces and plains	Marine	Continental deposits	Marine terraces are flat, wave-cut platforms that have been uplifted above sea-level. Marine plains are broad, flat areas adjacent to coastlines, often formed by sediment deposition in marine environments.
Uncompacted fill	Fill	Fill materials	Man-made deposits of soil, rock, or other materials that have not been compacted to increase their density and strength.
Compacted fill	Fill	Fill materials	Man-made deposits that have been mechanically compressed to reduce voids, increase density, and improve stability and load-bearing capacity.

For example, a certain polygon could be classified as:

- **Level 1**: Continental deposits.
- **Level 2**: Alluvial deposits.
- **Level 3**: River channel.
- **Level 4**: Holocene river channel.

Different levels of the schema can be viewed at varying scales, and higher levels (e.g. Level 2 and 3) can easily convert to lower levels (e.g. Level 1) for the purpose of grouping geotechnical information.

The adoption of geomorphology categories based on the YP78 qualitative system, along with a hierarchical classification structure, enables the NLM Geomorphology Model to integrate new and updated New Zealand geological maps. During the development of the NLM Geomorphology Model, GNS released QMAP v4. Thanks to the nationally standardised data schema, updating the model to incorporate data from the new QMAP v4 was a relatively straightforward process, requiring only a simple transformation from the previous QMAP v3 format.

6.3.3 QMAP conversion

The schema adopted for the NLM Geomorphology Model is presented in Section 6.1.1. The transformation from QMAP v4's simple_name to the standard schema was developed collaboratively by geologists and data scientists through detailed desktop study. Geologists applied local knowledge and compared definitions and descriptions to design the transformation, while data scientists employed semantic analysis of QMAP's simple_name against Level 3 categories. This iterative approach continued until both methodologies aligned. The resulting transformation is provided in Digital Supplement B: *simple_name_to_l3_yp.csv*.

The epoch was typically included in the QMAP simple_name and was generally straightforward to map to YP78 categories. In cases where the simple_name specified a broader date range, the most likely YP78 category was selected by identifying the largest overlap between QMAP's minimum and maximum date range and YP78 epochs. The epoch mapping is also included in *simple_name_to_l3_yp.csv*.

6.3.4 Merging of local refined maps

Local geomorphology maps were available for Christchurch, Hawke's Bay, Kapiti Coast, and Nelson. In areas where these local maps existed, they replaced overlapping QMAP data by substituting QMAP polygons with the more detailed local information. Each refined local map contained region-

specific classifications, which geo-professionals mapped to the corresponding adopted NLM geomorphology categories.

Most local maps included sufficient information to assign a geological epoch to each geomorphology classifications. Where epoch information was missing, it was inferred from the underlying QMAP base layer. The only exception was for units designated as compacted or uncompacted fill, which were consistently assigned to the modern epoch. When the "main_rock" field was absent in the local maps, it was similarly derived from the QMAP base layer.

6.3.5 Geometry refinement and incorporation of water bodies

Incorporating water bodies into the NLM Geomorphology Model presented several challenges due to voids that arose when merging the LINZ waterbody dataset (See Section 3.4.3) with the geomorphology dataset. These voids, where no geomorphology classification was assigned (due in part to inaccuracies within both datasets), led to visible gaps in the overall model. To ensure comprehensive coverage within the land area of New Zealand, areas not covered by the LINZ waterbody dataset were filled using a geospatial process.

As illustrated in Figure 6.4, this process involved expanding the boundaries of adjacent geomorphology polygons to encompass any voids. Specifically, each void was absorbed into the nearest, largest geomorphology polygon (based on longest bordering neighbour), thereby preserving alignment with the coastal boundary and promoting a consistent geomorphological representation across all areas.

Nevertheless, it is important to recognise that this approach has certain limitations. In particular, the example shown in Figure 6.4 represents a relatively extreme case intended to demonstrate the process rather than a typical occurrence. In most cases, the method of extending the longest bordering geomorphology polygon provides results that are consistent with the underlying geomorphology data. However, localised anomalies or irregularities in void shapes may not always be fully rectified, due to both dataset inaccuracies and the inherent generalisations of the mapping and merging processes.

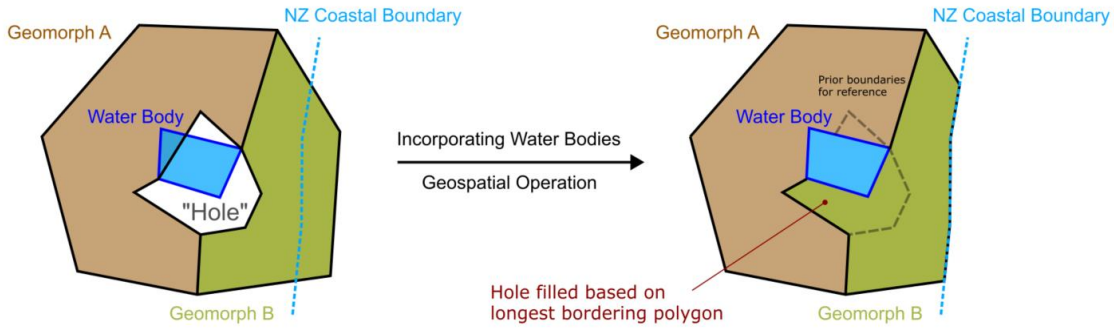

Figure 6.4: Incorporating water bodies into the geomorphology

6.4 Model validations

A series of validation exercises were conducted on the NLM Geomorphology Model which are summarised below. For each region listed in the sections below, a table is included presenting the change matrices which compare QMAP-based classifications with the classifications developed from selected refined local maps. Rows represent the transform from QMAP classifications, while columns represent the classifications from the refined maps. The values in the cells denote the area (in square kilometres) that corresponds to both classifications. The tables use the Level 3 YP78 categories. A legend for these in provided in Table 6.3.

For example, looking at Table 6.4, the value in the row labelled "EST" (Estuarine) and the column labelled "AFP" (Alluvial fan and plains) in is 2.84. This means that an area of 2.84 square kilometres classified as Estuarine in the QMAP model is classified as Alluvial fan and plains in the refined model. Each of these tables includes a "Total" column and row at the end, which represent the sums of the respective columns and rows, providing an overview of the total area for each classification across the compared models.

From the change matrices, there are significant areas that are remapped to different geomorphology classifications. However, most of these re-mappings are to similar geomorphology classifications. While this indicates the uncertainty in the process it also highlights the importance of the refined maps in improving LV estimates and gives confidence in the mapping as most changes were minimal (i.e. the majority of area does not change class).

Table 6.3: Level 3 YP78 abbreviations

Level 3 YP78 Category	Abbreviation
Alluvial fan and plains	AFP
Beach high wave energy	BHE
Beach low wave energy	BLE
Colluvium	CLV
Compacted fill	CFL
Estuarine	EST
Floodplain	FLP
Foreshore	FSH
Glacial till	GLT
Igneous	IGN
Lacustrine and playa	LAP
Landslide	LSD
Loess	LOS
Marine terraces and plains	MTP
Melange	MLG
Metamorphic	MET
River channel	RCH
Sedimentary	SED
Talus	TLS
Tuff	TUF
Uncompacted fill	UFL
Water body	WBY

6.4.1 Christchurch

The majority of Christchurch in QMAP is mapped as River channel, in the refined model this category is significantly split up with nearly a third remapped to alluvial fans and plains, and 48.4 km^2 of Lacustrine and playa, as well as small portions of other classifications. The other significant changes include remapping nearly all the Igneous area to Talus, as well as the majority of Loess and Sedimentary to Talus. The remapping to Talus was determined through the transform from “Undifferentiated hillslope landforms” used in the refined map. The remaining classification had only

minor changes, largely reflecting the more refined polygon boundaries in the higher resolution refined map. As a result of the numerous changes mentioned above, in total, only 39% of the area of the Christchurch refined map remained unchanged compared to the classification of QMAP. A full comparison is summarised in Table 6.4.

Table 6.4: Christchurch refined geomorphology mapping validation

(km²)		Categorisation from local refined maps															
		AFP	BHE	CFL	EST	FLP	FSH	IGN	LAP	LOS	MTP	RCH	SED	TLS	UFL	WBY	Total
Categorisation from QMAP	AFP																
	BHE																
	CFL																
	EST	2.84	2.68	1.22	3.93				2.07	<1		<1		<1		<1	14.6
	FLP			<1	1.04				8.07	2.56		2.45				<1	14.1
	FSH	1.27	67.2	<1	2.77				4.69	1.89	<1	2.31		<1		1.42	82.3
	IGN	5.15	<1	<1	<1				<1	<1		<1		790		<1	797
	LAP	1.57	6.81	<1	2.57				59.1	<1		2.24		<1		<1	74.1
	LOS	9.22	18	1.3	2.55				2.69	93.6		15.3		127		<1	270
	MTP																
	RCH	395	6.54	21.4	12.7				48.4	12.3	<1	867		13.7		<1	1380
	SED	<1		<1						<1	<1	<1		13.9			15
	TLS	<1	<1											12.2			12.3
	UFL	<1		3.62						<1		<1		<1		<1	4.96
	WBY																
	Total	**416**	**102**	**28.3**	**25.6**				**126**	**112**	**<1**	**891**		**958**		**4.36**	**2660**

6.4.2 Hawke's Bay

The Hawke's Bay refined map resulted in only small changes for most classifications (see Table 6.5), reflecting the more refined polygon boundaries. The most significant change was Foreshore being mostly remapped, primarily to Loess, as well as Estuarine, River channel and Sedimentary. In total, 82% of the area of the Hawke's Bay refined map remained unchanged compared to the classification of QMAP.

Table 6.5: Hawke's Bay refined geomorphology mapping validation

(km²)		Categorisation from local refined maps									
		AFP	CLV	EST	FLP	FSH	LOS	RCH	SED	UFL	Total
Categorisation from QMAP	AFP										
	CLV										
	EST			37.6			<1	5.0	<1		43.1
	FLP	<1		<1	<1			3.0	<1		4.03
	FSH	<1	<1	1.1		4.1	10.5	2.5	1.1	<1	15.5
	LOS				<1	4.2	<1		<1		<1
	RCH	12.7	1.6	5.7	<1	<1	1.0	361	60.4	<1	446
	SED	4.65	2.7	<1	<1		<1	12.1	191	<1	213
	UFL						<1			<1	<1
	Total	**17.7**	**4.5**	**45.7**	**<1**	**8.4**	**12.6**	**383**	**253**	**1.0**	**722**

6.4.3 Kapiti Coast

The main changes for Kapiti Coast included Foreshore being remapped, primarily to Marine Terraces and Plains, and about a quarter of River channel being remapped to Alluvial plains. See Table 6.6 for more details. In total, 61% of the area of the Kapiti Coast refined map remained unchanged compared to the classification of QMAP.

Table 6.6: Kapiti Coast refined geomorphology mapping validation

(km²)		Categorisation from local refined maps														
		AFP	CLV	CFL	EST	FLP	FSH	LSD	LOS	MTP	RCH	SED	TLS	UFL	WBY	Total
Categorisation from QMAP	AFP															
	CLV															
	CFL															
	EST															
	FLP															
	FSH	<1		<1		<1			<1	6.61	1.8	<1		<1	<1	10.2
	LSD															
	LOS	2.15	<1	5.13	<1	11.6		<1	61.8	<1	1.26	<1	<<1	7.06	1.55	90.8
	MTP															
	RCH	8.94	<1	<1	<1	1.51		<1	3.56	<1	19.3	1.14	<1	<1	<1	37.8
	SED	<1	<1	<1		<1		<1	<1	<1	<1	10.8	<1	<1	<1	12.4
	TLS	<1						<1			<1	<1				<1
	UFL															
	WBY															
	Total	**11.6**	**<1**	**6.38**	**<1**	**13.6**		**<1**	**66.1**	**7.51**	**22.5**	**12.1**	**<1**	**8.3**	**1.87**	**151**

6.4.4 Nelson

The most significant changes for Nelson were Floodplain remapped to Estuarine, and the small (~3 km²) area of Foreshore remapped to Beach high wave energy and Beach low wave energy. In total, 56% of the area of Nelson refined map remained unchanged compared to the classification of QMAP. See Table 6.7 for more details.

Table 6.7: Nelson refined geomorphology mapping validation

(km²)		Categorisation from local refined maps														
		AFP	BHE	BLE	EST	FLP	FSH	IGN	LSD	LOS	MET	RCH	SED	TLS	UFL	Total
Categorisation from QMAP	AFP															
	BHE															
	BLE															
	EST															
	FLP	<1	<1		3.15				<1				<1			3.35
	FSH	<1	1.21	1.39	<1				<1				<1			3.12
	IGN	<1						<1					9.15			10.2
	LSD															
	LOS	<1		2.86					<1							2.94
	MET	<1									<1		<1			<1
	RCH	29.2		<1	<1			<1	<1		<1		1.57		<1	31.5
	SED	5.18	<1		<1			<1	1.68		<1				<1	84.8
	TLS	<1			<1				1.35				1.52			3.05
	UFL	<1	<1	<1	1.41				<1				<1		1.62	3.43
	Total	**35.6**	**1.25**	**4.52**	**5.04**			**<1**	**3.3**		**<1**		**90.1**		**1.87**	**143**

6.4.5 Validation against existing geomorphology models

A final validation of the NLM Geomorphology Model was done by comparing it to the New Zealand wide geomorphology model from Foster et al., (2019) which uses the categories from Ahdi et al. (2017) and was based off QMAP version 2.

The difference matrix presented in Table 6.8 shows how sample points from a regular grid (with a resolution of 100 metres) are classified by both models. Each row in the table represents a geomorphology classification from Foster's model, while each column represents a level 3 category from the final Geomorphology Model for the NLM. For example, the value in the row labelled "Fan" and the column labelled "RCH" (River Channel) is 722,816, indicating that 722,816 grid points classified as "Fan" in Foster's model are classified as "River Channel" in the NLM's final Geomorphology Model.

A semantic comparison of the mapped terms shows general consistency between the mapping approaches used in the two models and provided confidence in the methodology used to create the NLM Geomorphology Model. Some of the discrepancies between the models is attributed to the difference in QMAP versions, the different definitions of the two geomorphology models and the inclusion of local refined maps in the NLM Geomorphology Model.

Table 6.8: Validation against geomorphology model from Foster et al. (2019)

Categorisation from Foster et al., (2019)	Categorisation from NLM Geomorphology Model (Level 3)														
	EST	FLP	FSH	GLT	IGN	LAP	LOS	MTP	MLG	MET	RCH	SED	TLS	TUF	UFL
Peat		206857	63		40		2				56	45		2	5
Fill		12		10	2		1				10	6			12694
Fluvial estuarine	9295	260	2								25	24121			
Alluvium	605	2853	621	4	437	2	198		2	19	2787258	1257	65	23	159
Lacustrine					14	37000				43	10				
Beach bar dune	4	1470	96841		909	1990	9869				280	12834		39615	5
Fan		5	430	9	72		1472		10	140	722816	97	63	32	
Loess	14	7	42		12		376265				114	45		3	
Outwash			1			3					229403	1			225
Flood gravel						2	2				143151				39
Moraine till		1	3	463271		20				13	9035	28	63001		195
Undiff. sediments & sed. rocks	69453	17117	2864	8474	187		5	53	395037	23	1140	5960162	268870	86857	9
Terrace		1	163522	65	1		5		1		767988	1937			104
Volcanic					8740							50925			
Crystalline		105	683	114	1923421	35	508		35033	3701835	5183	1609	331		105

6.5 Limitations

The NLM Geomorphology Model has several limitations that must be acknowledged.

1 One of the primary limitations is the reliance on the base layer QMAP, a regional scale geological map that may not capture local-scale geomorphology features critical for detailed liquefaction assessment. This coarse-scale resolution means that significant variations can exist in geomorphology classes, which can greatly influence liquefaction susceptibility and therefore may not be adequately represented in the model.

2 The model relies on QMAP (Heron, 2023) in many areas. The limitations on accuracy and disclaimers for QMAP are applicable to the NLM output.

3 The difficulty of defining the boundaries between terrains. This can result in the incorrect categorisation of the land. Where specified, the scale of mapping provides an indication of the accuracy. For some maps, areas where there is more uncertainty associated with the location of the boundary have been identified.

4 Unmapped anthropogenic landform changes. Some anthropogenic landform changes can result in changes to the underlying ground conditions. In some cases, these changes will reduce LV (e.g. ground improvements) and in some cases these changes will increase LV (e.g. reduction of the ground surface elevation resulting in a reduced depth to GW or increasing the ground surface elevation on top of liquefiable deposits adjacent to water bodies).

5 Inconsistency in the existing local refined geomorphology maps available for integration. The variability in quality, format, and scale of these maps poses challenges in terms of integration with the standardised nationally-consistent schema adopted. This inconsistency can lead to gaps or overlaps in geomorphology classifications, potentially affecting the accuracy and reliability of the model outputs.

6 Resource constraints also limit the model's comprehensiveness. Conducting high-resolution geomorphology mapping across the entire country requires significant manual effort and expertise, which may not be feasible for all areas. As a result, many regions may lack the detailed mapping necessary for more precise liquefaction assessments.

7 The dynamic nature of landscapes due to natural processes like erosion, sedimentation, and particularly human activities means that some data may become outdated over time. These dynamic changes necessitate regular updates to the model to maintain its accuracy and relevance.

The NLM Geomorphology Model has been developed for the purpose of assessing LV at a regional scale and has been developed with an emphasis on classifications that are important to liquefaction assessment, therefore it should not be relied upon for other purposes.

6.6 Potential future improvements

To enhance the NLM Geomorphology Model and address its current limitations, several potential future improvements have been identified:

1 **Incorporation of additional local refined maps.** As additional local refined maps become available (e.g. via GNS or TAs), these should be incorporated into the NLM Geomorphology Model since geomorphology categorisation is a significant predictor of LV, as covered in Section 8.

2 **Adopting the standardised nationally-consistent schema.** Standardisation of the local refined maps as some maps do not contain all the standardised attributes (e.g. main_rock).

3 **Specific consideration of pumiceous deposits**. Identify soil containing pumice as an attribute in the geomorphology model. Pumiceous soil is recognised as an important material type for

liquefaction response and identified in the LVM as an important category (see Section 7.8.1). Explicit identification and handling of these areas would improve the accuracy of LVM predictions.

4 Additional cross-validation of the difference between local refined maps and QMAP. Further understand why the differences occur and whether improvements can be made to the refined mapping or QMAP transform.

5 Further evaluate whether all Level 3 categories are needed, the remapping of Foreshore to Beach high wave energy and Low wave energy in Nelson indicates the classes could be combined.

6 Integrate additional geotechnical data into the NLM Geomorphology Model methodology such as GIs, high-resolution remote sensing imagery and updated geological maps to help improve the accuracy of the model. Regular data updates will allow the model to reflect the latest insights into the ground conditions encountered in different geomorphology classifications and their influence on liquefaction susceptibility.

7 Exploring automated mapping techniques. Implementing ML algorithms and GIS automation can expedite the mapping process, reduce manual effort, and handle large datasets more efficiently. Automation can also improve consistency in geomorphology classifications and facilitate rapid updates as new data becomes available.

8 Fostering stakeholder collaboration. Collaboration can significantly enhance the model's development and validation. Engaging with regional councils, territorial authorities, and other stakeholders can provide access to non-public geomorphology data and local expertise. Collaborative efforts can help validate model outputs, ensuring they align with regional observations and meet the needs of those involved in liquefaction risk management. This partnership approach can lead to a more comprehensive and accurate national geomorphology map, ultimately improving the effectiveness of the NLM.

7 Ground investigations module

GIs are used to generate LDMs, which are used for both providing liquefaction predictions at a local scale, and for the development of a liquefaction geospatial model to provide predictions of LDMs across the entire flatland area of New Zealand. LDMs (or manifestation severity index models) provide an index of the expected level of liquefaction-induced ground damage at the ground surface. In this report the LDM used is LSN (van Ballegooy, Malan, et al., 2014). LSN was chosen as it is currently the only supported input for the residential housing loss functions.

The GI module takes GIs (i.e. CPT and BH) as inputs, and outputs the calculated LDMs for those GIs. The values for all LDMs are precomputed at a series of different PGA, Mw and GWDs (GWD). Section 7.1 covers the output data structure, Section 7.2 covers the key development steps, Section 7.3 covers the calculation of the LDMs and Section 7.4 covers the selection of output increments. Sections 7.5, 7.6 and 7.7 respectively discuss the incorporation of CPTs, BHs, and short GIs into the calculation of LDMs. Section 7.8 then compares the LSN values calculated from the GIs. Limitations and potential future improvements are presented in Section 7.9 and Section 7.10.

7.1 Module output

The GI module produces the following outputs:

1 <LDM>-<PL>-<method>-per-GI: LDM for each GI for a range of PGA, Mw and GWD. The <LDM> is the LDM that is stored, <PL> corresponds to the adopted probability of liquefaction used in the triggering process and <method> corresponds to the specific details of the adopted triggering analysis, as outlined in Section 7.3. This is a large data frame which is stored as a parquet file. This file summarised 19,995,850 triggering analyses from 6,986 BH and 57,131 CPT.

2 Coordinates_per_GI: The coordinates of each of the GIs.

The process presented in Section 7.3 is referred to as m1 (or method 1). Recognising that there are many different decisions made to compute the LDM (e.g. triggering method, fines content correction factors etc.) and those decisions are collectively considered as a method. Identifying the method is critical for consistency, in that the geospatial model developed in Section 8.4 is specific to that method. When developing the liquefaction land damage functions in Section 8.7, it should be used with LDMs from GIs determined using the same method.

7.2 Key steps in model development

The key steps in this module are:

1 Develop LDMs from CPT (see Section 7.5).

2 Develop LDMs from BHs by converting BHs into an interpreted CPT profile which is then used to compute LDMs using the same process as the CPT (see Section 7.6).

3 Correct and filter for early depth termination of GIs (see Section 7.7).

7.3 Liquefaction Damage Measures (LDMs)

Liquefaction assessment was performed using a CPT-based liquefaction triggering analysis (Boulanger & Idriss, 2016) with the objective of calculating LDMs to quantify the probability of land damage.

The first step in this analysis was to identify the liquefaction susceptibility of each soil layer. The conventionally adopted criteria of soil behaviour index (Robertson & Wride, 1997), I_c, less than 2.6 was implemented to identify soils expected to behave in a sand-like manner and therefore able to liquefy.

The second step in the analysis was performing liquefaction triggering analyses for soil layers deemed susceptible to liquefaction. This process computed a normalised clean sand equivalent cone tip resistance (q_{c1Ncs}), calculated according to Boulanger & Idriss (2016), where q_{c1Ncs} is a measure of liquefaction resistance for any non-cohesive soil that has been converted to an equivalent clean sand. The q_{c1Ncs} was converted to a cyclic resistance ratio for a magnitude 7.5 event and effective vertical stress of 100 kPa, $CRR_{M7.5,\sigma=100kPa}$, using Equation 1. C_0 is a statistical term which was taken as 2.8 to provide a 50% probability of liquefaction (P_L = 50%), and 2.6 for a 15 % probability of liquefaction (P_L = 15%). At each depth in the CPT, the factor of safety against liquefaction triggering, FOS, was determined using Equation 2. *CSR* is the seismic demand represented as a cyclic stress ratio, *MSF* is an earthquake magnitude scaling factor to adjust the resistance ratio based on the magnitude of the event, and K_σ adjusts the resistance ratio based on the effective vertical stress of the layer.

Equation 1:

$$CRR_{M7.5,\sigma=100kPa} = exp\left[\frac{q_{c1Ncs}}{113} + \left(\frac{q_{c1Ncs}}{1000}\right)^2 - \left(\frac{q_{c1Ncs}}{140}\right)^3 + \left(\frac{q_{c1Ncs}}{137}\right)^4 - C_0\right]$$

Equation 2:

$$FOS = \frac{CRR_{M7.5,\sigma=100kPa}}{CSR} \cdot MSF \cdot K_{sigma}$$

All these parameters are computed using the process in Boulanger & Idriss (2016), with the following key assumptions and decisions:

- Soil below the GW table is fully saturated (i.e. can liquefy), and soil above the GW table is fully unsaturated (i.e. cannot liquefy).
- Unit weight of soil was assumed to be 18 kN/m^3.
- No correction factors were applied for ageing, ground slope, or the consideration of pumiceous material.
- Two probabilities of liquefaction triggering were considered: P_L = 15% and P_L = 50%. P_L = 50% is used throughout the report except for when explicitly stated, since it produces a median estimate. P_L = 15% outputs have also been produced since they are widely used and understood in the engineering profession.
- The correlation between fines content and I_c was applied with the correlation coefficient (error term) C_{FC} = 0 (i.e. default value).The triggering and subsequent calculations for LDMs are computed to a maximum depth of 20 m, or if the GI terminated before this depth, then the LDMs that are computed from the GI are adjusted to approximately account for the unsampled length.

While the above calculations result in a continuous evaluation of liquefaction triggering over the full CPT profile depth, it does not quantify potential effects of liquefaction (e.g. ground movement, ejecta, cracking, etc). The severity of land damage which manifests at the ground surface for a given seismic event can be estimated using one of several CPT-based LDMs that have been developed to estimate LV. This study uses the LSN (van Ballegooy, Malan, et al., 2014) to assess potential land damage caused by liquefaction. LSN is based on the premise that the less dense, the thicker and the shallower the depth of liquefying soils, the greater the expected damage and observed effects of liquefaction at the ground surface. LSN is calculated using Equation 3: where ε_v is the calculated post-liquefaction volumetric reconsolidation strain (based on the Zhang et al. (2002) strain equations), and z is the depth below the ground surface in metres.

Equation 3:

$$LSN = 1000 \int \frac{\varepsilon_v}{z} dz$$

7.4 Increments of seismic demand and Groundwater Depth (GWD)

The following increments were adopted for computing LDMs.

- PGA values (g): [0.05, 0.08, 0.11, 0.13, 0.16, 0.20, 0.27, 0.40, 0.60, 1.0].
- Mw values: [5, 6.5, 7.5, 8, 9].
- GWD values (m): [0.25, 0.5, 1, 1.5, 2.5, 4, 10].

The intention of the selected increments is to cover the expected range where liquefaction-induced damage is of interest while balancing interpolation error versus storage and runtime requirements. The combinations provided result in 350 triggering analyses per GI. The interpolation error for PGA, Mw, and GWD are covered in the following subsections.

7.4.1 Evaluation of error due to interpolation between PGA increments

The interpolation error in LSN due to discrete PGA increments was evaluated for a sample of 100 CPT with a depth of at least 20 m (Figure 7.1). The actual LSN was calculated from PGA = 0.06 g to PGA = 1.0 g in increments of 0.02 g, using GWD = 1.0 m and Mw = 7.5. Interpolated LSN was obtained by calculating LSN at each of the coarse increments outlined in Section 7.4, and linearly interpolating between the increments. The interpolation error is the log of the actual LSN, log(LSN), minus log of the interpolated LSN, log($LSN_{interpolated}$). LSN values below 1 were excluded prior to taking the log.

Negative values on the plot in Figure 7.1 represent an overestimation of interpolated LSN values and positive values represent an underestimation of interpolated LSN values The absolute log error for this example with shallow GWD is typically less than 0.2 and the 15th and 85th percentile are constrained within 0.1, except for between 0.1 and 0.15 g. There is a slight bias whereby for a PGA less than 0.17 g, the interpolated LSN values are overestimated. Conversely, above a PGA of 0.27 g, the interpolated LSN values are underestimated. This bias is geometrically expected (given that LSN vs PGA curves typically have an inflection point at moderate PGA values – see Section 8.4.5 for details) and was considered acceptable with reference to the uncertainty guidance outlined in Section 4.3.1.1.

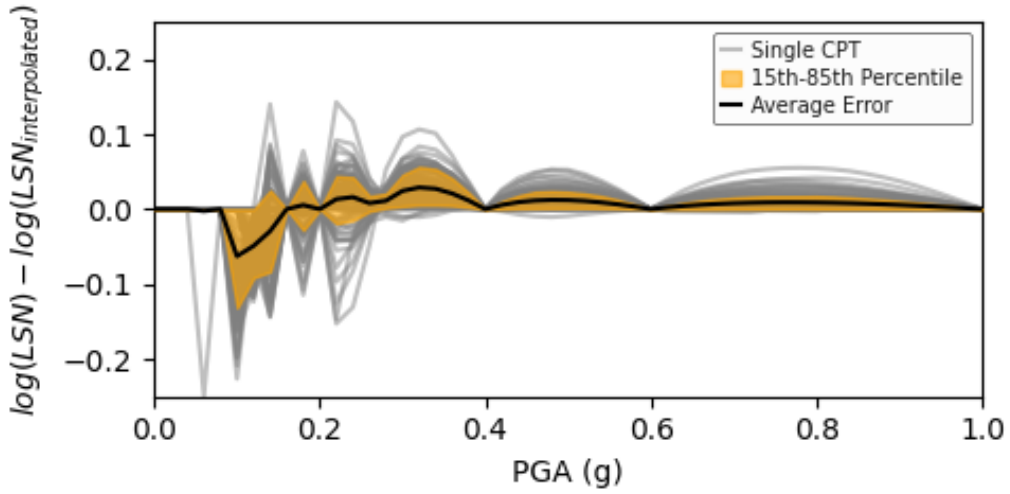

Figure 7.1: Difference in log(LSN) between interpolated and calculated values between PGA of 0.02 and 1 g

7.4.2 Evaluation of error due to interpolation between Mw increments

The interpolation error in LSN due to Mw was calculated in the same manner as for PGA (Section 7.4.1), with fine increments of Mw = 0.25 (Figure 7.2). This was calculated between Mw = 5.0 and Mw = 9.0 using GWD = 1.0 m and PGA = 0.6 g. The 15th and 85th percentile of the absolute log interpolated error in this exercise was less than 0.05 across the full magnitude range, so was considered acceptable with reference to the uncertainty guidance outlined in Section 4.3.1.1.

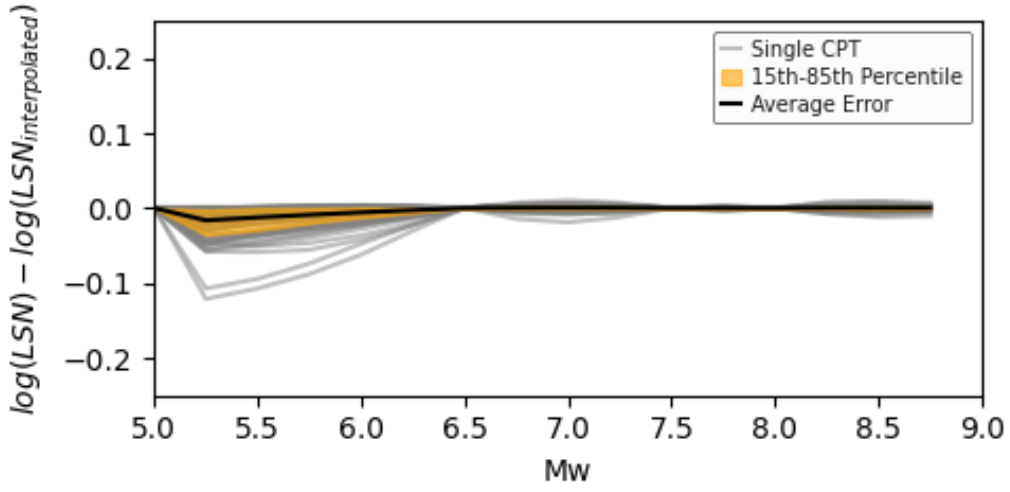

Figure 7.2: Difference in log(LSN) between interpolated and calculated values between Mw 5 and 9

7.4.3 Evaluation of error due to interpolation between GW increments

The interpolation error in LSN due to GWD was calculated in the same manner as for PGA (Section 7.4.1) and Mw (Section 7.4.2), with fine increments of 0.05 m (Figure 7.3). This was calculated between GWD = 0.2 m and GWD = 10 m using Mw = 7.5 and PGA = 0.6 g. The 15th and 85th percentile of the absolute log interpolated error in this exercise was typically less than 0.07, so was considered acceptable with reference to the uncertainty guidance outlined in Section 4.3.1.1. The exception to this is for GWD greater than 4 m; however, in these situations the thick crust is expected to significantly limit surface manifestation of liquefaction-induced damage, so this greater uncertainty is not expected to materially impact the model results. It is noted that the bias for interpolating

between GWDs is always negative because of the inverse proportional relationship between LSN and GWD (see Section 8.4.6).

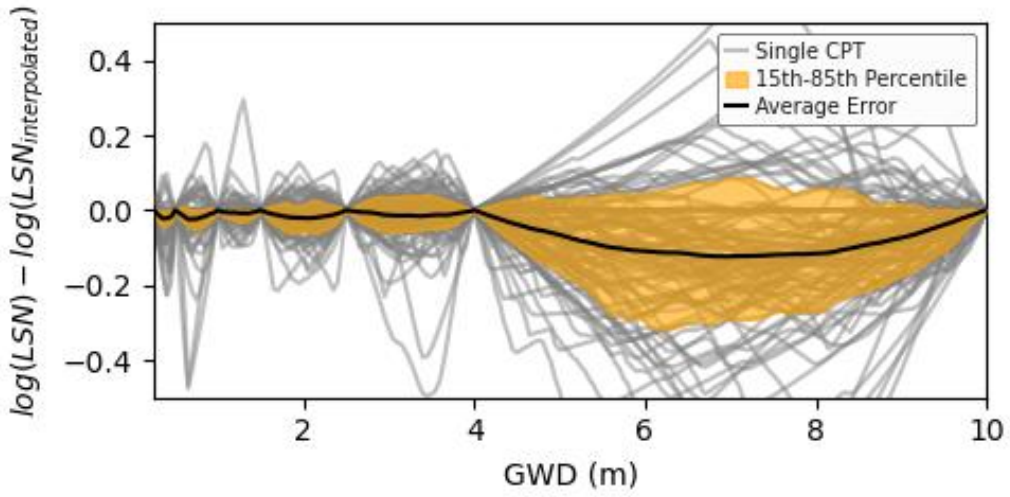

Figure 7.3: Difference in log(LSN) between interpolated and calculated values between GWD 0.2 m and 10 m

7.5 Cone Penetration Tests (CPT)

The CPT method to obtain LDMs consists of three high level steps with details provided in subsequent sections. The conversion of raw CPT data to a standard format is achieved using T+T's internal geotechnical database functions and is not covered in this report. The depth correction for short CPTs is provided in Section 7.7.

7.5.1 Key steps

The key steps for computing LDMs from CPT are:

1 Initial filter of CPTs to identify duplicate CPTs, CPTs with poor metadata and CPT with issues with readings (see Section 7.5.2).

2 Pre-process CPT readings to handle negative sleeve friction (f_s) and q_c values as well as predrill issues. (see Section 7.5.3).

3 Perform triggering analysis to compute LDMs as covered in Section 7.3.

7.5.2 Initial filter of CPTs

The CPT metadata and readings are pre-screened to identify potentially erroneous readings using a set of criteria.

Table 7.1 lists the number of CPT that match each criterion out of a total 61,509 CPTs that have no "known data issues" on the NZGD. Note that each CPT may meet multiple criteria. The total number of excluded CPTs is 4,378 or 7.1% of the total.

Table 7.1: CPT cleansing criteria

Condition	Reason	No. Excluded	% of total
Depth resolution of more than 3 cm	Indication of old readings that may be less reliable.	585	1.0
Less than 5 readings	Insufficient data.	8	0
4 consecutive error codes	Unreliable data.	0	0
Predrill or start depth over 2 m	Predrill obfuscates important near surface data for the purpose of liquefaction assessment.	1,455	2.4
q_c below –200 kPa for more than 0.2 m	Indication of issues with readings. Condition not applied to the predrill length or top 1 m or bottom 1 m of trace due to pre-process correction applied to top and bottom see Section 7.5.3.	191	0.3
f_s below –50 kPa for more than 0.2 m	Indication of issues with readings, generally a dirty CPT[19] cone. Condition not applied to the predrill length or the top 1 m or bottom 1 m of trace due to pre-process correction applied to top and bottom see Section 7.5.3.	192	0.3
Outside New Zealand boundaries	Not applicable.	514	0.8
Duplication	Avoid over-representation of a data point.	2,339	3.8

7.5.2.1 Handling of duplicate CPTs

Duplication errors generally occur in the geotechnical databases due to transcription error, most commonly when a CPT is assigned the wrong location metadata or is duplicated into the database. Another cause is when there are multiple attempts at a CPT at the same location. To identify potential duplication, CPTs that are very close together (< 0.5 m) are examined, and CPTs that have the same readings. Note that post ground improvement CPTs have been removed prior to performing this examination. The examination produces two types of duplication error:

1 Same location – same readings – all but one CPT is removed. Note CPTs are considered to have the same readings if all the readings match to within 0.1 Pa.

2 Same location (all different readings) – the CPT of the longest depth is kept.

7.5.3 Pre-process CPT readings

7.5.3.1 Adjustment of trace for predrill

When a predrill depth is specified in the metadata, the trace values are replaced with q_c = 18.0 MPa and f_s = 10 kPa. The predrill values represent a gravel material (i.e. non-liquefiable properties) since predrilling is either done to avoid services or due to dense gravel at the surface. Additionally, when readings are missing at the top of the trace (e.g. depth readings start at 0.4 m), the top of the CPT trace is extended to the ground surface using the predrill values.

7.5.3.2 Handling negative values at top and bottom of the trace

CPT readings often contain negative skin friction (f_s) and cone tip resistance (q_c) readings at the start and end of a trace due to the offset in depth between the cone tip and the sleeve, as well as

[19] A dirty CPT is a CPT that was performed with a cone that was not properly cleaned prior to the test. This can result in very low sleeve friction (f_s) values (sometimes negative), which usually results in soil appearing more liquefiable.

disturbances near the ground surface. These CPTs do not necessarily indicate a bad reading across the whole trace.

Negative q_c and f_s values were corrected as follows:

- For the top 0.5 m of the trace, readings with negative q_c or f_s are replaced. The replacement values were consistent with the predrill values (q_c = 18.0 MPa and f_s = 10 kPa), since the negative values near the surface generally correspond to a predrill section that was not recorded in the metadata.
- If negative q_c or f_s readings are present in the bottom 1 m of a CPT trace, the CPT is terminated 0.1 m before any negative values occur.
- For negative values that remain in the trace, these were handled during the calculation of LSN:
  - For the calculation of I_c, the negative values were clipped to the range of values provided in the charts by (Robertson, 2009).
  - For the calculation of q_{c1Ncs}, the negative q_c is used directly, however, due to the low q_c value, these layers had I_c>2.6, and therefore were considered non-liquefiable.

7.5.3.3 Adjustment of metadata

When there is no metadata of measured GWL for a given CPT, the median value from the NLM GW Model (see Section 9) is used instead. If no GW value is available (e.g. for a CPT outside the extent of the NLM GW Model), a replacement GWD value of 1.0 m is used.

When there is no metadata for cone tip area ratio, the value is assumed to be 0.8 (as this is typical for many cones used in New Zealand).

7.6 Conversion of Boreholes (BHs) to equivalent CPTs

The BH conversion process uses information from geotechnical BH and, when present, SPT data to develop an equivalent interpreted CPT (equivalent CPT) that allows the calculation of LDMs and the thickness of liquefiable material.

The development of the equivalent CPT follows a series of steps outlined in Section 7.6.2, including the development of several novel relationships. For simplicity of reading, the key steps are presented without the details of how the relationships were developed, and the development of each of the novel relationships are provided in Appendix A. Several comparisons between equivalent CPT from BH and adjacent CPT are presented in Section 7.6.6.

7.6.1 Context

The initial conceptual model development only considered CPT data for determining LDMs. This appeared to bias the model to predict significant LV in non-penetrable ground (since there were no CPT). However, unlike CPTs, BHs have been performed throughout New Zealand in a wider range of soil types than CPTs (including non-penetrable soil). Therefore, the NLM leverages information from BH investigations (i.e. drilling and logging of extracted subsurface soils) and SPT data to supplement the CPT dataset and provide insights into areas with limited or no CPT data. The process converts the BH log and SPT data into an equivalent CPT to be used within the process to calculate LDMs (Section 7.3) and for determining the thickness of liquefiable material for correcting short GI in Section 7.7.

New Zealand practice often logs BH information in accordance with standardised guidelines (NZ Geotechnical Society, 2005) which contain qualitative information regarding soil composition and its in-situ state. The conversion process takes advantage of the BH log descriptions to infer liquefaction resistance through correlations developed based on databases between BH and adjacent CPT and between SPT and BH logs.

7.6.2 Key steps

A schematic illustration of the BH conversion process is shown in Figure 7.4, with the key steps described as follows:

1 **Development of BH database** (see Section 7.6.3). This involved compiling BH files from various sources and pre-screening them.

2 **Development of simplified logs** (see Section 7.6.4). This involved extracting key information for each layer in the BH log (depth interval, *main_material*, *density_status*, *plasticity_status*).

3 **Develop interpreted log and interpreted SPT records** (see Section 7.6.5). This involved defining a q_{c1Ncs} range and percentage of $I_c > 2.6$ per BH layer and SPT layer.

4 **Join interpreted log and SPT records** to develop interpreted profiles. The interpreted profile was developed by preferentially using the interpreted SPT layers, backfilling any gaps with the interpreted log.

5 **Convert to an equivalent CPT**. This involved setting q_{cN1cs} and I_c at 0.1 m depth increments.

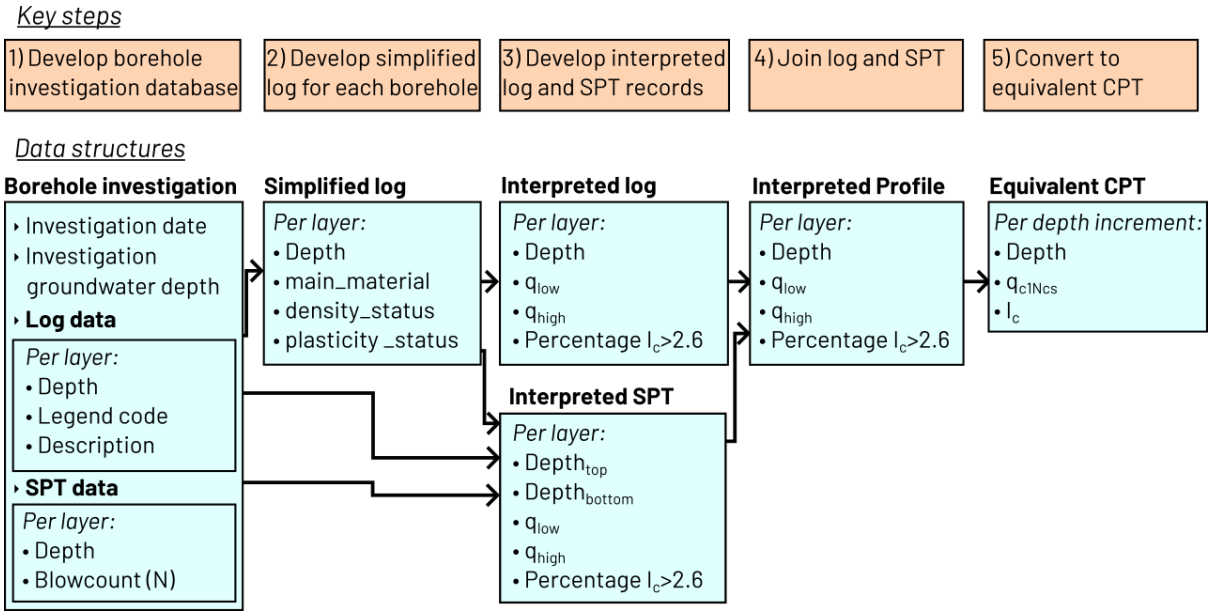

Figure 7.4: Flow chart of the key steps in the BH conversion process

The parameter Percentage $I_c > 2.6$ is used to account for the common practice of describing soil over significant thicknesses (typically 0.2-2 m) that often contain interbedded layers. Some of these layers may not be considered susceptible to liquefaction. While this parameter is derived from the *main_material* description, it's not a direct interpretation. Instead, it's established through correlations with nearby CPT traces.

A key challenge arises because soil descriptions, such as "Silty SAND," often refer to the overall composition of particles rather than distinct interbedded layers of sand and silt. Given that interbedding can occur at a very fine scale (e.g. 0.01 meters), the two meanings—composition and discrete layers—are frequently conflated. For this reason, the *main_material* and *plasticity_status* (both extracted from the soil description) are generally correlated with the percentage of the layer that has a soil with an I_c value greater than 2.6.

7.6.3 Development of BH database

This section outlines the source of the BH investigations and the filtering that was applied to develop the database.

7.6.3.1 Source of data

BH investigations were sourced from TTGD on 22 January 2025 and Aperion from Infinity Studio Logs on 8 August 2024 (Infinity Studio). Most of the data is in AGS4 format. Only 11 PDF-based BHs were manually extracted from PDFs to aid in the development of a CPT-BH database used for developing the novel relationships. The TTGD and Aperion datasets have a high degree of duplication. Out of the 6,689 BHs from the TTGD, 6,517 (97.4 %) were excluded for duplication.

7.6.3.2 Pre-screen BH dataset

The following data cleansing and filtering was applied to the raw data:

1 BHs were only considered if they had a single *.ags* file, the exception being the 11 manually extracted from PDFs which had no *.ags* file. BHs with multiple *.ags* files were removed due to potential for conflicting data.

2 BHs with coordinates outside of New Zealand were removed.

3 BHs taken after ground improvement were removed.

4 Duplicate BHs were removed by selecting a single BH from groups of potential duplicates. BHs were grouped if they are within 0.5 m of one another or if they have identical features. The features which were compared are top depth, bottom depth, number of depth increments and character count. There were many duplicates between the TTGD and Aperion datasets.

5 BHs were removed if they contain one or more layers of greater than 1 m thickness that have unknown material type in the top 20 m. Note that this filter was applied using the simplified log (see Section 7.6.4).

6 BHs were removed if they have any overlapping, missing or non-consecutive depth increments in the log data. These files caused issues with the developed algorithms and were indicative of issues with the data (e.g. data conflicts or incomplete data).

This reduced the dataset from 17,460 BHs to 6,986 BHs.

7.6.4 Development of simplified log

For each BH investigation, a simplified log was developed by converting the legend code and description into the following three simple attributes for each layer in the log:

- *main_material* (see Section 7.6.4.1). This categorises the material into one of 19 categories, which provide high-level information about the likely penetration resistance and plasticity.
- *density_status* (see Section 7.6.4.2). This categorises the layer into four relative soil density states.
- *plasticity_status* (see Section 7.6.4.3). This categorises the layer into three relative soil plasticity states.

7.6.4.1 *Main_material* classification

The *main_material* classification was developed to reduce the number of unique soil descriptions used in BH logs (~150 unique moderately-to-widely used abbreviated descriptions are in the database). The classification aims to provide simple and easily understood categories that reflect different liquefaction susceptibility features (i.e. grouped descriptions should have similar q_{c1Ncs} values and percentage $I_c > 2.6$). For example, one would expect all rock-based descriptors to be

equivalent in terms of liquefaction behaviour, and hence are all recorded as “ROCK” under *main_material*.

Table 7.2 summarises the categories as well as the descriptions and liquefaction susceptibility features.

Table 7.2: *Main_material* categories with descriptions and liquefaction susceptibility features

Main_material Category	General description	Liquefaction susceptibility features
ROCK	Solid or fractured rock	Considered non-liquefiable with very high penetration resistance
COARSE_GRAVEL_TO_BOULDER	The primary material is boulders, cobbles or coarse gravel	Considered non-liquefiable with very high penetration resistance
GRAVEL_WITH_CLAY	Gravel containing clay	High average penetration resistance with low to moderate content of high plasticity soil
GRAVEL_WITH_FINER	Gravel and gravel containing non-claylike finer material (e.g. sand or silt)	High average penetration resistance with no high plasticity soil
GRAVELLY_FILL	Fill material identified as gravelly	High average penetration resistance with no high plasticity soil
SANDY_FILL	Fill material identified as sandy	Moderate average penetration resistance with no high plasticity soil
FILL	Fill material that could not be identified as gravelly, clayey or sandy	A catch-all for unidentified fill
SAND_WITH_COARSER	Sand is the primary material with minor mixtures of material coarser than sand (e.g. gravel)	Moderate average penetration resistance with no high plasticity soil
SAND	Sand	Moderate average penetration resistance with low content of high plasticity soil
SAND_WITH_SILT	Sand is the primary material with minor mixtures of material coarser than sand (e.g. gravel)	Moderate average penetration resistance with low content of high plasticity soil
SILT_WITH_GRANULAR	Silt is the primary material with minor mixture of granular material (e.g. sand or gravel)	Moderate average penetration resistance with low content of high plasticity soil
SILT	Silt	Moderate average penetration resistance with low-to-moderate content of high plasticity soil
SILT_WITH_CLAY	Silt is the primary material with minor mixture of clayey material	Low-to-moderate average penetration resistance with moderate-to-high content of high plasticity soil
SAND_WITH_CLAY	Sand is the primary material with minor mixtures of clayey material	Moderate average penetration resistance with moderate-to-high content of high plasticity soil

Main_material Category	General description	Liquefaction susceptibility features
CLAY	Clay	Considered non-liquefiable with only high plasticity soil
CLAYEY_FILL	Fill material identified as clayey	Considered the same as CLAY
PEAT	Peat	Low-to-moderate average penetration resistance with low-to-moderate content of high plasticity soil
MISSING_UNKNOWN	Unidentified material	
OTHER_NL	Miscellaneous non-liquefiable material	Considered non-liquefiable with low resistance and high plasticity

The mapping of a layer to a main_material category followed the following steps:

1 If the legend code is in the *main_material_lookup* table (provided as Digital Supplement C: *main_material_lookup.csv*), then assign the corresponding main_material. The *main_material_lookup* table was developed by having both geo-professionals and large-language models map the legend codes to the *main_material* descriptions. Numerical legend codes were first converted to their abbreviated description based on the Core-GS conversion and further extended with additional conversions that were inferred by reading the full layer description (which usually provide the abbreviated description). The inferred legend code is also provided in the *main_material_lookup.csv*.

2 If the assigned *main_material* is "MISSING_UNKNOWN", read the description and extract the abbreviated description by identifying the upper-case words in the description (which identify the primary material), then read the preceding lowercase words related to the trace descriptors (e.g. Sandy, Silty). First try to obtain a match to the abbreviated descriptions in the *main_material_lookup* table using the full trace descriptor. If there is no match, then use only the primary material to infer the *main_material*.

3 If the *main_material* is classed as "AS_ABOVE", the *main_material* is taken from the layer above. This often happens when logs only provide a small change in detail at a given depth.

7.6.4.2 Identify *density_status*

To obtain the *density_status* for a BH log layer, a search within the description for a list of expressions associated with the words "density", "relative density", "packing", and "packed" is performed.

The words and assigned *density_status* are provided in Digital supplement D: *density_status_terms.csv.* The classification assigns one of the follow states: LOOSE, MEDIUM_DENSE, DENSE. If these words are not found, then the *density_status* is assigned as "NOT_FOUND". The word mapping was developed as follows:

1 Descriptions that indicate very loose or loose densities or packings (e.g. "loose packing", "loosely packed", "low density") correspond to a "LOOSE" *density_status*.

2 Descriptions that indicate medium density states (e.g. "moderately dense", "intermediate relative density") correspond to a "MEDIUM_DENSE" *density_status*. The same *density_status* is assigned also to expressions associated with tight packings (e.g. "tightly packed").

3 Descriptions that indicate dense states (e.g. "dense", "high relative density") correspond to a "DENSE" *density_status*.

4 For descriptions indicating a range of density states (e.g. “loose to medium dense”), the lowest density state described in this range is adopted.

7.6.4.3 Identify *plasticity_status*

The *plasticity_status* classification assigns one of the follow states: NON_PLASTIC, PLASTIC, NOT_FOUND. Key steps to identify *plasticity_status* are as follows:

1 A search within the material description for the words “plastic” and “plasticity” is performed. If these words are not found, then the *plasticity_status* is assigned as “NOT_FOUND”.

2 Otherwise it checks the preceding word of the first occurrence of “plastic” or “plasticity” and checks for a match in Digital Supplement E: *plasticity_status_terms.csv* which assigns the *plasticity_status*, there is an exception where it first checks the preceding three words and if “to” is the second word, then the three words are converted to a single word for the lookup by replacing “ to “ with “-“, e.g. (“medium to low” becomes “medium-low”).

3 If there is no match in the lookup table, then it is assigned “NOT_FOUND”.

7.6.5 Interpreted BH log and interpret SPT profiles

This step involves determining a suitable range of q_{c1Ncs} values for each BH log and SPT layer, and determining a percentage thickness of the layer that would have soil with $I_c > 2.6$. Note that the range of q_{c1Ncs} values corresponds to the soil that does not have $I_c > 2.6$.

7.6.5.1 Interpreted log

7.6.5.1.1 Range of q_{c1Ncs} values

The range of q_{c1Ncs} values in the interpreted BH log is defined as a uniform distribution between q_{low} and q_{high} from Table 7.3 on the *main_material* and *density_status*. Table 7.3 was developed based on the CPT-BH and CPT-SPT-BH databases covered in Appendix A[20]. In cases where only *density_status* of ALL is provided, then the *density_status* was not used to determine q_{low} and q_{high} and these values were considered representative of all *density_status* categories. Table 7.3 only provides values for *main_materials* that had sufficient data to constrain the estimate of the range of q_{c1Ncs}. In cases where the *main_material* is not listed in Table 7.3, instead of developing material-specific values of q_{low} and q_{high}, which would have greater uncertainty, the values were mapped from another *main_material* (see Table 7.4). The mappings in Table 7.4 were based on a review of the pairs in the CPT-BH and CPT-SPT-BH databases and engineering judgement. As additional data is added to the databases, the *main_material* can then be directly defined.

Table 7.3: q_{c1Ncs} ranges used for equivalent CPTs from BHs

Main_material Category	*density_status*	q_{low}	q_{high}
CLAY	LOOSE	140	140
CLAY	MEDIUM_DENSE	140	140
CLAY	DENSE	140	140
CLAY	NOT_FOUND	140	140
CLAYEY_FILL	LOOSE	124	225
CLAYEY_FILL	MEDIUM_DENSE	164	251

[20] Note that the *density_status* of NOT_FOUND in Table 7.3 corresponds to the q_{low} and q_{high} determined from considered all *density_status* categories (ALL in Appendix A), not from only using data from NOT_FOUND since the ALL category was considered more representative.

Main_material Category	*density_status*	q_{low}	q_{high}
CLAYEY_FILL	DENSE	201	283
CLAYEY_FILL	NOT_FOUND	154	255
COARSE_GRAVEL_TO_BOULDER	LOOSE	144	245
COARSE_GRAVEL_TO_BOULDER	MEDIUM_DENSE	184	271
COARSE_GRAVEL_TO_BOULDER	DENSE	221	303
COARSE_GRAVEL_TO_BOULDER	NOT_FOUND	174	275
FILL	LOOSE	124	225
FILL	MEDIUM_DENSE	164	251
FILL	DENSE	201	283
FILL	NOT_FOUND	154	255
GRAVELLY_FILL	LOOSE	124	225
GRAVELLY_FILL	MEDIUM_DENSE	164	251
GRAVELLY_FILL	DENSE	201	283
GRAVELLY_FILL	NOT_FOUND	154	255
GRAVEL_WITH_CLAY	LOOSE	124	225
GRAVEL_WITH_CLAY	MEDIUM_DENSE	164	251
GRAVEL_WITH_CLAY	DENSE	201	283
GRAVEL_WITH_CLAY	NOT_FOUND	154	255
GRAVEL_WITH_FINER	LOOSE	124	225
GRAVEL_WITH_FINER	MEDIUM_DENSE	164	251
GRAVEL_WITH_FINER	DENSE	201	283
GRAVEL_WITH_FINER	NOT_FOUND	154	255
OTHER_NL	LOOSE	100	100
OTHER_NL	MEDIUM_DENSE	100	100
OTHER_NL	DENSE	100	100
OTHER_NL	NOT_FOUND	100	100
PEAT	LOOSE	76	105
PEAT	MEDIUM_DENSE	76	105
PEAT	DENSE	76	105
PEAT	NOT_FOUND	76	105
ROCK	LOOSE	255	255
ROCK	MEDIUM_DENSE	255	255
ROCK	DENSE	255	255
ROCK	NOT_FOUND	255	255
SAND	LOOSE	89	137
SAND	MEDIUM_DENSE	126	184
SAND	DENSE	176	247
SAND	NOT_FOUND	120	182
SANDY_FILL	LOOSE	117	192
SANDY_FILL	MEDIUM_DENSE	145	228

Main_material Category	*density_status*	q_{low}	q_{high}
SANDY_FILL	DENSE	194	273
SANDY_FILL	NOT_FOUND	128	214
SAND_WITH_CLAY	LOOSE	89	137
SAND_WITH_CLAY	MEDIUM_DENSE	126	184
SAND_WITH_CLAY	DENSE	176	247
SAND_WITH_CLAY	NOT_FOUND	120	182
SAND_WITH_COARSER	LOOSE	117	192
SAND_WITH_COARSER	MEDIUM_DENSE	145	228
SAND_WITH_COARSER	DENSE	194	273
SAND_WITH_COARSER	NOT_FOUND	128	214
SAND_WITH_SILT	LOOSE	109	166
SAND_WITH_SILT	MEDIUM_DENSE	142	197
SAND_WITH_SILT	DENSE	180	227
SAND_WITH_SILT	NOT_FOUND	137	199
SILT	LOOSE	92	130
SILT	MEDIUM_DENSE	92	130
SILT	DENSE	92	130
SILT	NOT_FOUND	92	130
SILT_WITH_CLAY	LOOSE	92	130
SILT_WITH_CLAY	MEDIUM_DENSE	92	130
SILT_WITH_CLAY	DENSE	92	130
SILT_WITH_CLAY	NOT_FOUND	92	130
SILT_WITH_GRANULAR	LOOSE	88	118
SILT_WITH_GRANULAR	MEDIUM_DENSE	112	155
SILT_WITH_GRANULAR	DENSE	172	226
SILT_WITH_GRANULAR	NOT_FOUND	96	139

Table 7.4: *Main_material* mappings for cases with limited CPT-BH comparison data

Main_material Category	Use qlow and qhigh from
SILT_WITH_CLAY	SILT
GRAVEL_WITH_CLAY	GRAVEL_WITH_FINER
COARSE_GRAVEL_TO_BOULDER	GRAVEL_WITH_FINER (however, +20 was added to both q_{low} and q_{high})
FILL	GRAVEL_WITH_FINER
SANDY_FILL	SAND_WITH_COARSER
CLAYEY_FILL	GRAVEL_WITH_FINER
SAND_WITH_CLAY	SAND
GRAVELLY_FILL	GRAVEL_WITH_FINER

The limited data for some less common *main_materials* meant that the q_{c1Ncs} values were derived from similar *main_materials*. An alternative solution would have been to reassign the layers corresponding to these *main_materials* to the similar *main_material* (i.e. have less *main_material* categories, only ones with sufficient data). This approach was not adopted for two reasons:

1 The additional data from the less common categories could unduly influence the distribution of values for the similar *main_material.*

2 The less common and similar *main_material* may have different expected percentage $I_c > 2.6$.

7.6.5.1.2 Percentage $I_c > 2.6$

Like the relationships for q_{c1Ncs}, for each *main_material* and *plasticity_status*, the percentage of the layer with I_c greater than 2.6 is computed from the CPT-BH database and rounded to the nearest 10%. Table 7.5 summarises the map of *main_material* and *plasticity_status* to percentage $I_c > 2.6$. Note that in some cases, the *plasticity_status* does not adjust the percentage. This was because there was insufficient data to quantify the behaviour. Further details on the development of Table 7.5 are provided in Appendix A. Note, that the *plasticity_status* values corresponding to NOT_FOUND in Table 7.5 were determined from all readings without filtering for *plasticity_status*, since these were considered more representative than only using the readings corresponding to NOT_FOUND.

Table 7.5: Adopted percentage of layer with $I_c > 2.6$ for various *main_material* and *plasticity_status* combinations

Main_material Category	*Plasticity_status*		
	NOT_FOUND	NON_PLASTIC	PLASTIC
CLAY	80	60	80
COARSE_GRAVEL_TO_BOULDER	10	10	10
GRAVEL_WITH_CLAY	40	40	40
GRAVEL_WITH_FINER	10	0	30
OTHER_NL	100	100	100
PEAT	90	90	90
ROCK	0	0	0
SAND	10	0	40
SAND_WITH_CLAY	30	30	60
SAND_WITH_COARSER	10	0	10
SAND_WITH_SILT	10	10	40
SILT	70	70	80
SILT_WITH_CLAY	70	70	70
SILT_WITH_GRANULAR	50	50	80
FILL	0	0	0
CLAYEY_FILL	80	60	80
GRAVELLY_FILL	0	0	0
SANDY_FILL	0	0	0

7.6.5.1.3 Handling MISSING_UNKNOWN

For layers in the simple log that were identified as "MISSING_UNKNOWN", the q_{low}, q_{high} and percentage $I_c > 2.6$ were obtained from the average of the properties directly above and below the layer. This approach was adopted because there are some situations where the missing material (e.g. lost core) could be associated with the layer above, some where it could be associated with the layer below, and some where it is a completely different material – so in the absence of evidence to select a particular layer it was considered more appropriate to take a simple average.

7.6.5.2 Interpreted SPT

This section outlines how the range of q_{c1Ncs} values, percentage $I_c > 2.6$ and depth range for each layer of the interpreted SPT are obtained.

7.6.5.2.1 Range of q_{c1Ncs} values

To obtain a range of q_{c1Ncs}, Equation 4 was used (developed in Appendix A). It converts normalised corrected SPT blow count, $(N_1)_{60}$ to lower, q_{low}, and upper, q_{high}, estimate of q_{c1Ncs}. In Equation 4, q_{offset} is 70 for all *main_materials* that contain the word "silt", and 55 for all other materials. The different value for silty *main_materials* is for the clean sand correction that is applied in BI2014 (these details are provided in Appendix A).

Equation 4:

$$q_{low} = q_{offset} + 3 \cdot (N_1)_{60} \text{ and } q_{high} = q_{offset} + 5 \cdot (N_1)_{60}$$

To apply the correlation, the following steps are applied:

1 Compute the effective vertical overburden pressure, σ'_v, where the GWD is taken as the investigation GWD, where available. When not available, the median GWD from the NLM GW Model (see Section 9) is taken instead. The dry and buoyant unit weights are taken as 17 kN/m3 and 9 kN/m3 respectively.

2 Convert the SPT blow count, N, to (N1)60 using Equation 5. The overburden correction ratio, CN, is computed using Equation 6 from Robertson & Wride (1997), with Pa being the atmospheric pressure. The energy correction ratio CE is taken as 1.0 for SPTs performed before 2012 and 1.33 for SPTs performed after 2012 (based on energy efficiency ratios of 60% and 80% respectively). This is to reflect the change in SPT hammer equipment typically used in New Zealand because of the uplift in drilling activity and hammer calibration requirements following the Canterbury Earthquakes. The assumed hammer efficiencies are based on SPT hammer calibration testing undertaken by T+T across New Zealand over the past 20 years.

3 Obtain q_{low} and q_{high} from Equation 4.

Equation 5:

$$(N_1)_{60} = C_N \cdot C_E \cdot N$$

Equation 6:

$$C_N = \left(\frac{P_a}{\sigma'_v}\right)^{0.5}$$

Note that blow counts of 0 were taken as 'null' and not used. 3.5% of SPT blow counts were recorded as 0. Inspection of these in relation to the log description at the same depth suggested there were many cases where 0 corresponded to no SPT being performed (e.g. the layer abbreviated description is basalt). There were also quite a few that described the soil as very loose, or as soft clay. The decision to ignore readings of 0 was based on this producing the least error, in that the *main_material* and *density_status* would still result in a reasonable estimate of q_{low} and q_{high} for situations where the soil was soft/loose. However, assigning q_{low} and q_{high} from $(N_1)_{60}$ = 0 for a rock layer results in a major misrepresentation. Further analysis of the descriptions could be applied in the future to ascertain whether 0 or 'null' should be used on a layer-by-layer basis, similar to the judgement applied by an engineer.

7.6.5.2.2 Percentage I_c > 2.6

The percentage I_c > 2.6 was obtained from the interpreted BH log (see Section 7.6.5.1) at the depth corresponding to the SPT layer.

7.6.5.2.3 Depth range

The depth range for each SPT reading is applied at most 0.5 m before the depth of the reading and 1.0 m after the depth of the reading. However, if the *main_material* changes across this depth range, the thickness is truncated to this depth. This is illustrated in Figure 7.5. Note that the

interpreted SPT layers take precedence over the interpreted BH log layers, so this step establishes when to use the interpreted SPT and every depth where there is no interpreted SPT layer the Interpreted BH log layers are used.

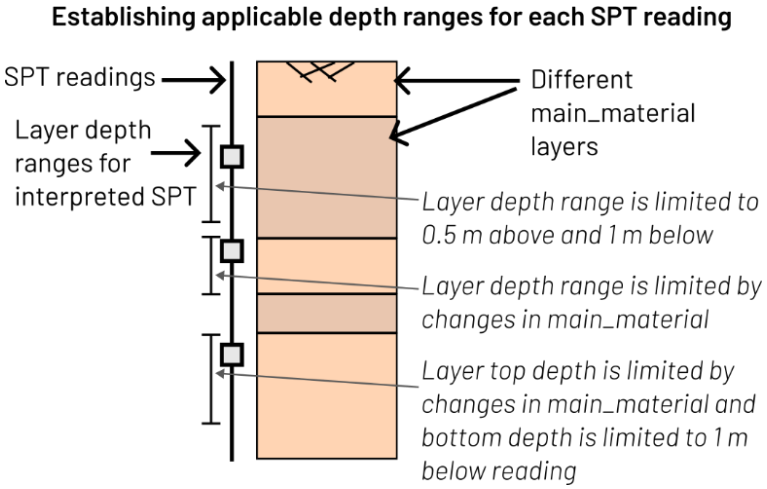

Figure 7.5: Schematic example of assigning layer depths for interpreted SPT

7.6.5.3 Conversion to equivalent CPT

Each interpreted profile is converted to an equivalent CPT using the following steps:

1 The entire profile is discretised into 0.1 m slices and a q_{low}, q_{high}, and percentage $I_c > 2.6$ are assigned at each depth based on the interpreted profile.

2 Layers are then determined at any change in any q_{low}, q_{high}, and percentage $I_c > 2.6$

3 For each layer:

- The total number of slices, n, in each layer is determined and the slices are numbered from 1 to n from the middle. The upper slice is numbered first if two slices are equidistant from the middle.
- The number of slices that should have $I_c > 2.6$, is determined based on the total number of slices and the percentage $I_c > 2.6$ (rounded to the nearest integer). The slices, from 1 to number of slices that should have $I_c > 2.6$, are set to $I_c = 3.0$ and $q_{c1Ncs} = q_{low}$
- The remaining slices are then assigned q_{c1Ncs} values in order at equal increments from q_{low} to q_{high}. I_c is arbitrarily assigned 1.8 (though it is not used in any further calculations).

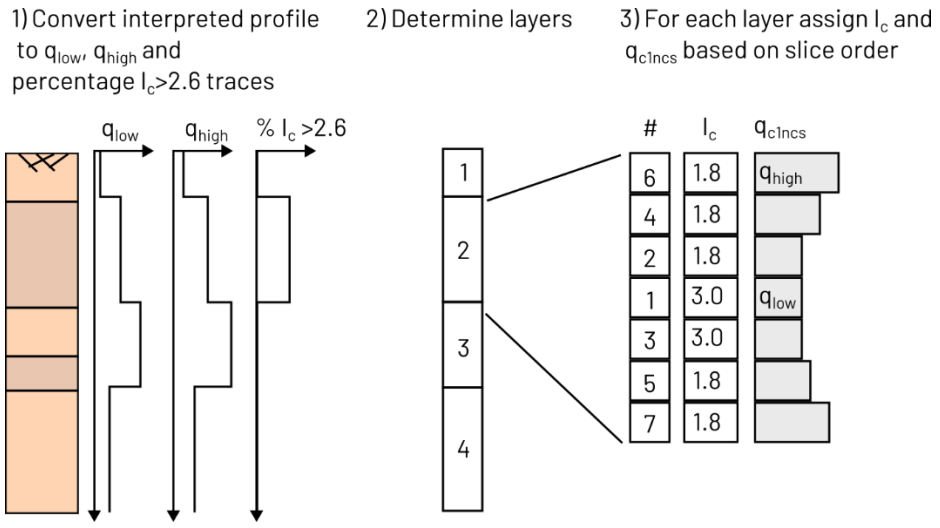

Figure 7.6: Process to develop an equivalent CPT from an interpreted BH profile

The use of equal increments from q_{low} to q_{high} (i.e. a uniform distribution) and the choice of numbering from the middle to have weakest soil in the centre of the layer was primarily to have a simple, repeatable and non-biased approach. An alternative, using a normal or lognormal distribution with values randomly selected may better represent the range and distribution of the q_{c1Ncs} values from the databases in Appendix A, but would lose repeatability and be hard to visually validate implementation.

7.6.6 Example equivalent CPT traces compared to adjacent CPT traces

Three BH-CPT pairs are compared in Figure 7.7 to Figure 7.9 to demonstrate the BH conversion process. The red line shows q_{c1Ncs} values that were derived from SPT, and the blue lines shows values inferred from the BH log. The LSN was computed for PGA = 0.6 g, Mw = 7.5, and GWD = 1 m. The comparison of all BH-CPT pairs from the NZGD have been included as Digital Supplement F: - *BH-CPT-comparisons*.

The comparison in Figure 7.7 shows that the BH generally has higher percentage I_c > 2.6, and for most of the profile provides reasonably similar estimates of q_{c1Ncs} compared to the adjacent CPT. The notable exception is from 3-7 m where low SPT values result in significantly lower q_{c1Ncs} values (100-160) compared to the CPT (160-250). This difference only results in minor differences in LSN across the full trace.

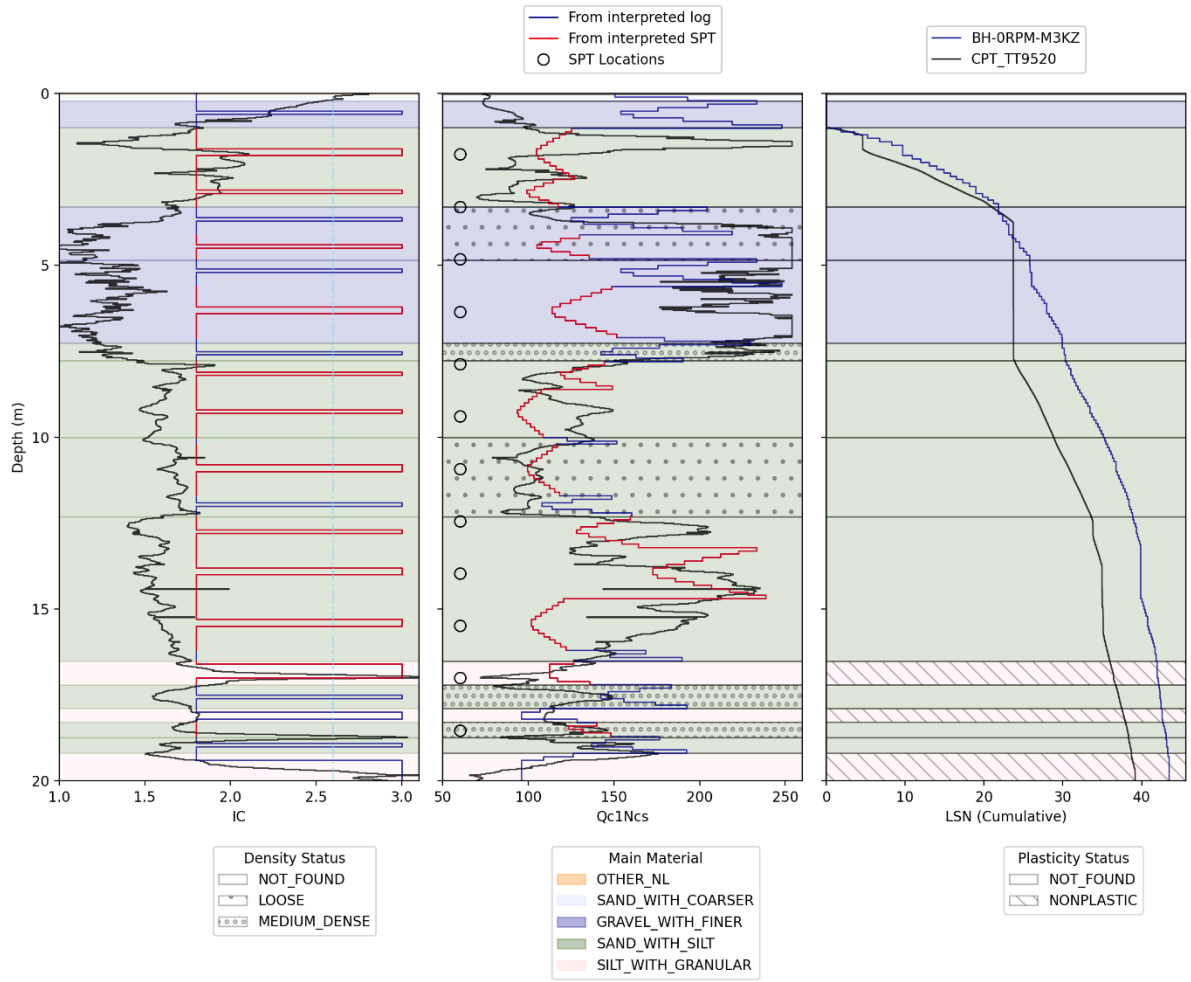

Figure 7.7: Comparison between a BH (shaded background), equivalent CPT (blue line for BH log-derived and red line for SPT-derived), and a CPT (black line) from within 10 m of each other

Figure 7.8 shows the q_{c1Ncs} trace is reasonably similar between the BH and CPT across the whole profile, however, the BH has more $I_c > 2.6$. This results in substantially lower LSN of 31 versus 50.

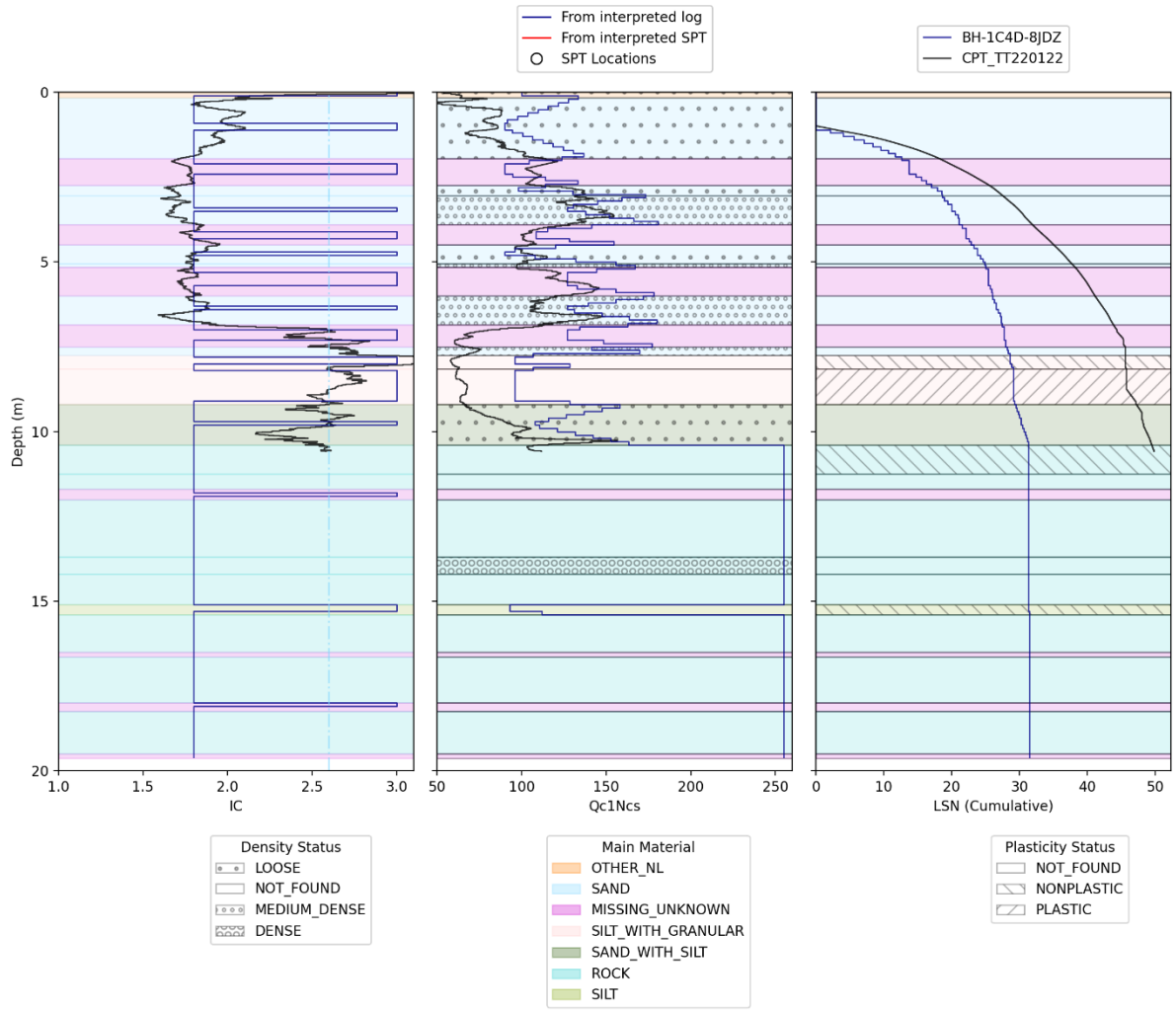

Figure 7.8: Comparison between a BH (shaded background), equivalent CPT (blue line for BH log-derived and red line for SPT-derived), and a CPT (black line) from within 10 m of each other

Figure 7.9 shows the percentage $I_c > 2.6$ is reasonably similar between the CPT and BH. There are some notable differences in q_{c1Ncs} profile where the high q_{c1Ncs} values at 7-8.5 m in the CPT potentially correspond to the high q_{c1Ncs} values at 8.5-10 m in the BH. The high q_{c1Ncs} values at 15-18 m in the CPT appear to be thinner in the BH. Overall, the LSN values are different, 35 for the BH and 45 for the CPT.

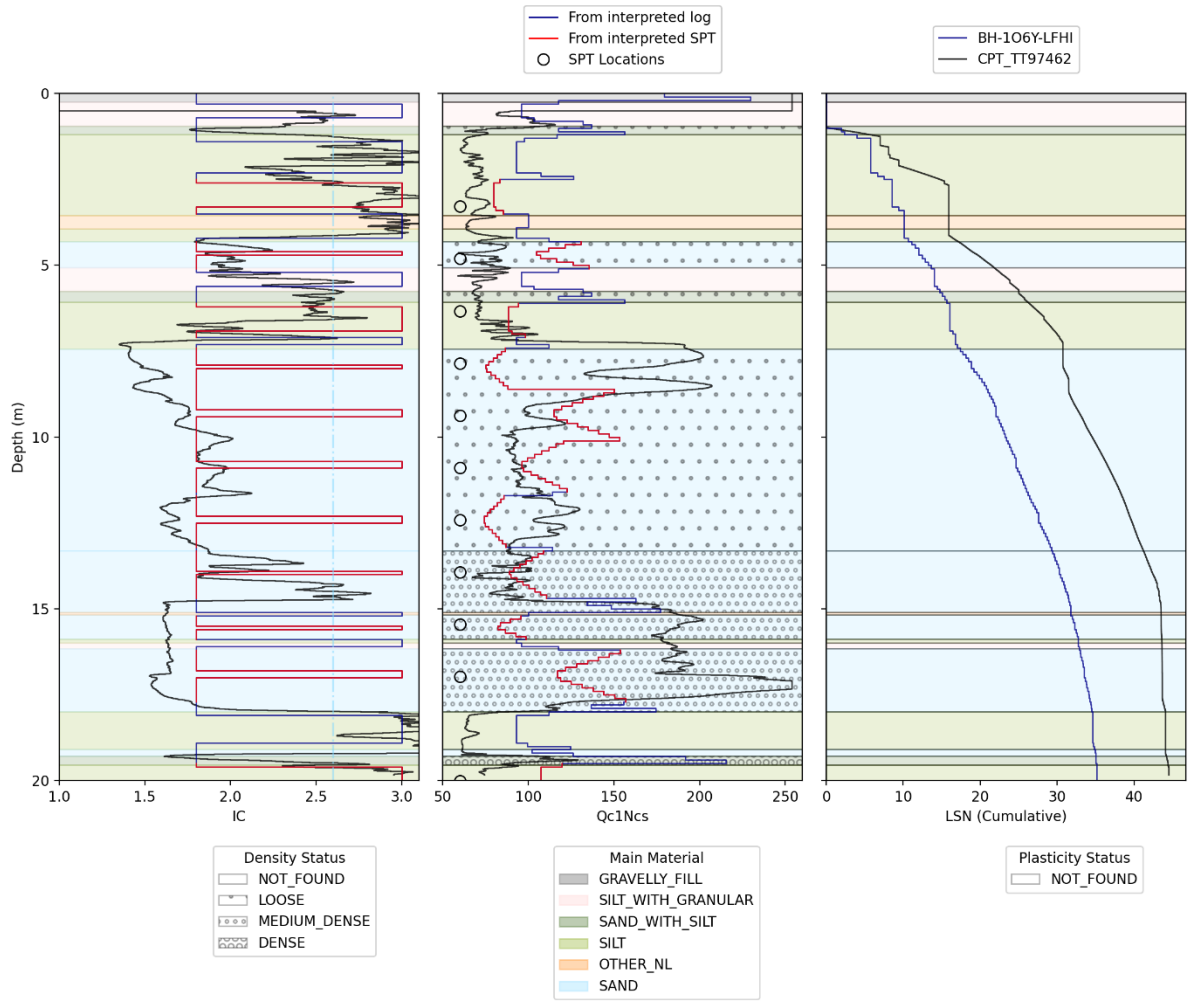

Figure 7.9: Comparison between a BH (shaded background), equivalent CPT (blue line for BH log-derived and red line for SPT-derived), and a CPT (black line) from within 10 m of each other

7.7 Correction of short GIs

Short GIs are GIs that terminate before the maximum calculation depth for LSN. For the purpose of this model, the maximum calculation depth is 20 m. CPTs are often terminated due to hitting a denser sand or gravel layer, or terminated since the investigation reached its target depth. Rather than excluding these GIs from the liquefaction assessment, a correction process is applied to make use of the valuable near-surface data available from short GIs. This methodology is presented in the sections below along with an example of the application in Section 7.7.8.

7.7.1 Context

Many GIs terminate before the maximum calculation depth for LSN (in this case 20 m). Excluding short CPTs can result in over-prediction of liquefaction in a given area, since many GIs are terminated because they have sampled sufficient competent material or hit a thick layer of dense material. These GIs would typically have lower than average LSN values due to the presence of non-liquefiable material. However, directly including these CPTs without a depth correction can result in an under-prediction if there are liquefiable soils present beneath the layer on which the CPT refused, or if the CPT was terminated at a target depth while still within liquefiable material.

The correction process makes an adjustment based on many different data sources and therefore appears to be quite complex, however, it has been designed to automate the general steps that an

engineer may apply when handling a single short GI at a site. Specifically, the correction is informed by the geomorphology, nearby GIs, the termination depth, the termination conditions, LSN and the thickness of liquefiable material calculated from the short GI, and two databases that provide insights into how LSN changes with depth and thickness of liquefiable material in the trace. The process was also validated using CPT that were full length (i.e. 20 m) to quantify the expected error from the correction.

In previous studies (e.g. Tonkin + Taylor, 2015), the short CPT problem was handled by splicing LSN contributions from nearby CPT records (i.e. for a given location, take the average of the LSN contributions of all nearby CPT at depth increments, such that if a CPT had a short termination depth it would stop contributing to the average LSN). Geyin & Maurer (2020) addressed the short CPT problem by excluding CPT based on Anselin Local Moran's analysis (Anselin, 1995). The process excluded the CPT if, based on the trace, it was deemed that the CPT was terminated prematurely. These previous approaches were applied for obtaining a best estimate at a specific location and where there was a high density of CPTs (i.e. applied to the Christchurch dataset).

The approach for handling short GIs in the NLM needs to be applicable also when data is scarce. If data is scarce, then the exclusion of short GIs should be avoided as the little data that they do provide is very informative. To overcome the limitations of previous approaches and reduce the bias, the two methods mentioned above have been used in conjunction with the national GI dataset and Geomorphology Model to correct most short GIs and only exclude a subset. To make use of both nearby CPT and BHs, and general trends from geomorphology, the process corrects short CPT based on an estimation of missing thickness of liquefiable soil.

7.7.2 Key steps

Only GIs that had termination depths less than 15 m were considered short, GIs that were greater than or equal to 15 m in length were used unadjusted. This approach was adopted because the bottom 5 m typically makes only a relatively small contribution to the calculated LSN value. Overall, 16,460 CPTs (28.8 %) and 1,498 BHs (21.44 %) were adjusted. The key steps (as shown in Figure 7.10) are:

1 Determine the termination conditions of CPTs and BHs (Section 7.7.3).

2 Compute the thickness of liquefiable material from CPTs and BHs (Section 7.7.4).

3 Determine the range of expected missing thickness of liquefiable material based on geomorphology, nearby GIs and the computed thickness in the trace up to the termination depth (see Section 7.7.5).

4 Determine the depth adjusted LSN based on the expected missing thickness of liquefiable material, the LSN in the trace for GWD = 1.0 m, the termination depth, and the current GWD (see Section 7.7.6).

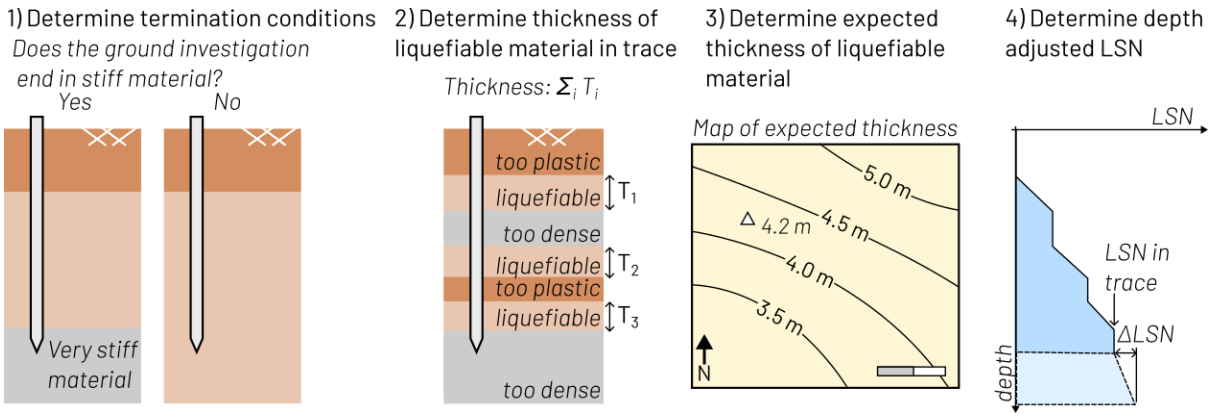

Figure 7.10: Key steps for correction of short GIs

Note, "trace" refers to the recordings per depth in the GI. It is referred to in this section to be specific to the unadjusted values for the thickness of liquefiable material and LSN.

The correction process is specific to the LDM and the maximum calculation depth of the LDM. The process outlined here is for LSN computed to 20 m and uses several unique relationships that have been developed for that purpose. As an example, the calculation of thickness of liquefiable material is only to a depth of 15 m even though the calculation of LSN is to 20 m. This difference is because LSN has a strong depth weighting factor such that deeper depths have a very minor contribution to LSN. Evaluating the thickness of liquefiable material to only 15 m means that this metric captures the most influential liquefiable material for the LSN calculation. Different maximum depths and different LDM may require a different definition of thickness of liquefiable material.

7.7.3 Determine the termination conditions

7.7.3.1 CPT

If the end of the CPT trace contains high cone tip resistance (q_c), then this is an indicator that the CPT was terminated due to hitting a dense layer. The expected increase in LSN beyond this depth is less than for a CPT that terminates at the same depth but without high cone tip resistance, since there is a higher chance of high q_{c1Ncs} beyond the termination depth. The condition, referred to as term_high_q, is a Boolean variable. If the median q_{c1Ncs} >= 200 in the last 0.3 m of the trace, then term_high_q is true. This classification determines the extent and suitability of the depth correction applied (i.e. if term_high_q is false, a larger correction is applied).

7.7.3.2 BH

For BHs, the term_high_q condition was always taken as false (because BHs can typically drill through even very dense/strong material).

An additional criterion was set to identify substantial competent material at the end of the trace that did not require adjustment. These BH were identified as BHs that are 7 m or longer and where q_{c1Ncs} >= 170 for the last 2 m of the equivalent CPT trace. If the BH satisfy the criteria, they were considered full length and do not have any adjustments applied.

7.7.4 Compute thickness of liquefiable material

The definition of thickness of liquefiable soil, $T_{liq1-15}$, in this context is defined as:

- Soil between 1-15 m depth;
- I_c < 2.6; and
- q_{c1Ncs} < 130.

The criteria were ultimately selected because this definition of thickness of liquefiable soil strongly correlates to LSN for GWD = 1.0 m and high seismicity. Specifically, the start depth of 1 m was selected because near surface material can be poorly characterised by CPT. The depth end of 15 m was selected because the lower depths have limited influence on calculated LSN, and setting this deeper would reduce the number of deep GIs available to calibrate the correction. Note that liquefaction can occur under strong shaking for q_{c1Ncs}>130, so this is not a true definition of liquefiable material, but this threshold provided the best correlation to LSN.

$T_{liq1-15}$ was computed for all GI and referred to as $T_{liq1-15,trace}$, where the $T_{liq1-15,trace}$ for BHs was computed from the equivalent CPT traces. When the termination depth was less than 15 m, $T_{liq1-15,trace}$ was computed to the termination depth.

7.7.5 Determine range of expected thickness of liquefiable material

The range of expected thickness of liquefiable material for a GI was determined from a map of the expected thickness (Section 7.7.5.1) and standard deviation of the expected thickness, then adjusted based on the termination depth and the thickness of liquefiable material in the trace (Section 7.7.5.2). An additional filter to remove GI from the NLM database was then applied to exclude GI that would have a very uncertain correction based on the upper estimate of $T_{liq1-15}$ (see Section 7.7.5.3).

7.7.5.1 Determine map of expected thickness of liquefiable material

A map of the estimated thickness of liquefiable material, $T_{liq1-15,est}$, was created by considering each l4_yp geomorphology class (see Section 6.1.1) separately and applying the following steps. For each l4_yp geomorphology class:

1 Determine the mean $T_{liq1-15}$ from all GIs within the l4_yp polygons that have termination depths of 15 m or more. If the GI is a BH, include it if:
   - The BH has a continuous 2 m or greater thickness of material in the base of the trace that has equivalent q_{c1Ncs} >= 170; and
   - The termination depth exceeds 7 m.
2 Compute the residual for each GI versus the mean for the appropriate l4_yp.
3 Krig the residuals into a prediction grid of points at a 100 m resolution for each l4_yp layer, using a partial sill of 2, nugget of 0.2 and range of 2000 m with the PyKrige Python package.
4 Add the mean values to the residuals at each point to obtain $T_{liq1-15,est}$ at each point and the uncertainty in $T_{liq1-15,est}$
5 Determine the standard deviation at each residual point from the variance in the kriged output.

7.7.5.2 Adjust estimated thickness of liquefiable material using trace

This step adjusts $T_{liq1-15,est}$ if the ratio of $T_{liq1-15,trace}/T_{liq1-15,est}$ is outside expected ranges for the termination depth (e.g. if $T_{liq1-15,trace} > T_{liq1-15,est}$ this is clearly not a realistic estimate). The likely bounds were the 10th and 90th percentiles of the databases discussed in Section 7.7.7, and shown in Figure 7.11 (a) and (b) for when *term_high_q* is true and false respectively. Note, for BHs, the term_high_q condition was always taken as false. Even though the kriging could often provide reasonable $T_{liq1-15,est}$, this correction was necessary since sometimes there were no nearby GIs for

the kriging, and the use of more information (i.e. the $T_{liq1-15,trace}$) was deemed to improve estimates.

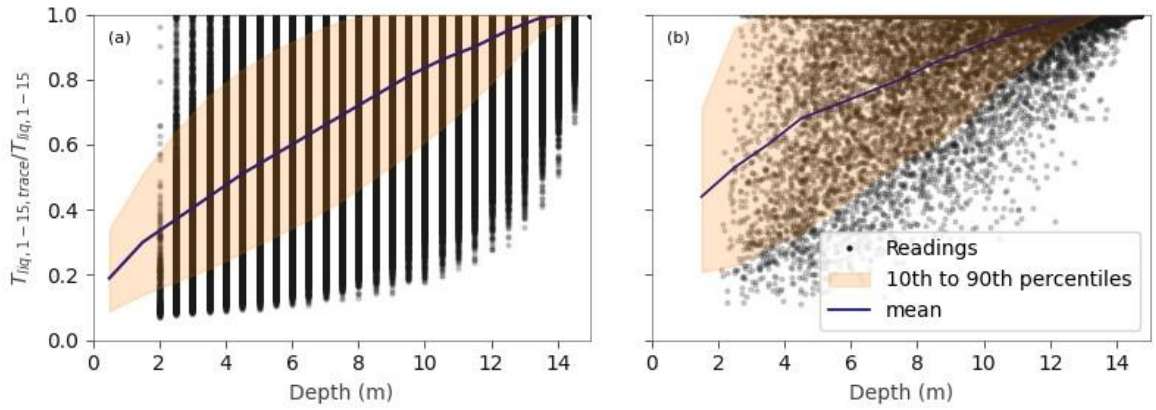

Figure 7.11: Percentile bounds of ratio of T_{liq} versus depth for (a) term_high_q is true, and (b) term_high_q is false

If $T_{liq1-15,trace}/T_{liq1-15,est}$ falls outside the likely bounds for the given termination depth, then the expected $T_{liq1-15}$ is adjusted such that the ratio is on the edge of the bounds. This adjustment is applied to reflect that the short CPT is a good indication of the likely total $T_{liq1-15}$, especially in cases where the expected $T_{liq1-15}$ is poorly constrained in the kriged output. The adjustment is applied to both the mean expected $T_{liq1-15}$ and an upper estimate.

7.7.5.3 Remove short GI with high uncertainty in the depth correction

Three additional filters were applied to the GI database to reduce the extrapolation error from the depth adjustment. Short GIs that met any of the following criteria were removed from the database:

1 $T_{liq1-15,trace}$ is less than 1 m.

2 The ratio of $T_{liq1-15,trace}$ divided by the upper estimate of $T_{liq1-15}$ is less than 0.4 when term_high_q is true or 0.5 when term_high_q is false.

3 The termination depth is less than 6 m and term_high_q is false.

These limits were developed by evaluating long GIs and artificially truncating the record then estimating the LSN and comparing it to the true LSN. Specifically, Figure 7.12 shows the error from applying the short GI correction to every entry in the termination condition databases (Section 7.7.9), after removing entries that met any of the criteria above. The extrapolation error is quantified as the true LSN (total LSN in the databases) minus the predicted LSN in log space, $\log(LSN)_{true} - \log(LSN)_{pred}$. Figure 7.12(a) shows that when term_high_q is true, this results in a log(LSN) extrapolation error of +0.05 and -0.2 for the 15th and 85th percentiles at LSN values less than 10 and decreases to approximately +/- 0.05 at LSN values greater than 40. Figure 7.12(b) shows the resulting error from the term_high_q is false database, where the trend and magnitude of error is similar to the term_high_q is true results. The error appears to be slightly biased (see mean line), with low LSN being overpredicted on average by ~0.04 and a similar magnitude of underprediction for LSN values greater than 60. Note, LSN was computed with PGA = 0.6 g, Mw = 7.5, GWD = 1.0 m. Noting that this analysis was performed with the exact $T_{liq1-15}$, not an estimate, therefore the filter uses the upper estimate of $T_{liq1-15}$. Overall, the error fulfils the uncertainty and bias guidance in Section 4.3.1.1, however, the uncertainty is slightly higher than the 0.17 guidance value for some LSN ranges.

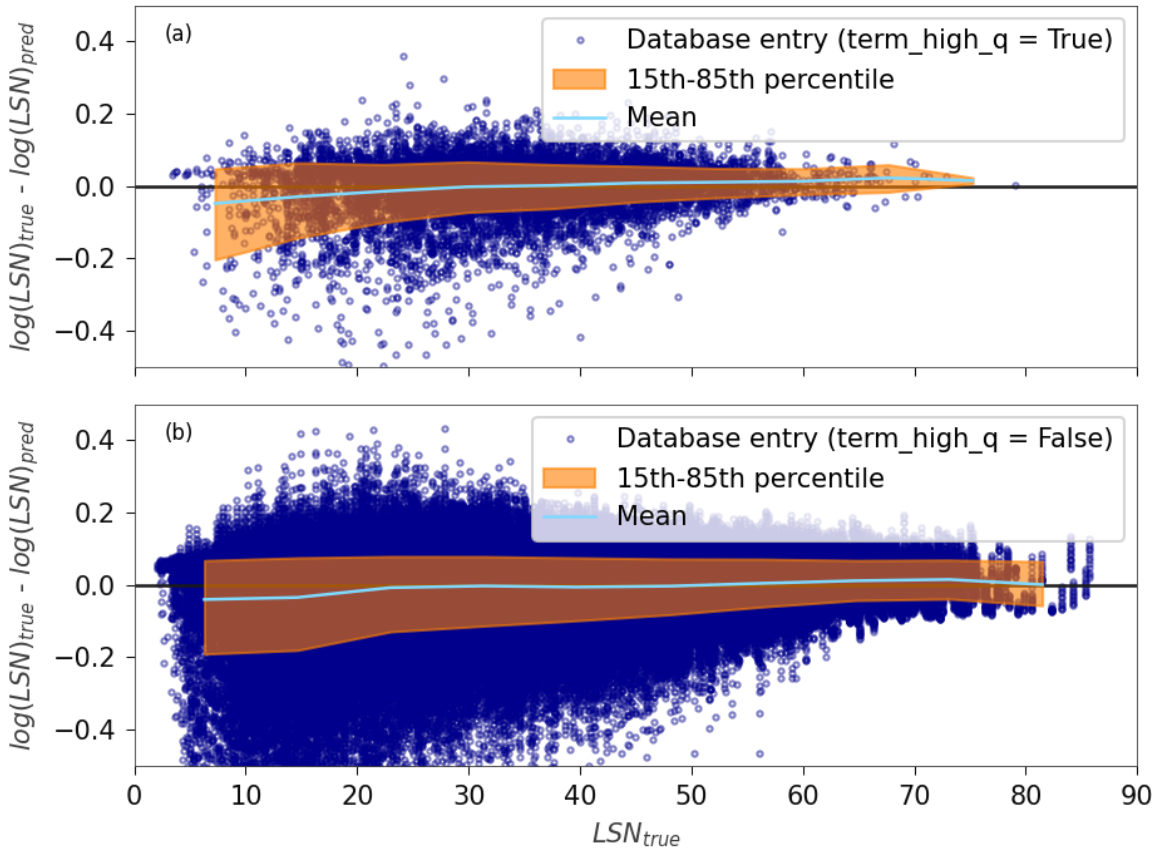

Figure 7.12: Error from short GI correction for (a) term_high_q is true and (b) term_high_q is false, using the termination condition databases for PGA = 0.6 g, Mw = 7.5, GWD = 1.0 m

7.7.6 Determine depth adjusted LSN

The depth-adjusted LSN is determined using the following steps outlined in Figure 7.13:

1 Determine the expected fraction of missing LSN (see Section 7.7.6.1).

2 Determine the missing LSN for a GWD of 1 m (see Section 7.7.6.2).

3 Determine missing LSN for all GWDs and adjust LSN accordingly (see Section 7.7.6.3).

Steps 2 and 3 address a challenge for deep GW, in that scaling up LSN that was calculated with different GWDs using some ratio that is based only on the termination depth and $T_{liq,1-15,trace}$ would result in different additional LSN. Whereas the additional LSN (provided it is below the GW) should be reasonably similar for different GWDs. Therefore, the additional LSN is determined using the GWD = 1 m case and this additional component is assumed to the same for other GWDs with a correction made if the termination depth is shallower than the GWD. This final correction is because the additional LSN should be less in this case since some of the missing soil is not saturated.

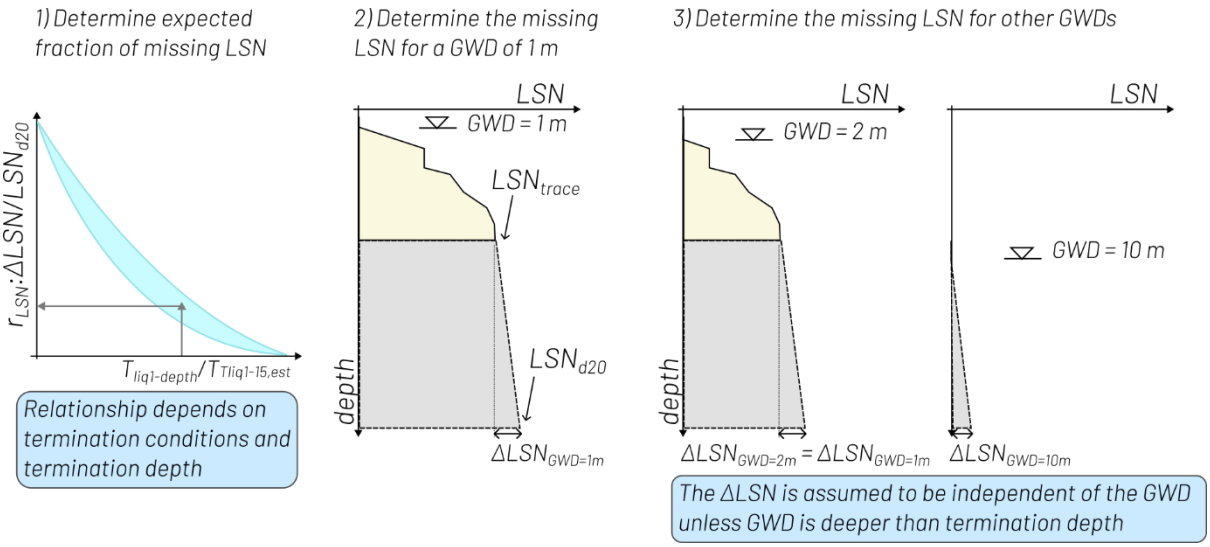

Figure 7.13: Conceptual depiction of the steps to apply a short termination correction to LSN

7.7.6.1 Determine the expected fraction of missing LSN

For the first step, the expected fraction of missing LSN from the trace for different GWDs, $r_{LSN,GWD}$ is determined using Equation 7 and Equation 8 when term_high_q is true and false respectively. The two equations were developed using multi-linear regression from the two databases discussed in Section 7.7.9 to predict the ratio of LSN contribution below a depth divided by the total LSN.

Equation 7:

$$r_{LSN,GWD} = 0.740 \cdot e^{-1.26\frac{T_{liq1-\mathrm{depth}}}{T_{liq1-15,est}}} - 0.0125 \cdot depth + 0.00283$$

Equation 8:

$$r_{LSN,GWD} = 0.972 \cdot e^{-1.08\frac{T_{liq1-depth}}{T_{liq1-15,est}}} - 0.00552 \cdot depth - 0.203$$

Depth is the maximum of the termination depth and the GWD. $T_{liq1-\mathrm{depth}}$ should be $T_{liq1-15,trace}$ when the GWD is less than the termination depth, and calculated using Equation 9 for other situations. Equation 9 scales up the thickness of material in the trace (i.e. decreases the missing thickness) by the scaling parameter, $sf_{GW,trace}$, from Equation 10. The scaling is based on the assumption that the liquefiable material is uniformly distributed in the profile and that only material below the GWD can contribute to LSN.

Equation 9:

$$T_{liq1-depth} = T_{liq1-15,trace} \cdot (1 + sf_{GW,trace})$$

Equation 10:

$$sf_{GWD,trace} = \frac{GWD - depth_{term} - 1}{14 - term_{depth}}$$

7.7.6.2 Determine the missing LSN for GWD of 1.0 m

The LSN and the missing LSN assuming GWD = 1.0 m can be determined using Equation 11 and Equation 12 respectively, where $r_{LSN,\mathrm{GWD=1m}}$ is the missing LSN ratio for GWD = 1 m.

Equation 11:

$$LSN_{GWD=1m} = \frac{1}{1 - r_{LSN,GWD=1m}} LSN_{trace,GWD=1m}$$

Equation 12:

$$\Delta LSN_{GWD=1m} = LSN_{GWD=1m} - LSN_{trace,GWD=1m}$$

These equations are only applicable for GWD = 1.0 m since $r_{LSN,GWD}$ equations were only developed using databases for GWD = 1.0 m.

7.7.6.3 Determine missing LSN for all GWDs and adjust LSN accordingly

To obtain LSN for other depths, it is assumed that the contribution of missing LSN for a given depth is independent of the GWD provided it is below the GWD. Therefore, the additional LSN contribution beyond the termination depth (ΔLSN) for all GWD (and all PGA and Mw values) can be computed using Equation 13, and the depth adjusted LSN from Equation 14. Note that in Equation 13, $r_{LSN,GWD}$ and $r_{LSN,GWD=1m}$ are equal to each other unless the termination depth is shallower than the GWD.

Equation 13:

$$\Delta LSN = \frac{r_{LSN,GWD}}{r_{LSN,GWD=1m}} \cdot \Delta LSN_{GWD=1m}$$

Equation 14:

$$LSN = LSN_{trace} + \Delta LSN$$

The decision to base the depth correction off GWD = 1.0 m allowed for a single set of equations for r_{LSN} and was confirmed as a suitable assumption by developing additional databases with GWD = 5.0 m. An alternative method where the r_{LSN} was a function of the GWD led to larger error in the prediction of total LSN for deeper GW. This was attributed to the correction being highly sensitive to small contributions of LSN at depth.

7.7.7 Evaluation of depth adjusted LSN

Figure 7.14 shows the depth corrected LSN versus uncorrected LSN (i.e. LSN_{trace}) for CPTs and BHs. The 1:1 line in the top row of plots shows that many GI were not corrected. The 1:2 line shows that the ΔLSN correction for GWD = 1.0 m is always less than 100% of LSN_{trace}, due to the filters on minimum termination depth. Conversely, the middle row of Figure 7.14 shows that for deep GW (e.g. 10 m), the correction can be very substantial relative to the uncorrected trace LSN. This is because the assumed missing content below the termination depth may be the main liquefiable material below the GWD. The bottom row of Figure 7.14 shows that the depth correction to LSN for deep GW is always less than or equal to the correction applied for GWD = 1.0 m.

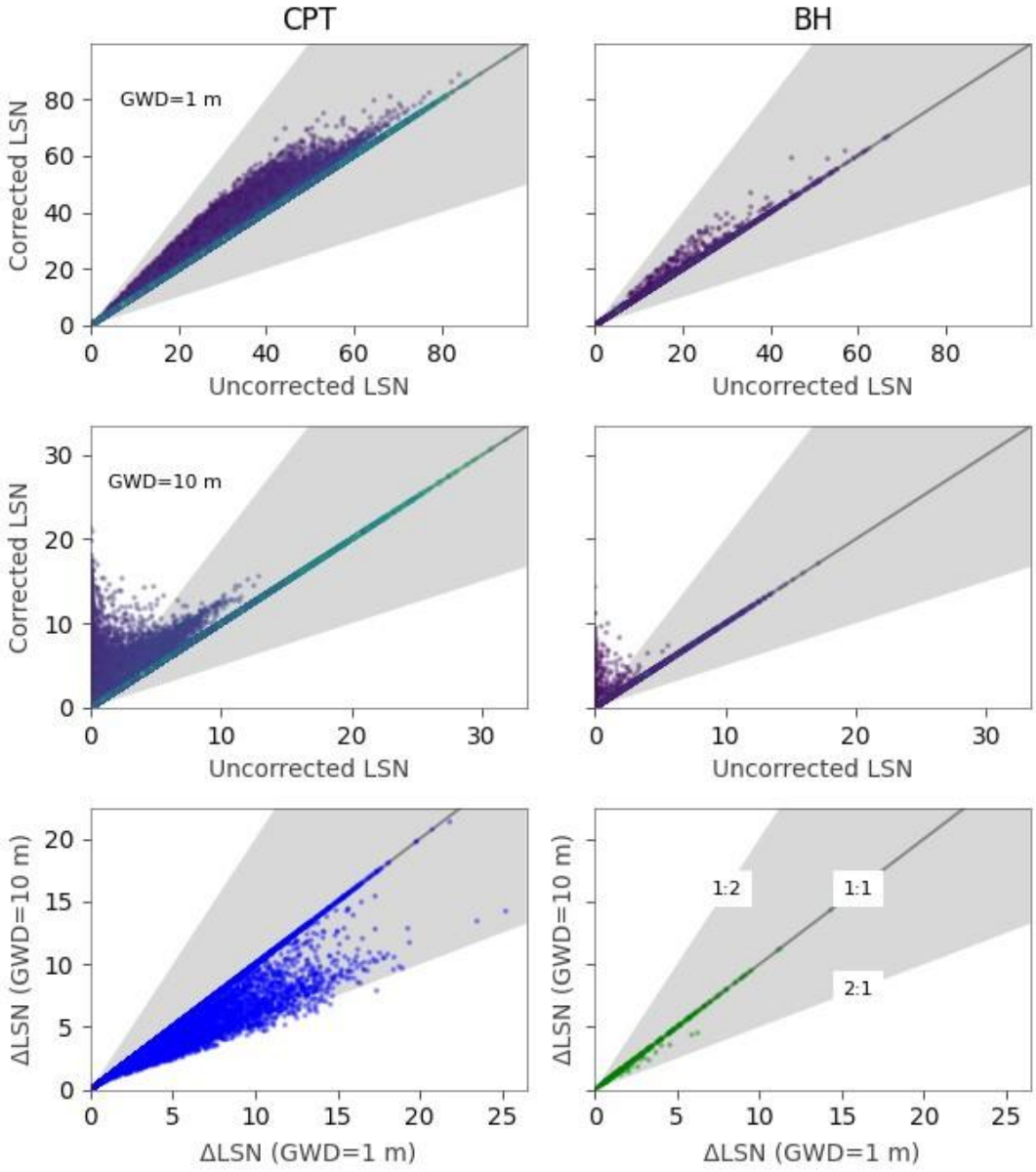

Figure 7.14: Summary of adjustments to LSN due to early termination for all CPTs (left) and all BHs (right). The top two rows have the adjustment amount versus the uncorrected LSN for 1 m and 10 m GWD, while the last row compares the correction amounts between the two GWD

7.7.8 Example application of short GI process

Figure 7.15 presents the application of the short GI process for an example CPT. In this example, the CPT is assumed to terminate at 9.4 m instead of going the full 20 m. Figure 7.15(a) and (b) present the I_c and q_{c1Ncs} traces respectively, showing the portion above and below the assumed termination depth. Figure 7.15(c) shows the cumulative calculation of $T_{liq,1-15}$ with depth. In this example the $T_{liq,1-15,est}$ is taken as the true value of 3.7 m. Figure 7.15(d) shows cumulative LSN contribution versus depth, where the red star shows the predicted value at 20 m depth using only the trace up to 9.4 m depth and applying the short GI correction process. The LSN contribution from the full trace is also shown as a dashed line.

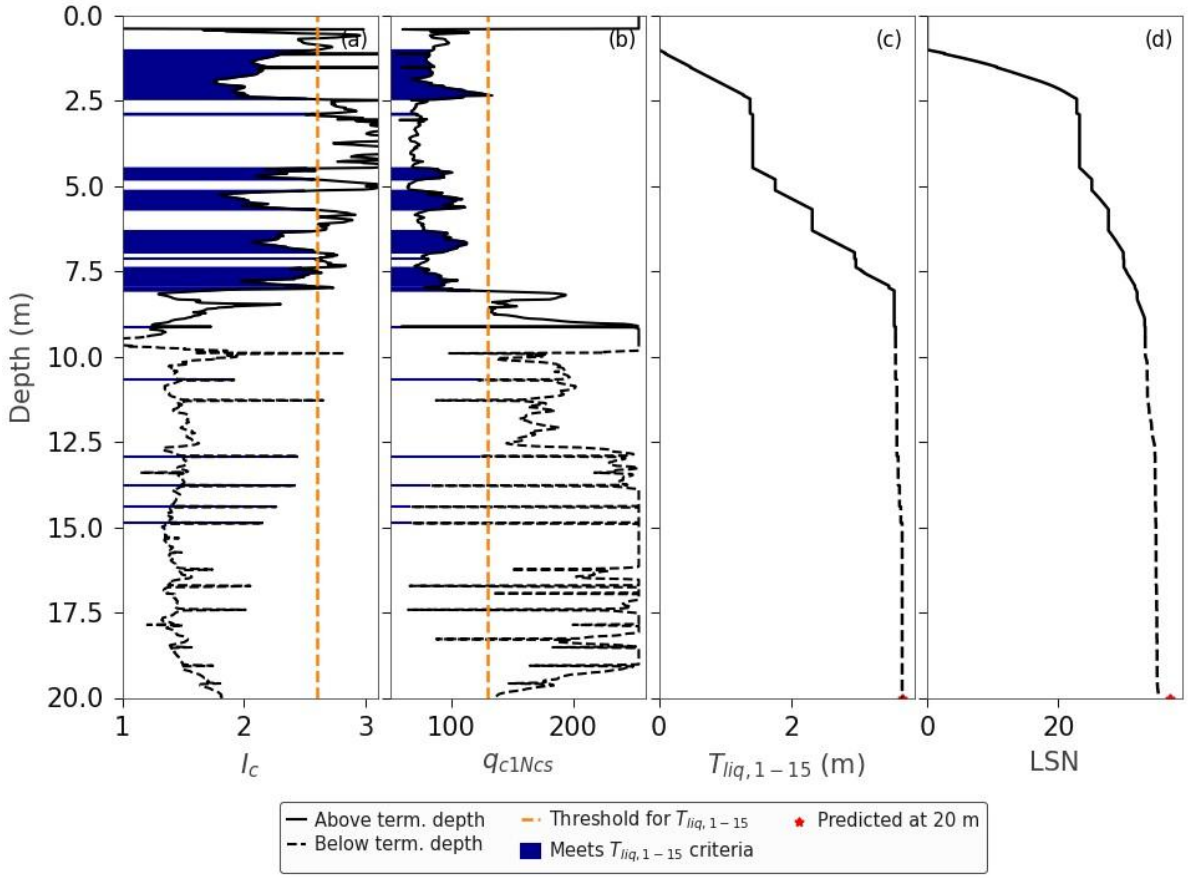

Figure 7.15: Example application of short GI process for a CPT that terminated at a depth of 9.4 m where the LSN at 20 m is approximated versus the true LSN at depth 9.4 m

7.7.9 Development of termination condition databases

Two databases were generated to quantify relationships needed to adjust for short GIs. The first database (referred to as the "term_high_q is true" database) was developed using all CPTs with a termination depth of 15 m or more, where each row in the database corresponds to a depth of the trace where q_{c1Ncs} >= 200 for a 0.3 m thickness. The second database (referred to as the "term_high_q is false" database) was developed using all CPTs with a termination depth of 15 m or more, where each row is for a 0.5 m depth increment. However, if that depth increment corresponded to conditions of "term_high_q is true", then than depth is omitted. The different databases were used to develop the equations for the short GI process presented in the preceding sections, where the equations were dependent on the termination conditions.

For each row in each database the following is stored:

- Depth.
- $T_{liq1-15,\text{trace}} - T_{liq1-15}$ computed using only the trace above the specific depth.
- LSN in trace – computed LSN using only the trace above the specific depth, where LSN is computed for PGA = 0.6 g, Mw = 7.5 and GWD = 1.0 m.
- Total $T_{liq1-15}$ to the depth of 15 m.
- Total LSN to a maximum depth of 20 m, where LSN is computed for PGA = 0.6 g, Mw = 7.5 and GWD = 1.0 m.

A depiction of the database creation is provided in Figure 7.16 where for a single trace, there are many points stored in each database. The figure shows a particular entry at a depth of

approximately 13 m. The middle image shows how the $T_{liq,1-15,trace}$ and total $T_{liq,1-15}$ are determined. The last image shows the LSN in trace and the total LSN.

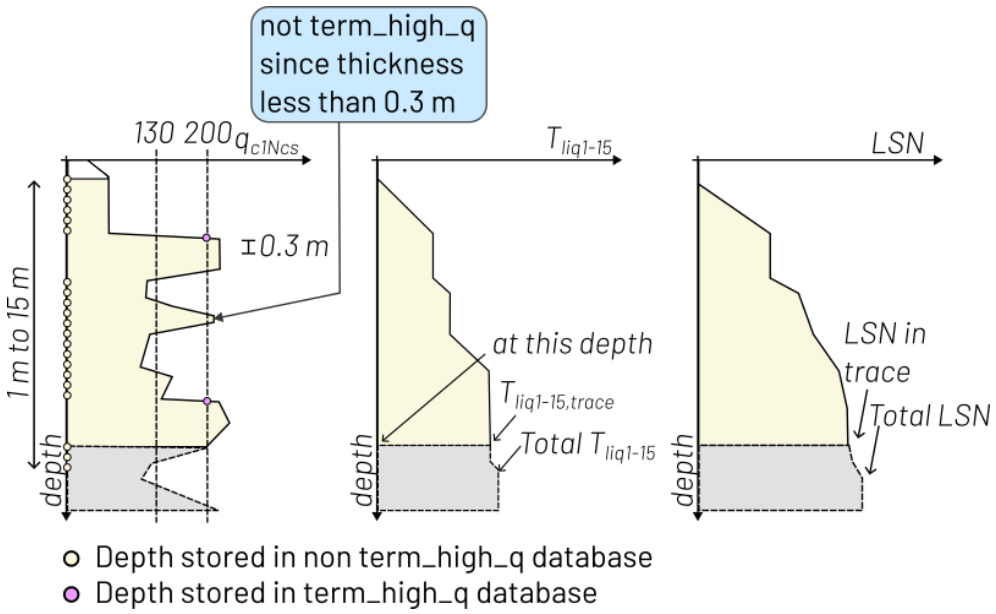

Figure 7.16: Illustration of the development of the termination conditions databases for the GI correction process where a row in the database is computed at the end of the yellow shading

7.8 Model validations

Three different validations were performed to understand differences between LSN from CPT versus BH. There are notable differences between the LSN values from the two different GI. However, not including BH data means that non-penetrable soils are not included in the model, which biases the model toward overestimating liquefaction. Therefore, we have opted to accept these differences and include the BH data to address this bias.

7.8.1 Comparison of liquefaction classes against GIs

Figure 7.17 shows the distribution of LSN (for PGA = 0.6 g, Mw = 7.5, GWD = 1 m) as calculated for the GIs for each l4_yp. Each LSN is weighted by the weightings described in Section 8.4.3. These weightings are used to ensure GIs that are very close together are not over-represented. These weightings scale down the count of each observation in the histogram (scaling from 1 through to 0.1) and aim to reduce bias from areas with a high spatial density of GIs.

Notably the BHs and CPTs have similar distributions; however, the BHs provide more readings in the classes with lower LV. Most distributions are consistent with expected output interpreted from YP78. Some notable exceptions are:

- The small number of high LSN readings for the Pre-Pleistocene Metamorphic class (plot #30) and Pleistocene Glacial Till class (plot #20). These samples are not representative of expected behaviour and may represent a sampling of more penetrable soil or a misalignment of the boundary of the geomorphology polygons.
- The Pleistocene River Channel class (plot #24) has a very wide liquefaction response and higher than the Holocene liquefaction response which is inconsistent with the expected relativity between these classes.

The first issue is dealt with specifically in the LVM geospatial model (see Section 8.4). To address the second issue, an exploration of the spatial distribution of the data showed that high LSN values in

Pleistocene River channel polygons were in polygons that also contained descriptions that the soil contained pumice. Figure 7.18 compares the LSN values from polygons considering all data (top row), those that have pumice in their descriptions (middle row) and those that do not (bottom row). Figure 7.18 shows that after the de-aggregation due to pumice the LSN values from the Holocene polygons have higher values on average than the Pleistocene values for both pumiceous soils and non-pumiceous soils. For the LVM geospatial model, the pumice polygons were considered as separate l3_yp (and l4_yp) categories due to this difference as covered in Section 8.4.

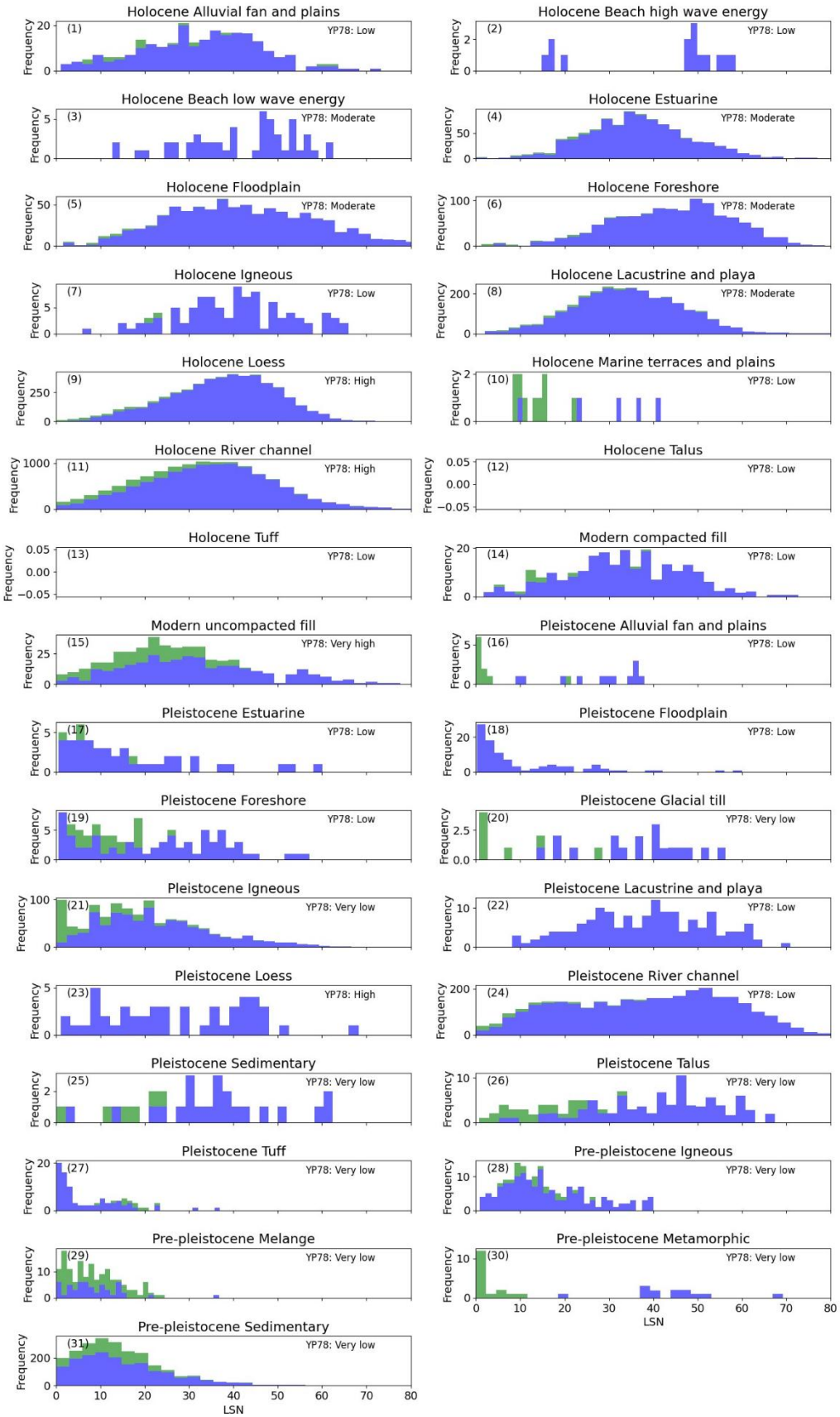

Figure 7.17: Stacked histograms of weighted LSN distributions from GIs (CPT = blue; BH =green) for each l4_yp category

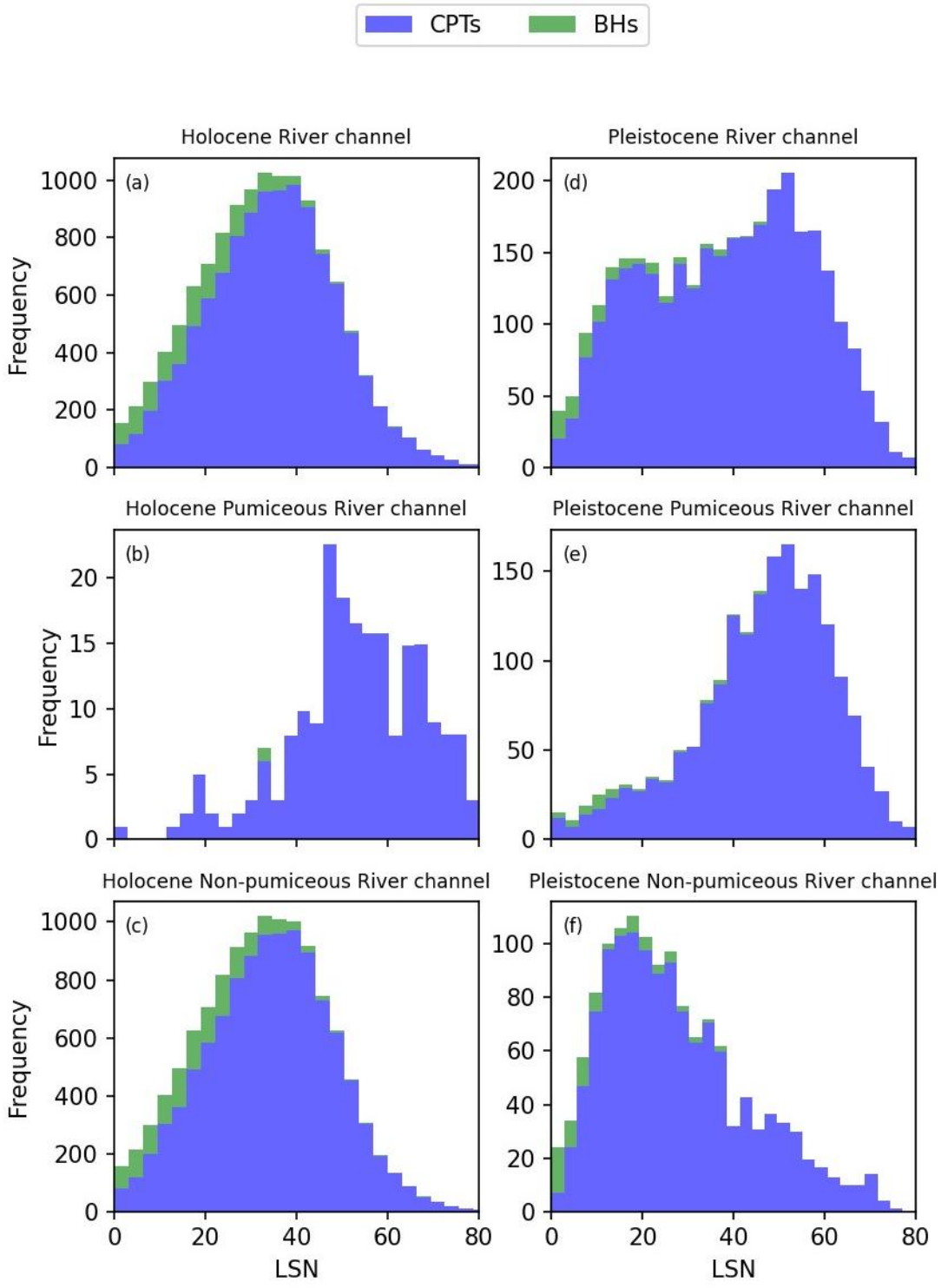

Figure 7.18: Stacked histograms showing the LSN comparison of GIs (CPT = blue; BH =green) in l4_yp River channel de-aggregated by Epoch with polygons that have pumice in their descriptions (middle row) compared to those that do not (bottom row)

7.8.2 Comparison of LSN from BH and CPT

Figure 7.19 shows the difference between LSN computed from CPT-BH pairs located within 10 m of each other, to evaluate whether there is a significant bias and/or inaccuracy from LSN computed from BH. The LSN calculation was applied to the minimum of 20 m or the termination depth of the CPT or BH, therefore this comparison does not apply the short GI correction. Additionally, the results are only shown if the calculation depth exceeds 5 m and the predrill is 1 m or less, to be consistent with the filters applied in this module. From Figure 7.19 it can be seen that a large portion of the pairs fall within the 2:1 and 1:2 bounds (corresponding to $\Delta \log(LSN)$ of 0.35). However, there is a notable portion of pairs where LSN from the BH is significantly higher than from the CPT, in many cases due to incorrectly determining the percentage I_c<2.6. For the cases where the CPT LSN was significantly higher, these were generally due to a thin layer of very low q_{c1ncs} near the surface that was not seen in the trace of the equivalent CPT developed from the BH. Overall, for this dataset of 934 pairs the calculated LSN values were on average 3.4 LSN units higher for the BH than the CPT.

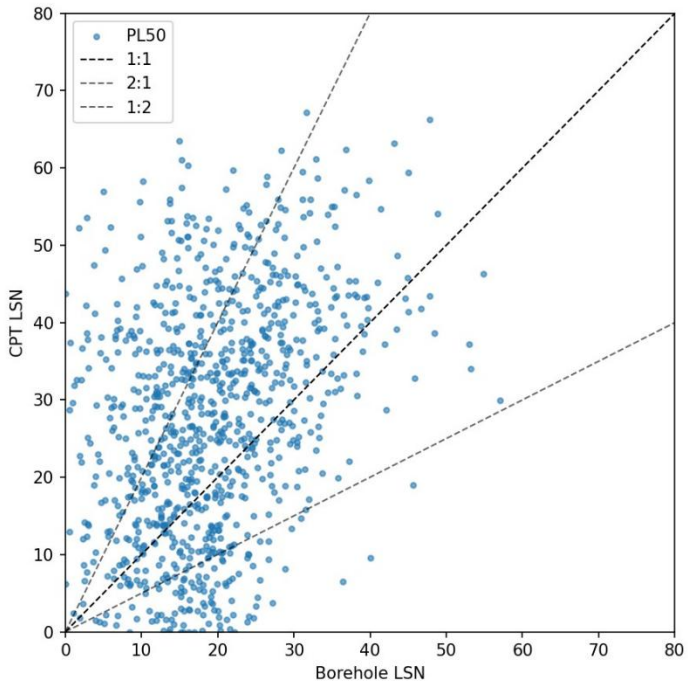

Figure 7.19: Comparison of LSN values calculated from CPT-BH pairs within 10 m of each other. LSN was computed using PGA = 0.25g, Mw = 7.5, GWD = 1.0 m down to a depth of 20 m, or the shortest depth of the BH and CPT pair if less than 20 m

7.8.3 LSN spatial variability comparison

A validation exercise was undertaken to identify whether BH-to-BH comparisons had a similar variability to CPT-to-CPT comparison, to identify anomalies in the comparisons (e.g. data cleaning issues can often be identified by looking at outliers from these analyses), and to evaluate any bias between CPT and BH calculations. The spatial variability of LSN calculated from pairs of nearby BHs is compared to the spatial variability for pairs of CPTs, as well as between BH-to-CPT pairs. These three comparisons were made by computing the difference in log(LSN) using the depth corrected LSN values. The comparisons identify GI pairs at different distances and compute the difference in LSN.

All l4_yp geomorphology categories (that had at least 1000 pairs within 100 m) were evaluated and the two with the worse bias in terms of differences between CPT and BH are shown as examples in Figure 7.20 and Figure 7.21, the remainder are provided in Digital Supplement G: – *LSN-diff*. The BH-to-BH plot for Holocene Loess in Figure 7.20 shows the limited data available to produce variograms

for BHs. In contrast, Figure 7.21 for Holocene River Channel has sufficient BH-to-BH pairs to show that the BH-to-BH variability is slightly higher than for CPT-to-CPT. As expected, the variability increases with distance, particularly notable for the CPT plot. The difference between BH-to-CPT shows a notable bias, with CPT producing higher LSN than BH. This is the opposite trend to the comparison using the LSN values that have not been depth corrected in Section 7.8.2. This trend was observed across these two geomorphologies and Holocene Estuarine. However, for some it was the opposite (e.g. Pre-Pleistocene Sedimentary), where BH tended to have lower LSN values than CPT. Some confirmed causes and potential causes for the bias are:

1 Confirmed cause: Some BH were included uncorrected if they had a depth of 7 m or more and where q_{c1Ncs} >= 170 for the last 2 m of the equivalent CPT trace.

2 Potential cause: There are differences and potentially biases in $T_{liq1-15}$ between BH and CPT, which means that the correction relationship developed for CPT may have resulted in a too small correction of LSN for BH.

3 Potential cause: When term_high_q is true, shorter GI are corrected, whereas when false they are rejected. term_high_q was only considered for CPT thus potentially biasing to rejecting more BH that would have low LSN.

4 Potential cause: The adopted values for determining the equivalent CPT from BH, e.g. the conversion from SPT blow count to q_{c1Ncs}, may estimate too high q_{c1Ncs} values.

5 Potential cause: Difficulties and potential biases with establishing a representative percentage I_c > 2.6 for the BH layers

6 Potential cause: CPT are not performed in non-penetrable ground and therefore this bias partially reflects the ground sampling bias of CPT.

In Section 10.4.1.1 this bias is shown to manifest in different predictions of the land damage from BH versus CPT for the same LSN. This suggests that the approach adopted for establishing the equivalent CPT or the depth correction is biased.

Figure 7.20 and Figure 7.21 both show there is reasonably high variability in log(LSN) (mean of approximately 0.2) from CPT-CPT pairs at short distances ~15-20 m. The analysed data here includes decisions around the database filtering, predrill adjustments and the short GI correction process which may have increased variability. However, the high variability shows that uncertainty guidance for the development of the NLM (Section 4.3.1.1) is on par with the variability of LSN that could be expected to occur over short distances due to natural variability from depositional processes in the types of environments where liquefaction is generally expected to occur.

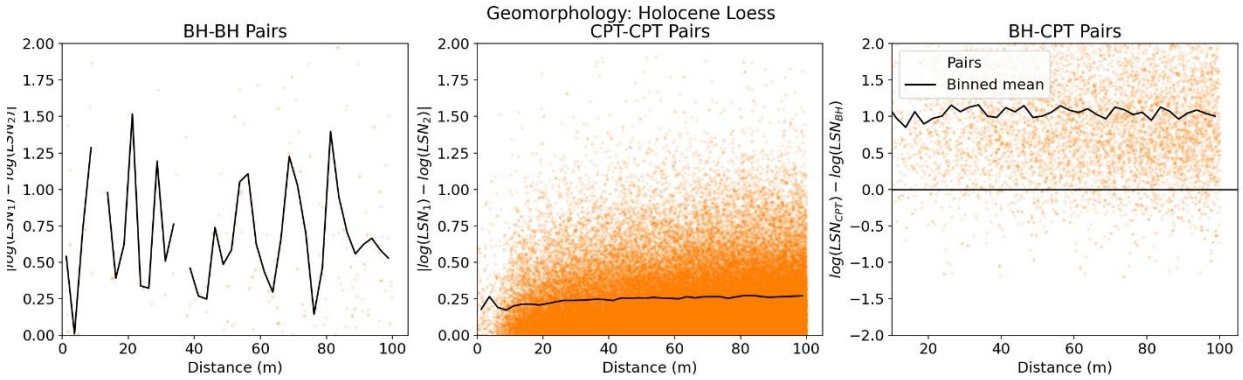

Figure 7.20: Comparison of spatial variability, to 100 m, for the Holocene Loess geomorphology

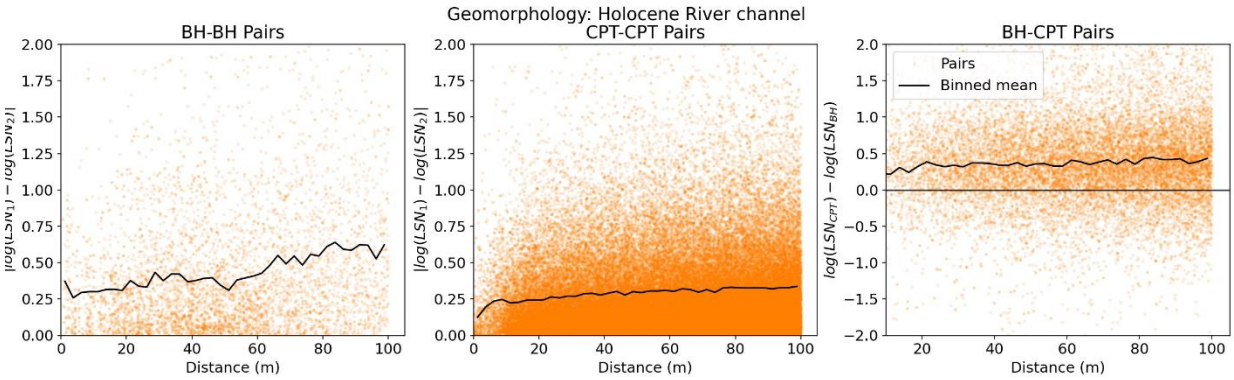

Figure 7.21: Comparison of spatial variability, to 100 m, for the Holocene River Channel geomorphology

7.9 Limitations

1 The LDMs developed here are not suitable for site-specific design because they have only been evaluated in aggregate without specific quality checks on data and processing.

2 LDMs are only an index of likely liquefaction damage at the ground surface and therefore only represent likely damage in a probabilistic sense.

3 There are some known limitations of the triggering methods (e.g. they do not account for system response effects as described in Cubrinovski et al. (2019) or highly interbedded deposits as described in (Upadhyaya et al., 2023)). These limitations impact the accuracy of liquefaction damage predictions developed herein.

4 The majority of GIs were sourced from the NZGD. The limitations on accuracy and disclaimers for the NZGD are applicable to the NLM output. These include but are not limited to:

   a No warranties are provided in relation to the accuracy or fitness for any purpose of Geotechnical Data uploaded to the NZGD. You must exercise reasonable care and perform due diligence when using Geotechnical Data obtained from the NZGD.

   b Users acknowledge that Geotechnical Data uploaded to the NZGD may have been compiled for a purpose other than the purpose for which you intend to use the Geotechnical Data.

5 The large scale processing of the dataset means that individual GIs were not checked, instead outlier analysis was used to detect obvious issues and develop the filters and pre-processing steps outlined in Sections 7.5.2 and 7.5.3. However, additional filters of data (e.g. identification of traces from dirty CPT that result in lower-than-expected skin friction) have not been fully considered.

6 748 CPTs that are marked as being undertaken post ground improvements are currently not excluded or handled differently to those that are taken on natural ground. Ground improvements are undertaken in very localised areas so in case where these form a Tier 3 (higher confidence smaller) polygon (discussed in Section 8.6) these CPTs would provide a reasonable representation of the ground. Their inclusion in non-made geomorphologies for the geospatial model would have a minor impact since the post ground improvement CPTs represent only 1% of total CPTs.

7 For BH the MISSING_MATERIAL currently only interpolates the q_{low} and q_{high} from the layers above and below, it does not interpolate percentage I_c>2.6 which is set to 0 for these layers (i.e. missing material is assumed to be susceptible to liquefaction).

8 The triggering calculations rely on the assumptions outlined in Section 7.3, which may result in mispredictions when conditions differ from those assumed. In particular, the assumption of fully saturated soils only below the GWL, and no explicit consideration of the influence of pumice.

9 The model contains a large number of GIs where depth corrections are applied to address early termination. The adjustment attempts to provide an unbiased (best estimate) correction and may over or underestimate LSN. The greater the extrapolation of this correction, the larger the potential inaccuracy.

10 BH have larger uncertainty and potentially bias for the depth correction since the depth correction process was developed for CPT and directly applied to the "equivalent CPTs" derived from BH.

11 The BH-based LDMs are anticipated to have greater uncertainty compared to CPT-based LDMs due to the additional process that involves converting a BH to a CPT equivalent trace, as well as the lower resolution data that BH provide.

12 The current version of the BH conversion process is subject to the following additional limitations:

a It assumes that geo-professionals across New Zealand are consistent when logging BHs, and that different loggers assign consistent descriptions to soil cores. Soil cores exhibit varying degrees of disturbance to soil structure, depending on the coring method, so a visual assessment of soil composition will retain a level of subjectivity, despite all loggers referencing the same guidelines. There is also expected to be a great level of uncertainty regarding the evaluation of soil density.

b The liquefaction behaviour of a specific soil is affected by many factors which cannot all be captured by relatively simple qualitative assessments of soil cores (i.e. grain size composition, plasticity, and density).

c An extensive analysis of terms associated with plasticity and density within the BH database has been performed to compile the reference lists used in the model to define *plasticity_status* and *density_status*. However, there is the possibility that relatively uncommon descriptions, not included in the reference lists, or descriptions containing misspelled terms, are not identified, thus resulting in "NOT_FOUND" plasticity or density descriptors. Furthermore, silt-dominated soils can be accompanied by descriptive terms such as "soft" and "stiff" rather than "loose" or "dense", which were not used in the *density_status*.

13 The NLM GI model has been developed for the purpose of regional scale LV assessment and should not be relied upon for other purposes.

7.10 Potential future improvements

To enhance the GI module and address its current limitations, several potential future improvements have been identified:

1 **Additional LDMs**. Include additional LDMs that account for the PGA, Mw, GWD and liquefaction triggering calculations in a different manner, e.g. LPI (Iwasaki et al., 1981). Different LDMs may be more predictable (e.g. lower spatial variability (see 7.8.3)) and higher efficiency and sufficiency for predicting land damage (i.e. better correlated to land damage (see Section 10)). Therefore, they could provide an improved basis for estimating liquefaction induced damage. Even if the additional LDMs provide similar predictability, efficiency and sufficiency, the prediction of probability of land damage would differ from an LSN-based prediction. The differences in probabilities can be used to infer uncertainty and compute an average probability from multiple LDM.

2 **Obtain non NZGD GIs**. Include additional data held by others (e.g. councils and other asset owners), particularly in areas where data is scarce.

3 **Convert more BH from PDF into the Simple BH format**. BHs can provide predictions in non-penetrable ground which reduces the bias due to using CPT.

4 **Cross-check dataset of LSN values**. Perform additional validation on the GIs and corresponding LSN values by comparing results to published datasets, e.g. the dataset from Geyin & Maurer (2020) with LSN values for the Christchurch earthquake events.

5 **Include different liquefaction triggering methods.** Liquefaction triggering can be calculated using a range of different triggering methods. For the purposes of this model, Boulanger & Idriss (2016) has been used. In the future, the model could be more flexible so that other liquefaction triggering methods can be used.

6 **Handle CPTs which appear to have a dirty cone (i.e. dirty CPT)**. Dirty CPT result in lower-than-expected skin friction and higher LSN values. The filter to identify them is currently very simple and could be improved by considering nearby GI, additional trace features and metadata associated with the GI. The dirty CPT are currently removed from the database, however, these could be corrected if a suitable correction can be developed.

7 **Consider the inclusion of post ground improvement GI**. The 748 post ground improvement CPTs are currently included in the LV geospatial model, some of which are not in Compacted or Uncompacted fill geomorphology polygons. These GI modify the distributions of the geospatial model.

8 **Address potential differences in the short GI correction process between BH and CPT**. The short GI process appears to provide a greater correction to CPT than BH.

9 **Update the criteria for evaluating termination conditions for the short GI correction process**. The direct inclusion of BH without depth correction when q_{c1Ncs} >= 170 for the last 2 m of the equivalent CPT trace may be biasing BH to lower LSN values. The criteria for this condition could be updated to be based on the *main_material*, e.g. if the *main_material* in the last layer is ROCK then no depth correction is needed.

Potential updates specific to the conversion of BH to equivalent CPT:

10 **Improved filter for comparison databases.** For the development of the CPT-BH, CPT-SPT-BH and SPT-BH databases, develop a methodology to include BH that were filtered out because they contained a section of MISSING_MATERIAL greater than or equal to 1 m. These BH often contain a lot of useful data to inform the relationships used in the BH method.

11 **Regional specific corrections**. The current process does not account for the presence of non-routine soil fractions (e.g. cemented soils, pumice, residual soils). Zone-based classifications to recognise specific characteristics of soil deposits encountered in certain areas of New Zealand could be used to refine the estimates of q_{c1Ncs} and percentage $I_c > 2.6$.

12 **Age of deposit**. Account for the geological unit recorded in the BH log to infer the age of the deposit and apply a geological-unit specific modifier to q_{c1Ncs} based on the age of the deposit.

13 **Update percentage Ic > 2.6 values**. Update Table 7.5 to use the latest CPT-BH database

14 ***Density_status* for silt**. Include terms related to silt-dominated soils such as “soft” and “stiff” for determining the *density_status*.

8 Liquefaction Vulnerability (LV) module

The Liquefaction Vulnerability (LV) module combines the Flatland Model, Geomorphology Model and the GI Model to provide predictions of LDMs across the full extent of the flatland for a range of PGA, Mw and GWD combinations. The flatland area is divided into polygons defined as SSP. For each SSP, the predictions are provided using three different distributions. The distributions provide an unbiased estimate of the LDM, and for a given PGA, Mw and GWD combination, three distributions are provided[21]:

- Geospatial distribution: A probability distribution of an LDM that reflects the typical range of an LDM based on similar geomorphology across the country. This distribution is directly taken from the geospatial model and is constructed using P50_geospatial and P85_geospatial.
- Spatial variability distribution: A probability distribution of an LDM that represents a best estimate of the expected differences of LDM values across a polygon. This distribution accounts for the geomorphology, the likely spatial variability of soil conditions, and LDM values of the local GIs within the polygon. It is constructed using P50_spatial_var and P85_spatial_var.
- Sample uncertainty distribution: A probability distribution of an LDM that represents the total modelled uncertainty of an LDM value for a randomly sampled point in the polygon. It accounts for the uncertainty due to the finite number of local GIs, as well as the geomorphology, the likely spatial variability of soil conditions, and the LDM values of the local GIs within the polygon. It is constructed using P50_sample_unc and P85_sample_unc.

Why provide 3 distributions?
Section 4.2 outlines that the NLM must support multiple different end use cases. These different end use cases may need different representations of uncertainty and variability. For example, land use planning exercises may only consider the sample uncertainty distribution when there are enough nearby GIs and may default to use the geospatial distribution in other cases. On the other hand, research or loss modelling may want a best estimate of the likely variability in a LDM and therefore adopt the spatial variability distribution.

Each of these distributions are conceptually shown in Figure 8.1, where the geospatial distribution represents the distribution from all GIs that have the same geomorphology as the polygon. The spatial variability distribution provides a best estimate of the distribution by considering the geospatial estimate, the likely standard deviation and the local GIs. The sample uncertainty distribution sits between the geospatial model and the spatial variability; in that it considers that there is some uncertainty in the best estimate.

[21] The definitions of the distributions provided here should not be confused with the general terms defined in Section 4.3.1.

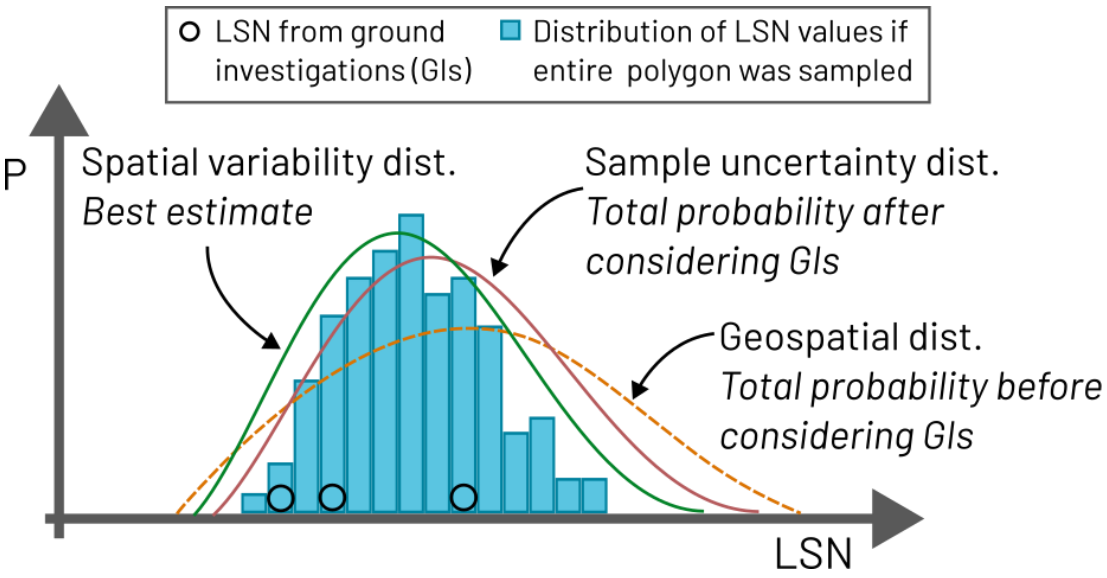

Figure 8.1: Conceptual explanation of the different distributions provided by the LVM

In situations where a polygon is well characterised by local GIs, the spatial variability and sample uncertainty distributions are very similar. However, when there are no local GIs, the sample uncertainty distribution is equal to the geospatial model uncertainty. The three distributions allow the end user to adopt estimates suitable for their purpose (e.g. land-use planning or loss modelling) where boundary and liquefaction response uncertainty may be handled differently.

This section provides details of the module outputs listed in Section 8.1. The key steps are covered at a high level in Section 8.2, and the details on how spatial variability and uncertainty were handled are discussed in Section 8.3. The remaining sections provide additional details on the key steps, limitations and potential future improvements of this module. The validations for this module are provided in the simulation of historical events (see Section 11.1). For this report the LDM used is LSN.

8.1 Module output

The main output from the LV module is the LVM which includes the following:

1 Similar-soil-polygons (SSP): A geopackage file with each row corresponding to an SSP with a unique ID (SSP ID) and the polygon geometry.

2 <LDM>-<PL>-<method>-per-SSP (referred to as LDM-per-SSP): A parquet file defining the LDM response for different SSP for a range of PGA, Mw and GWD combinations. <LDM> corresponds to the LDM that is produced (in this case LSN) and method is the liquefaction triggering method detailed in Section 7.1. The data structure is presented in Table 8.1. The predictions are provided for the same PGA, Mw and GWD increments as produced in the GI module (See Section 7.4).

Table 8.1: Data structure for LDM-per-SSP

Column name	Units	Description
ssp_id		The ID of the SSP
PGA	*g*	Peak Ground Acceleration
Mw		Moment magnitude
GWD	m	Groundwater Depth
P50_spatial_var		The median LDM from the SSP considering only spatial variability, used with P85_spatial_var to produce a lognormal distribution
P85_spatial_var		The 85th percentile LDM considering only spatial variability, used with P50_spatial_var to produce a lognormal distribution
P50_sample_unc		The median LDM considering both spatial variability and uncertainty in the median estimate, used with P85_sample_unc to produce a lognormal distribution
P85_sample_unc		The 85th percentile LDM considering both spatial variability and uncertainty in the median estimate, used with P50_sample_unc to produce a lognormal distribution
P50_geospatial		The median LDM from the geospatial model output, used with P85_geospatial to produce a lognormal distribution
P85_geospatial		The 85th percentile LDM from the geospatial model output, used with P50_geospatial to produce a lognormal distribution

Note: P50 and P85 in the table above represent the uncertainty in the LV model (not the probability of liquefaction (P_L) triggering, which is set to P_L = 50% throughout this report unless stated otherwise)

There are 6 output variables and 350 seismicity and GW combinations, which results in 2,100 unique outputs per polygon. There are 164,914 polygons in the final model. Figure 8.2 provides a sample output for the LVM at national scale.

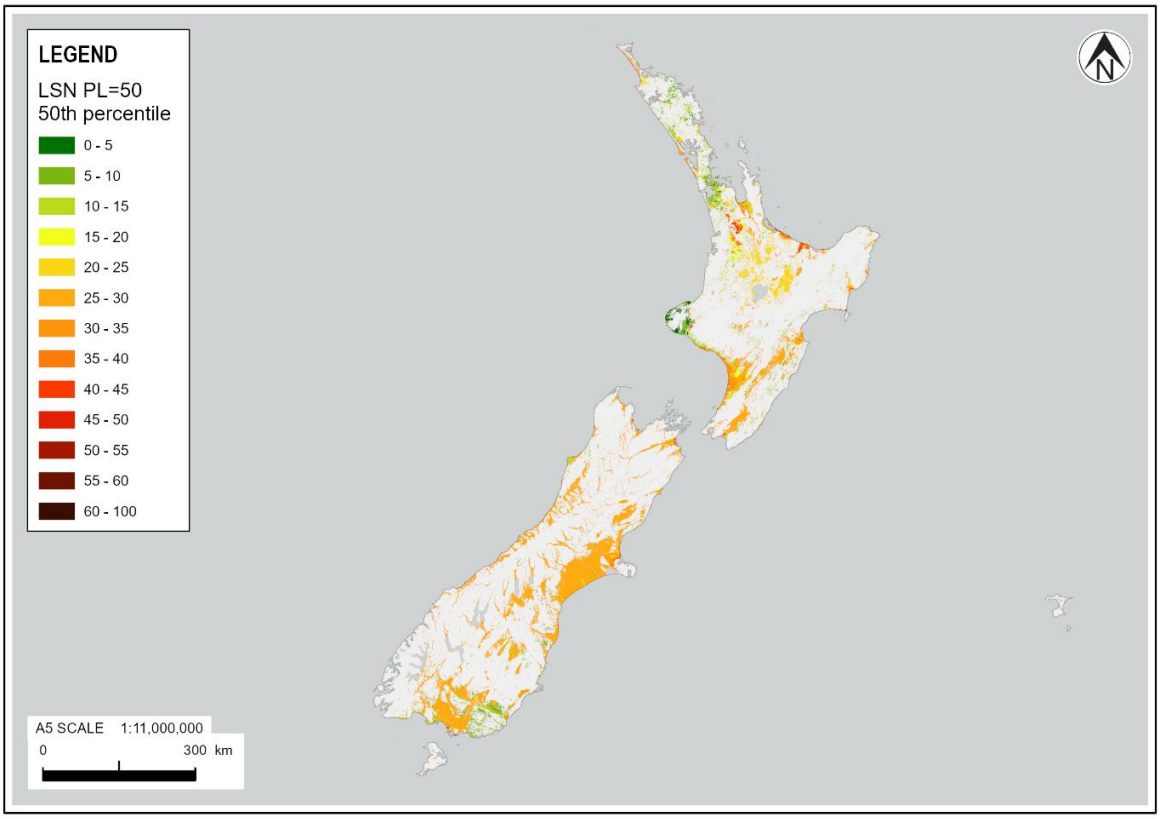

Figure 8.2: LVM output for LSN 50th percentile of the spatial variability distribution for P_L = 50%, PGA = 0.6 g, Mw = 7.5 and GWD = 1 m

A note regarding quantifying distributions using percentiles

Lognormal distributions are used in three parts of the NLM to quantify the behaviour and each one deliberately adopts different percentiles to quantify the distribution. The different percentiles are due to the context of their use (although the use of different percentiles provides a convenient measure to avoid unintended misuse). The three specific uses are:

- ***LV geospatial model (Section 8.4)***
  Distribution of LSN per geomorphology category for different PGA, Mw, GWD.
  15th and 85th percentiles were used since these percentiles have different relationships with PGA and GWD which are independently fitted. Using 50th percentile instead of 15th or 85th would not be as effective at capturing this difference.
- ***LDM-per-SSP table (Section 8.1)***
  Distribution of LSN per SSP for different PGA, Mw, GWD.
  50th and 85th percentiles were used since the median (50th) is a useful metric to compare different polygons. The 85th was chosen instead of the 15th since for most use cases of the LVM there would be more interest in the upper range in LSN than the lower range.
- ***LDFCs (Section 10.2)***
  Cumulative distribution function for probability of a land damage state.
  15th and 50th percentiles were used since the median is useful metric to compare different curves. The 15th was chosen instead of the 85th since for loss and land-use planning the expected behaviour at low probabilities is more important than at higher probabilities. Notably both the 15th and 50th percentiles for land damage are used with the MBIE/MfE Guidance (2017).

These percentiles should not be confused with the probability of liquefaction (P_L). Where the adoption of different P_L values adjusts the calculation of the factor of safety against triggering of liquefaction. This report adopts P_L=50%, except for when explicitly stated that P_L=15% is used.

The percentiles are primarily used as a convenient and highly interpretable way to store a lognormal distribution to allow it to be reproduced. Different software packages generate lognormal distributions using different input variables. The SciPy Python package requires the mean and standard deviation of a normal distribution in log space. To obtain these values the log space mean is simply:

$$mean = \log\left(P50\right)$$

And the log space standard deviation, σ_{log}, is:

$$\sigma_{log} = \frac{\log(P85) - \log(P50)}{1.036}$$

Where P50 and P85 are the 50th and 85th percentiles, and 1.036 is the z-score for the 85th percentile. If using the 15th percentile instead of 85th percentile then change the z-score to negative 1.036.

8.2 Key steps

The high-level LV module workflow is provided in Figure 8.3 and consists of four main steps:

1 The development of a geospatial model to predict LDMs across all flatland areas based on the geomorphology (see Section 8.4).

2 The quantification of spatial variability (see Section 8.5).

3 The identification of SSP to allow more refined predictions both spatially and in the output distributions (see Section 8.6).

4 The development of the liquefaction-induced land-damage measure lookup tables per SSP. This combines the geospatial model predictions with the GIs within each polygon using the likely spatial variability and provides distributions for different use cases (see Section 8.7).

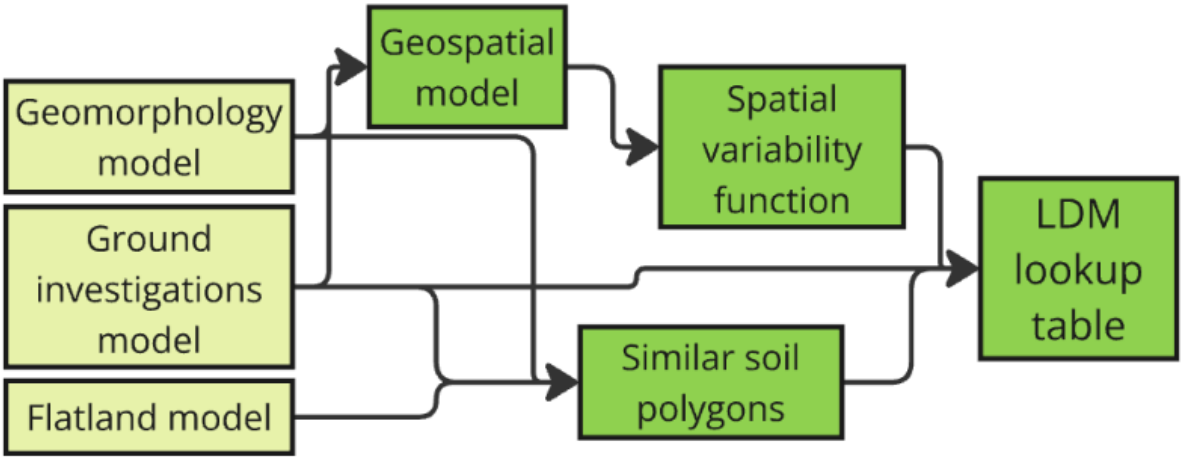

Figure 8.3: LV module design

8.2.1 Inputs

The key inputs to the module are:

1 National Flatland Model.

2 National Geomorphology Model.

3 National GI Model.

8.3 Framework for spatial quantification and uncertainty

8.3.1 Use of polygons for spatial quantification

The structure of the LV module is based around a series of polygons that are intended to maximise homogeneity of LV within polygons, and heterogeneity between them. The use of a polygon is convenient in that a single set of LV parameters can be assigned to the whole polygon. An alternative approach using points/raster at 100 m spacing would require ~7 million points, which when combined with the six output values for each of the 350 different seismicity and GWD combinations, would result in 14.7 billion unique values (~40x more than the polygon-based model) and significant computational challenges.

Polygon assignment is a form of classification or digitisation that inherently results in some data loss at the point-of-interest level (i.e. increased uncertainty). This loss of information can be captured through a distribution that would represent the expected spatial variability within the polygon. Given the underlying soil is poorly known (due to a limited amount of GIs) and there may be significant ground variability even over the smallest area of interest (e.g. footprint of a dwelling), the "data loss" from the digitisation process does not necessarily result in a significant increase in response uncertainty.

To reduce data loss, the maximum size of polygons was limited to reflect observed trends in the underlying data. For example, a large geomorphology polygon covers most of Lower Hutt, however, the LV is higher near the coast than up the valley. If the polygon used the geomorphology boundary and ignored this trend, it would result in loss of information and increased dispersion of the

expected LV values. Instead, if the polygon is split into several polygons with different median values, these polygons would have smaller dispersion of LV values than the large polygon and more information would be retained. The process to identify polygon boundaries is provided in Section 8.5.

8.3.2 Consideration of spatial variability and sampling error

Soil variability is often described by the simple mathematical model given in Equation 15. The model consists of a deterministic component, t(x), a randomly varying component w(x), and some error term, ϵ, and is a common spatial variability model adopted for soil (Bong & Stuedlein, 2018; Ching et al., 2022; Stuedlein & Bong, 2017).

Equation 15:

$$S(x) = t(x) + w(x) + \epsilon$$

The deterministic component can be considered as large spatial trends, whereas the random component can be local fluctuations caused by unpredictable local factors in the deposition. The model is a convenience, since both components are driven by physical processes, and therefore could be considered deterministic. However, the ability to estimate the first component is far greater than the second component.

The LVM adopts the same mathematical model, however, the deterministic component is a piece-wise constant (i.e. it is constant over a polygon and changes between polygons), while the randomly varying and error components are modelled as a probability distribution. The LVM outputs several different distributions, of which the spatial variability distribution adopts an error term of 0, whereas the geospatial distribution and the sample uncertainty distribution aggregate the local fluctuations and error term together in the distribution.

Given that LV variability increases with distance, the spatial variability distribution should increase as the polygon area increases and should tend towards the sample uncertainty distribution. In other words, the expected difference in LDM across a very large polygon could be considered representative of the range of expected LDM for those geomorphological attributes, therefore would have no sampling error but a large spatial variability. This concept is implemented in the model with details provided in Section 8.7.

8.3.3 Reduction in sampling error due to local GIs

The geospatial model provides predictions by grouping GIs by geomorphological attributes and fitting distributions to the aggregated values. These distributions are then used to provide an initial (prior) estimate of the response of individual polygons. The distributions reflect the national average for those particular geomorphological attributes. However, a small polygon would have a small spatial variability distribution, therefore the difference in two distributions is due to the sampling error (defined here as the uncertainty in the median). If more information is known about the actual LV of the polygon (i.e. local GIs) this can be used to update the estimate of the median and reduce the uncertainty of its value. Therefore, polygons with more GIs have lower uncertainty associated with them. The details of how this is handled through Bayesian updating are provided in Section 8.7.

8.3.4 Balancing liquefaction response uncertainty and spatial variability using different tiers of SSP

There are three classifications of SSPs, reflecting an increasing understanding of the ground conditions:

- **Tier 1 polygons** are based on the geomorphology polygon boundaries and have limited or no GI data.
- **Tier 2 polygons** split large Tier 1 polygons based on GIs if there is a sufficient difference in liquefaction response of the GIs.
- **Tier 3 polygons** identify closely spaced clusters of GIs that have similar liquefaction response.

Figure 8.4 shows a conceptual example of a polygon where the true response for a cross-section differs based on the following situations:

1 **In Case 0 –** there are no GIs in the polygon and the distribution of expected response can only be constrained by the geospatial model (which relies on the geomorphology classes). The polygon is not split, and it is considered Tier 1.

2 **In Case 1** – there are a few GIs, however, the readings do not show a detectable spatial trend or significant benefit to split the polygon. The polygon is not split, and it is considered Tier 1.

3 **In Case 2** – there are a few GIs, and the readings show a detectable spatial trend. The polygon is split, and it is considered Tier 2.

4 **In Case 3** – there is a high density of GIs, and the readings show a detectable spatial trend as well as a closely spaced consistent set of readings. The polygon is split to become a Tier 2 polygon, and the closely spaced set is identified as a Tier 3 polygon.

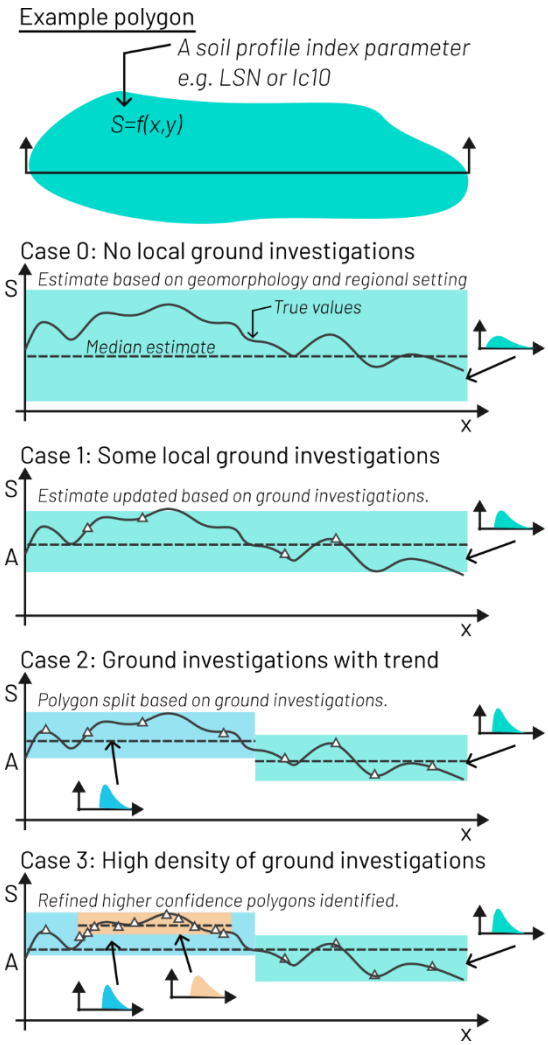

Figure 8.4: Conceptual example of how a geomorphological polygon is classified into SSPs based on different amounts of GIs. The cross-sections show x as the horizontal distance, plotted against the soil profile index parameter, S

8.3.5 Approximate liquefaction response and boundary uncertainty levels in the LVM

Table 8.2 provides a description and indication of the level of liquefaction response uncertainty and boundary uncertainty.

Table 8.2: Indicative liquefaction response uncertainty and boundary uncertainty for different tiers of SSPs and non-flatland

Tier	Description	Indicative liquefaction response uncertainty*	Boundary uncertainty[+]
Non-flatland	Identifies land that is considered non-liquefiable due to material and composition typical of steep land. Boundary uncertainty largely a function of ground steepness and geology.	Corresponding to the MBIE/MfE LV category ***"Liquefaction Damage is Unlikely"*** MBIE/MfE Guidance (2017)	50 m to 500 m
Tier 1	Predictions are based on the geospatial model which relies on the geomorphology classes. The predictions generally have large liquefaction response uncertainty, and boundary uncertainty is driven by the uncertainty in the geomorphology model. Polygons are generally very large.	0.35 to 1.0	100 m to 500 m
Tier 2	Predictions based largely on the geospatial model with some consideration of local GI. Polygons are generally large which means the influence of GIs is extrapolated across a wide area resulting in large boundary uncertainty.	0.35 to 0.80	500 m to 2 km
Tier 3	Predictions are based nearly entirely on the local GIs. Polygons are small and have significantly lower uncertainty than other polygon tiers.	0.18 to 0.25	10 m to 20 m

* Defined here as using the standard deviation in natural log(LSN) for PGA = 0.6 g, Mw = 7.5 and GWD = 1.0 m

[+] Land within this distance of the polygon boundary would have larger sampling uncertainty due to uncertainty in the position of the boundary.

The different polygons serve different purposes within the framework of predicting liquefaction-induced losses:

- Non-flatland polygons exclude large areas from the loss process due to their low probability of contributing to liquefaction-induced losses.
- Tier 1 polygons provide a baseline broad prediction as no additional information (i.e. GIs or local knowledge) have been considered to adjust predictions. They are deliberately as large as possible to be efficient for data storage.
- Tier 2 polygons provide spatial variability and spatial correlation, and capture trends across a large geomorphology polygon.
- Tier 3 polygons provide higher accuracy predictions, thus reducing the scatter in the predictions of loss (since these polygons produce similar levels of liquefaction-induced damage across different realisations of the same seismic event).

Tier 2 polygons are the most problematic, in that there is a significant potential for a biased prediction at a suburb level due to the potential for large extrapolation. The extrapolation is shown conceptually in Figure 8.5 which is an extension from the example in Figure 8.4. In this example, the polygon split is based on two GI in each Tier 2 polygon and the extent of the Tier 2 polygons extends far beyond the GIs.

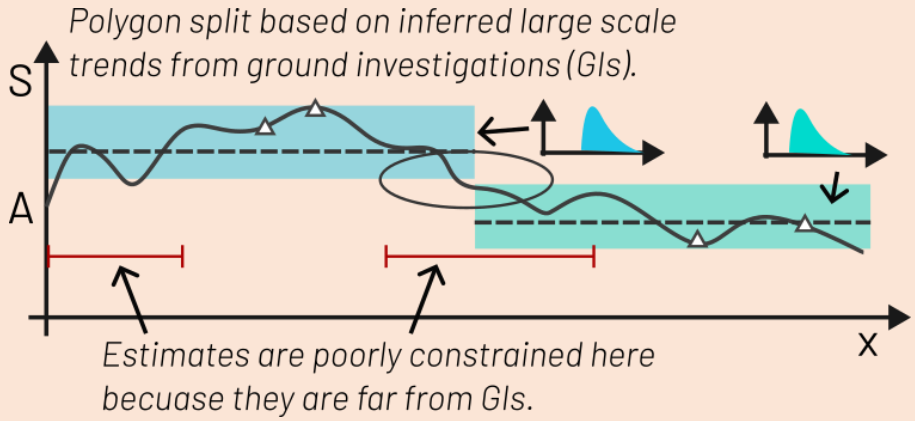

Figure 8.5: Conceptual drawing of potential for extrapolation error in Tier 2 polygons

At a regional scale, this extension or extrapolation is considered unbiased since both low vulnerability and high vulnerability polygons are extrapolated. Additionally, there are further mitigating factors:

- The spatial variability estimate increases with area (Section 8.5). Therefore, large extensions result in larger expected standard deviation of the spatial variability. A larger standard deviation means that individual GI have less influence on the updated distributions.
- The spatial weighting factors used for the Bayesian updating (Section 8.7.3) reduce the impact of several closely spaced GI's influencing a large area.
- The Bayesian updating process updates both the mean and the standard deviation. Therefore, if a single GI deviates substantially from the geospatial estimate, this results in only a modest change in the mean and increase in the standard deviation. This reduces the impact of a small number of GI having large changes to predictions.

For the development of MBIE/MfE guidance maps, the boundary uncertainty is more important and the estimated LDMs from these would not be directly applicable for liquefaction mapping for land-use planning (e.g. MBIE/MfE Guidance (2017)) as discussed in Section 12.2.

8.4 Development of the geospatial model

The geospatial model provides an estimate (15th and 85th percentile values to produce a lognormal distribution) of an LDM at any point of interest based on geomorphological attributes (i.e. without taking account of local GIs).

8.4.1 Background

There are three common approaches to estimate LDMs: geospatial models, triggering approaches and effective stress analyses. The latter requires ground motion records, is highly site specific, and has a large computational demand. It is therefore not compatible with the national scale liquefaction model. The triggering approach is common for site-specific assessments but only provides a point estimate of liquefaction, therefore making it challenging to generalise across a broad area with

limited data. The geospatial approach is well suited to regional scale mapping, however, it suffers from limited case history data (Zhu et al., 2017).

Geyin et al. (2022) recently proposed a hybrid approach where geospatial models could be used to approximate triggering approaches using ML. This approach leverages the extensive knowledge embedded in the triggering methods and generally overcomes the lack of data issue (with some exceptions). This powerful approach provides point-wise estimates of any CPT-based LDM and probabilistic bounds.

The main limitation of this approach is that the model cannot provide an estimate in conditions where there are no CPTs (e.g. gravelly riverbeds are unlikely to liquefy but also unlikely to have CPT records). Furthermore, even within a geomorphology, the CPT readings are biased towards more penetrable soils which are more likely to be liquefiable. Finally, depending on the prediction model adopted, the high correlation of some input features (e.g. geomorphology and distance to river or coast) can result in unusual trends. An adapted version of the approach by Geyin et al (2022) is adopted here, where the adaptions are made to address these issues. The key changes were:

1 The use of BH and CPT to develop predictions to reduce the issues around under-representing non-penetrable soils.
2 The use of a deterministic process to develop the decision tree for predictions, allowing rules to be directly implemented to avoid overfitting on small datasets and to correct for trends that are inconsistent with literature.
3 Hierarchical features that allow improved precision when sufficient data is available by using a more extensive set of geomorphological features and reduced precision by aggregating data from similar features.
4 The use of functions to define the relationships between the LDM and PGA, Mw and GWD. This enables the whole model to be saved into csv file in ~150 rows and enables easy review of the model. Furthermore, the functions could be constrained to produce sensible trends for each of these features.
5 A down-scaling of the data prior to model fitting using two factors, one to reduce GIs when over-representing a very localised area, and a second factor to reduce over-representation of a region.

8.4.2 Key steps

To develop the LV geospatial model, the following steps were undertaken:

1 Retrieve the precomputed LDMs from all GIs from the GI model.
2 Assign weighting values to each GI (See Section 8.4.3).
3 Fit distributions to precomputed LDMs for characteristic geomorphology groupings (see Section 8.4.4).
4 Fit relationships for LDM versus PGA (see Section 8.4.5).
5 Fit relationships for LDM versus GWD (see Section 8.4.6).
6 Cross-check LDM distributions (see Section 8.4.7).

The data structure of the model is provided in Table 8.1 in Section 8.1.

8.4.3 Geospatial model weighting factor

GIs are not uniformly distributed and therefore some ground conditions are over-represented in the dataset. To reduce the bias introduced to the model by areas with very high densities of GIs, such as Christchurch, the influence of each GI point is weighted. Specifically, the weight of a GI is a number between 0 and 1 which is inversely proportional to the square root of the number of nearby

investigations. This means a GI has less influence on the geospatial model if it is surrounded by other GIs, and the influence of a small area only increases by the square root of the number of GIs in that area (once above a minimum count). The weights are used to reduce histogram counts prior to fitting the geospatial distributions in Section 8.4.4 and the cross-checking of the geospatial distributions for overfitting in Section 8.4.7.

The weighting factor was determined using two characteristic buffer distances of 100 m and 1 km. The first buffer distance is to reduce the impact of dense clusters of GIs that sample a very localised area (e.g. a subdivision with many GIs). The second distance is to reduce the impact of regions with a higher number of GIs (e.g. Canterbury), since regional differences could be expected.

The calculation for the weight factor, w, is presented in Equation 16, where n_{100m} and n_{1km} are the number of GIs within 100 m and 1 km respectively. Equal weighting is given to both these measures. The coefficients of 10 and 100 for the two components were determined to have no reduction for the majority of low-density readings. Comparisons of the two components of the equations versus the histograms of n_{100m} and n_{1km} are provided in Figure 8.6.

Equation 16:

$$w = \frac{0.5}{\sqrt{\frac{\max(10, n_{100m})}{10}}} + \frac{0.5}{\sqrt{\frac{\max(100, n_{1km})}{100}}}$$

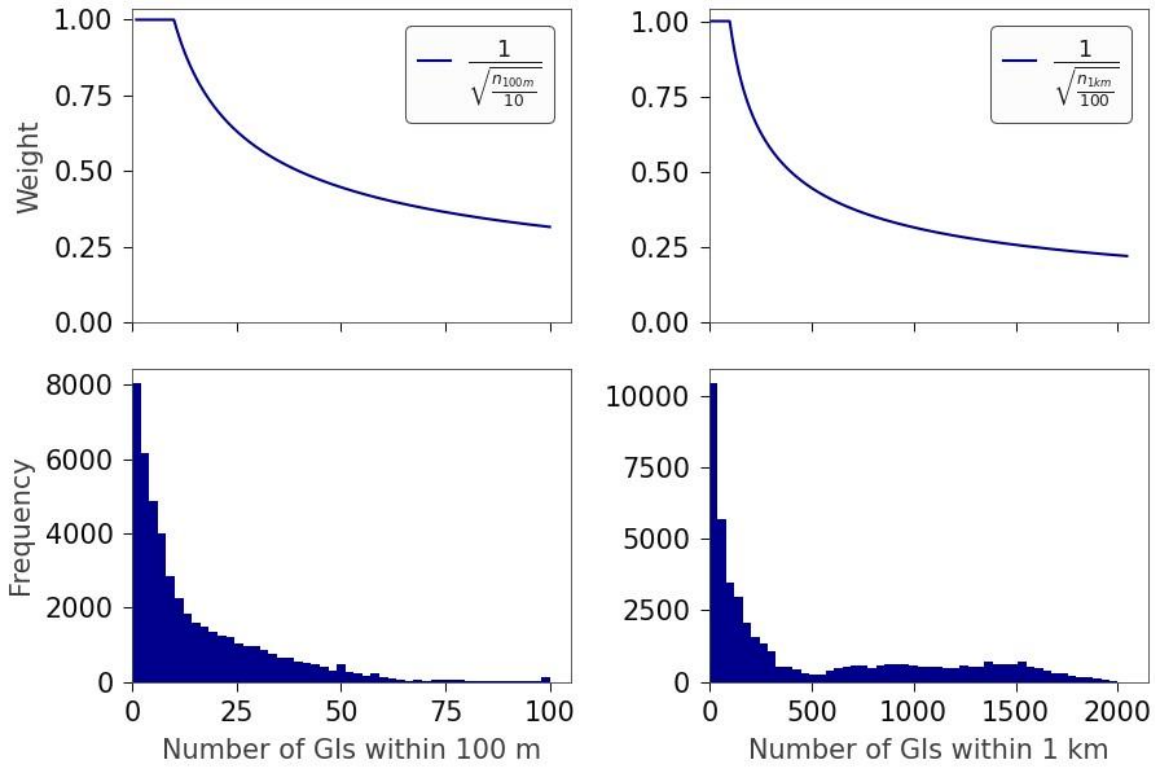

Figure 8.6: (Top row) GI weighting functions for 100 m and 1 km radius for the geospatial model. (Bottom row) Count of GIs that have a certain number of GIs within 100 m and 1 km radius.

Over-representation bias

The choice of buffer distances for the geospatial model were selected to represent the scale of subdivisions and cities, and the coefficients of 10 and 100 were selected as convenient and sensible numbers (noting that the variograms show high variability in LSN even at distances less than 10 m (see Figure 7.20)). The use of weighting factors did result in changes to the geospatial model compared to not using weighting factors, however, adopting alternative coefficients of 20 and 200 resulted in only a minor difference. On investigation of geomorphology categories with few data points (< 50), the use of the smaller coefficients was preferred since it reduced the development of categories that were based on very localised soil sampling (see Section 8.4.4 for details). In the future, further analysis using variograms and comparisons across regions could identify more appropriate weighting factors that would most likely be dependent on the geomorphology category.

The issue of over-representation or narrow sampling of small areas is also addressed by enforcing a minimum log(P85/P15) of 0.7 for polygons with a weighted sample count less than 50 (in Section 8.4.7), and addressed again in the Bayesian updating in Section 8.7.3 although handled in a different manner due to the focus in that case on a single polygon.

8.4.4 Fit distributions for LDMs

The weighted GIs were spatially joined to the geomorphology model. A lognormal distribution was fitted to the weighted LDMs for each PGA and GWD combination (see Section 7.4) with Mw = 7.5. Note that Mw is handled in the geospatial model using a simple scale factor defined in Section 8.4.9. The distribution was fitted first to all GIs within each l3_yp (geomorphology) category, then to each

l4_yp (geomorphology + epoch) category, and finally to l4_yp with main_rock from the NLM Geomorphology Model (referred to as L5 for simplicity). Additionally, the l3_yp, l4_yp and L5 categories were split if there were polygons where the geomorphology description contained the word “pumice”. As an example, this created distributions for both Holocene River channel and Pumiceous Holocene River channel.

A lognormal distribution was chosen due to it being simple (stored using just two values), interpretable, the scale is constrained to above 0 (consistent with LSN), and it allows for a simple update of the distribution using Bayesian updating (see Section 8.7.4). A normal distribution was not adopted due to the distribution producing values below zero, while a truncated normal distribution cannot easily be updated with Bayes updating. The distribution was stored as the 15th and 85th percentile of the fitted distribution (P15 and P85 respectively) to allow this distribution to be reconstructed for forward prediction. Figure 8.7 shows an example of the fitting for l4_yp category of Holocene Alluvial fan and plains.

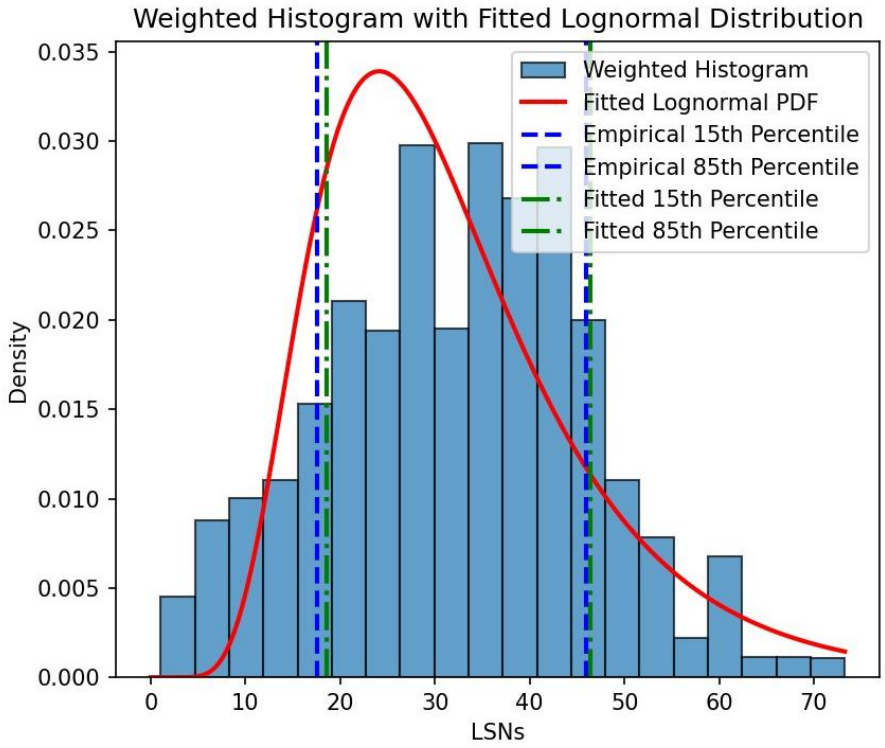

Figure 8.7: Example fit of lognormal distribution using the Gompertz function against a weighted histogram for Holocene Alluvial fan and plains at PGA = 0.6 g, Mw = 7.5 and GWD = 1.0 m

8.4.5 Fit relationship with PGA

Once the fitted P15 and P85 was determined for all PGA and GWD combinations and all L3, L4, and L5 categories, a relationship was fitted to both percentiles as a function of PGA where GWD = 1.0 m and Mw = 7.5. The relationship adopted the Gompertz function defined in Equation 17 and was fitted with least squared error.

$LSN_{ref_{gw}}$ in Equation 17 is the LSN at PGA = 0.6 g, Mw = 7.5 for a specific GWD (for fitting the coefficients GWD = 1.0 m was used), $PGA_{M7.5}$ is the PGA for Mw = 7.5, b and c are equation coefficients that were constrained to produce reasonable trends. b was constrained to be between 1 and 10, while c was constrained to be between $\log(b) + 10$ and 30, the limits are shown in Figure 8.8. The constraints do not force LSN to be equal to LSN_{ref} at PGA = 0.6 g, Mw = 7.5, GWD = 1.0 m

(e.g. see lower limit in Figure 8.8), since a better fit to the full range of PGA values can be achieved by not forcing this constraint. Figure 8.9 shows an example of the fitting for l4_yp category of Holocene River channel.

Equation 17:

$$\frac{LSN}{LSN_{ref_{gw}}} = e^{-b \cdot e^{-c \cdot PGA_{Mw7.5}+2}}$$

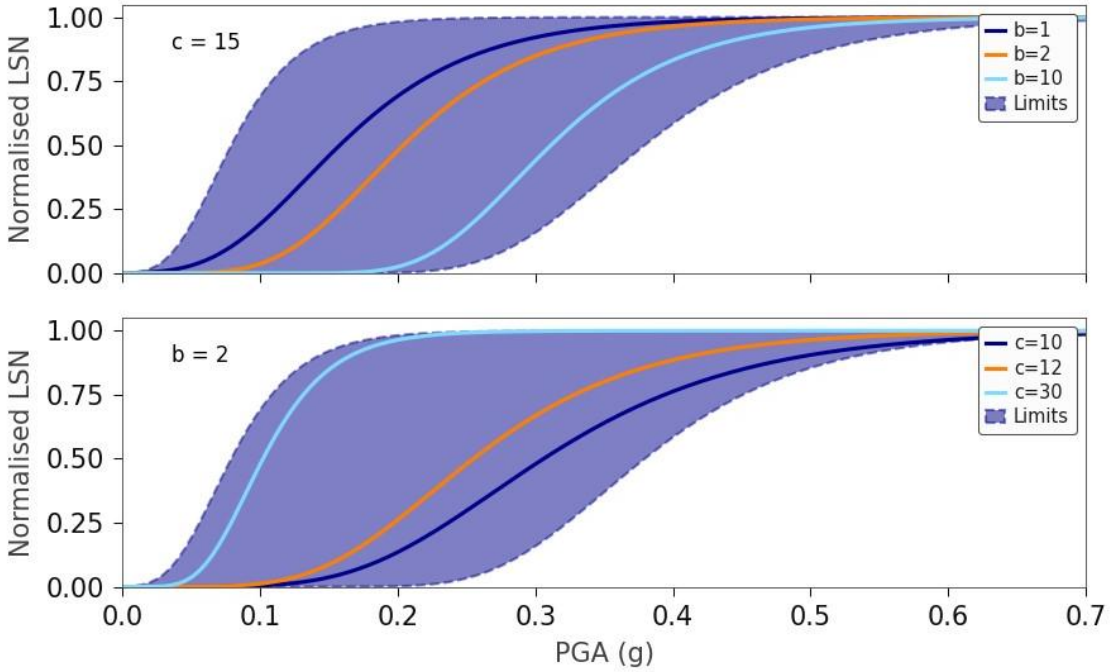

Figure 8.8: Limits on Gompertz function coefficients

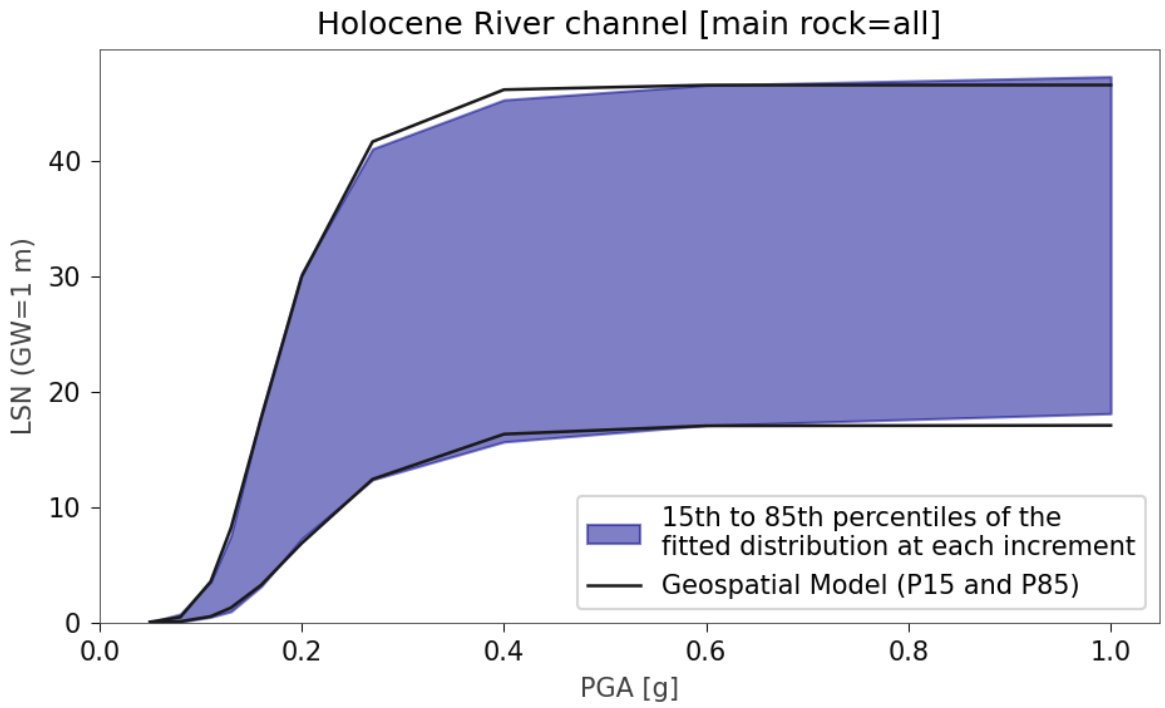

Figure 8.9: Example fitting of Gompertz function for PGA relationship for Holocene River channel for Mw = 7.5

The LSN to PGA relationship was fitted in linear LSN space (i.e. not log(LSN)) and therefore put greater relative weighting to larger PGA values in terms of the framework outlined in Section 4.3.1.1. This decision was deemed appropriate since the function was fitted across all of the PGA increments outlined in Section 7.4.1, which has many points at the low PGA range and therefore the range of PGAs was considered well balanced when fitting in linear LSN space.

8.4.6 Fit relationship with GW

The influence of GW was determined by fitting the coefficient, a, in Equation 18 to the percentiles from the fitted distributions for different GWDs, as shown in Figure 8.10a. GWD is the GWD in metres, LSN_{ref} is the LSN at PGA = 0.6 g and Mw = 7.5 and GWD = 1.0 m and $LSN_{ref_{gw}}$ is the LSN at a specific GWD for PGA = 0.6 g and Mw = 7.5. The coefficient a was fitted to both P15 and P85 and then the average of a was adopted as the final value. Figure 8.10b shows the fitted P15, fitted P85 and average for a normalised LSN.

Equation 18:

$$\frac{LSN_{ref_{gw}}}{LSN_{ref}} = \frac{a}{GWD + a - 1}$$

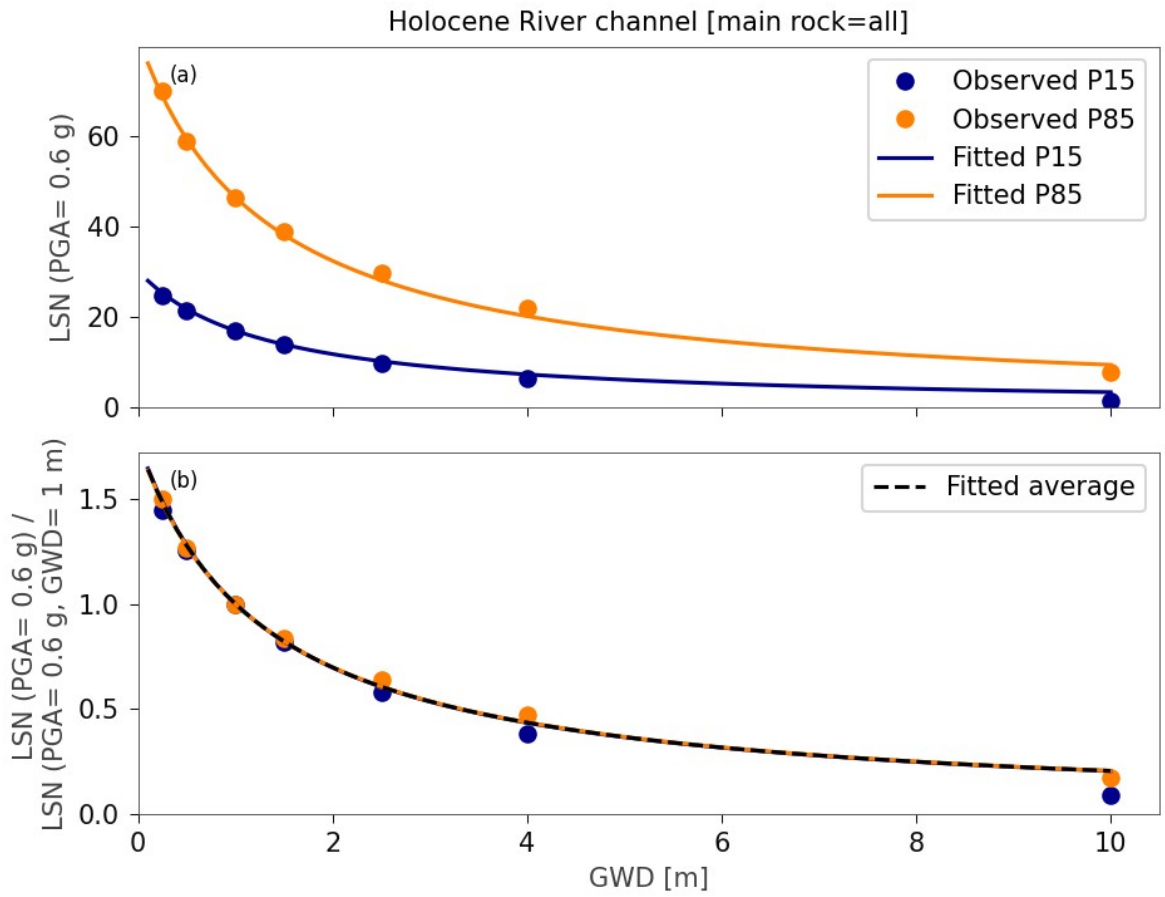

Figure 8.10: Example fitting of the GW influence coefficients for P15 and P85 for Holocene River channel

8.4.7 Cross-check distributions

The following cross-checks and corrections were applied to the model to better constrain the outputs:

1 All distributions that consisted of a weighted count of readings less than 20 were then excluded. This rule was applied to avoid over fitting to categories that had insufficient data.

2 In some cases, there was insufficient data to produce a distribution even at the l3_yp level. In these cases, data from a similar l3_yp category was added to the category to allow a prediction to produced. The following aggregations were applied:

- Marine Terraces and Plains had insufficient data and Talus was added.
- Beach High Wave Energy had insufficient data and Foreshore was added.

3 When P85 for main_rock = gravel exceeded P85 of a main_rock = sand for the same geomorphology and epoch (at any GWD and any PGA greater than 0.1 g), the data from both categories was merged. The same approach was applied for P15. This was indicative of a bias since the results were inconsistent with expected behaviour. The merge resulted in a wider distribution for both categories and therefore greater uncertainty.

4 When the average of P15 and P85 of an early epoch exceeded the average of P15 and P85 of a later epoch (at any GWD and any PGA greater than 0.1 g), the data from both categories were merged. This was indicative of a bias since the results were inconsistent with expected behaviour. The merge resulted in a wider distribution for both categories and therefore greater uncertainty.

5 When the readings count was less than 50 and log(P85/P15) was less than 0.7, the P15 was reduced and P85 increased equally in log space until this ratio was achieved. This was to avoid narrow distributions due to limited data, and the ratio was chosen based on ratios from large datasets.

8.4.8 Data structure

The LV geospatial model is a single csv file with the headers detailed in Table 8.3.

Table 8.3: LV geospatial model headers

Column name	Description
l3_yp	Geomorphology category from NLM Geomorphology Model
epoch	Epoch category from NLM Geomorphology Model, or "all" if all epoch categories have been aggregated
main_rock	Main rock from NLM Geomorphology Model, or "all" if all main_rock categories have been aggregated
n_gi	Number of GIs corresponding the l3_yp, l4_yp, or L5 category
n_cpt	Number of CPT
n_bh	Number of BH
n_weighted	Weighted number of GIs
lsn_ref_p15	The 15th percentile of a fitted lognormal distribution corresponding to LSN for PGA = 0.6 g, Mw = 7.5, GWD = 1.0 m
lsn_ref_p85	The 85th percentile of a fitted lognormal distribution corresponding to LSN for PGA = 0.6 g, Mw = 7.5, GWD = 1.0 m
gomp_p15_b	The Gompertz function coefficient b for 15th percentile LSN
gomp_p15_c	The Gompertz function coefficient c for 15th percentile LSN
gomp_p85_b	The Gompertz function coefficient b for 85th percentile LSN
gomp_p85_c	The Gompertz function coefficient c for 85th percentile LSN
ktop	The coefficient for the GW relationship for 15th percentile LSN

The geospatial model is provided as Digital Supplement H - *lsnpl50_m1_gs_model.csv*.

8.4.9 Implementation details

To enable the highest precision distribution from the hierarchical system, the model is accessed for predictions in the following order: L5, l4_yp, l3_yp. That is:

1 Attempt to load the row that matches all the geomorphology, epoch and main_rock for a given polygon.

2 If there is no match, then set main_rock to "all".

3 If there is still no match, then set epoch to "all" and only use the geomorphology.

Note that the pumice categories are not used in forward prediction since the CPT-based liquefaction triggering analysis was developed for hard grained soils. While future model versions may make use of the pumice categories, the identification of them at this point is simply to remove them from the geospatial model.

Once the matching row is identified, the LSN_{ref} as well as PGA and GWD coefficients for the two percentiles are extracted from the row. The LSN_{ref} percentiles are then converted to the specific

GW and PGA and Mw of interest. Figure 8.11 shows an example for L5 category of Holocene River channel with main_rock = gravel, for PGA = 0.22 g, Mw = 6.6, GWD = 2.5 m. The key steps shown in Figure 8.11 and are:

1 Obtain the LSN_{ref} for P15 and P85 for the specific geomorphology class.

2 The LSN_{ref} percentiles are corrected to the specific GW of interest ($LSN_{ref_{gw}}$) using Equation 18 (Figure 8.11(a)).

3 PGA is adjusted to an equivalent PGA at Mw = 7.5 ($PGA_{Mw7.5}$) using Equation 19, where MSF is a magnitude scale factor defined in Equation 20 from Idriss & Boulanger (2008)

4 The $LSN_{ref_{gw}}$ percentiles are used in Equation 17 to determine the percentile values for the given $PGA_{Mw7.5}$ (i.e. the blue dots in Figure 8.11(a) correspond to the blue dots in Figure 8.11(b), and the orange dots in Figure 8.11(b) are the intercept of the equivalent PGA with the LSN-to-PGA relationships for the two percentiles).

5 Produce a lognormal distribution from the provided percentiles (Figure 8.11(c)) (Note that the orange dots in Figure 8.11(b) and correspond to the orange dots in Figure 8.11(c)).

Equation 19:

$$PGA_{Mw7.5} = \frac{PGA}{MSF}$$

Equation 20:

$$MSF = 6.9e^{-\frac{M_w}{4}} - 0.058 \leq 1.8$$

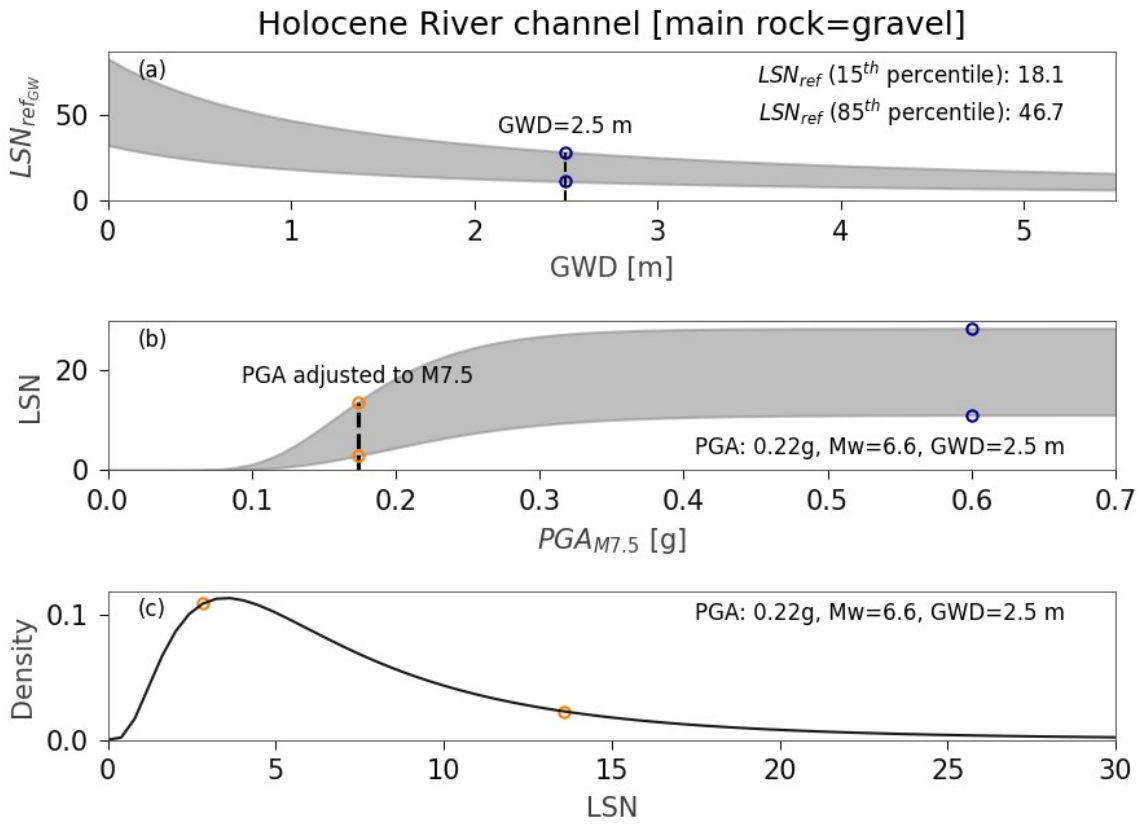

Figure 8.11: Example of accessing the geospatial model to produce a prediction, a) Determine the GWD corrected LSN_{ref}, b) Determine LSN percentiles for given seismicity, and c) Produce a lognormal distribution

Note that the MSF from Idriss & Boulanger (2008) was adopted for correcting the magnitude since it provides a single equation for sand, whereas the magnitude correction from Boulanger & Idriss (2014)is dependent on the q_{c1Ncs} value, making it not directly applicable to a distribution of GIs.

8.5 Development of spatial variability function

An estimate of spatial variability of a polygon is needed as a prior estimate for the Bayesian updating process, specifically, the standard deviation in log(LSN). To estimate the spatial variability of a polygon, the spatial variability was first quantified through variogram functions which quantify the semi variance as the distance between measurement increases. Note that the semi variance tends towards the standard deviation squared divided by 2 at large distances. The variograms were then converted to standard deviation versus area through random field theory. However, for LSN there are two significant challenges:

1 LSN is dependent on PGA, Mw and GWD and therefore variogram functions would be dependent on the selected PGA, Mw and GWD.

2 LSN is significantly different for different geomorphologies.

To overcome these challenges, a normalised variogram function was developed and normalised by the variance of the whole population to yield a sill of 1. The normalised variogram function could then be multiplied by the variance for a given PGA, Mw, GWD and geomorphology to establish the spatial variability. To establish the normalised variogram function, four geomorphology categories were selected that had large amounts of data and represented a range of geomorphologies. The normalised empirical variograms for log(LSN_{ref}) for Holocene Loess, Holocene River channel, Holocene Lacustrine and playa, and Pleistocene Igneous are all shown in Figure 8.12. Note that GIs in

pumiceous soils were excluded for this analysis and that the variance in the population differs from the variance of the fitted lognormal functions in the geospatial model since lognormal distributions are not a perfect fit to the data.

An approximate normalised variogram was fitted to the empirical curves (Equation 21), where x is the distance in metres, $\sigma^2_{\log(\mathrm{LSN})}$ is the variance of the whole population, and $\sigma^2_{\log(\mathrm{LSN}),x}$ is the covariance at some distance x. The exponential shape of the function was dictated by the ability of the GSTools Python package to simulate within a random field. Note that the relationship overestimates variability for the Holocene River channel geomorphology. This means that there is lower variability across small distances (up to 30 km based on Figure 8.12) than what is estimated from the geospatial model using the l4_yp geomorphology category and the fitted normalised variogram relationship. The additional refined classification using the l5_yp (i.e. using main_rock) would partially reduce this difference, and potentially future work could provide further spatial refinement (e.g. at the catchment level).

Equation 21:

$$\frac{\sigma^2_{log(LSN),x}}{\sigma^2_{log(LSN)}} = 0.6(1 - e^{-0.001\mathrm{x}}) + 0.4$$

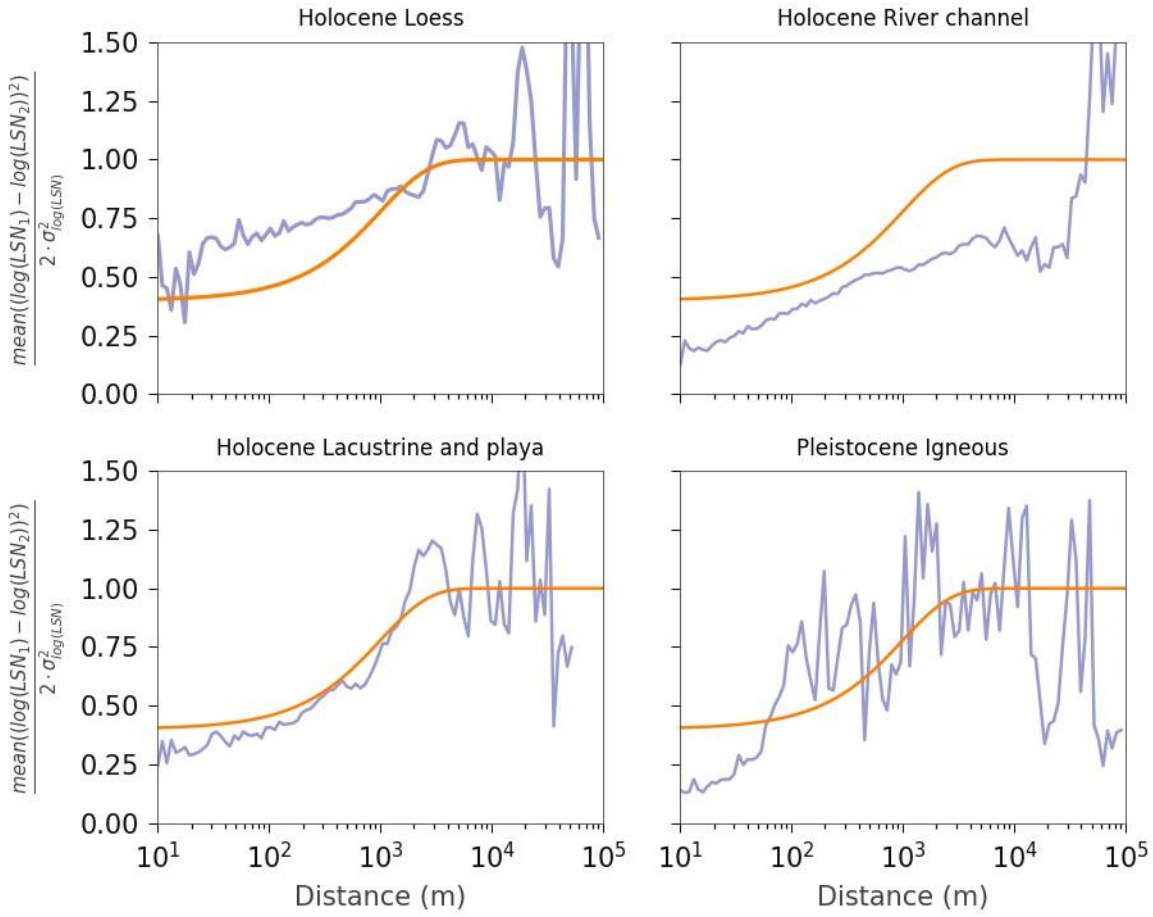

Figure 8.12: General variogram function versus empirical variograms for four types of geomorphologies

To convert from a variogram to a standard deviation versus area relationship, the following steps were taken:

1 Generate a 2D 4000 km by 4000 km spatial random field using the GSTools Python package with a covariance model equal to the fitted variogram (Equation 21) with grid spacing of 10 m. The use of the covariance model means that points within the random field would approximate the variogram.

2 Randomly sampling the field with square samples, with increasing edge size from 32 m to 25,000 m, where 100 samples were taken for each edge size. For each sample, compute the standard deviation and mean of the values in the square.

3 For each edge size, compute the area and the mean, 15th and 85th percentiles of the standard deviation across the 100 samples for each edge size.

4 Plot the mean, 15th and 85th percentiles of the standard deviation versus area (Figure 8.13), and fit an expression to quantify the relationship (Equation 22). Note that the equation produces the normalised standard deviation since the normalised variogram function was used in the random field. The 15th and 85th percentiles were fitted as +/- 0.05.

Equation 22:

$$\frac{\sigma_{log(LSN),polygon}}{\sigma_{log(LSN),geospatial}} = \sqrt{0.6\left(1 - e^{-0.001\sqrt{Area/\pi}}\right) + 0.4}$$

In Equation 22, $Area$ is the polygon area in metres. This equation assumes that polygons are square in shape, so would underestimate likely variability for more irregular shaped polygons and overestimate more circular polygons. Equation 22 shows that for small areas (~<0.01 km^2), the expected spatial variability in LSN, $\sigma_{log(LSN),polygon}$, is equal to 0.63 of the variability from the geospatial model, and for large areas (~100 km^2), the expected spatial variability equals the geospatial model. This means that as polygons get larger, the local GIs have less and less impact on the estimated LSN distributions. This is because for large polygons, it is expected that the full range of the geospatial model prediction is present within the polygon.

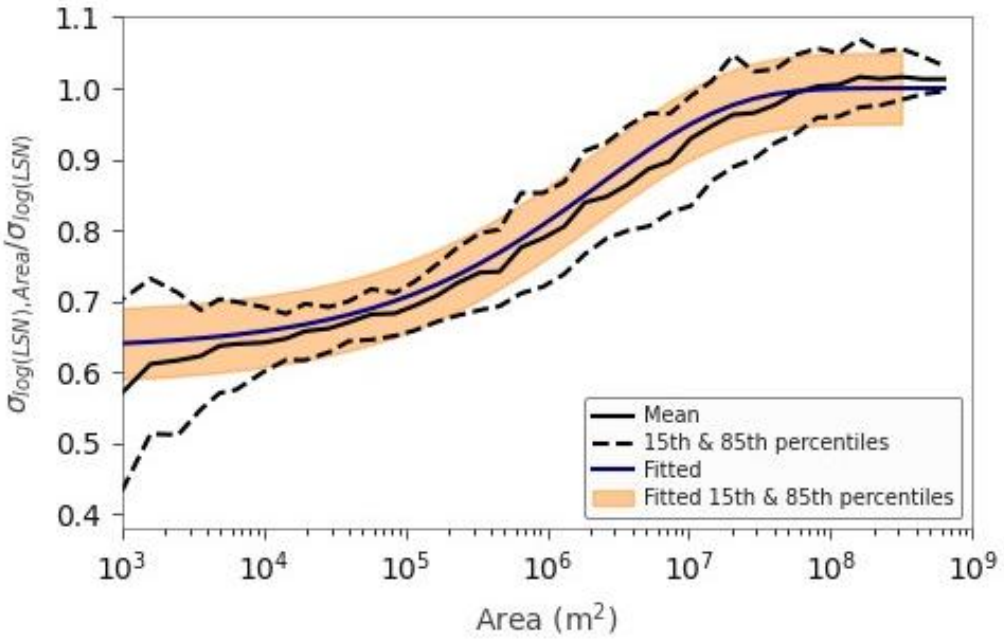

Figure 8.13: Normalised standard deviation versus area relationship derived from simulation of a random field

8.6 Development of SSPs

The use of SSPs allows an efficient and readily interpretable approach to define the ground response to liquefaction. The SSP is formulated around an assumption that the ground conditions anywhere within the polygon can be described by a single distribution.

However, if there is a notable spatial trend, then that would invalidate the spatial independence assumption and that would increase the error in the model. Therefore, the key variables that control the extent of an SSP are the estimated level of spatial variability, and the level of confidence in the ground conditions (largely controlled by spatial density of GIs). The different categories of SSP are identified based on the evaluation of spatial variability and density of the GIs.

Previously developed liquefaction models have typically adopted a similar polygon-based approach. However, the process is normally manual and therefore subject to the typical drawbacks associated with all manual processes (e.g. time-consuming, costly and inconsistent). The adopted automated approach attempts to replicate many of the steps that are performed manually without being subject to these drawbacks.

While the full automation may create unusual artifacts (e.g. small gaps between polygons and polygons that are large circles), the full automation means that as more GI are included in the database they can automatically be updated (and improved). Furthermore, full automation provides consistent national handling of polygon creation and bias can be evaluated based on the implemented automated process. Manual processes can take advantage of additional local knowledge; however, this could potentially bias the model to over or underestimate liquefaction if this local knowledge is more concentrated on particularly areas.

8.6.1 Key steps

The following process was followed for developing the SSP file.

1 Identify Tier 1 polygons (see Section 8.6.2).

2 Identify Tier 2 and Tier 3 polygons in parallel (see Sections 8.6.3 and 8.6.4).

3 Combine the different tiers and handle spatial overlaps (see Section 8.6.5).

8.6.2 Tier 1 polygon algorithm

Tier 1 polygons are the geomorphology model polygons clipped to the flatland area. Waterbodies are also filtered out in this step. To perform the clip, a spatial overlay is performed between the geomorphology and the flatland datasets.

The overlay can result in small polygons along the edge of the Flatland Model, which are below the small area threshold defined in Section 5.3.5. These small polygons are created where the edges of geomorphology polygons lie closely but not perfectly along the boundary of the flatland area.

A small polygon is defined as any polygon with an area less than 40,000 m^2. These small polygons are either merged into adjacent polygons or removed entirely if there are no adjacent polygons within the flatland overlay to merge them with. The small polygon is merged with the polygon with the longest adjacent length determined by the polygon with the largest intersection area of the polygon's buffer, at a buffer distance of 0.01 metres. This distance is small and is mostly to ensure an area is created by the intersection, and to avoid any floating-point errors. A visual representation of this process is shown in Figure 8.14 below.

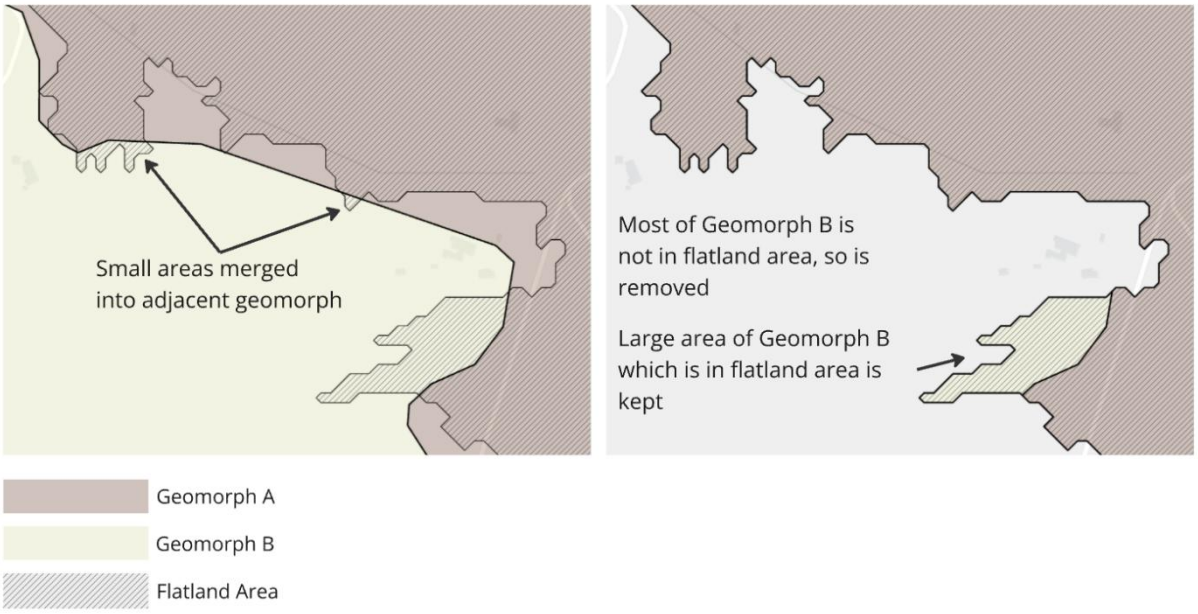

Figure 8.14: Tier 1 Polygon method

8.6.3 Tier 2 polygons algorithm

Tier 2 polygons are created to reduce the size of the tier one polygons where there are sufficient GIs to better quantify the soil profile. The Tier 2 process was applied independently to each Tier 1 polygon (as shown in Figure 8.15):

1 **Identify clusters of very closely spaced GIs**. Find GIs that were close together to prevent polygon boundaries between them. The agglomerative clustering algorithm from scikit-learn with a distance threshold of 100 m and linkage rule of "complete" was used. This algorithm merges GIs into clusters, it identifies the closest GIs first and continues to merge until a merge would result in the maximum distance exceeding 100 m between any two GIs.

2 **Use Voronoi expansion of GI points to create initial Tier 2 polygons**, where the expansion is constrained by the boundary of the Tier 1 polygon and a buffer distance of 5 km. Dissolve the polygons together where they are in the same closely spaced GI clusters, as identified in Step 1 of Figure 8.15. Dissolve in this context means to iteratively merge adjacent or overlapping polygons that share a common boundary into a single larger polygon.

3 If the area of the smallest polygon is less than a small area threshold, $\text{Area}_{\text{thres}}$ of 2.25 km^2 then, **order the polygons by area**, starting with the smallest area.

4 **For each polygon, calculate the average** within the polygon as the mean of $\log(LSN_{ref})$ from all GIs in the polygon.

5 **Merge polygons**. Iterate over the polygons, performing the following steps:

   a Find all adjacent polygons which share a border with the current polygon.

   b Calculate the weighted difference metric between each adjacent polygon and the current polygon. This is calculated as the difference in mean between the two polygons, divided by the intersection length between the two polygons. A merge is then prioritised where the two polygons share a large border, and the liquefaction response is similar.

   c Find the adjacent polygon with the lowest weighted distance metric. This will be referred to as the merge candidate.

      i Assess whether to merge the polygons using the following logic:

ii Always merge if the current polygon area is less than a minimum area threshold of 250,000 m2.

d If the difference in the mean $\log(LSN_{ref})$ is less than 0.05, merge.

e Depending on the output from steps a to d, merge the current polygon with the merge candidate polygon. Then calculate the new average liquefaction response for the merged polygon.

6 Steps 3 – 5 are repeated until there are no polygons less than $Area_{thres}$, or until there are no viable merge candidates for all remaining polygons.

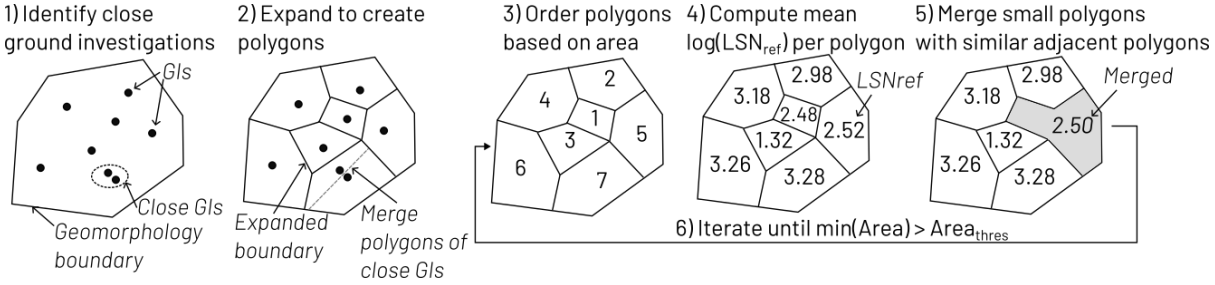

Figure 8.15: Key steps for developing Tier 2 polygons shown for a single geomorphology polygon

The algorithm parameters (i.e. distance threshold of 100 m for the agglomerative clustering algorithm, the $Area_{thres}$ of 2.25 km^2, the minimum area threshold of 250, 000 m^2, minimum difference in mean $\log(LSN_{ref})$ of 0.05), and the calculation of the weighted difference metric, were all established through trial and error by applying the algorithm to different urban areas. The selection of parameter values attempted to balance identifying trends in LSN at the scale of ~200 m to 2 km, while minimising artifacts in the model (e.g. small gaps between polygons, or excessive polygons when there was little difference in LSN values). The selected parameter set generally results in quite large polygons (which are associated with large uncertainty) even in areas with a high density of GI. Further calibration of this process could result in improved polygon selection that reduces overall uncertainty.

8.6.4 Tier 3 polygons algorithm

Tier 3 polygons identify areas of higher confidence in liquefaction response. These high confidence areas are areas with a high density of GIs with similar liquefaction response. To identify these areas GIs, within a Tier 1 polygon are evaluated for how close and similar in liquefaction response they are using a clustering algorithm. Tier 3 polygons are then established around clusters of similar GIs. The specific steps for the Tier 3 identification process are outlined below and shown in Figure 8.16:

1 **Identify all GIs within a Tier 1 polygon.**

2 **Develop a connectivity matrix for the GIs** (see Section 8.6.4.1). This identifies the nearest GIs in six equal angular sectors. It is used to prevent the clustering algorithm from making connections with non-adjacent GIs (i.e. skipping over a GI in the middle of two similar GIs).

3 **Identify clusters of GIs** that are both similar in $\log(LSN_{ref})$ and nearby to one another (see Section 8.6.4.2).

4 **Develop polygons around the identified clusters** (see Section 8.6.4.3).

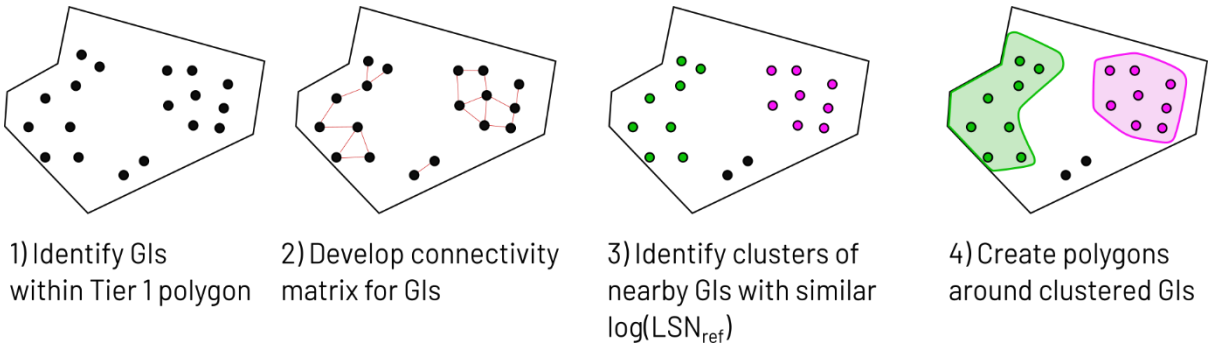

Figure 8.16: Key steps for developing Tier 3 polygons shown for a single geomorphology polygon

8.6.4.1 Connectivity matrix

A connectivity matrix is generated for all GI points within the geomorphology polygon. The matrix defines whether any two points are "connected" and is used within the hierarchical clustering algorithm to force clusters between connected points before not connected points (i.e. prevent skipping over a GI in the middle of two similar GIs). We define two points as connected if, for either point, the other is within 100 m and is the closest point in the sector in which it lies, where each point has six even sectors around it. That is, each sector represents a 60 degree "slice" which has side lengths of 100 m. This is shown in Figure 8.17 to Figure 8.19.

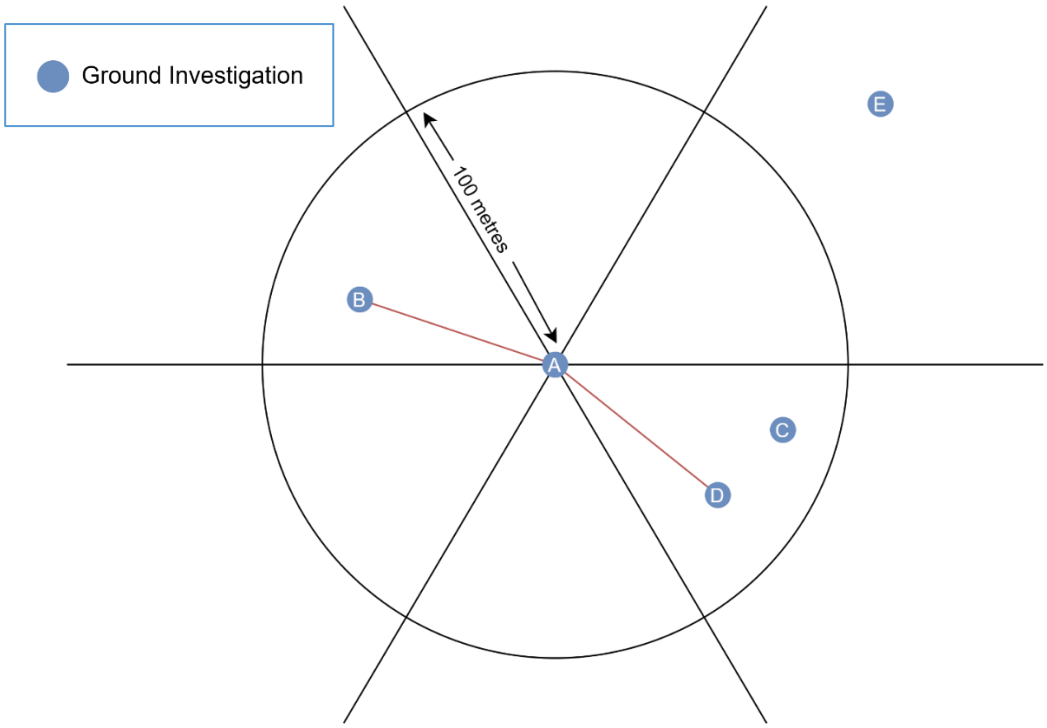

Figure 8.17: Connectivity as from GI A's perspective. In this diagram, A is connected to points B and D, but not C and E. It is not connected to C as D is closer to A than C while being within the same sector, and it is not connected to E as E is outside the 100 m radius.

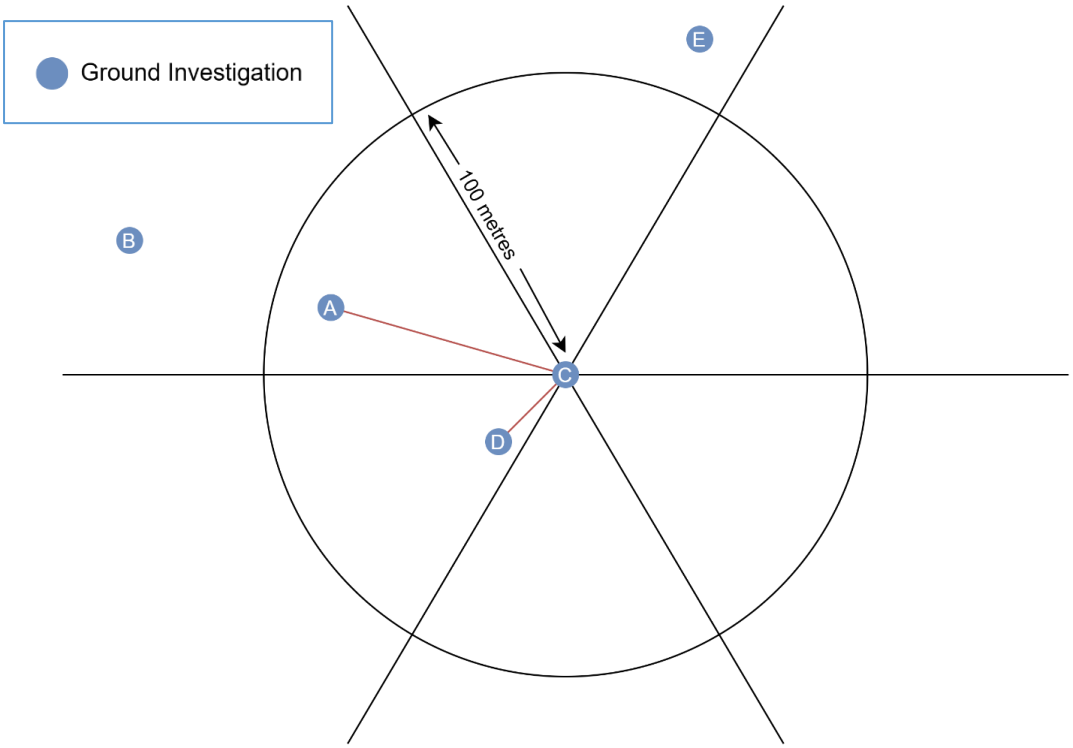

Figure 8.18: Connectivity as from GI C's perspective. In this diagram, C is connected to points A and D, but not B and E as they are both outside the 100 m radius

	A	B	C	D	E
A	-	1	1	1	0
B	1	-	0	0	0
C	0	0	-	1	0
D	1	0	1	-	0
E	0	0	0	0	-

Figure 8.19: Connectivity Matrix of GI A-E, based on Figure 8.17 and Figure 8.18. A green square or "1" shows a connection is present from the column to the row points, e.g. A is shown to be connected with B and D

8.6.4.2 Cluster identification

To identify clusters of GIs with very similar $\log(LSN_{ref})$, the individual GIs were compared for similarity both spatially (i.e. how close are they) and in terms of difference in $\log(LSN_{ref})$. The comparison process develops connections between the most similar GIs and eventually builds a full hierarchical tree of ordered connections. This process was performed using scikit-learn's agglomerative clustering algorithm with the linkage rule set to "single", the connectivity defined using the connectivity matrix outlined in Section 8.6.4.1, and a weighting of 0.05 was applied to

$\log(LSN_{ref})$ to adjust the relative importance of LSN differences against the Euclidean distance between points when evaluating similarity.

The hierarchical tree has a top node (this is the last formed connection) which represents a cluster with all the GIs and has as many leaf nodes as there are GIs. The final clusters were determined from the hierarchical tree by travelling down each branch and evaluating each connection, starting with the last connection (top node). Each connection was evaluated as to whether it should be split or not based on the following criteria. If the standard deviation in $\log(LSN_{ref})$ of all the values in the cluster is above 0.2 then split and move to the child nodes (since the variability is too high). If the standard deviation is less than or equal to 0.2, then consider the following additional criteria:

- If the cluster has less than eight GIs, then reject the cluster since there are insufficient points. Rejecting the cluster means that those GI are no longer potentially part of a Tier 3 polygon.
- Create a concave hull of the cluster using Shapley's concave hull function, and if this shape is not fully contained within the geomorphology, then split the cluster (i.e. if the new SSP polygon would cross into another geomorphology polygon then the polygon would be split, see Figure 8.21).

Figure 8.20 provides a simple example showing only the top-most nodes, starting with 40 GIs in the first node. Since the standard deviation was above 0.2, this node was split into 2 clusters. The nodes down each of the two branches are then evaluated. The right node satisfies the requirements for a Tier 3 polygon and therefore this cluster of GIs is evaluated for the concave hull check before finalising as a Tier 3 polygon. The left node still had a standard deviation above 0.2, so was split further. The left branch below this split only had 4 GIs, so was rejected and those GIs were not used for a Tier 3 polygon. The right branch satisfied the requirements and was evaluated for the concave hull check before being used to developing a Tier 3 polygon.

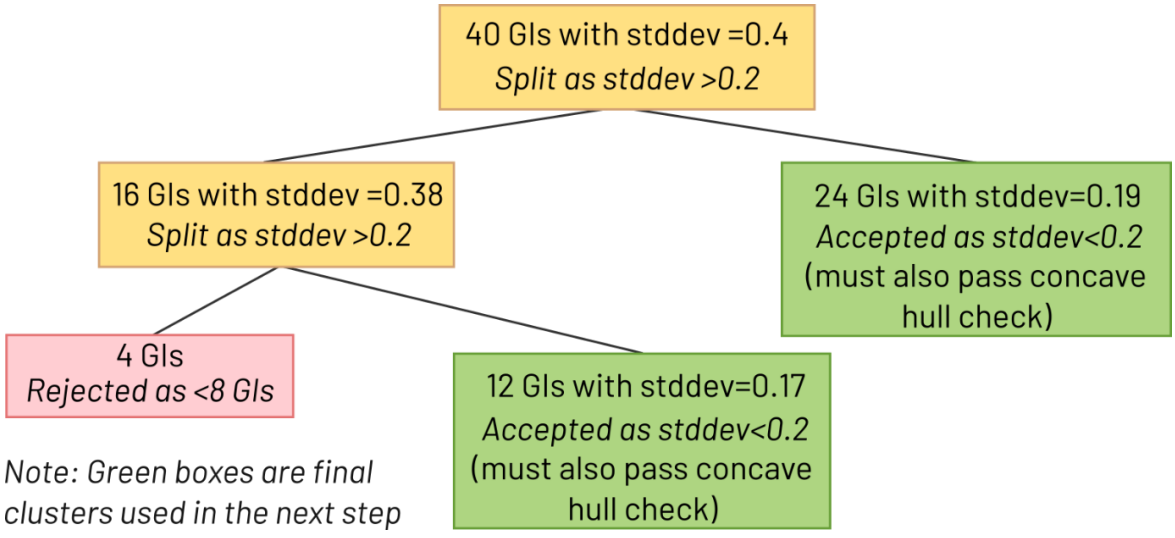

Figure 8.20: Cluster splitting algorithm for Tier 3 polygons

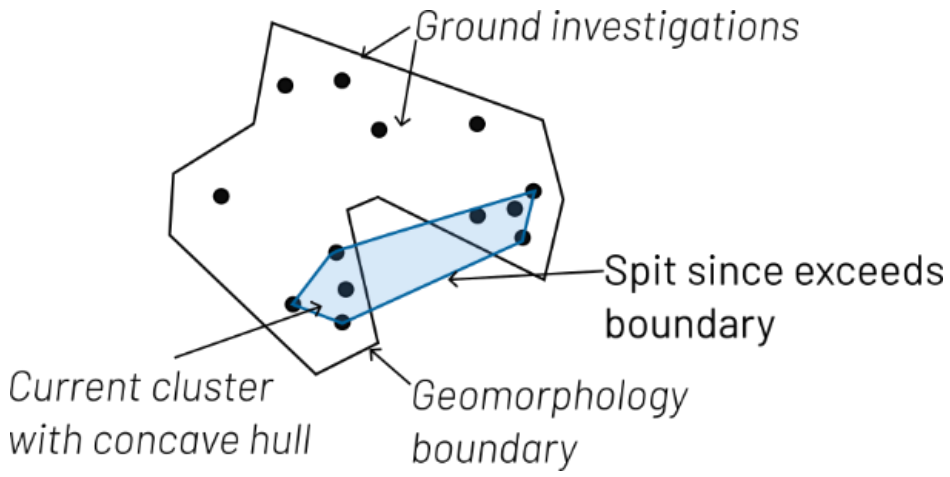

Figure 8.21: Handling clusters that exceed the geomorphology polygon boundary

Tier 3 polygon clustering parameters

The threshold standard deviation for $\log(LSN_{ref})$ to evaluate low variability was set at 0.2 because this was lower than any of the standard deviations from geospatial models using the l5_yp categories, which generally range from 0.3 to 1.0. When comparing the standard deviation ratio of the GIs over the standard deviation of the geospatial model, these polygons would have significantly higher confidence than an average polygon. In the future, this threshold could be lowered to increase the number of Tier 3 polygons and potentially the threshold could be a dependent variable of the geospatial model category assigned to the polygon.

The decision to use a minimum of eight GIs for a Tier 3 polygon was made as eight GIs was generally sufficient to control the final LSN distributions assigned to the polygon with only very little influence from the geospatial model. Future work may revisit this assumption since selecting a smaller number may result in more Tier 3 polygons that would still have sufficiently high confidence.

The $\log(LSN_{ref})$ weight of 0.05 was determined by visually checking the output and balancing the generation of highly spatially irregular clusters when the weight was high, versus higher variability in LSN in the more regular shaped clusters. Future work could be done to objectively calibrate this parameter based on an understanding of the spatial variability of LSN. It may also need to be adjusted if other parameters in the clustering algorithm are adjusted.

8.6.4.3 Creating polygons from clusters

The clusters of GI points were used to establish the boundary of each Tier 3 polygon by evaluating a representative area that those GIs represent. This was done by enclosing them in a single polygon, establishing a buffer zone around the polygon, and handling potential overlaps and edge cases. These steps were achieved using a combination of concave hulls and Voronoi expansion.

To establish the enclosing polygon, concave hulls of the GIs were created. A concave hull is like a convex hull but allows inward pointing "dents" or "caves", thereby representing a more natural boundary for the group of GIs. The shapely concave_hull function was used to establish the concave hulls using a ratio parameter of 5/6. The ratio parameter was set using trial and error with visual inspection to reduce irregular polygons, since a higher value reduces the number of vertices.

The concave hulls were then buffered by 10 m to create representative areas which do not spread too far away from the GIs. An example of how a buffered concave hull is constructed is shown in Figure 8.22, and an example of how these develop side by side is presented in Figure 8.23.

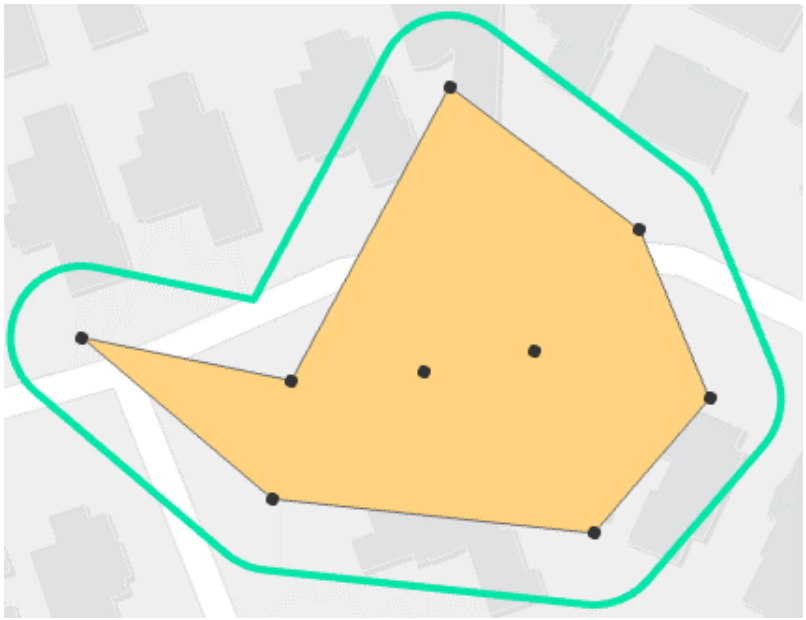

Figure 8.22: Constructing a buffered concave hull, orange showing the initial concave hull, and green outline showing the buffered hull

These buffered concave hulls frequently overlap. An example of this is shown in Figure 8.23 (left). To avoid overlaps in the final polygons, expanded GI polygons were generated by applying Voronoi expansion to all GI and merging the expanded GI polygons based on their cluster. The expanded GI polygons never overlap, so when a buffered polygon had an overlap, the expanded GI polygons from the overlapping polygon cluster was used to remove area from the buffered polygon. The final Tier 3 polygons were then established from the buffered polygons after all overlaps had been addressed (see Figure 8.23 right).

Figure 8.23: Overlapping concave hulls and dissolved Voronoi on the left, final Tier 3 polygon boundaries on the right

The parameters used for the creation of the polygons from clusters were established from trial and error with visual inspection of the outputs. While increasing the buffer zone and the concave hull ratio produces larger and more regular polygons, it also results in more overlaps. The process to handle overlaps results in thin strips between Tier 3 polygons. This is a reasonable approximation since the response between the adjacent Tier 3 polygons is different. However, it results in large model files. Future work would be required to further optimise the selection of these parameters and how the overlap is handled.

8.6.5 Combination of polygons

Two separate SSP files were generated: the *similar-soil-polygons* file (which is one of the module outputs listed in Section 8.1) and an intermediate *ssp-w-overlaps* file. The first file provides spatial coverage of the flatland area, and is used for identifying the unique ID of the SSP that corresponds to the location of interest for using the LDM-per-SSP. This file was generated using the following rules:

1 Where Tier 2 polygons exist, they replace Tier 1 polygons; and

2 Where Tier 3 polygons exist, they replace Tier 2 and Tier 1 polygons.

The *ssp-w-overlaps* file is only used within the LV module and is utilised to identify which GIs should be used within the Bayesian updating process in Section 8.7. For this purpose, GIs that are in Tier 3 polygons are also considered to belong to the underlying Tier 1 and/or Tier 2 polygons (i.e. a GI can be in both a Tier 2 and Tier 3 polygon). This is because the Tier 3 polygons still provide information on the likely LDM distribution within a Tier 2 polygon. However, due to the different spatial weighting applied for Tier 3 versus Tier 2 (see Section 8.7.3) and the larger polygon area leading to a larger distribution for spatial variability, the GIs that are in both have less influence in the Tier 2 polygon. To generate this file only rule 1 above was applied, enabling Tier 3 polygons to overlap Tier 1 and Tier 2.

8.7 Development of LDM-per-SSP table

The LDM-per-SSP table is a table containing different distributions (spatial variability, sample uncertainty, and geospatial) to quantify an LDM for every combination of PGA, Mw, GWD a given SSP (see Table 8.1). The geospatial distribution is simply the prediction from the geospatial model, whereas the spatial variability and sample uncertainty distributions are constructed by combining the geospatial model (Section 8.4), spatial variability function (Section 8.5) and a Bayesian updating process to consider local GI data in each SSP outlined Section 8.7.2.

8.7.1 Basis for Bayesian update

Ideally, each polygon would contain sufficient GI data to completely resolve the distribution of an LDM; however, this is often not possible. The geospatial model can provide an approximation of the LDM for a given polygon; however, it represents the distribution across the whole country. Small polygons would generally have smaller variability and deviate from the geospatial model response due to localised effects. To achieve reasonable estimates, an initial estimate can be made based on the geospatial model and expected spatial variability. It can then be updated using Bayesian updating when there are local GIs within a polygon. The local GIs therefore can reduce uncertainty and potentially capture local effects that were not mapped by the geospatial model.

Given that soil is inherently highly variable, a single GI should have a small impact on the refinement process, and as the area increases the expected variability increases and the influence of a single GI should reduce. Therefore, a significant improvement in estimates could only be expected when there are several local GI, there is a small area, and the geospatial model is not capturing a local trend.

Figure 8.24 conceptually shows the probability distribution of an LDM for a given polygon computed directly from the geospatial model, as well as the true distribution (if we had perfect data), and three GI from within the polygon of interest. Note that the true distribution is narrower than the geospatial prediction, in that the geospatial model does not fully capture the deterministic component of soil variability and therefore the model represents this unmapped variability as an additional error. The Bayesian updating process allows the combination of the geospatial prediction with the local GI data to provide two additional estimates. The spatial variability distribution is the best estimate of the true distribution, whereas the sample uncertainty distribution is the probability of sampling an LSN from that polygon considering the geospatial distribution and the local GI (see start of Section 8 for definitions of these distributions).

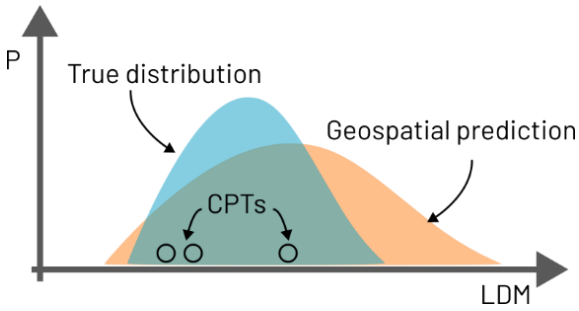

Figure 8.24: Probability and true distributions of an LDM for a given polygon

8.7.2 Key steps

The key steps for implementing a Bayesian updating process were as follows:

1 Identify GIs within polygon using the *ssp-no-overlap* file (see Section 8.6.5). Note that GIs within Tier 3 polygons are also used in Tier 2 polygons, though due to the weighting function and larger standard deviation they have reduced influence in Tier 2 polygons.

2 Compute weights for each GI to handle closely spaced GIs (see Section 8.7.3).

3 Apply Bayesian updating of prediction.

4 Provide different distributions to reflect uncertainty.

8.7.3 Handling closely spaced GIs

In the Bayesian updating approach, the GIs are assumed independent; however, this is not valid if GIs are closely clustered. For example, if there is a polygon with 20 GIs and they are all very closely clustered in the polygon, those 20 GIs should not have as much influence compared to if those GIs were spatially distributed throughout the polygon. This is a very common case with the GI dataset available in the NZGD and TTGD and if not addressed, it significantly biases the model by putting too much weighting on some GI and insufficient weighting on the background model.

To determine the weighting for each GI, a circle of influence is buffered around each GI within a polygon. The radius is 50 m for Tier 1 and 2 polygons and 25 m for Tier 3. A Voronoi expansion is applied when creating these circles of influence to prevent overlapping areas between multiple GIs. The expanded area of influence is then compared to the total potential area of influence if there were no overlaps. This ratio of unique influence is used to calculate the weighting for each GI. An example of this expansion and weightings for five GIs is shown in Figure 8.25 below.

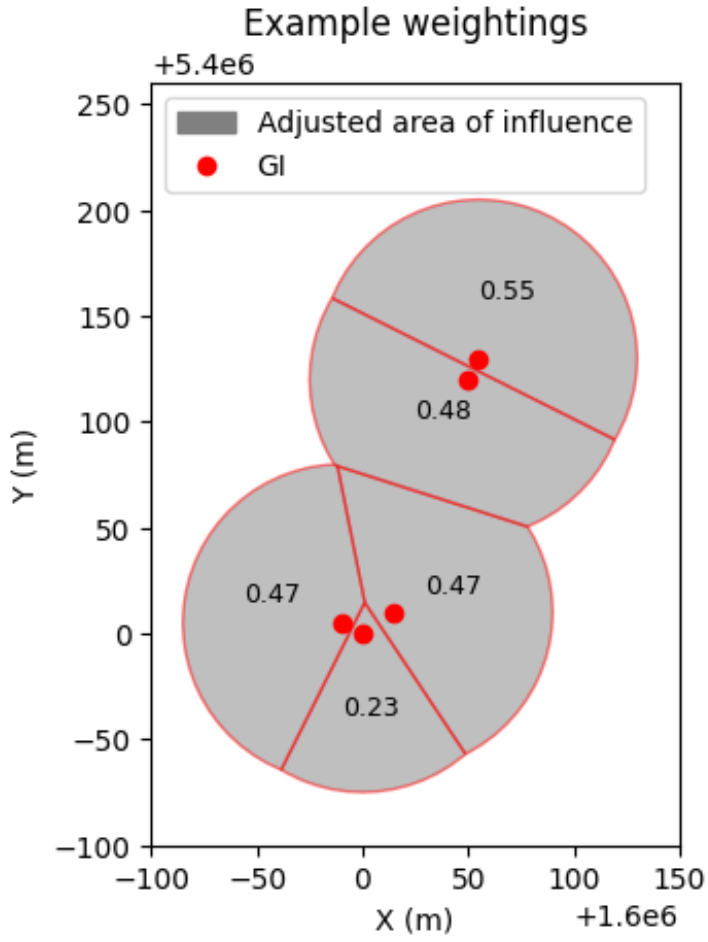

Figure 8.25: Example of determining weighting values for GIs for Bayesian update based on Voronoi expansion, weightings are shown for each GI

The use of a smaller radius for Tier 3 polygons is because these polygons cover small areas where there is a high concentration of GI data, which provides greater confidence in categorising the ground conditions within these polygons. Since there is reasonably good GI coverage in these areas, there is more confidence in using GI data to classify the ground conditions. As a result, greater weighting is applied to the GI data compared to the background model. The 25 m radius ensures that each GI maintains a meaningful area of influence, despite the high data density.

The Bayesian update works by using maximum likelihood estimation to determine which distribution, θ, maximises the probability of observing the observed data. Due to the small probabilities being worked with, the log-likelihood is used to avoid overflow errors. When weightings are applied to the observations, the likelihood function is modified to incorporate these weights. The modified equation which is used is shown in Equation 23. Each weight, w_i, represents the relative importance of the corresponding observation x_i. For example, if $w_i = 0.5$, the observation, x_i, will contribute half as much to the likelihood as an observation with $w_j = 1$. A GI has a weighting between 0 and 1.

Equation 23:

$$\log L_{weighted}(\theta) = \sum_{i=1}^{n} w_i \log p(x_i|\theta)$$

8.7.4 Bayesian updating process

Bayesian updating requires a "prior" estimate which is updated based on observations to provide a final ("posterior") estimate. In this case, the "prior" actually consists of multiple estimates and is a collection of potential distributions of LSN defined using a mean and standard deviation of a normal distribution in log(LSN) space. These distributions are estimates of the true LSN distribution for the polygon. Different combinations of standard deviation and mean were created to establish the collection of distributions, with each distribution having different "prior" likelihood. The "prior" likelihood was taken as the product of the likelihood of the standard deviation and the product of the mean as covered in the steps below.

The LSN from local GI are used to update the likelihood of each distribution. This process is demonstrated in Figure 8.26 for initial P15 and P85 values of LSN of 5 and 30 respectively from the geospatial model, giving a mean of 2.5 and standard deviation, $\sigma_{\log(LSN)}$, of 0.86 in log space. Assuming a mean $\frac{\sigma_{\log(LSN),polygon}}{\sigma_{\log(LSN),geospatial}}$ of 0.6 to account for the polygon area, the mean $\sigma_{\log(LSN),polygon}$ is therefore 0.52 with the 15th and 85th percentiles of the distribution as 0.52 +/- 0.043. The "prior" probability of obtaining various mean and standard deviations is depicted in Figure 8.26a.

The full details for obtaining the "posterior" are presented in the key steps below. For the example in Figure 8.26, two LSN values of 2 and 30 are used to update the distribution. Given these values are far apart and skew slightly lower than P15 and P85, the likely distribution to represent the spatial variability would have a higher-than-average standard deviation and lower mean. Figure 8.26b shows that the higher probabilities for the distribution are for the lower mean values with higher standard deviation. The details of the update and converting to a single distribution for spatial variability as well as obtaining the full sample uncertainty distribution are provided in the key steps below. Note that the calculations are all performed in log space.

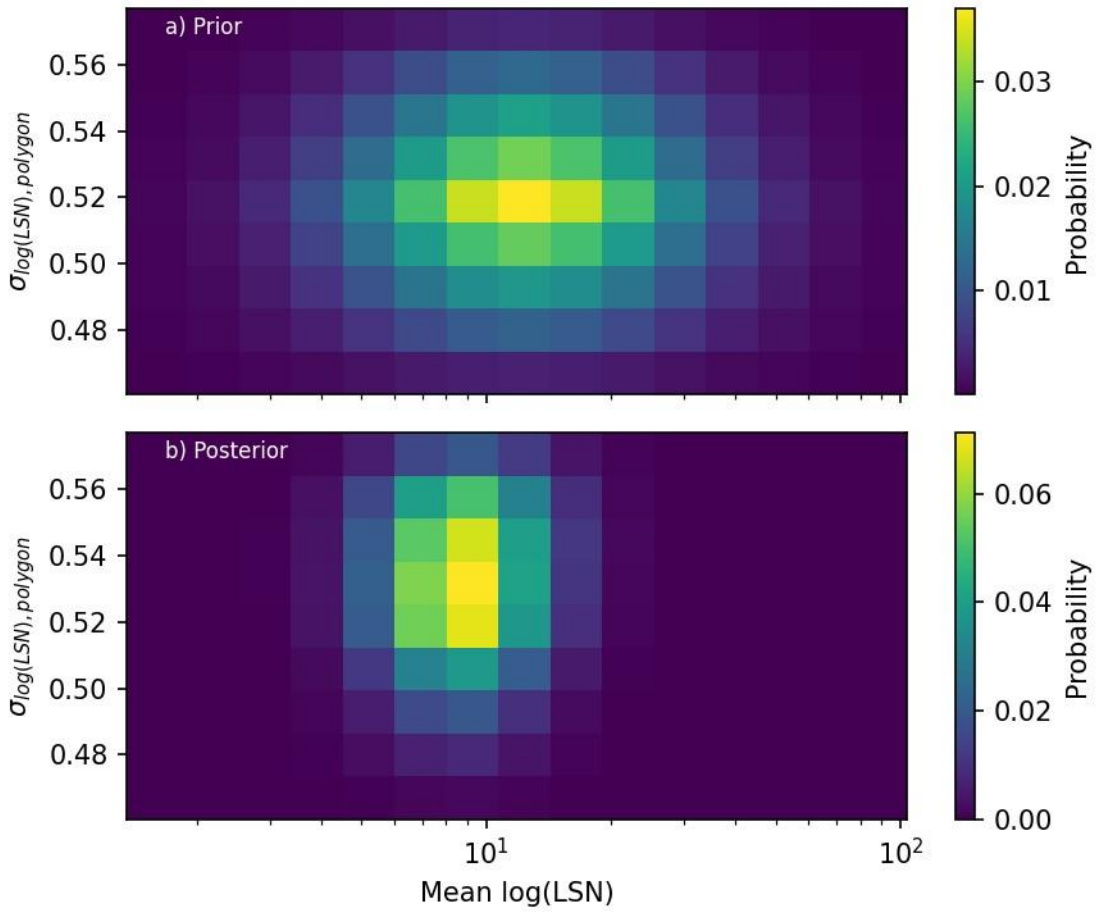

Figure 8.26: Example of Bayesian update showing the change in the probability of the mean and standard deviation between a) The "prior" estimate, and b) The "posterior" estimate

The key steps in applying the Bayesian updating process are:

1 Obtain a geospatial model prediction of the LDM distribution (see example in Section 8.4.9). This provides a lognormal distribution for a given PGA, Mw and GWD (normal distribution in log space).

2 Obtain a probability distribution of the likely value of the standard deviation of the spatial variability of the polygon based on the polygon area and geomorphology. The spatial variability is defined as normalised standard deviation, where the standard deviation of log(LSN) of the polygon is normalised by standard deviation of the geospatial model, $\frac{\sigma_{\log(LSN),polygon}}{\sigma_{\log(LSN),geospatial}}$. The mean estimate of that normalised standard deviation was obtained using Equation 22. The probability distribution of the normalised standard deviation was modelled as a triangular distribution, where the 15th and 85th percentiles of that distribution were set at +/- 0.05 of the mean estimate as fitted in Figure 8.13.

3 Sample the triangle distribution of normalised standard deviations equally at 9 points from -0.1 to 0.1 to obtain potential normalised standard deviations and their corresponding likelihood.

4 Unnormalise (i.e. reverse the normalisation process) the potential standard deviations for the spatial distribution by multiplying by the geospatial standard deviation, $\sigma_{\log(LSN),geospatial}$.

   – For each potential standard deviation, determine the "prior" probability of several different potential mean values. The "prior" probability of each mean for a particular

potential standard deviation was determined by generating a normally distributed probability distribution of potential mean values ($\sigma_{\mu,prior}$, $\mu_{\mu,prior}$), then obtaining the likelihood of each mean directly from that distribution. The $\sigma_{\mu,prior}$ was taken from Equation 24. This was determined as the remainder of $\sigma_{log(LSN),geospatial}$ after removing $\sigma_{log(LSN),polygon}$ with a minimum of 5% of $\sigma_{log(LSN),geospatial}$. $\mu_{\mu,prior}$ was taken as equal to the mean from the geospatial model. The potential means were set as 15 equal increments in log(LSN) space ranging from +/- 2.5 times the standard deviation of the geospatial model either side of the mean of the geospatial model.

Equation 24:

$$\sigma_{\mu,prior} = \min\left(\sqrt{\sigma^2_{log(LSN),geospatial} - \sigma^2_{log(LSN),polygon}}, 0.05 \cdot \sigma_{log(LSN),geospatial}\right)$$

5 The "prior" probability of each potential distribution (mean and standard deviation pair) was taken as the "prior" probability of the standard deviation multiplied by the "prior" probability of the mean (see Figure 8.26a).

6 The "posterior" probability of each potential distribution was computed using Bayesian theory with the weighted LSN values from the local GIs (Figure 8.26b).

7 The spatial variability distribution was determined as the centre of mass of the "posterior" probability of each potential distribution. This essentially represents a best estimate of the distribution.

8 The sample uncertainty distribution was taken as the probability of sampling an LSN given the "posterior" probability of each distribution (i.e. the probability of LSN considers the probability of each distribution that could produce that LSN value, and the probability of that distribution being the true distribution).

9 The 50th and 85th percentiles of the spatial variability and sample uncertainty distributions were stored along with the geospatial distribution.

- In the absence of any local GIs, the 50th percentile of the spatial variability and sample uncertainty distributions was set to the 50th percentile of the geospatial distribution, the 85th percentile of the spatial variability was set by obtaining the distribution using Equation 22, and 85th percentile for the sample uncertainty distribution was taken as the 85th percentile of the geospatial model. This avoided the rounding error and numerically intensive calculations in the Bayesian updating process.

8.7.5 Worked example

In Figure 8.27, the example from Figure 8.11 in Section 8.4.9 is extended to include the Bayesian updating. This example demonstrates how to obtain the different LSN distributions for a location where the l5_yp geomorphology category is Holocene River channel with main_rock = gravel, PGA = 0.22 g, Mw = 6.6, and GWD = 2.5 m. As discussed in Section 8.4.9, Figure 8.27(a)-(c) outline the steps undertaken to obtain the geospatial model distribution.

Figure 8.27d shows the expression for the normalised standard deviation of spatial variability, $\frac{\sigma_{log(LSN),polygon}}{\sigma_{log(LSN),geospatial}}$, versus area (i.e. Equation 22), and for this example a polygon area of 1.4 km^2 is adopted which corresponds to approximately to a normalised standard deviation of 0.8. This allows the best estimate of polygon spatial variability, $\sigma_{\log(LSN),polygon}$, to be computed by multiplying the normalised standard deviation by the standard deviation from the geospatial model distribution, $\sigma_{log(LSN),geospatial}$ (taken from the black line in Figure 8.27(c)).

Figure 8.27(e) shows the black line from the geospatial model for reference (same as the black line in Figure 8.27(c)), as well as three other distributions. The "No GI" shows the adopted spatial variability

distribution if there were no local GI. This is distribution is constructed from the best estimate of $\sigma_{\log(LSN),polygon}$ from above, and the mean of log(LSN) of the geospatial model. The reduction in $\sigma_{\log(LSN)}$ for this distribution (spatial variability) is purely due to the size of the polygon. The third distribution (spatial variability with GI - light blue) is the Bayesian updated estimate of the spatial variability distribution that considered the three LSN values from local GI (shown as red dots in Figure 8.27(e) and have values of 7.1, 8 and 12.5 with weights of 0.7, 1.0 and 0.7 respectively). Note that this distribution has shifted to higher LSN values due to the LSN values of the local GI. The final distribution (sample uncertainty with GI – purple) provides the probability of sampling LSN from the distribution after the Bayesian update. Note that this distribution is wider than the spatial variability distribution due to this additional uncertainty.

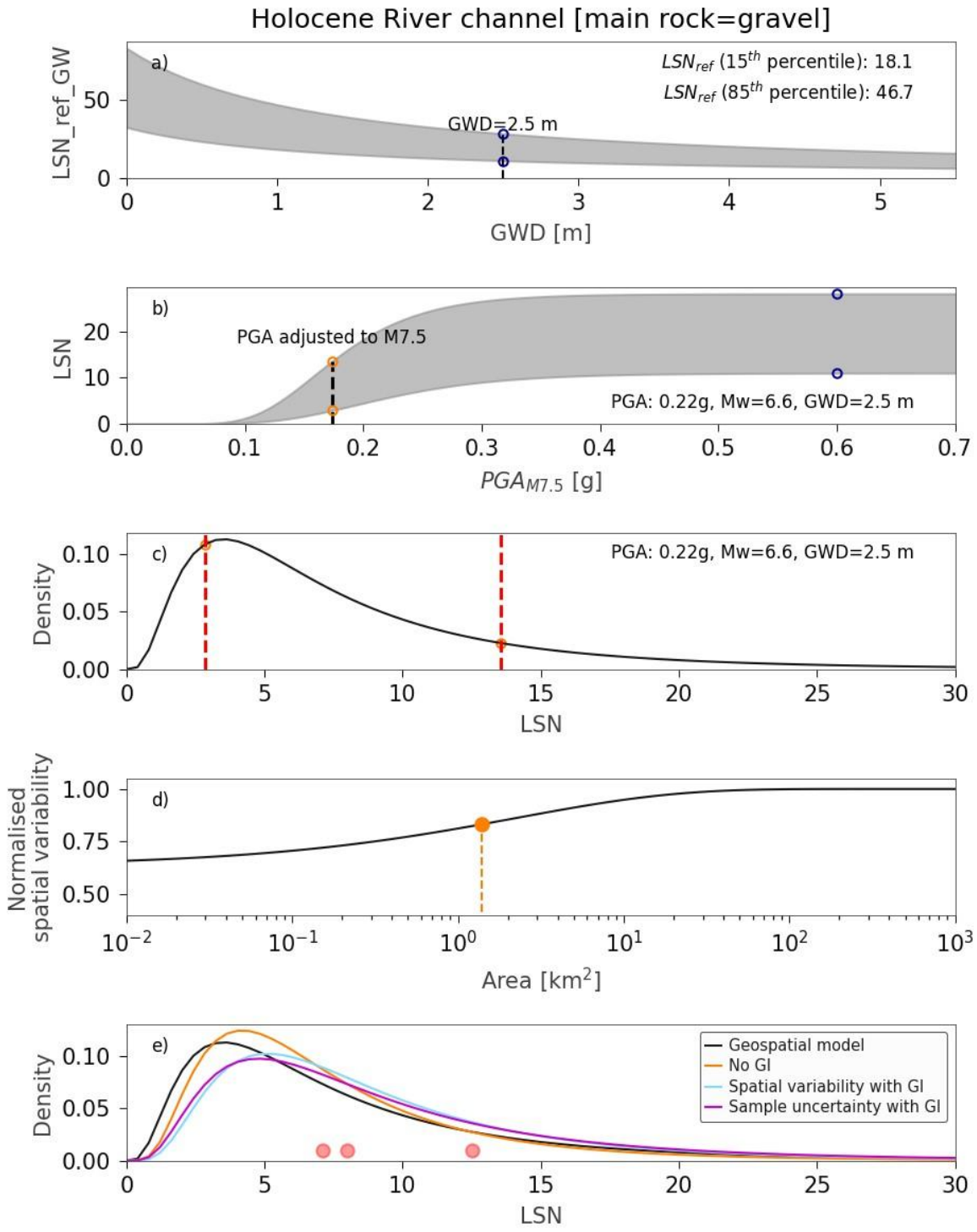

Figure 8.27: Example of functions to support worked example for determining LSN distributions using the geospatial model and Bayesian updating

8.7.6 Further examples

Given the complex nature of the updating process, a series of examples have been produced in Table 8.4 to illustrate how different observations influence the final distributions. Table 8.4 describes and provides inputs and outputs for different scenarios. The "case" column describes the scenario how the output differs compared to the baseline case of "No GIs". The inputs for the example

calculations are presented in the next four columns, where geospatial model parameters are distribution parameters from the geospatial model, norm. stddev. is the normalised standard deviation accounting for the area of the polygon (i.e. Equation 22), LSN values are the local GI within the polygon, and weights are the weighting factors for the Bayesian update due to spatial density of the local GI as determined in Section 8.7.3. The last two columns provide the calculated spatial variability and sample uncertainty distributions.

Table 8.4: Examples of Bayesian update calculations

Case	Geospatial model	Norm stddev.	LSN values	Weights	Spatial variability	Sample uncertainty
No GIs	15th: 8.93 50th: 12.2 85th:16.6	0.7			50th: 12.2 85th: 15.1	50th: 12.2 85th: 16.6
2 GIs at mean – shows a narrow distribution with unchanged mean	15th: 8.93 50th: 12.2 85th:16.6	0.7	12, 12	1, 1	50th: 12.2 85th: 15.1	50th: 12.2 85th: 15.7
2 GIs at +2x the standard deviation – shows a shift in the mean	15th: 8.93 50th: 12.2 85th:16.6	0.7	22, 22	1, 1	50th: 18.3 85th: 22.7	50th: 18.3 85th: 23.1
3 GIs at +2x the standard deviation with two at 50% weight – shows similar behaviour to case with only 2 GI	15th: 8.93 50th: 12.2 85th:16.6	0.7	22, 22, 22	1, 0.5, 0.5	50th: 19.2 85th: 23.9	50th: 19.1 85th: 23.9
2 GIs at +2x the standard deviation for a big area – shows less narrowing of distributions than for cases with smaller area.	15th: 8.93 50th: 12.2 85th:16.6	0.95	22, 22	1, 1	50th: 13.8 85th: 18.5	50th: 13.8 85th: 18.9
2 GIs at +/- 2x the standard deviation (i.e. widespread) – shows an increase in width of the spatial variability and decrease in the width of the sample uncertainty distribution	15th: 8.93 50th: 12.2 85th:16.6	0.7	6.7, 22	1, 1	50th: 12.2 85th: 15.2	50th: 12.2 85th: 15.8

8.8 Outputs for PL=15%

The NLM produces output for P_L=50% and P_L=15%. In the majority of steps the calculations are run in parallel, e.g. two separate <LDM>-<PL>-<method>-per-GI files are generated in the GI module (see Section 7.1). For the LV module the geospatial model and Bayesian update steps are done separately for PL=50% and PL=15%. However, the spatial variability function and SSP were only developed based on PL=50% data since they were quantifying normalised liquefaction behaviour and therefore the expectation was that the outputs would be similar. The LVM P_L=15% outputs may be more familiar with geotechnical engineers since P_L=15% is commonly used in practice. When considering the combination of LVM outputs with LDFCs produced with P_L=15%, the end user should familiarise themselves with the discussion and limitations of these in Section 11.2.1.

8.9 Limitations

The LV model is based on the NLM Flatland, NLM Geomorphology and NLM GI models, and therefore all the limitations associated with those models are also applicable to this model. Limitations specific to the LV module are:

1 The LV geospatial model has been developed based on GIs that are not evenly distributed across the country. This means that regions with more GIs may be over-represented in the geospatial model, however, the weighting factors developed in Section 8.4.3 are employed to help address this issue. Notably, the large number of GIs in Christchurch means that Holocene River channel, Holocene Loess, and Holocene Lacustrine and playa categories have a high representation from Christchurch.

2 The high-density clusters of GIs for recent subdivisions and other infrastructure means that these areas could be over-represented in the predictions, although this has been partially mitigated in the geospatial model using spatial density based reduced weighting. Likewise, a Bayesian updating process and spatial density based reduced weighting has been used in the LV module.

4 The spatial bias that CPT are not performed in non-penetrable ground means that the geospatial model predictions may be biased towards more liquefiable ground. The inclusion of BH (which can be performed in penetrable ground) was to both quantify the issue and partially offset it. Figure 7.17 compares the distributions from CPT and BH, which for many geomorphology categories had similar distributions; however, there are some with notable differences (e.g. Pleistocene Igneous). If the CPT and BH distributions are the same then it indicates that there is no apparent bias due to sampling technique (although other sampling biases may exist, e.g. GIs in general are more regularly performed in poor ground conditions). For geomorphology categories where the BH distribution produces lower LSN values than the CPT distribution, and there are considerably more CPT readings, it could be expected that these distributions are over-influenced by liquefiable ground. Polygons in these geomorphology categories may over-predict liquefaction if there are no local GIs to constrain the prediction.

3 The LV model produces an expected uncertainty; however, the GI in each geomorphology is not uniformly distributed. In cases where there are no local GI to constrain estimates these areas may have larger uncertainty than what is captured by the geospatial model, and may have significant changes to predictions in the future releases of the model (e.g. as additional data is added). Areas with no refined geomorphology model and very few digital CPT and BH are particularly associated with higher uncertainty (e.g. Upper Hutt).

4 The LV model spatially quantifies liquefaction using polygons. The use of polygons can result in sharp contrasts in liquefaction response across polygon boundaries. In reality, the transition is expected to be more gradual. Furthermore, the position of the boundaries can be sensitive to small changes in calibration parameters and the addition of more GIs. While these sharp contrasts have little impact (and can improve) regional loss estimates, they provide a significant limitation for other uses.

5 The geomorphology model provides initial boundaries for the SSP. This means that local GIs that are just outside the boundary are not considered in the predictions. This can be particularly limiting when a GI is next to a river but is not considered since it is within the mapped water bodies layer.

6 The SSP provide a spatial constraint on the prediction of similarity of ground response. In locations with limited data, the boundary is poorly defined and has been set as 5 km from the nearest GI to reduce the number of polygons, but this could be refined. Predictions in areas away from the local GIs should be considered as having lower accuracy.

7 The Bayesian updating process relies on an expected spatial variability that is a function of the polygon area. The standard deviation of the spatial variability in log space is not influenced by the LDM values of the GI; however, more consistent LDM values should result in reduced spatial variability.

8 Pumiceous material can be crushed during CPT and SPT testing which can lead to estimating that the deposit has a lower relative density and therefore higher liquefaction susceptibility than what may be the case. The triggering method does not account for the influence of pumiceous material and therefore may misinterpret these deposits.

9 The NLM LV module has been developed for the purpose of regional LV assessment and therefore it should not be relied upon for other purposes.

8.10 Potential future improvements

To enhance the LV module and address its current limitations, several potential future improvements have been identified:

1 **Geospatial model features.** Include additional features in the geospatial model (e.g. steepness of slope) to refine estimates, particularly categories that have many GI and a wide distribution of response.

2 **Account for areas with ground improvement**. A potential process to account for ground improvement could include: for the LV geospatial model, exclude all GIs that have been marked as post ground improvement from geomorphology categories that are of natural deposits. Consider additional LV geospatial model categories for post ground improvement. Identify polygons with ground improvement using cluster analysis of GI (i.e. an adaption of the Tier 3 polygon algorithm). Use the post ground improvement GI within these polygons when performing the Bayesian update.

3 **Review SSP algorithm parameters**. Examples include:

- Clustering thresholds for Tier 3. Potentially increasing the standard deviation threshold and lowering the minimum number of GI would benefit the overall model. This would increase the uncertainty in the Tier 3 polygons but would also increase their size and how many there are (i.e. more flatland area would be covered with Tier 3 polygons).
- Buffer distance of Tier 3 polygons. Currently the buffer is 10 m, however, the variograms shown in Figure 7.20 indicate that a large buffer out to 50 – 100 m may be justifiable. This would result in more area being covered with Tier 3 polygons.
- Buffer distance for Tier 2 polygons. Currently the buffer is 5 km, however, this distance may be too large based on the normalised variograms in Figure 8.12 and a distance of 500 m to 2 km may be more appropriate.

4 **Review of process to handle closely spaced GIs in Bayesian update.** The current process uses fixed buffer distances for the Voronoi expansion. However, the buffer distances could be adjusted based on the polygon size and/or standard deviation of the geospatial model.

5 **Handle pumiceous soil.** Make specific corrections for the presence of pumice in soil in the GI model, the geospatial model, and the Bayesian updating.

6 **Handling borderline GIs.** Consider including GIs within the nearest polygon if they are in a water body and within a certain distance from a polygon.

7 **Smooth polygon boundaries.** The *similar-soil-polygon* geopackage file is very large (>1 GB) and results in slow loading and rendering times. Some smoothing of boundaries to a scale of 5 to 20 m may significantly reduce the file size.

8 **Use magnitude corrected PGA in LDM-per-SSP lookup table**. The use of magnitude corrected PGA (Equation 19) may only have a small change in the interpolation error but would significantly reduce the *LDM-per-SSP* file size.

9 Groundwater (GW) module

Understanding shallow GW conditions is critical for assessing LV, as liquefaction only occurs in saturated soils. The depth to GW directly influences the extent of liquefaction-induced ground damage during seismic events, making GW modelling a key component of national liquefaction hazard assessments.

To address this, a national median shallow GW Model has been developed to provide estimates of GWD across New Zealand's flatland regions. This model serves as a key input for the NLM.

This section begins with an overview of the data structure and model outputs (Section 9.1). Sections 9.2 and 9.3 cover the core model development and GW response to SLR. Validation results and comparisons to other models are presented in Section 9.4. Limitations and potential future improvements are discussed in Sections 9.5 and 9.6 respectively.

9.1 Module output

The NLM GW Model is configured to make predictions on a 100 x 100 m grid. Outputs are generated as raster GeoTIFF files. The five main outputs are described in Table 9.1.

Table 9.1: GW output files with units and description

File name	Units	Description
NLM_gwl.tif	m	Median GWL.
NLM_gwd.tif	mbgl	Median GWD (i.e. depth below the ground surface).
NLM_gw_std_wo_seasonal.tif	m	Standard deviation of GW (depth/level) when "seasonal trend" has not been considered.
NLM_gw_std_w_seasonal.tif	m	Standard deviation of GW (depth/level) when "seasonal trend" has been considered.
NLM_gw_delta_d.tif	Days	Days to peak of GWL of sinusoidal "seasonal trend".
NLM_gw_delta_h.tif	m	Amplitude of "seasonal trend".

Figure 9.1 shows the NLM GW Model output of median GWD (mbgl) in the flatland regions of New Zealand, categorised into different depth classes.

Examples from two of the regions with a locally refined GW Model, Lower Hutt and Hawke's Bay, are shown in more detail in Figure 9.2 and Figure 9.3. Note that the process of making locally refined models results in boundary effects (as seen in the Hawke's Bay model, Figure 9.3), where the national base model and the locally refined models meet. This is an expected result and is discussed in the sections that follow.

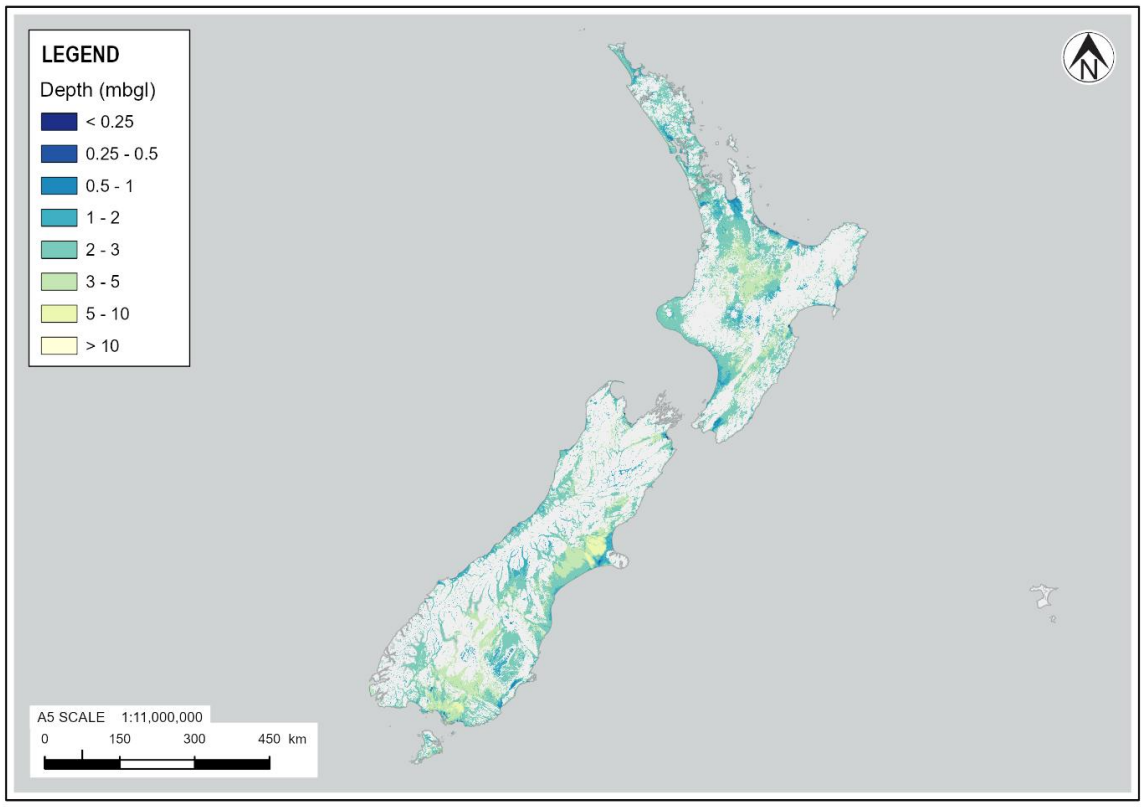

Figure 9.1: National NLM GW Model for New Zealand

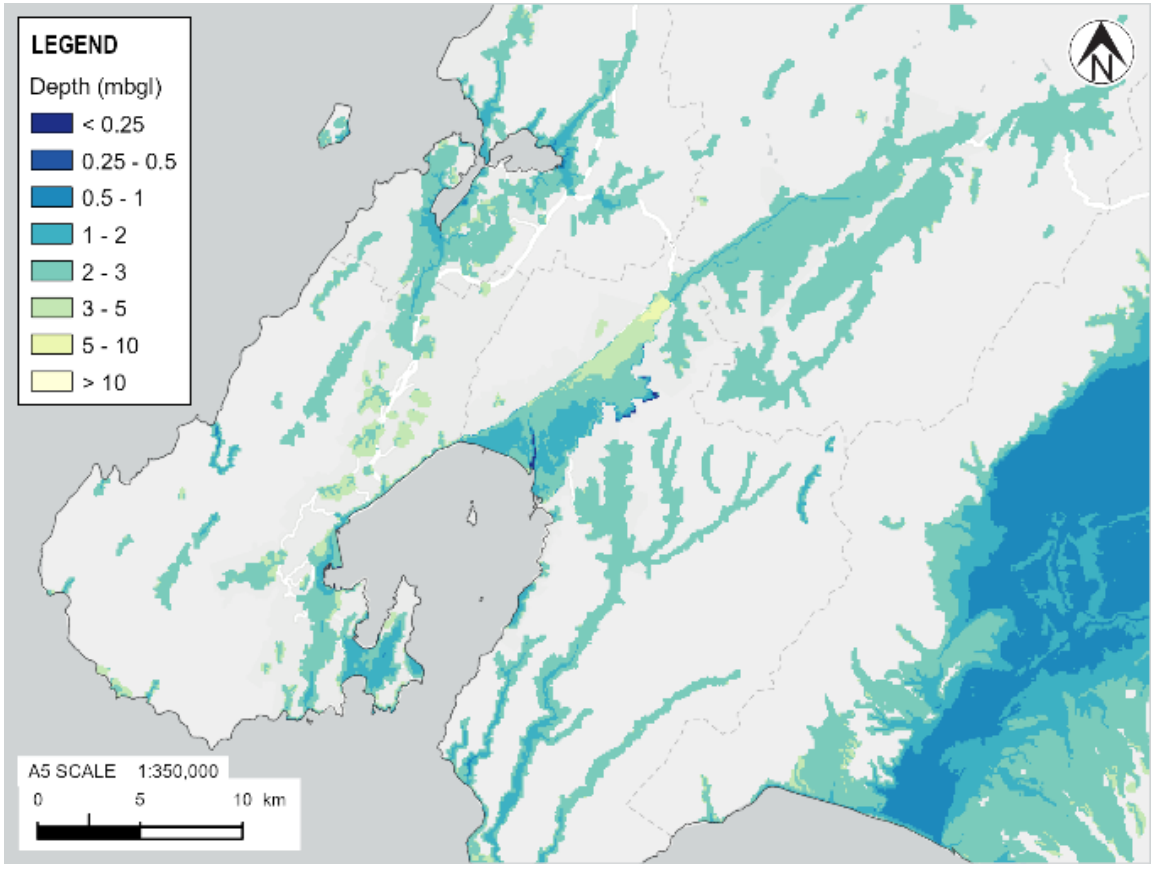

Figure 9.2: GW model – Lower Hutt

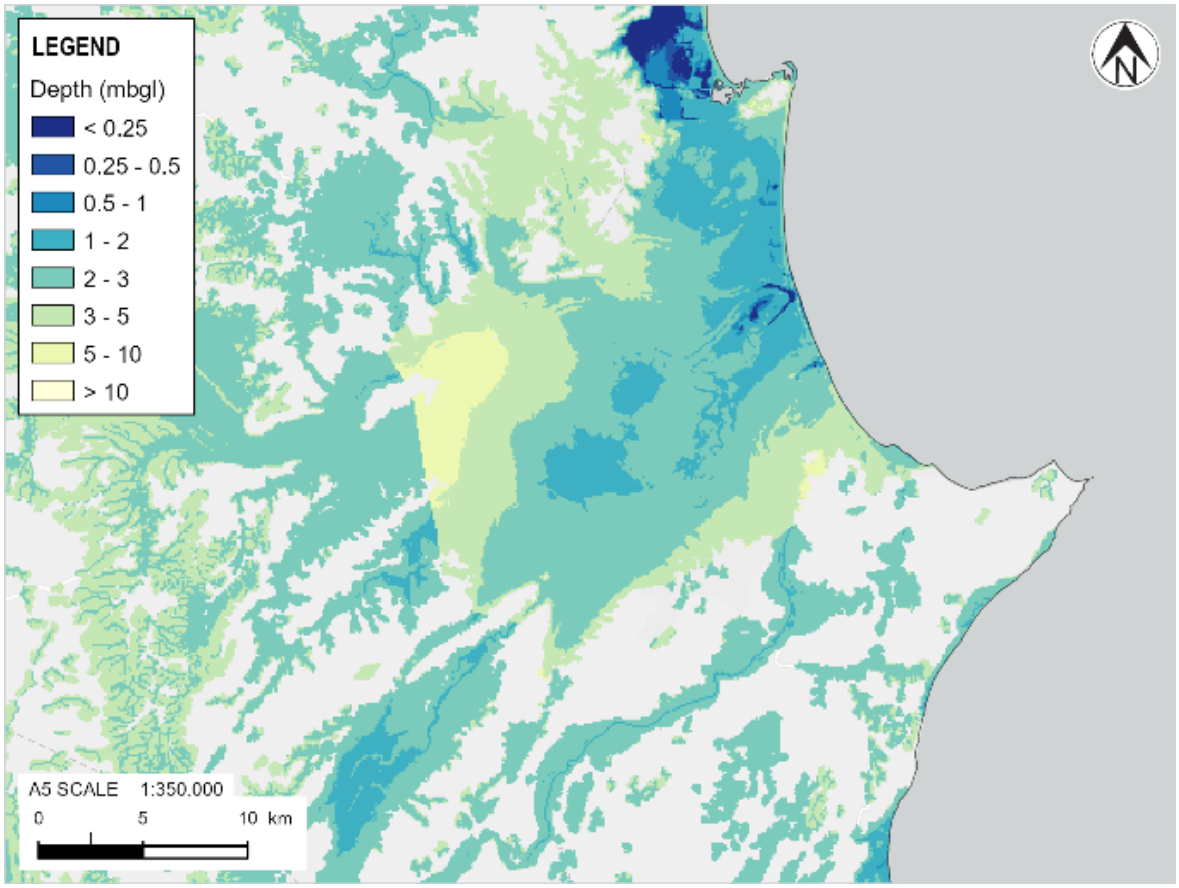

Figure 9.3: GW model – Hawke's Bay, note the sharp boundary effect present

9.2 Model development

Consistent with the philosophy applied to other modules, a data-driven approach to predict shallow GWD across the country has been adopted. The final model output is a continuous, spatially distributed surface of GWD at a 100 m resolution. At a high level, the modelling approach can be summarised as:

1 Collate and preprocess data and modelling features (Sections 9.2.1 and 9.2.2).

2 Develop a national GW Model (Section 9.2.3).

3 Develop and add in refined regional models (Section 9.2.4).

4 Apply post processing of predictions, including error quantification (Section 9.2.5.1).

The following sections provide more detail about each step.

9.2.1 Model inputs

9.2.1.1 GW data

The primary source of observed depth to GW data comes from the NZGD, a digitised collection of BH data (see Section 3.3.1). Additional data is sourced regionally from public council portals and through information requests made to regional councils and governing bodies. Static GW data is more readily available than temporal monitoring well data, due to the cost and complexity of storing/maintaining a temporal monitoring network. The key variables from these sources are the spatial location, date of measurement, depth of the BH, and depth to GW.

The table below lists the access locations of the GW data used in the model.

Table 9.2: Links to GW data used in the model

Name	Link to database
NZGD	https://www.nzgd.org.nz/
Northland	https://data-nrcgis.opendata.arcgis.com/datasets/NRCGIS::bore-logs/explore
Waikato	https://data-waikatolass.opendata.arcgis.com/datasets/219e0a0ef6224b5db25dc61c8f14322f_0/explore
Bay of Plenty	https://maps.boprc.govt.nz/datasets/BOPRC::well-bore-locations-in-the-bay-of-plenty/explore
Hawke's Bay	https://hbrcopendata-hbrc.opendata.arcgis.com/datasets/849f36ba4af14e599456f8f4fd9e8ec1_0/explore
Manawatu-Whanganui	https://data-horizonsrc.opendata.arcgis.com/datasets/1f53ca0f492248e3b0433d20a5630687_0/explore
Wellington	https://data-gwrc.opendata.arcgis.com/datasets/wells-and-bores/explore
Marlborough	https://data-marlborough.opendata.arcgis.com/datasets/7c4ff7d25e164c39aa853294efc727ee_13/explore
Canterbury	https://opendata.canterburymaps.govt.nz/datasets/ecan::wells-and-bores-all-1/explore
Southland	https://data-esgis.opendata.arcgis.com/datasets/24fb7bb2a3a649b1a0767c7c33dbfaae/explore
Otago	Received via email
Tasman	Received via email

9.2.1.2 Regression features

Table 9.3 below lists the input files used during the GW modelling process, as well as those used to generate secondary features. These features serve as the predictive variables in the regression model.

Table 9.3: Links to input files for GW modelling and creating secondary features in the model

Name	Source
T+T national DEM	See Section 3.1.3.
T+T national slope	See Section 3.1.3.
LINZ: New Zealand Coastline	See Section 3.4.3 - https://data.linz.govt.nz/layer/105085-nz-coastline-mean-high-water/
LINZ: New Zealand Lakes	See Section 3.4.3 - https://data.linz.govt.nz/layer/50293-nz-lake-polygons-topo-150k/
LINZ: New Zealand River Polygons	See Section 3.4.3 - https://data.linz.govt.nz/layer/50328-nz-river-polygons-topo-150k/
LINZ: New Zealand River Centrelines	See Section 3.4.3 - https://data.linz.govt.nz/layer/50327-nz-river-centrelines-topo-150k/
LINZ: Land Cover Database version 5.0	https://lris.scinfo.org.nz/layer/104400-lcdb-v50-land-cover-database-version-50-mainland-new-zealand/

In addition to these base datasets, a Wetness Index dataset has been created from the T+T national DEM model. Flatter areas with larger upstream catchments have a higher Wetness Index, whereas steeper areas with smaller upstream catchments have a smaller value. The Wetness Index was developed by Beven & Kirkby (1979) and is commonly used to quantify topographic influences in GW modelling. The Wetness Index is described by the following equation:

Equation 25:

$$Wetness\ Index = \log\left(\frac{A_s}{\tan(Slope)}\right)$$

Where A_s is defined as the upslope contributing area per unit length. Note that the Wetness Index is calculated at a 100 m resolution for use as a feature.

9.2.2 Preprocessing of GW measurements

The key steps involved in preprocessing the GW measurements are as follows:

1 Standardise formatting of GWD, well depth, date, location, and well ID attributes.

2 Filter well depth <= 20 mbgl, because bores of greater depth may not be representative of the shallow unconfined GW.

3 Filter GWD < 0 m (GW above ground surfaces) and GWD >= 10 mbgl (GW deeper than 10 m), to filter out any artesian wells and any bores with potential measurement errors.

4 Determine GW elevation by differencing the GWD from the T+T National DEM.

The table below shows the number of GW measurements available by region following the filtering process.

Table 9.4: Number of static GW measurements used from each region for the development of the GW Model

Region	NZGD	Regional Council Data
Auckland Region	17509	0
Bay of Plenty Region	4955	769
Canterbury Region	26720	8820
Gisborne Region	580	0
Hawke's Bay Region	1660	1118
Manawatu-Whanganui Region	791	566
Marlborough Region	774	1246
Nelson Region	532	1
Northland Region	739	239
Otago Region	729	999
Southland Region	341	1984
Taranaki Region	991	0
Tasman Region	367	1549
Waikato Region	6764	2085
Wellington Region	2220	688
West Coast Region	437	0

9.2.3 Build national scale GW Model

The national scale GW Model predicts the GW elevation (rather than GWD) using a multi-linear regression (MLR). The GWD is then determined as the difference between GW elevation and the ground surface elevation. To establish the national MLR model, the following steps were followed:

1 Fit an initial MLR model for GW elevation (see Section 9.2.3.1)
2 Seasonally correct the observation data based on the seasonal trend (see Section 9.2.3.2)
3 Fit a final MLR model (see Section 9.2.3.3)
4 Quantify the residuals to allow estimation of uncertainty (see Section 9.2.3.4)
5 Apply to a national prediction grid (see Section 9.2.3.5)

9.2.3.1 Fit initial MLR model

Forward selection was used for developing the MLR model to identify relevant features for predicting GWLs. This method builds the model step-by-step, starting with no features, then including one feature at a time based on its impact on model performance. At each step, the remaining features were tested and the feature that improves the model most (measured by the Akaike Information Criterion) is added. The Akaike Information Criterion helps balance model accuracy with simplicity, preventing overfitting by adding only meaningful features.

The process continues until no further features significantly improve the model or until a certain number of features is reached. This approach creates a simpler, more effective model with only the most important predictors. Features that were likely to influence GW trends were explored (as well as their log transform), including:

- Elevation;
- Slope;

- Distance to coast;
- Distance to lakes;
- Distance to rivers;
- Distance to wetlands;
- Distance to surface water;
- Wetness index;
- Downslope distance to coast;
- Downslope distance to stream;
- Elevation above stream; and
- Geomorphology.

The following seven features were selected from this process, used both for the initial and final national model as well as for the local models (presented in Section 9.2.1.2):

- Elevation;
- Log of elevation;
- Log of wetness index;
- Distance to coast;
- Log of distance to coast;
- Distance to wetlands; and
- Elevation above stream.

Both regular and log-transformed versions of the same variables (distance to coast and elevation) were included in the final model because they capture different aspects of the relationship with GWD. Including both forms allows the model to account for both linear and non-linear effects of these variables.

For distance to coast, the regular term captures the linear relationship where GWD changes at a constant rate with increasing distance, while the log-transformed term captures the non-linear effect where the influence diminishes with increasing distance (stronger influence near the coast and weaker influence farther inland). This dual representation improves model performance by capturing both immediate and distant coastal influences on GW systems.

Similarly, for elevation, both regular and log-transformed versions were retained because they represent different aspects of how elevation affects GWD. The inclusion of both terms was validated through the Akaike Information Criterion based forward selection process, which indicated that each term contributed unique explanatory power to the model.

9.2.3.1.1 Regression model issue with DEM derived inputs

Note that the Wetness Index is dependent on the slope, and as mentioned in Section 3.1.3, the stitching of the 1 m LiDAR and 8 m DEM results in some sharp unrealistic transitions in slope. This results in unrealistic predictions along the stitched boundary. This was particularly noticeable between Palmerston North and Levin as shown in Figure 9.4 and Figure 9.5.

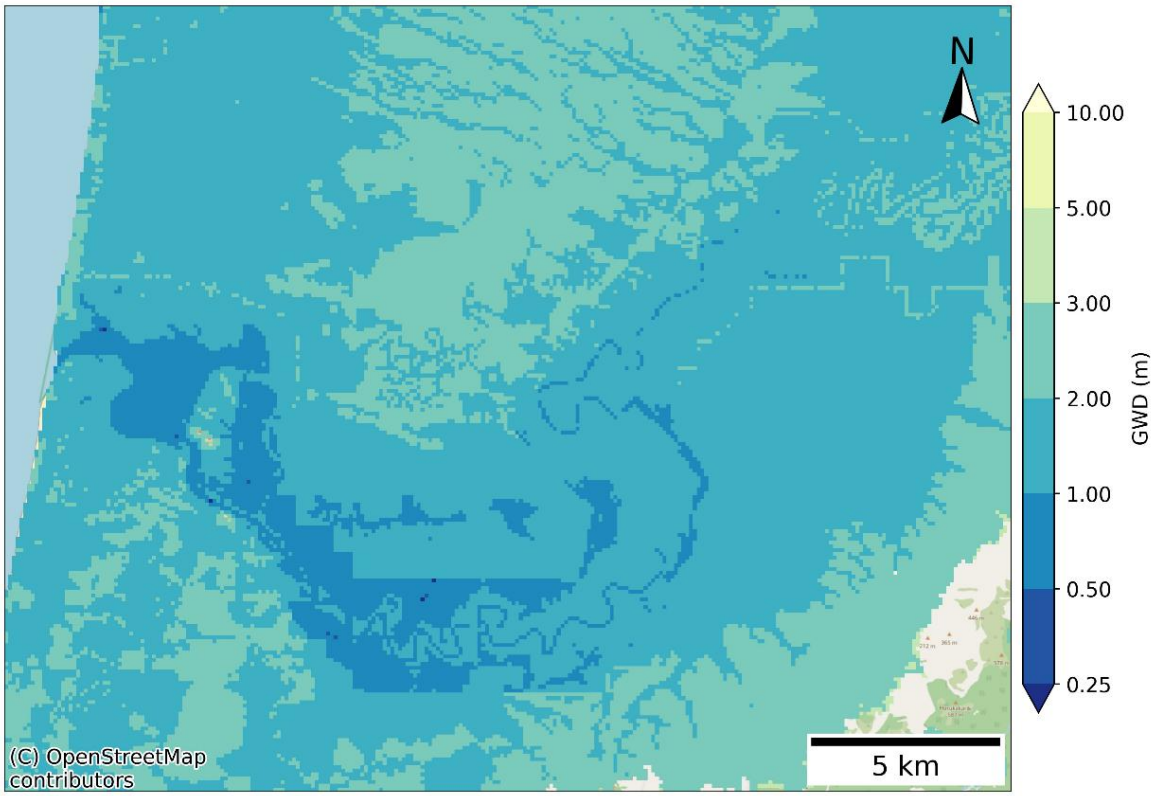

Figure 9.4: GWD showing boundary artifacts due to stitching of DEMs near Palmerston North

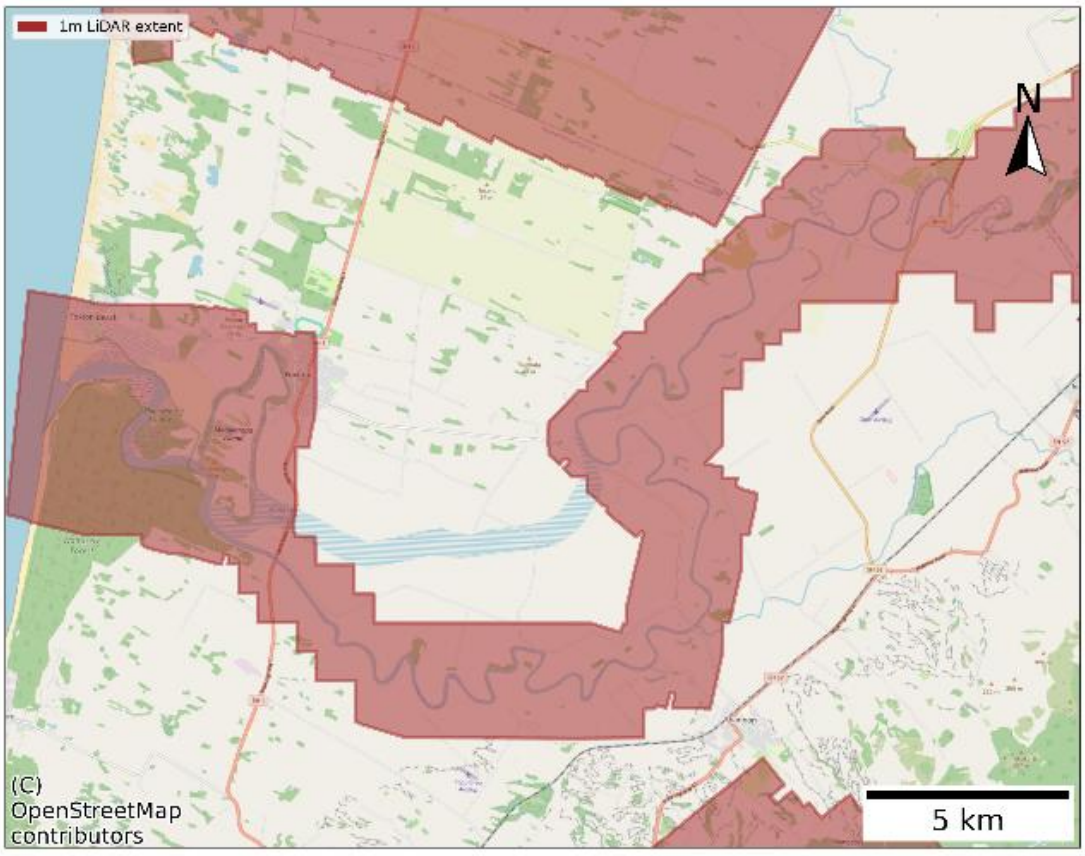

Figure 9.5: Mapped extent of 1 m LiDAR revealing the underlying cause of artifacts

9.2.3.2 Seasonal correction of in-situ GW observation data

GWLs often rise and fall with the seasons, typically going up in wet months and down in dry ones. To correct this, the difference between the initial MLR predictions and actual values (the residuals) were calculated. These residuals often show a seasonal pattern, which can be observed when plotted against the day of year (Figure 9.6). By removing this "seasonal trend", the training data becomes more stable and accurate for building the final model.

To remove the observed trend, a sinusoidal function was fitted to the residuals. The parameters of this function (i.e. peak deviation (delta_h), timing of the peak (delta_d), and median level) define the seasonal cycle (see Equation 26). Once identified, this seasonal variation was subtracted from the original GWLs, providing seasonally corrected data. This corrected data was used in further analysis.

Equation 26:

$$GWL_{seasonal_{trend}} = \boldsymbol{delta_h} \cdot \cos\left(2\boldsymbol{\pi} * \frac{\left(\boldsymbol{day_{of_{year}}} - \boldsymbol{delta_d}\right)}{\mathbf{365.25}}\right) + \boldsymbol{GWL_{median}}$$

Figure 9.6 shows the residuals and modelled trend for the initial MLR model, showing how the sinusoidal model aligns with the data. The residual trend model (for the national dataset) has a maximum amplitude of 0.2 m occurring in late August, indicating the time where the GWL is at its highest.

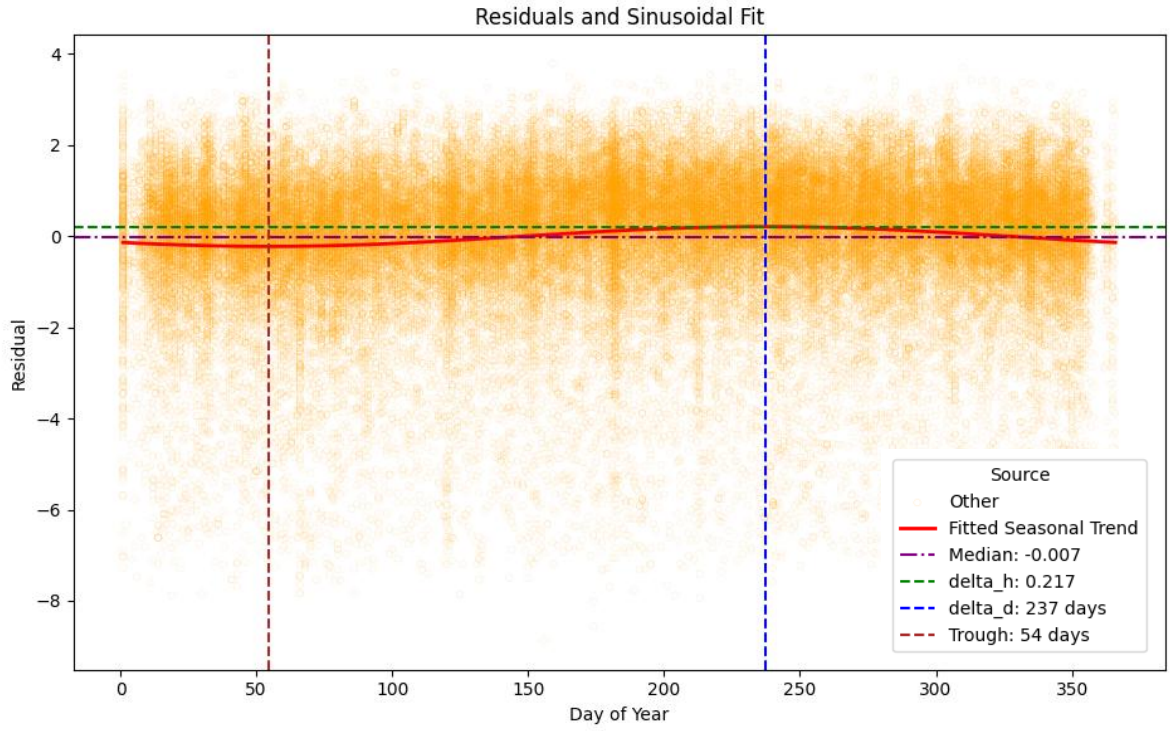

Figure 9.6: Seasonal GW trend for national dataset

9.2.3.3 Seasonally corrected MLR model

This step applies the same steps as in Section 9.2.3.1 for the initial MLR, however, the observations were seasonally corrected as described in Section 9.2.3.2. This second MLR model is provided in Equation 27 below.

Equation 27:

$$GWL_{national,MLR,SC} = 1.0034 \cdot Elevation - 1.73 \cdot 10^{-5} \cdot Distance_{coast} - 3.04 \cdot 10^{-5} \cdot Distance_{wetlands} - 0.00276 \cdot Elevation_{abovestream} - 0.407 \cdot \log(Elevation) + 0.570 \cdot \log(Wetness\ Index) + 0.112 \cdot \log(Distance_{coast}) - 3.32 .$$

The GWD corresponding to this GWL prediction, $GWD_{national,MLR,SC}$, was then computed from Equation 28.

Equation 28

$$GWD_{national,MLR,SC} = Elevation - GWL_{national,MLR,SC}$$

This model was then corrected further in Section 9.2.3.4 due to a trend observed in the residuals.

9.2.3.4 Residual model fitting

The residuals of the seasonally corrected MLR model were quantified to both apply corrections to the predictions and allow the model uncertainty to be quantified for different future use cases. Figure 9.7 shows the residuals plotted against a selection of features. Figure 9.7(a) to (c) show no significant trend in the mean of the residuals for elevation, distance to coast and log wetness index. However, Figure 9.7(d) shows that the model has a positive trend for shallow predictions (up to ~1 m deep) and is over-predicting GWL in this range. A trend like this is often due to underfitting or a constraint that is not captured in the regression model. In this case, it appears to be due to the physical constraint that unconfined GWLs cannot exceed the ground surface. Equation 29 (plotted in black in Figure 9.7(d)) was applied to manually correct predictions and remove this trend. The adjusted predictions are shown in Figure 9.8, where the mean and median trends of GWL (bottom right) are now zero (or close to zero) for all GWD.

The final national mean GWD was then computed from Equation 30.

Equation 29:

$$\Delta GWD_{mean} = \begin{cases} 1 - GWD_{national,MLR,SC}, GWD_{national,MLR,SC} < 1 \\ 0, GWD_{national,MLR,SC} \geq 1 \end{cases}$$

Equation 30:

$$GWD_{national,final,mean} = GWD_{national,MLR,SC} + \Delta GWD_{mean}$$

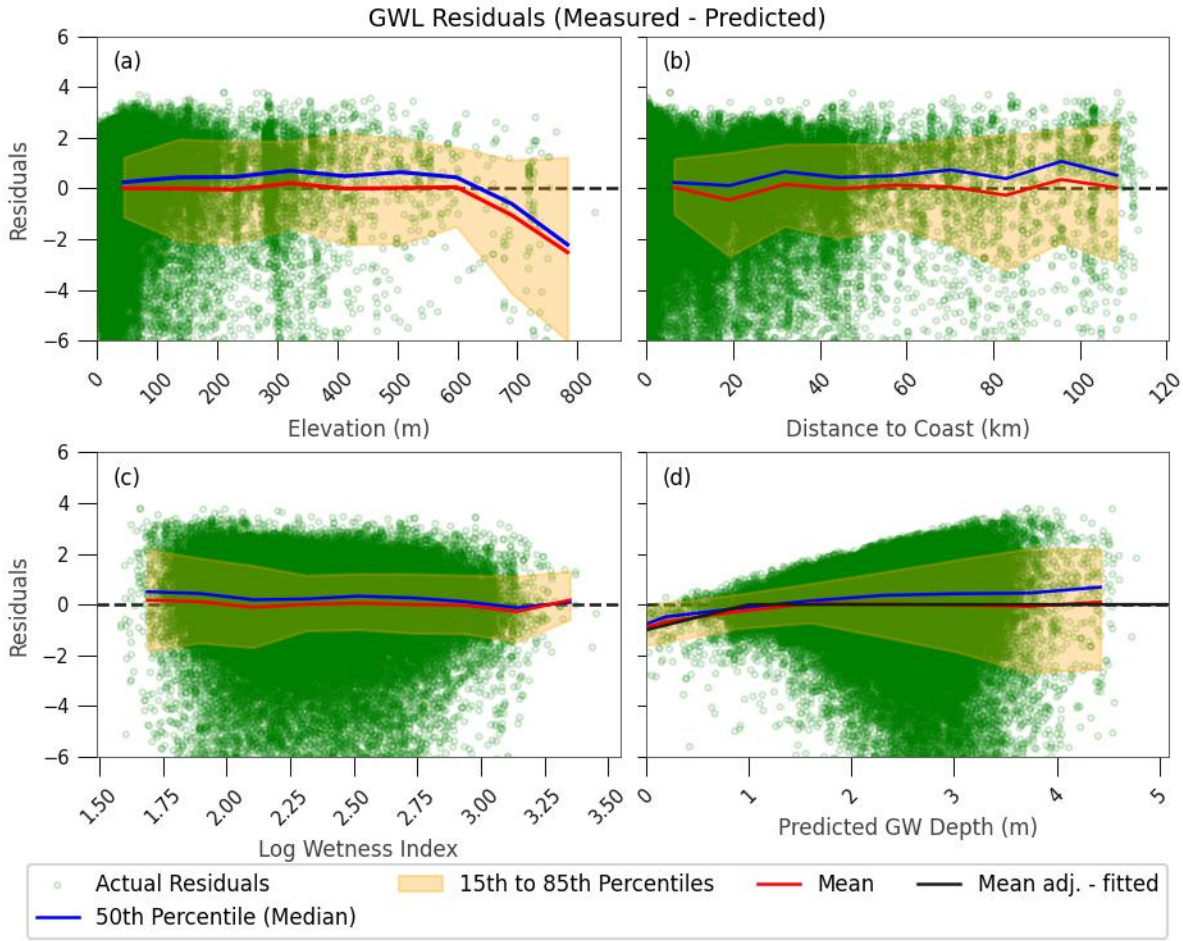

Figure 9.7: Raw GWL residuals for a selection of features

To quantify the median and prediction error / uncertainty in this regression model, the adjusted GWL residuals were plotted (i.e. residuals after applying Equation 30). The median GWD was determined as 0.3 m less than the mean GWD. Note, from Figure 9.8 it can be seen that the measured GWL was 0.3 m higher than predicted mean GWL. The uncertainty was quantified using Equation 31 by fitting to the 85th percentile of the GWL residuals as a function of the predicted GWD (black line in Figure 9.7(d)). In summary, the uncertainty in the GWD or GWL generally increases with increasing GWD. The 85th percentile and difference between the median and mean were used to obtain a standard deviation for a normal distribution prediction of the uncertainty (Equation 32). Note that Equation 32 takes the median GWD as the centre of the normal distribution not the mean. Using the mean for quantifying the residuals or fitting a normal distribution directly to the residuals would skew the estimates of the residuals because it is a clipped normal distribution (due to the limit of GWD > 0). The use of the median and 85th can be reasonably assumed to not be influenced by the clipping at the ground surface and provides suitable parameters to quantify the distribution. To be consistent with the assumptions adopted here, the residuals should be clipped at the ground surface in forward use, consistent with how the mean and median estimates should be handled.

Equation 31:

$$\Delta GWD_{85th} = \begin{cases} 1, GWD_{national,final,mean} < 1.75 \\ 1 + 0.75(GWD_{national,final,mean} - 1.75), 1.75 \leq GWD_{national,final,mean} \leq 3.75, \\ 2.5, GWD_{national,final,mean} > 3.75 \end{cases}$$

Equation 32:

$$\sigma_{GWL} = \frac{\Delta GWD_{85th} + 0.3}{1.038}$$

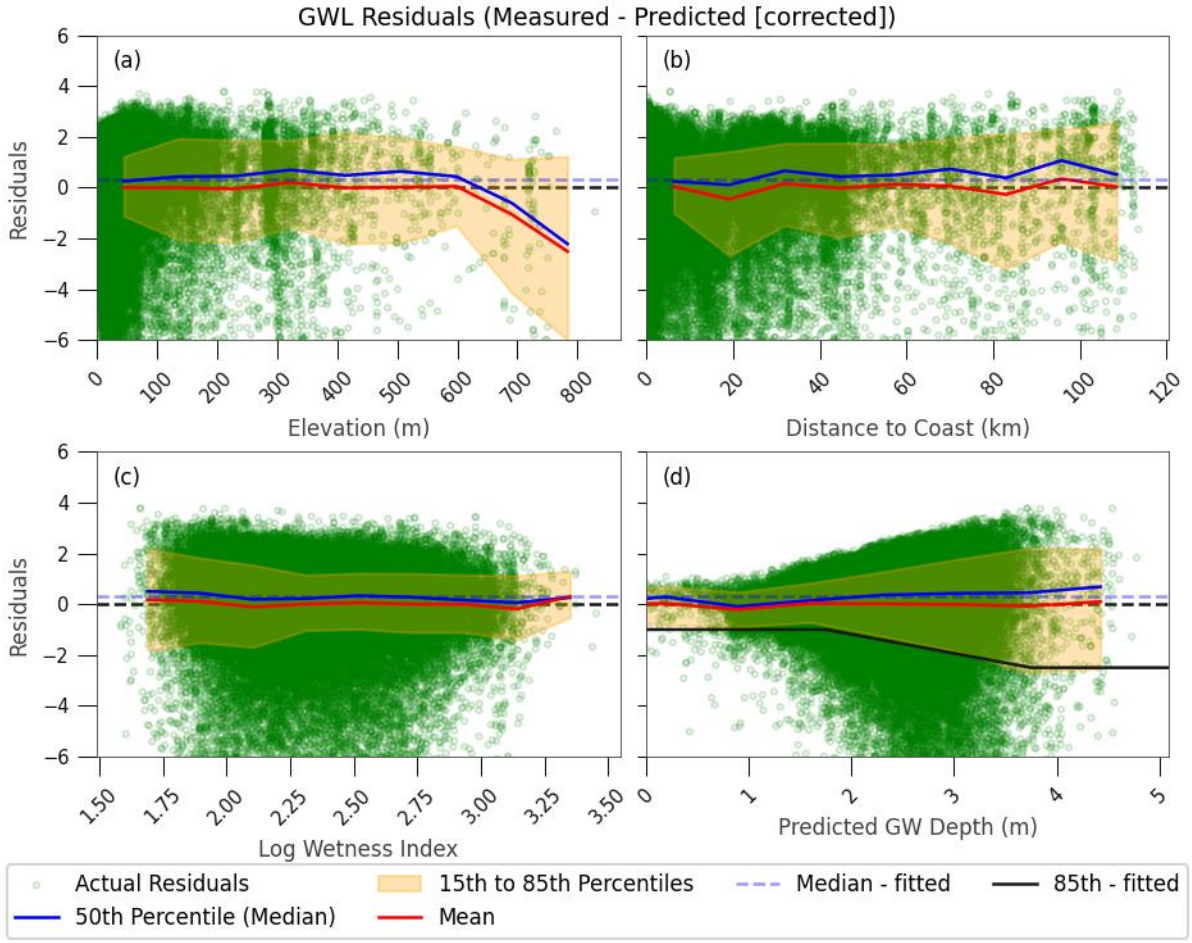

Figure 9.8: Corrected GWL residuals for a selection of features

The coefficients for the national model and the locally refined models are provided as Digital Supplement I: *GW-regression-coefficients*.

9.2.3.5 Apply to a national prediction grid

Each of the MLR features were approximated across a 100 m regular grid in all flatland areas. Equation 30 was used to estimate the mean GWD, the median was taken as 0.3 m below the mean, and the standard deviation was taken from Equation 32. This model was further modified to include the local refined models and the post-processing steps in Section 9.2.5.1.

9.2.4 Refined regional models

Locally refined models were computed for areas within New Zealand with a high density of GW observations. In these areas, the same MLR model methodology and model features as in Section 9.2.3 were applied but to a local subset of the observation data to best represent local conditions. The last step on residual model fitting was not applied. Instead, the residuals were krigged to capture some of the unaccounted-for spatial heterogeneity. Areas were selected based on the

location and density of data points, with a preference for populated areas. Appendix B shows the selected refinement areas.

The “seasonal trend” (discussed in Section 9.2.3.2) was recalculated for each local area. Figure 9.9 shows the fitted trend for Hawke’s Bay. As expected, there are much fewer observation points compared to the national plot.

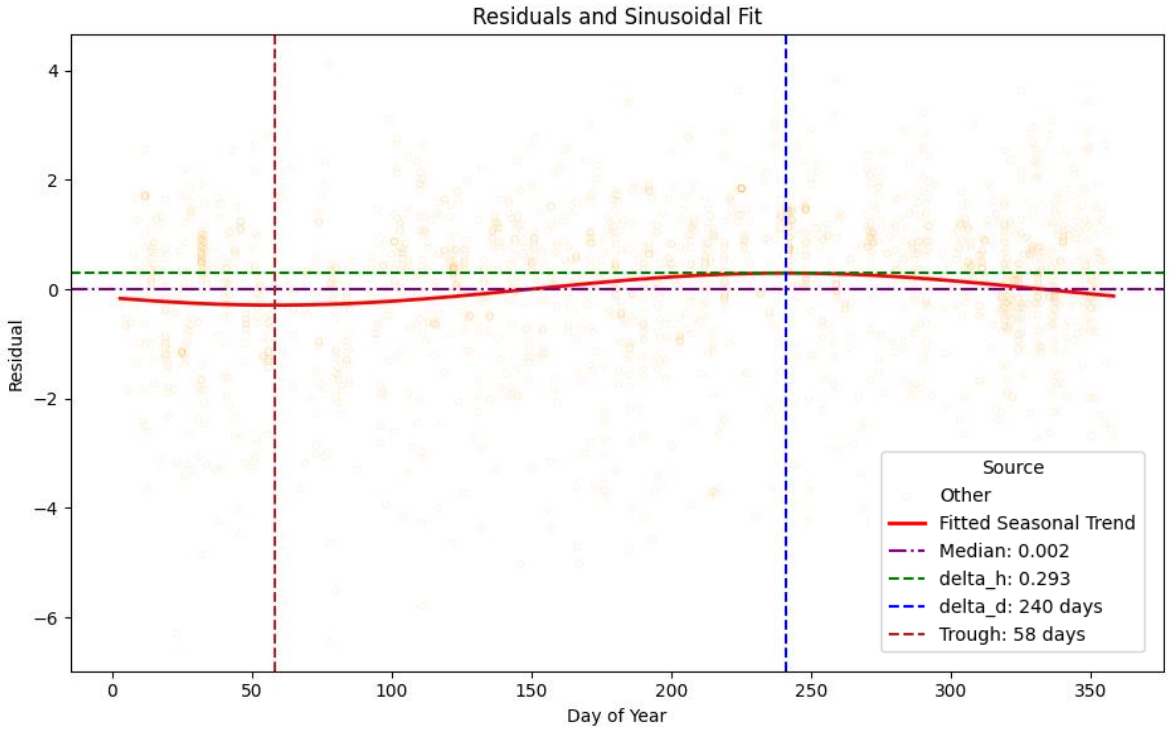

Figure 9.9: Seasonal GW trend for Hawke’s Bay locally refined area

The kriging process provided both an adjustment to the GW elevation and an associated variance. This adjustment was added to the regression-based GW elevation to produce a final elevation surface within the region. The variance from kriging was converted into a standard deviation, representing the interpolation uncertainty. This is the uncertainty associated with estimating the residuals at unsampled locations based on their spatial structure and distribution. It is important to note that this standard deviation reflects only the uncertainty introduced through the kriging process and does not account for other sources of uncertainty, including those from the regression model (e.g. parameter or model specification uncertainty), or measurement errors in the observed GWLs. As such, the kriging-derived uncertainty represents a partial view of total model uncertainty, limited to the interpolation of residuals. The PyKrige Python package was used for “ordinary” kriging with a gaussian variogram. The Variogram Range was set to 10 km. The Nugget and Partial Sill were set to 1.0 and 0.2 respectively. Kriging was not applied nationally to avoid modelling inter-regional spatial trends that were unlikely to exist.

9.2.5 Combined model

The locally refined model was stitched into the national model by replacing the region with the locally refined GW estimates (i.e. mean and mean GWD and GWL, seasonal adjustment and standard deviation). While this process does result in sharp changes at some of the boundaries, it makes best use of the available data at each location, without trying to hide the limitations of that data.

9.2.5.1 Post processing of model predictions

The post-processing phase improves and formats the model's predictions to prepare outputs for practical use. This addresses potential over-predictions in GWL by correcting any cases where predicted GWLs exceed surface elevation but there is no mapped water body. This adjustment prevents unrealistic GWLs in these areas. Any GWL that exceeded the surface elevation was reduced to 0.1 m below it.

The GWD was calculated by subtracting the GWL from the surface elevation. This provides a direct measure of GWD relative to the terrain, which was then stored as a new attribute in the prediction grid. Further fine-tuning occurred through surface water corrections, correcting GWD in lakes to zero to reflect the presence of surface water.

The prediction grid, containing both GWL and GWD predictions, was saved in a final data structure. The predictions were converted into raster files, with the GWL and depth data saved as (100 m) GeoTIFF files.

The uncertainty in model predictions from the national and locally refined models were both defined as standard deviations for a clipped normal distribution, where predictions were clipped to 0.1 m below the ground surface in the same manner as the median estimate.

9.3 Sea-level rise (SLR)

9.3.1 SLR influence on GW systems

SLR impacts GWLs where GW is in hydraulic connection to the sea. Under SLR, the two mechanisms by which GW rises over a continuum are:

1 Flux-controlled (or recharge-limited) – where GWLs rise by the same amount as SLR, where the GWD can accommodate the rise.

2 Head-controlled (or topography limited) – where GWLs rise less than SLR and instead there is increased discharge through new or existing drainage networks as well as potentially a relative reduction in flux.

Refer to Figure 9.10 for a schematic of these two modes.

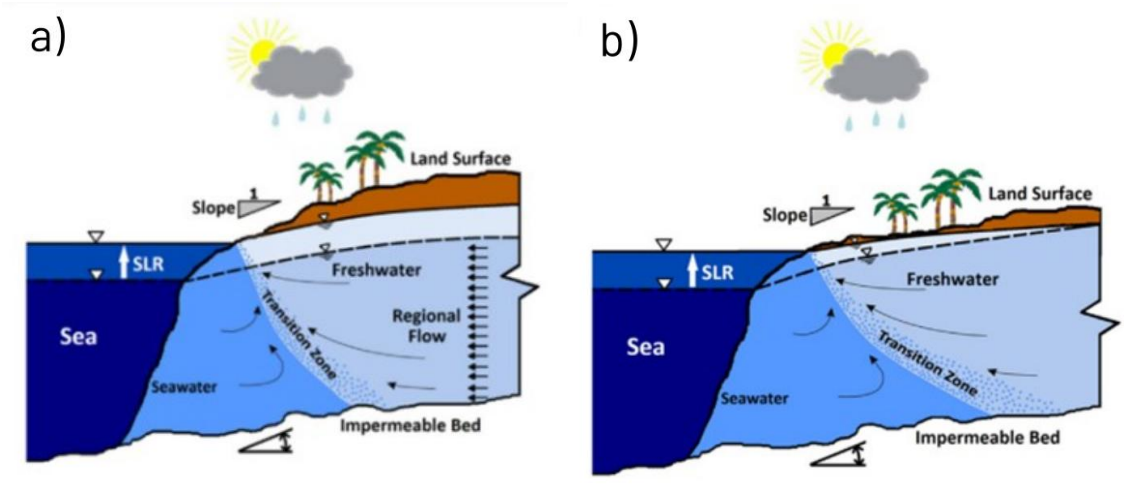

Figure 9.10: a) Flux-controlled system, where GWLs rise as the same amount as SLR, and b) Head-controlled system, where GWLs rise less than SLR (Ketabchi et al., 2016)

The extent of GW elevation rise due to SLR is still a topic of considerable research, and there is minimal observational evidence to support different models (Bosserelle et al., 2022). Numerical

models are the primary means to indicate whether or not a coastal aquifer is flux-controlled or head-controlled (Befus et al., 2020; Bosserelle et al., 2022; Gesch, 2018; Michael et al., 2013). Many assessments which model the impacts of sea-level on GW using numerical methods have found that the majority of coastal aquifers are topography limited, therefore, GWLs will rise less than SLR (Befus et al., 2020; Michael et al., 2013; Ramesh et al., 2023). Michael, Russoniello, and Byron (2013) also show that coastal regions with high recharge or high freshwater discharge (i.e. from modified river channels and drainage networks) are more likely to experience lower increases in GWLs compared to the coast.

Future Coasts (https://niwa.co.nz/hazards/future-coasts-aotearoa) is a five-year MBIE Endeavour research program which aims to help lowland coastal communities adapt to climate change. It is anticipated that this research program will develop a national coastal GW model which considers absolute SLR due to both increase in ocean levels and coastal vertical land movement. However, currently there is no nationally-consistent estimate to increases in GWLs as a result of SLR. Therefore, for the purpose of the NLM, a first order estimate of GWL response to SLR was developed. In the future, it is anticipated that the modelled results from Future Coast Aotearoa could be used for additional validation/calibration or in place of this model.

9.3.2 NLM SLR model

For this assessment, a GW-centric approach is taken, whereby the modelled median GWL characteristics were used to predict the impact of SLR. Given the extent and number of drainage features (natural, agricultural, and anthropogenic) within the coastal urban flatland areas of New Zealand, it can be expected that GW head will rise less than a 1:1 ratio with SLR for areas not immediately along the coast (i.e. head controlled). To reflect the likelihood of drainage limiting SLR, the extent of rise was set to be a function of the current GW head.

A zonal approach has been developed, whereby the zone closest to the coast experiences a bathtub-like increase to GWLs at a 1:1 ratio with anticipated SLR estimates. Following this is a transitional zone, whereby there is a linear decrease in SLR impacts (as a function of current GWLs). The extent of the transition zone is constrained by a threshold elevation which is assumed to control GWLs, whereby there is no longer any influence from SLR (Figure 9.10). Simply put, the greater the current GWL, the less likely the GWL is controlled by the sea-level.

The approach adopted for the change in GWL due to SLR increment, ΔGWL_{SLR}, is provided in Equation 33, and shown in Figure 9.11. Where ΔH_{SLR} is the change in sea-level, GWL is the current GWL above the current sea-level, $GWL_{bathtub}$ is the GWL where the full increment in sea-level is added to the GWL (commonly referred to as the bathtub point), GWL_{noinfl} is the GWL where there is no longer any SLR influence on GW.

Equation 33:

$$\Delta GWL_{SLR} = \begin{cases} \Delta H_{SLR}, GWL < GWL_{bathtub} \\ \Delta H_{SLR} \cdot \dfrac{GWL - GWL_{bathtub}}{GWL_{noinfl} - GWL_{bathtub}}, GWL_{bathtub} \leq GWL > GWL_{noinfl} \\ 0, GWL \geq GWL_{noinfl} \end{cases}$$

Both $GWL_{bathtub}$ and GWL_{noinfl} for $\Delta H_{SLR} = 1\ m$ were informed by comparison to previous SLR studies conducted in Christchurch and South Dunedin, and have been assumed to be 0.3 m and 3.5 m respectively (Figure 9.11). These two numbers are only for $\Delta H_{SLR} = 1\ m$ and would need to be recalibrated for different SLR scenarios. Further regional comparisons to modelled GW response to SLR are discussed in Sections 9.4.4 and 9.4.5.

ΔGWL_{SLR} was additionally post-processed to limit the GWL after SLR (i.e. $GWL + \Delta GWL_{SLR}$) to be 0.1 m below the ground surface. This post-processing step was consistent with the post-processing applied to the current median NLM GW Model. The post-processing was performed partly due to limitations of the liquefaction triggering method for modelling liquefaction in the very near surface (e.g. less than 0.5 m depth) and since the evapotranspiration rate would substantially increase if the GWL is near ground surface (which was not explicitly accounted for in the adopted SLR approach or median NLM GW Model).

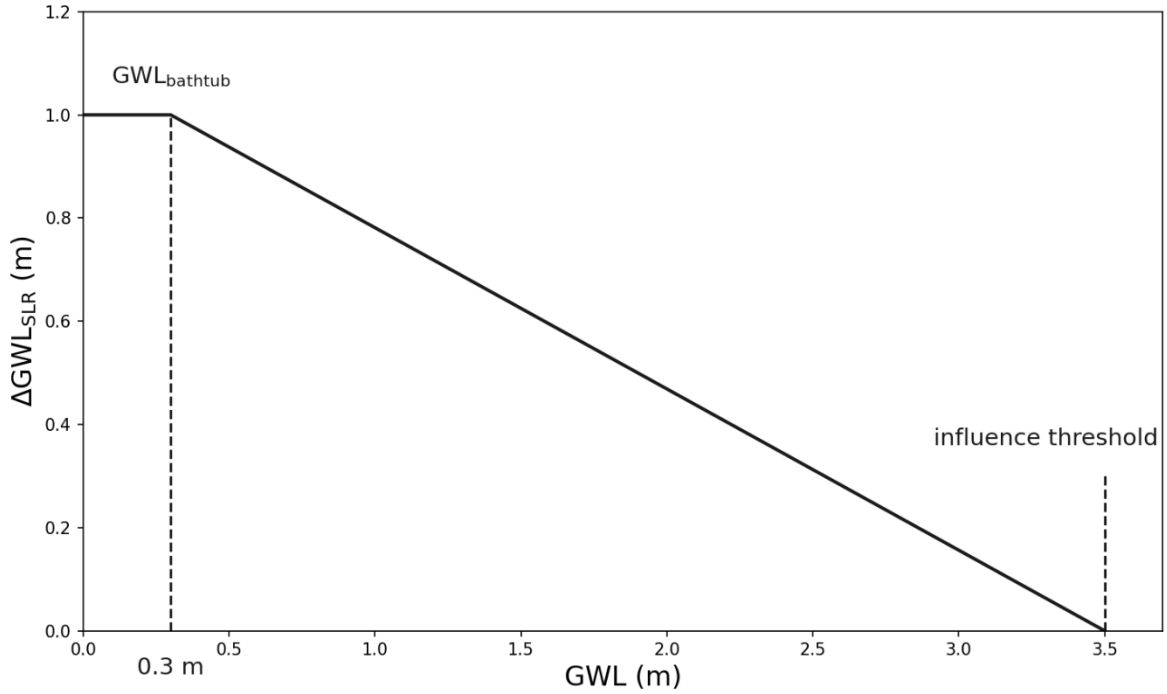

Figure 9.11: SLR model showing change in GWL for 1 m SLR

The increase in GWL is shown in Figure 9.12 and Figure 9.13. These figures highlight how SLR may have significantly different inward extents in different regions. In Napier, the increase in GW elevation extends inland 4-6 km in most areas, compared to the 2-3 km inland extent for Lower Hutt.

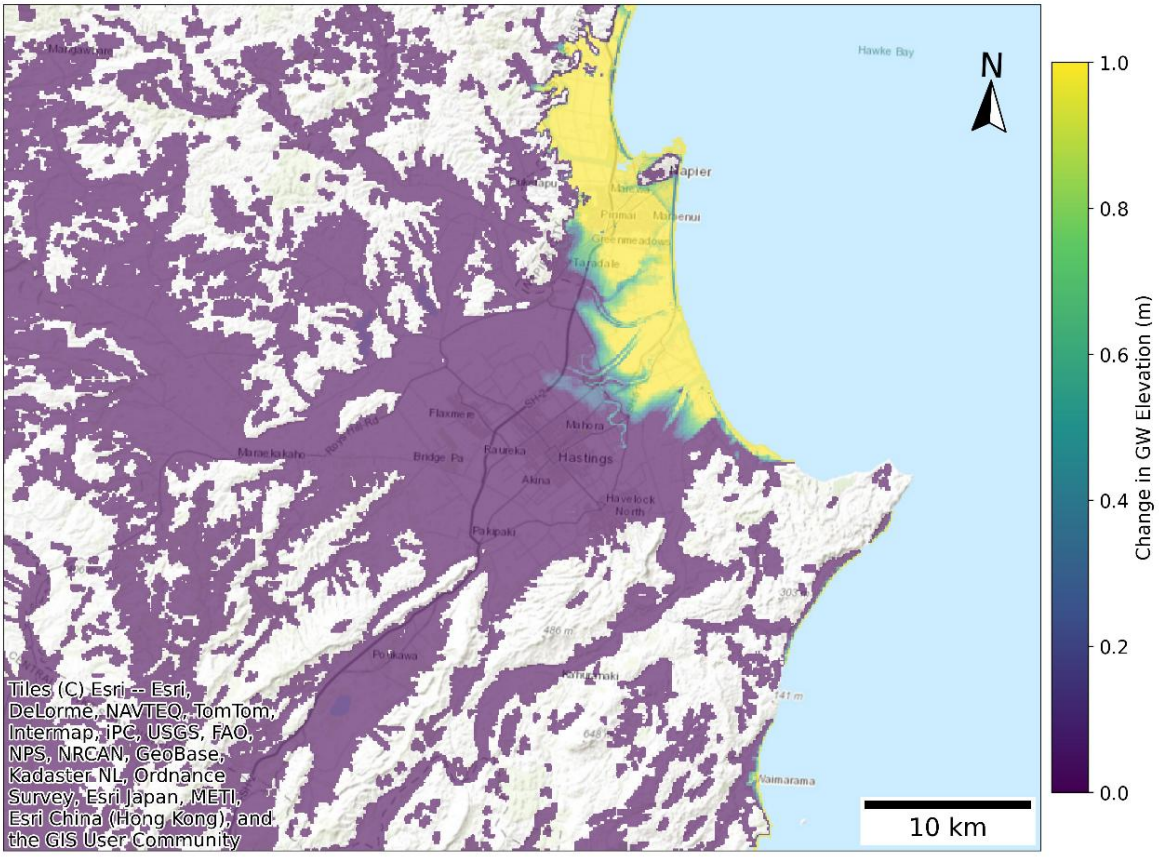

Figure 9.12: Increase in GWL assuming 1 m SLR, Hawke's Bay

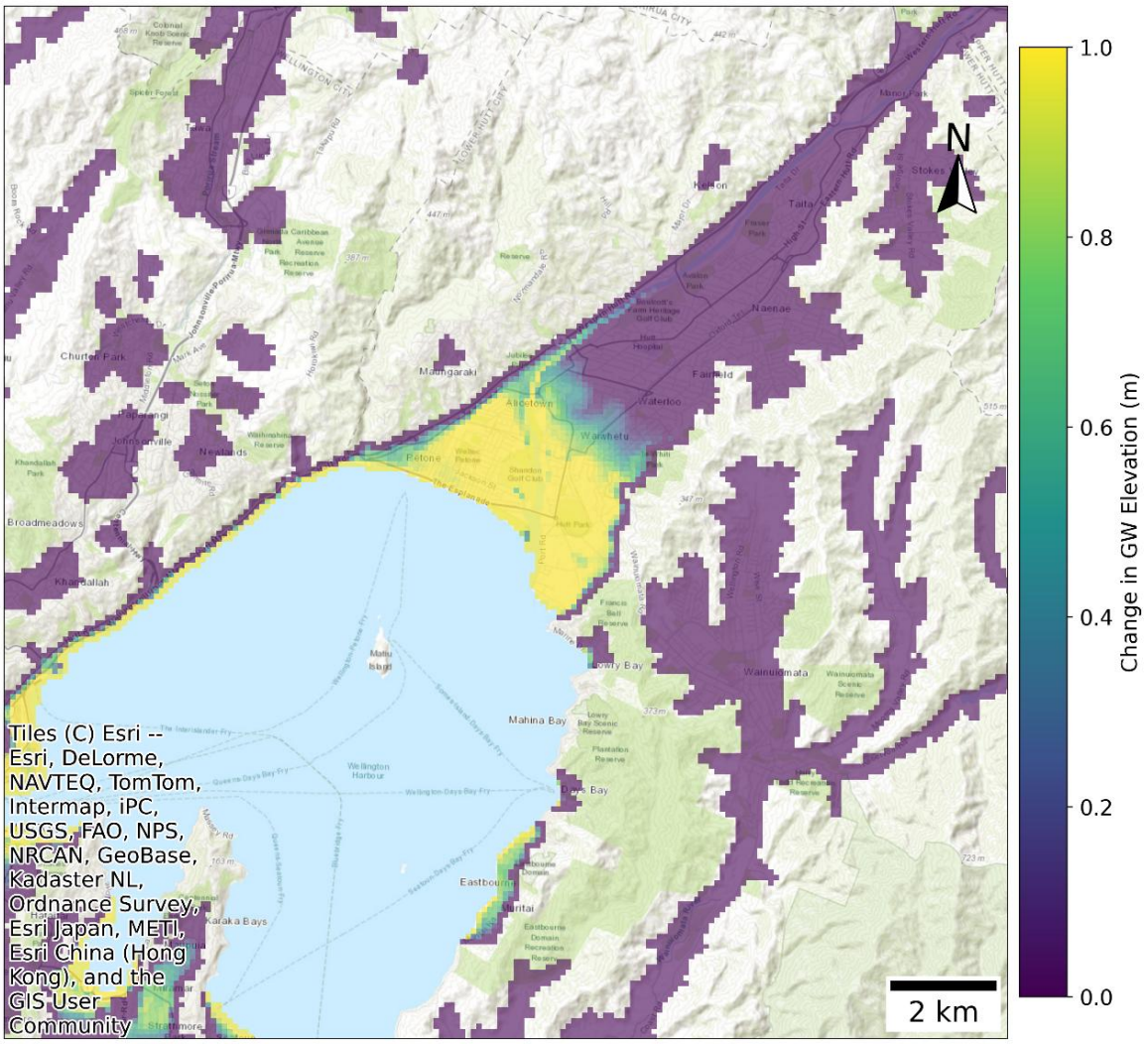

Figure 9.13: Increase in GWL assuming 1 m SLR, Lower Hutt

9.4 Model validations

This section begins by comparing the NLM GW Model to observed GW measurements at key locations. GWD outputs are then compared with the NWT model. Three regional models are included for comparison: Hawke's Bay (GWD), South Dunedin (both GWD and SLR), and Christchurch (SLR). The final part of the validation focuses on several earthquake-specific GW models in Christchurch.

9.4.1 Comparison to observation points

Figure 9.14 shows a cross-section in Lower Hutt, indicating how the modelled GWL and ground surface elevation varies in space. The seasonally corrected data used in training the model is also presented, which shows that while there are outliers in certain regions with limited data, overall, the modelled surface follows the measured readings well. Note that the cross-section does not capture the 3D surfaces (into-the-page direction) which is why some observations appear above the ground surface.

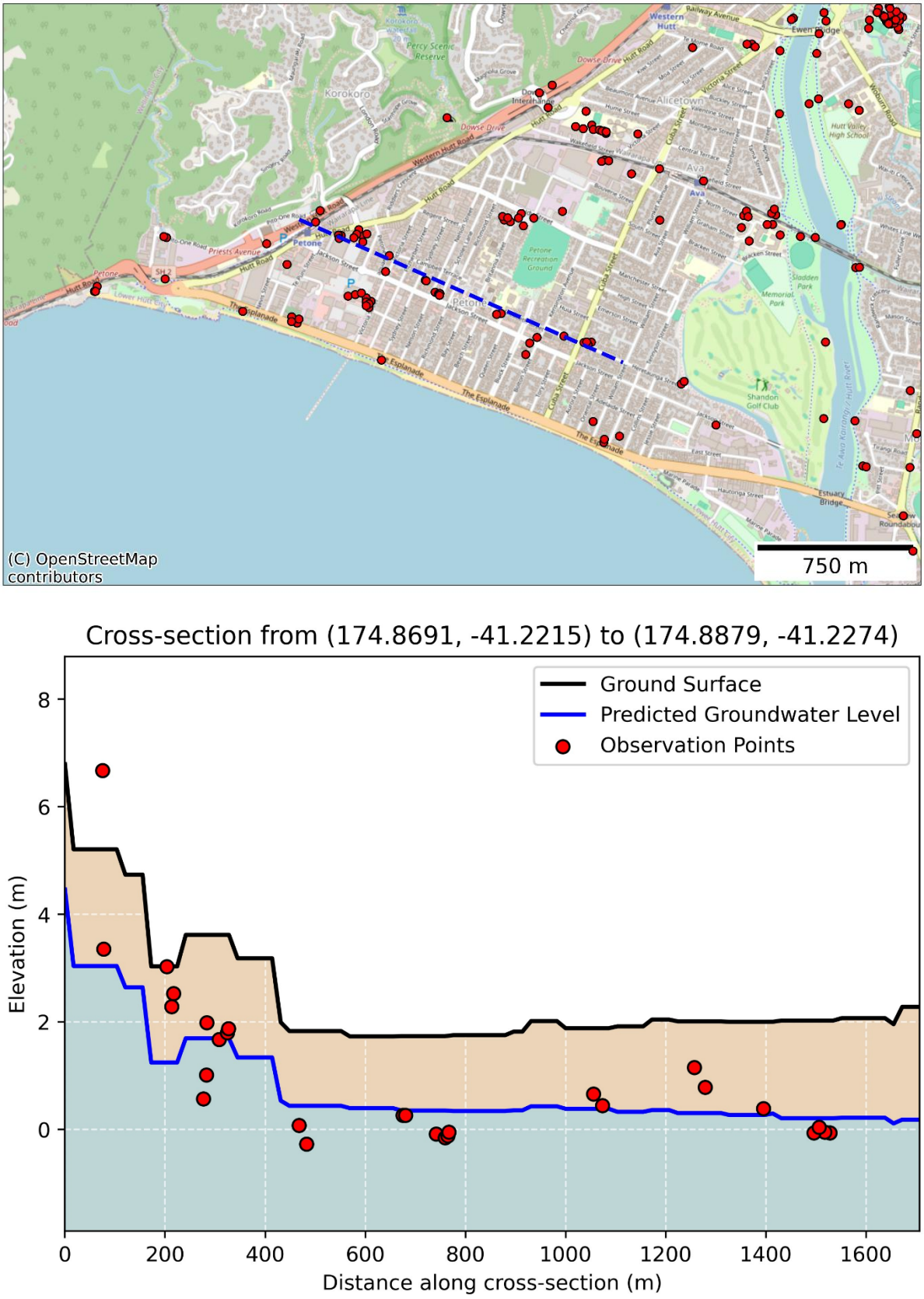

Figure 9.14: Cross-section through Lower Hutt showing modelled GWL (blue), ground surface elevation (black) and GW readings within 100 m of the cross-section

Figure 9.15 shows a cross-section in Napier, the cross-section again shows the relation between the modelled GWL and the ground surface elevation. In some cases, the data points appear to be a considerable distance from the modelled surface. This may be either due to the large out-of-plane distance between the cross-section and some readings (up to 100 m), or because of seasonal variation, or other unknown reasons.

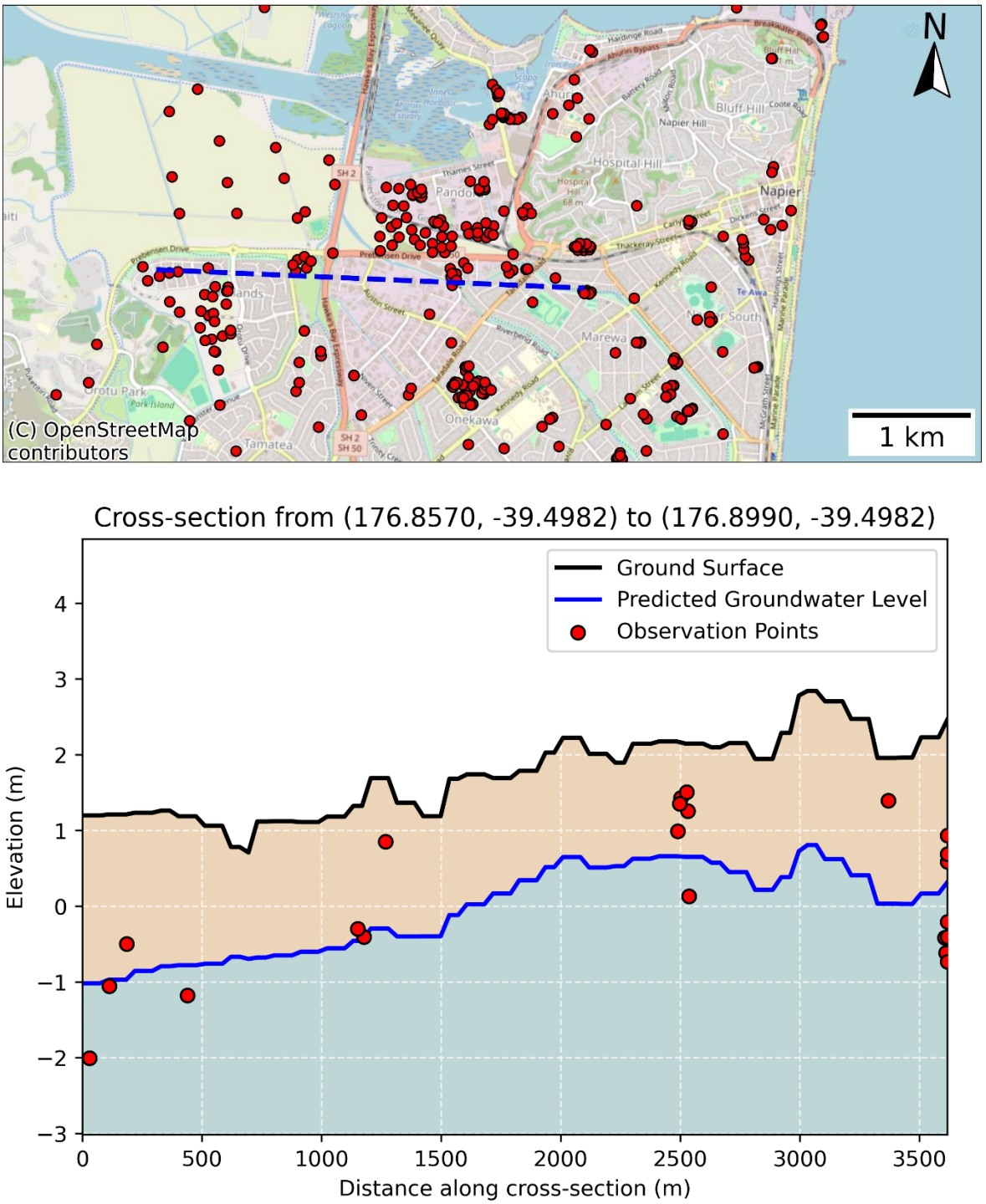

Figure 9.15: Cross-section through Napier showing modelled GWL (blue), ground surface elevation (black) and GW readings within 100 m of the cross-section

Figure 9.16 shows a cross-section in Christchurch, where a lot more data is available and as such, the model creates an “average” in the areas with a higher density of GW readings. This highlights the importance of having more data to better ground-truth the model. In the future, as more data becomes available throughout the country, the NLM GW Model is also be expected to improve.

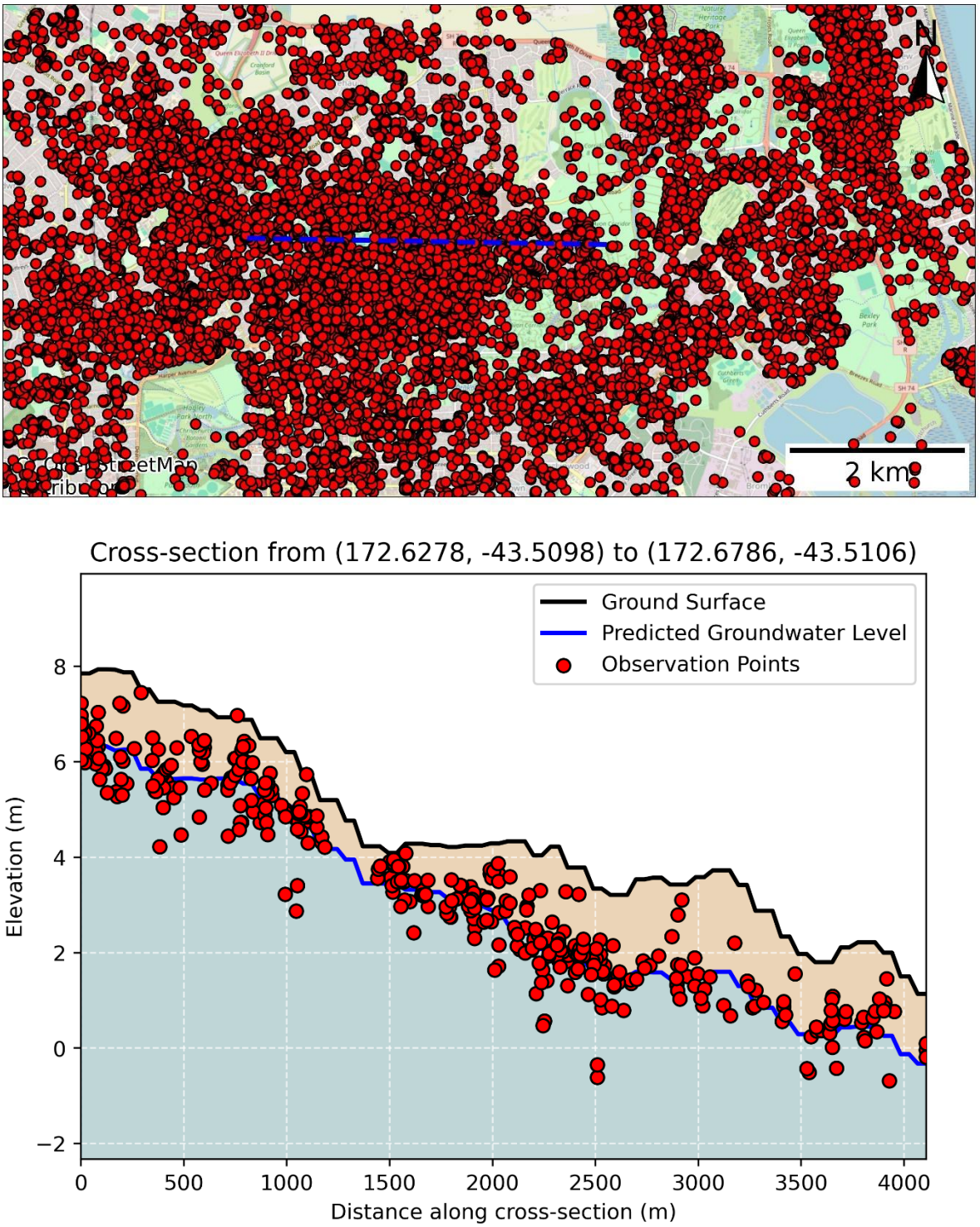

Figure 9.16: Cross-section through Christchurch showing modelled GWL (blue), ground surface elevation (black) and GW readings within 100 m of the cross-section

9.4.2 Comparison to NWT model

Figure 9.17 shows a set of validation plots between the NLM GW Model and the NWT model (GNS Science, 2018). Figure (a) shows actual measured GWDs from all the wells and bores used as input data and cover all of New Zealand. Figure (b) shows NLM GW Model values and (c) shows NWT model values at the same locations as the actual measured GWDs from all the wells and bores. Figures (d) and (e) show the residuals between modelled and actual values for the NLM GW Model and NWT model. While the NLM model residuals are roughly symmetrical and centred on 0 with minor deviations in edge cases, the NWT model residuals appear more skewed and have larger variation against the raw data, over-predicting the depth to GW in a significant number of cases. Figure (f) shows the difference between the NLM GW Model and the NWT model.

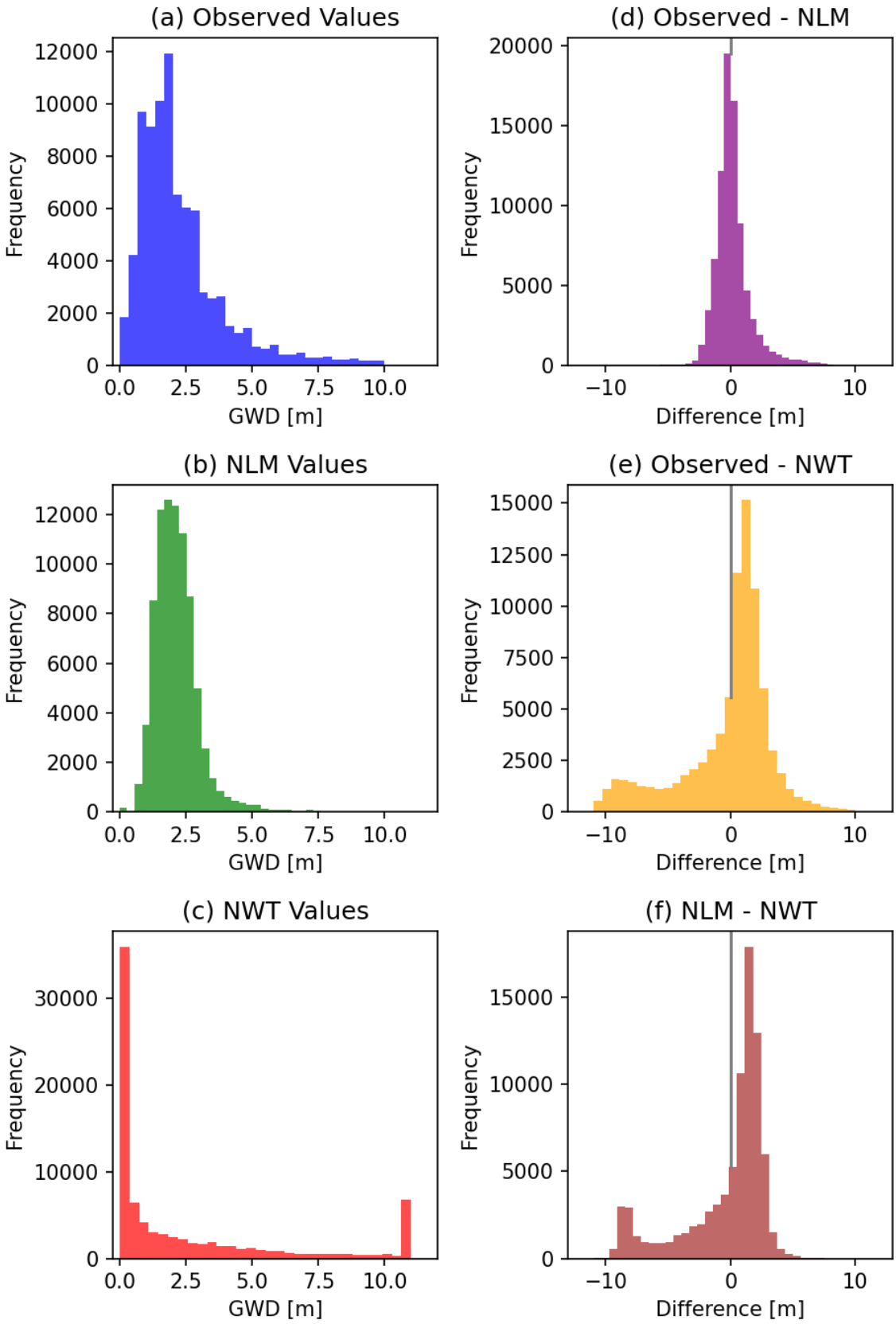

Figure 9.17: Comparison between NLM GW Model and the NWT model, where a) Shows the observed values, b) NLM model predicted values at the observation locations, and c) NWT model predicted values at the observation locations. The differences are shown on the right-hand side, where d) shows residuals for the NLM GW Model, e) shows the NWT model residuals, and f) shows a comparison between the NLM and NWT models for values taken at 100 m grid spacing.

The NLM GW Model appears to better represent in-situ observation data compared to the NWT model based on modelled residuals. The NWT model has a larger distribution of residual values compared to the NLM. These discrepancies are likely due to the lower resolution of the model, as well as the NLM GW Model's ability to capture local scale variability reflected in static well observations. This comparison for in-situ observations only represents areas with data or a higher density of data. As the NLM model is data-driven, it is difficult to validate the model in data-scarce areas.

9.4.3 Comparison to Hawke's Bay regional model

Figure 9.18 shows the previously modelled depth to the unconfined GW surface by GNS (Rosser & Dellow, 2017) compared to the predictions from the NLM GW Model. The two models are presented in the same colour palette for comparison purposes.

Both models show a gradual increase in GWD from the coast going inland. The shallowest GW conditions are near Hastings, Napier and the coastline. The GNS model predicts a greater extent of shallow GW conditions (GWD < 2.5 m), particularly in the centre of the plains through to the coast compared to the NLM GW Model. In addition, the NLM GW Model shows greater spatial heterogeneity in GWD within the Heretaunga Plains. The NLM GW Model tends to predict slightly deeper GW conditions along the periphery of the basin although there are few observation points to constrain the model. This is likely due to modelled features correlating to GWL, such as topography.

Discrepancy between the GNS and NLM modelled shallow GW conditions may be attributed to differences in observation data and/or modelling methodology. The GNS surface modelled three zones across the Hawke's Bay region and used a combination of time series data (n = 35), static water levels (n = 449), and surface water feature data. A kriging model with linear drift was used to predict the depth to GW from observations. The GNS model used a different classification methodology from the NLM GW Model to identify unconfined static water level observations, and this may explain some of the differences in output surfaces. In addition, the GNS model has a lower 250 m resolution, which may dampen some local spatial heterogeneity.

The GNS model extents were limited to the major unconsolidated sediments of the Heretaunga Plains based on QMAP geology. In contrast, the NLM GW Model has a greater coverage. The sharp transition in the NLM GW Model from deeper to shallower GW conditions observed on the western extent of the plains is an artifact of the stitching together of the national and locally refined GW models underlaying the NLM GW Model.

In general, based on this semi-quantitative comparison, the NLM GW Model has a relatively similar performance in this region based on a visual comparison to observational data used in NLM GW Model. Due to the differences in input datasets, a field-based survey would likely be required to help constrain shallow unconfined GWLs which have been used in the models. In addition, as new observational data becomes available, the NLM GW Model can be updated, thereby improving the uncertainty associated with the model prediction in areas that are scarce in data.

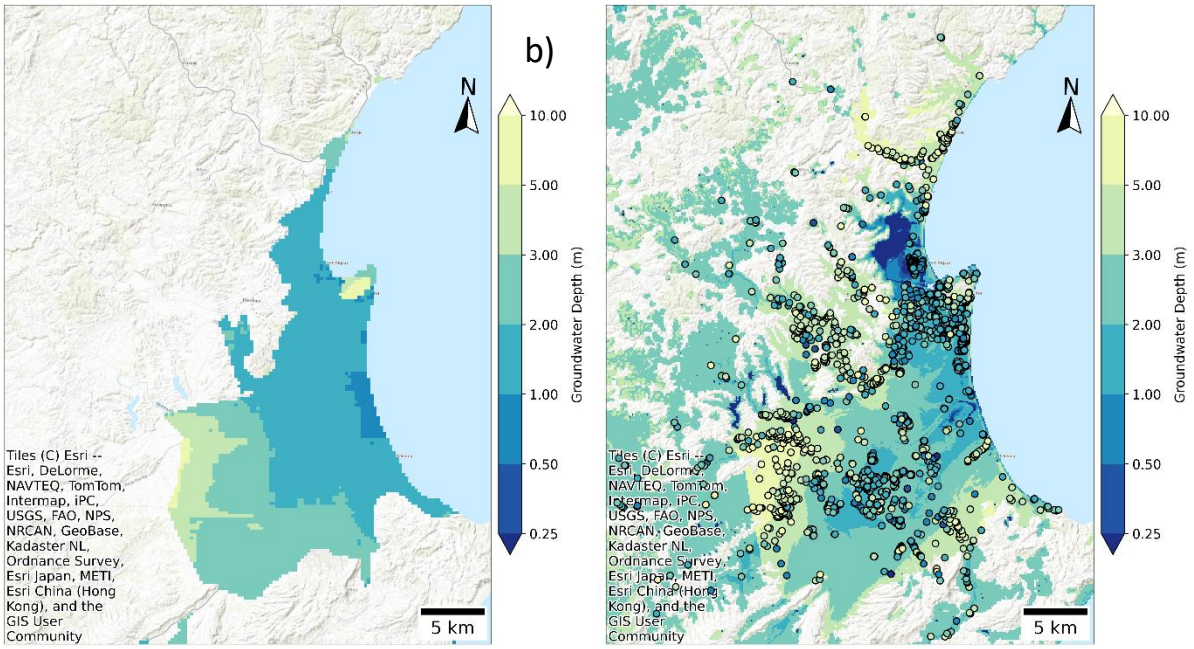

Figure 9.18: Comparison between GNS unconfined GW surface: a) Figure 4.2 from (Rosser & Dellow, 2017), and b) T+T NLM GW Model with GW observations shown as an overlay

9.4.4 Comparison to South Dunedin regional model

The maps of current unconfined GWL and the GWL with 1 m SLR from the South Dunedin GW models by GNS (Cox et al., 2023) were used as a benchmark validation for the NLM GW Model. Figure 9.19 (a) and (b) below show the NLM GW Model. Figure 9.19 (c) to (f) show the two GNS models (numerical in the middle row and geometric in the bottom row) for the current GWLs (left-hand side) and the GWLs assuming 1 m of SLR (right-hand side). GWL is compared and presented in the same colour palette as the original report Cox et al. (2023) for comparative review. The numerical and geometric models represent two different methods of estimating the GWL. The geometric model adopts a statistical approach with smoothing, while the numerical model is determined from a physics-based simulation. Both models were augmented to provide estimates of GWL for different SLR conditions, including a 1 m SLR scenario.

A comparison for the current conditions (SLR = 0 m) between the GNS model and the NLM GW Model shows that they generally agree, especially with the geometric model, noting that the NLM has greater spatial variability and noise. This is likely due to a combination of the modelled resolution and the underlying spatial variability of the input features. A notable difference is higher GWLs in the NLM GW Model along the southern coast, which is associated with an increase in ground surface to ~7 mRL compared to surrounding areas of ~1 mRL.

For the 1 m SLR scenario, the predicted GWLs from the NLM SLR GW Model are between the numerical and geometric GNS models. The differences along the southern coast for the median GWL model are also present and amplified in the NLM SLR GW Model.

Overall, the NLM GW Model appears to predict slightly higher GW elevation values compared to the two GNS models in terms of median current elevations, and predictions in between the two GNS models for SLR predictions.

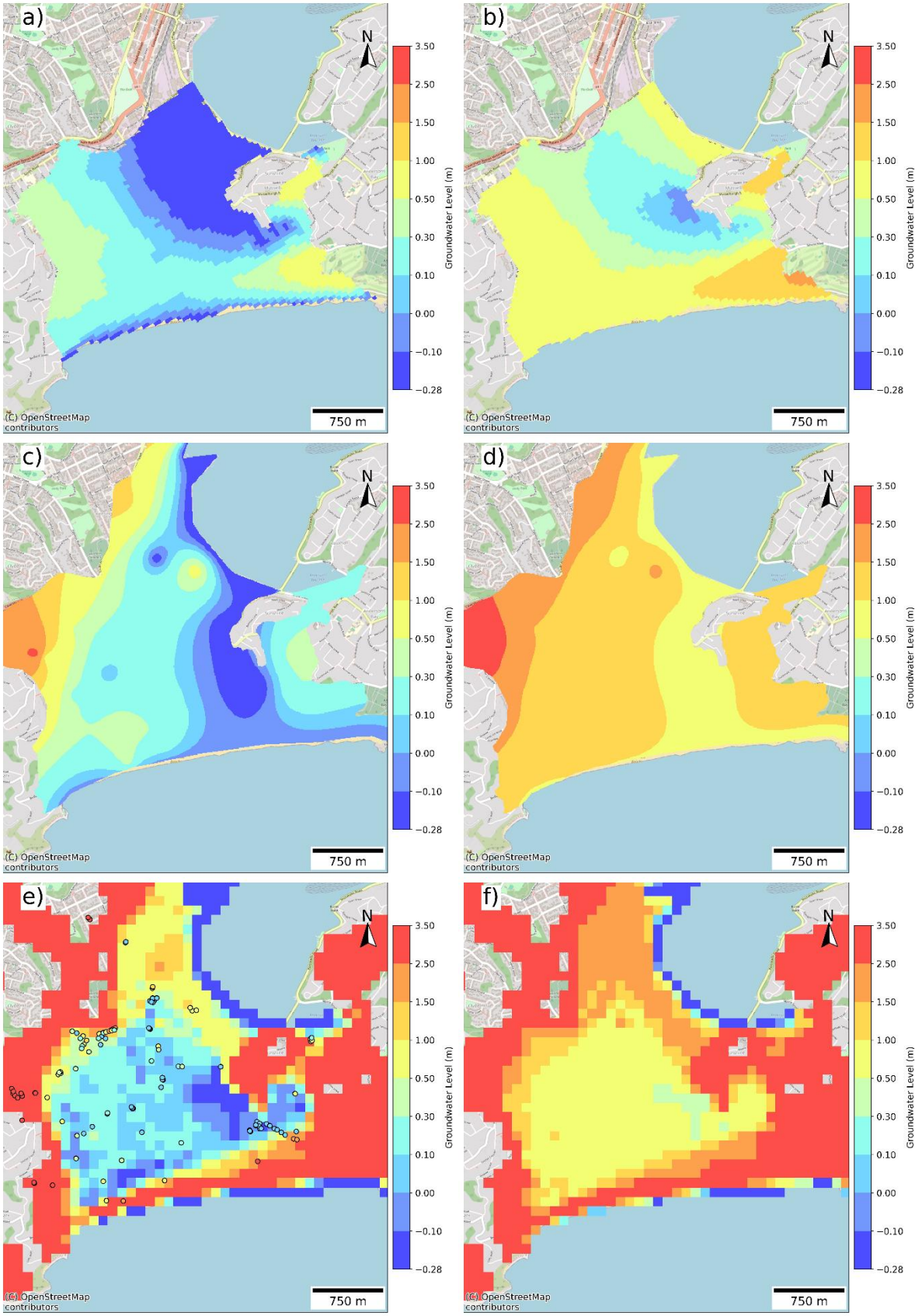

Figure 9.19: (a,b) South Dunedin NLM GW Models, (c,d) GNS numerical model, (e,f) GNS geometric model. GNS model from Cox et al. (2023). (a,c,e) Current GWLs and (b,d,f) GWLs with 1 m SLR

9.4.5 Comparison to Christchurch SLR regional model

The impact of 1 m SLR on shallow GW in the Christchurch region was previously modelled by Aqualinc (Rutter, 2020) (see Section 3.4.2.5). This model was used as a benchmark validation for the NLM SLR GW Model.

Figure 9.20 shows two maps of Christchurch and the change in GW surface that would be expected assuming 1 m of SLR. The Aqualinc model models SLR through a change in constant head boundary conditions along the estuary and coastlines equal to the SLR projection. The change in GW heads is calculated as a difference in steady-state model runs pre- and post- SLR.

Figure 9.20 shows that SLR is affecting GWL for a similar extent in both models. The NLM SLR GW Model predicts a greater impact of SLR on GWLs for areas close to the Avon River compared to the Aqualinc model. In general, the NLM SLR GW Model predicts slightly larger GW head changes within proximity of the coast, except for the area south of the Waimakariri River, where the NLM SLR GW Model predicts little impact from SLR.

The difference between the NLM SLR GW Model and the Aqualinc model generally explained by differences in modelling approach. The NLM SLR GW Model uses a data-driven approximation to SLR based on predicted GWLs, whereas the Aqualinc model uses a process-based approach using numerical modelling and SLR projections. As numerical modelling of SLR is considered out of scope at a national scale, based on these comparisons, the conclusion is that the NLM SLR model approach generally captures the spatial variability and magnitude of SLR projections.

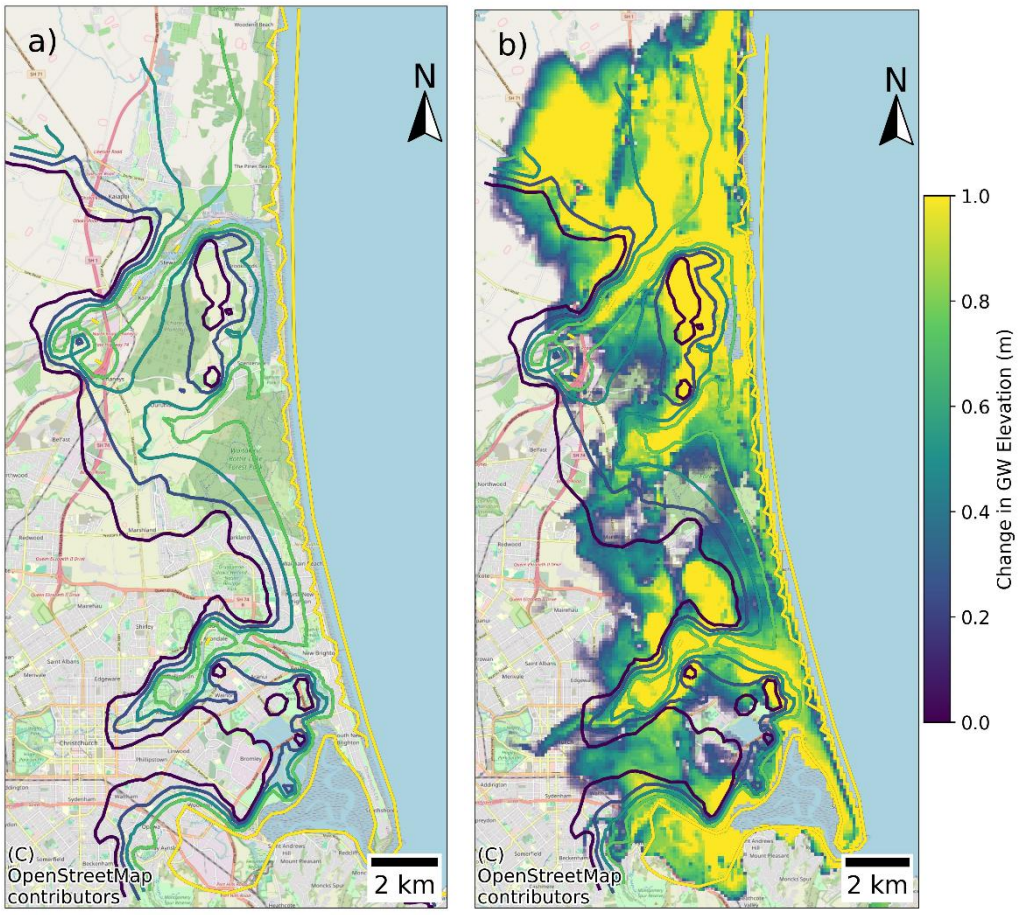

Figure 9.20: Comparison between a) Aqualinc 1 m SLR map with 0.2 m contours, and b) overlaid on top of the NLM predicted GW change assuming 1 m of SLR

9.4.6 Comparison to Christchurch earthquake-specific GW models

In order to compare the NLM GW Model with the Christchurch earthquake-specific GW models, a "seasonal trend" version of the NLM GW Model was computed by adding the daily offset value computed from the regional "seasonal trend" (see Section 9.2.3.2) to the median GW surface. Additionally, the measured GWDs were seasonally corrected (using the NLM seasonal trend - Equation 26).

Figure 9.21 to Figure 9.24 show the comparison between the NLM GW Model with the "seasonal trend" offset applied and the event-specific GW models (Tonkin + Taylor, 2013). Figure 9.21 spatially compares the 4 September 2010 models, with distributions of observations and differences compared in Figure 9.22. Figure 9.23 spatially compares the 22 February 2011 models, with distributions of observations and differences compared in Figure 9.24.

Both the NLM "seasonal trend" GW outputs and the event-specific T+T GW models were created by first developing a shallow median GW model (using different methodologies) and then applying an offset (once again using two different methodologies) to calculate a season/event-based GW model.

Comparison of the respective NLM "seasonal trend" GW outputs and the previously modelled event-based GW surfaces show a relatively large difference in modelled GWD between both models. The NLM "seasonal trend" GW outputs show a lower spatial variability in GWD compared to the event-based models created by T+T (2013). This is because the methodology used to create the median NLM GW Model follows topographic features more closely, thereby resulting in lower spatial variability of the GWD surface. The similarities between Figure 9.21(b) and Figure 9.23(b), and Figure 9.21(c) and Figure 9.23(c) suggest the main difference between the NLM "seasonal trend" GW outputs and the event-specific T+T GW models stem from the base median model, rather than the offsets applied to account for the "seasonal trends".

When the GW observations are compared to both the NLM "seasonal trend" GW outputs and the event-specific T+T GW models, both the spatial variability and distribution of residuals is lower in the NLM "seasonal trend" models compared to the residuals from the event-specific T+T models (Figure 9.22(e)(f), and Figure 9.24(e)(f)). However, the NLM seasonal trend correction does bias this evaluation. Overall, the NLM model produces GWDs generally within 0 to 2.5 m which is largely consistent with both the observation points, and the prediction of the event models.

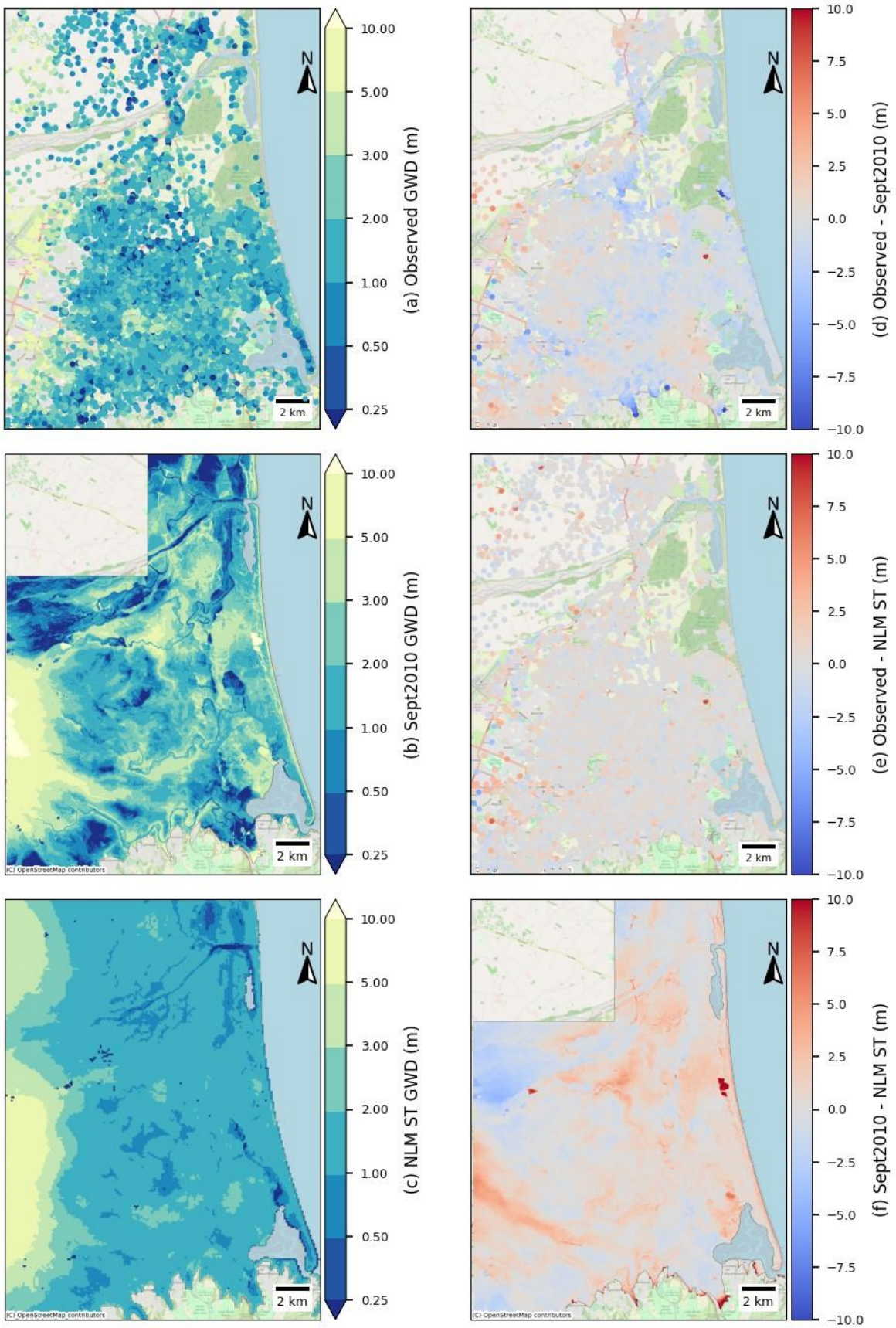

Figure 9.21: a) GW observations, b) 4th September 2010 specific GW model, c) NLM ST GW Model for 4th September, and d) e) and f) The differences between a) b) and c)

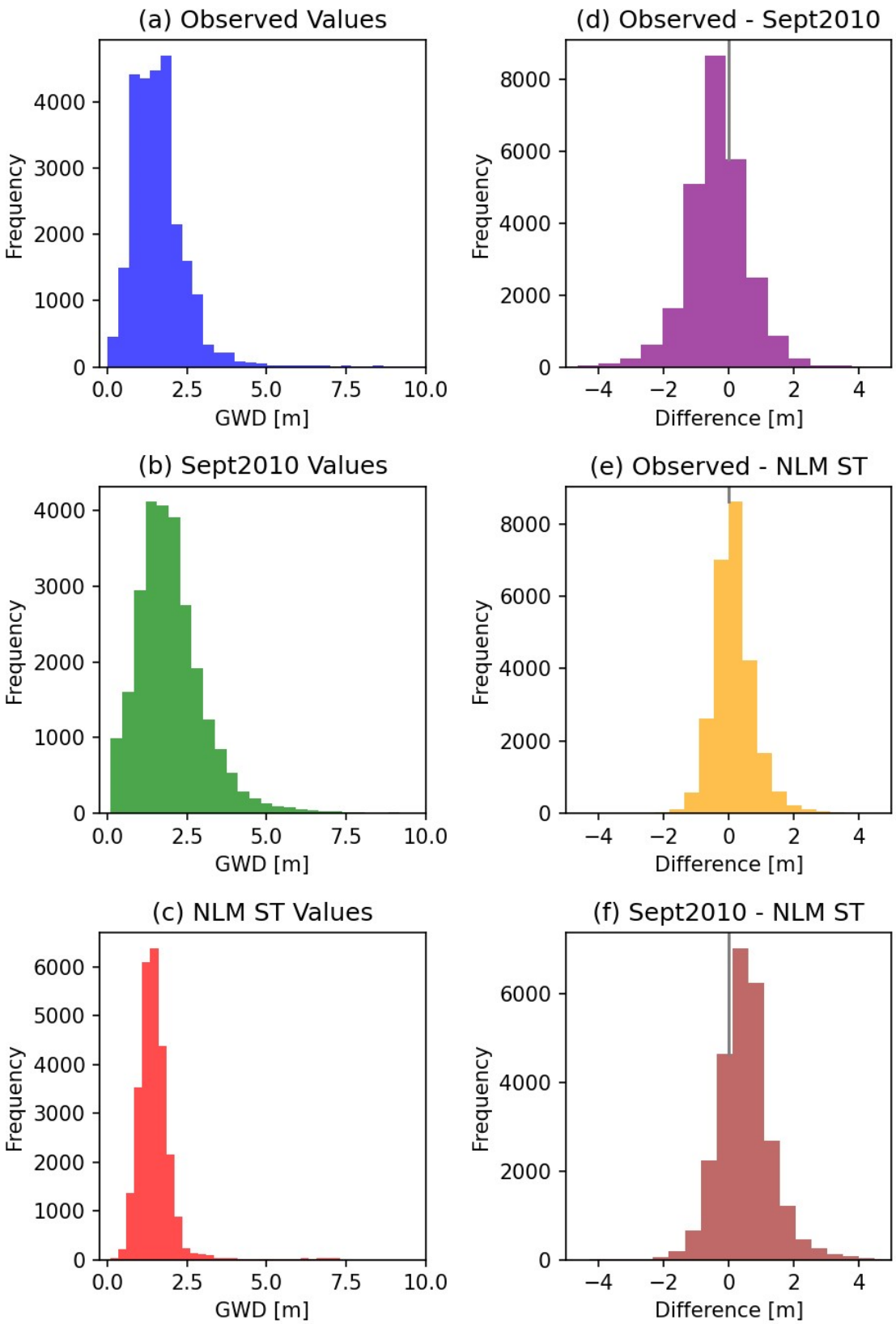

Figure 9.22: a) Histogram of observed GWD values, b) Histogram of 4th September 2010 specific GW model values, c) Histogram of ST NLM GW Model values for 4th September, and d) e) and f) Histograms of differences between a) b) and c)

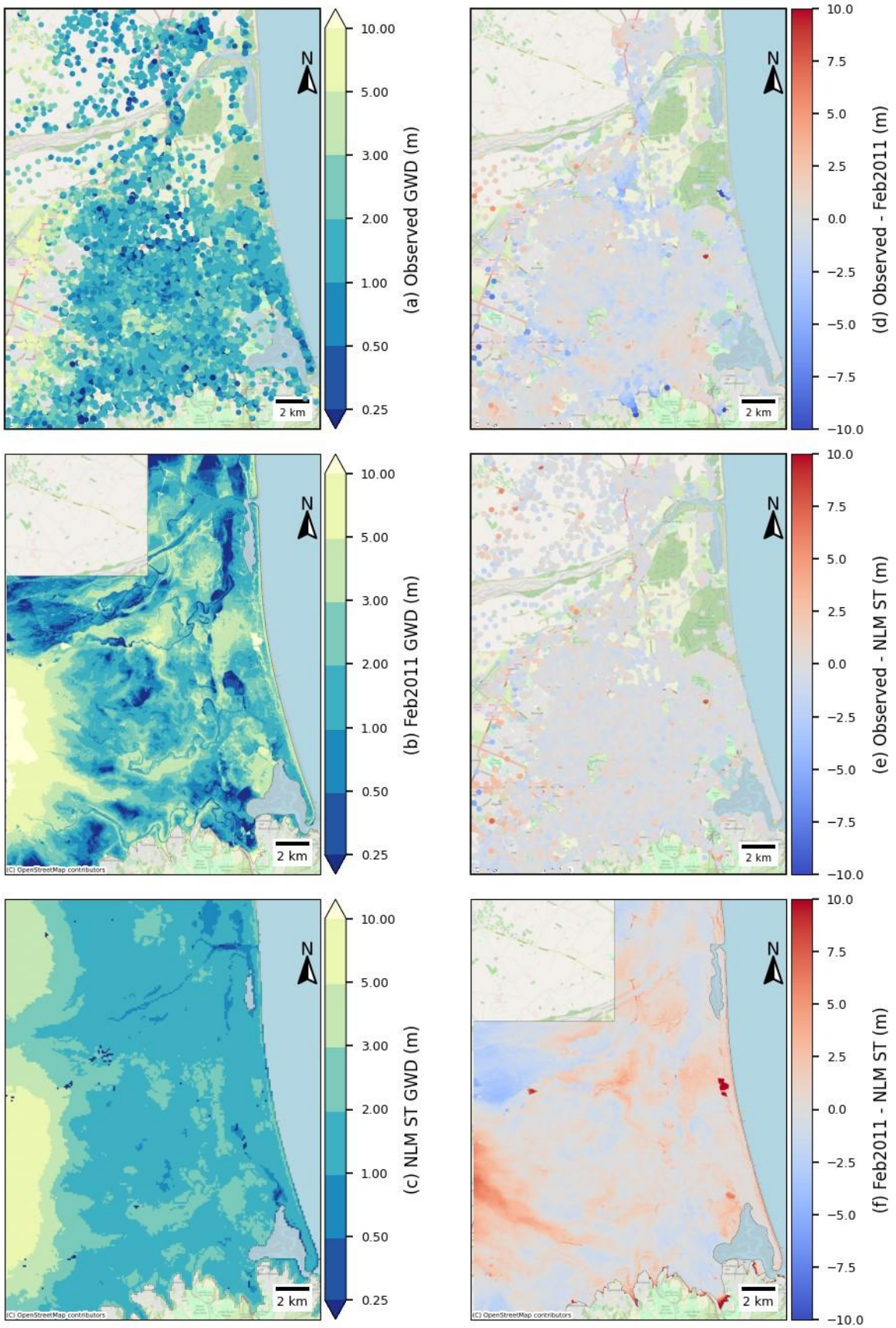

Figure 9.23: a) GW observations, b) 22nd February 2011 specific GW model, c) NLM ST GW Model for 22nd February, and d) e) and f) The difference between a) b) and c)

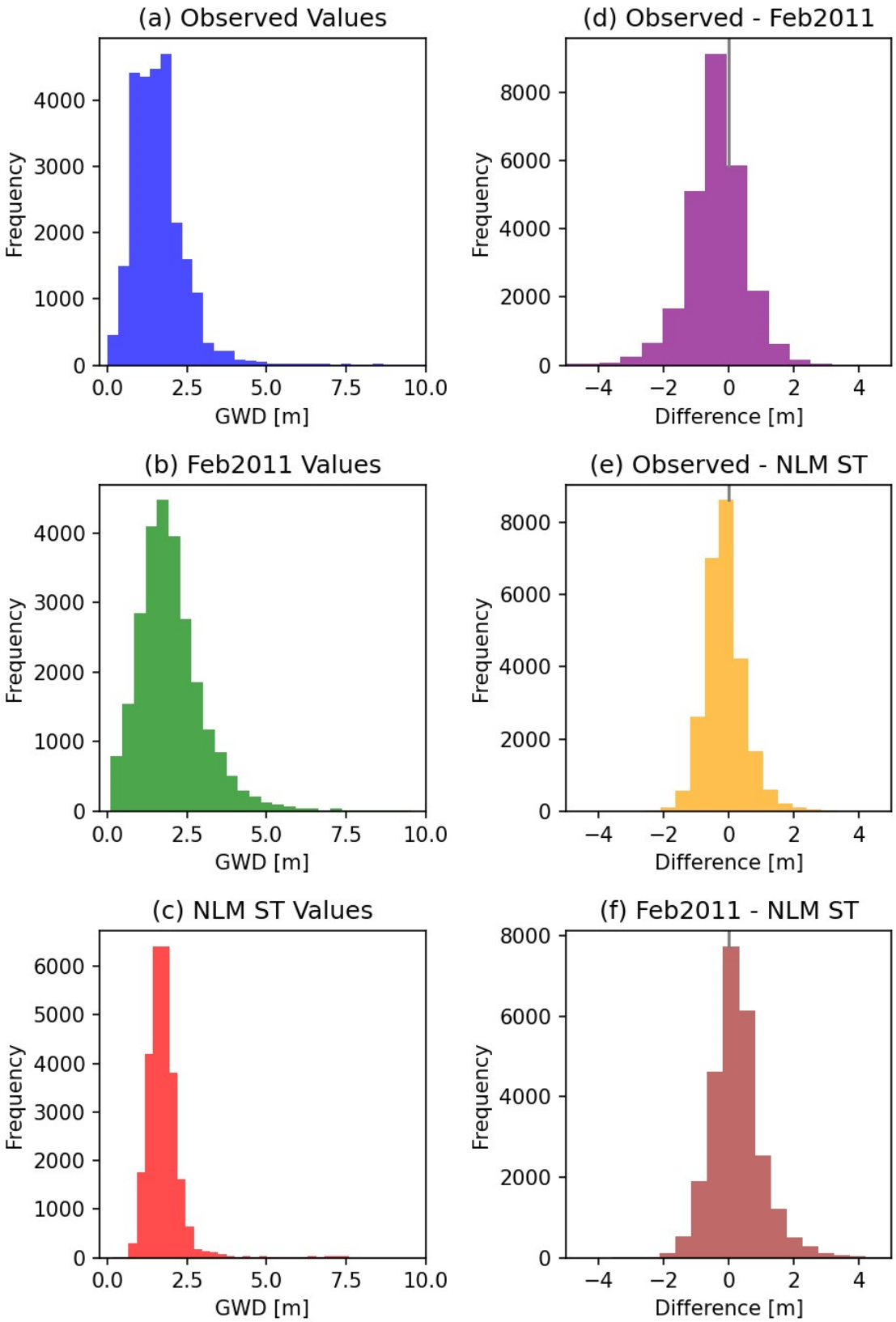

Figure 9.24: a) Histogram of observed GWD values, b) Histogram of 22nd February 2011 specific GW model values, c) Histogram of ST NLM GW Model values for 22nd February, and d) e) and f) Histograms of differences between a) b) and c)

9.5 Limitations

This model uses data-driven techniques to approximate GW behaviour via regression modelling and kriging with some post-processing corrections. This is a simplified statistical representation of a complex system based on static GW observations and national datasets to inform spatial heterogeneity of median shallow GWDs and the expected range of uncertainty. Predicting GWLs is challenging because GW systems are highly variable and time dependent, and the supporting data is often sparse, inconsistent, or incomplete.

The following limitations should be noted:

1 The model provides a prediction of GW elevation and depth at specific points on a 100 m grid. The use of this prediction for surrounding areas (i.e. between points) comes with additional uncertainty and error especially in areas with sharp changes in ground surface topology.

2 The regression model does not account for the spatial density of data points and therefore over-represents areas if there is a high reading density in the predictions.

3 Data scarcity across many regions and uncertainties in the GW measurements used to train the model further reduce its reliability. Much of the data cannot be fully verified, and problems such as measurement errors, uncalibrated sensors, and inconsistent sampling methods will affect the model's accuracy. In some areas, particularly those with few or no observations, it is impossible to accurately represent GWLs. As a result, the model relies on extrapolation and broad assumptions, which can lead to less reliable (and in some cases unreliable) predictions in those regions. While these limitations will be less important in some areas (e.g. non-liquefiable soils or low population density), others could be significantly impacted given shallow GW plays a major role in assessing liquefaction hazard.

4 In the process of integrating the national model with locally refined regression kriging-based models, there can be sudden and "unnatural" boundary shifts. These abrupt transitions highlight the model's limitations in seamlessly connecting various data scales and are an inherent limitation of the modelling approach.

5 The kriging interpolation is locally sensitive to nearby observations, and when stitched together with coarser national-scale predictions, mismatches can occur at the edges where different models meet. These boundary effects are particularly noticeable where local models are constrained by dense, high-quality data and adjacent national models rely on sparse, uncertain inputs. As such, care must be taken when interpreting outputs near these boundaries as sharp transitions are likely to be artefacts of the modelling framework, rather than real hydrogeological conditions.

6 The national and local regression models often cover areas with significant changes in ground surface elevation (i.e. from sea-level to 400 m elevation). This makes the predicted GW elevation very sensitive to ground surface elevation and may overestimate the influence of small changes in the ground surface.

7 The stitching of the 1 m LiDAR and 8 m DEM across the country results in some sharp unrealistic transitions in the national elevation model (see Section 3.1.3) which affects DEM-derived features like slope and wetness to index. This results in visible artifacts along the stitched boundary for the depth to GW predictions (see Figure 9.5). As coverage of the higher resolution 1 m LiDAR increases, this boundary effect between DEMs should diminish. This boundary effect may result in discontinuity of the modelled liquefaction hazard.

8 The SLR model is a simple approximation of a complex process, with limited data available for calibration. It uses a zonal approach, where areas closest to the coast are assumed to have a 1:1 rise in GW with sea-level, tapering off inland based on current GW elevation. Because the model uses predicted GWLs as input, any errors in those predictions are directly carried into the SLR outputs. While this method reflects general expectations about the role of drainage

features, the thresholds used are based on assumptions rather than site-specific data. As a result, predictions should be seen as broad indicators rather than precise forecasts.

9 The majority of static water depths were sourced from the NZGD. The limitations on accuracy and disclaimers for the NZGD are applicable to the NLM output. These include but are not limited to:

- No warranties are provided in relation to the accuracy or fitness for any purpose of Geotechnical Data uploaded to the NZGD. You must exercise reasonable care and perform due diligence when using Geotechnical Data obtained from the NZGD.
- Users acknowledge that Geotechnical Data uploaded to the NZGD may have been compiled for a purpose other than the purpose for which you intend to use the Geotechnical Data.

10 The NLM GW Model has been developed for the purpose of providing input into the LV module and has been developed with an emphasis on outputs that are important to liquefaction assessment, therefore it should not be relied upon for other purposes. Given the highlighted assumptions and limitations, it cannot be seen as a replacement for more specific local GW assessments and any use outside the explicit NLM modelling purposes detailed here have not been explored and are highly uncertain.

9.6 Potential future improvements

To enhance the NLM GW Model and address its current limitations, several potential future improvements have been identified:

1 **Include continuous monitoring data**. Incorporate time-series data from continuous monitoring stations to improve understanding of seasonal and long-term GW trends.

2 **Multiple national models for uncertainty quantification**. Developing models with different methods and input features would allow for comparison of results and better estimate the uncertainty in predictions.

3 **Regular model updates with improved data**. As higher-resolution and more reliable datasets become available (e.g. LiDAR, GWLs), updating the model provides more accurate and current outputs. Over time, this may help resolve some of the boundary issues listed in the limitations section above.

4 **Addition of features unavailable nationally**. Including features (such as river levels) only available at local scales enhances prediction where this data exists, even if not uniformly available nationwide.

5 **Create more locally refined models.** Identifying and refining additional regions allows better local accuracy, especially where the national model is reliant on scarce data and hence lacks detail.

6 **Use of local expert knowledge**. Experts can provide context-specific insights on GW behaviour that can improve model relevance and performance in their regions.

7 **Down-sampling in dense data areas**. Reducing the influence of over-sampled regions helps to reduce model bias. This could be achieved by assigning reduced weightings to GW measurements located in areas of high measurement density, as is currently done with GIs in the LV module.

8 **Adjust uncertainty in low-data areas**. Recognising and increasing uncertainty estimates in regions with sparse data since these areas may be extrapolations rather than interpolations and the uncertainty defined through the regression model would therefore underestimate the uncertainty.

9 **Smoothing model transitions**. Improving consistency at the boundaries between refined local models and the national model avoids unrealistic discontinuities in liquefaction hazard

predictions. While this obscures a significant limitation of the method, smoothing the national model predictions towards the regional estimates would most likely improve estimates of the GWD.

10 **Smoothing GW elevation surface**. The GW elevation may be oversensitive to localised changes in ground surface elevation due to the regression model predictions. The surface could be smoothed prior to computing the GWD.

11 **Refine shallow GWD threshold for obtaining unconfining aquifer depth measurements**. The depth to confined aquifers varies considerably by region, whereas currently the unconfined depth threshold is set nationally to 10 m. By adjusting the threshold regionally, additional data could be included.

10 Land damage fragility assessment

The assessment of liquefaction-induced land damage is an important measure for evaluating the impacts of liquefaction and is an important output for many end users (e.g. it is an integral step in the MBIE/MfE mapping process). Additionally, land damage observations from historical events can be compared against predicted land damage from the NLM for the purposes of validation.

A LDFC provides a function that returns a probability of a land damage state being reached or exceeded for a given LDM. Geyin & Maurer (2020) have developed LDFCs using LSN as the LDM. However, these are based on different land damage categories to those used in the MBIE/MfE mapping process, and a different liquefaction susceptibility I_c cut-off was used for computing LSN. To address these differences, this section presents the development of LDFCs using the NLM GI dataset and a subset of the land damage observation dataset from Bastin et al. (2021), adapting the methodology from Geyin & Maurer (2020).

10.1 Module output

The LDFCs module produces LDFCs for the Minor-to-Moderate and Moderate-to-Severe land damage categories as defined in the MBIE/MfE Guidance (2017). Different sets of LDFCs are produced for different input LDM (i.e. LSN with P_L=50% and P_L=15%). There are two different sets of LDFCs for different situations (only the adjusted curves are demonstrated in the scenario outputs in Section 11):

1 Fitted: The uncertainty in GWD is not explicitly accounted for in the calculation of the input LDM (i.e. a mean or median GWD is adopted with no consideration of uncertainty in the GWD depth). In this case, the directly fitted LDFCs could be adopted which implicitly include GWD uncertainty.

2 Adjusted: The uncertainty in GWD is explicitly considered (i.e. the calculation of the LDM considers a range of GWDs based on the uncertainty in GWD). In this case the adjusted LDFCs could be adopted. These curves are an adjusted version of the fitted curves that have had the uncertainty in GWD removed.

The data schema for the LDFCs is a structured set of nest objects (i.e. dictionaries) as outlined below. The LDFCs are stored in json file format where a different json file is produced for each LDM. The data schema is provided below where the Land damage category is either Minor-to-Moderate or Moderate-to-Severe, the LDM GWD uncertainty is either “fitted” or “adjusted”. The percentiles are the 15th and 50th percentiles which can be used to produce a cumulative lognormal distribution.

Data schema of LDFC json file:

<Land damage category>: <LDM GWD uncertainty>:<percentiles>

Note that the None-to-Minor land damage category from the MBIE/MfE Guidance (2017) is not provided since this is the complement of the Minor-to-Moderate LDFC (i.e. one minus probability of Minor-to-Moderate).

10.2 Development of fragility curves

10.2.1 Inputs

The development of LDFCs was based on a database of three historical earthquake events, with the event and observation details provided in Table 10.1. The augmentation of the event observations for the purposes of developing LDFCs is provided in Section 10.2.2. Additional events from Bastin et al. (2021) could be used in future revisions, however, the augmentation process in Section 10.2.2 would need to be revised and the complexity of handling multiple closely spaced events (e.g. June

2011 initial tremor and aftershock of Mw 5.3 and 6.0 respectively) would need to need to be addressed.

Table 10.1: Event information (reference numbers refer to list below)

Event ID	Event	GeoNet ID	PGA source	GWD source	Mw	Damage observations source	Case history count (LSN > 0.1)
Sept2010	September 2010 Darfield Earthquake	3366146	[1]	[2] (Sept)	7.1	[3]	14,539
Feb2011	February 2011 Christchurch Earthquake	3468575	[1]	[2] (Feb)	6.2	[3]	14,404
Feb2016	Valentine's Day Earthquake (February 2016 Christchurch)	3528839	[4]	[5] – extended with NLM GW	5.7	[6]	19,014

Case history data source references from Table 10.1**:**

- [1] Bradley (2014) and Bradley (2012), in some areas choosing to defer to kriging on strong motion station data (O'Rourke, T. & Milashuk, S., 2012).
- [2] (Tonkin + Taylor, 2013). "Liquefaction Vulnerability Study". #52020.0200/v1.0, Earthquake Commission, Wellington, New Zealand, 59p.
- [3] (Tonkin + Taylor, 2015). "Canterbury Earthquake Sequence: Increased Liquefaction Vulnerability Assessment Methodology". #52010.140.v1.0, Chapman Tripp acting on behalf of the Earthquake Commission, Wellington, New Zealand, 204pp.
- [4] Model developed using a similar methodology to [1] by Bradley (2016).
- [5] Model developed using a similar methodology to [2] by T+T.
- [6] Comprehensive reconnaissance mapping performed by T+T.

10.2.1.1 Land damage categories

The land damage categories used in the MBIE/MfE mapping process are the simplified land damage observation categories in Table 10.2: "None-to-Minor", "Minor-to-Moderate", and "Moderate-to-Severe".

Table 10.2: Land damage observation categories used for MBIE/MfE mapping

Category	Descriptions from MBIE/MfE Guidance (2017)
None-to-Minor	• No signs of ejected liquefied material at the ground surface (Note: An absence of ejecta at the ground surface does not necessarily mean that liquefaction has not occurred. Liquefaction may still occur at depth, potentially causing ground settlement.) • No more than minor differential settlement of the ground surface (e.g. undulations less than 25 mm in height). • No apparent lateral spreading ground movement (e.g. only hairline ground cracks). • Liquefaction causes no or only cosmetic damage to buildings and infrastructure (but damage may still occur due to other earthquake effects).
Minor-to-Moderate	• Minor to Moderate quantities of ejected liquefied material at the ground surface (e.g. less than 25 percent of a typical residential site covered); and/or • Moderate differential settlement of the ground surface (e.g. undulations 25–100 mm in height). • No significant lateral spreading ground movement (e.g. ground cracks less than 50 mm wide may be present, but pattern of cracking suggests the cause is primarily ground oscillation or settlement rather than lateral spreading). • Liquefaction causes moderate but typically repairable damage to buildings and infrastructure. Damage may be substantially less where liquefaction was addressed during design (e.g. enhanced foundations).
Moderate-to-Severe	• Large quantities of ejected liquefied material at the ground surface (e.g. more than 25 percent of a typical residential site covered); and/or • Moderate to Severe differential settlement of the ground surface (e.g. undulations more than 100 mm in height); and/or – Significant lateral spreading ground movement (e.g. ground cracks greater than 50 mm wide, with pattern of cracking suggesting direction of movement downslope or towards a free-face). • Liquefaction causes substantial damage and disruption to buildings and infrastructure, and repair may be difficult or uneconomic in some cases. Damage may be substantially less, and more likely to be repairable, where liquefaction was addressed during design (e.g. enhanced foundations and robust infrastructure detailing).

The LDFCs developed herein correspond to the land damage states in Table 10.2, because they are published in national guidance and are widely used in practice. However, the land damage observations for events were mapped by others using different categories which further subdivide these three simplified categories (see Table 10.3 and Table 10.4).

For the 4 September 2010 and 22 February 2011 earthquake events (referred to as Sept2010 and Feb2011 from here on), the refined categories in Table 10.3 were used for mapping land damage, while for the 14 February 2016 earthquake event (i.e. Feb2016), the categories in Table 10.4 were used. The transforms between the observed categories and the LDFC categories are also provided in Table 10.3 and Table 10.4.

Notably, there was only one polygon for Moderate-to-Severe for the Feb2016 event. This category may be under-represented, however, there were relatively few instances of more severe liquefaction-induced ground damage for this event compared to the other events, and therefore this under-representation is expected to be small.

Table 10.3: Land damage observation categories used for the Sept2010 and Feb2011 events (Table adapted from Appendix B of Tonkin + Taylor (2015))

Land damage observation categories	Criteria / description	Simplified land damage observation categories
None	• No observed cracks, undulation/deformations at the ground surface; • No signs of ejected liquefied material at the ground surface; and • No apparent lateral movement.	None-to-Minor
Minor	• Shaking-induced damage resulting from cyclic deformation and surface-waves causing ground surface damage. Ground surface damage likely limited to minor cracking (tension) and buckling (compression) and/or minor undulations at the ground surface; • No signs of ejected liquefied material at the ground surface; and • No apparent lateral movement.	None-to-Minor
Moderate	• Minor to moderate quantities of ejected liquefied material on ground surface (generally < 25% of site covered with ejected material); and/or • Small cracks from ground oscillations (< 50 mm) may be present, but little to no vertical displacement across cracks; and • No apparent lateral movement.	Minor-to-Moderate
Major	• Large quantities of ejected liquefied material on ground surface (generally > 25% of site covered with ejected material); and/or • Severe observed ground surface subsidence; and/or • Small cracks from ground oscillations (< 50 mm) may be present, but little to no vertical displacement across cracks; and • Limited evidence of lateral movement.	Moderate-to-Severe
Severe	• Moderate to major lateral spreading (< 1 m cumulative); and/or • Large cracks extending across the ground surface, with horizontal and/or vertical displacement (> 50 mm, but generally < 200 mm); and • Ejection of liquefied material at the ground surface may also be observed.	Moderate-to-Severe
Very Severe	• Extensive lateral spreading (≥ 1 m cumulative); and/or • Large open cracks extending through the ground surface, with very severe horizontal and/or vertical displacements (≥ 200 mm); and • Ejection of liquefied material at the ground surface may also be observed.	Moderate-to-Severe

Table 10.4: Transforms from Feb2016 land damage observation dataset to the adopted categories

Land damage observation categories	Simplified Land Damage Observation Category from Feb2016 in Kennerley & McDougall (2023)
Lateral spreading	Moderate-to-Severe
Liquefaction Ejecta	Minor-to-Moderate
Observed Water	None-to-Minor
No Visible Damage Observed	None-to-Minor
None Observed	None-to-Minor

10.2.2 Augmentation of the observation dataset

The assignment of land damage, PGA, Mw, GWD and event LSN to the GIs is outlined below and is a modified approach from the process developed by Kennerley & McDougall (2023). Note that the land damage observations for the events were spatially defined using polygons. The assignment process for the Sept2010 and Feb2011 events is outlined briefly here:

1 Apply an outward buffer of 10 m around all observation polygons. Where there was a conflict (specifically, where the None-to-Minor land damage category overlap with the Minor-to-Moderate or Moderate-to-Severe categories) the area was assigned Borderline. Where there was no conflict, the area was assigned the observation category. Where Moderate-to-Severe overlapped Minor-to-Moderate, this was assigned Moderate-to-Severe. The Borderline area removed data that were potentially misclassified. It also meant that GIs that were along roadways were assigned a damage observation (since roadways were not mapped in the original observation dataset).

2 For all GIs, sample the PGA, Mw, GWD and observation category at the location of the GI. Note Borderline areas and areas with no observation were not used.

3 Compute the event LSN using the <LDM>-<PL>-<method>-per-GI file (see Section 7.1).

For the Feb2016 event, large parts of Christchurch were not mapped for land damage (because there was no obvious damage visible from initial reconnaissance). To account for this, the assignment process differed slightly to the other events. In this case, only Minor-to-Moderate and Moderate-to-Severe were buffered by 15 m. A 15 m buffer was used since the observations of liquefaction were mapped in terms of soil ejecta, not ground distortion so were considered to likely under-represent the spatial extent of damage. The remaining area was classified as None-to-Minor. The None-to-Minor observations were not buffered since they overlapped the observed liquefaction, and the presence of liquefaction was considered more accurate than no observed damage due to the focus on mapping soil ejecta.

10.2.3 Pre-processing filter

Ideally the LDFCs should use known LSN values, however, due to significant uncertainties both in the PGA and GWD, the LSN is not fully constrained. Some event LSN calculations are highly sensitive to changes in GWD due to thin liquefiable layers near the surface, while others can be highly sensitive to changes in PGA. These event LSN values are highly uncertain compared to LSN values that are not sensitive to changes in PGA and GWD.

To identify these sensitive points, perturbed LSN values, $LSN_{perturb}$, were calculated by individually considering GWD +/- 0.5 m, and PGA +/- 20%[22]. The changes in LSN for the perturbed GWD and PGA

[22] These perturbation values were chosen to approximate the typical uncertainties associated with GWD and PGA for the events used to develop the fragility curves. For instance, the NLM GW Model's standard deviation for Northern Canterbury is approximately 0.9 m.

are plotted against the original LSN in Figure 10.1 respectively. A sensitivity threshold was defined in log(LSN) space as $|\Delta \log(LSN)_{perturb}| > 0.85$ (using Equation 34). 0.85 roughly corresponding to 2.5 times the standard deviation of $\Delta \log(LSN)$ for the GW sensitivity. This threshold is also shown on the plots in Figure 10.1 for positive and negative changes.

Equation 34:

$$|\Delta\, log(LSN)_{perturb}| = |\, log\left(LSN_{perturb}\right) - log\ (LSN)|$$

From Figure 10.1(a), there were a considerable number of points that exceed the sensitivity threshold due to GWD, many of which would appear to be misclassifications (i.e. high LSN assigned None-to-Minor and low LSN assigned Moderate-to-Severe). For PGA sensitivity in Figure 10.1(b), there were points that exceeded the sensitivity threshold, however, most of these points do not appear to be misclassifications (i.e. they had low LSN and had a damage observation of None-to-Minor) and therefore no pre-processing was applied for PGA). To apply some constraint on the estimate of LSN, all points exceeding the sensitivity threshold for GW sensitivity were dropped from the dataset.

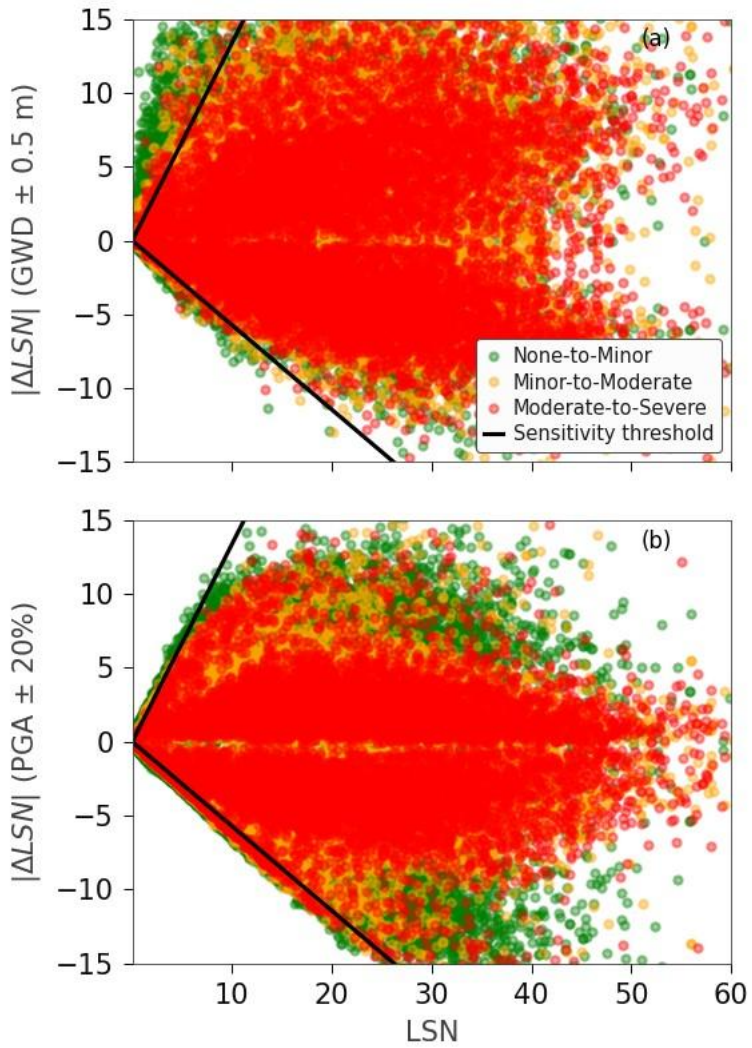

Figure 10.1: Evaluation of absolute sensitivity of LSN to a) Changes in GWD, and b) Changes in PGA; vs the original LSN value

10.2.4 Process to fit curves

To generate the LDFCs, the following steps were followed:

1 For all LSN-land damage observation pairs, the LSN values were log-transformed and binned into equal log space intervals. Equal log space bins were used instead of equal linear space bins since this puts greater emphasis on the lower LSN range where differences are more critical for loss modelling.

2 For each bin, the proportion of data points corresponding to each land damage category was calculated. The proportions for the Minor-to-Moderate and Moderate-to-Severe damage categories are shown in Figure 10.2(a).

3 A normal distribution curve was then fitted to the logged data to generate the fragility curves.

4 The 15th and 50th percentile values (P15 and P50) of the fitted curves were determined and stored to allow the curves to be reproduced (see Table 10.5 and Table 10.6).

5 To account for uncertainty in the input variable (i.e. the uncertainty in GWD for the calculation of LSN), the fragility curves were adjusted using the process in Section 10.2.6.

Notes:

1 The fitted curves are lognormal distribution curves with respect to LSN for P_L = 50%. By fitting a normal distribution to binned data in log space (instead of fitting a lognormal distribution in linear space), the fitting process had greater weighting to the smaller percentiles – which is typically the more important part of the LDFCs.

2 The damage categories are cumulative, in that Minor-to-Moderate refers to the probability of Minor-to-Moderate or greater land damage, hence also contains all data points for Moderate-to-Severe.

3 The None-to-Minor category is 1 minus the probability of Minor-to-Moderate.

4 The curves shown in Figure 10.2(a) and adopted for this report are based on both CPT and BH data.

5 The data that the curves are fitted to are per GI per event

10.2.5 Fitted and adjusted curves

Figure 10.2(a) shows the fitted LDFCs with and without the uncertainty adjustment and Table 10.5 provides the values for the fitted relationships.

The values in Table 10.5 directly correspond to the MBIE/MfE Guidance (2017) criteria for assigning LV categories:

1 Liquefaction Damage is Possible: “There is a probability of more than 15 percent that liquefaction-induced ground damage will be Minor-to-Moderate (or more) for 500-year shaking.”

2 High LV: “There is a probability of more than 50 percent that liquefaction-induced ground damage will be Moderate-to-Severe for 500-year shaking and/or Minor-to-Moderate (or more) for 100-year shaking.”

3 The unadjusted percentiles in Table 10.5 could be used as thresholds when LSN for PL = 50% is computed as a single value (e.g. from a single GI) without consideration of spatial variability or GW uncertainty, and the adjusted values would be used when considering the likely distribution of LSN values. Note, the LSN values in Table 10.5 are quoted to two decimal points to allow an accurate recreation of the fragility curves but do not imply accuracy to this level.

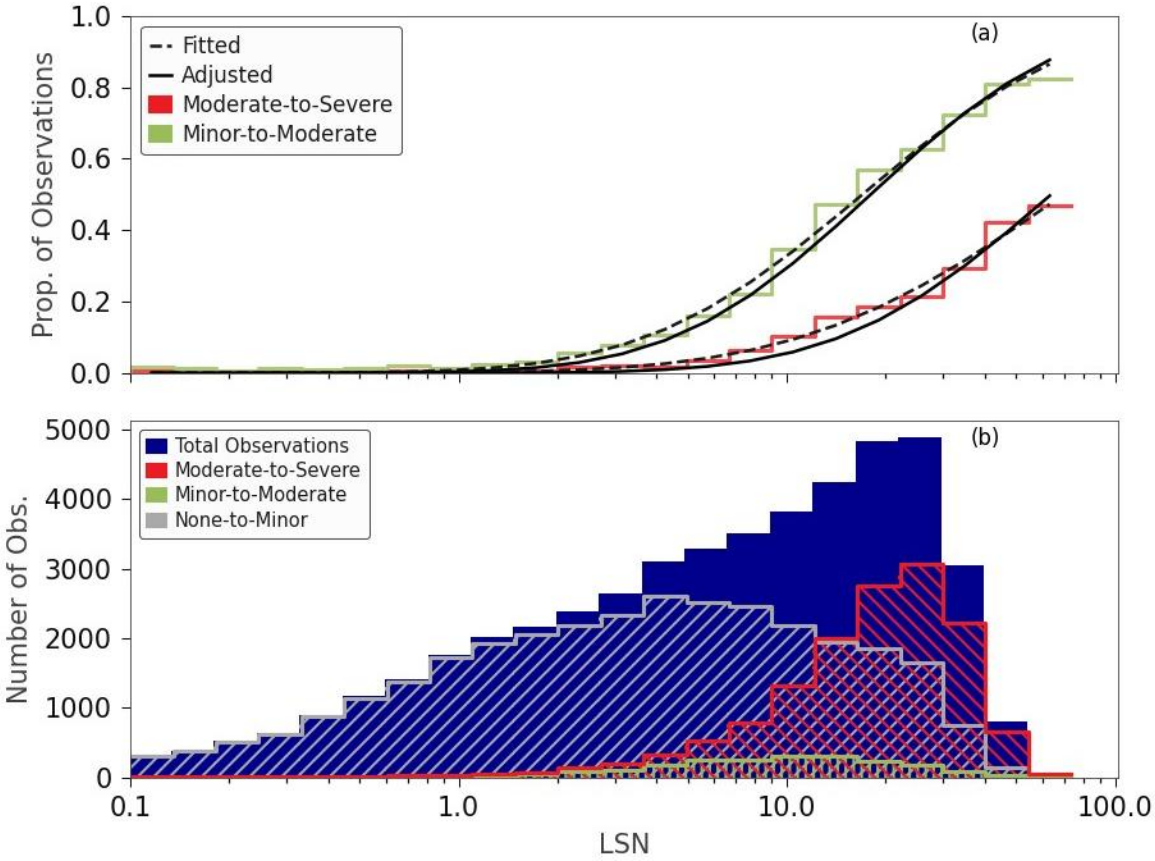

Figure 10.2: a) Minor-to-Moderate (or worse) and Moderate-to-Severe LDFCs with the proportion of each damage category per LSN bin, and b) Distribution of LSN values in the observation dataset

Table 10.5: LSN (P_L = 50%) values for 15th and 50th percentiles for LDFCs using lognormal cumulative distribution curves

Land damage category	15th percentile	50th percentile
Minor-to-Moderate [fitted]	4.95	17.01
Moderate-to-Severe [fitted]	15.65	69.81
Minor-to-Moderate [adjusted]	5.87	17.01
Moderate-to-Severe [adjusted]	19.26	69.81

To convert the percentile values presented in Table 10.5 to the cumulative log normal distribution curves. The mean and standard deviation of a normal distribution in log space can be obtained using Equation 35 and Equation 36. P15 and P50 are the 15th and 50th percentiles, and -1.036 is the z-score for the 15th percentile. If using the 85th percentile instead of 85th percentile then change the z-score to positive 1.036.

Equation 35:

$$\mu_{log} = \log(P50)$$

Equation 36:

$$\sigma_{log} = \frac{\log(P15) - \log(P50)}{-1.036}$$

Fragility curves for P_L = 15% are compared to the P_L = 50% curves in Figure 10.3 and Table 10.6. As expected, the P_L = 15% curve plots to the right of the P_L = 50% curve (i.e. higher LSN value for a given probability of land damage), due to the bias towards predicting liquefaction triggering.

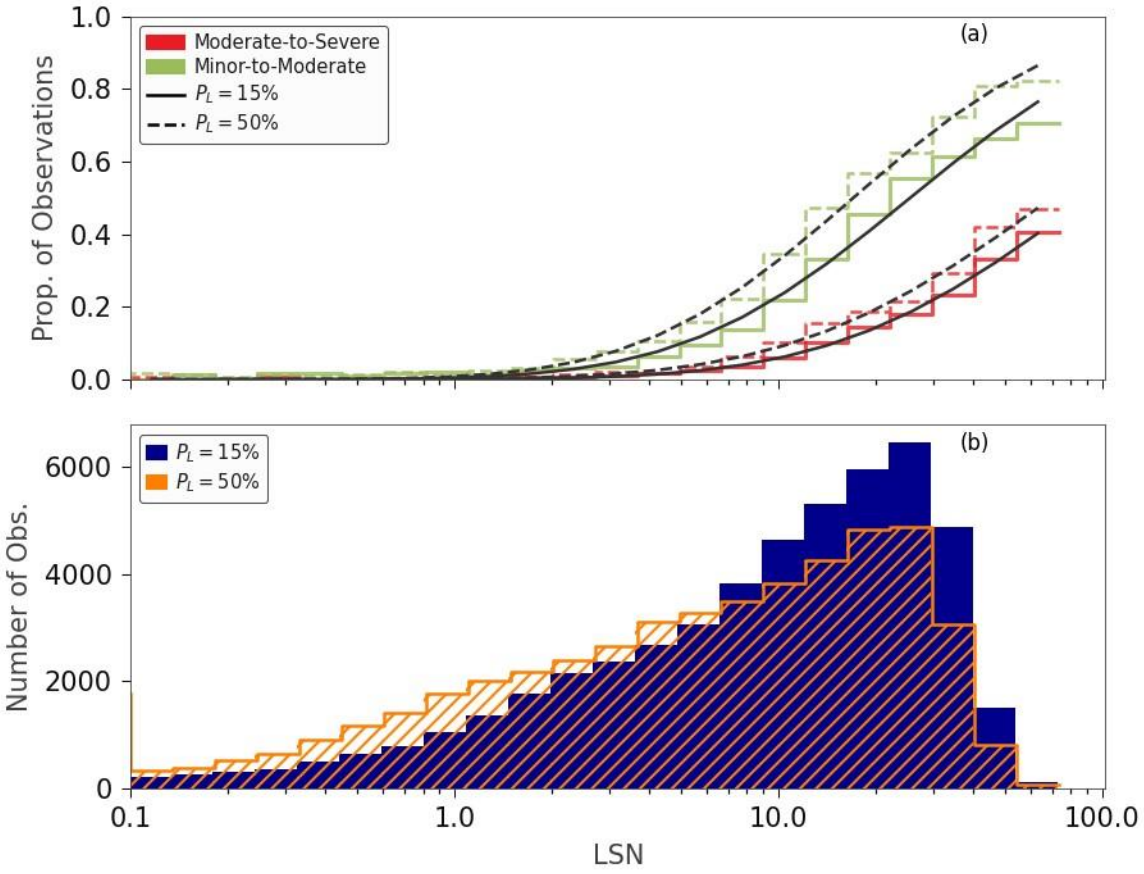

Figure 10.3: a) PL=15% and PL=50% LDFC's for Minor-to-Moderate (or worse) and Moderate-to-Severe damage with portions of each damage category per LSN bin, and b) Distribution of LSN values in the observation dataset

Table 10.6: LSN (P_L = 15%) values for 15th and 50th percentiles for LDFCs using lognormal cumulative distribution curves

Land damage category	15th percentile	50th percentile
Minor-to-Moderate [fitted]	6.92	25.49
Moderate-to-Severe [fitted]	20.91	89.25
Minor-to-Moderate [adjusted]	8.37	25.49
Moderate-to-Severe [adjusted]	25.36	89.25

10.2.6 Removing GW input uncertainty in fragility curves

The LDFCs were built with inherent uncertainties in PGA and GWD values for the observation data. These uncertainties are implicitly included in the LDFCs and result in higher response uncertainty. Excessive response uncertainty in loss modelling can result in biased estimates of loss as outlined in Section 4.2.1.1. To reduce double counting uncertainty in GWD (both implicitly within the LDFCs and in the estimate of GWD for calculating LSN in future predictions), a set of LDFCs were generated

where the GWD uncertainty was removed. These curves could be used in place of the directly fitted curves in certain situations and are used in Section 11.

10.2.6.1 Uncertainty quantification

To quantify the impact of GWD uncertainty, the uncertainty in LSN was determined using the sensitivity analysis described in Section 10.2.3. This analysis involved perturbing GWD by +/- 0.5 m and PGA by +/- 20% for each GI and subsequently recalculating the LSN. From this analysis the GWD was shown to produce a larger variation in LSN values than PGA for the perturbations considered. For simplicity, and due to difficulties in obtaining the uncertainty in PGA for many applications, only the uncertainty in GWD for LSN was considered and removed from the LDFCs.

The difference between the perturbed and original log(LSN) values, $\Delta \log(LSN)_{perturb}$, was adopted as a measure of the relative sensitivity of LSN to variations in GWD. This sensitivity metric represents the proportional change in LSN due to GWD perturbations. Figure 10.4 shows the relationship between the sensitivity metric and LSN. Notably, the magnitude of sensitivity decreases as LSN increases. The flat top and bottom of the scatter highlights the effect of the sensitivity threshold cutoff applied in Section 10.2.3.

To model the uncertainty, the standard deviation of the sensitivity metric, denoted as σ, was computed within 50 LSN bins. A linear relationship was fitted between LSN and the uncertainty, yielding Equation 37 and shown in Figure 10.4. Figure 10.4 also shows the 15th and 85th rolling percentiles for reference. Note that the decision in Section 10.2.3 to perturb the GWD by +/- 0.5 m impacts the quantified uncertainty, and the extent of adjustment to the LDFCs. Future work may revise the development of the uncertainty relationship to better reflect GWD uncertainty.

Equation 37:

$$\sigma\left(\Delta\, log(LSN)_{perturb}\right) = 0.298 - 0.0014 \cdot LSN$$

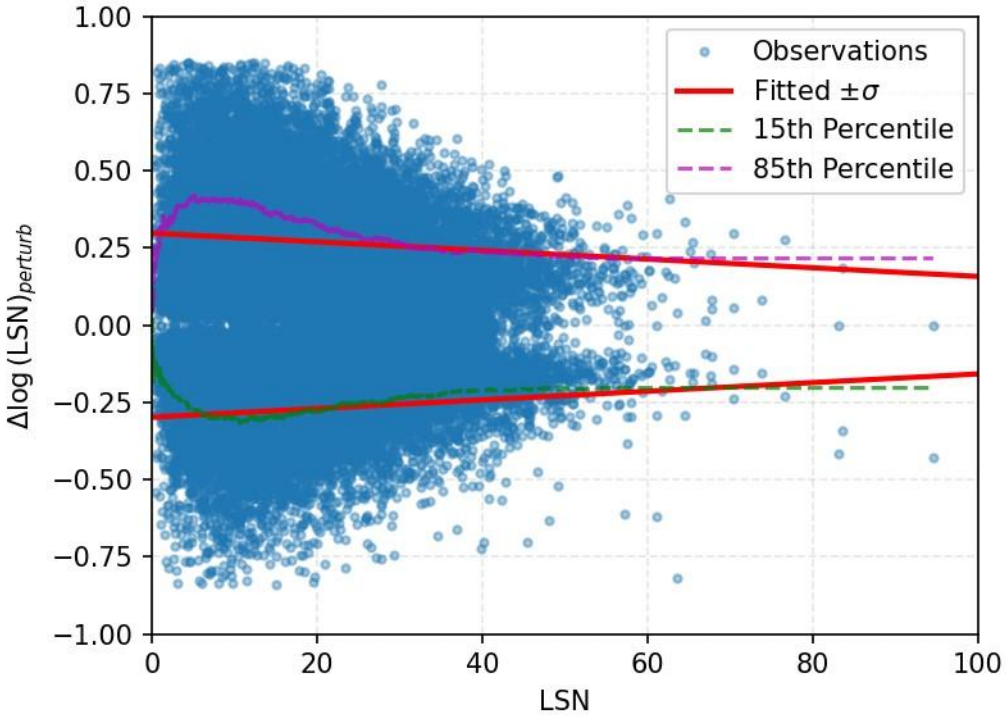

Figure 10.4: Sensitivity of log(LSN) due to changes in GWD by +/- 0.5 m

10.2.6.2 Uncertainty Removal

The process to remove uncertainty was achieved through reverse engineering. This involved the following steps:

1 Start with some initial underlying fragility curves and convert the fragility curves back to a pseudo-observation dataset (i.e. consider increments of LSN, for each LSN increment generate 1000 points, assign observations to those points based on the probability of land damage corresponding to that LSN value).

2 Add uncertainty to the observation dataset. For each LSN value, adjust the LSN by a random sample based on the range in Equation 37.

3 Fit a new set of curves (fitted curves) to the observation data with uncertainty.

4 Compare the fitted curves to the original curves that were obtained from the empirical data and iterate by adjusting the underlying fragility curves until the fitted curves match the original curves. Therefore, the underlying curves are the fragility curves with the uncertainty removed.

This process was applied to the Minor-to-Moderate and Moderate-to-Severe fragility curves and resulted in a notably higher gradient at the point of inflection (i.e. lower liquefaction response uncertainty for a given LSN) as shown in Figure 10.2).

10.3 Validations

Several validation exercises are presented in this section, the first set in Section 10.3.1, is focused on efficiency and sufficiency of LSN as an LDM. Section 10.3.2 performs additional sufficiency analysis of LSN and is focused on whether LSN adequately quantifies differences in the ground profile. Section 10.3.3 provides a brief cross-check by comparing to existing LDFCs.

10.3.1 Efficiency and sufficiency of LSN

Index parameters for fragility curves are often investigated in terms of both the efficiency (i.e. steepness of curve), and sufficiency (i.e. are there other features of the demand that are influential to the response). For example, for structural analysis, a fragility curve for drift might use spectral acceleration as the index and could check sufficiency by confirming the curves are independent of magnitude.

The section evaluates the sensitivity of the LDFCs to the inputs of the LSN calculation, particularly GWD and PGA. LDFCs were also produced independently for each of the three events to evaluate the event-to-event variability (which was used to explore whether other demand features such as Mw and distance-to-source may influence the LDFCs).

Typically, sufficiency of a primary parameter is evaluated using secondary parameters that are not explicitly considered in the primary parameter. In this case, the calculation of LSN (Equation 3) does not explicitly use GWD, PGA or Mw, however, the liquefaction factor of safety (FOS_{liq}) does, which is an input to LSN. The sufficiency analysis is still valid since FOS_{liq} is not developed as a measure of land damage. However, adjustments to the consideration of GWD, PGA and Mw within the FOS_{liq} calculation may improve the sufficiency of LSN.

In this study, efficiency is inferred by P15/P85, the ratio of LSN for the 15^{th} percentile divided by 85^{th} percentile of the fitted LDFC (where the maximum value of 1.0 would indicate a very efficient index parameter). Sufficiency is determined by splitting the dataset based on some secondary input parameter and evaluating whether the efficiency increases. The split is performed at many different thresholds for the secondary parameter and efficiency is evaluated for both portions of the dataset (above and below the threshold). An additional measure is the difference between the 50^{th} percentiles of the two portions of the dataset. A final measure for improving predictive power is if

the split has significant portions of the data both above and below the threshold (since trends observed on small subsets of the total dataset are less likely to be generalisable or meaningful). For the purposes of evaluating the portion of data in each subset, only results with LSN > 0.1 were considered.

The efficiency and sufficiency were only evaluated for the Minor-to-Moderate land damage category. The Moderate-to-Severe category was not used due to the smaller amount of data, particularly to constrain the 85th percentile.

To demonstrate the influence of the secondary parameter, fragility curves are shown for values above and below a selected threshold of the secondary parameter. Given the limitations of the empirical dataset, particularly that the results are all from Canterbury, the direct use of the split fragility curves is not recommended. They are produced to highlight the potential for over- and under-prediction for different GWDs and seismic demands.

10.3.1.1 GWD

Figure 10.5 shows that splitting the dataset by the event GWD results in improved predictive power of the LDFCs. Improved prediction is when at least one of the P15/P85 ratios increases, and both the difference in P50 is significant and the two portions of the dataset have a reasonable portion of the total dataset. These conditions are true for any event GWD splitting threshold value between 1.0 m and 2.0 m.

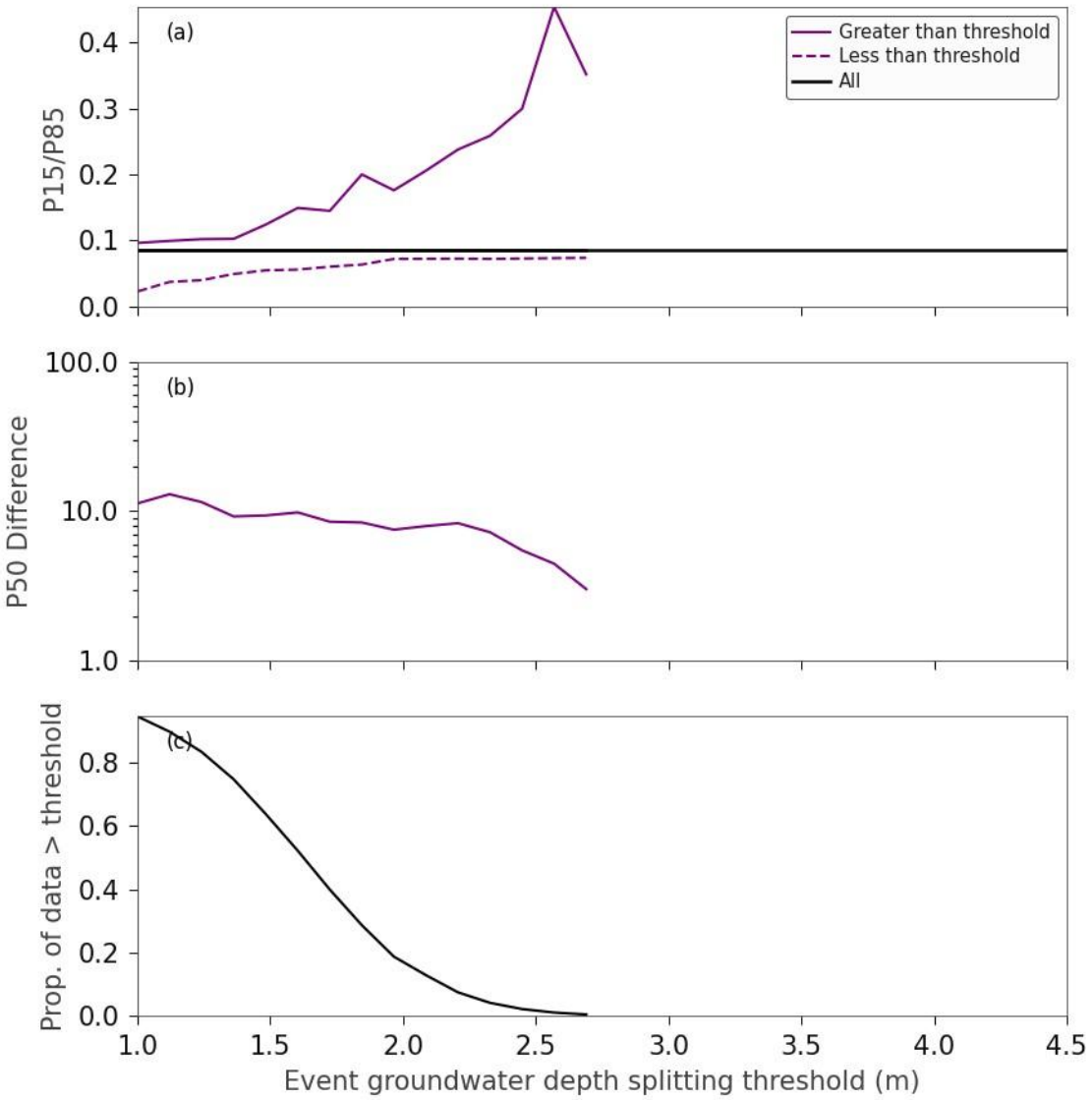

Figure 10.5: Comparison of efficiency and sufficiency of Minor-to-Moderate LDFCs using LSN, evaluated using change in a) Ratio of 15th to 85th percentile LSN, b) Difference in 50th percentile LSN, and c) Portion of data above the threshold; for changing values of event GWD splitting threshold

A splitting threshold of GWD = 1.5 m was provisionally chosen based on Figure 10.5 to produce the empirical LDFCs shown in Figure 10.6 that demonstrate the potential influence of GWD. Based on this threshold, the influence of event GWD on the LDFC can be seen. When LSN is 10, the probability of Minor-to-Moderate (or worse) land damage is ~25% if the event GWD is less than 1.5 m, compared to ~45% if the event GWD is greater than 1.5 m. This comparison suggests that the LSN based fragility curves are not sufficient in terms of the influence of GWD, potentially with too strong of a weighting to near surface liquefaction.

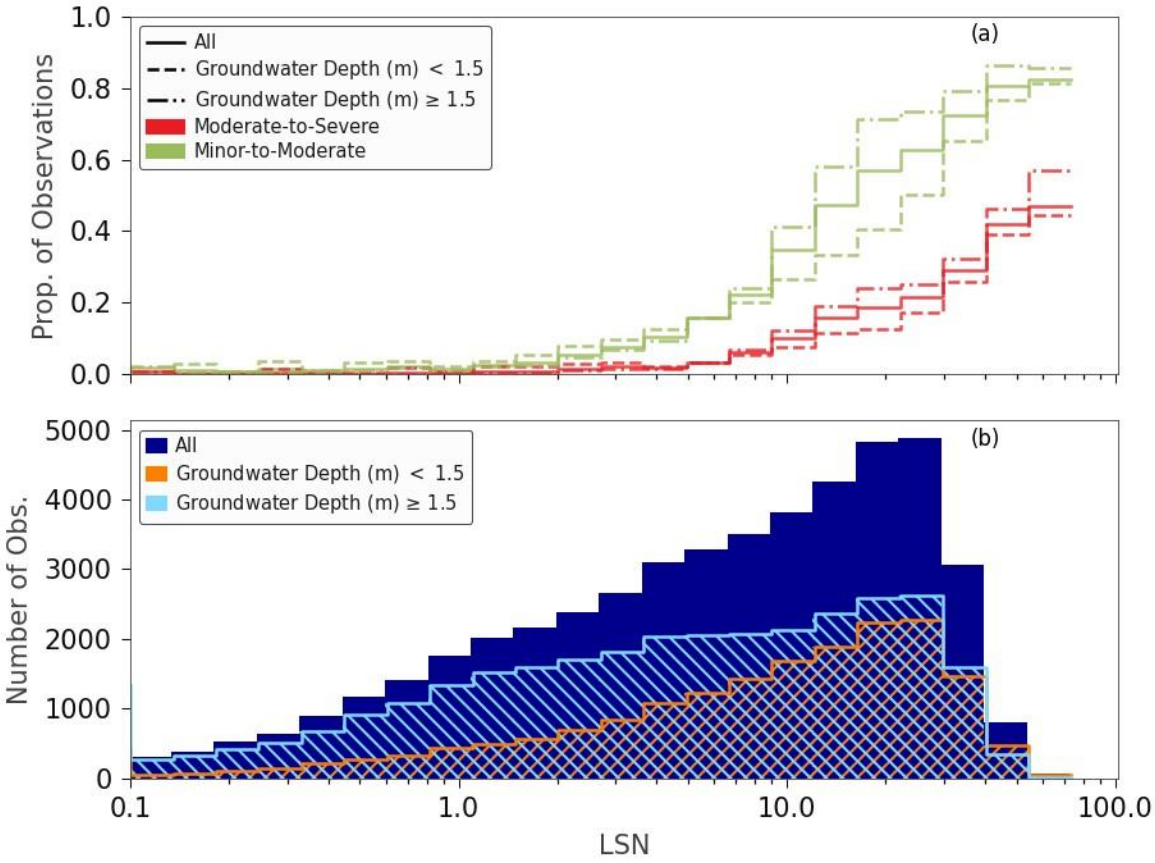

Figure 10.6: a) Comparison of empirical Minor-to-Moderate and Moderate-to-Severe LDFCs for event GWD above and below 1.5 m, and b) Distribution of observations with respect to LSN

10.3.1.2 Peak Ground Acceleration (PGA)

Figure 10.7 shows a very strong influence from PGA, with a threshold PGA from 0.22 to 0.36 g resulting in a flat fragility curve for the greater than threshold subset (e.g. the P50 increases so much that the P50 difference exceeds 100).

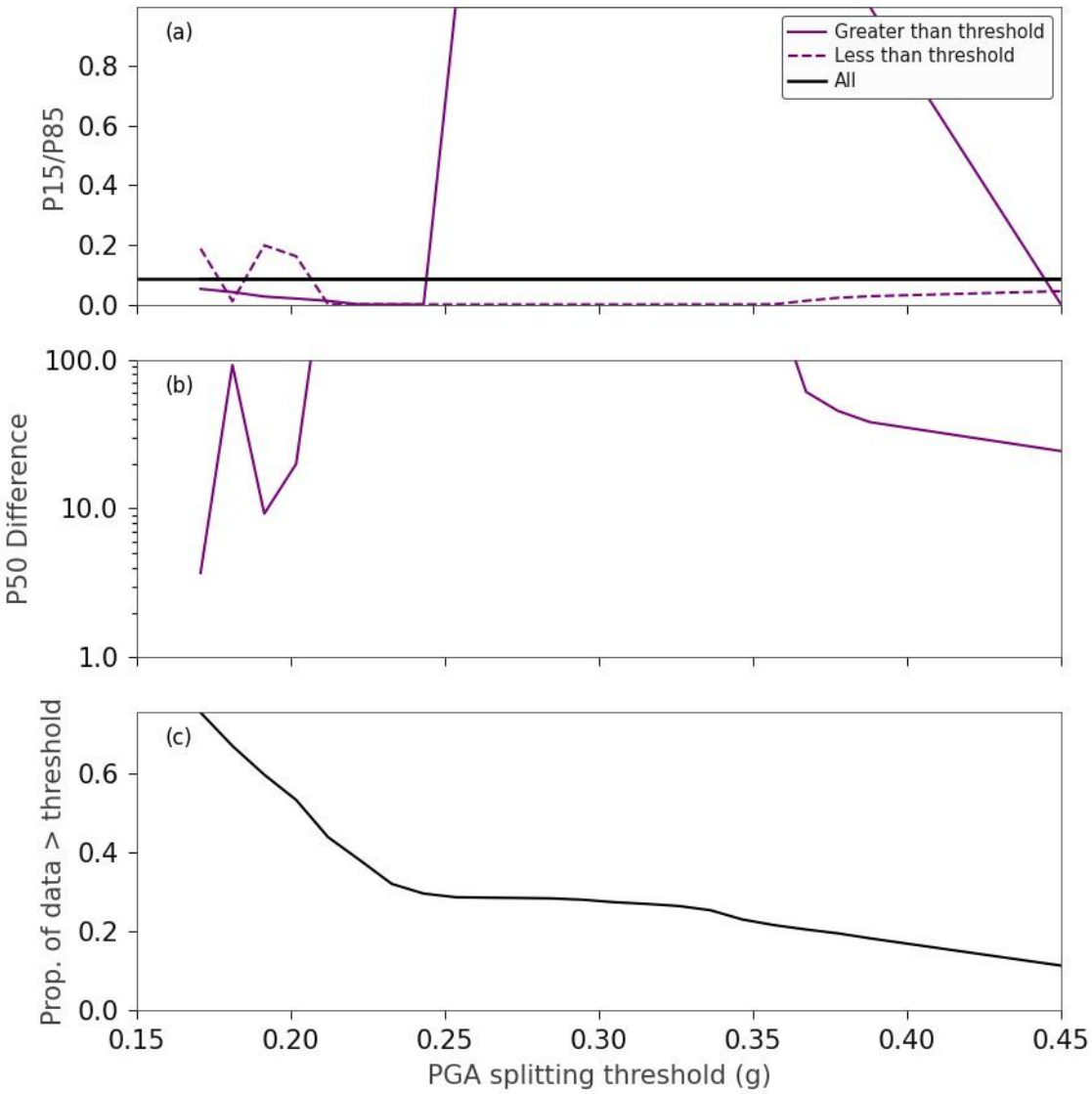

Figure 10.7: Comparison of efficiency and sufficiency of Minor-to-Moderate LDFCs using LSN, evaluated using change in a) Ratio of 15th to 85th percentile LSN, b) Difference in 50th percentile LSN, and c) Portion of data above the threshold; for changing values of event PGA splitting threshold

A threshold of 0.25 g was used to split the dataset and create the LDFCs in Figure 10.8. It appears that there is a strong influence of PGA. When LSN is 10, the probability of Minor-to-Moderate (or worse) land damage is ~15% if the event PGA is less than 0.25 g, compared to ~80% if the event PGA is greater than 0.25 g. This difference is significant and suggests that LSN is not sufficient as an LDM, however, other factors may have influenced these results as discussed in Section 10.3.1.4. Figure 10.8(a) should also be interpreted with the context of Figure 10.8(b), which shows that there were very few observations with high PGA and low LSN. While the trend for the high PGA dataset is significant, the limited amount of data makes the trend highly sensitive to small biases. Some biases that may have impacted this trend include:

- Misclassification of land damage, i.e. a few cracks being classified as liquefaction-induced when they were actually not liquefaction-induced would significantly change the proportions.
- Calculation variability in LSN, e.g. differences from different testing equipment, different correction factors, and uncertainty in PGA and GWD. In fact, manual inspection of many of the

observations with Minor-to-Moderate or Moderate-to-Severe damage were associated with GIs that had a liquefiable layer just above the event GWD. Re-analysing these points with a higher GWD resulted in a significant jump in LSN. Therefore, GWD depth uncertainty may partially explain the observed trend.

- Mapping biases of ground conditions with greater focus on damaged areas than areas with no damage.
- Physical effects not captured by the simplified liquefaction triggering method that may or may not be generalisable, such as lateral spreading causing damage to sites that have low LV.

More detailed evaluation of this data, and the inclusion of data from other events is recommended to better understand the role of PGA on ground damage.

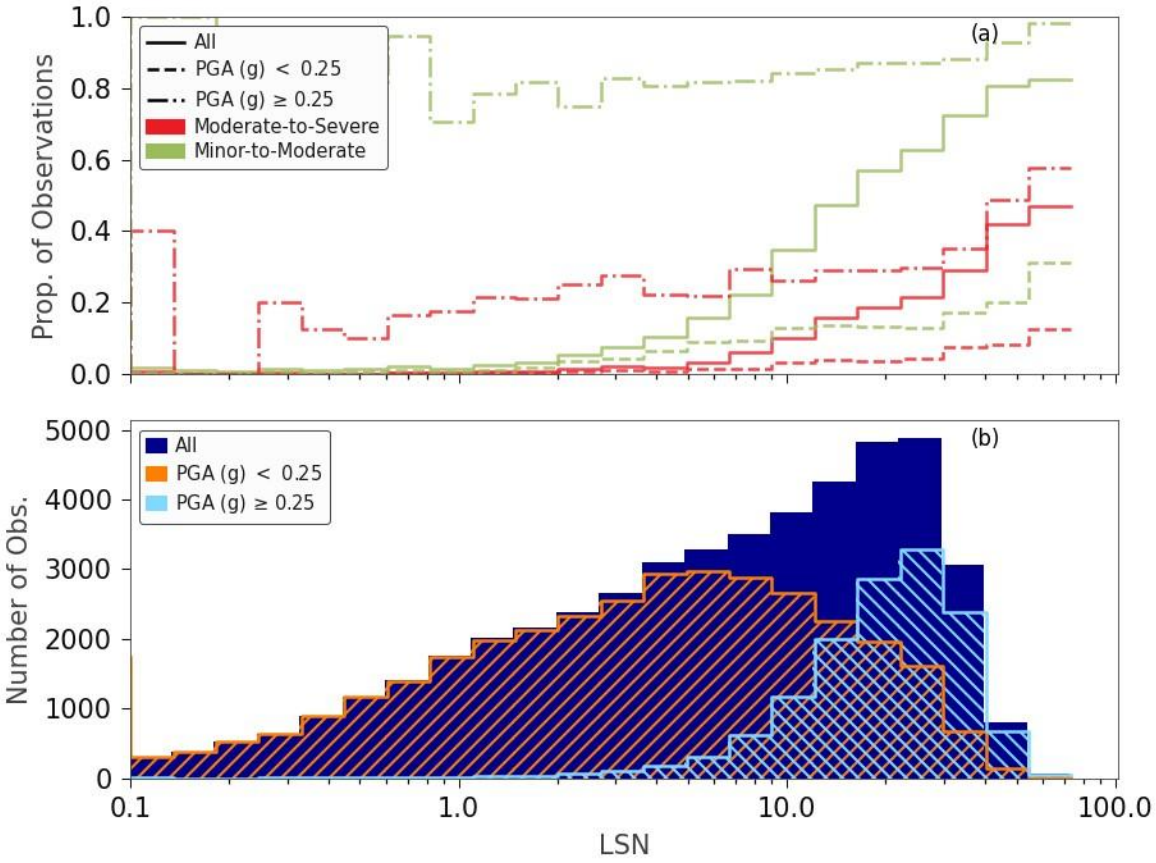

Figure 10.8: a) Comparison of empirical Minor-to-Moderate and Moderate-to-Severe LDFCs for PGA above and below 0.25 g, and b) Distribution of observations with respect to LSN

10.3.1.3 Comparison by event

Figure 10.9 compares LDFCs for Minor-to-Moderate land damage produced for each of the three events presented in Section 10.2.1. From Figure 10.9, it is apparent that the different events have very different proportions of land damage for the same LSN values. This highlights that forward prediction of these events would result in significant under- and over-prediction of land damage when the "All" LDFCs are used. For example, when LSN is 10, "All" corresponds to ~40% Minor-to-Moderate (or worse) land damage. However, the Feb2011 event resulted in ~80% Minor-to-Moderate (or worse) land damage and the Valentine's Day earthquakes had near zero damage. Despite the differences, the "All" LDFCs are the most justifiable option for future events, given that

there are many potential causes for the difference in response and many of those may not be known a priori for a future event.

As discussed in Section 10.3.1.2, the significant land damage for the Feb2011 event even at low LSN values (< 1) is unexpected. Many of these data points were manually investigated and were clustered in several areas. Notably, in many cases, the estimated event GWD was directly below a near surface liquefiable layer, suggesting that the modelled GWD may have been deeper than the actual GWD at time of the event.

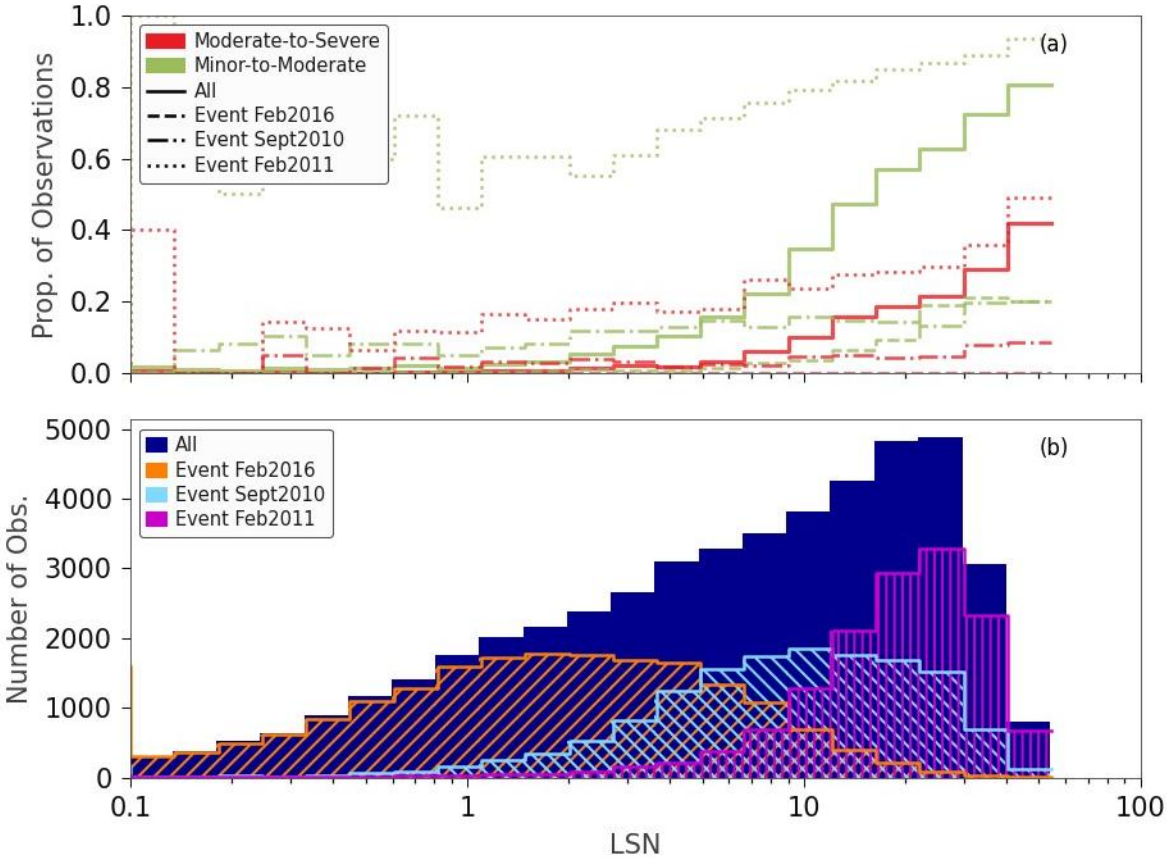

Figure 10.9: a) Comparison of empirical Minor-to-Moderate and Moderate-to-Severe LDFCs for the Sept2010, Feb2011 and Feb2016 events, and b) Distribution of observations with respect to LSN

10.3.1.4 Summary

While the use of LSN appears to be insufficient in how it addresses GWD, PGA, and differences between events (potentially due to differences in distance to fault and magnitude), the observed differences may be amplified by the following potential causes:

1 Lateral spread induced ground damage (e.g. lateral spreading in Feb2011 amplified damage, especially at lower LSN values). This could be investigated in the future by considering the proximity of Moderate land damage category with low LSN values to Major, Severe and Very Severe land damage categories using the original mapping from (Tonkin + Taylor, 2015).

2 Sampling bias (e.g. strongest shaking in most liquefiable soil in Feb2011). This could be investigated by adding more events to the dataset and/or more observation points with low LSN for the Feb2011 event.

3 1D system response effects resulting in amplified liquefaction in some deposits that had stronger relative shaking in the Feb2011 event (e.g. hydraulic connectivity of soil layers amplifying response, see Cubrinovski et al. (2019)). This could be investigated in the future by

considering different LDMs, such as the ejecta potential index, EPI (Hutabarat & Bray, 2022), or applying factors to the liquefaction triggering calculations to account for system response.

4 3D spatial interaction (e.g. horizontal porewater flow, see Hutabarat & Bray (2021)). This could be investigated in the future by adjusting the buffer zone used (see Section 10.2.2) to decide whether observations are included in the dataset.

10.3.2 Other ground profile indices

This section evaluates whether the relationship between LSN and land damage correlates with other ground profile indices. This is an adaption on the conventional sufficiency analysis to determine whether the LSN calculation sufficiently considers identifiable measures of the ground profile that may influence land damage.

10.3.2.1 Median I_{c10}

The median I_{c10}, a modified version of I_{c10} proposed by Upadhyaya et al. (2023)[23], was computed for all CPT. It was computed by calculating the median I_c value in the top 10 m of the soil profile. If the trace was less than 10 metres or included a predrill section, the median I_c was computed over the non-predrill section and over the available length of trace, up to the maximum depth of 10 m. Figure 10.10 shows the spatial distribution of median I_{c10} across Christchurch, where most of the event observation dataset is.

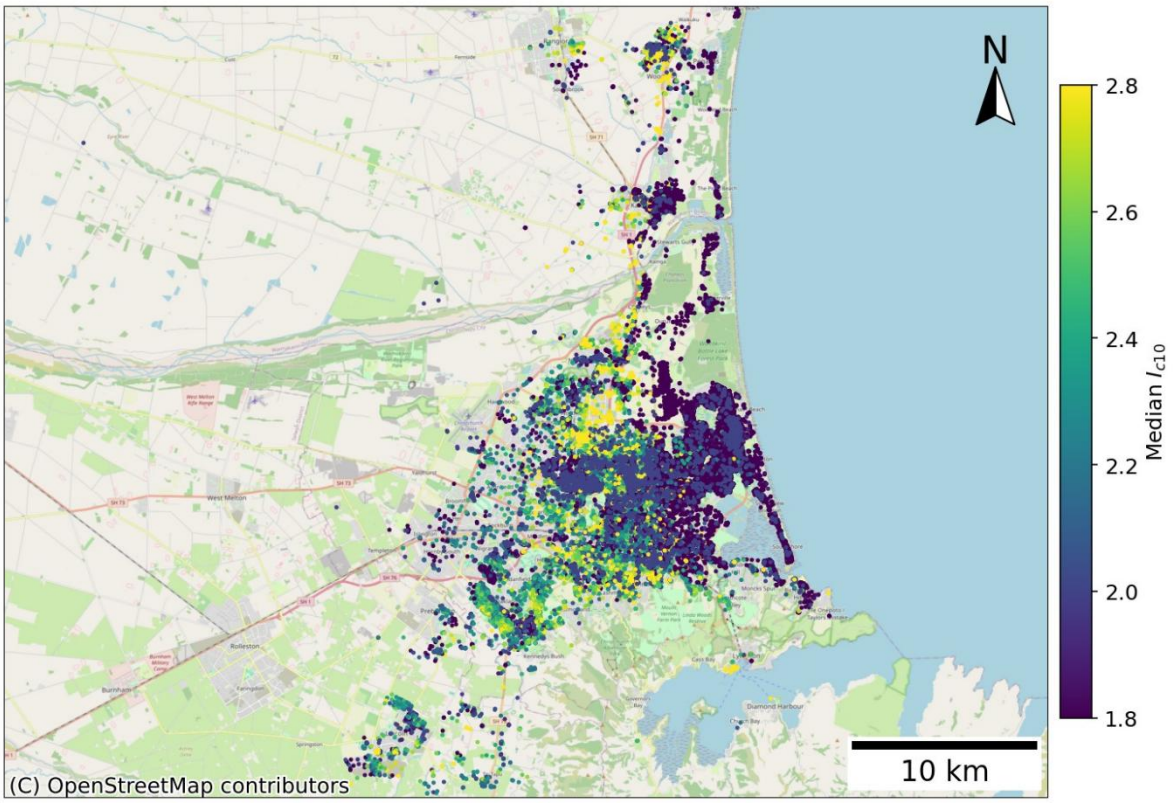

Figure 10.10: Spatial distribution of median I_{c10} for all CPT in Christchurch

The efficiency (P15/P85) and the sufficiency (P50 difference) were evaluated for varying values of median I_{c10}. Based on the results shown in Figure 10.11, it appears there is a trend change around the median I_{c10} value of 2. Hence a threshold of 2.05 was chosen to subset the data, consistent with

[23] Upadhyaya et al. (2023) calculated the mean average I_c over the top 10 m of the soil profile whereas the analyses presented in this report calculate the median I_c over the top 10 m of the soil profile.

Upadhyaya et al. (2023). Figure 10.12 shows LDFCs with the dataset split by the 2.05 threshold. For a given LSN, the difference in portion of land damage between the two different subsets is considerable. When LSN is 10, the probability of Minor-to-Moderate (or worse) land damage is ~20% if the median I_{c10} is greater than 2.05, compared to ~40% if the median I_{c10} is less than 2.05.

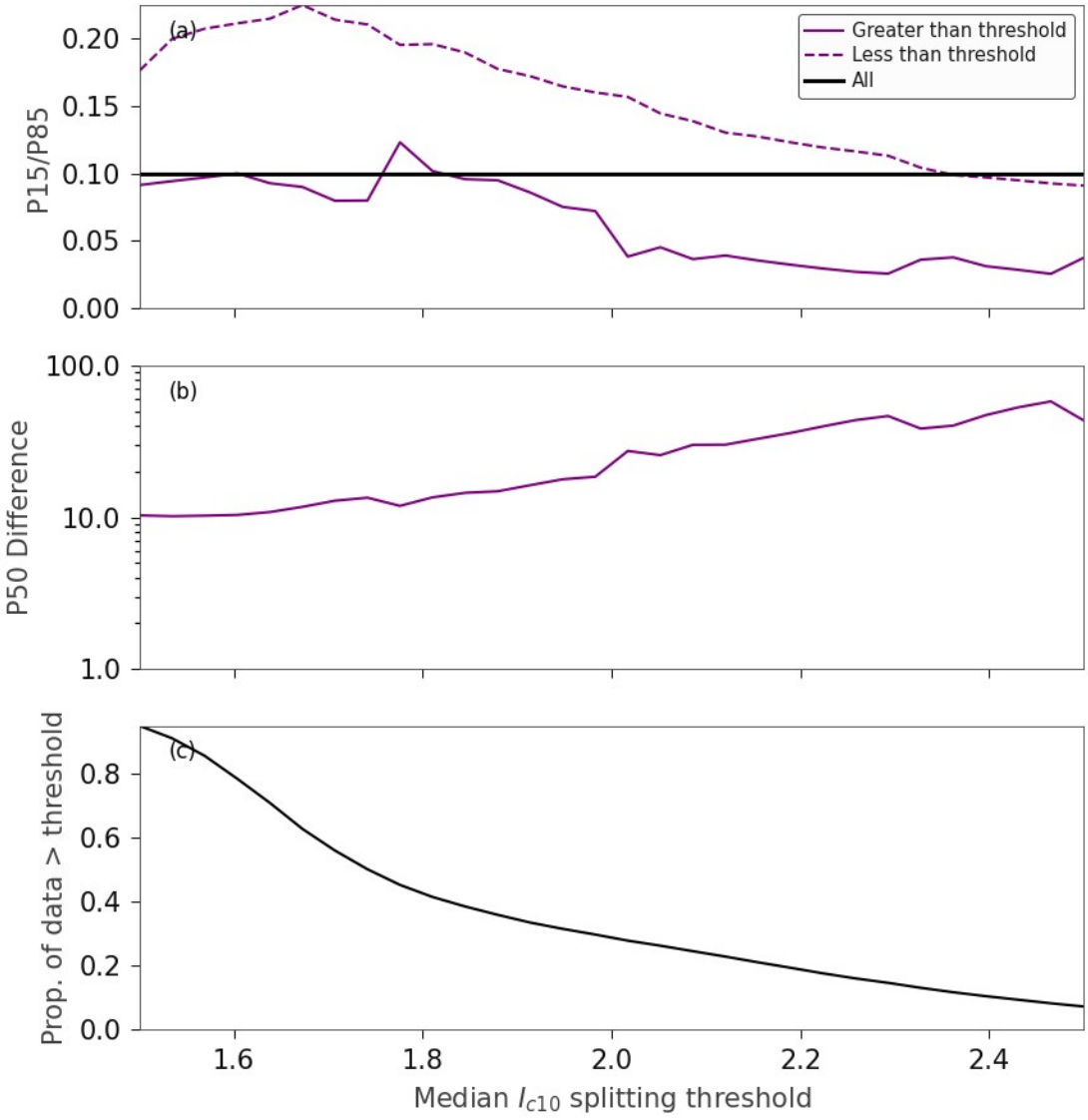

Figure 10.11: Comparison of efficiency and sufficiency of Minor-to-Moderate LDFCs using LSN, evaluated using change in a) Ratio of 15th to 85th percentile LSN, b) Difference in 50th percentile LSN, and c) Portion of data above the threshold; for changing values of median I_{c10} splitting threshold

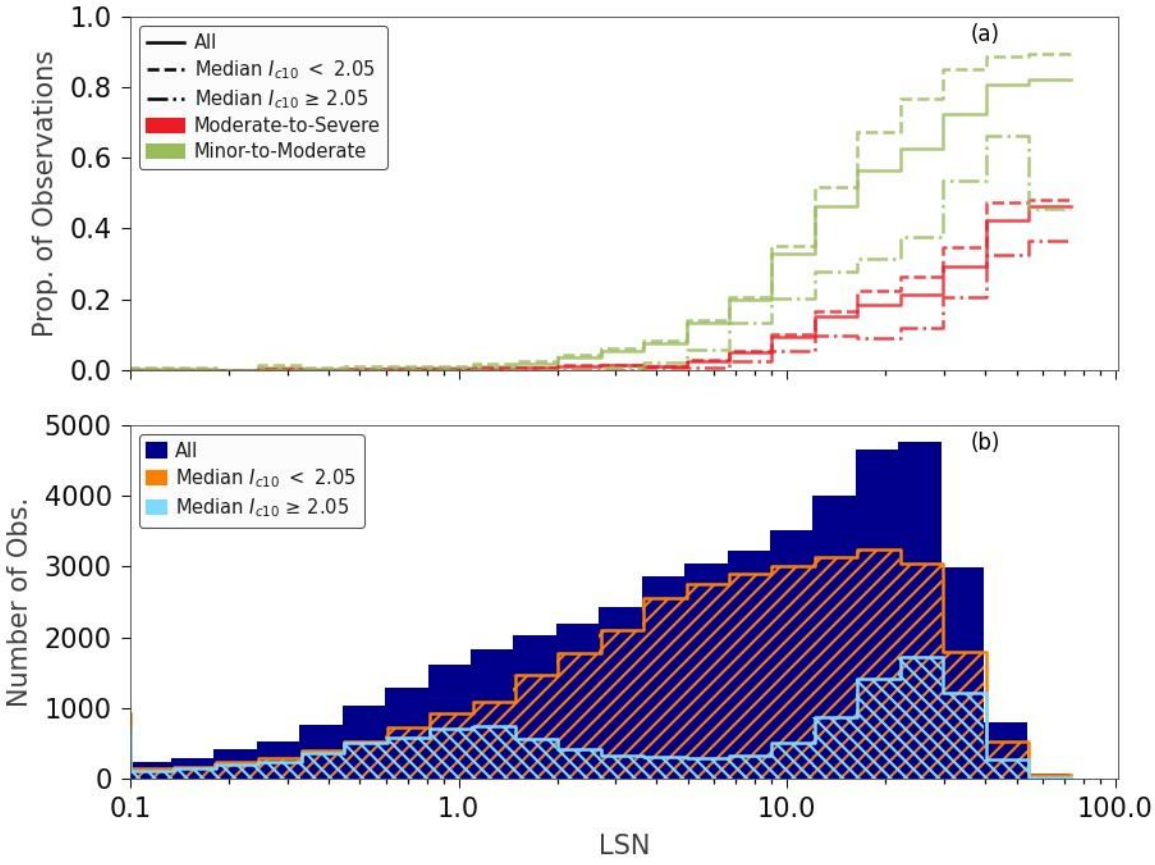

Figure 10.12: a) Comparison of empirical Minor-to-Moderate and Moderate-to-Severe LDFCs for median I_{c10} above and below 2.05, and b) Distribution of observations with respect to LSN

10.3.2.2 Percentage of $I_c > 2.6$ in top 10 m of soil profile

An additional metric was determined as the percentage of readings in the top 10 m of the soil profile that had $I_c > 2.6$, denoted as $(I_c > 2.6)_{10}$. If the trace was less than 10 metres or included a predrill section then $(I_c > 2.6)_{10}$ was computed over the non-predrill section and over the available length of trace, up to the maximum depth of 10 m. $(I_c > 2.6)_{10}$ is shown spatially across Christchurch in Figure 10.13 for all CPT locations. This index was chosen since it can be computed directly from both CPTs and the equivalent CPT derived from BHs (see Section 7.6 for details).

The efficiency and sufficiency were evaluated across a range of values (see Figure 10.14). Based on this, a threshold of 20% $(I_c > 2.6)_{10}$ was chosen. The LDFC's shown in Figure 10.9 were produced using this threshold and it appears that $(I_c > 2.6)_{10}$ has a very similar influence to median I_{c10} (see Figure 10.8). When LSN is 10, the probability of Minor-to-Moderate (or worse) land damage is ~25% if $(I_c > 2.6)_{10}$ is greater than 20%, compared to ~35% if $(I_c > 2.6)_{10}$ is less than 20%. The influence does not appear to be as large as for median I_{c10}.

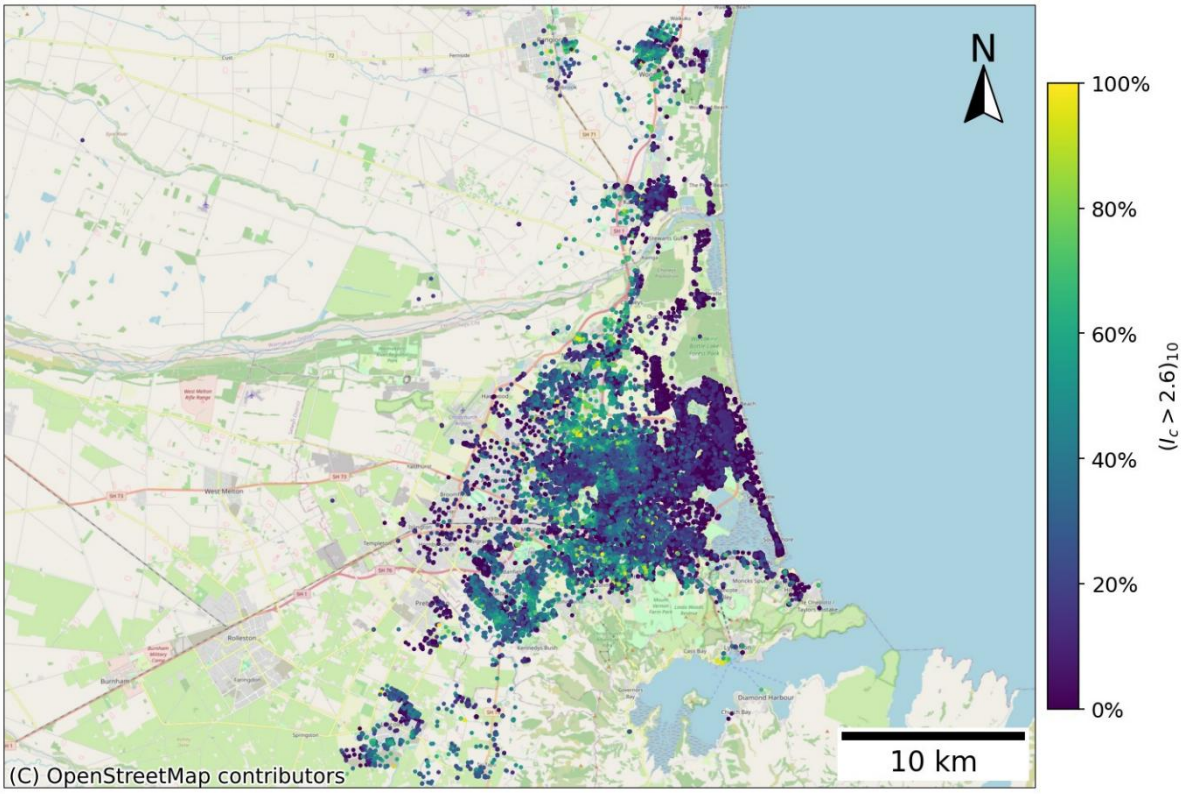

Figure 10.13: Spatial distribution of $(I_c > 2.6)_{10}$ for all CPT in Christchurch

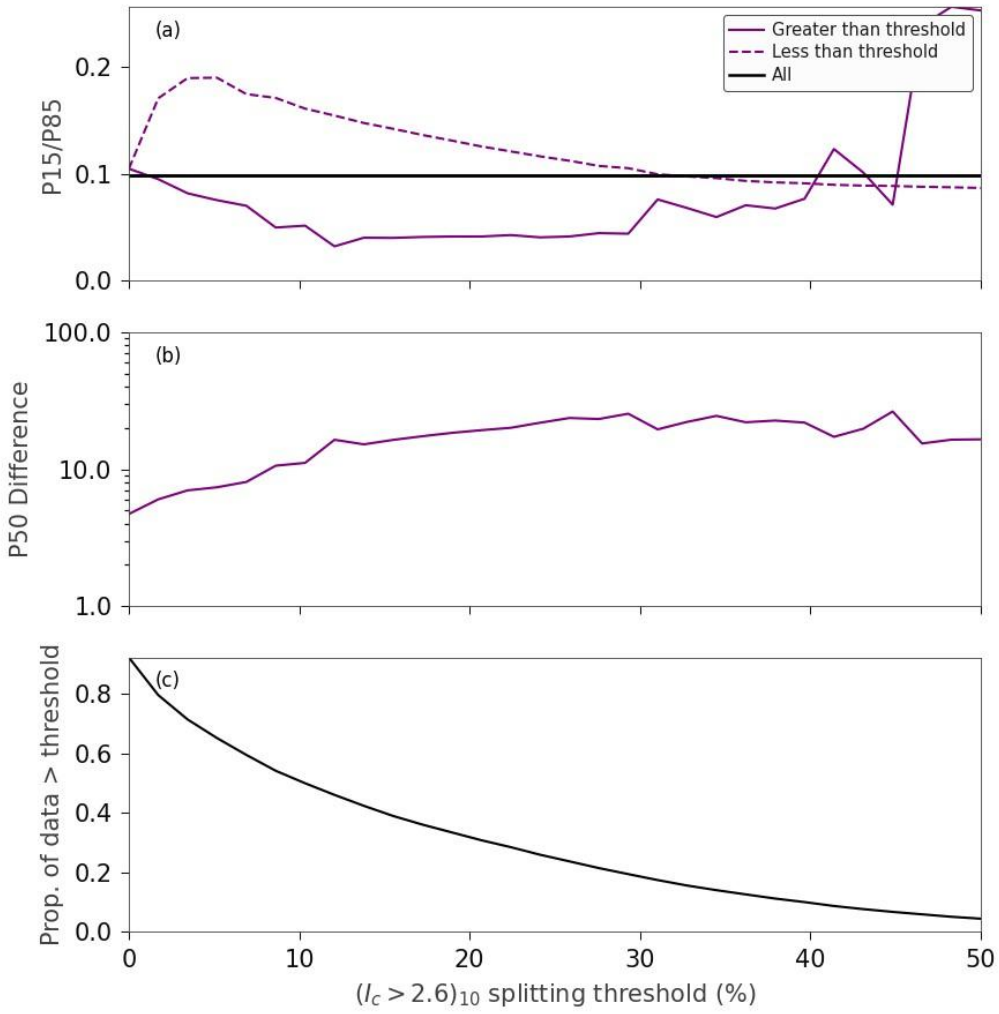

Figure 10.14: Comparison of efficiency and sufficiency of Minor-to-Moderate LDFCs using LSN, evaluated using change in a) Ratio of 15th to 85th percentile LSN, b) Difference in 50th percentile LSN, and c) Portion of data above the threshold; for changing values of percentage I_{c10} > 2.6 splitting threshold

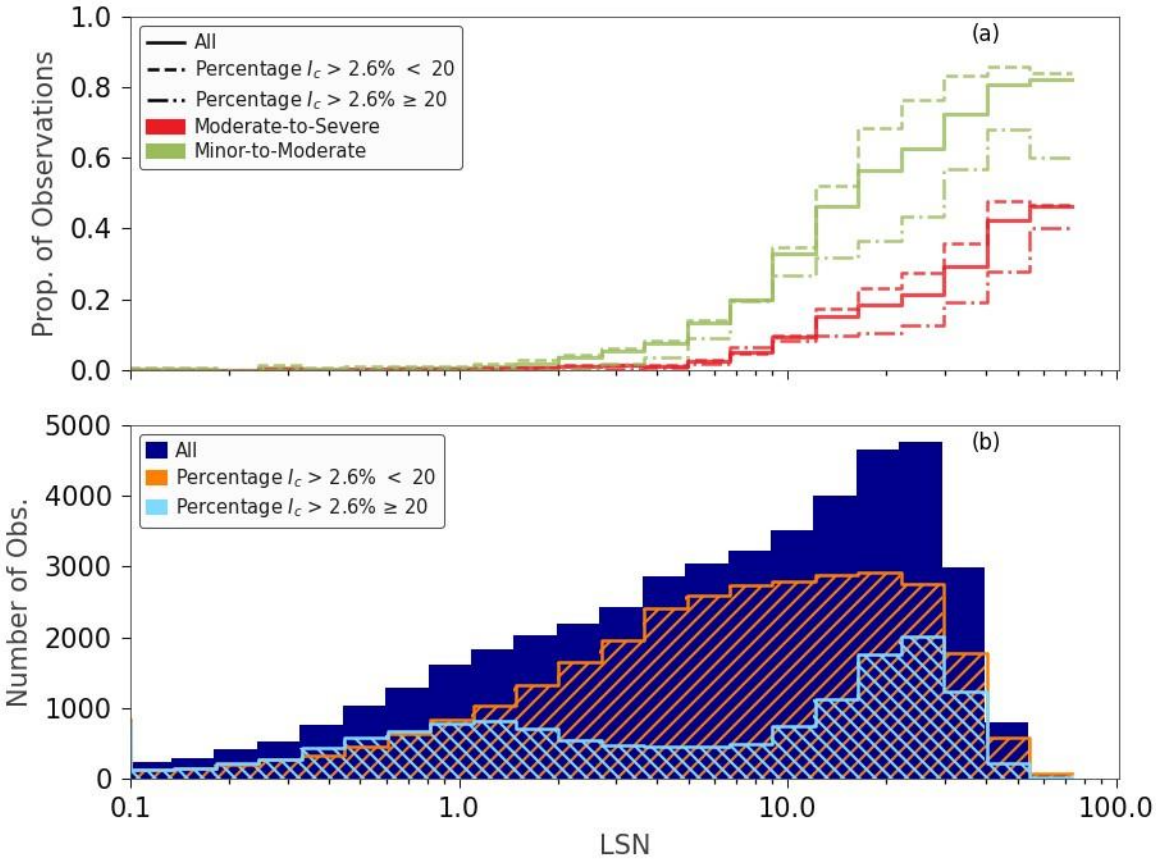

Figure 10.15: a) Comparison of empirical Minor-to-Moderate and Moderate-to-Severe LDFCs for when $(I_c > 2.6)_{10}$ is less than 20% vs greater than or equal to 20%, and b) Distribution of LSN

10.3.2.3 Machine Learning (ML) based identification of misprediction

The first two ground profile indices considered above, I_{c10} and $(I_c > 2.6)_{10}$, were easily computed and highly interpretable. Alternative indices can be determined through ML based evaluations. This section develops an index based on a ML model that evaluates CPT trace features to estimate relative land damage. The purpose was to understand whether there are further improvements to land damage prediction that can be achieved through alternative LDMs to LSN.

The developed index was the "ML over-prediction rate", which is based on the ML model from Kennerley & McDougall (2023). Kennerley & McDougall (2023) develop a ML model that uses CPT data to predict cases where LSN is high and yet no liquefaction-induced land damage is expected. More specifically, for a given CPT and earthquake scenario parameters for PGA, Mw, and GWD that give LSN ≥ 15, the ML model predicts whether any liquefaction-induced land damage is to be expected. The ML model was trained using land damage observation data from past New Zealand earthquake case histories. Whether the case history was associated with land damage or not was given by the "None" land damage category in Table 10.3.

To align the ML model with the specific LSN calculation method adopted in the NLM, the ML model was re-trained on the NLM database with the following updates to the dataset originally outlined by Kennerley & McDougall (2023):

1 **Extended GW coverage:** A limiting factor in obtaining case histories from historical events was the availability of GW models (ideally matching the time of those events). For sites with CPTs,

land damage observations and event seismicity but no GWD value, the GWD was taken from the NLM median GW Model.

2 **Updated LSN values:** LSN values were obtained using three-way linear interpolation of PGA, Mw, and GWD against pre-calculated values of LSN at fixed increments (see Sections 7.1 and 7.4).

ML over-prediction rate was developed as a measure of the general tendency of a CPT towards over-prediction land damage. Over-prediction was defined for this purpose as LSN > 15 (for P_L=50%) but no observed damage. The ML model outputs whether over-prediction is expected for a given PGA, Mw, GWD and CPT. The ML over-prediction rate index was computed by evaluating the ML model output for a range of PGA, Mw and GWD combinations to evaluate the tendency for over-prediction. Specifically, it was the proportion of PGA, Mw, and GWD combinations (nearly all possible parameter combinations on the parameter grid in Section 7.4) for which the ML model identified over-prediction. A restriction was applied that GWD must lie between 1 m and 4 m. The rationale for excluding GWDs less than 1 m is that the ML model was not trained on depths shallower than this. The rationale for excluding GWDs greater than 4 m is that over-prediction is very uncommon in this case. The use of LSN>15 means that generally no over-prediction is identified for small seismic demands directly from the ML model. However, using the aggregate of many seismic demand combinations means the CPT can have a high ML over-prediction rate which can then be used to infer overprediction at low LSN values. Note that it was only developed for CPT and efforts to train a similar model for BH lacked sufficient data.

The spatial distribution of the ML over-prediction rate for the CPTs across Christchurch is shown in Figure 10.16. Parts of the high over-prediction rate occur in the same area as high median I_{c10} (see Figure 10.11), however, there are notable differences (e.g. there are distinct pockets of high ML over-prediction rate in north-eastern Christchurch).

The influence of ML over-prediction rate on LDFCs was evaluated using the efficiency and sufficiency plots in Figure 10.17. Based on this a threshold of 0.2 was chosen as the splitting threshold. The LDFCs shown in Figure 10.18 were produced using this threshold, and there is a notable difference between the subsets. Compared to median I_{c10}, the influence is lower at lower LSN values but has a greater influence at high LSN values, i.e. for the ML over-prediction rate there is a clear difference in predicted damage beyond LSN of 15.

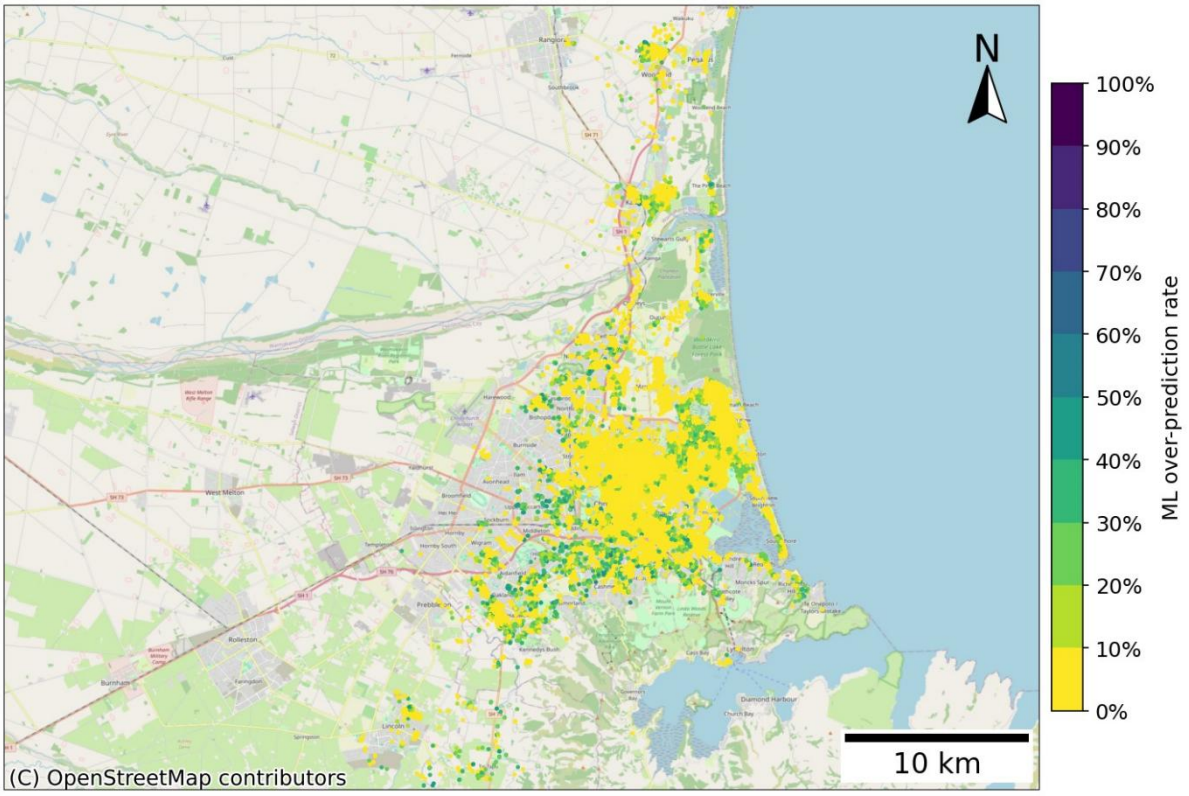

Figure 10.16: Spatial distribution of ML over-prediction rate across Christchurch

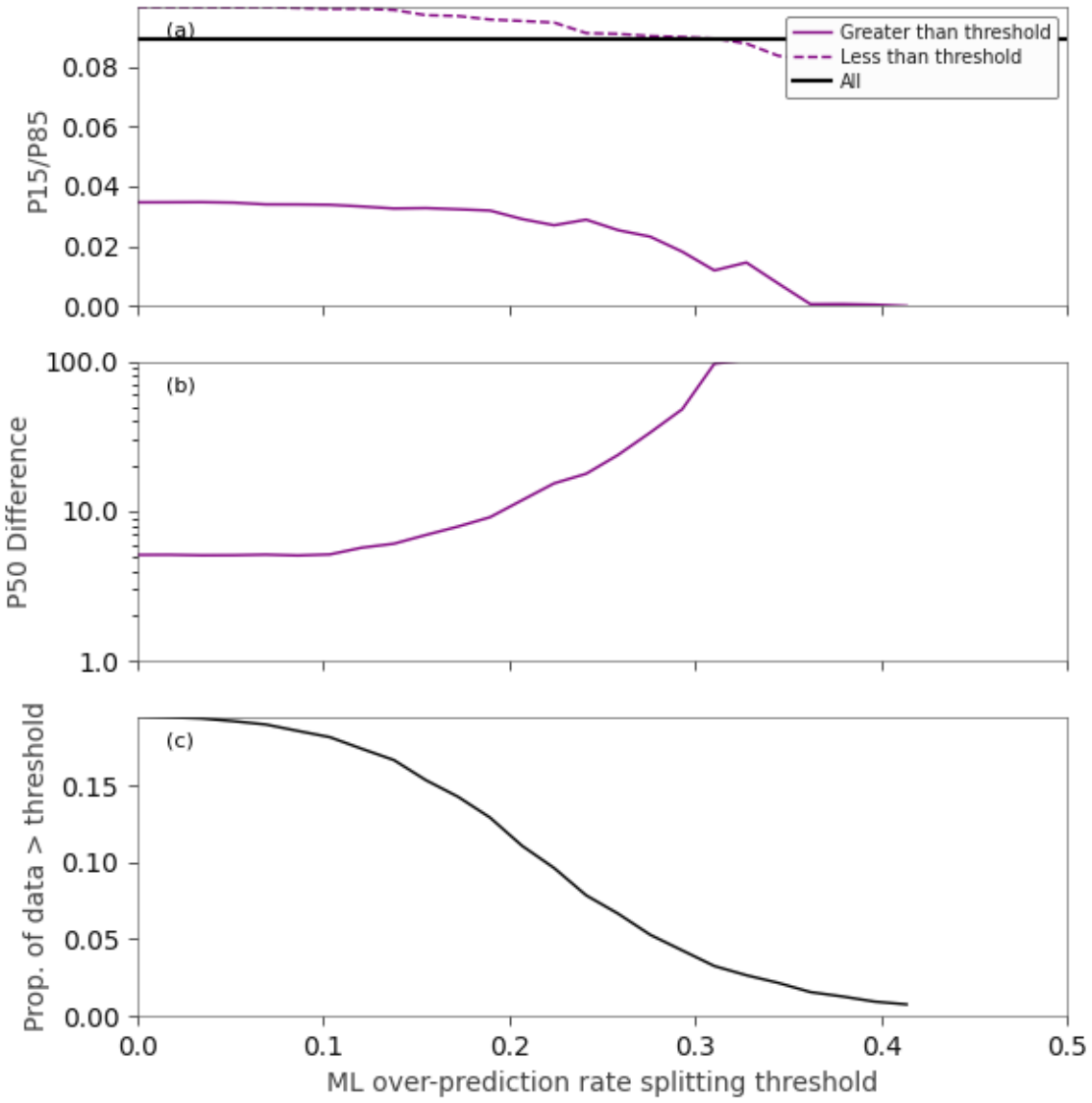

Figure 10.17: Comparison of efficiency and sufficiency of Minor-to-Moderate LDFCs using LSN, evaluated using change in a) Ratio of 15th to 85th percentile LSN, b) Difference in 50th percentile LSN, and c) Portion of data above the threshold; for changing values of rate of ML over-prediction splitting threshold

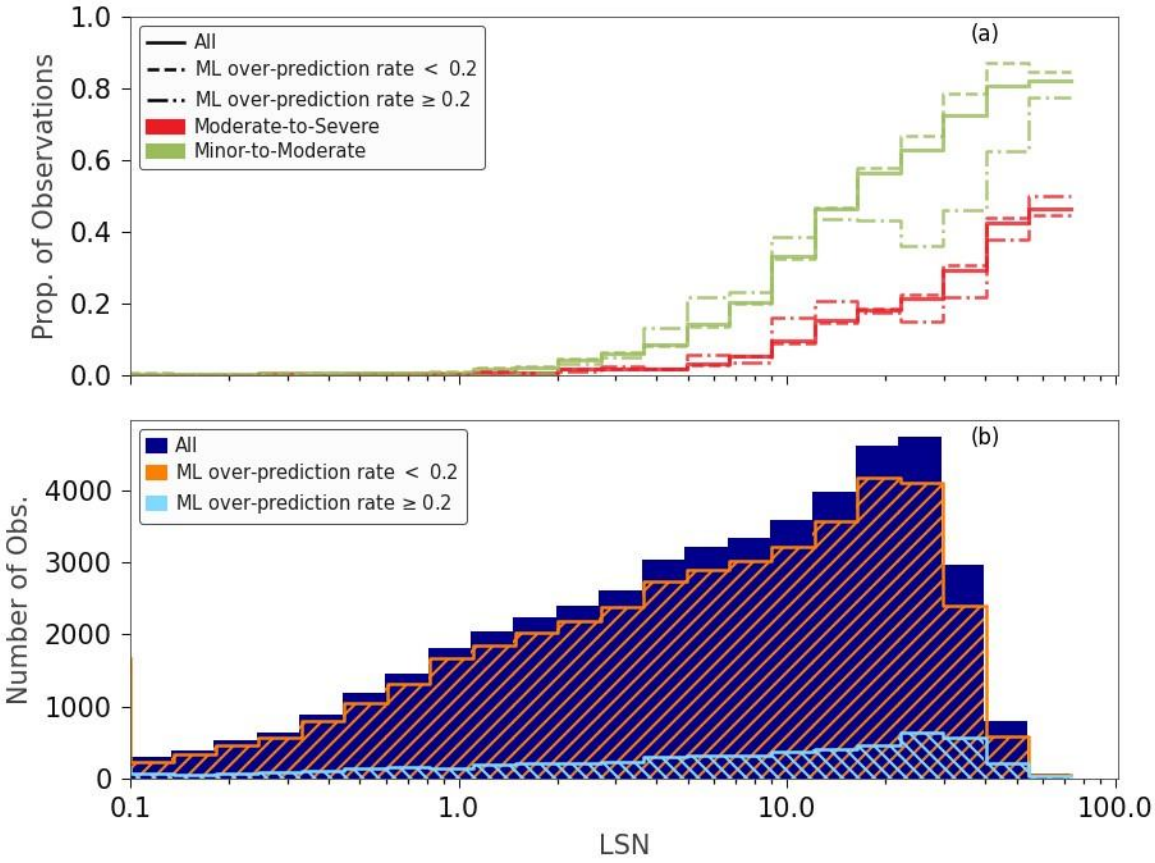

Figure 10.18: a) Comparison of empirical Minor-to-Moderate and Moderate-to-Severe LDFCs for ML over-prediction rate above and below 0.2, and b) Distribution of LSN with respect to ML over-prediction rate

10.3.2.4 Comparison of index measures

Figure 10.19 and Figure 10.20 show the correlation between ML over-prediction rate versus median I_{c10} and $(I_c > 2.6)_{10}$ respectively. There appears to be only a minor correlation between both index measures and ML over-prediction rate. This suggests that the ML over-prediction rate uses different features of the CPT trace than those captured by the I_c-based indices.

For comparison purposes, Figure 10.21 shows the median I_{c10} plotted against $(I_c > 2.6)_{10}$ for the full NLM dataset. The correlation between these two measures is strong. Note that, by definition, CPTs with median I_{c10} of 2.6 correspond exactly with 50% $(I_c > 2.6)_{10}$. Most striking about Figure 10.21 is the high percentage of CPTs (48% of the national dataset) which have median $I_{c10} > 2.05$, and similarly 51% for $(I_c > 2.6)_{10}$ above 20%. These portions notably exceed the portions in the event dataset for Christchurch which is approximately 35% for median $I_{c10} > 2.05$. These CPTs are particularly prevalent in the North Island around Tauranga and Hawke's Bay. An adjustment to land damage probabilities based on these indices would result in significant changes in these areas.

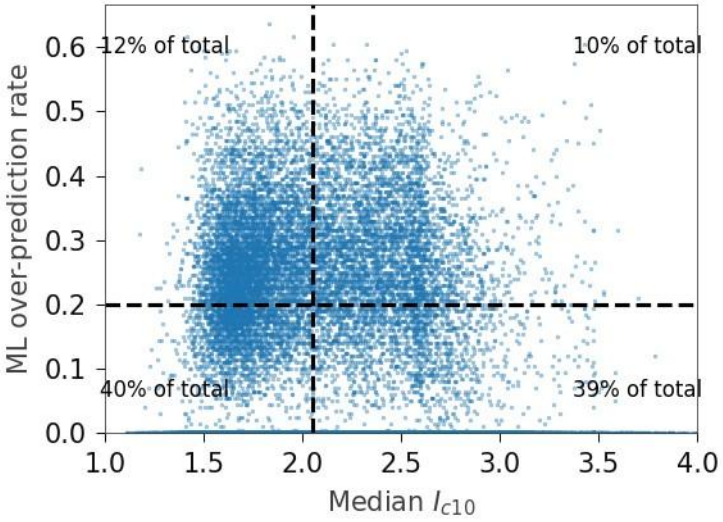

Figure 10.19: Median I_{c10} vs ML over-prediction rate for all CPTs in the full NLM dataset

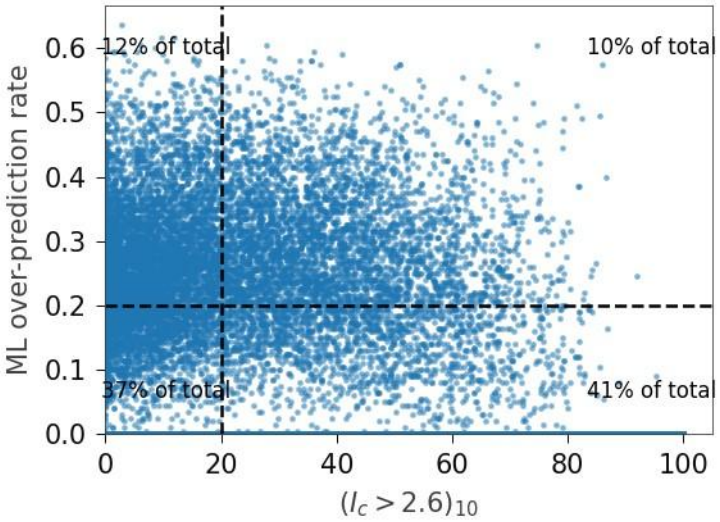

Figure 10.20: $(I_c > 2.6)_{10}$ versus ML over-prediction rate for all CPTs in the full NLM dataset

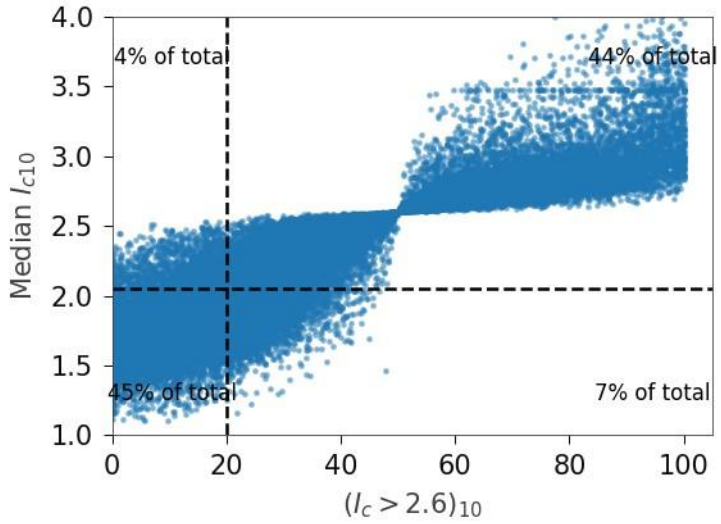

Figure 10.21: $(I_c > 2.6)_{10}$ versus median I_{c10} for individual CPTs within the full NLM dataset

10.3.3 Comparison to existing Land Damage Fragility Curves (LDFCs)

Figure 10.22 compares the NLM P_L = 15% fitted LDFCs to the LDFCs determined by Geyin & Maurer (2020). P_L = 15% fitted curves were used since this was the approach adopted by Geyin & Maurer (2020). The two sets of curves appear to be generally consistent. The main differences between the approaches to develop the curves are the differences in calculation of the LSN estimates, particularly:

- Geyin & Maurer (2020) used a liquefaction susceptibility limit of $I_c < 2.5$ compared to 2.6 adopted for the NLM curves;
- Geyin & Maurer (2020) used only CPT, whereas the NLM curves also use BH;
- Geyin & Maurer (2020) removed CPT that were deemed to have terminated prematurely, whereas the NLM curves used a depth corrected LSN for short GI; and
- Geyin & Maurer (2020) used the event GW models from Table 10.1, whereas the NLM curves used the seasonally corrected NLM GW Model.

Another important difference is that different definitions were used for the land damage categories. For example, “Moderate” in Geyin & Maurer (2020) corresponds to 5-40% ground coverage by liquefaction ejecta, while the NLM “Minor-to-Moderate” category corresponds to < 25% coverage. These differences make a quantitative comparison difficult, however, the NLM Minor-to-Moderate curve falls between the Minor and Moderate curves from Geyin & Maurer (2020). Similarly, the NLM Moderate-to-Severe curve is between the Moderate and Severe land curves from Geyin & Maurer (2020).

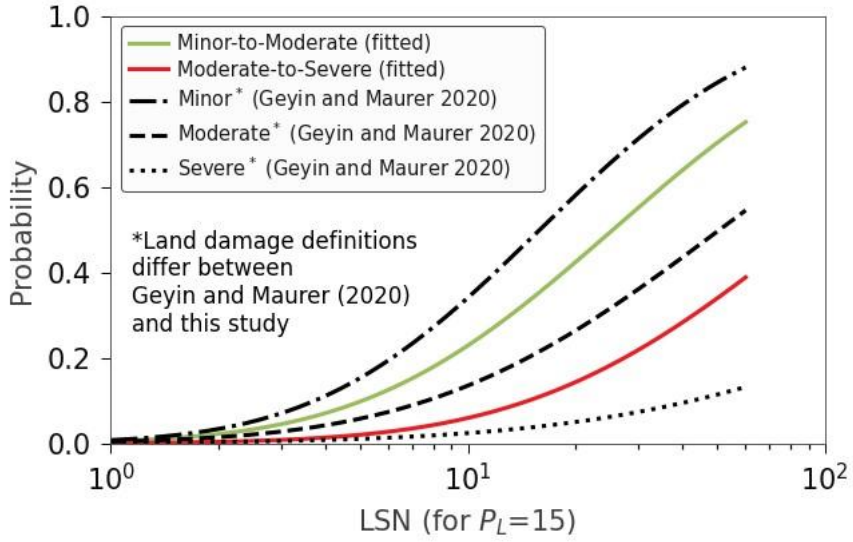

Figure 10.22: Comparison between LDFCs from Geyin & Maurer (2020) versus the NLM for P_L=15%. Note that these curves are cumulative – e.g. Minor-to-Moderate also includes Moderate-to-Severe, so could be thought of as "Minor-to-Moderate (or worse)"

10.4 Validations of other parts of model

10.4.1.1 Evaluation of prediction differences between GI types

The LDFCs have been produced in Figure 10.23 using just BH and just CPT to evaluate whether prediction performance is lower for the novel BH method. The LDFC for BH are notably flatter showing lower efficiency than CPT. This result is unsurprising, as the higher resolution and precision of CPT data is one of the reasons why CPT testing is typically preferred (where practical) over BHs for liquefaction assessment. The BH method generally has lower LSN for the same level of damage, this is a reflection of the bias noted in Section 7.8.3 for LSN from BH being lower than from CPT in the Holocene River channel, Holocene Loess and Holocene Estuarine geomorphologies (which are prevalent in Christchurch). Since these geomorphologies typically have a large amount of CPT (~10x more than BH), any bias from BH in these geomorphologies is expected to be limited.

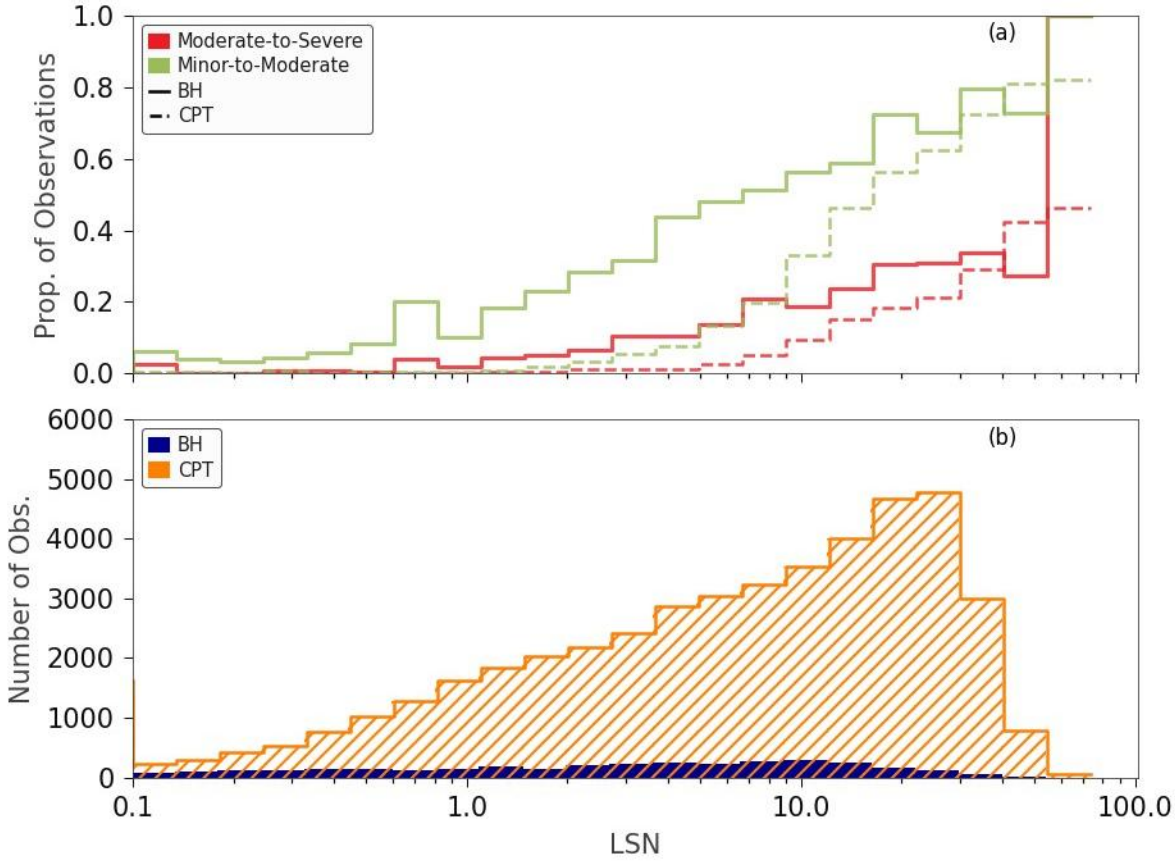

Figure 10.23: a) Comparison of empirical Minor-to-Moderate and Moderate-to-Severe LDFCs for BH only and CPT only, and b) Distribution of observations with respect to LSN

10.4.1.2 Evaluation of prediction differences between GW models

Figure 10.24 shows empirical, fitted and adjusted curves generated using the NLM GW Model to estimate LSN versus using the event GW model from Table 10.1. The NLM GW Model produces improved efficiency with steeper curves for both land damage categories.

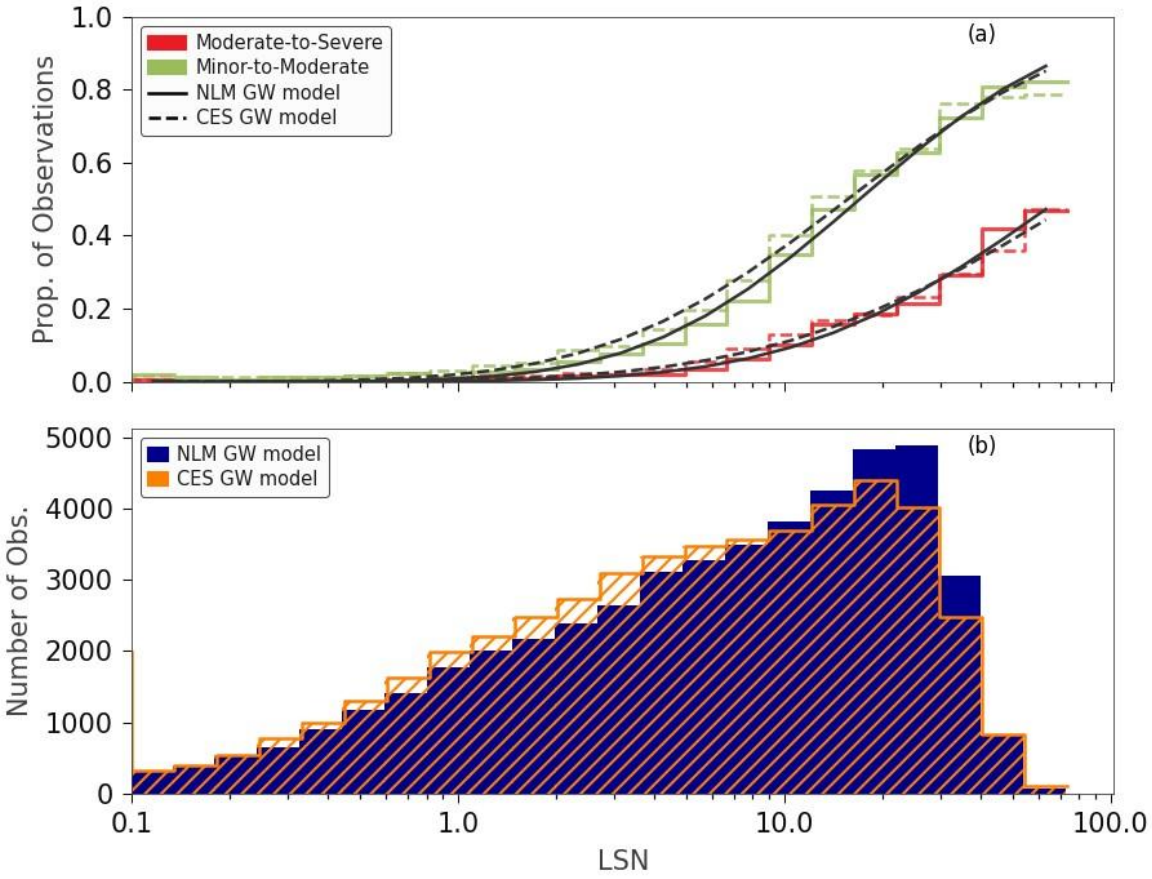

Figure 10.24: a) Comparison of empirical Minor-to-Moderate and Moderate-to-Severe LDFCs using the NLM GW Model versus the CES event GW models, and b) Distribution of observations with respect to LSN

10.4.1.3 Use of log transform of LSN for evaluating accuracy and bias

The guidance for establishing thresholds and processes in the NLM model to reduce output uncertainty and bias was based on $\log(LSN)$ (see Section 4.3.1). The primary basis for the use of $\log(LSN)$ is due to the correlation between $\log(LSN)$ and the change in the ratio of probability of land damage, as presented in this section. Figure 10.25 shows the LDFCs in log-log space, where the slope is approximately 2 up to a probability of 35% for both land damage categories. This corresponds to Equation 38, where $P_{LD,1}$ and $P_{LD,2}$ are two different land damage probabilities corresponding to two different LSN values, and $\Delta \log(LSN)$ is the difference between the LSN values in log space. Notably, using Equation 38 the doubling or halving of the probability of a land damage state corresponds to an absolute $\Delta \log(LSN)$ of 0.35, and a tenfold increase or decrease corresponds to $\Delta \log(LSN)$ of 1.15. Essentially the use of log(LSN) for evaluating errors means that the practical implications of errors are better conveyed across a range of land damage probabilities. For example, a 5% error in probability could have a significant practical implication if the modelled probability was 5%, but would have little practical implication if the modelled probability was 50%. The use of log(LSN) means that a change from 5% to 10% is considered as important as from 10% to 20% or from 20% to 40%, which is a common framework for evaluating natural hazards such as USGS hazard maps (United States Geological Survey (USGS)). An alternative approach of evaluating errors using LSN in linear scale would mean that a change in LSN from 1 to 2 would be seen as of equal importance as the difference between 51 and 52, but the former results in a more impactful change in the probability of land damage. Error evaluation using linear scale LSN would therefore put

greater focus on reducing errors for higher probabilities of damage, whereas the accuracy of low probabilities are typically of greater interest to loss modelling and many other applications.

Equation 38:

$$\frac{P_{LD,2}}{P_{LD,1}} = e^{2 \cdot \Delta \log(LSN)}$$

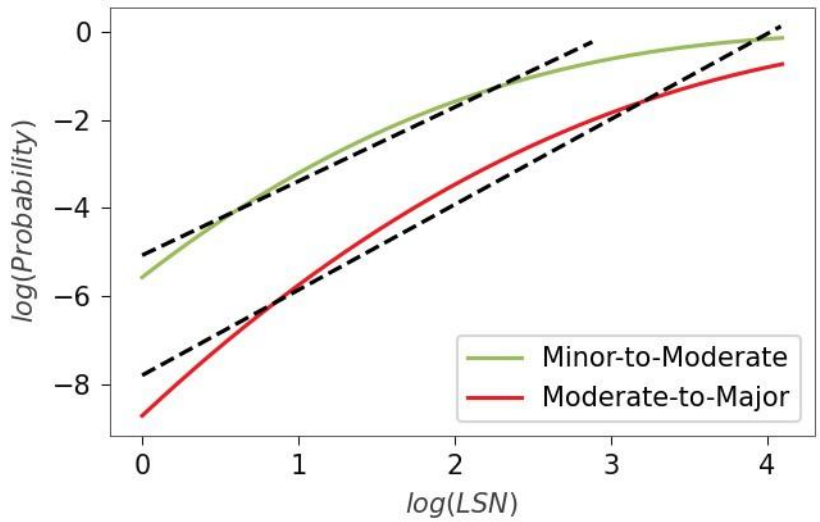

Figure 10.25: Fitted LDFCs in log-log space

Note that while Equation 38 only approximates Minor-to-Moderate and Moderate-to-Severe land damage up to about a probability of 35%, it also approximates the reduction in the probability of the None-to-Minor land damage state from 35% tending to zero. For example, a change in probability of None-to-Minor land damage from 10% to 5% occurs across the same $\Delta \log(LSN)$ as a change in Minor-to-Moderate land damage from 5% to 10%.

10.5 Limitations

The LDFCs developed herein are subject to the following limitations:

1 A limited dataset constrained to three earthquake events near Christchurch was used, therefore the LDFCs may be inaccurate (i.e. under- or over-predicting) for other areas.

2 There are notable differences in the empirical LDFCs between the three events, as well as when comparing LDFCs from subsets of the data at different levels of PGA and GWD. This suggests that while LSN is strongly correlated with land damage there is some inter-event and intra-event variability that make the LDFCs non-unique, and would differ for other events and different ground conditions.

3 The LDFCs have been derived from CPT and BH, where BH have notable lower efficiency in predicting land damage.

10.6 Potential future improvements

To enhance the LDFCs and help address their current limitations, several potential future improvements have been identified:

1 **Filter for short GI**. Investigate whether the extent of short GI correction reduces predictive performance. GIs with significant short GI correction could be filtered out of the dataset used for developing LDFCs to remove this uncertainty and potentially improve the prediction accuracy of the LDFCs.

2 **Shallower depth for LSN calculation**. Investigate whether improved prediction can be achieved by changing the total depth for the LSN calculation from 20 m to a shallower depth (e.g. 10 m).

3 **Reduce the mislabelled data percentage**. Consider further data validation and updating the buffers for assigning land damage observations.

4 **Add more earthquake events**. Add the observation dataset from the 2016 Mw 7.8 Kaikōura earthquake event and several smaller NZ events, and observations from the international events in the Next Generation Liquefaction database (www.nextgenerationliquefaction.org). More events would help constrain the position of the LDFCs and provide insight into the different potential biases that were noted in Sections 10.3.1 and 10.3.2.

5 **Revise the LSN uncertainty removal method**. The current method uses perturbed GWDs of +/- 0.5 m. This is an approximation of the uncertainty in GWD and could be revised to better reflect the normal distribution estimate from the NLM GW Model. Additionally, the removal of other uncertainties should be considered (e.g. uncertainty in PGA and variation from different drilling equipment).

6 **Cross-validation of observations against existing databases.** E.g. the database from Geyin & Maurer (2020) uses a different land damage classification schema but the cross-validation may identify some misclassifications and improve the NLM database.

7 **Include system response effects.** Include corrections for system response effects in the triggering analysis to potentially address noted issues with dependency of LDFCs on PGA, GWD, inter-event variability and ground profile indices.

8 **LDM from 1D effective stress analysis.** Perform 1D effective stress analysis on all GIs to compute an LDM that accounts for 1D system response effects.

9 **Alternative LDM.** Different LDMs have been developed that may improve predictive performance (e.g. ejecta potential index from Hutabarat & Bray (2022), or could be used in conjunction with LSN to estimate land damage and potentially improve estimates.

10 **Threshold-based LSN modification.** Develop modified LSN values based on secondary indices (see Section 10.6.1 for more details).

11 **Multi index land damage estimate**. An extension of threshold-based LSN modification would be to develop modifications to LSN that are continuous for a given secondary index (e.g. the LSN adjustment would increase with increasing I_{c10}) – this would avoid a sharp change in LSN across the selected threshold.

10.6.1 Modification of LSN values

To improve the predictive capability of LSN the LSN values could be modified based on a secondary index (thus producing a new index). This new index could then be calculated in the NLM GI and LV modules to predict the new index across the country. In conjunction with the development of a new index, the magnitude of the changes and how they are spatial distributed compared to the dataset used for the LDFC should be quantified. This is important for evaluating the applicability of such corrections.

10.6.1.1 Modification transform

Any of the above indices as well as input parameters (e.g. PGA or GWD) can be used to modify LSN using the method outlined here. The method modifies LSN values in one subset to match the LSN

values of a reference subset at the same probability of land damage. As an example, reducing the LSN values for all CPT where median I_{c10} > 2.05, so that they would have the same land damage probability as the dataset with median I_{c10} <= 2.05. This correction means both subsets can adopt the steeper LDFC of the median I_{c10} <= 2.05, however, locations that have median I_{c10} > 2.05 would now have lower LSN values.

The development of a transform to modify the LSN values can be achieved by fitting LDFC to the Minor-to-Moderate land damage curves for both subsets, then pairing the LSN values from each LDFC at various percentiles. Note that the LDFC for Minor-to-Moderate land damage is preferred over the Moderate-to-Severe since it has more data and covers high percentiles thus improving the resolution of the transform. A significant drawback of this modification transform is the step change that occurs across the threshold, where a small change in median I_{c10} could significantly change the LSN value.

11 Scenario outputs

This section provides three different kinds of outputs for three different purposes:

1 Simulations of historical events, where comparisons are made with the post-event observed land damage for the purpose of validating the LV and GW models.

2 Simulation of a potential Alpine Fault event, the purpose is to demonstrate the use of the model for evaluating liquefaction for future events (commonly done in loss modelling and can support pre-event planning).

3 Simulations for different return periods of seismicity as well as different GW and LSN calculations. These outputs could be used to support the development of MBIE/MfE Guidance (2017) maps, where uncertainties from multiple different sources should be considered.

To generate the scenarios, outputs are produced for a 100 m x 100 m grid. The following steps were applied at each grid point:

1 Obtain the PGA, Mw, GWD and SSP ID at the location of the grid point. PGA was obtained from a map of PGA, Mw was either the event magnitude or the mean magnitude corresponding to that location and return period, and GWD was taken from the NLM GW Model (for the historical events the seasonal correction was applied to produce GWDs that corresponded to the date of the event), and SSP was obtained from the *LVM SSP parquet* file.

2 Obtain the lookup values for specific SSP ID from the <LDM>-<PL>-<method>-per-SSP file (see Section 8.1 for the data and naming schemas). Note that LSN for PL=50% was used unless explicitly stated in the report.

3 Perform three-way linear interpolation of the PGA, Mw and GWD on the lookup table to obtain the P50 and P85 LDM distribution parameters. Note that the percentiles for the sample uncertainty distribution were used unless explicitly stated in the report.

4 Land damage probabilities were computed by integrating the LDFCs from Section 10 with the distribution of LSN (see Section 8.7). Note that only the "adjusted" LDFCs were used in these scenario outputs. The "adjusted" LDFCs do not implicitly consider the GWD uncertainty, compared to the "fitted" LDFCs which implicitly consider GWD uncertainty. Equation 39 presents the integration where P_{damage} is the probability of the damage state, $Damage$, and f_{LSN} is the probability distribution of LSN.

Equation 39:

$$P_{damage} = \int_{\{-\infty\}}^{\{\infty\}} P(Damage|LSN) \cdot f_{LSN}(LSN)\, dLSN$$

The scenario output is provided as maps of probability of Minor-to-Moderate (or greater) land damage and probability of Moderate-to-Severe land damage. The outputs for historical and potential future events are generated for the extent of the PGA layer. The outputs for the return periods are generated for the whole country. For reporting purposes only select areas are shown.

11.1 Historical events

Four historical events have been simulated: three events from the Canterbury earthquake sequence (see Section 11.1.1) and the 2016 Mw 7.8 Kaikōura earthquake event (see Section 11.1.2). The Canterbury events are used for model validation with additional comparisons made to the observed damage at the suburb level. Validation was not performed for the Kaikōura event since the observed data was less comprehensive so could not easily be compared at the suburb level. The simulations were performed using the spatial variability LSN distributions from the LVM (see Section 8.1).

11.1.1 Canterbury events simulation

The seismicity inputs used for simulating these events, as well as the post-event observation datasets, are summarised in Table 10.1. Quantitative comparisons were made between simulations (i.e. results from the NLM liquefaction model) and post-event observations at the suburb level (suburb polygons obtained from LINZ (2023) using the following steps for each suburb (as illustrated in Figure 11.1). Note that the portion of each observed land damage category is taken as equivalent to the probability of each land damage category at a suburb level. While this comparison attempts to provide a relative measure of error for forward prediction, the limitations of this comparison are detailed later in this section. The following steps are undertaken for each suburb:

1 Sample observed land damage map using a 25 m by 25 m point grid.

2 Determine the percentage of valid points that correspond to each land damage category. Valid points are points where observations were made.

3 Simulate the event to generate the Minor-to-Moderate and Moderate-to-Severe land damage probability raster grid at 100 m spacing.

4 Extract the probabilities of Minor-to-Moderate and Moderate-to-Severe land damage from the simulation output at each valid sample point.

5 Compute the average of the probabilities of Minor-to-Moderate and Moderate-to-Severe (referred as simulated average probabilities).

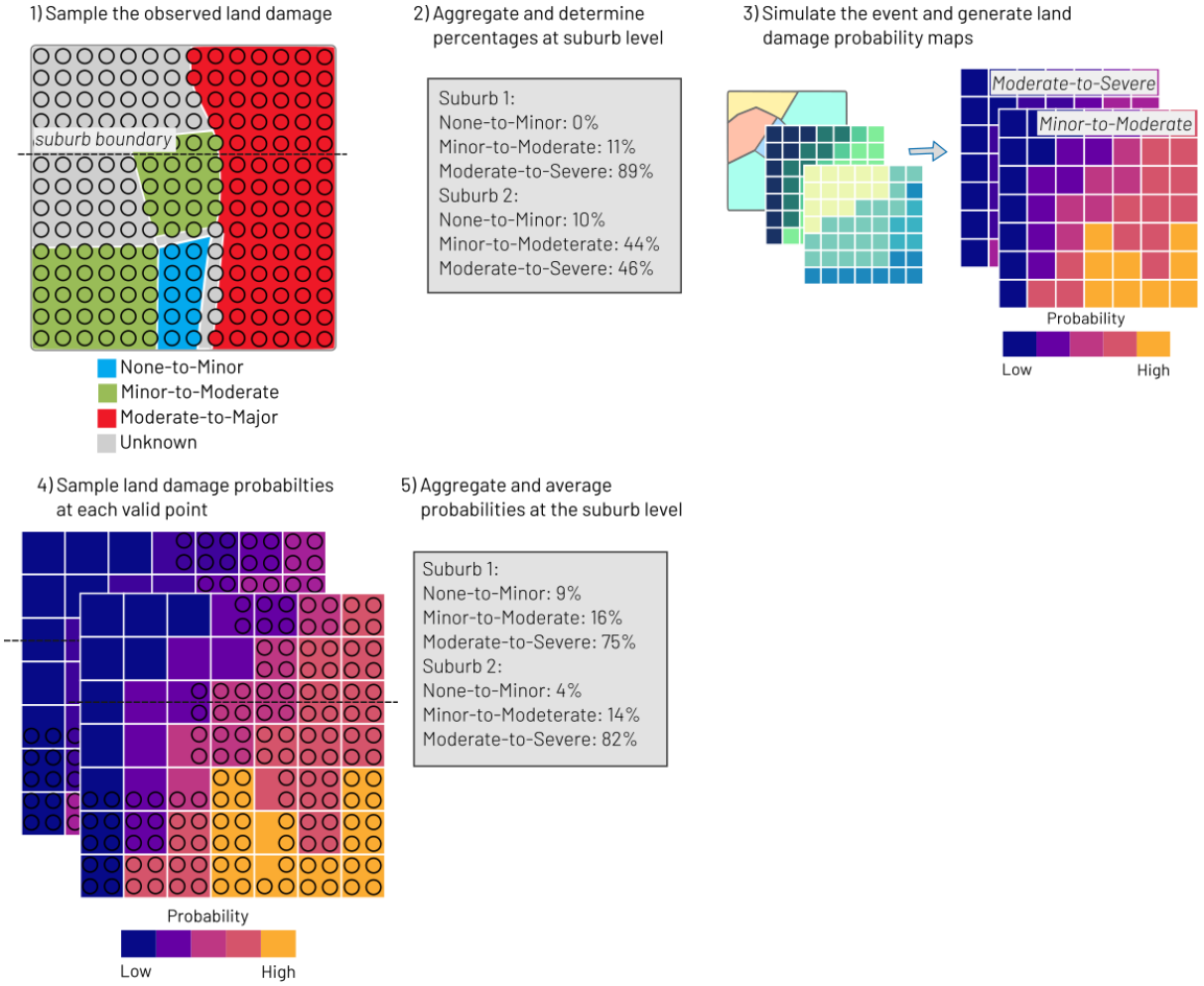

Figure 11.1: Historical event validation process

For each event, a figure with six subplots is created. PGA and observed land damage maps are in the top row. The second row has the land damage probability maps, and the third row shows the difference in land damage probabilities to proportions of sampled observation points in each suburb. A positive value in the bottom maps indicates the simulation is over-predicting, whereas a negative value indicates the simulation is under-predicting.

The comparison of differences provides an objective way to evaluate whether the model would over or under predict damage in a suburb for a particular event. Suburb-scale is used as the area to aggregate data for this exercise, since average house sizes and prices (and thus the cost of building damage) tend to vary between suburbs. Therefore, when evaluating likely losses, the overprediction of land damage in one suburb is not necessarily balanced by an equal and opposite underprediction in another. While close agreement between simulated average probabilities and proportions of observations is desirable at the suburb scale, it should not be expected due to the following caveats:

1 The proportions from the event observations are for a single event, whereas the simulated average probabilities consider all possible event realisations, (i.e. the event observations have an inter-event variability effect that may shift the proportions for that event, which is not considered in simulated average probabilities).

2 The uncertainties and biases in PGA estimates vary at the suburb-scale (e.g. liquefaction at some strong motion stations in February 2011 increases the uncertainty in the PGA for North-Eastern Christchurch).

3 The NLM GW Model was developed at a regional level and could be expected to have biases at the suburb-scale.

4 The uncertainty and bias guidance has some acceptable level of bias at the suburb level (see Section 4.3.1.1). This bias could be generated in several parts of the model build. Some examples that could influence suburb-scale results are: the misclassification and boundary uncertainty in the geomorphology model; local bias in GWD from the NLM GW Model; three-way interpolation of LSN distributions for a given PGA, Mw and GWD; the Voronoi expansion of SSP in the Tier 2 development.

5 There could be biases in the extent of land damage observation mapping. In particular, there are notable unmapped areas – if an unmapped area had a larger proportion of None-to-Minor damage than the rest of the suburb then the observed proportions are not fully representative. This issue is only partially mitigated by only comparing the simulation and observations at points where land damage was observed.

6 The augmentation of the observation dataset does not filter the land damage categories equally (see Section 10.2.2). Particularly, the Minor land damage category is considered liquefiable for evaluating Borderline observations which results in the removal of a greater proportion of None-to-Minor observations. Conversely, for the Feb2016 event the unmapped land is considered None-to-Minor, which would most likely bias the proportions to overrepresent None-to-Minor. Furthermore, the transform of the observation categories for Feb2016 event had only a single polygon assigned as Moderate-to-Severe and therefore this category may be underrepresented in this comparison.

7 The limitations in the LDFCs as outlined in Section 10.5, mean that some ground profiles and some demands may over and under predict in terms of land damage

8 The process to obtain LSN and the process to obtain the probability of land damage from LSN have some double counting of uncertainty, as discussed in the orange box at the end of this subsection.

Figure 11.2 shows the comparison for the September 2010 event, where the simulation results in high probabilities of Minor-to-Moderate land damage compared to the corresponding observed proportion, except for a few suburbs in the North-East. Conversely, the low simulation probabilities

of Moderate-to-Severe land damage are reasonably consistent with the observations (mostly within 10%), in that most suburbs had no observed Moderate-to-Severe land damage.

Figure 11.3 shows the comparison for the February 2011 event, where there are significantly higher probabilities of land damage from the simulation than observed proportions for the North-East. However, the opposite is true for the South-West. The distribution of over-prediction and under-prediction is similar to the distributions of median I_{c10}, percentage $I_c > 2.6$ and ML over-prediction rate (see Section 10.3.2).

Figure 11.4 shows the comparison for the February 2016 event. Note that the map of the observed data does not show the buffer augmentation applied in Section 10.2.2, but the augmented data was used to determine the comparison at the suburb level. Also note that due to the data transform adopted (Table 10.4), there was only 1 observation of Moderate-to-Severe land damage. For this event, damage was localised to a few suburbs in eastern Christchurch and hence, the simulation provided a reasonable estimate of the concentrated damage.

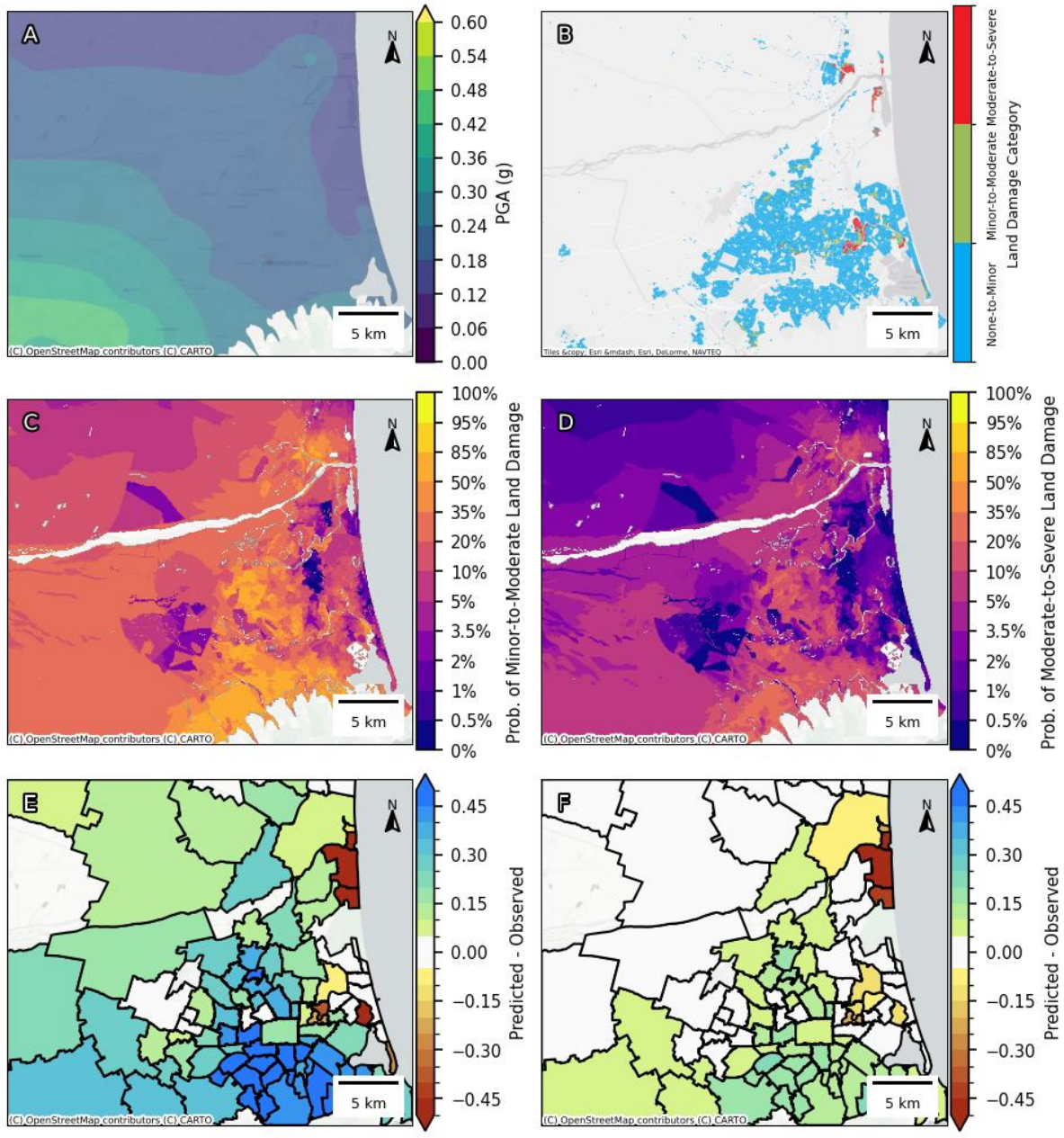

Figure 11.2: September 2010 event comparison maps, (A) PGA, (B) observed land damage, (C) probability of Minor-to-Moderate land damage, (D) probability of Moderate-to-Severe land damage, (E) difference between predicted land damage probabilities, map C, and sampled observation points per suburb, (F) difference between predicted land damage probabilities, map D, and sampled observation points per suburb

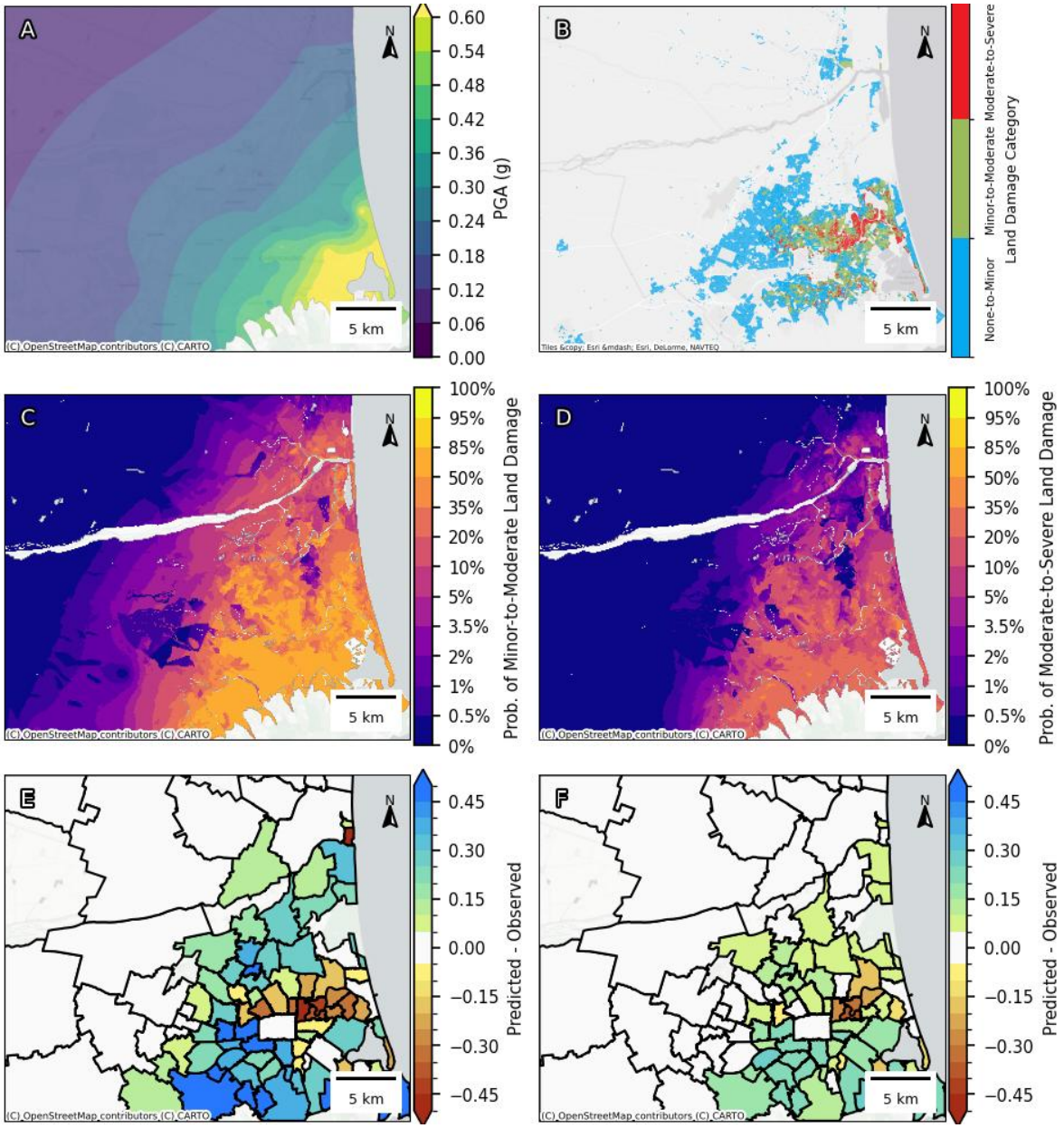

Figure 11.3: February 2011 event comparison maps, (A) PGA, (B) observed land damage, (C) probability of Minor-to-Moderate land damage, (D) probability of Moderate-to-Severe land damage, (E) difference between predicted land damage probabilities, map C, and sampled observation points per suburb, (F) difference between predicted land damage probabilities, map D, and sampled observation points per suburb

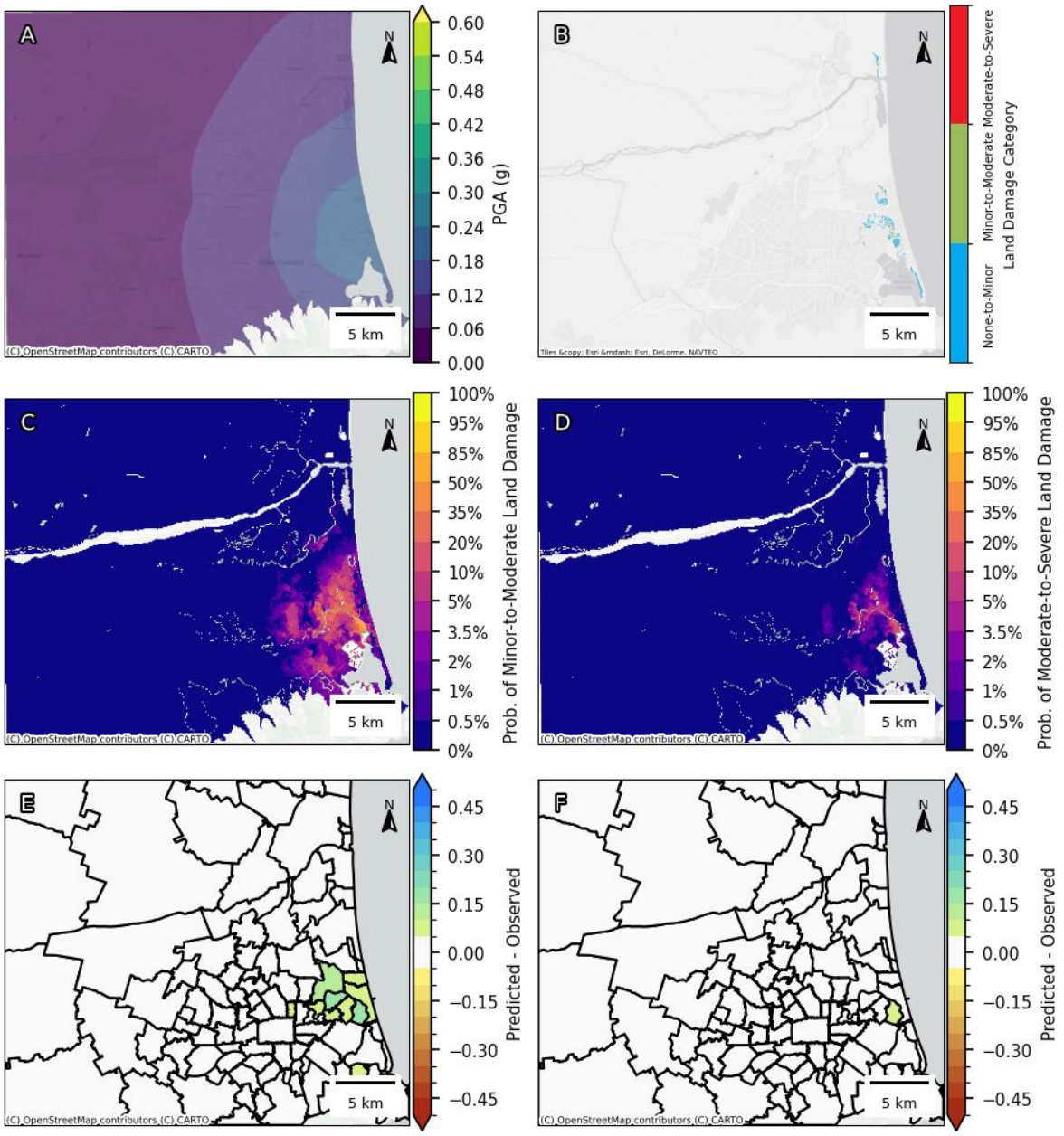

Figure 11.4: February 2016 event comparison maps, (A) PGA, (B) observed land damage, (C) probability of Minor-to-Moderate land damage, (D) probability of Moderate-to-Severe land damage, (E) difference between predicted land damage probabilities, map C, and sampled observation points per suburb, (F) difference between predicted land damage probabilities, map D, and sampled observation points per suburb

The simulated average probabilities of land damage per suburb versus the proportions of observed land damage are compared in Figure 11.5. The star symbol for each land damage category represents the average of all valid land damage observation points for the event (not the average of the points in Figure 11.5). The following can be noted from Figure 11.5:

- The September 2010 event shows over-prediction of Minor-to-Moderate land damage for most suburbs, with most points below the 2:1 line. The average for all points for Minor-to-Moderate (i.e. star symbol) was over-predicted by more than double. The Moderate-to-Severe land damage shows some under-prediction for several suburbs, however, the average of all points was over-predicted by 2:1. Note that the overall Moderate-to-Severe land damage was low (<10%).

- For the February 2011 event, the average of all points was closer to the 1:1 correlation line for both land damage categories, though there were notable over and under-predictions at the suburb level. Interestingly, the variation in proportions from the observations is higher than the variation in simulated percentages (i.e. the observed percentages are scatter from 0-100% for Minor-to-Moderate whereas the simulated average probabilities fall within a narrow range, mostly 30-60%). This could be expected since the observations represent a single event realisation, while the simulations use the integration of the distributions and therefore represent the average of all realisations. Potentially the under-prediction of scatter may suggest that uncertainty is over-represented in the simulations – in that averaging of uncertainty causes results to tend towards median values (see Section 4.2.1.1). This could be addressed by increasing the steepness of the LDFCs to produce more scatter in the simulation results[24] or using narrower distributions of LSN. Other potential causes of under representation of suburb-by-suburb variability may be due to:
  - Biases in the observations (e.g. North of Christchurch there are only select pockets where observations were made, primarily of None-to-Minor, and these may be a biased sample. Furthermore, in areas of widespread damage, small pockets of None-to-Minor damage may not have been captured).
  - Spatial interaction of liquefaction (e.g. lateral spreading) where early onset of liquefaction in an area of low liquefaction resistance results in increased land damage nearby. For the February 2016 event, the simulation generally predicts low probabilities of land damage, consistent with the outputs shown in Figure 11.4.

A note regarding the use of steeper LDFCs and narrow LSN distributions

Given the numerous steps involved in the determination of LSN it is likely that there is significant double counting of uncertainty. For example, differences in LSN caused by the depth correction, three-way interpolation for the parameters of the LSN distribution from a lookup table, or different corrections applied to CPT cone areas in the liquefaction triggering calculations. All these differences result in increased uncertainty in the LDFCs and in the LSN distributions.

Unlike uncertainty in the GWD which influences both the LSN and the event land damage, the uncertainty due to differences in the calculation of LSN could be removed from both the input LSN and the LDFCs as they do not impact event land damage. Unfortunately, the removal is not trivial – and so a simple nominal reduction in uncertainty in the LSN distributions and/or the LDFCs could be warranted instead. This issue is particularly important for fragility curves that use highly interpreted inputs, whereas for fragility curves that use directly measurable parameters (e.g. PGA) the uncertainty should be considered in either the fragility curves or explicitly in the estimate of the parameter.

[24] Steeper fragility curves mean the output probability is more sensitive to changes in the input variable. In this case, small variations in LSN across suburbs would result in more significant differences in probabilities (i.e. more scatter).

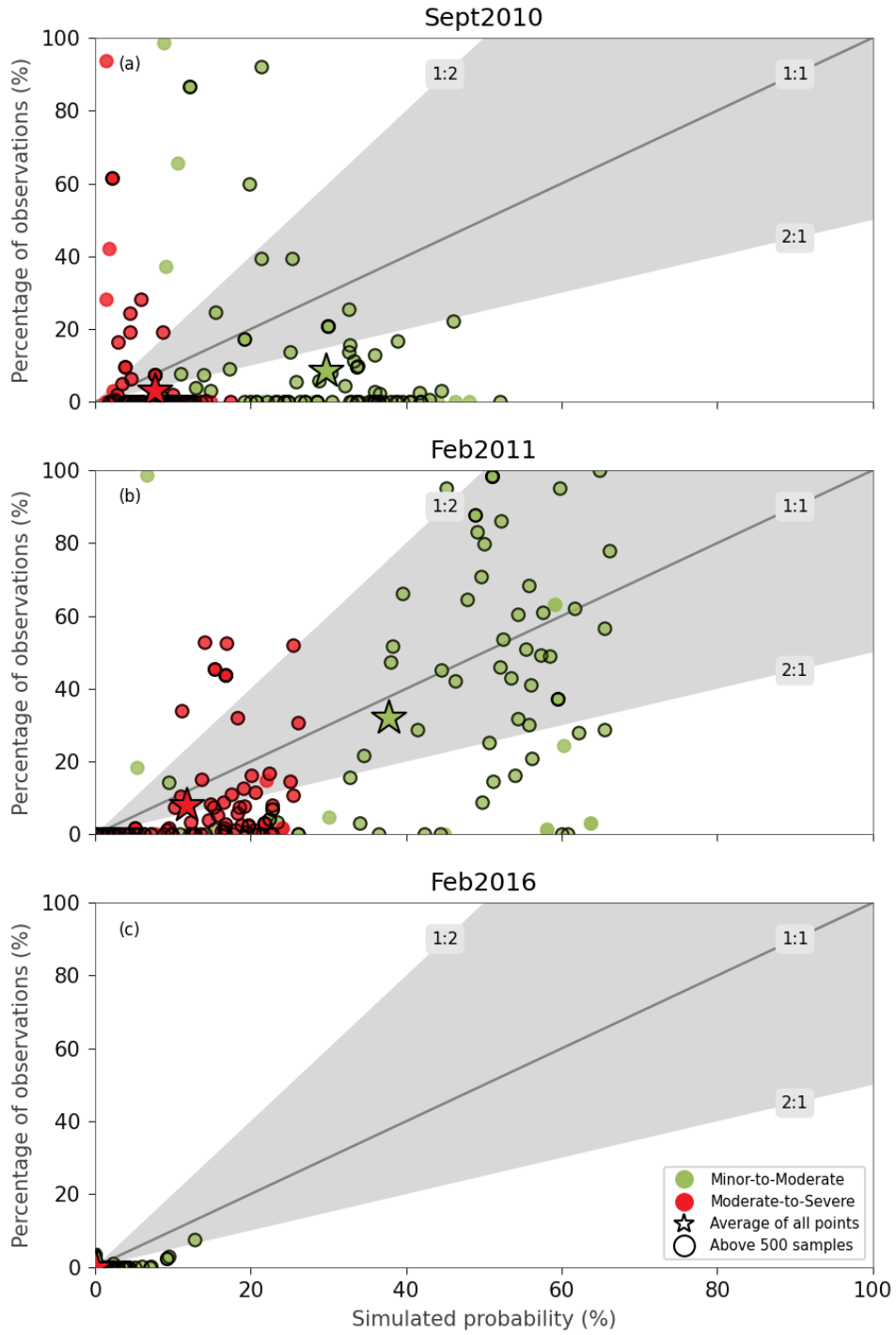

Figure 11.5: Comparison of simulated probability of land damage versus proportion of land damage observations at the suburb level, a) September 2010 event, b) February 2011 event, and c) February 2016 event

11.1.2 Kaikōura 2016 event simulation

The 2016 Mw 7.8 Kaikōura earthquake event was simulated using the NLM GW Model and the PGA shake maps from GeoNet GNS Science (2016). The simulated output is shown in Figure 11.6 (a) for Christchurch, Figure 11.6 (b) for the Wellington area and Figure 11.6 (c) for the Wairau Valley (Blenheim). The most extensive simulated land damage was in the Wairau Valley, closest to the

epicentre, and consistent with the observations post event, whereas there were no observations of land damage in Christchurch and localised areas in Wellington.

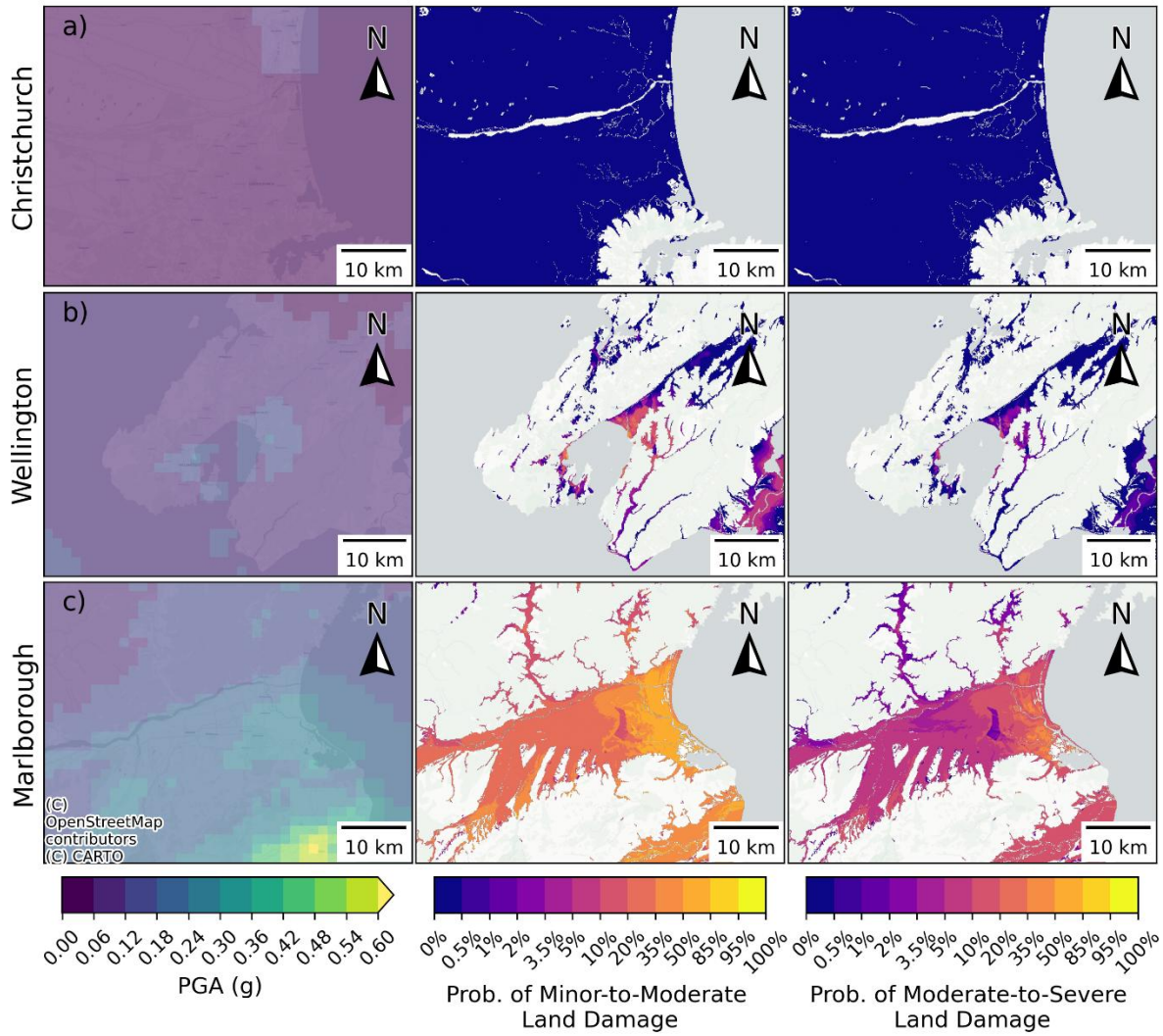

Figure 11.6: (left) PGA map, (centre) probability of Minor-to-Moderate land damage, (right) probability of Moderate-to-Severe land damage, for (a) the Christchurch area, (b) the Wellington area and (c) the Wairau Valley (Blenheim) for the 2016 Mw 7.8 Kaikōura earthquake event

11.2 Future Alpine Fault event

The seismic map for a simulation of a future Mw 7.9 Alpine Fault rupture was obtained from the QuakeCore SeisFinder website with simulation attributed to Bradley et al. (2017). The simulated PGA values are quite low for Christchurch and Wairau Valley (Blenheim), resulting in very low probability of land damage (see Figure 11.7 and Figure 11.8 below). The higher land damage probability near Oxford (north-west area in the figures) corresponds to higher predicted PGA from the Alpine Fault simulation.

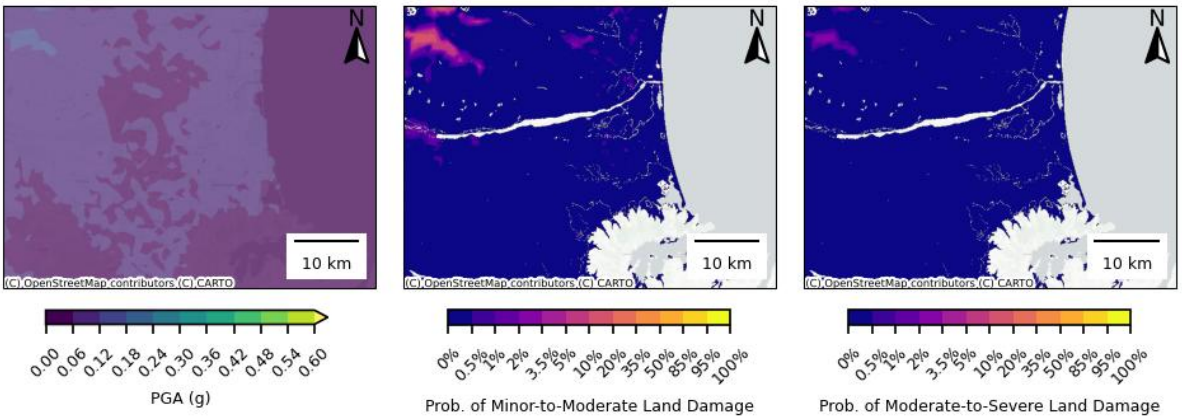

Figure 11.7: (left) PGA map, (centre) probability of Minor-to-Moderate land damage, (right) probability of Moderate-to-Severe land damage, for the Christchurch area for a simulated Alpine Fault earthquake event

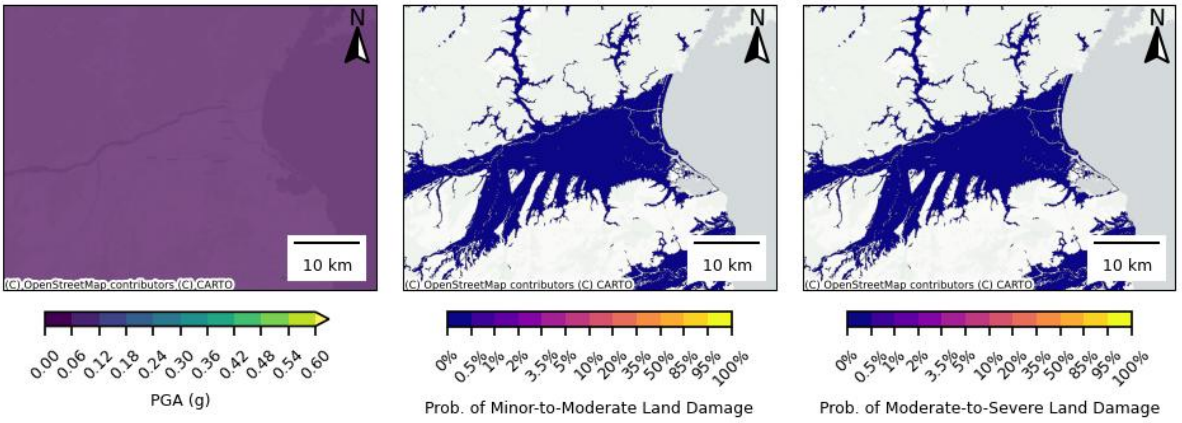

Figure 11.8: (left) PGA map, (centre) probability of Minor-to-Moderate land damage, (right) probability of Moderate-to-Severe land damage, for the Wairau Valley (Blenheim) area for a simulated Alpine Fault earthquake event

11.2.1 Simulation using PL=15%

The Alpine Fault event was also simulated using the LSN distributions and LDFCs for P_L=15% as shown in Figure 11.9. Notably, the Minor-to-Moderate predicted damage is higher than for the P_L=50% output. This higher damage is more consistent with simulation output from Geyin & Maurer (2020) which predicted pockets of >10% probability of Moderate land damage for the same event in similar areas to the higher probability areas in Figure 11.9.

The difference between P_L=15% and P_L=50% is unexpected since the higher LSN values for P_L=15% (not shown) should be balanced by P_L=15% fragility curves having lower probability of damage for the same LSN value (see Figure 10.3). Further comparisons between P_L=50% and P_L=15% showed that P_L=15% generally generates larger probabilities of land damage for small shaking and vice-versa for strong shaking (such as 500-year shaking in Wellington presented Figure 11.15). This suggests the differences may be due to the potential biases explored in Section 10.3.1 and 10.3.2, or due to LSN plateauing at large PGA values. This highlights an unusual quirk of adopting non median parameters (i.e. P_L=15%) at an intermediate step, which resulted in an unintended outcome (the opposite of the original intention of adopting lower liquefaction resistance).

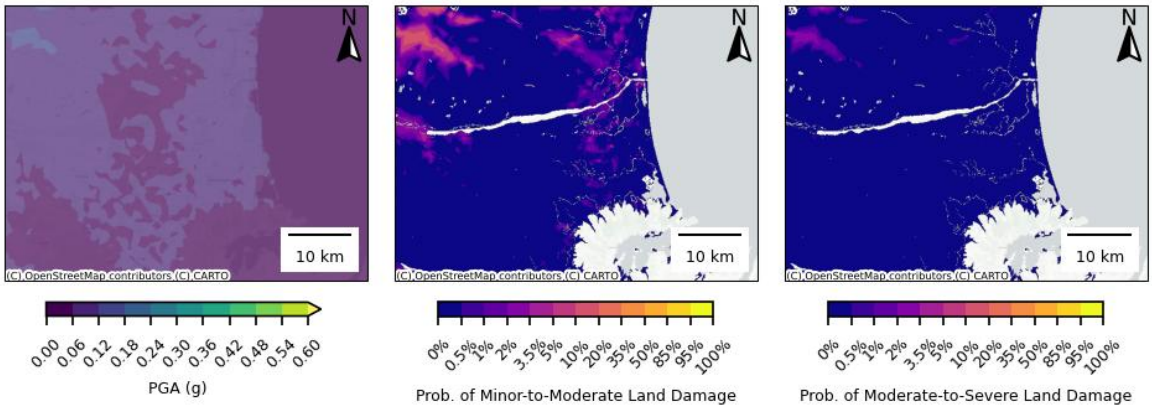

Figure 11.9: (left) PGA map, (centre) probability of Minor-to-Moderate land damage, (right) probability of Moderate-to-Severe land damage, for the Christchurch area for a simulated Alpine Fault earthquake event using P_L=15%

11.3 Return period calculations

11.3.1 Outputs for different return period seismicity

The seismic demands (PGA and mean Mw) for Site Class V (soft or loose soil) from the Draft TS1170.5 (Standards New Zealand, 2024) for different return periods of seismic shaking were used to evaluate the probability of land damage. The outputs for 25-year, 100-year, 500-year, and 2,500-year return periods are provided below for Christchurch (Figure 11.10), Wellington (Figure 11.11) and Hawke's Bay (Figure 11.12).

Some of the key observations from these scenario outputs include:

- In Christchurch, the probability of Minor-to-Moderate (or more) land damage in Christchurch is near zero for 25-year return period seismic shaking. The probability increases significantly between 25-year and 100-year shaking and then plateaus beyond 500-year seismic shaking.
- In Wellington and Hawke's Bay, the probability of Minor-to-Moderate (or more) land damage varies between ~10-20% for 25-year return period seismic shaking. The probability increases and then plateaus beyond 100-year shaking.
- There is a sharp change in probabilities on the eastern edge of the Hawkes Bay maps (Figure 11.12). This was caused by the change in GWD across the refined GW model boundary and does not reflect reality.
- Comparative analysis between return periods identified two situations where the probability of land damage may decrease with increasing return period, the first is at very low LSN values caused by the geospatial model having a minimum P85/P15 ratio (see Section 8.4.7 step 5), this can cause land damage probabilities to decrease when transitioning out of this minimum ratio. This impacts less than 0.005% of polygons and the decrease in probability is on the order of 0.01%. The second occurs when a ground investigation has a LSN that is an extreme outlier compared to the geospatial distribution. The limits on the possible range of posterior mean and standard deviations in the Bayesian updating process (see Section 8.7.4 steps 3 & 4) combined with the typical plateau in LSN at high PGA can result in higher PGA having a narrower LSN distribution but the same mean LSN than at lower PGA, this narrower distribution can result in lower probability of land damage. This impacts less than 0.03% of polygons and the decrease in probability is in the order of 0.01-1%.

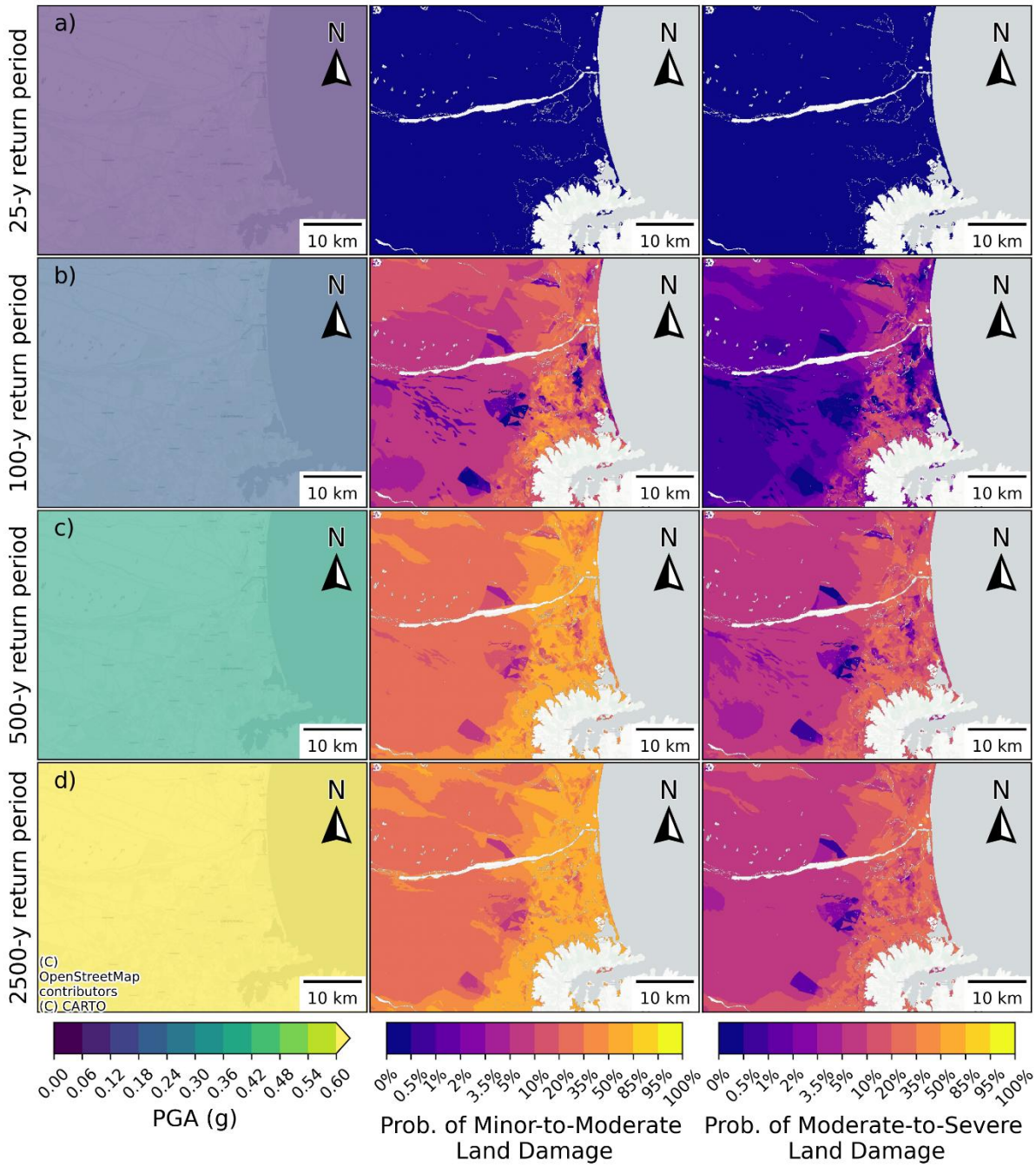

Figure 11.10: (left) PGA, (centre) probability of Minor-to-Moderate land damage (right) probability of Moderate-to-Severe land damage, for the Christchurch area for the a) 25-year, b) 100-year, c) 500-year, and d) 2,500-year return period seismic shaking

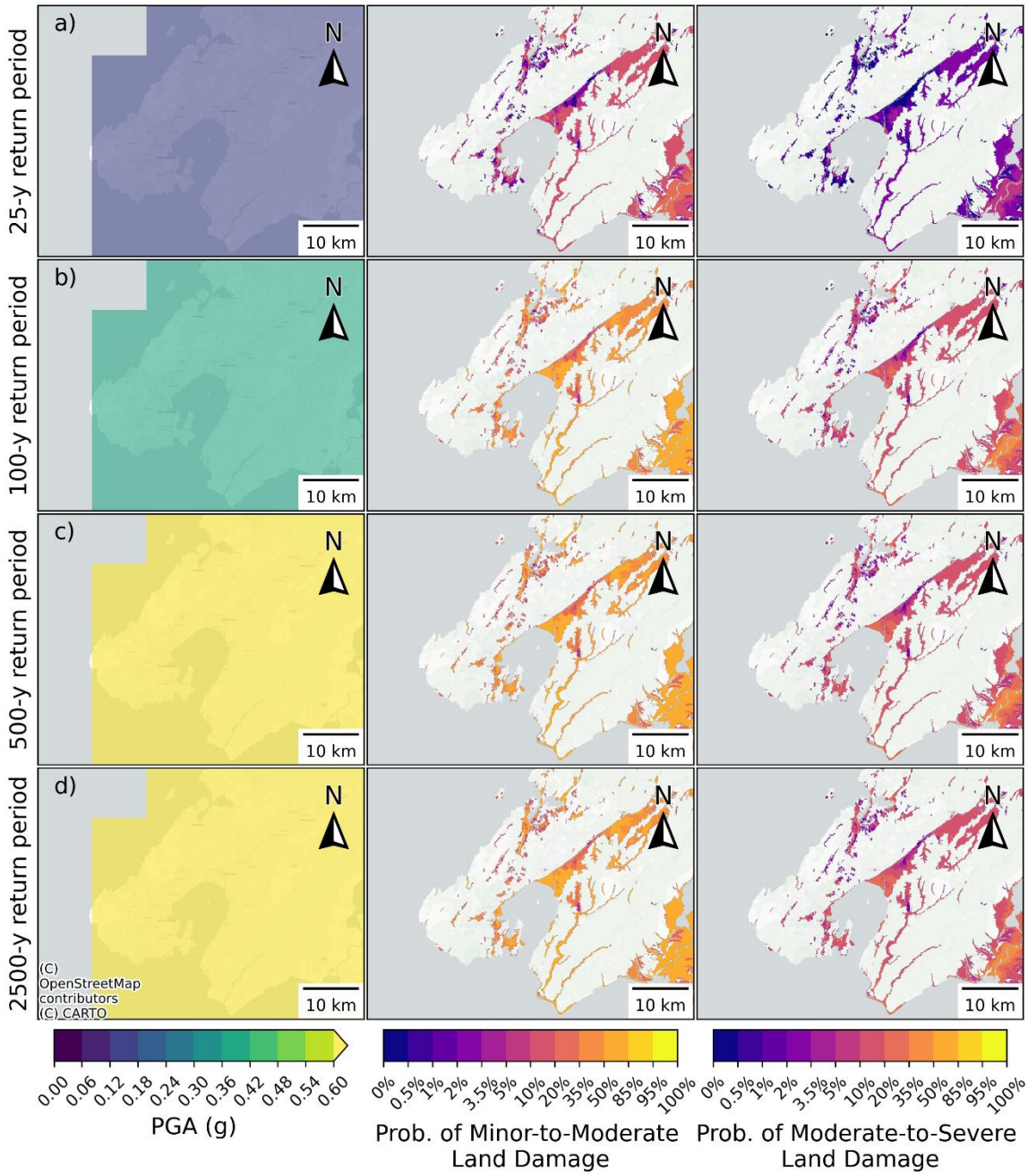

Figure 11.11: (left) PGA, (centre) probability of Minor-to-Moderate land damage (right) probability of Moderate-to-Severe land damage, for the Wellington area for the a) 25-year, b) 100-year, c) 500-year, and d) 2,500-year return period seismic shaking

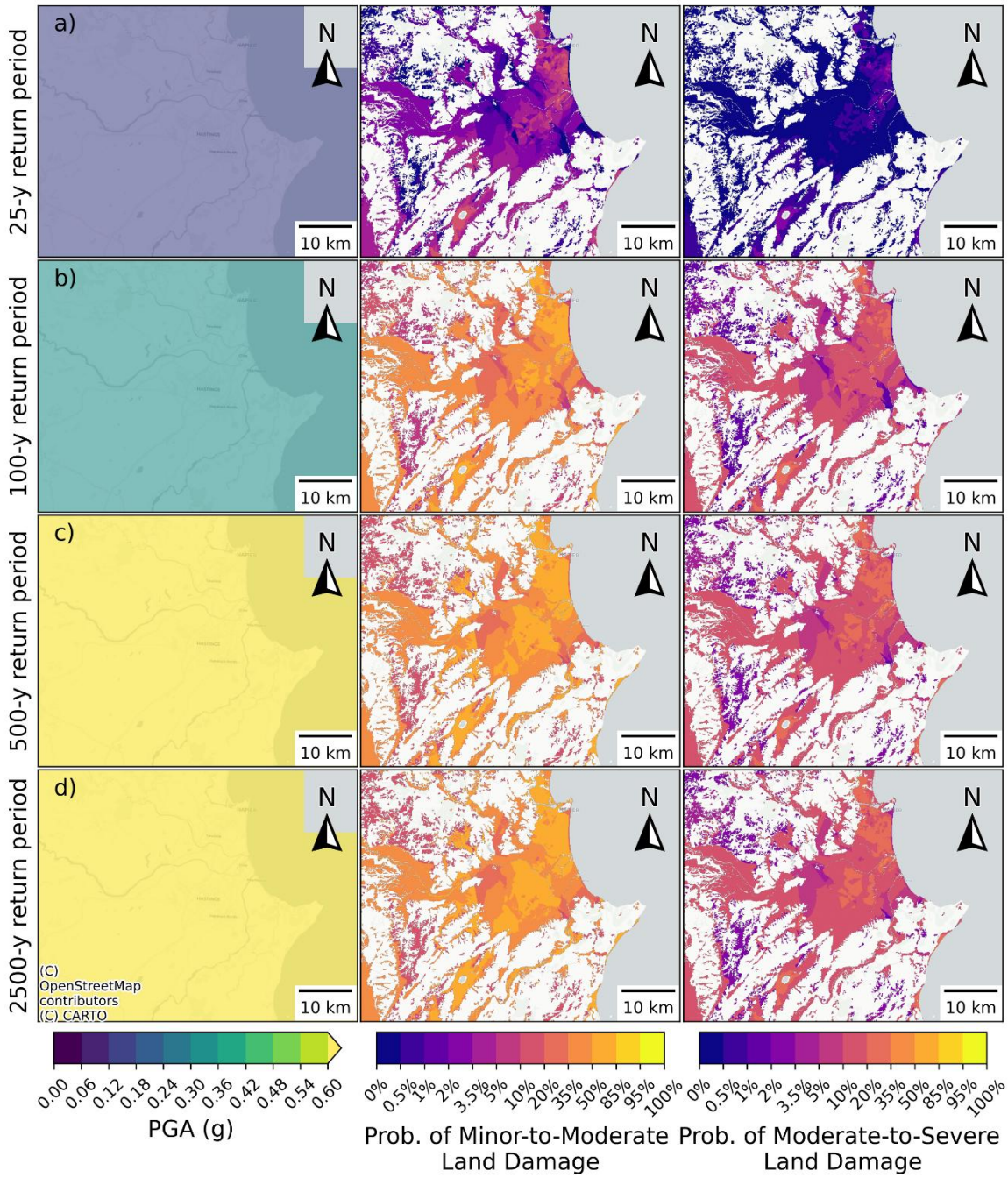

Figure 11.12: (left) PGA, (centre) probability of Minor-to-Moderate land damage (right) probability of Moderate-to-Severe land damage, for Hawke's Bay area for the a) 25-year, b) 100-year, c) 500-year, and d) 2,500-year return period seismic shaking

11.3.2 Outputs for different GW

Uncertainty in GWD is a key factor in the development of MBIE/MfE guidance maps. This section presents several different outputs that can be used to evaluate the influence of GWD.

11.3.2.1 Outputs for uncertainty in the NLM GW Model

The probability of land damage for 500-year return period shaking for one standard deviation deeper than median GWD, the median GWD and one standard deviation shallower than median GWD was determined and shown for the Wellington area in Figure 11.13. The GWD values for each

evaluation are shown in the left map. There are modest differences in the probability of Moderate-to-Severe land damage across the region when alternative GWDs are adopted. Note that the GW in the Lower Hutt area was modelled with a refined GW model and therefore has less uncertainty than the national model and thus a smaller standard deviation in GWD than Upper Hutt. The impact of changes in GW depth varies significantly across the country depending on the soils, PGA level, and median GWD.

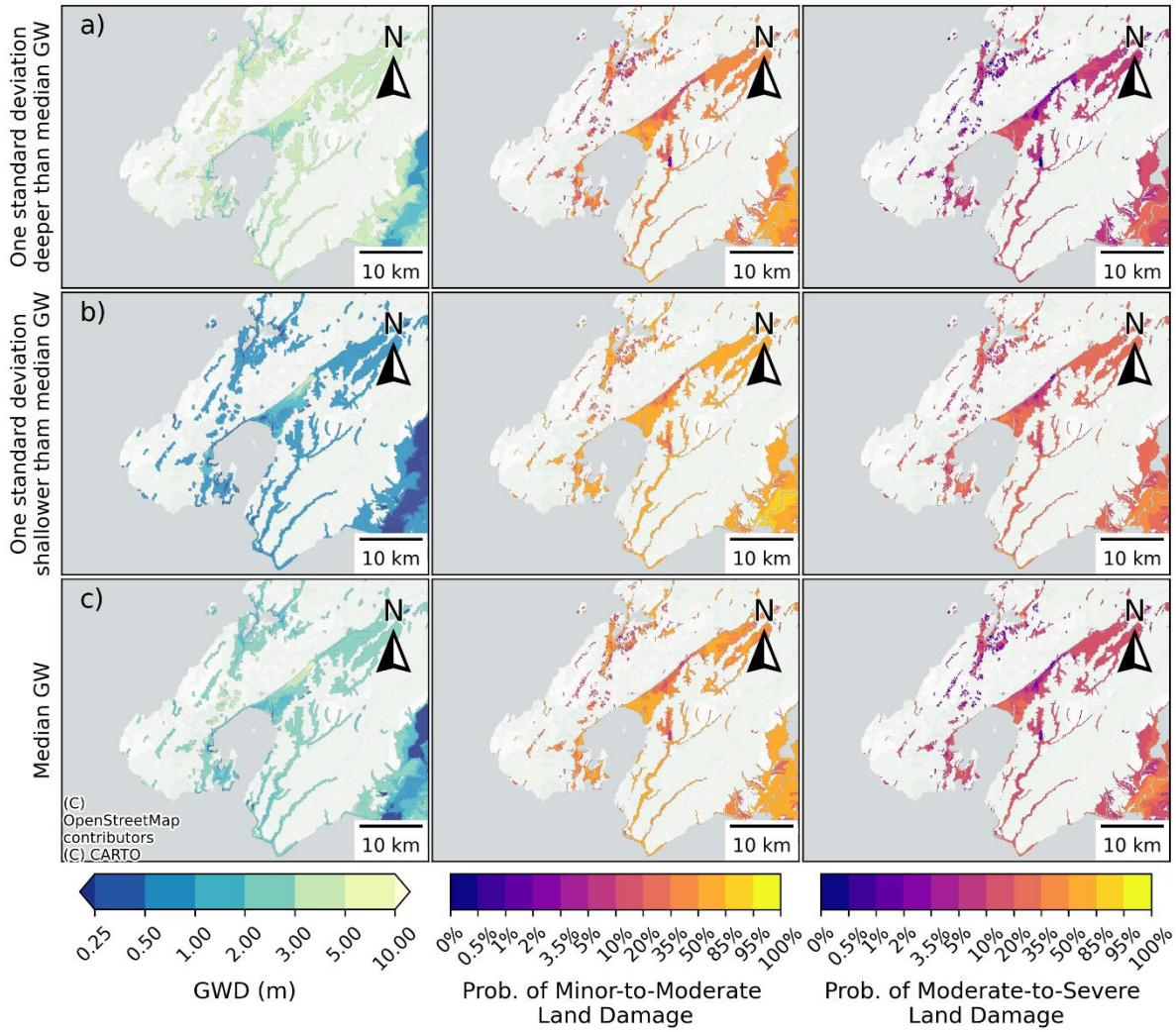

Figure 11.13: (left) GWD for various GW scenarios as labelled, (centre) corresponding probability of Minor-to-Moderate and (right) Moderate-to-Severe land damage computed using the sample uncertainty distributions, for the Wellington area for 500-year return period seismic shaking

11.3.2.2 Outputs using the 1 m sea-level rise NLM GW Model

The probability of land damage for 500-year return period seismic shaking for the median GWD assuming 1 m of SLR was determined and shown for the Wellington area in Figure 11.14 b). In comparison to Figure 11.14 a), which shows the results for current median GWD, there is a notable increase in Moderate-to-Severe land damage along the coast in Lower Hutt. The changes to Minor-to-Moderate land damage are less significant for this return period since the probability is already very high when evaluating with the current median GWD, however, other coastal areas show a greater increase in land damage probability (not shown in the report).

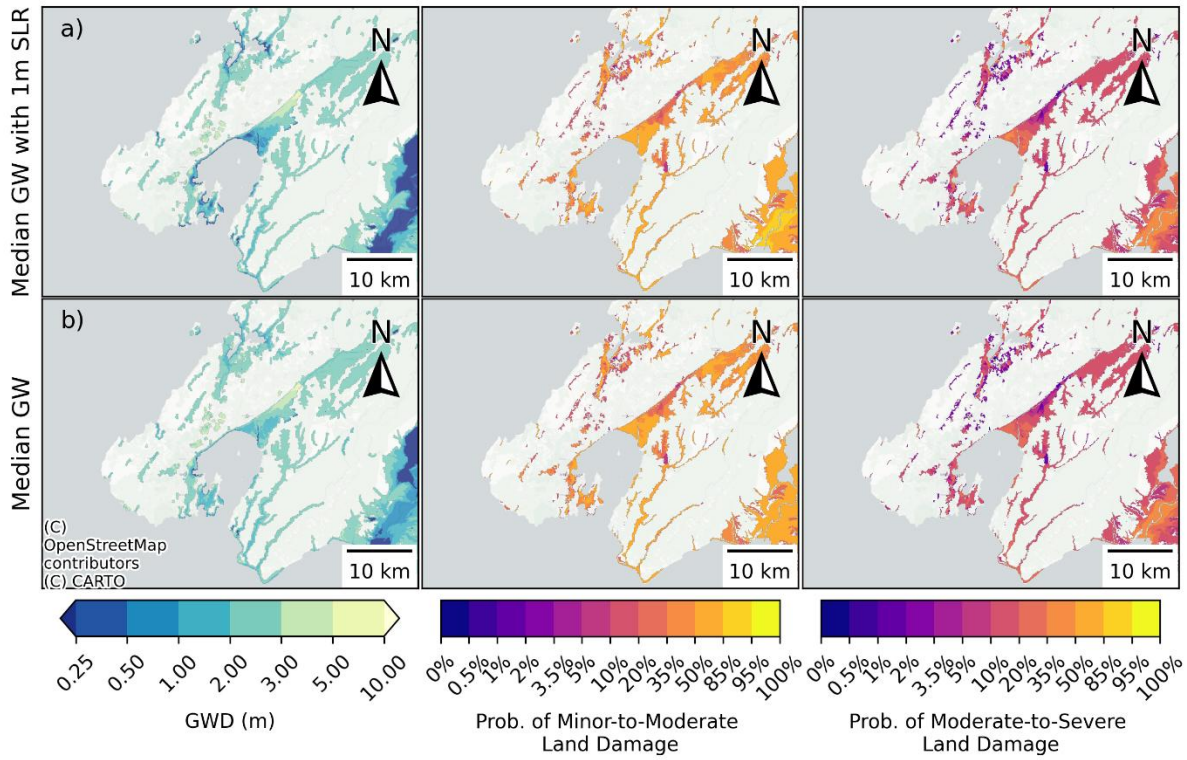

Figure 11.14: (left) Median GWD, (centre) corresponding probability of Minor-to-Moderate and (right) Moderate-to-Severe land damage computed using the sample uncertainty distributions, for the Wellington area for 500-year return period seismic shaking, for a) Median GW, and b) Median GW with 1 m SLR

11.3.3 Different LSN distributions

This section presents outputs for LSN using P_L=15% and outputs using the LV geospatial model. The P_L=15% outputs are primarily produced to demonstrate difference between adopting P_L=50% and P_L=15%, of which the differences are perhaps unexpected. The geospatial model outputs demonstrate the influence of the SSP and Bayesian updating step. In some areas the differences can be significant and can be based on GI that are located several km away (due to the Tier 2 Voronoi expansion see discussion in Section 8.6.3). These differences would need to be considered for development of MBIE/MfE guidance maps.

11.3.3.1 Outputs for P_L=15%

The probability of land damage for 500-year return period shaking for the median GWD, was derived using LSN and LDFCs calculated using P_L=15% and shown for the Wellington area in Figure 11.15 b). This can be compared to the outputs derived from LSN and LDFCs calculated using P_L=50% for the same GWD and seismicity shown in Figure 11.15 a). There are some differences between the land damage probability maps, with the P_L=15% output generally producing lower probabilities of land damage than the P_L=50%, similar to the findings discussed in Section 11.2.1. Notably, the probabilities in parts of Lower Hutt are >10% higher for the PL=50% simulations, while land in Whitemans Valley in the Northeast of the figure has lower probabilities for the P_L=50% simulations.

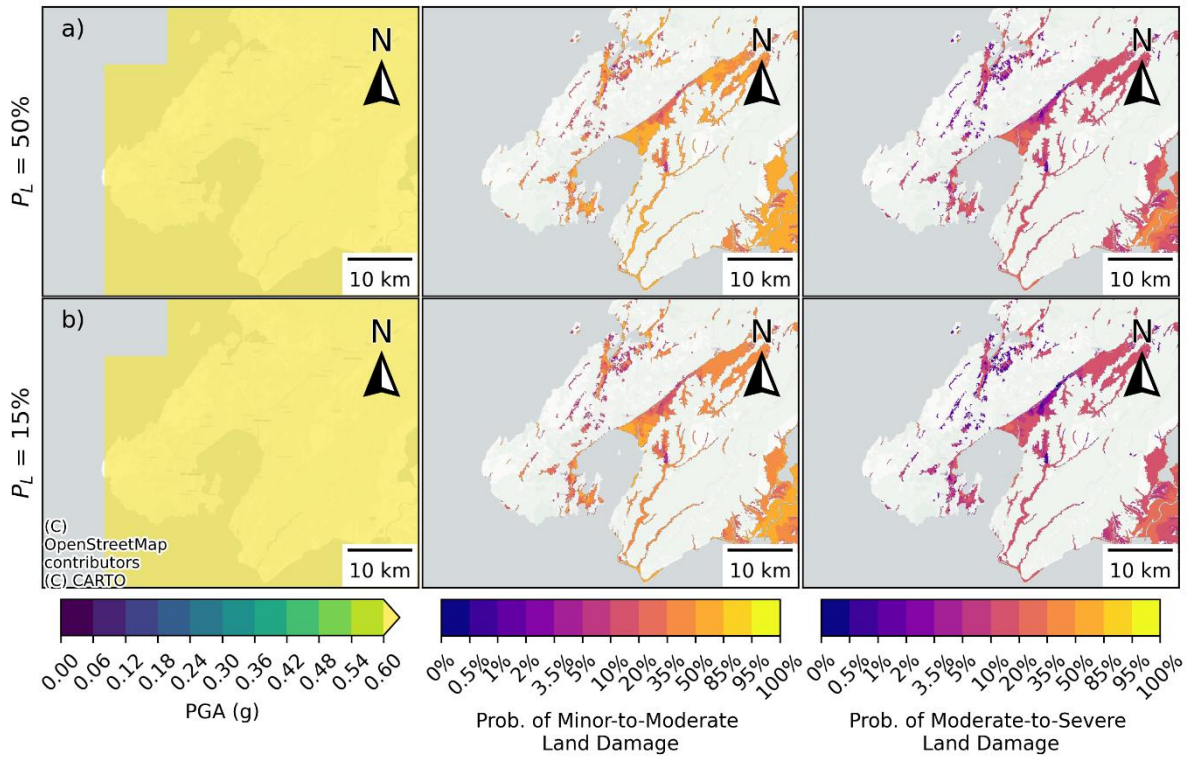

Figure 11.15: (left) PGA, (centre) probability of Minor-to-Moderate land damage (right) probability of Moderate-to-Severe land damage, computed for a) P_L=50%, and b) P_L=15% for the Wellington area for 500-year return period seismic shaking

11.3.3.2 Outputs using the LV geospatial model

The probability of land damage produced using LSN distributions from the geospatial model (using P_L=50% and the median GWD) was determined and shown for the Wellington area in Figure 11.16 b). This can be compared to Figure 11.16 a), which used the sample uncertainty distribution that has the Bayesian update to include local GI. The land damage probabilities using the geospatial model shows less variability with slightly higher land damage in Lower Hutt and Porirua. These differences are important to consider for the development of MBIE/MfE maps.

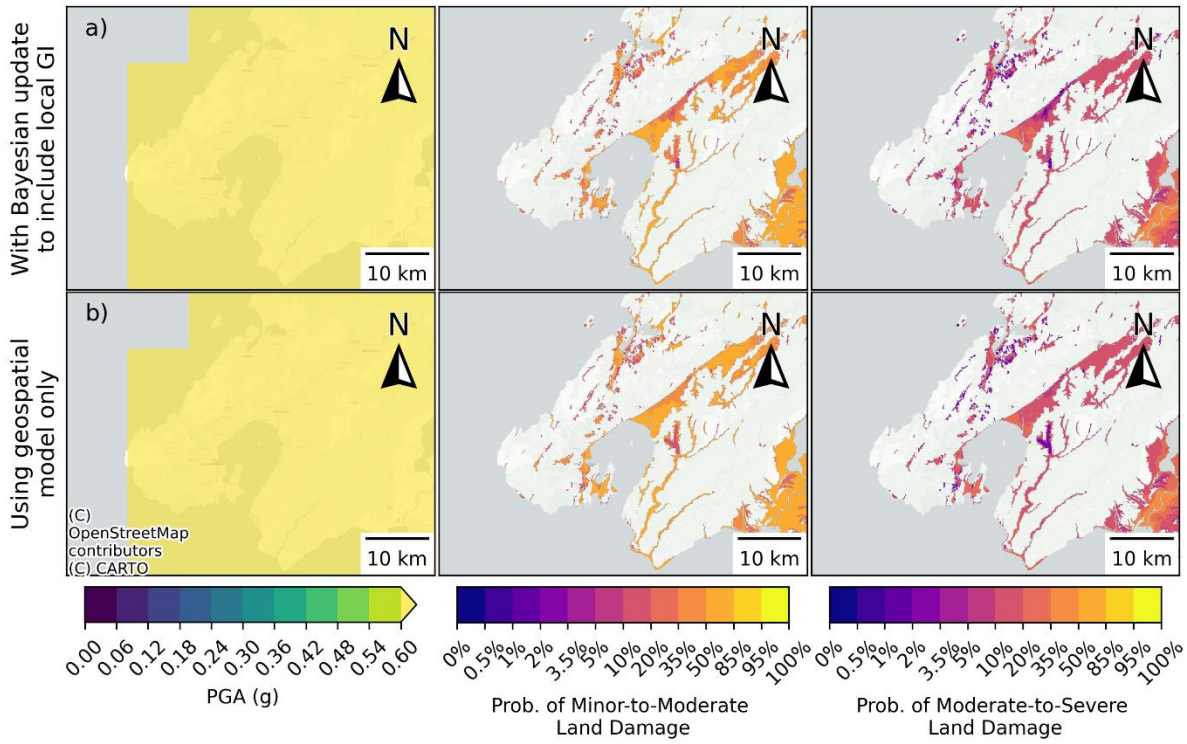

Figure 11.16: (left) PGA, (centre) probability of Minor-to-Moderate land damage (right) probability of Moderate-to-Severe land damage computed using the LV geospatial model distributions, for the Wellington area for 500-year return period seismic shaking, a) With Bayesian update to include local GI, and b) Using geospatial model only

11.4 Limitations

The scenario outputs make use of all of the NLM modules, and therefore all the limitations that apply those modules are also applicable here. Additional limitations that should be noted for the scenario outputs include:

1 Outputs are produced using a 100 m raster grid, however, the output is only determined for the centre point of each raster cell and is not necessarily representative of the 100 m wide cell.

2 Liquefaction predictions are dependent on estimates of the seismicity (i.e. PGA, and Mw). The estimation of PGA typically has large uncertainty for historical, future and return period-based calculations. This uncertainty has not been reflected in the outputs but should be considered for the specific end use. Specifically, the uncertainty in PGA for the February 2011 event is particularly high due to the close proximity of the epicentre to the observation dataset. Furthermore, several strong motion stations in Christchurch experienced liquefaction during the event which modified the ground motion and PGA at those sites. The Alpine Fault simulation requires assumptions about the specific event, in this case a Mw 7.9 event, as well as simulations of low frequency ground motions from the source to site, and an approximation of the high-frequency content. This process results in a large amount of uncertainty in the estimated PGA for a similar future event, readers are referred to the publication by Bradley et al. (2017) for details.

3 The return period land damage estimates are produced with PGA and Mw demands from the Draft TS1170.5 which at the time of writing is still under review and subject to change. Additionally, the PGA estimate did not account for the characteristics of the site, it was based on Site Class V.

4 Suburb-based historical comparisons may suffer from bias in the observation dataset, in that greater focus may have been put to mapping damaged areas.

5 The simulations provide land damage estimates using a 1D liquefaction triggering method that does not account for 3D interactions in the ground e.g. lateral spreading.

6 When interpreting spatial outputs, it should be noted that there are occasionally sharp changes. These originate from the polygon boundaries in the LVM and sharp transitions between the refined and national GW models. They are artifacts of the modelling approach and do not represent reality.

11.5 Potential future improvements

1 **Cross-validation using additional historical earthquake events**. Quantitative comparison of the simulation output versus observation data from the 2016 Mw 7.8 Kaikōura earthquake event would provide insight into the different potential biases that were noted in Sections 10.3.1 and 10.3.2. Additionally, simulating several smaller events where no liquefaction was observed would establish performance for these more common events.

2 **Cross-validation of historical events at the geomorphology polygon level**. Cross-validation for different geomorphologies could identify whether particular geomorphologies are mis predicted. This could then be used to improve the LV geospatial model and help inform the focus of future research and model updates.

3 **Compare NLM simulations to existing simulations**. Cross-checking NLM output against existing published simulations of events (e.g. Geyin & Maurer (2020) simulation of the Alpine Fault event) to understand similarities and differences. The cross-check would help with evaluating biases in the NLM approach.

4 **Produce additional future event simulations**. The simulation of additional potential future events (e.g. Wellington Fault, Hikurangi subduction zone) helps understand the impact of liquefaction from these events and focus research and event preparedness.

5 **Higher resolution output**. Simulations are currently produced using a 100 m raster grid, consistent with the output from the NLM GW Model. Higher resolution (e.g. 50 m raster grid) would improve details near sharp changes in geomorphology, e.g. near rivers and hills.

6 **Investigate causes for the difference between P_L=50% and P_L=15% output**. P_L=15% is widely adopted in practice for design because it is generally considered conservative. However, as noted in Section 11.3.3.1, the combination of LSN distributions and LDFCs both generated with P_L=15% do not always produce a conservative estimate of land damage probability. A clear explanation on why there are differences between P_L=15% and P_L=50% would help the engineering profession understand the NLM outputs which are primarily produced using P_L=50%.

7 **Produce land damage probabilities as the average of multiple LDMs**. Currently land damage is estimated using LSN as the LDM. Different LDMs produce different estimates of probability of land damage. Probabilities of land damage from multiple different LDMs can be averaged to provide a more informed estimate of probability.

8 **Produce a potential model error overlay for land damage probabilities**. Currently uncertainty is only propagated to the LSN distributions and then different probability estimates are produced for different LSN distributions (i.e. spatial variability distribution and sample uncertainty distribution). The scenario maps only produce total modelled probability of land damage, they do not consider the uncertainty in that probability for a specific event or specific site (typically referred to as site or event specific effects). his means that well-constrained estimates of LSN from small polygons with many nearby GI can have the same probability as large polygons that are entirely based on a geospatial model estimate. While this is suitable for regional loss modelling, it may be less informative for other uses cases and does not

identify areas where the model is poorly constrained. An overlay could be developed that would quantify how the uncertainty in LSN could impact the estimated probability of land damage (i.e. contours of +/- percentage change in probability). This could be used to inform end users of where probability estimates are poorly constrained.

12 Use of outputs

The NLM has been developed to support three key uses: to help inform NHC's loss modelling programme, to provide nationally-consistent outputs to support the development of MBIE/MfE maps, and to enhance the understanding of liquefaction-related risk. This section provides a summary of considerations for each of these use cases (Sections 12.1 to 12.3) as well as additional discussion regarding future model updates (Section 12.4) and research needs (Section 12.5).

12.1 Loss modelling

The NLM has been developed as an input into PRUE, NHC's catastrophe loss model suite, to assess consequential liquefaction damage to one and two-storey residential buildings across the flatland areas of New Zealand. This model is probabilistic and uses the expected level of liquefaction severity to predict the extent and additional cost of damage caused by liquefaction (i.e. the additional cost over and above the cost of the building shaking damage). The liquefaction loss model therefore requires maps of liquefaction severity as a key input. The NLM will enable this loss modelling to be carried out nationally, both for future loss estimation and for event response.

In a general sense, the outputs from the NLM could be used for other regional loss modelling purposes (e.g. for council or utility infrastructure networks). The scenario outputs presented in Section 11 outline how a scenario earthquake or return period-based output can be produced as a raster of either LSN (randomly sampled from the LSN distribution) or probability of different land damage states. The expected liquefaction hazard can be obtained by directly sampling the raster at each asset location. Alternatively, the GW, SSP and associated LDM could be sampled at each asset location.

The raster output from Section 11 was produced on a 100 m grid, the same resolution as the NLM GW Model. If larger grid spacing is used, there would be some loss in accuracy from both the LVM and GW Model. Another issue that needs to be considered is the spatial correlation length in asset value and liquefaction spatial variability versus grid spacing. Other important considerations include:

- Whether outputs should be produced using the spatial variability distribution or sample uncertainty distribution, or some modification of them. This largely depends on whether the loss functions already include some implicit uncertainty in the liquefaction hazard that should not be compounded.
- Whether the outputs should be produced with the median GWD or a consideration of the uncertainty in GWD. This largely depends on whether the loss functions already include some implicit uncertainty in the GWD that should not be compounded.
- All users of the model should understand the limitations outlined in Section 2.7 and the limitations associated with the sub-model (see discussion at the end of each report section).

12.2 MBIE/MfE maps

The RMA requires an assessment of natural hazard risk to support applications for subdivision consent, and therefore there is a need for consenting authorities and applicants to understand whether that land is likely to be affected by liquefaction. The MBIE/MfE Guidance (2017) provides a nationally-consistent methodology to carry out liquefaction assessments, with a specific focus on RMA and Building Act aspects. While the driver for the NLM is primarily in relation to regional scale

loss modelling, the model may also be able to help inform the development of a territorial authority's MBIE/MfE Guidance (2017) maps[25].

The MBIE/MfE Guidance (2017) is important because territorial authorities and regional councils had previously taken varying approaches to this assessment. To date 43 of the 67 territorial authorities across New Zealand have published new maps using criteria/categories consistent with the guidance. Some of these also have published information about the interpretation of these maps to support the resource consent and building consent process. The remaining 24 either have not published new maps or are reliant on previously published maps using criteria/categories that are not consistent with the MBIE/MfE Guidance (2017).

The NLM creates outputs to support the generation of LV maps in the MBIE/MfE Guidance (2017) format. **However, the automated NLM outputs are not suitable for direct application without further manual review** (and likely localised adjustments) by suitably qualified and experienced geo-professionals. This is because the MBIE/MfE Guidance (2017) is a risk-based approach that includes stakeholder engagement and consideration of the local context and other relevant information, which is outside of the scope of the NLM. Nonetheless, the ability for the NLM to support the generation of these maps provides significant benefit. It facilitates the validation and refinement of existing maps, and provides a nationally-consistent baseline for new maps in terms of rigor, methodology and criteria/categorisation. It will also be readily updateable to accommodate future changes (e.g. improved understanding of seismic hazard), which will allow the potential implications of these changes to be more readily assessed across the country.

The scenario outputs presented in Section 11 outline how the probability of Minor-to-Moderate and Moderate-to-Severe land damage can be produced for different return periods, in line with the MBIE/MfE Guidance (2017). However, there are several non-trivial decisions that need to be made within the context of the MBIE/MfE Guidance (2017), specifically:

- The choice of LSN distribution to determine the probabilities (e.g. see Figure 11.11 versus Figure 11.16).
- Whether to develop probabilities of land damage using P_L=15% or P_L=50%.
- The MBIE/MfE guidance was written for regional-level mapping and therefore recommendations such as the numbers of ground investigations within geomorphology units are not directly applicable to the NLM outputs.
- The choice of which LSN distribution and whether to use the LDFCs that implicitly or consider GWD uncertainty or not.
- The handling of GW variability, GW uncertainty and SLR (e.g. see Figure 11.13 to Figure 11.14).
- The boundary uncertainty, particularly related to the classification of flatland, geomorphology boundaries, GW and SSP boundaries.
- The incorporation of local knowledge and context as well as calibration/validation using information from previous seismic events.

[25] It is not appropriate to apply the NLM at an individual property level, or to directly translate the model outputs to MBIE/MfE liquefaction vulnerability (LV) categories or vulnerability maps. Rather, the NLM can be one source of information which if used to help inform MBIE/MfE regional mapping, must be critically assessed and verified by suitably qualified and experienced geo-professionals, alongside other relevant information such as factual data specific to the area in question. Where the NLM is used to help inform development of MBIE/MfE guidance maps, it is important to appreciate the low level of detail in the input data and the significant uncertainties in the model outputs, including the limitations detailed in Section 2.7 and further details provided in this Section. The NLM model outputs are likely to only be relevant to help inform development of Level A maps (basic desktop assessment), or Level B maps (calibrated desktop assessment) in conjunction with additional ground truthing and qualitative analysis. Development of Level C and Level D maps requires location-specific mapping of geology and geomorphology, subsurface investigations and quantitative analysis (refer Table 3.2 of MBIE/MfE Guidance (2017)), and this more detailed information would supersede any outputs from the NLM.

Perhaps the most challenging difference between the framework for loss modelling and land-use planning maps is the handling of boundary uncertainty. In the context of regional loss assessment, which typically involves a large number of assets distributed over a large area, boundary uncertainty has relatively little impact on the aggregate result provided that any potential spatial extrapolations are not biased to be more over-predicting than under-predicting. However, in land-use planning, the over-predictions and under-predictions can result in significant areas being misclassified. This challenge is most significant for Tier 2 polygons which have large spatial extrapolation and cover a large portion of the urban environment. The extent of potential bias due to spatial extrapolation can be inferred by comparing different LSN distributions, as well as evaluating the spatial density of GIs.

Another significant difference between loss modelling and land-use planning maps is how uncertainty is handled. In loss modelling, excessive uncertainty may obfuscate results or trends and so best estimates are sometimes adopted. For land-use planning maps there is an option to simply assign a category of ***Liquefaction Category is Undetermined*** for high uncertainty cases, which means that more detailed assessment will be required in the future before a resource or building consent is issued. The choice of when to assign ***Liquefaction Category is Undetermined*** based on national scale predictions is not simple since the guidance is written in relation to the understanding of different geomorphologies at a regional scale or smaller.

12.3 Contributions to enhanced understanding of liquefaction-related risk

Given the unique challenges and scale of the analysis, the NLM project made several novel contributions to the understanding and quantification of liquefaction-related risk, such as:

1 The variogram and standard deviation to area relationships provide guidance on the level of variability of LSN.

2 The LV geospatial model provides LSN estimates for any New Zealand geomorphology for a range of PGA, Mw and GWD. This provides nationally-consistent baseline estimates of expected liquefaction response which can be a useful starting point for local studies, or for examining trends across the country.

3 Development of a novel method to provide a depth correction for LSN to a set depth of 20 m. This is applicable to GI that terminate before 20 m depth and reduces biases caused by filtering out short GI or using them without a depth correction.

4 Development of a novel method to convert a BH log into an equivalent CPT for the purpose of evaluating liquefaction. This is particularly relevant in areas where there are few CPT.

5 Development of a process to combine local GIs with geospatial estimates to estimate likely LSN for an area, accounting for the influence of closely spaced GIs.

6 Development of an automated process for local GW model creation and a regression equation for providing nationally-consistent baseline estimates.

7 Development of LDFCs, which allow a calculated LSN value to be used to estimate land damage categories based on probability of damage as specified in Section 10. This included a process to remove the uncertainty associated with the input estimate of LSN.

8 Quantified the difference in estimated LSN from pumiceous soils versus non-pumiceous soil when comparing the same geomorphology.

9 Highlighted and resolved several challenges with data storage, and the automation of many steps in the liquefaction evaluation process that engineers would typically do with a bespoke manual approach.

12.4 Future updates

It is intended for the NLM to be updated periodically to:

- Include new data (e.g. LiDAR DEM, GW, GIs).
- Include new research and processes.
- Produce additional outputs for the evaluation of liquefaction impacts on other infrastructure.
- To refine the framework and model build process.

As described in Section 4.2, the model has been deliberately built with a modular software architecture to facilitate these updates. Each version of the model will have details on how the model was updated in the form of version release notes or a short technical report. Potential future steps have been identified in each of the modules to highlight ways in which the model is intended to be updated in the future and to help set the future direction of those updates. End users that adopt the NLM should be prepared for these updates. While there is an intention to maintain backwards compatibility for the data schemas, some updates may necessitate changes to the data schemas, and therefore that cannot be guaranteed.

The NLM GW Model and LVM provide an estimate of the uncertainty in the outputs. However, the results following an update may significantly differ from the previous version, especially in areas with low data density. These differences may be due to local data better constraining predictions, or changes in the LV geospatial model or GW regression or kriging models. The modular framework means that improvements in one sub-model are expected to improve estimates in other areas (e.g. improvements in the geomorphology model would reduce mislabelled GIs that inform the geospatial model, which results in less variability in these predictions across the country).

12.5 Research needs

Many of the potential future updates and improvements to predicting liquefaction-induced damage would benefit from significant research. These include, but are not limited to:

- Improvements in soil profile characterisation (e.g. how to define q_{c1ncs} and percentage I_c>2.6 in the BH method; how pumiceous soils are characterised from CPT).
- Improvements to the prediction of land damage states from CPT and BH (e.g. accounting for system response effects).
- Development of additional refined geomorphology maps to improve the characterisation of LV in the newly refined areas and to reduce the mislabelling of GIs that inform the geospatial model.
- Additional research efforts that adopt the NLM for understanding the impact of liquefaction for different end-uses in land-use planning, post-disaster reconnaissance and recovery (both within New Zealand and internationally) would be beneficial to increase the impact and awareness of the NLM.

13 Data attributions

1 **LINZ 8 m DEM** – Digital elevation model, flatland and the groundwater model were derived from the 8 m Digital Elevation Model dataset © LINZ created by Geographx (geographx.co.nz), licensed under Creative Commons Attribution 4.0 International (CC BY 4.0). Modifications and analysis by Tonkin + Taylor. Accessed from https://data.linz.govt.nz/layer/51768-nz-8m-digital-elevation-model-2012/

2 **LINZ 1 m LiDAR** – Digital elevation model, flatland and the groundwater model were derived from the LINZ 1 m LiDAR dataset © LINZ, licensed under Creative Commons Attribution 4.0 International (CC BY 4.0). Data processed and modelled by Tonkin + Taylor. Accessed from https://registry.opendata.aws/nz-elevation/

3 **QMAP v4** – Geomorphology model derived from the GNS Science QMAP v4 dataset © GNS Science (Earth Sciences New Zealand), licensed under Creative Commons Attribution 4.0 International (CC BY 4.0). Derivatives by Tonkin + Taylor. Accessed from https://shop.gns.cri.nz/maps/qmap-digital-download/

4 **Geomorphology of Kapiti Coast** – Geomorphology model derived from the GNS Science 'Geomorphology of Kapiti Coast' dataset © GNS Science (Earth Sciences New Zealand), licensed under Creative Commons Attribution 4.0 International (CC BY 4.0). Modifications and analysis by Tonkin + Taylor. Accessed from https://shop.gns.cri.nz/sr_2016-037-pdf/

5 **Geomorphology of Eastern Canterbury** – Geomorphology model derived from the GNS Science 'Geomorphology of Eastern Canterbury' dataset © GNS Science (Earth Sciences New Zealand), licensed under Creative Commons Attribution 4.0 International (CC BY 4.0). Modifications and analysis by Tonkin + Taylor. Accessed from https://shop.gns.cri.nz/gnsgm3a/

6 **Geological Map of Napier–Hastings** – Geomorphology model derived from GNS Science 'Geological Map of Napier–Hastings' dataset © GNS Science (Earth Sciences New Zealand), licensed under Creative Commons Attribution 4.0 International (CC BY 4.0). Modifications and analysis by Tonkin + Taylor. Accessed from https://shop.gns.cri.nz/gnsgm7a/

7 **Geological Map of Nelson** – Geomorphology model derived from GNS Science 'Geological Map of Nelson' dataset © GNS Science (Earth Sciences New Zealand), licensed under Creative Commons Attribution 4.0 International (CC BY 4.0). Processed by Tonkin + Taylor. Received by email.

8 **Foster Geomorphology Model** – Reference geomorphological model utilised for validation, developed by Kevin Foster (fostergeotech /Vs30_NZ). Used with author approval. Accessed from https://github.com/fostergeotech/Vs30_NZ

9 **New Zealand Geotechnical Database (NZGD)** – Cone Penetration Test, borehole data, and groundwater data was sourced from NZGD (nzgd.org.nz). *The success of NZGD relies on users submitting data, which is helped by many local authorities and central government agencies contractually requiring their partners to submit data."*

10 **Northland Static Water Data** – Static water dataset and the groundwater model were developed using the Northland Regional Council dataset © NRC, licensed under Creative Commons Attribution 4.0 International (CC BY 4.0). Modifications and analysis by Tonkin + Taylor. Accessed from https://data-nrcgis.opendata.arcgis.com/datasets/NRCGIS::bore-logs/explore

11 **Waikato Static Water Data** – Static water dataset and the groundwater model were developed using the Waikato Regional Council dataset © WRC, licensed under Creative Commons Attribution 4.0 International (CC BY 4.0). Modifications and analysis by Tonkin + Taylor. Accessed from https://data-waikatolass.opendata.arcgis.com/datasets/219e0a0ef6224b5db25dc61c8f14322f_0/explore

12 **Bay of Plenty Static Water Data** – Static water dataset and the groundwater model were developed using the Bay of Plenty Regional Council, permission granted to use, adapt, and share. Accessed from https://maps.boprc.govt.nz/datasets/BOPRC::well-bore-locations-in-the-bay-of-plenty/explore

13 **Hawke's Bay Static Water Data** – Static water dataset and the groundwater model were developed using the Hawke's Bay Regional Council dataset © HBRC, licensed under Creative Commons Attribution 4.0 International (CC BY 4.0). Analysis and modelling by Tonkin + Taylor. Accessed from https://hbrcopendata-hbrc.opendata.arcgis.com/datasets/849f36ba4af14e599456f8f4fd9e8ec1_0/explore

14 **Manawatu–Whanganui Static Water Data** – Static water dataset and the groundwater model were developed using the Horizons Regional Council dataset © Horizons, licensed under Creative Commons Attribution 4.0 International (CC BY 4.0). Modifications by Tonkin + Taylor. Accessed from https://data-horizonsrc.opendata.arcgis.com/datasets/1f53ca0f492248e3b0433d20a5630687_0/explore

15 **Wellington Static Water Data** – Static water dataset and the groundwater model were developed using the Greater Wellington Regional Council © GWRC, permission granted to use, adapt and share. Used unchanged by Tonkin + Taylor. Accessed from https://opendata.gw.govt.nz/datasets/b52e4f95910141118fce229f33928d4c_1/explore

16 **Marlborough Static Water Data** – Static water dataset and the groundwater model were developed using the Marlborough District Council dataset © MDC, licensed under Creative Commons Attribution 4.0 International (CC BY 4.0). Model development by Tonkin + Taylor. Accessed from https://data-marlborough.opendata.arcgis.com/datasets/7c4ff7d25e164c39aa853294efc727ee_13/explore

17 **Canterbury Static Water Data** – Static water dataset and the groundwater model were developed using the Environment Canterbury data © CRC, licensed under Creative Commons Attribution 4.0 International (CC BY 4.0). Analysis by Tonkin + Taylor. Accessed from https://opendata.canterburymaps.govt.nz/datasets/ecan::wells-and-bores-all-1/explore

18 **Southland Static Water Data** – Static water dataset and the groundwater model were developed using the static water dataset from Environment Southland © licensed under Creative Commons Attribution 4.0 International (CC BY 4.0). Analysis by Tonkin + Taylor. Accessed from https://data-esgis.opendata.arcgis.com/datasets/24fb7bb2a3a649b1a0767c7c33dbfaae/explore

19 **Otago Static Water Data** – Static water data and the groundwater model were developed with permission using the groundwater dataset received from Otago Regional Council via email.

20 **Tasman Static Water Data** – Static water data and the groundwater model were developed with permission using the groundwater dataset received from Tasman District Council via email.

21 **Coastlines Topo150k** – Coastal boundary layer derived from LINZ 'NZ Coastlines Topo150k' dataset © LINZ, licensed under Creative Commons Attribution 4.0 International (CC BY 4.0). No modifications made. Accessed from https://data.linz.govt.nz/layer/50258-nz-coastlines-topo-150k/

22 **Lake Polygons Topo150k** – Waterbodies layer derived from LINZ 'NZ Lake Polygons Topo150k' dataset © LINZ, licensed under Creative Commons Attribution 4.0 International (CC BY 4.0). Derivatives by Tonkin + Taylor. Accessed from https://data.linz.govt.nz/layer/50293-nz-lake-polygons-topo-150k/

23 **Land Cover Database v5.0** – Waterbodies layer derived from Landcare Research (LRIS) Land Cover Database v5.0 © Landcare Research, licensed under Creative Commons Attribution 4.0 International (CC BY 4.0). Derivatives by Tonkin + Taylor. Accessed from

https://lris.scinfo.org.nz/layer/104400-lcdb-v50-land-cover-database-version-50-mainland-new-zealand/

24 **Coastlines and Islands Polygons** – Waterbodies layer derived from LINZ 'NZ Coastlines and Islands Polygons Topo150k' dataset © LINZ, licensed under Creative Commons Attribution 4.0 International (CC BY 4.0). Modified for use by Tonkin + Taylor. Accessed from https://data.linz.govt.nz/layer/51153-nz-coastlines-and-islands-polygons-topo-150k/

25 **Regional Councils 2023 Boundary** – Regional boundary layer derived from Stats NZ 'Regional Council 2023 Generalised' dataset © Stats NZ, licensed under Creative Commons Attribution 4.0 International (CC BY 4.0). No modifications, derivatives by Tonkin + Taylor. Accessed from https://datafinder.stats.govt.nz/layer/111182-regional-council-2023-generalised/

26 **GNS Dunedin Groundwater Models** – Validation with permission of the National Groundwater model using the GNS Groundwater models received from GNS Science via email.

27 **Hawke's Bay Groundwater Model** – Validation with permission of the National Groundwater model using the Hawke's Bay Groundwater Model derived from GNS Science Report "Assessment of Liquefaction Risk in the Hawke's Bay" © B. Rosser and S. Dellow (2015).

28 **National Water Table** – Validation of the National Groundwater model using the GNS Science National Water Table © GNS Science (2022) (Earth Sciences New Zealand), licensed under Creative Commons Attribution 4.0 International (CC BY 4.0). No modifications. Analysis by Tonkin + Taylor.

29 **Christchurch City Council Groundwater models** – Validation with permission of the National Groundwater model and sea-level rise using the Christchurch City Council groundwater models developed by Aqualinc relating to sea-level-rise groundwater modelling.

30 **Future and Historic Earthquake Scenarios** – Seismic scenario data (PGA map and magnitude) provided by Brendon Bradley and QuakeCore (SeisFinder) https://quakecoresoft.canterbury.ac.nz/seisfinder/, used for fragility curve development and model validation, citations:

- Bradley, B. A., Bae, S. E., Polak, V., Lee, R. L., Thomson, E. M., & Tarbali, K. (2017). Ground motion simulations of great earthquakes on the Alpine Fault: Effect of hypocentre location and comparison with empirical modelling. New Zealand Journal of Geology and Geophysics, 60(3), 188–198. https://doi.org/10.1080/00288306.2017.1297313
- Bradley, B. A. (2012). Strong Ground Motion Characteristics Observed in the 4 September 2010 Darfield, New Zealand Earthquake. Soil Dynamics and Earthquake Engineering, 42, 32–46. https://doi.org/10.1016/j.soildyn.2012.06.004
- Bradley, B. A. (2014). Seismic hazard analysis for urban Christchurch accounting for the 2010-2011 Canterbury earthquake sequence. Technical report prepared for the New Zealand Earthquake Commission (EQC) and Tonkin and Taylor Ltd by Bradley Seismic Ltd.
- Bradley, B. A. (2016). Strong ground motion characteristics observed in the 13 June 2011 Mw6.0 Christchurch, New Zealand earthquake. Soil Dynamics and Earthquake Engineering, 91, 23–38. https://doi.org/10.1016/j.soildyn.2016.09.006
- Brendon A. Bradley, Hoby N. T. Razafindrakoto,Viktor Polak; Ground-Motion Observations from the 14 November 2016 Mw 7.8 Kaikoura, New Zealand, Earthquake and Insights from Broadband Simulations. Seismological Research Letters 2017;; 88 (3): 740–756. doi: https://doi.org/10.1785/0220160225

31 **Canterbury Events Observations** – Validation of models using "Canterbury Events Liquefaction and Lateral Spreading Observations" from NHC / NZGD (Downloaded 1 June 2025 from https://www.nzgd.org.nz/Map/MapContent.aspx)

32 **Seismic Return Period Maps** – PGA and Mw hazard was determined from Draft TS1170.5 (2024) by the NZ Standards Committee (standards.govt.nz).

33 **Suburbs and Localities** – Boundary layer from LINZ 'NZ Suburbs and Localities' dataset © LINZ, licensed under Creative Commons Attribution 4.0 International (CC BY 4.0). No modifications. Accessed from https://data.linz.govt.nz/layer/113764-nz-suburbs-and-localities/

34 **Territorial Authority Boundaries** – Boundary layer derived from Stats NZ 'Territorial Authority 2022 Generalised' dataset © Stats NZ, licensed under Creative Commons Attribution 4.0 International (CC BY 4.0). No modifications. Accessed from https://datafinder.stats.govt.nz/layer/106668-territorial-authority-2022-generalised/

35 **TTGD CPTs** – Cone penetration test data from Tonkin + Taylor used to inform liquefaction vulnerability model, used with permission.

36 **TTGD Boreholes** – Borehole data from Tonkin + Taylor used to inform liquefaction vulnerability model, used with permission.

37 **TTGD Static Water Data** – Static water level information from Tonkin + Taylor used to inform national groundwater model, used with permission.

38 **Canterbury Earthquake Sequence GW Layers –**
Groundwater layers developed by Tonkin + Taylor and GNS Science (2013) for the Earthquake Commission (now Natural Hazards Commission) were used with permission to compare against the National Groundwater model.

39 **Event Observations** –
Liquefaction and event observation data managed by Tonkin + Taylor, used with permission to develop land-damage fragility curves and compare against scenario outputs.

14 Conclusions

The National Liquefaction Model (NLM) represents a major step forward in New Zealand's capacity to assess and manage liquefaction hazard at a national scale. The NLM provides a nationally-consistent data-driven approach to the evaluation of liquefaction-related risk, producing tangible outputs to support key use cases across disaster risk reduction, planning, and research.

The key conclusions of this technical report are:

1 The project delivered the core components for loss modelling, including the national Liquefaction Vulnerability Model (LVM) and Groundwater (GW) Model.

2 The project delivered land damage probability maps and quantification of output uncertainty to support the development of MBIE/MfE maps.

3 The project delivered several sub-models which are key inputs to the quantification of liquefaction, including the national Flatland Model and Geomorphology Model, as well as Land Damage Fragility Curves (LDFCs).

4 The NLM provides a nationally-consistent approach to evaluating liquefaction hazard, which helps to address historical variability in assessments. The NLM is underpinned by over 15 million liquefaction triggering analyses derived from more than 50,000 GIs. All model processes are fully prescribed and driven by input data, eliminating manual intervention and increasing repeatability (albeit acknowledging that local knowledge and judgement from geo-professionals are critical as part of more detailed liquefaction assessments).

5 As with all models, there are many limitations that should be noted when interpreting the NLM outputs or making use of the models. The limitations related to each module are outlined near the end of each of their corresponding technical sections (4 to 11). Additionally, there are broad limitations outlined in Section 2.7 and some guidance on interpreting the outputs for different use cases in Section 12. While the NLM is a multi-use model, the limitations have different impact for different use cases. Most notably, the NLM has been developed at a regional scale. It is not appropriate to apply the NLM to higher resolution assessment (e.g. individual property or subdivision scales). The modular architecture of the model supports scalability and integration of new datasets such as updated GW measurements or refined geomorphology classifications, enabling continuous refinement of outputs. Its modular design ensures flexibility, allowing components to be updated or replaced as liquefaction science and data evolve, without impacting the overall integrity of the system. For example, by decoupling the liquefaction model from seismic hazard inputs, the NLM is future-proofed against inevitable updates to the National Seismic Hazard Model (NSHM). It is also positioned to support emerging applications, such as modelling liquefaction effects on underground infrastructure.

6 The development of the NLM overcame significant challenges in geotechnical, software and data engineering. Innovative solutions were developed for the following:

- New methods for modelling spatial variability;
- Handling short Ground Investigations (GIs);
- Handling variable spatial density of GIs;
- Converting Borehole (BH) logs to equivalent Cone Penetration Tests (CPTs) for the purpose of liquefaction triggering; and
- Predicting the future probability of land damage for multiple seismic scenarios.

7 This first phase of model development has primarily focused on the development of the model framework to support regular updates and produce useable outputs for multiple end use cases. Throughout the report, potential future improvements have been identified to guide future development of the model. These are not recommendations for updates within

the current phase of work but should be considered and prioritised for inclusion in the future model updates. The intention is for the model to be maintained and updated for years to come, and accordingly NHC is taking a long-term view on its investment.

8 The project was supported by a strong governance structure comprising a Peer Review Team (PRT), Steering Group (SG), and End User Group (EUG). This helped to facilitate scientific rigor, policy alignment, and practical usability. Early engagement of end users was also undertaken to support the long-term adoption and ongoing relevance of the model.

15 References

Ahdi, S. K., Stewart, J. P., Ancheta, T. D., Kwak, D. Y., & Mitra, D. (2017). Development of V_S Profile Database and Proxy-Based Models for V_{S30} Prediction in the Pacific Northwest Region of North America. *Bulletin of the Seismological Society of America*, *107*(4), 1781–1801. https://doi.org/10.1785/0120160335

American Society of Civil Engineers. (2023). *Seismic Evaluation and Retrofit of Existing Buildings*. American Society of Civil Engineers. https://doi.org/10.1061/9780784414859

Anselin, L. (1995). Local Indicators of Spatial Association—LISA. *Geographical Analysis*, *27*(2), 93–115.

Bastin, S. H., van Ballegooy, S., & Ogden, M. (2021). The past is key to the future; Collating historical cases of liquefaction to supplement liquefaction hazard assessments. *21st New Zealand Geotechnical Society Symposium*, *2021/3*, 24–26.

Befus, K. M., Barnard, P. L., Hoover, D. J., Finzi Hart, J. A., & Voss, C. I. (2020). Increasing threat of coastal groundwater hazards from sea-level rise in California. *Nature Climate Change*, *10*(10), 946–952. https://doi.org/10.1038/s41558-020-0874-1

Beven, K. J., & Kirkby, M. J. (1979). A physically based, variable contributing area model of basin hydrology / Un modèle à base physique de zone d'appel variable de l'hydrologie du bassin versant. *Hydrological Sciences Bulletin*, *24*(1), 43–69. https://doi.org/10.1080/02626667909491834

Bong, T., & Stuedlein, A. W. (2018). Effect of Cone Penetration Conditioning on Random Field Model Parameters and Impact of Spatial Variability on Liquefaction-Induced Differential Settlements. *Journal of Geotechnical and Geoenvironmental Engineering*, *144*(5), 04018018. https://doi.org/10.1061/(ASCE)GT.1943-5606.0001863

Bosserelle, A. L., Morgan, L. K., & Hughes, M. W. (2022). Groundwater Rise and Associated Flooding in Coastal Settlements Due To Sea-Level Rise: A Review of Processes and Methods. *Earth's Future*, *10*(7), e2021EF002580. https://doi.org/10.1029/2021EF002580

Boulanger, R. W., & Idriss, I. M. (2014). *CPT and SPT based liquefaction triggering procedures* (No. UCD/CGM-14/01; pp. 1–138). The University of California. https://www.ce.memphis.edu/7137/PDFs/Notes/i3Boulanger_Idriss_CPT_and_SPT_Liq_triggering_CGM-14-01_20141.pdf

Boulanger, R. W., & Idriss, I. M. (2016). CPT-Based Liquefaction Triggering Procedure. *Journal of Geotechnical and Geoenvironmental Engineering*, *142*(2), 04015065. https://doi.org/10.1061/(ASCE)GT.1943-5606.0001388

Bradley, B. A. (2012). Strong Ground Motion Characteristics Observed in the 4 September 2010 Darfield, New Zealand Earthquake. *Soil Dynamics and Earthquake Engineering*, *42*, 32–46. https://doi.org/10.1016/j.soildyn.2012.06.004

Bradley, B. A. (2014). *Seismic hazard analysis for urban Christchurch accounting for the 2010-2011 Canterbury earthquake sequence*. Technical report prepared for the New Zealand Earthquake Commission (EQC) and Tonkin and Taylor Ltd by Bradley Seismic Ltd.

Bradley, B. A. (2016). Strong ground motion characteristics observed in the 13 June 2011 Mw6.0 Christchurch, New Zealand earthquake. *Soil Dynamics and Earthquake Engineering*, *91*, 23–38. https://doi.org/10.1016/j.soildyn.2016.09.006

Bradley, B. A., Bae, S. E., Polak, V., Lee, R. L., Thomson, E. M., & Tarbali, K. (2017). Ground motion simulations of great earthquakes on the Alpine Fault: Effect of hypocentre location and comparison

with empirical modelling. *New Zealand Journal of Geology and Geophysics*, *60*(3), 188–198. https://doi.org/10.1080/00288306.2017.1297313

Building Act 2004, Pub. L. No. 2004 No 72 (2004). https://www.legislation.govt.nz/act/public/2004/0072/latest/DLM306036.html

Building Regulations 1992 (1992). https://www.legislation.govt.nz/regulation/public/1992/0150/latest/DLM162576.html

Chambers, L. A., Hemmings, B., Cox, S. C., Moore, C., Knowling, M. J., Hayley, K., Rekker, J., Mourot, F. M., Glassey, P., & Levy, R. (2023). Quantifying uncertainty in the temporal disposition of groundwater inundation under sea level rise projections. *Frontiers in Earth Science*, *11*, 1–17. https://doi.org/10.3389/feart.2023.1111065

Ching, J., Phoon, K.-K., Yang, Z., & Stuedlein, A. W. (2022). Quasi-site-specific multivariate probability distribution model for sparse, incomplete, and three-dimensional spatially varying soil data. *Georisk: Assessment and Management of Risk for Engineered Systems and Geohazards*, *16*(1), 53–76. https://doi.org/10.1080/17499518.2021.1971256

Cox, S. C., Ettema, M. H. J., Chambers, L. A., Easterbrook-Clarke, L. H., & Stevenson, N. I. (2023). Dunedin groundwater monitoring, spatial observations and forecast conditions under sea level rise. *GNS Science Report*, *2024/43*, 111. https://doi.org/10.21420/5799-N894

Cubrinovski, M., Rhodes, A., Ntritsos, N., & van Ballegooy, S. (2019). System response of liquefiable deposits. *Soil Dynamics and Earthquake Engineering*, *124*, 212–229. https://doi.org/10.1016/j.soildyn.2018.05.013

Earthquake Commission Act 1993. https://www.legislation.govt.nz/act/public/1993/0084/latest/DLM305968.html

Foster, K. M., Bradley, B. A., McGann, C. R., & Wotherspoon, L. M. (2019). A VS30 Map for New Zealand Based on Geologic and Terrain Proxy Variables and Field Measurements. *Earthquake Spectra*, *35*(4), 1865–1897. https://doi.org/10.1193/121118EQS281M

GeoNet GNS Science. (2016). *M 7.8 Kaikōura Mon, Nov 14 2016* [Dataset]. https://www.geonet.org.nz/earthquake/felt/2016p858000

Gesch, D. B. (2018). Best Practices for Elevation-Based Assessments of Sea-Level Rise and Coastal Flooding Exposure. *Frontiers in Earth Science*, *6*, 230. https://doi.org/10.3389/feart.2018.00230

Geyin, M., & Maurer, B. W. (2020). Fragility Functions for Liquefaction-Induced Ground Failure. *Journal of Geotechnical and Geoenvironmental Engineering*, *146*(12). https://doi.org/10.1061/(ASCE)GT.1943-5606.0002416

Geyin, M., Maurer, B. W., & Christofferson, K. (2022). An AI driven, mechanistically grounded geospatial liquefaction model for rapid response and scenario planning. *Soil Dynamics and Earthquake Engineering*, *159*, 107348. https://doi.org/10.1016/j.soildyn.2022.107348

GNS Science. (2015). *Christchurch Urban Geological Map* [Dataset]. https://www.gns.cri.nz/our-science/land-and-marine-geoscience/te-riu-a-maui-our-continent/geology-of-new-zealand/urban-geological-maps/christchurch/

GNS Science. (2016). *Detailed geomorphological mapping of the coastal plain of the Kapiti Coast District* (Version 10.2) [Dataset]. https://geodata.nz/geonetwork/srv/api/records/CCD1C820-4020-40FA-BB95-37F116C823CB

GNS Science. (2018). *National Water Table model* [Dataset]. https://doi.org/10.21420/KZ52-NT28

GNS Science. (2022a). *Napier-Hastings Urban Geological Maps* [Dataset]. https://www.gns.cri.nz/our-science/land-and-marine-geoscience/te-riu-a-maui-our-continent/geology-of-new-zealand/urban-geological-maps/napier-hastings/

GNS Science. (2022b). *New Zealand National Seismic Hazard Model* (Version v1.0.4) [Dataset]. https://nshm.gns.cri.nz/

GNS Science. (2022c). *NSHM - National Seismic Hazard Model*. GNS Science | Te Pū Ao. https://www.gns.cri.nz/research-projects/national-seismic-hazard-model/

Heron. (2023). *Geological map of New Zealand 1:250,000. 4th ed* [Dataset]. GNS Science. https://doi.org/10.21420/5XTJ-5718

Hutabarat, D., & Bray, J. D. (2021). Seismic Response Characteristics of Liquefiable Sites with and without Sediment Ejecta Manifestation. *Journal of Geotechnical and Geoenvironmental Engineering*, *147*(6), 04021040. https://doi.org/10.1061/(ASCE)GT.1943-5606.0002506

Hutabarat, D., & Bray, J. D. (2022). Estimating the Severity of Liquefaction Ejecta Using the Cone Penetration Test. *Journal of Geotechnical and Geoenvironmental Engineering*, *148*(3), 04021195. https://doi.org/10.1061/(ASCE)GT.1943-5606.0002744

Idriss, I. M., & Boulanger, R. W. (2008). *Soil liquefaction during earthquakes*. Earthquake Engineering Research Institute (EERI).

Infinity Studio. (n.d.). *Apeiron*. https://apeiron.infinitystudio.ai/

Iwahashi, J., & Pike, R. J. (2007). Automated classifications of topography from DEMs by an unsupervised nested-means algorithm and a three-part geometric signature. *Geomorphology*, *86*(3–4), 409–440. https://doi.org/10.1016/j.geomorph.2006.09.012

Iwasaki, T., Tokida, K., & Tatsuoka, F. (1981). *Soil Liquefaction Potential Evaluation with Use of the Simplified Procedure*. First International Conference on Recent Advances in Geotechnical Earthquake Engineering & Soil Dynamics, St. Louis, Missouri. https://scholarsmine.mst.edu/cgi/viewcontent.cgi?params=/context/icrageesd/article/2503/&path_info=_Soil_liquefaction_potential_eval.pdf

Ketabchi, H., Mahmoodzadeh, D., Ataie-Ashtiani, B., & Simmons, C. T. (2016). Sea-level rise impacts on seawater intrusion in coastal aquifers: Review and integration. *Journal of Hydrology*, *535*, 235–255. https://doi.org/10.1016/j.jhydrol.2016.01.083

LAWA. (2020). *Groundwater basics*. Land, Air, Water Aotearoa (LAWA). https://www.lawa.org.nz/learn/factsheets/groundwater/groundwater-basics/

LENZ. (2010). *LENZ - Slope* [Dataset]. Landcare Research. https://doi.org/10.26060/TBMR-RE43

Lin, A., Wotherspoon, L., Blake, D., Bradley, B., & Motha, J. (2019). National-scale infrastructure network exposure to liquefaction using geospatial models. *Japanese Geotechnical Society*, *6*(2), 61–66. https://doi.org/10.3208/jgssp.v06.GIZ09

LINZ. (2011a). *NZ Coastlines (Topo, 1:50k)* [Dataset]. https://data.linz.govt.nz/layer/50258-nz-coastlines-topo-150k/

LINZ. (2011b). *NZ Lake Polygons (Topo, 1:50k)* [Dataset]. https://data.linz.govt.nz/layer/50293-nz-lake-polygons-topo-150k/

LINZ. (2011c). *NZ River Centrelines (Topo, 1:50k)* [Dataset]. https://data.linz.govt.nz/layer/50327-nz-river-centrelines-topo-150k/

LINZ. (2011d). *NZ River Polygons (Topo, 1:50k)* [Dataset]. https://data.linz.govt.nz/layer/50328-nz-river-polygons-topo-150k/

LINZ. (2012). *NZ 8m Digital Elevation Model (2012) | LINZ Data Service*. https://data.linz.govt.nz/layer/51768-nz-8m-digital-elevation-model-2012/

LINZ. (2023). *NZ Suburbs and Localities: Suburb Locality* [Dataset]. https://data.linz.govt.nz/layer/113763-suburb-locality/

MBIE. (2012). *Guidance: Repairing and rebuilding houses affected by the Canterbury earthquakes* (3rd edition). Ministry of Business Innovation & Employment. https://www.building.govt.nz/building-code-compliance/canterbury-rebuild/repairing-and-rebuilding-houses-affected-by-the-canterbury-earthquakes/

MBIE. (2019). *November 2019 Building Code update*. Building Performance. https://www.building.govt.nz/building-code-compliance/annual-building-code-updates/november-2019-building-code-update/

MBIE. (2021). *Earthquake geotechnical engineering practice (Module 1—Overview of the guidelines)* (Rev 0). New Zealand Geotechnical Society : Ministry of Business Innovation & Employment.

MBIE/MfE. (2017). *Planning and engineering guidance for potentially liquefaction-prone land: Resource Management Act and Building Act aspects* (Rev 0.1). Ministry of Business, Innovation & Employment. https://www.building.govt.nz/assets/Uploads/building-code-compliance/b-stability/b1-structure/planning-engineering-liquefaction.pdf

MfE. (2023, September 18). *Proposed National Policy Statement for Natural Hazard Decision-making 2023*. Ministry for the Environment. https://environment.govt.nz/publications/proposed-national-policy-statement-for-natural-hazard-decision-making-2023/

Michael, H. A., Russoniello, C. J., & Byron, L. A. (2013). Global assessment of vulnerability to sea-level rise in topography-limited and recharge-limited coastal groundwater systems. *Water Resources Research*, *49*(4), 2228–2240. https://doi.org/10.1002/wrcr.20213

Natural Hazards Commission Toka Tū Ake. (2024, July 1). *About natural hazards cover*. Naturalhazards.Govt.Nz. https://www.naturalhazards.govt.nz/insurance-and-claims/about-nhcover/

Natural Hazards Insurance Act 2023. https://legislation.govt.nz/act/public/2023/0001/latest/LMS546422.html

New Zealand Standards Executive. (2004). *Structural design actions—Part 5: Earthquake actions—New Zealand* (No. NZS 1170.5:2004 (Excludes Amdt 1)). New Zealand Standards Executive. https://www.standards.govt.nz/shop/nzs-1170-52004-excludes-amdt-1

NZ Geotechnical Society. (2005). *Field guide sheet description of soil and rock*. https://fl-nzgs-media.s3.amazonaws.com/uploads/2022/06/Field-guide-sheet-description-of-soil-and-rock-2005-3.pdf

O'Rourke, T. & Milashuk, S. (2012). *Spatial Distribution of Ground Motion During Earthquakes affecting Christchurch, New Zealand*.

QuakeCore. (n.d.). *New Zealand Historical Earthquake Dataset* [Dataset]. https://projectorbit.maps.arcgis.com/apps/webappviewer/index.html?id=140265d6f8754f28851c92dee5491c9a

Ramesh, K., Srinivasamoorthy, K., Rajesh Kanna, A., Gopalakrishnan, V., Supriya Varshini, D., & Subramanian, S. (2023). Simulation of the impact of sea level rise groundwater flooding along the south-eastern coast of India. *Urban Climate*, *52*, 101732. https://doi.org/10.1016/j.uclim.2023.101732

Rekker, J. (2012). *The South Dunedin coastal aquifer & effect of sea level fluctuations.* Otago Regional Council. https://www.orc.govt.nz/media/3801/south-dunedin-coastal-aquifer-study-final.pdf

Resource Management Act 1991, Pub. L. No. 1991 No 69. https://www.legislation.govt.nz/act/public/1991/0069/latest/DLM230265.html

Ristau, J. (2008). Implementation of Routine Regional Moment Tensor Analysis in New Zealand. *Seismological Research Letters*, *79*, 400–415.

Robertson, P. K. (2009). Interpretation of cone penetration tests—A unified approach. *Canadian Geotechnical Journal*, *46*(11), 1337–1355. https://doi.org/10.1139/T09-065

Robertson, P. K., & Wride, C. E. (1997). Cyclic liquefaction and its evaluation based on SPT and CPT. *NCEER Workshop on Evaluation of Liquefaction Resistance of Soils*. https://www.researchgate.net/publication/284757005_Cyclic_liquefaction_and_its_evaluation_based_on_SPT_and_CPT_Proc_NCEER_Work-shop_on_Evaluation_of_Liquefaction_Resistance_of_Soils

Rosser, B., & Dellow, S. (2017). *Assessment of liquefaction risk in the Hawke's Bay* (No. Volume 1: The liquefaction hazard model; p. 126). GNS Science. https://ref.coastalrestorationtrust.org.nz/site/assets/files/11709/cr-2015-186.pdf

Rutter, H. (2020). *LDRP45: Impacts of Earthquakes and Sea Level Rise on Shallow Groundwater Levels* (No. 1). Christchurch City Council, Aqualinc Research Limited. https://ccc.govt.nz/assets/Documents/Environment/Coast/Aqualinc-Groundwater-Report_Final_August-2020-multi-hazard-gap-filling.pdf

Scikit-image. (n.d.). *Contour finding*. Scikit-Image.Org. Retrieved April 3, 2025, from https://scikit-image.org/docs/stable/auto_examples/edges/plot_contours.html

Standards New Zealand. (2011). *NZS3604:2011 Timber-framed buildings*. 1–448.

Standards New Zealand. (2024). *TS1170.5 Public consultation Draft—Structural design actions Part 5: Earthquake actions—New Zealand* (No. DZ TS 1170.5:2024). https://consultations.standards.govt.nz/draft-standards/ts1170-5-public-consultation/user_uploads/20240215-ts-1170.5---public-comment-draft_v2.pdf

Stepinski, T. F., & Jasiewicz, J. (2011). Geomorphons—A new approach to classification of landforms. *Geomorphometry 2011*. https://gisandscience.wordpress.com/2011/12/12/geomorphons-a-new-approach-to-classification-of-landforms/

Stuedlein, A. W., & Bong, T. (2017). Effect of Spatial Variability on Static and Liquefaction-Induced Differential Settlements. *Geo-Risk 2017*, 31–51. https://doi.org/10.1061/9780784480694.003

Tonkin + Taylor. (2013). *Liquefaction Vulnerability Study* (No. 1.0; p. 59). https://canterburygeotechnicaldatabase.projectorbit.com

Tonkin + Taylor. (2015). *Canterbury Earthquake Sequence: Increased Liquefaction Vulnerability Assessment Methodology*. https://www.eqc.govt.nz/assets/Publications-Resources/CES-Increased-Liquefaction-Vulnerability-Assessment-Methodology-T+T-Report.pdf

Tonkin + Taylor. (2020). *TC52/19 Liquefaction Analysis and Hazard Mapping for Eastern Zone, prepared for Tauranga City Council* (No. 109973.v1; p. 116).

Tonkin + Taylor. (2022a). *Glenorchy Liquefaction Vulnerability*. https://www.orc.govt.nz/media/12457/glenorchy-liquefaction-vulnerability_tonkinplustaylor_final-report-issued-26-may-2022.pdf

Tonkin + Taylor. (2022b). *Wairarapa Councils: Probable maximum loss estimate for three waters infrastructure, prepared for Aon New Zealand* (No. 29730.1013 v1.0; p. 35).

Tonkin + Taylor. (2023). *Machine Learning Correction of Overpredicted Liquefaction Manifestation using Liquefaction Severity Number*. Tonkin + Taylor Ltd.

United States Geological Survey (USGS). (n.d.). *Earthquake Hazards Program* [Dataset]. https://www.usgs.gov/programs/earthquake-hazards/earthquakes

Upadhyaya, S., Maurer, B. W., Green, R. A., Rodriguez-Marek, A., & van Ballegooy, S. (2023). Surficial liquefaction manifestation severity thresholds for profiles having high fines-content, high-plasticity soils. *Canadian Geotechnical Journal*, *60*(5), 642–653. https://doi.org/10.1139/cgj-2022-0092

van Ballegooy, S., Cox, Simon C., Reynolds, T., Thurlow, C., Rutter, H. K., Scott, D. M., Harrington, G., Fraser, J., & Smith, T. (2014). *Median water table elevation in Christchurch and surrounding area after the 4 September 2010 Darfield Earthquake* (Version 2). https://natlib.govt.nz/records/35101932

van Ballegooy, S., Malan, P., Lacrosse, V., Jacka, M. E., Cubrinovski, M., Bray, J. D., O'Rourke, T. D., Crawford, S. A., & Cowan, H. (2014). Assessment of Liquefaction-Induced Land Damage for Residential Christchurch. *Earthquake Spectra*, *30*(1), 31–55. https://doi.org/10.1193/031813EQS070M

Westerhoff, R., White, P., & Miguez-Macho, G. (2018). Application of an improved global-scale groundwater model for water table estimation across New Zealand. *Hydrology and Earth System Sciences*, *22*(12), 6449–6472. https://doi.org/10.5194/hess-22-6449-2018

Youd, T. L., & Perkins, D. M. (1978). Mapping Liquefaction-Induced Ground Failure Potential. *Journal of the Geotechnical Engineering Division*, *104*(4), 433–446. https://doi.org/10.1061/AJGEB6.0000612

Zevenbergen, L. W., & Thorne, C. R. (1987). Quantitative analysis of land surface topography. *Earth Surface Processes and Landforms*, *12*(1), 47–56. https://doi.org/10.1002/esp.3290120107

Zhang, G., Robertson, P. K., & Brachman, R. W. I. (2002). Estimating liquefaction-induced ground settlements from CPT for level ground. *Canadian Geotechnical Journal*, *39*(5), 1168–1180. https://doi.org/10.1139/t02-047

Zhou, H., Wotherspoon, L. M., Hayden, C. P., McGann, C. R., Stolte, A., & Haycock, I. (2021). Assessment of Existing SPT–CPT Correlations Using a New Zealand Database. *Journal of Geotechnical and Geoenvironmental Engineering*, *147*(11), 04021131. https://doi.org/10.1061/(ASCE)GT.1943-5606.0002650

Zhu, J., Baise, L. G., & Thompson, E. M. (2017). An Updated Geospatial Liquefaction Model for Global Application. *Bulletin of the Seismological Society of America*, *107*(3), 1365–1385. https://doi.org/10.1785/0120160198

16 Applicability

This report has been prepared for the exclusive use of our client Natural Hazards Commission Toka Tū Ake, with respect to the particular brief given to us and it may not be relied upon in other contexts or for any other purpose, or by any person other than our client, without our prior written agreement.

As with all models, there are important limitations that need to be understood when using the model. Many of these stem from the fact that the model has been developed at a national to regional scale, and as a result it is not appropriate to directly apply the NLM at an individual property scale. The limitations subsections outline specific limitations related to each module, and should be read in conjunction with the general limitations. These limitations are important and should be clearly understood and adhered to before the model is implemented for any particular purpose.

Liquefaction assessment is a complex and highly specialised undertaking. Furthermore, this model and the associated codebase are complex and outside the scope of routine geotechnical engineering expertise. Therefore, if this model and its outputs are utilised by others it is important that the context for any work is clearly defined, and that it is undertaken by a team with suitable competency and experience in earthquake geotechnical engineering and data science.

Tonkin & Taylor Ltd

Environmental and Engineering Consultants

Report prepared by:	Technical review by:
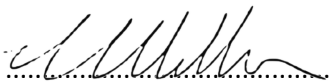	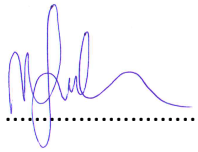
Maxim Millen	Mike Jacka
Project Manager & Technical Lead	Technical Director, Earthquake Geotechnical Engineering

Authorised for Tonkin & Taylor Ltd by:

James Russell

Project Director

t:\auckland\projects\1017473\issueddocuments\20260521 Technical report with monocity fix\nlm final technical design report_v5.2.docx
Tonkin + Taylor

Appendix A Development of relationships for conversion of Boreholes (BH)

This expands on Section 7.6.

The process to convert a BH into an equivalent CPT (Figure 7.4) requires a number of novel relationships, which were developed using the Ground Investigation (GI) database. Specifically, three sub databases were developed:

1 A CPT-BH database (Section A1)

2 A CPT-SPT-BH database (Section A2)

3 A SPT-BH database (Section A3)

These databases were used to derive the following:

- The SPT blow count to q_{c1Ncs} relationship (Section 7.6.5.2.1)
- The *main_material* and *density_status* to q_{c1Ncs} lookup table (Section 7.6.5.1.1)
- The *main_material* and *plasticity_status* to percentage $I_c > 2.6$ lookup table (Section 7.6.5.1.2)

A1 Development of CPT-BH database

The following steps were applied to generate the CPT-BH database (consisting of 1,210 unique CPT-BH pairs):

1 Identify the closest CPT to each BH that was not filtered out of the database.

2 If the CPT and BH are within 10 m of each other, then for each layer in simple log (see Section 7.6.4 for details on the simple log):

  – Obtain all interpreted CPT readings (i.e. I_c and q_{c1Ncs}) that are within the depth range of the log layer except 0.1 m below the top of the layer and 0.1 m above the bottom of the layer, and any readings in the top 0.5 m or last 0.1 m of the CPT. These exceptions were to reduce collecting data that was not representative of log layer.

  – For each CPT reading, store the I_c, q_{c1Ncs}, depth of CPT reading, layer number, *main_material*, *density_status*, *plasticity_status*, BH ID, CPT ID.

A2 Development of CPT-SPT-BH database

The CPT-SPT-BH database was based on 928 unique CPT-BH pairs and is very similar to the CPT-BH database. However, in this case, instead of cycling through the layers of the simple log, the database entries were based on the SPT readings. The specific steps were:

1 Identifying the closest CPT to each BH that contains SPT readings.

2 If the CPT and BH are within 10 m of each other, then for each SPT reading:

- Obtain all interpreted CPT readings (i.e. I_c and q_{c1ncs}) that are from the start depth of the SPT to 0.5 m below the start depth.
- For all valid CPT readings, compute the mean q_{c1Ncs} from the readings with $I_c < 2.6$.
- Obtain the BH layer number, *main_material* and *density_status* at the depth corresponding to the SPT start depth.
- Store the mean q_{c1ncs}, layer number, *main_material*, *density_status*, SPT blow count, $(N_1)_{60}$, SPT start depth, BH ID, CPT ID, provided the layer has at least 15 CPT readings with $I_c < 2.6$.

The approach adopted here is similar to that applied by Zhou et al. (2021) to develop a New Zealand SPT-CPT database using 230 CPT-BH pairs. The differences are briefly discussed in Table Appendix A.1 which can primarily be attributed to the different purposes of the databases. Zhou et al. (2021) aimed to evaluate existing CPT cone tip resistance (q_c) to SPT blow count correlations, whereas this database was to estimate the range of q_{c1Ncs} and percentage of $I_c > 2.6$ for different *main_materials*.

Table Appendix A.1: Comparison between the SPT-CPT database from Zhou et al. (2021) and the NLM SPT-CPT-BH database

This database	Zhou et al. (2021)	Reasoning for difference
CPT-BH pairs were considered if within 10 m	CPT-BH pairs were considered if within 12 m	At larger distances the assumption that soil at the same depth is representative across both investigations becomes less valid (e.g. due to dipping and discontinuous layers, variable deposition). The minor difference in distance was because sufficient data could be obtained using the smaller distance.
Store CPT readings from the start depth of the SPT to 0.5 m below the start depth	Stored CPT readings from 0.15 m below to 0.45 m below the SPT reading start depth, this only took readings from the drive length and disregarded the 0.15 m seating drive.	To compute percentage $I_c > 2.6$ and median q_{c1Ncs} from soil with $I_c < 2.6$ there needed to be a sufficient number of readings. The larger thickness of the CPT trace was still deemed representative provided that the *main_material* did not change.
All non-zero SPT blow counts were considered	All blow counts > 50 or 0 were removed.	The readings above 50 were still considered useful for obtaining representative q_{c1Ncs} values
Filters for CPT in Section 7.5.2 were applied	Locations where drillers noted heave or artesian water effects were removed due to potential soil disturbance. CPT readings less than zero were removed.	This heave and artesian filters were not applied as the metadata to capture these details was not processed, however, the CPT readings less than zero were addressed in a similar way.
Median of q_{c1Ncs} for readings where $I_c < 2.6$	Arithmetic mean of cone tip resistance was stored	Different use cases

A3 Development of SPT-BH database

The SPT-BH database was considerably larger (4,013 BH) than the CPT-BH and CPT-SPT-BH databases since it used all BH that had SPT readings. The specific steps for each SPT reading were:

- For each SPT reading define a region of influence from the SPT reading depth to 0.5 m below the SPT reading depth. Take the *main_material*, *density_status* and *plasticity_status* for the layer which has the most overlap with the region of influence.
- Store the layer number, *main_material*, *density_status*, *plasticity_status*, SPT blow count, $(N_1)_{60}$, SPT start depth, BH ID.

A4 Development of relationship between q_{c1Ncs} and SPT

The database of CPT-SPT-BH pairs was used to develop a relationship between q_{c1Ncs} and $(N_1)_{60}$. The median q_{c1Ncs} was plotted against $(N_1)_{60}$ in Figure Appendix A.1 for all *main_material*, that had more than 150 data points. Additionally, the black line was drawn corresponding to equivalent $CRR_{M7.5}$ when computed from q_{c1ncs} (Equation 1) from BI2014 and from $(N_1)_{60cs}$, using BI2014. There is no notable trend in the data, which is similar to results presented by Zhou et al. (2021). The equivalence line from the BI2014 does provide one option, however, the line uses $(N_1)_{60cs}$ not $(N_1)_{60}$. To provide a

simple expression, linear relationships for the q_{low} and q_{high} lines were established either side of BI2014 equivalence line (Equation 40). For all non-silty *main_materials*, q_{offset} was set to 55. The effect of fines content was only considered for *main_materials* that contain the word "silt", where q_{offset} was set to 70.

Equation 40:

$$q_{c1Ncs,lower} = q_{offset} + 3 \cdot (N_1)_{60} \text{ and } q_{c1Ncs,upper} = q_{offset} + 5 \cdot (N_1)_{60}$$

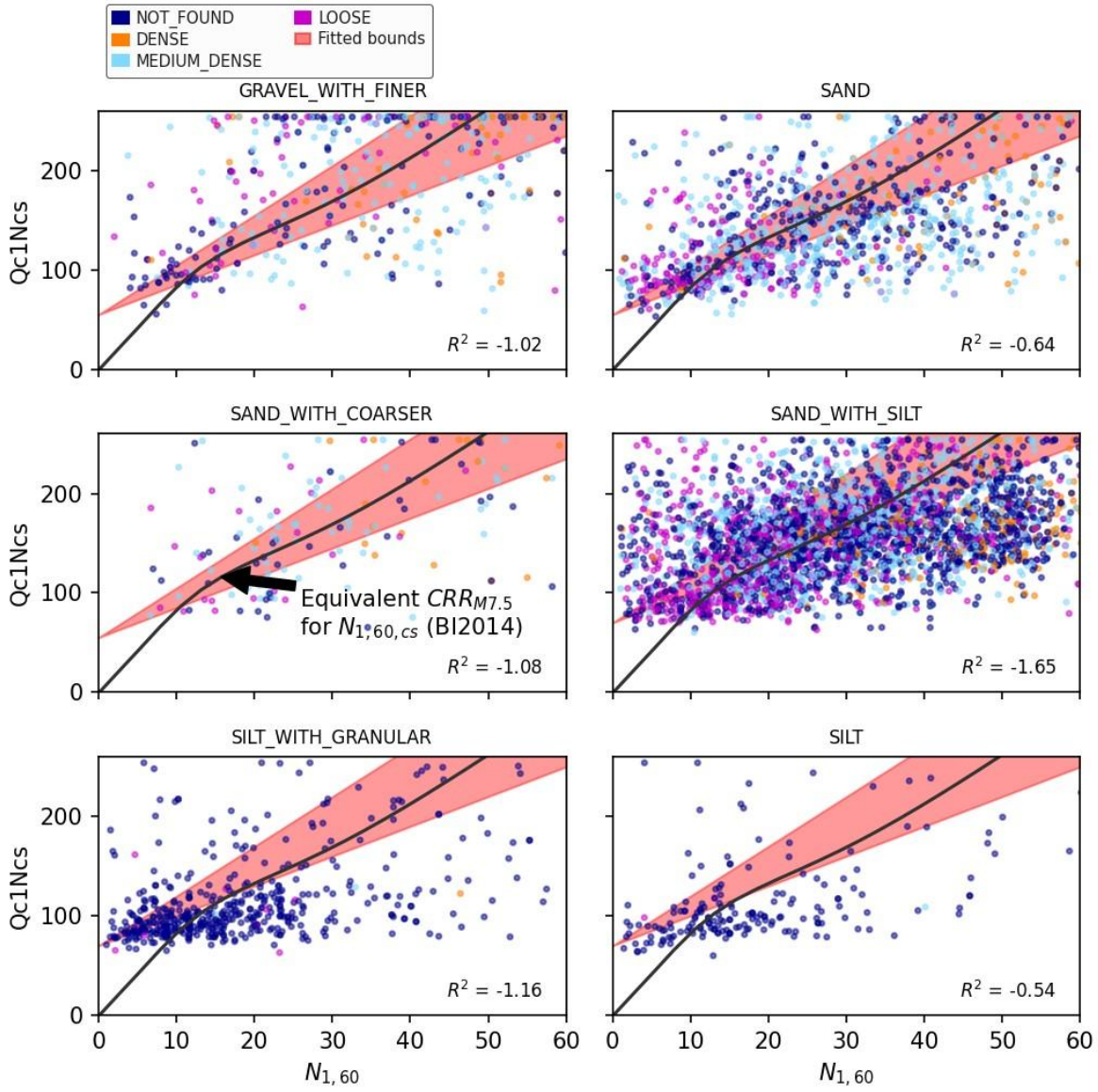

Figure Appendix A.1: SPT-CPT relationships for different main_material and density_status categories

A5 Development of main_material to q_{c1Ncs} lookup table

The *main_material* and *density_status* lookup table for q_{c1Ncs} was developed using both the CPT-BH database and the SPT-BH database. The specific steps were:

1 For each *main_material* and *density_status* determine the mean q_{c1Ncs} for all points in a layer where $I_c < 2.6$ from the CPT-BH database.

2 Determine the 30th and 70th percentile of the mean q_{c1Ncs} (Example shown in Figure Appendix A.2).

3 For each *main_material* and *density_status* determine the corresponding $(N_1)_{60}$ values in the SPT-BH database and convert them to an equivalent q_{c1Ncs} using Equation 41. Equation 41 was taken as the average of q_{low} and q_{high} from Equation 40.

4 Determine the 30th and 70th percentile of q_{c1Ncs} from the converted SPT values (Example shown in Figure Appendix A.3).

5 Take the q_{low} as the average of the CPT-based and SPT-based 30th percentile values, and the same for q_{high} for the 70th percentile.

Equation 41:

$$q_{c1Ncs,mid} = q_{offset} + 4 \cdot (N_1)_{60}$$

where q_{offset} is as defined in Appendix A4 above.

Table Appendix A.2 provides the percentiles from SPT and CPT for *main_material* and *density_status* as well as the adopted q_{low} and q_{high} values.

Notes:

- The *density_status* category of "ALL" is for when the data was only filtered by *main_material* not *density_status*.
- In the conversion of BHs to equivalent CPTs, layers that had *density_status* of NOT_FOUND used the q_{low} and q_{high} values from "ALL" rather than NOT_FOUND since these were considered more representative.
- When there was not enough data to generate reliable differences between the *density_status* categories, only the "ALL" category was produced (e.g. PEAT).

Table Appendix A.2: Percentiles of q_{c1Ncs} from SPT and CPT for each group of *main_material* and *density_status*

main_material	*density_status*	q_30_spt	q_30_cpt	q_low	q_70_spt	q_70_cpt	q_high
GRAVEL_WITH_FINER	LOOSE	111	136	124	197	254	225
GRAVEL_WITH_FINER	MEDIUM_DENSE	170	158	164	247	254	251
GRAVEL_WITH_FINER	DENSE	232	169	201	312	254	283
GRAVEL_WITH_FINER	NOT_FOUND	166	142	154	255	254	255
GRAVEL_WITH_FINER	ALL	181	151	166	274	254	264
SAND_WITH_COARSER	LOOSE	100	134	117	153	230	192
SAND_WITH_COARSER	MEDIUM_DENSE	159	131	145	234	222	228
SAND_WITH_COARSER	DENSE	224	164	194	291	254	273
SAND_WITH_COARSER	NOT_FOUND	142	114	128	241	187	214
SAND_WITH_COARSER	ALL	161	131	146	253	235	244
SAND	LOOSE	87	92	89	130	143	137
SAND	MEDIUM_DENSE	138	114	126	199	168	184
SAND	DENSE	209	143	176	272	221	247
SAND	NOT_FOUND	120	120	120	188	176	182
SAND	ALL	128	111	119	209	169	189
SAND_WITH_SILT	LOOSE	105	112	109	158	175	166
SAND_WITH_SILT	MEDIUM_DENSE	150	133	142	209	184	197
SAND_WITH_SILT	DENSE	214	146	180	273	182	227
SAND_WITH_SILT	NOT_FOUND	147	126	137	220	178	199
SAND_WITH_SILT	ALL	139	128	133	217	180	198
SILT_WITH_GRANULAR	LOOSE	94	83	88	124	112	118
SILT_WITH_GRANULAR	MEDIUM_DENSE	132	92	112	196	114	155
SILT_WITH_GRANULAR	DENSE	183	161	172	268	185	226
SILT_WITH_GRANULAR	NOT_FOUND	105	87	96	164	115	139
SILT_WITH_GRANULAR	ALL	105	87	96	166	115	140
SILT	ALL	100	84	92	149	112	130
PEAT	ALL	74	79	76	113	97	105

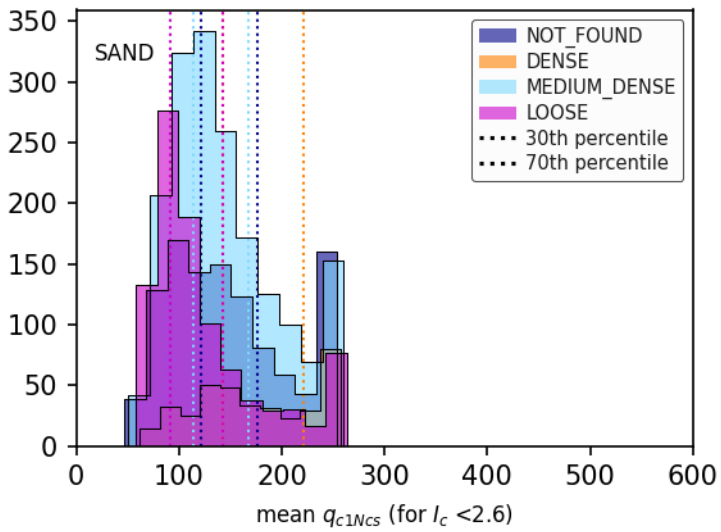

Figure Appendix A.2: Distribution of mean q_{c1Ncs} from CPT for SAND for four density_status computed using BH-CPT pairs

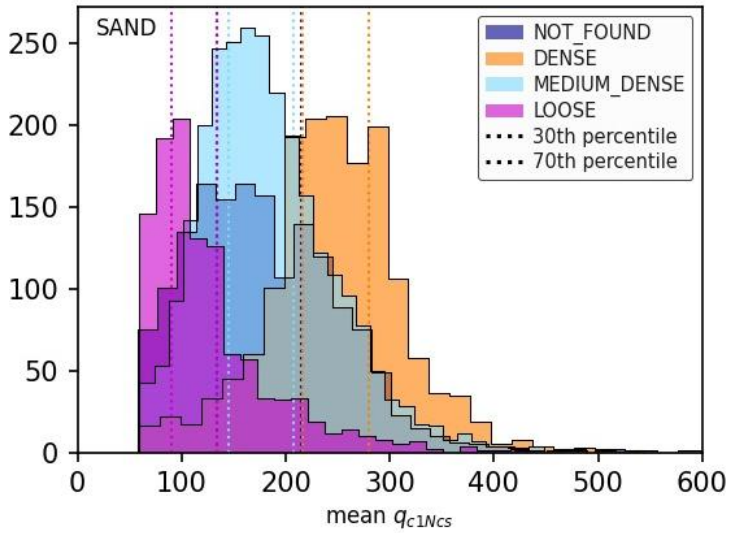

Figure Appendix A.3: Distribution of estimated q_{c1Ncs} from SPT blow count for SAND for four density_status computed using BH-SPT pairs

A6 Relationship for Percentage $I_c > 2.6$

The percentage $I_c > 2.6$ for each *main_material* and *plasticity_status* was determined from the CPT-BH database using the following steps:

1 All layers are grouped by *main_material* and *plasticity_status*.

2 The mean percentage $I_c > 2.6$ is taken for each group rounded to the nearest 10%.

3 *Main_materials* with high q_{c1Ncs} that were unlikely to have clay-like material were set to zero (e.g. COARSE_GRAVEL_TO_BOULDER, ROCK).

4 For some *main_material* where the percentage $I_c > 2.6$ for a given *plasticity_status* had insufficient points (less than 20 layers) then the *plasticity_status* was not used, and values were set based on all layers regardless of *plasticity_status*. Also, the *plasticity_status* values corresponding to NOT_FOUND (adopted) were determined from ALL (i.e. all readings regardless of *plasticity_status*), since these were considered more representative than only using the readings corresponding to NOT_FOUND. Finally, the extent of change in percentage due to *plasticity_status* was limited to +/- 30% from ALL percentages, since some *plasticity_status* categories were not based on large amounts of data.

5 Table Appendix A.3 shows the mean values and the adopted values for each *main_material* and *plasticity_status*.

Table Appendix A.3: Mean percentage $I_c > 2.6$ for each group of *main_material* and *plasticity_status*

Main_material	ALL (Mean)	Not Found (Adopted)	Non-Plastic (Mean)	Non-Plastic (Adopted)	Plastic (Mean)	Plastic (Adopted)
CLAY	82	80	66	60	86	80
COARSE_GRAVEL_TO_BOULDER	11	10	-	10	-	10
GRAVEL_WITH_CLAY	38	40		40	-	40
GRAVEL_WITH_FINER	10	10	2	0	31	30
MISSING_UNKNOWN	40	40	-	40	-	40
OTHER_NL	100	100	100	100	100	100
PEAT	92	90	93	90	86	90
ROCK	49	0	25	0	65	0
SAND	11	10	5	0	95	40
SAND_WITH_CLAY	26	30	37	30	72	60
SAND_WITH_COARSER	7	10	0	0	-	10
SAND_WITH_SILT	9	10	30	10	79	40
SILT	72	70	69	70	81	80
SILT_WITH_CLAY	73	70	75	70	72	70
SILT_WITH_GRANULAR	49	50	48	50	79	80
FILL	3	0	-	0	-	0
CLAYEY_FILL	-	80	-	60	-	80
GRAVELLY_FILL	39	0	49	0	43	0
SANDY_FILL	-	0	-	0	-	0

Appendix B Boundaries of refinement areas

Table Appendix B.1: Boundaries of refinement areas (shown as red polygons), with GW measurements (shown as dots)

Refinement Area	Map
Auckland	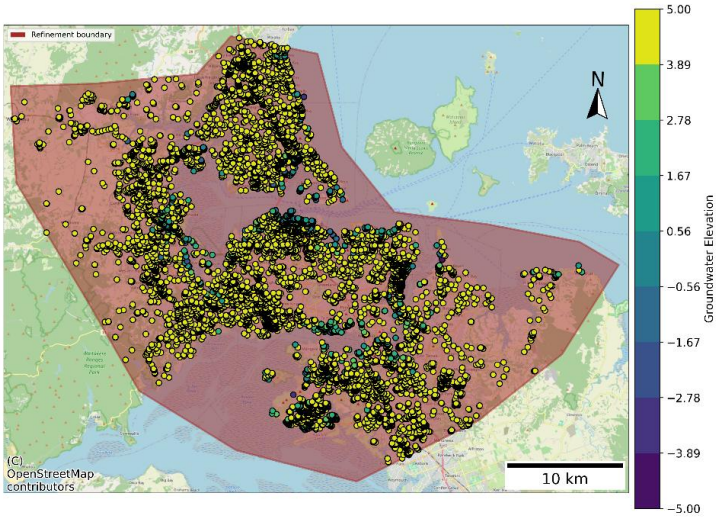
Hamilton	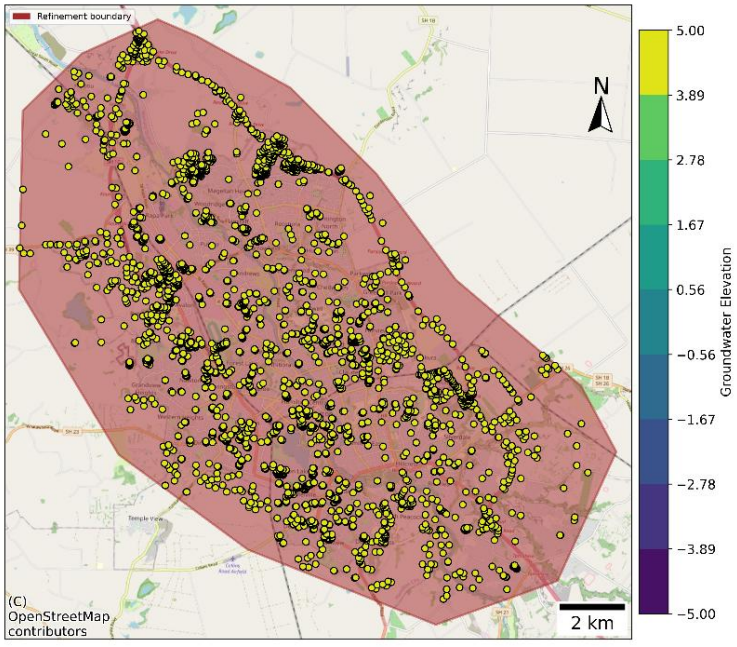

Appendix B: Boundaries of refinement areas

Refinement Area	Map
Bay of Plenty	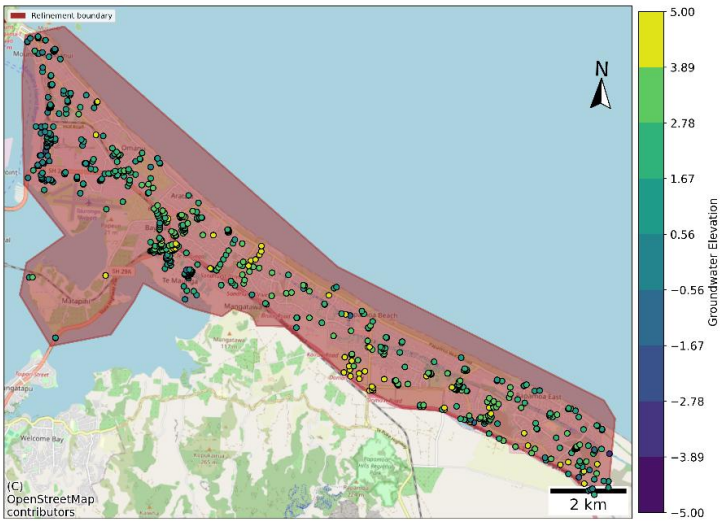
Gisborne	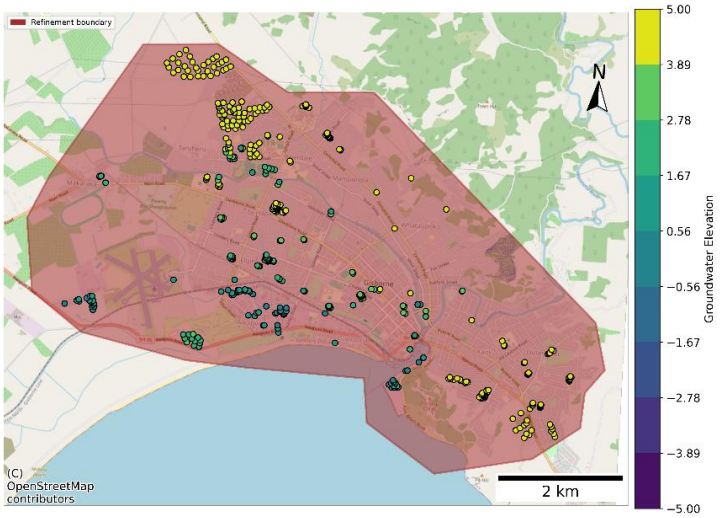
Hawke's Bay	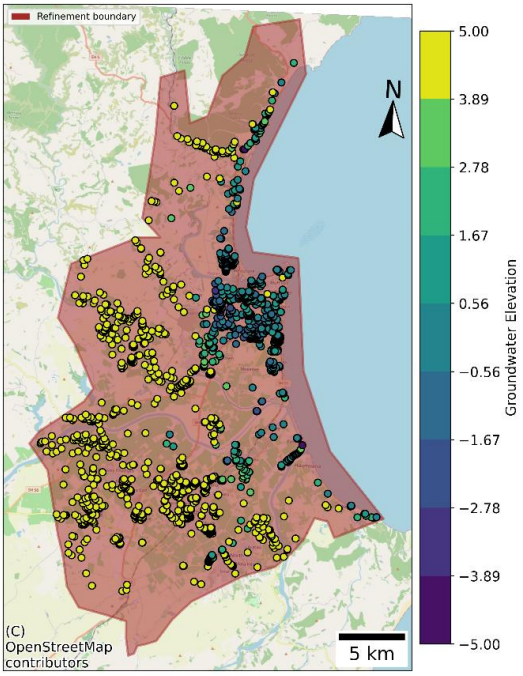

Appendix B: Boundaries of refinement areas

Refinement Area	Map
Lower Hutt	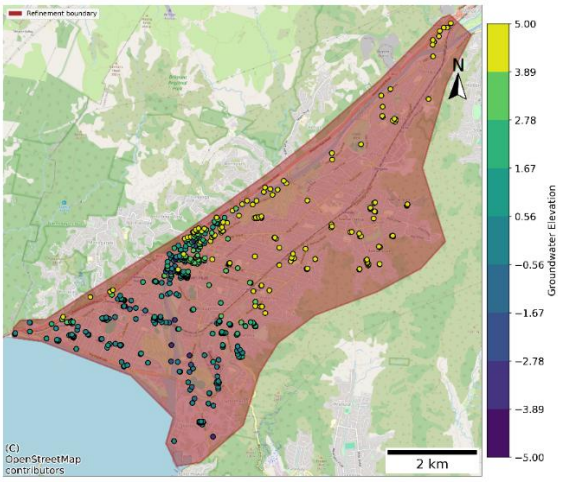
Wellington	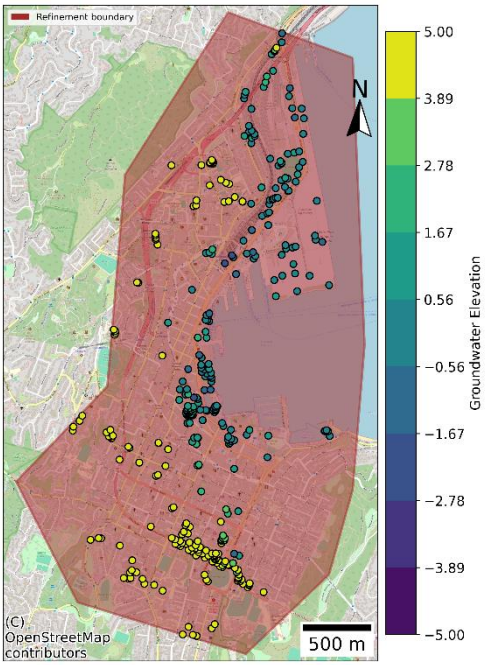
Marlborough	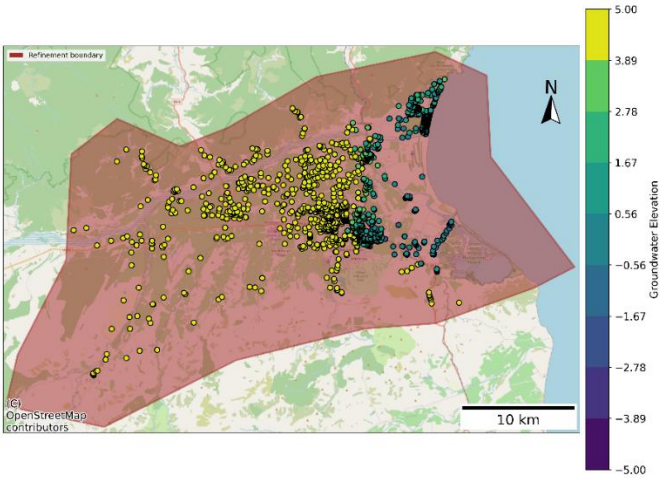

Appendix B: Boundaries of refinement areas

Refinement Area	Map
Nelson Tasman	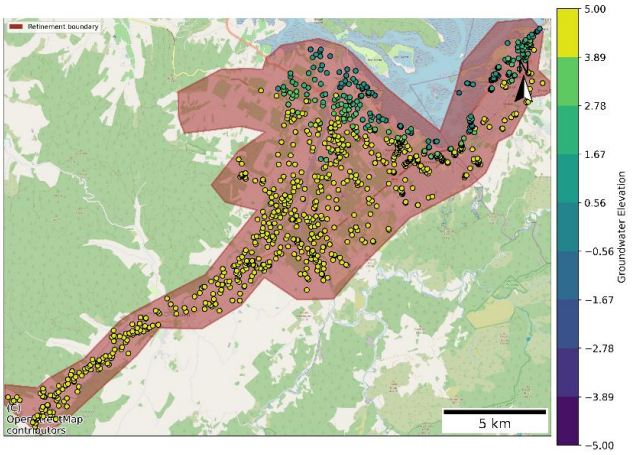
Motueka	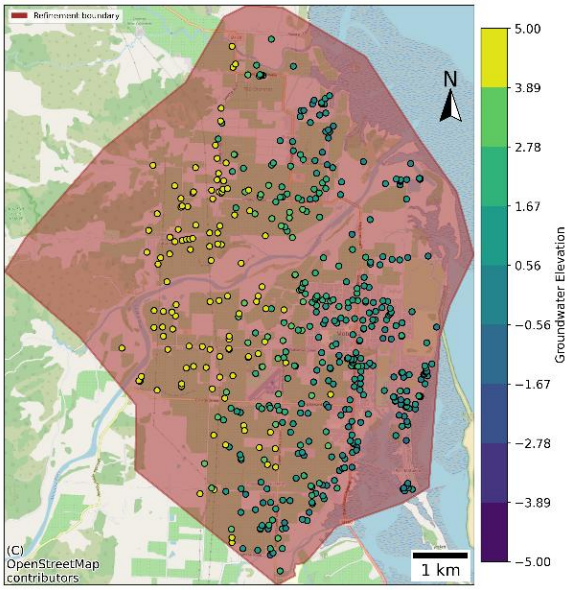
Christchurch	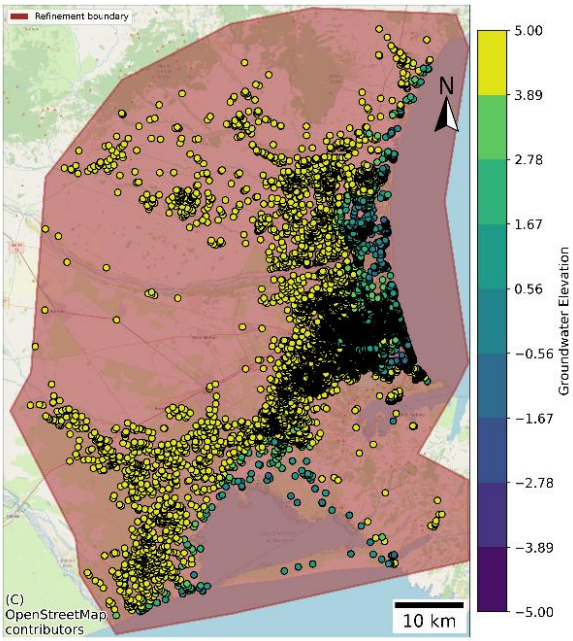

Appendix B: Boundaries of refinement areas

Refinement Area	Map
Invercargill	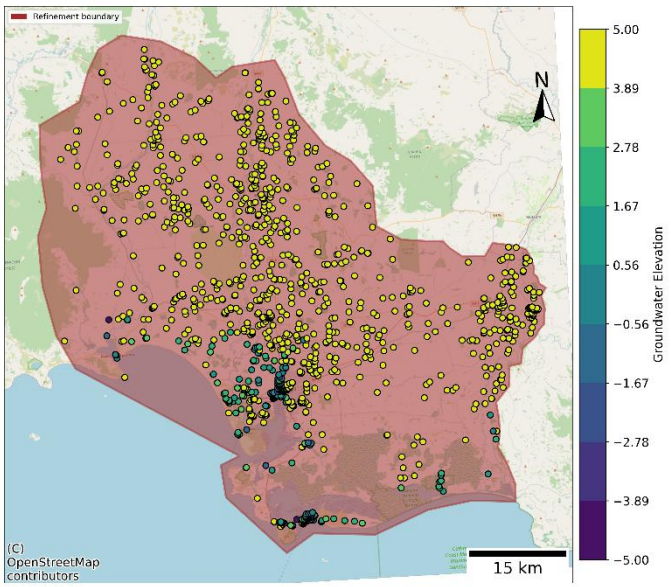

www.tonkintaylor.com